PREDICTION OF SOIL REINFORCEMENT LOADS IN MECHANICALLY STABILIZED EARTH (MSE) WALLS

by

Tony M. Allen, P.E.
Washington State Department of Transportation
FOSSC Materials Laboratory Geotechnical Branch
Olympia, Washington

and

Richard J. Bathurst, Ph.D., P.Eng.
Professor of Civil Engineering
Royal Military College of Canada
Kingston, Ontario, Canada

TECHNICAL REPORT STANDARD TITLE PAGE

1. REPORT NO.	2. GOVERNMENT ACCESSION NO.	3. RECIPIENT'S CATALOG NO.
WA-RD 522.1		

4. TITLE AND SUBTITLE	5. REPORT DATE
Prediction of Soil Reinforcement Loads in Mechanically Stabilized Earth Walls	October 2001
	6. PERFORMING ORGANIZATION CODE

7. AUTHOR(S)	8. PERFORMING ORGANIZATION REPORT NO.
Tony M. Allen, Richard J. Bathurst	

9. PERFORMING ORGANIZATION NAME AND ADDRESS	10. WORK UNIT NO.
Washington State Transportation Center (TRAC) University of Washington, Box 354802 University District Building; 1107 NE 45th Street, Suite 535 Seattle, Washington 98105-4631	
	11. CONTRACT OR GRANT NO.

12. SPONSORING AGENCY NAME AND ADDRESS	13. TYPE OF REPORT AND PERIOD COVERED
Research Office Washington State Department of Transportation Transportation Building, MS 47370 Olympia, Washington 98504-7370 Keith Anderson, Project Manager, 360-709-5405	Research report
	14. SPONSORING AGENCY CODE

15. SUPPLEMENTARY NOTES

This study was conducted in cooperation with the U.S. Department of Transportation, Federal Highway Administration.

16. ABSTRACT

Proper estimation of soil reinforcement loads and strains is key to accurate design of the internal stability of geosynthetic and steel reinforced soil structures. Current design methodologies use limit equilibrium concepts to estimate reinforcement loads for internal stability design, with empirical modifications to match the prediction to observed reinforcement loads at working stresses. This approach has worked reasonably well for steel reinforced walls but appears to seriously overestimate loads for geosynthetic walls.

A large database of full-scale geosynthetic walls (16 fully instrumented, full-scale geosynthetic walls and 14 walls with limited measurements) and 20 fully instrumented, full-scale steel reinforced MSE wall sections was utilized to develop a new design methodology based on working stress principles, termed the K_0-Stiffness Method. This new methodology considers the stiffness of the various wall components and their influence on reinforcement loads. Results of simple statistical analyses to evaluate the ratio of predicted to measured peak reinforcement loads in geosynthetic walls were telling: the AASHTO Simplified Method results in an average ratio of predicted to measured loads of 2.9 with a coefficient of variation (COV) of 86%, whereas the proposed method results in an average of 1.12 and a COV of 41%. The proposed method remains accurate up until the point at which the soil begins to fail (approximately 3 to 5% strain). For steel reinforced MSE walls the improvement was more modest: AASHTO's Simplified Method results in an average ratio of predicted to measured loads of 1.04 with a (COV) of 51%, whereas the new K_0-Stiffness Method results in an average of 1.12 and a COV of 35%. The objective of the method is to design the wall reinforcement so that the soil within the wall backfill will not reach a state of failure consistent with the notion of working stress conditions. This soil failure limit state is not considered in the design methods currently available, yet, given the research results presented herein, is likely to be a controlling limit state for geosynthetic structures.

The fruit of this research is a more accurate method for estimating reinforcement loads, thereby reducing reinforcement needs and improving the economy of MSE walls. The scope of this research was limited to MSE walls that utilize granular (non-cohesive, relatively low silt content) backfill.

17. KEY WORDS	18. DISTRIBUTION STATEMENT
Reinforcement, walls, loads, strains, creep, design	No restrictions. This document is available to the public through the National Technical Information Service, Springfield, VA 22616

19. SECURITY CLASSIF. (of this report)	20. SECURITY CLASSIF. (of this page)	21. NO. OF PAGES	22. PRICE
None	None		

DISCLAIMER

The contents of this report reflect the views of the authors, who are responsible for the facts and the accuracy of the data presented herein. The contents do not necessarily reflect the official views or policies of the Washington State Transportation Commission, Department of Transportation, or the Federal Highway Administration. This report does not constitute a standard, specification, or regulation.

TABLE OF CONTENTS

FIGURES

TABLES

EXECUTIVE SUMMARY

This report is the culmination of over ten years of research on the estimation of reinforcement loads and strains in mechanically stabilized earth (MSE structures). This effort began as a Federal Highway Administration (FHWA) Experimental Features Project (the I-90 Rainier Avenue Geotextile Wall in Seattle), progressed into a multi-phase research project on geosynthetic walls at the University of Washington, continued with the development of a database of both geosynthetic and steel reinforced MSE walls in support of proposed revisions to the AASHTO Standard Specifications for Highway Bridges, and is continuing at present as a multi-agency pooled fund research project at the Royal Military College of Canada. This pooled fund project involves construction and analysis of full-scale, reinforced soil test walls subjected to surcharge loading in excess of working stress levels. The focus of all this effort is to develop a new design methodology based on working stress principles that provides more accurate estimates of reinforcement loads and strains. This is especially important for geosynthetic walls, as engineers have long recognized that current geosynthetic wall designs are excessively conservative, given observed performance to date. It is also important to consider the behavior of steel reinforced MSE walls, to ensure that any new design method will encompass the full range of soil reinforcement properties and not be limited to geosynthetic reinforced soil wall structures. Such a new method could also help to remove the somewhat arbitrary distinctions made between various reinforcement types, as is currently done to attempt to match the empirical data. A seamless design approach with consistent limit states and levels of safety for all reinforcement materials is desirable.

Proper estimation of soil reinforcement loads and strains is key to the accurate design of internal stability for reinforced soil structures. Accurate estimation of reinforcement loads and strains will result in more accurate estimation of reinforcement strength and spacing requirements, facing connection strength, facing design, and reinforcement length required to resist pullout.

Because current design specifications, such as the AASHTO Load and Resistance Factor Design (LRFD) Bridge Design Specifications and the Eurocode, now utilize a limit states approach, an objective of any new methodology must be to make it fully adaptable to limit states design. To this end, adequate statistical information that demonstrates the accuracy of the

design, both for loads and resistances, is an important objective. Such data can be used to develop accurate load and resistance factors so that a consistent and known overall level of safety can be quantified. Currently, the true level of safety in these systems is not very well known, as empirical or theoretical assumptions have been combined with poorly defined material properties, resulting in "hidden" safety factors. Furthermore, the true limit states for MSE wall systems need to be better defined to accurately understand the true performance limits of these structures.

Research Approach

The scope of this study was limited to MSE walls that utilize granular (non-cohesive, relatively low silt content) backfill. The scope of this study was also limited to static conditions (i.e., no seismic loading). Extension of the methodology developed herein to non-select fills and seismic load environments can only be carried out once the behavior of MSE walls is well defined for the simplest soil and loading conditions.

To develop an improved design approach, a database of numerous case histories of both geosynthetic and steel reinforced MSE walls was assembled (28 fully instrumented, full-scale, field wall case histories comprising 37 different wall sections and surcharge conditions, plus five fully instrumented, full-scale, laboratory test walls, plus an additional six field wall case histories comprising 14 different wall sections that were not fully instrumented). For each wall, this database included the wall geometry, reinforcement properties and spacing, measured soil properties (strength and unit weight), any available long-term performance data, and for the fully instrumented walls the measured reinforcement strains or loads. The range of material properties and wall geometries encompassed by this database included the following:

- For the geosynthetic wall case histories, reinforcement products included geotextiles and geogrids, different polymers (polypropylene (PP), high density polyethylene (HDPE) and polyester (PET)), strip and continuous reinforcements, and a range of tensile strengths from 12 to 200 kN/m and reinforcement stiffness values from 65 to 7,603 kN/m. Reinforcement vertical spacing varied from 0.3 to 1.6 m. Wall facing batter angles varied from 0° (vertical) to 27°, although most of the walls had facing batter angles of 8° or less. Wall heights vary from 3.0 m to 12.6 m, with surcharge heights of up to 5.3 m of soil. Facing types included geosynthetic wrapped-face, welded wire, pre-cast concrete

panels, and modular concrete blocks. Plane strain peak soil friction angles, estimated from measured triaxial or direct shear test data, varied from 42° to 57°. Some of these walls have been in service for up to 25 years, although long-term strain measurements were available only for walls up to 11 years old.

- For steel reinforced MSE wall case histories, reinforcement products included steel strip, bar mat, and welded wire reinforcement, and reinforcement stiffness values of from 18,000 kN/m to 166,000 kN/m. Most of the steel walls utilized pre-cast concrete panel facings, although one wall had a welded wire facing. The facing for all of the steel reinforced MSE walls was near vertical. Walls with and without significant soil surcharges, narrow base and wide base-width walls, walls with trapezoidal cross-sections, and very tall walls of up to 18 m high were included in the database. Reinforcement coverage ratios varied from 0.053 to 1.0, while vertical spacing of the reinforcement varied from 0.3 to 0.75 m. The wall backfill materials had a range of peak plane strain soil shear strengths (35° to 56°).

The new design methodology proposed herein, called the K_0-Stiffness Method, was developed empirically through analysis of these full-scale wall case histories within a working stress framework. In most cases, reinforcement loads in these case histories had to be estimated through measured reinforcement strains converted to load with reinforcement modulus values. Therefore, the correct modulus as a function of both time and temperature was estimated, at least for geosynthetic walls, to accurately determine the reinforcement loads. For steel reinforced walls, the conversion of strain to load was relatively straightforward.

The soil reinforcement in geosynthetic walls is loaded at a very slow rate during construction in contrast to the loading rate in typical index tensile test methods. Typically, wall construction takes 500 to 1,500 hours to be completed. To account for this slow loading rate, the analysis of the long-term load-strain properties of geosynthetics determined that the geosynthetic reinforcement modulus could be accurately estimated by using isochronous creep data. Stress relaxation tests, very slow constant rate of strain, or constant rate of stress tests may be more appropriate for quantifying the long-term modulus of geosynthetic reinforcement than constant load tests. However, from a practical point of view, for most geosynthetics little difference was found in the reinforcement stiffness at the times of interest, regardless of the type of test used. The accuracy of the method used to estimate the correct time-dependent geosynthetic modulus

was verified by comparing the loads predicted from measured strains to load cell readings, typically at the reinforcement-facing connection but in one case within the backfill. The accuracy of the reinforcement loads was also verified by comparing the measured post-construction creep strains and rates to laboratory in-isolation creep data obtained at the reinforcement load level estimated from measured strain data. In most cases, the laboratory creep strains and rates were found to be the same as or greater than (i.e., more conservative for design than) the creep strains and rates measured in the full-scale walls. An important implication of this result is that reinforcement loads estimated from strain readings with the reinforcement stiffness at the end of construction are reasonably accurate.

Once the correct load levels in the reinforcement layers had been established, the reinforcement loads obtained from the full-scale wall case histories were compared to values predicted by the current methodologies found in design guidelines and design codes, including the Coherent Gravity Method and the Simplified Method (AASHTO, 1999), and by the new proposed methodology. All of the existing design methodologies were found to provide very poor predictions of reinforcement load for geosynthetic walls and only marginally acceptable predictions for steel reinforced structures. The average and coefficient of variation (COV) of the ratio of predicted to measured peak reinforcement load (T_{max}) calculated by the Simplified Method (Allen and Bathurst, 2001) was 2.9 and 85.9 percent, respectively, for geosynthetic walls, and 0.9 and 50.6 percent, respectively, for steel reinforced MSE walls. These statistics were based on the use of the plane strain friction angle of the soil to calculate reinforcement loads. Note that the Simplified Method was developed to yield an average of just over 1.0 for steel reinforced MSE walls when more conventional triaxial or direct shear strength test results are used (the average when using the triaxial or direct shear friction angle was found to be 1.04, and the COV was 50.7 percent). The K_0-Stiffness Method was found to give average and coefficient of variation values for this ratio of 1.12 and 40.8 percent, respectively, for geosynthetic walls, and 1.12 and 35.1 percent, respectively, for steel reinforced MSE walls. This was a marked improvement, regardless of which soil friction angle was chosen for use with the Simplified Method.

Sources of variability in the measured strains used to estimate loads in reinforcements and in the modulus used to convert strains to load were also investigated. Although the variability in the measurements can be considerable, with variations of ±5 to 30 percent possible in each

primary variable (combined uncertainty in the actual reinforcement loads of approximately 20 to 35 percent, assuming that variability in parameter values are uncorrelated), redundancy in the measurements, careful data interpretation, and a large quantity of data can be used to reduce the effect of this variability. While it can be argued that some sources of uncertainty are correlated, the treatment of the variability of primary parameters as uncorrelated values follows conventional practice in bridge design and simplifies the investigation of parameter variability on predicted design loads. The authors believe that the best overall practical indicator of uncertainty in the new method is the comparison of the predicted loads to the best estimates of the actual loads in the reinforcement.

K_0-Stiffness Method

This new methodology considers, directly or indirectly, the stiffness of all wall components relative to the soil stiffness to estimate the distribution and magnitude of T_{max}. As such, it uses working stress principles to estimate the load and strain in the reinforcement. However, the method is empirical in nature, since it was calibrated to accurately predict the reinforcement loads in nine full-scale field geosynthetic wall cases (13 different wall sections and surcharge conditions with 58 individual data points) and 19 full-scale field steel reinforced MSE wall cases (24 different wall sections and surcharge conditions with 102 individual data points). An additional five full-scale test wall cases were also analyzed to assess the effect of variables that could not be easily assessed with only the field case studies. This new methodology was determined to provide a reasonably accurate prediction up to the point at which the soil begins to fail, making it possible to use the load predictions from this method for both a serviceability and strength limit state prediction.

The K_0-Stiffness Method considers the following variables:

- for wall geometry, H (the total height of the wall), S (the average surcharge height above the wall), S_v (tributary area, equivalent to the average vertical spacing of the reinforcement near each layer location when analyses are carried out per unit length of wall), and Φ_{fb} (a factor to account for the effect of wall face batter)
- for reinforcement properties, S_{local} (the local reinforcement stiffness, equal to J/S_v where J is the reinforcement stiffness), and S_{global} (the global wall stiffness, equal to $J_{ave}/(H/n)$

where J_{avg} is the average stiffness for all reinforcement layers and n is the number of layers)

- for facing stiffness, Φ_{fs} (facing stiffness factor)

- for soil properties, γ (the backfill soil unit weight), and K_0 (the at-rest earth pressure coefficient based on the peak plane strain soil friction angle).

The K_0-Stiffness Method was developed by first considering the conventional equation for earth pressure behind walls, assuming nothing about the distribution of that pressure, as follows:

$$\sigma_h = \frac{1}{2}K\gamma(H+S) \tag{1}$$

"K", a lateral earth pressure coefficient, was set equal to K_0. For steel reinforced systems, a lower bound cap for $K_0 = 0.3$ (this corresponds to an approximate plane strain soil friction angle of 44°) was required to provide the best correlation between K_0 and T_{max}. The distribution of maximum tensile forces in the wall reinforcement layers was determined empirically from the case history data and through limited analytical modeling. A trapezoidal distribution was found to work well for the geosynthetic walls, but a distribution that was more triangular in shape worked best for steel reinforced MSE walls. A factor (D_{tmax}) was introduced to characterize these distributions. Therefore, applying D_{tmax} to Equation 1 resulted in a distributed earth pressure of the proper shape. Applying the vertical spacing of the reinforcement, S_v, which in effect would become a tributary area if reinforcement loads were being evaluated on the basis of unit of wall width, converted Equation 1 to represent the force carried by the reinforcement layer, as shown below:

$$T_{max} = \frac{1}{2}K\gamma(H+S)S_v D_{tmax}\Phi \tag{2}$$

All that was left to do at this point was to empirically adjust this equation using the function Φ to accurately fit the equation to the empirical reinforcement load data. This function, Φ, was found to be affected by the global wall stiffness, the facing stiffness, the facing batter, and the local stiffness of the reinforcement. Using simple regression techniques to fit the equation to the empirical data, the final expanded form of the equation to predict the maximum load, T_{max}, in each reinforcement layer was determined as follows:

$$T_{max} = 0.5 S_v K_0 \gamma \ (H + S) D_{t \, max} \left(\frac{S_{local}}{S_{global}} \right)^a \left(\frac{K_{abh}}{K_{avh}} \right)^d \Phi_{fs} 0.27 \left(\frac{S_{global}}{p_a} \right)^{0.24} \tag{3}$$

where "a" is a coefficient (currently set equal to 1 for geosynthetic walls and 0 for steel reinforced walls); K_{abh} is the horizontal component of active earth pressure coefficient accounting for wall face batter; K_{avh} is the horizontal component of active earth pressure coefficient, assuming the wall is vertical; d is a constant coefficient (currently set equal to 0.5), p_a is the atmospheric air pressure (a constant equal to 101 kPa); and all other variables are as defined previously. Φ_{fs}, the facing stiffness factor, is set equal to 0.5 to 1.0, depending on the stiffness of the facing, the wall height, and the reinforcement type (geosynthetic or steel). $(S_{local}/S_{global})^a$ is a factor that accounts for the effects of local stiffness, and $(K_{abh}/K_{avh})^d$ is the batter factor Φ_{fb}. This equation is applicable to both geosynthetic and steel reinforced MSE walls. This equation can be used to estimate both reinforcement loads and strains, since strain can be estimated by simply dividing T_{max} by the reinforcement modulus.

To properly apply this equation to design, it must be used with conceptually correct limit states. The research found that this equation predicts the reinforcement loads accurately for geosynthetic reinforced structures up until the soil begins to fail, at which point the reinforcement load begins to increase. When the soil begins to fail, its modulus begins to decrease rapidly, causing the reinforcement to carry more load to maintain equilibrium in the wall system. In the past, failure has been defined in terms of reinforcement rupture, as it has been assumed that all wall components reached a state of failure at the same time (i.e., limit equilibrium). For geosynthetic reinforced structures, the soil will fail first, and then eventually, if destabilizing loads are great enough, the reinforcement will fail. Although steel reinforcements reach yield well before the soil begins to fail, rupture of the steel will most likely occur after the soil has reached a failure state. Therefore, one limit state that must be considered for MSE walls is failure of the wall backfill. Reinforcement failure is a second limit state that must be considered. In most cases, at least for granular soils, if the reinforcement strains can be kept below approximately 3 to 5 percent strain, soil failure will be avoided. The K_0-Stiffness Method can be used to design the reinforcement to limit the strain so that soil failure is avoided. Furthermore, the reinforcement load predicted by this method can be used to estimate the ultimate tensile strength required to prevent reinforcement rupture. This method can also be

used to estimate reinforcement requirements to meet serviceability criteria, although more research is required to link the estimated reinforcement strains to short-term and long-term wall face deformations.

<u>Additional Research</u>

Additional research will be needed to refine the magnitude of parameters needed to calculate T_{max} by this method and possibly to develop more accurate expressions for the factors that appear in the fundamental equation introduced as Equation 3. The available data at the time of this study suggest that best estimates of parameter values are based on a reasonable fit to the empirical data, so that the method can be used with confidence. Additional research is recommended in the following areas:

- improved quantification of how facing stiffness and wall toe restraint affect reinforcement loads, especially for steel reinforced MSE walls

- better quantification of the load distribution factor, D_{tmax}, especially for very soft or very stiff foundation conditions and for intermediate values of global wall stiffness (i.e., is the distribution a function of global wall stiffness?), as well as how local reinforcement stiffness affects the distribution of reinforcement load

- better quantification of the effect of reinforcement coverage ratio on reinforcement loads

- better quantification of the effect of wall face batter on reinforcement loads, especially for steel reinforced systems

- better quantification of the relationship between reinforcement strain and the shear strain needed to reach the soil peak strength

- improved methods of characterizing the soil to deal with working stress conditions (i.e., is the effect of the soil strength and stiffness characteristics on reinforcement load also related to the global reinforcement stiffness?)

- improved methodology for predicting global deformation of MSE walls

- quantification of wall face connection loads, considering all mechanisms of load development at the connection

- quantification of load and resistance factors for designing limit states through the assessment of the variability in key parameters

- additional analytical modeling, properly calibrated to match the existing case history data, to provide some theoretical verification of the trends observed herein, and to extrapolate the available case history data to a broader range of wall geometries and conditions.

1.0 THE PROBLEM

Accurate prediction of loads, strains, and their distribution for mechanically stabilized earth (MSE) wall backfill reinforcement is necessary to produce cost effective, internally stable MSE wall designs. The predicted reinforcement loads affect the strength and spacing required for the reinforcement as well as the reinforcement length required to resist pullout. Predicted strains affect the assessment of MSE wall serviceability.

The methods identified in the most recent design codes and design guidelines in North America for estimating reinforcement loads in MSE walls (e.g., the Simplified Method in AASHTO 1999) are semi-empirical in nature. They use limit equilibrium concepts to develop the design model but working stress observations to adjust the model to fit what has been observed in full-scale structures. These approaches have worked reasonably well for typical steel reinforced MSE walls, but they appear to be overly conservative for predicting loads in geosynthetic reinforced structures and their performance (Bell et al. 1983, Rowe and Ho 1993; Allen, et al. 2001). Furthermore, these methods cannot be used to accurately estimate reinforcement strains and deformations. Given that problems with current design methodologies have tended to result in excessively conservative designs, especially for geosynthetic walls, design method improvements should result in cost savings for these types of structures.

The reasons for the lack of reinforcement load and strain prediction accuracy appear to be two-fold:

- Limit equilibrium concepts do not accurately reflect mechanisms of load and strain development in a mass composed of elements that are vastly different in their load-strain properties and that are seldom at incipient collapse under operating conditions in the field. Modifications to limit equilibrium-based methods to improve the prediction of reinforcement loads by using measured reinforcement load and strain data are fundamentally impossible.

- The properties of the reinforcement, especially the geosynthetic reinforcement, have not been correctly characterized to provide an accurate estimate of the reinforcement loads and strains under typical operating conditions in the field.

In general, loads in MSE wall soil reinforcements must be estimated from strain measurements and converted to load by using the modulus of the reinforcement material. There are two requirements for estimating reinforcement load:

1. accurate determination of the strain in the reinforcement, accounting for sources of strain measurement error due to gauge location, calibration, and redundancy in the measurements

2. accurate determination of the modulus of the reinforcement, accounting for the time dependence of the modulus, the effect of soil confinement, the effect of installation damage, and other sources of modulus measurement error. The selection of an appropriate modulus value is mainly an issue for geosynthetic reinforcement, as the modulus of steel reinforcement is constant with time and temperature and is relatively straightforward to determine.

Selection of the correct modulus value to calculate actual reinforcement loads in full-scale MSE walls will provide an accurate basis for developing any improved methodology for designing the internal stability of MSE walls. The interpretation of empirical reinforcement load data using the appropriate modulus values also enables analytical models to be properly calibrated. Finally, empirical data also provide a baseline against which any new design methods can be compared and their accuracy quantified.

The accuracy of any new design methodology can be assessed by its ability to predict reinforcement loads, as well as its ability to predict performance of the wall over the service life of the structure. Ultimately, the goal is to produce a wall design with the least cost, but with acceptable and predictable long-term performance.

The following approach has been taken to systematically evaluate the current methodologies for designing the internal stability of MSE walls so that improvements can be made:

1. Develop a comprehensive database of wall case histories that will allow reinforcement loads, long-term performance, or both to be assessed. Chapter 2.0 presents the basic database for geosynthetic walls. The report by Allen et al. (2001) contains the corresponding database for steel reinforced MSE walls. Additional key measurements and properties (e.g., short- and long-term strain gauge measurements, stiffness properties, estimated reinforcement loads, etc.) for both types of walls are provided in subsequent chapters.

2. Evaluate how heavily reinforced walls have been built in the past and for which long-term performance data are available. Then compare that level of reinforcement to what would be required by current design methodologies, considering both short-term and long-term stability and performance relative to the demand the reinforcement must resist. From this comparison, begin to assess the sources of conservatism in the design of MSE walls. This comparison is also provided in Chapter 2.0.

3. Evaluate measured reinforcement strains and how they were obtained to assess their accuracy and reliability so that further analysis and interpretation of the data can be conducted with confidence. This is accomplished for geosynthetic walls in Chapter 3.0. Allen et al. (2001) address this issue for steel reinforced walls.

4. Evaluate the time dependency of the modulus for geosynthetics, considering all potential load-strain-time regimes for geosynthetic reinforcement confined in the wall backfill. Develop a model to predict the modulus near the end-of-wall construction and beyond. Next, assess the accuracy of the long-term modulus prediction model through comparison with direct reinforcement load cell measurements recorded in laboratory and full-scale structures. This evaluation is described in Chapter 4.0 and applied in Chapter 5.0.

5. Verify the accuracy of reinforcement loads estimated from strain measurements based on long-term creep measurements by using the relationship between load level and creep rate. If the load levels are accurate, the creep rate observed should be reasonably close to the laboratory creep rate at that same load level, given the effect of load application rate and soil confinement. This is described in Chapter 6.0.

6. Geosynthetic walls have been viewed by the civil engineering profession, in general, as a new technology whose performance has not been established. Yet geosynthetic walls have been in use for almost 25 years. Is enough case history data available and has the science of geosynthetic material degradation prediction advanced enough to demonstrate the long-term performance of geosynthetic walls? The long-term creep data obtained from full-scale geosynthetic walls mentioned previously will also be used to answer this question, so that any new design approach developed can be tied directly to the long-term performance expected. This is also described in Chapter 6.0.

7. Compare the "measured" reinforcement loads to the loads predicted by the current design methodologies for both geosynthetic and steel reinforced walls to assess any patterns that

develop in prediction error, sources of conservatism, and appropriateness of the design model used. This will form the baseline of comparison from which to evaluate design model improvements. The primary emphasis of these analyses will be on full-scale field walls. Full-scale laboratory test walls will also be considered for controlled evaluation of specific variables, provided the test wall boundary conditions are well enough understood to know how to extrapolate the test wall behavior regarding those controlled variables to field wall conditions. This is described in Chapter 5.0 for geosynthetic walls and in the report by Allen et al. (2001) for steel reinforced walls.

8. Develop a new design approach for estimating reinforcement loads in MSE walls. Compare predicted to measured loads and strains for the full-scale field wall case histories and evaluate all variables observed to influence reinforcement loads and strains. The approach used will be empirical in nature but will consider, from a theoretical standpoint, what should influence the development of reinforcement loads and strains at working stresses. The approach should also consider MSE walls as a whole, providing as much as possible a "seamless" design approach across all reinforcement types. This new methodology is developed for geosynthetic walls in Chapter 7.0 and extended to steel reinforced walls in Chapter 8.0.

9. Finally, implement the new reinforcement load prediction methodology for designing the internal stability of MSE walls. Use a limit states approach that will be suitable for load and resistance factor design (LRFD) and use key examples to illustrate how the new method compares to current practice. This is done in a companion report by Allen and Bathurst (2001).

Because of the complexity of the analysis required, the scope of the development of this new methodology is limited to granular backfill materials. Silt and clay backfills add complexity to the prediction of reinforcement load and long-term wall performance. Therefore, the application of the proposed design methodology to silt and clay backfills is reserved for a future study.

2.0 GLOBAL LEVEL OF SAFETY AND PERFORMANCE OF GEOSYNTHETIC WALLS: A HISTORICAL PERSPECTIVE

2.1 Introduction

The first geosynthetic reinforced soil walls were built in France in 1970 and 1971 (Leflaive 1988, Leclercq et al. 1990, Puig et al. 1977). Geosynthetic reinforced walls have been in use in the United States since 1974. Bell and Steward (1977) described some of these early applications, which were primarily geotextile wrapped-face walls that supported logging roads in the northwestern United States. Since these early examples, the use of geosynthetic walls has increased steadily, both in the private and public sectors (Yako and Christopher 1987, Elias et al. 2001). The history of geosynthetic wall design in North America has been summarized by Allen and Holtz (1991) and Berg et al. (1998).

Procedures for designing the internal stability of geosynthetic walls, which define the required strength, spacing, and length of the reinforcement, have become more conservative over the past 20 years, primarily because of the increase in knowledge regarding the durability of geosynthetics (Berg et al. 1998). Attention to the resistance element of internal stability equations has produced more accurate (though likely conservative) estimates of reduction factors for installation damage, creep (at least in air), and durability (at least in the laboratory). This knowledge has generally caused an increase in the magnitude of strength reduction factors that are used to calculate the long-term strength of geosynthetics (Allen and Elias 1996). However, design methods for estimating reinforcement loads have changed little in the past 20 years, resulting in generally more conservative design over time (Berg et al. 1998).

A careful reexamination of the global "level of safety" of older, carefully documented geosynthetic reinforced soil walls and their observed performance over many years offers the possibility to quantify the expected global level of safety and performance of geosynthetic reinforced soil walls constructed today. The performance of older geosynthetic structures will provide a conservative indication of the performance that should be expected for geosynthetic structures built today.

The first objective of this chapter is to provide a database of selected, well-documented geosynthetic reinforced soil walls constructed as long as 25 years ago. The walls selected in this

study were constructed with granular backfill materials to simplify interpretation and analyses. Only case histories that have a post-construction wall performance evaluation were selected.

The second objective of this chapter is to quantify the global level of safety for the one or more wall sections or loading conditions corresponding to each wall case history, and to compare these values to visual observation of wall behavior. Global level of safety is quantified in terms of a resistance-demand ratio, RD, which is the ratio of the sum of reinforcement strengths required to prevent reinforcement rupture to the total horizontal load in the soil reinforcement layers. This global level of safety or "resistance to demand ratio" concept was originally introduced by Allen (1997) and Berg et al. (1998) to provide a common basis of comparison between wall structures and design methods. The calculation of global level of safety values is explained in detail in Section 2.3.

The resistance-demand ratio for existing geosynthetic retaining walls is calculated and compared to the resistance-demand ratio that would be required by current design practice and the AASHTO (1999) design code in the USA. This comparison, together with observed post-construction wall performance, allows the identification of potential sources of current design conservatism, and the proposal of directions for improving current geosynthetic reinforced wall design methodologies.

2.2 Summary of Geosynthetic Wall Case Histories

The first geosynthetic wall in the world was built near Poitiers, France, in 1970 using woven polyester straps. Leflaive (1988) and Leclercq et al. (1990) reported on the long-term durability observed for the polyester reinforcement and provided some details about this wall. The polyester straps were of a type similar to safety belts and were anchored directly to the concrete facing units. The total wall height was approximately 4.5 meters, with six levels of straps installed at a vertical spacing that varied from 0.6 m to 1.1 m. The particle size distribution and soil type were not reported, but in a published photograph (Leclercq et al. 1990) the soil appeared to be gravelly. The pH of the soil was reported to be 8.5, and near the back of the facing panels, the pH was as high as 13 to 14. Samples of the straps taken nine years after the wall had been constructed indicated that the straps had lost significant strength near the connections to the concrete panels. Consequently, an earth berm was placed in front of the wall to prevent the possibility of collapse should the strength loss continue. Samples were taken and

tested again 17 years after the wall had been built. Significant losses on the order of 45 to 50 percent relative to the original strength of the straps had occurred near the wall face, but no significant strength loss was observed in the straps in the backfill away from the face (Leclercq et al. 1990). Observers concluded that at least a portion of this strength loss was due to hydrolysis caused by a high pH level at the wall face, with the remainder of the strength loss due to mechanical damage.

The second geosynthetic wall built, in 1971, was also located in France, at Rouen, on the A15 motorway. Details of this wall are provided by Delmas, Blivet and Matichard (1987), Gourc and Matichard (1992) and Leclercq et al. (1990). The wall was vertically faced and 4 m in height with a geotextile face. This temporary wall was considered experimental and was backfilled with earth in front of the wall after nine months of service. A nonwoven, needlepunched, polyester geotextile with a tensile strength of 10 kN/m was placed at a vertical spacing of 0.5 m. The fill material was a fine grained mixture of chalk, clay, and flint, with a soil pH of 9 to 10. The wall was placed over a compressible layer of peat and settled more than 1 meter, making interpretation of the wall strains, estimated to be in the order of 1.5 to 2 percent, very difficult (Gourc and Matichard 1992). After the wall had been in place for 15 years, samples of the geotextile were exhumed and tested. Samples revealed a loss in strength of 20 to 30 percent (Gourc and Matichard 1992, Leclercq et al. 1990). Since no chemical changes in the geotextile had occurred, all of the strength loss was attributed to mechanical damage that had occurred during construction.

Additional, more detailed geosynthetic wall case histories are summarized in Table 2.1 and Figures 2.1 through 2.20. The table provides information on material types, material properties, wall geometry, and surcharge details. Additional project details and performance observations are provided in the following sections. A total of 19 different projects, with data from 35 analysis cases (i.e., combinations of wall geometry and loading condition), are presented in the database. The writers were directly involved in many of the project case studies described below. For other walls the writers contacted the original investigators to confirm project details and to collect unpublished information.

Table 2.1. Summary of wall height and material properties for geosynthetic wall case histories.

Case Study	Project	Height and Surcharge	Soil Description	Soil Gradation d_{max} d_{50} <75μm (mm/mm/%)	Soil Unit Weight γ (kN/m³)	Design ϕ_{des} (°)	Triaxial or Direct Shear ϕ_{trx} or ϕ_{ds} (°)	Estimated Plane Strain ϕ_{ps} (°)	Project Section or Panel Number	Depth Zone	Geosynthetic Product Name/ Mass/unit area	Product Type/ Polymer	Index Strength T_{ult} (kN/m)
GW1	Snailback Wall, 1974	2.9 m plus 0.9 m soil surcharge	uniform subrounded fine to medium sand.	4.76 1.2 2	21.2[1]	34°	38°[8]	43°	NA	All	Fibretex 420 (420 g/m²)	NW-NP-GT/PP	19.0
GW2	Olympic National Forest Wall, 1975	5.6 m	crushed rock	75 35 -	18.1[2]	40°	NA	50°[3]	A	1 & 2	Bidim C-28 (200 g/m²)	NW-NP-GT/PET	14.4
										3 & 4	Bidim C-38 (420 g/m²)	NW-NP-GT/PET	24.7
									B	1 & 2	Fibretex 420 (420 g/m²)	NW-NP-GT/PP	15.8
										3 & 4	Fibretex 600 (600 g/m²)	NW-NP-GT/PP	22.1
GW3	CDOT Glenwood Canyon Walls, 1982	4.8 m	pit run, well-graded, clean sandy gravel (rounded)	100 19 -	22.3[1]	35°	42°[7]	46°	1 & 9	1 & 2	Typar 3601	HB-NW-GT/PP	12.6[5]
										3	Trevira 1155	NW-NP-GT/PET	28.9[5]
									2 & 10	1 & 2	Trevira 1127	NW-NP-GT/PET	16.6[5]
										3	Trevira 1155	NW-NP-GT/PET	28.9[5]
									3	1 & 2	Supac (200 g/m²)	NW-NP-GT/PP	24.3[5]
										3	Trevira 1155	NW-NP-GT/PET	28.9[5]
									4	1 & 2	Fibretex 400	NW-NP-GT/PP	9.9[5]
										3	Trevira 1155	NW-NP-GT/PET	28.9[5]

Case Study	Project	Height and Surcharge	Soil Description	Soil Gradation d_{max} d_{50} <75μm (mm/mm/%)	Soil Unit Weight γ (kN/m³)	Design ϕ_{des} (°)	Triaxial or Direct Shear ϕ_{trx} or ϕ_{ds} (°)	Estimated Plane Strain ϕ_{ps} (°)	Project Section or Panel Number	Depth Zone	Geosynthetic Product Name/ Mass/unit area	Product Type/ Polymer	Index Strength T_{ult} (kN/m)
GW3	CDOT Glenwood Canyon Walls, 1982	4.8 m plus 2 m soil surcharge 4.8 m	pit run, well-graded, clean sandy gravel (rounded)	100 19 -	22.3[1]	35°	42°[7]	46°	5	1	Typar 3401	HB-NW-GT/PP	7.7[5]
										2	Typar 3601	HB-NW-GT/PP	12.6[5]
										3	Trevira 1155	NW-NP-GT/PET	28.9[5]
									6	1	Trevira 1115	NW-NP-GT/PET	6.8[5]
										2	Trevira 1127	NW-NP-GT/PET	16.6[5]
										3	Trevira 1155	NW-NP-GT/PET	28.9[5]
									7	1 & 2	Supac (135 g/m²)	NW-NP-GT/PP	12.1[5]
										3	Trevira 1155	NW-NP-GT/PET	28.9[5]
									8	1	Fibretex 200	NW-NP-GT/PP	5.8[5]
										2	Fibretex 400	NW-NP-GT/PP	9.9[5]
										3	Trevira 1155	NW-NP-GT/PET	28.9[5]
GW4	Devils Punch Bowl Wrap-Faced Wall, 1982	8.8 m	crushed basalt	50 4 to 5 10	22.0[3]	40°	NA	50°[3]	NA	All	Tensar SR-2	E-GG/HDPE	73.0[4]
GW5	Tanque Verde Wall, 1984	4.9 m	clean well graded gravelly sand	75[3] 0.7[3] 3[3]	19.6[1]	34°	53°[6][10]	53°[1]	Wall 26-32	All	Tensar SR-2	E-GG/HDPE	73.0[4]

9

Case Study	Project	Height and Surcharge	Soil Description	Soil Gradation d_{max} d_{50} <75μm (mm/mm/%)	Soil Unit Weight γ (kN/m³)	Design ϕ_{des} (°)	Triaxial or Direct Shear ϕ_{trx} or ϕ_{ds} (°)	Estimated Plane Strain ϕ_{ps} (°)	Project Section or Panel Number	Depth Zone	Geosynthetic Product Name/ Mass/unit area	Product Type/ Polymer	Index Strength T_{ult} (kN/m)
GW6	Lithonia Georgia Wall, 1985	6.1 m	well graded sandy gravel	NA	21.2[3]	40°	43°[3]	48°	NA	All	Tensar SR-2	E-GG/ HDPE	79.0[5] (x 0.60 for partial coverage)
GW7	Oslo, Norway Wall, 1987	4.8 m plus 3 m soil surcharge (70° facing batter from horizontal)	uniformly graded fine to medium sand	205 0.2 -	17.0[1]	33°	41°[8]	46°	J	All	Tensar SR-55 (primary)	E-GG/ HDPE	47.0[5]
									J	All	Tensar SS1 (secondary)	E-GG/ PP	19.6[5]
									N	All	Tensar SR-55 (primary)	E-GG/ HDPE	47.0[5]
									N	All	Tensar SS1 (secondary)	E-GG/ PP	19.6[5]
GW8	Algonquin HDPE Wall, 1988	6.1 m plus 2.1 m soil surcharge	well graded clean gravelly sand	50 4 0	20.4[1]	40°	40°[7]	43°	FHWA Wall 2	All	Tensar SR-2	E-GG/ HDPE	67.8[5]
GW9	Algonquin PET Wall, 1988								FHWA Wall 9	All	Miragrid 5T	W-GG/ PET	39.2[5]
GW10	Algonquin Geotextile Wall, 1988	5.9 m but supported by 2.1 m of water at base of wall							FHWA Wall 6	All	Quline 160	W-GG/ PET	19.3[5]
		5.9 m after water removed								All	Quline 160	W-GG/ PET	1 9.3[5]

Table 2.1, Continued.

Case Study	Project	Height and Surcharge	Soil Description	Soil Gradation d_{max} d_{50} <75μm (mm/mm/%)	Soil Unit Weight γ (kN/m^3)	Design ϕ_{des} (^{o})	Triaxial or Direct Shear ϕ_{trx} or ϕ_{ds} (^{o})	Estimated Plane Strain ϕ_{ps} (^{o})	Project Section or Panel Number	Depth Zone	Geosynthetic Product Name/ Mass/unit area	Product Type/ Polymer	Index Strength T_{ult} (kN/m)
GW11	RMCC Geogrid Wrapped-Face Wall, 1986	2.85 m plus 0.6 m soil surcharge	clean uniform-size washed sand with some gravel	8 1.2 0	17.6[1]	40°	46° to 53[08]	55[o(11)]	NA	All	Tensar SS2	E-GG/PP	16.0[5]
GW12	RMCC Timber Propped Panel Wall, 1987	3 m plus effective surcharge of 42 kPa			18.0[1]					All	Tensar SR2	E-GG/ HDPE	67.0[5]
GW13	RMCC Timber Incremental Panel Wall, 1987	3 m plus effective surcharge of 42 kPa								All	Tensar SR-2	E-GG/ HDPE	67.0[5]
GW14	RMCC Full-Height Aluminum Propped Panel Wall, 1989	3 m	clean uniform-size washed sand with some gravel	8 1.2 0	18.0[1]	40°	46° to 53[08]	55[o(11)]	NA	All	Tensar SS1	E-GG/PP	12.0[5]
		3 m plus effective surcharge of 70 kPa									Tensar SS1	E-GG/PP	12.0[5]
GW15	RMCC Incremental Aluminum Panel Wall, 1989	3 m								All	Tensar SS1	E-GG/PP	12.0[5]
		3 m plus effective surcharge of 60 kPa									Tensar SS1	E-GG/PP	12.0[5]

Table 2.1, Continued.

Case Study	Project	Height and Surcharge	Soil Description	Soil Gradation d_{max} d_{50} <75μm (mm/mm/%)	Soil Unit Weight γ (kN/m³)	Design ϕ_{des} (°)	Triaxial or Direct Shear ϕ_{trx} or ϕ_{ds} (°)	Estimated Plane Strain ϕ_{ps} (°)	Project Section or Panel Number	Depth Zone	Geosynthetic Product Name/ Mass/unit area	Product Type/ Polymer	Index Strength T_{ult} (kN/m)
GW16	WSDOT Rainier Ave. Wall, 1989	12.6 m plus 5.3 m soil surcharge	well graded gravelly sand	60 2 -	21.1[1]	36°	45°[7][9]	54°	NA	1 2 3 4	Exxon GTF200 Exxon GTF375 Exxon GTF500 Exxon GTF1225T	W-GT/PP W-GT/PP W-GT/PP W-GT/PET	31.0[5] 62.0[5] 92.0[5] 186[5]
GW17	London, Ontario Propped Panel Wall, 1989	7.1 m	silty sand and gravel	27 4.75 10	20.4	36°	NA	45°[3]	Panel 39	All	Tensar UX1600	E-GG/HDPE	118[4]
GW18	Fredericton, New Brunswick Propped Panel Wall, 1990	6.1 m	pit run coarse sand and gravel	76 - 12	20.4[3]	40°	NA	45°[3]	NA		Tensar SR2 (except 2nd layer from top is SR1)	E-GG/HDPE	73.0[4] 55.0[4] for SR-1 (x 0.77 for partial coverage)
GW19	PET Strip St. Remy Test Wall, 1993	6.4 m	uniform size fine to medium (Fontaine-bleu) sand	1.5 0.15 to 0.2 4	16.4	37°	39°[7][10]	42°	NA	All	Paraweb 2S	PET	200

Table 2.1, Continued.

Case Study	Project	Height and Surcharge	Soil Description	Soil Gradation d_{max} d_{50} <75μm (mm/mm/%)	Soil Unit Weight γ (kN/m³)	Design ϕ_{des} (°)	Triaxial or Direct Shear ϕ_{trx} or ϕ_{ds} (°)	Estimated Plane Strain ϕ_{ps} (°)	Project Section or Panel Number	Depth Zone	Geosynthetic Product Name/ Mass/unit area	Product Type/ Polymer	Index Strength T_{ult} (kN/m)
GW20	Vicenza, Italy Wall, 1998	4 m	clayey, sandy gravel	50 10 10	21.1[2]	40°	49°[7][10]	57°	1	All	Tenax TT 201 SAMP	E-GG/ HDPE	58.0[5]
		4 m plus 3.5 m soil surcharge									Tenax TT 201 SAMP	E-GG/ HDPE	58.0[5]
		4 m							2		Tenax LBO 220 SAMP	E-GG/PP	23.7[5]
		4 m plus 3.5 m soil surcharge									Tenax LBO 220 SAMP	E-GGPP	23.7[5]

Notes:
(1) Measured in-situ during compaction of backfill
(2) Estimated from laboratory compaction tests
(3) Estimated based on data for similar soil
(4) From manufacturer product testing not specific to project wall
(5) From project-specific testing of geosynthetic materials
(6) Multiaxial cubic triaxial test results
(7) Triaxial compression test
(8) Direct shear test
(9) Plane strain test
(10) (c-φ) soil peak strength envelopes corrected to equivalent peak secant friction angle using $\tan\phi_{secant} = c/\gamma H + \tan\phi$ where c = soil cohesion
(11) peak direct shear friction angle corrected to peak plane strain shear angle using method by Bolton (1986)

NW-NP-GT = nonwoven needlepunched geotextile
HB-NW-GT = heat bonded nonwoven geotextile
E-GG = extruded geogrid
W-GG = woven geogrid
W-GT = woven geotextile
PP = polypropylene
PET = polyester
NA = not available.

2.2.1 Snailback Geotextile Shotcrete Wrapped-Face Wall, 1974 (Case GW1, Figure 2.1)

The Snailback Wall, built by the US Forest Service in 1974 near Cave Junction, Oregon, in the Siskyou National Forest, was the first geosynthetic wall built in North America and the third geosynthetic wall built in the world. Details regarding the Snailback Wall and its performance after 25 years were reported by Greenway et al. (1999), and their paper is the primary source of information on this structure. Direct shear tests were conducted on the backfill to determine its shear strength (Bell 1998). The wall reinforcement was placed to develop tensile load in the cross-machine direction. The ultimate wide-width tensile strength of the reinforcement layers was estimated from the results of the Oregon State University (OSU) ring test, grab tensile tests, and correlation with wide width tensile tests. Because of the unusually long overlap of the geotextile behind the wrapped face (1.5 m), the facing overlaps were considered to contribute to the internal stability of the reinforced zone. Post-construction evaluation of the geotextile strength and durability has not been carried out. However, the non-aggressive nature of the backfill soil and wall environment is believed to have kept installation damage and long-term strength losses to a minimum.

Recent observations of the long-term performance of the wall after 25 years of service reported by Greenway et al. (1999) indicate that the wall has performed well. Although no deformation measurements are available, they concluded that little if any deformation has occurred since the shotcrete facing was installed. They reported no evidence of facing distortion or significant cracking. Forest Service records reveal that no maintenance has been performed on the wall since its construction.
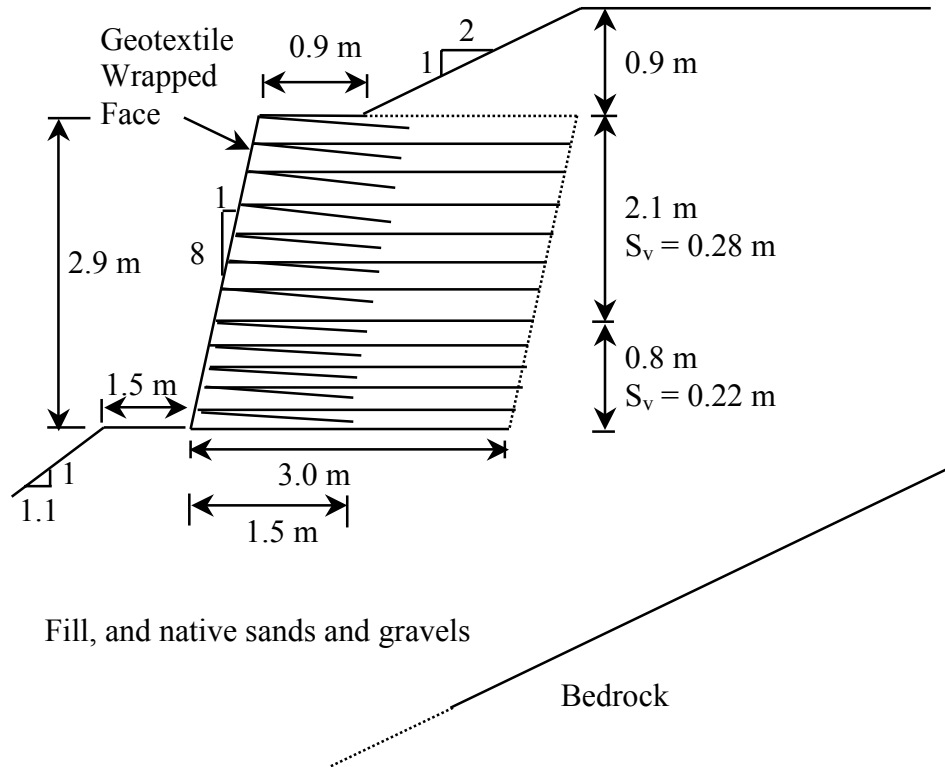
Figure 2.1. Cross-section for Snailback Wall.

2.2.2 Olympic National Forest Geotextile Wrapped-Face Wall, 1975 (Case GW2, Figure 2.2)

The Olympic National Forest wall located near Shelton, Washington, built in 1975, was the second geosynthetic reinforced soil wall built in the USA (Steward et al. 1977). The wall backfill is a crushed rock. The wall was built using two different reinforcement designs (Sections A and B). The ultimate wide-width tensile strength of the reinforcement layers was estimated from the results of OSU ring tests, grab tensile tests, and correlation with wide-width test results (Powell and Mohney 1994).

Lateral movements of 25 to 50 mm were measured with magnet extensometers attached to horizontal inclinometers. These deformations occurred during the first 1.5 years of service and within 1 meter of the front of the wall (Steward et al. 1977). This movement is attributed, in part, to downhill creep of the foundation that was seated on a relatively steep slope. In 1993, 18 years after construction, the wall was surveyed by the US Forest Service (Powell and Mohney 1994). They observed that wall movements had ceased. Nevertheless, the geotextile at the wrapped face had degraded significantly under exposure to ultraviolet radiation because of the poor performance of the spray-coated asphalt emulsion that was originally applied to the facing.

15

A facing repair with shotcrete is planned. Samples of the geotextile reinforcement were exhumed to measure strength degradation and to identify the cause of any degradation. The geosynthetic revealed obvious signs of installation damage (holes and punctures), and a strength loss based on tensile test results on the order of 50 percent for the polyester geotextile and 40 percent for the polypropylene geotextile. Powell and Mohney concluded that most of this strength loss could be attributed to installation damage.
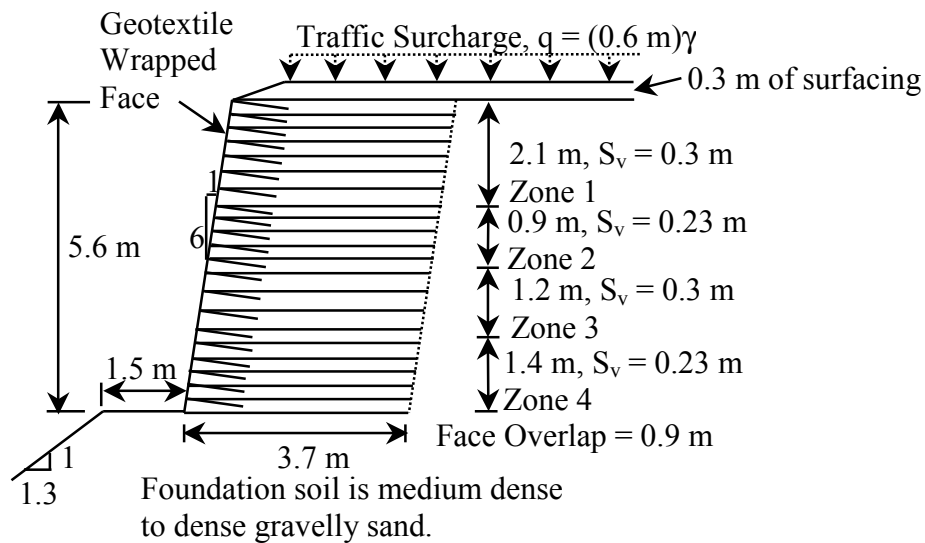
Figure 2.2. Cross-section for Olympic National Forest wall.

2.2.3 Glenwood Canyon Geotextile Shotcrete Faced Walls, 1982 (Case GW3, Figure 2.3)

A full-scale test wall was constructed by the Colorado Department of Transportation (CDOT) in 1982 (Bell et al. 1983). This wall consisted of ten different test sections and used a large number of different nonwoven geotextile products. Sections 2 and 9, at the opposite ends of the wall, used identical designs. Two of the wall sections (sections 5 and 6) were surcharged with soil after wall construction had been completed in an attempt to fail the wall. Soil shear strength was determined from the results of large diameter (100-mm) triaxial compression tests (Bell 1998). Wide-width tests using a precursor to the ASTM 4595 test method were conducted by the first writer in 1982 to determine the ultimate strength of the geotextile products. A low mass per area geotextile was used as a separator at the top of all reinforced wall sections, but these layers are not considered to have contributed to wall internal stability.

Lateral movements of 50 to 75 mm or less were measured. Most of this movement occurred during construction (Bell et al. 1983). The greatest lateral movements occurred at the top of the wall, but this may be due to the 150 to 450 mm of vertical foundation settlement recorded at the site. All of the walls appeared to be stable with respect to lateral movements within 6 months after construction, including the surcharged sections. Post-construction strains in the geotextile were too small in magnitude to be measurable.

Portions of the wall were excavated in 1986 to obtain samples of the geotextile reinforcement. Tensile test results indicated strength losses on the order of 15 to 38 percent, which appeared to be primarily due to installation damage (Allen and Bathurst 1994, Bell and Barrett 1995). The wall sections were buried in 1993. At that time visual observations by the first writer revealed no signs of distress.

Geotextile Wrapped Face with Shotcrete Covering

1.3

1

4 m max., 2 m ave. (Wall Sections 5 & 6)

$\gamma = 19.5$ kN/m^3

20:1 slope

Light weight cover fabric

Wall Sections 1 to 4 and 7 to 10

0.3 m

1

5

4.5 m

2.2 m, S_v = 0.23 to 0.30 m, Zone 1

1.6 m, S_v = 0.23 to 0.30 m, Zone 2

0.7 m, S_v = 0.30 to 0.37 m, Zone 3

0.9 m

2.4 m

3.7 m

Back of Wall, Sections 9 and 10 only

Foundation soil is compressible silt and clay.
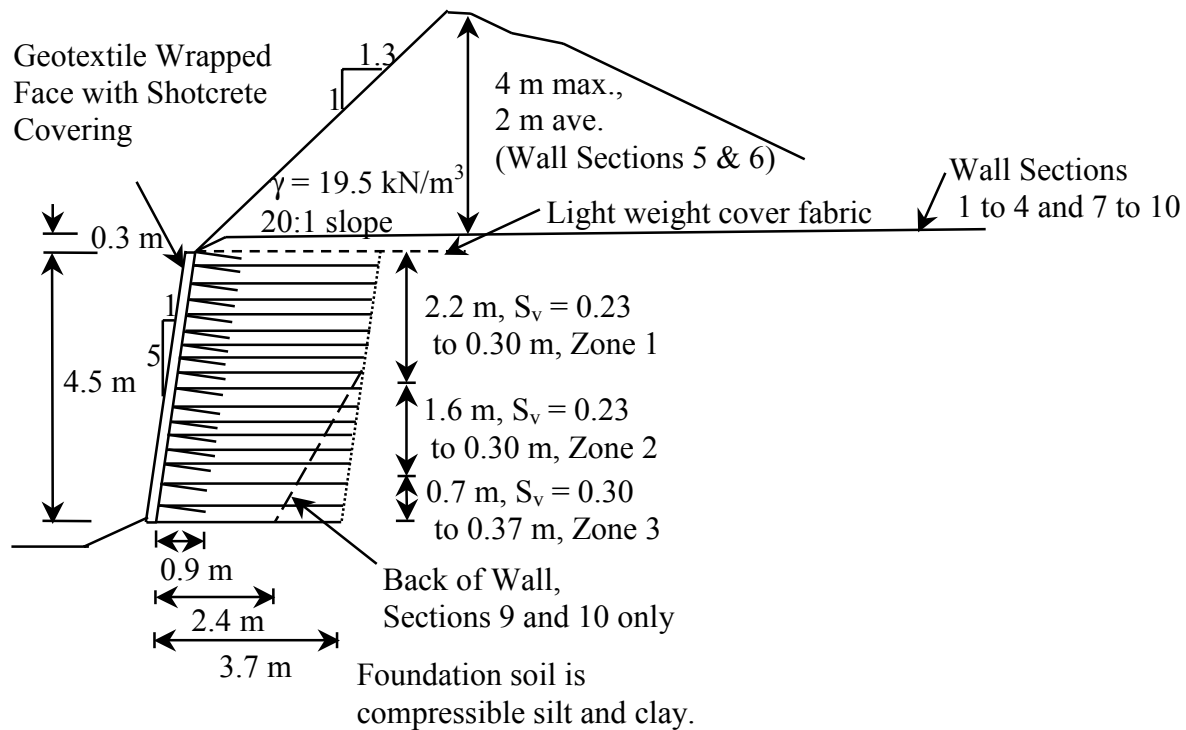
Figure 2.3. Cross-section for Colorado Department of Transportation Glenwood Canyon shotcrete faced walls.

2.2.4 Devils Punch Bowl Wrapped Face Geogrid Wall, 1982 (Case GW4, Figure 2.4)

The first permanent geogrid wall constructed in the US was built in 1982 to support a roadway access to Devils Punch Bowl State Park on the central Oregon coast (Bell et al. 1985). Personal observations by the first writer in 1993 indicated that little wall movement had occurred

since construction and that the geogrid reinforcement still appeared shiny and new, with no apparent degradation.
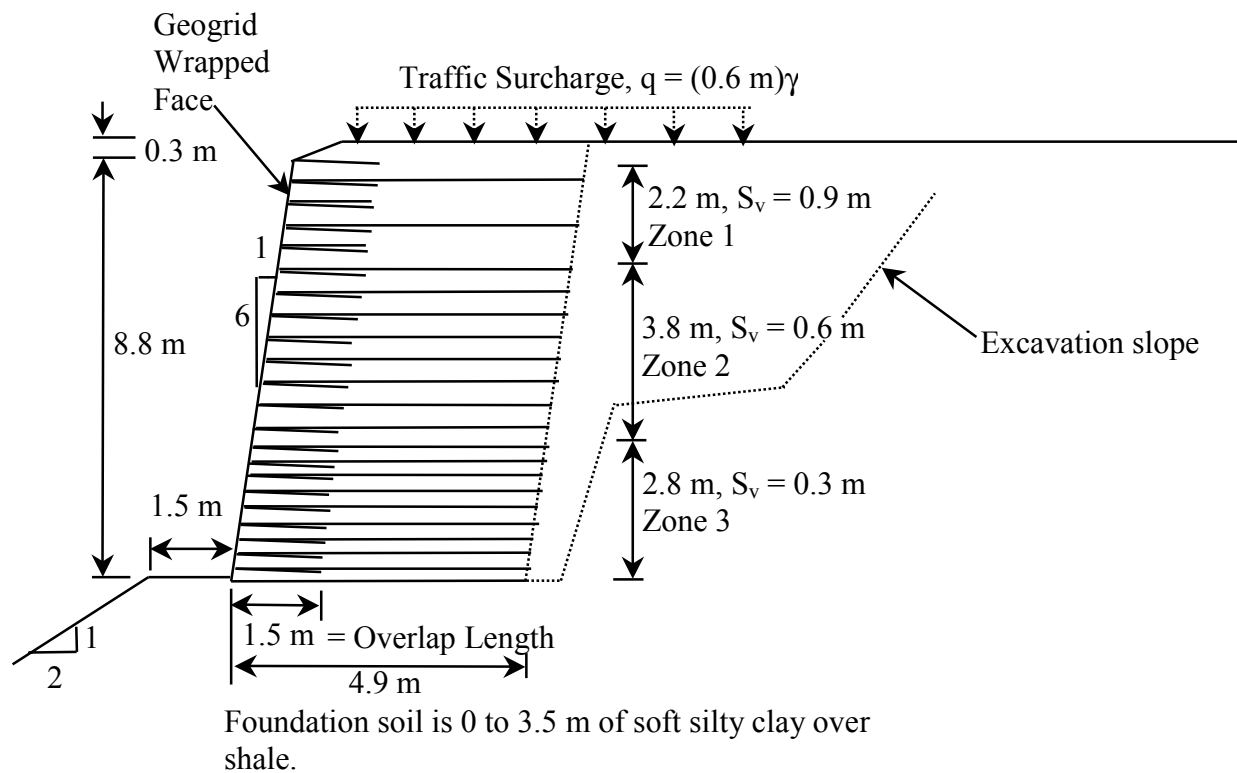
Figure 2.4. Cross-section for Devils Punch Bowl wrapped face HDPE geogrid wall.

2.2.5 Tanque Verde Geogrid Concrete Panel Wall, 1984 (Case GW5, Figure 2.5)

Forty-six geogrid reinforced retaining wall sections (1600 lineal meters of wall) were constructed to provide grade separations for the Tanque Verde-Wrightstown-Pantano Roads intersection in Tucson, Arizona (Bright et al. 1994). Full-height, precast concrete panels were used for the facing. The panels were externally braced (propped) until two-thirds of the backfill behind the panels was in place.

Multiaxial cubic triaxial tests were carried out on specimens of the granular backfill soil screened to a No. 4 sieve (Desert Engineering 1987). Interpretation of these data by the writers gave a peak friction angle of 53°. This value was not adjusted to give an equivalent peak plane strain angle (see Section 2.3.3), as the cubic triaxial test was considered to adequately approximate plane strain conditions.

The southwest USA location of these structures made the temperature within the wall backfill unusually high. The measured temperatures were as high as 38° C, with an average of 25

18

to 30° C. The maximum strains at the end of construction were about 0.3 percent and were located at the connections between the panel facing and the reinforcement layers (Desert Engineering 1987). After eight years, the maximum geogrid strains were 1 percent, most of which had occurred during wall construction. Maximum deformation of the face at the top of the wall was approximately 65 mm (Berg et al. 1986).   Exhumation of geogrid reinforcement samples in 1992 indicated that no significant change in tensile strength had occurred relative to the virgin material strength as a result of installation and eight years of in-service loading (Bright et al. 1994).
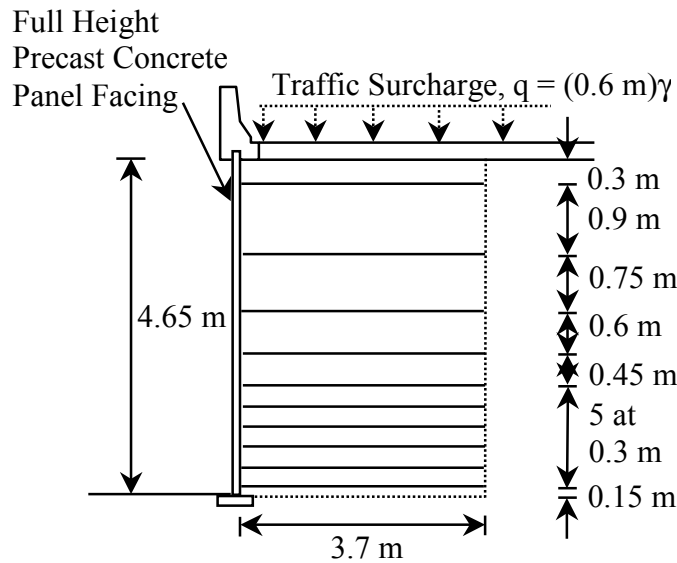
Figure 2.5. Cross-section for Tanque Verde HDPE geogrid concrete panel wall.

2.2.6 Lithonia Geogrid Concrete Panel Wall, 1985 (Case GW6, Figure 2.6)

An incremental concrete panel demonstration wall was constructed near Lithonia, Georgia, in 1985 (Berg et al. 1986). In this structure the concrete facing panels were not directly attached to the soil reinforcement layers. Geogrid tabs, 1.3 m long, were cast directly into concrete facing units and overlapped with the primary reinforcement layers. The overlap lengths were separated vertically by a 75-mm thickness of soil. At the bottom of the wall, three additional layers of reinforcement were installed that were not connected to the facing units.

The structure is now in service as a materials handling platform, with trucks dumping quarry stone over the top of the wall into bins located at the front of the structure. Maximum lateral

movement of the wall face during construction and during the first year of service was on the order of 100 to 150 mm. Wall performance has been acceptable, with no signs of deterioration or unacceptable deformation.
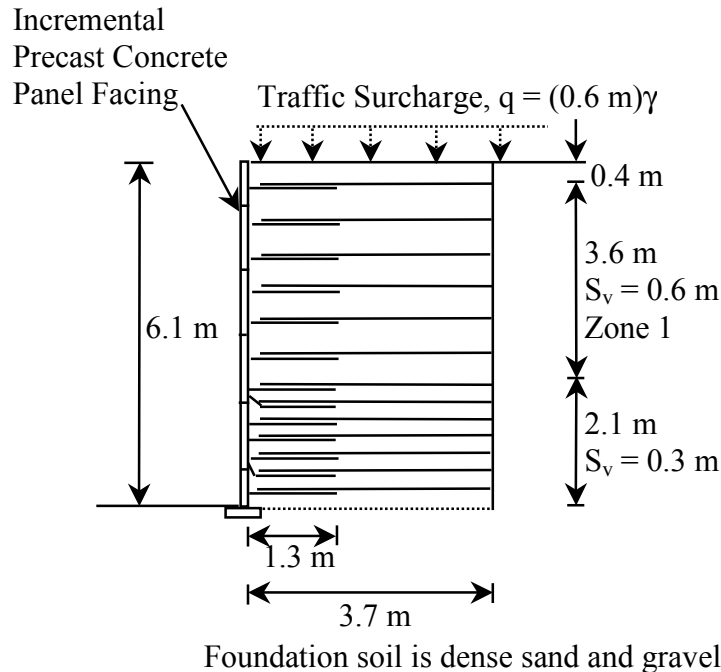
Figure 2.6. Cross-section for Lithonia, Georgia, demonstration HDPE geogrid concrete panel wall.

2.2.7 Oslo, Norway, Geogrid Walls, 1987 (Case GW7, Figures 2.7 and 2.8)

A full-scale, welded, wire-faced test wall was constructed in Oslo, Norway, in 1987 (Fannin and Hermann 1990). This wall was designed in two sections with different reinforcement spacing and lengths. The wall face is inclined at an angle of about 63° from the horizontal. In practice, this structure could be classified as a slope. However, because of the high quality data for this structure and because earth force calculations described later in this paper were carried out by using Coulomb theory (i.e., the wall facing angle is included explicitly in the calculation of earth forces), this case study is included. Note that the primary reinforcement layers simply abut against the back of the welded wire facing form, and did not wrap back into the backfill as is typical of wrapped-face wall systems. Material properties for the wall, including direct shear testing for the wall backfill, were reported by Fannin (1988). The wall has been monitored continuously for 12 years for deformations and load. Total maximum strains in the

reinforcement are less than 1 percent and occurred largely during construction. Strains in the reinforcement have stabilized (Fannin and Hermann 1991; Fannin 1994, 2001).
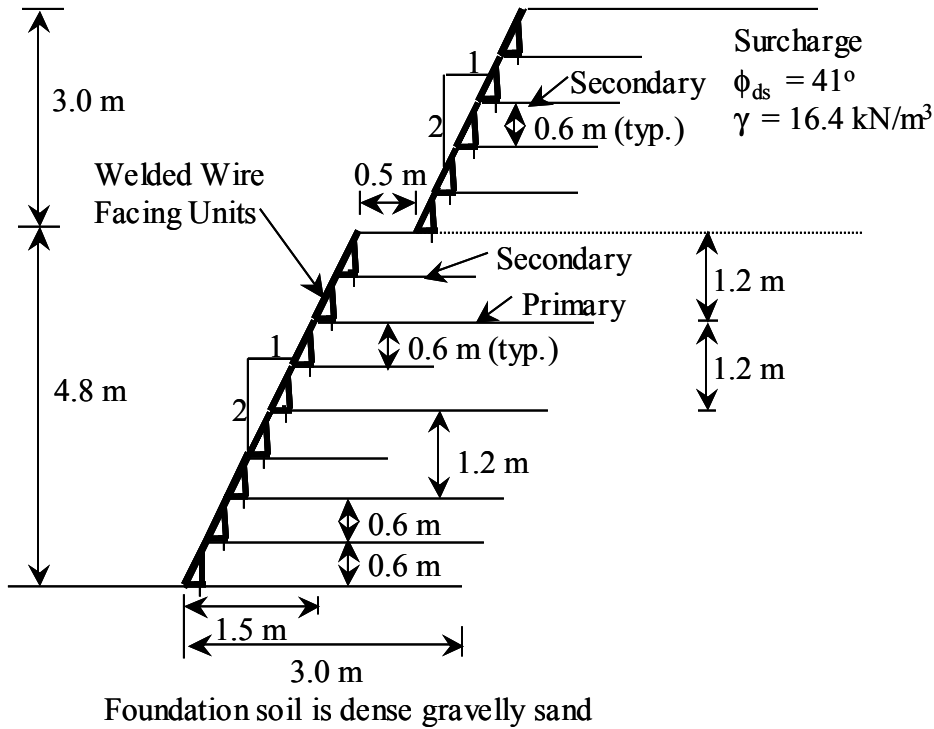
Figure 2.7. Cross-section for Oslo, Norway, (HDPE geogrid) walls, Section J.
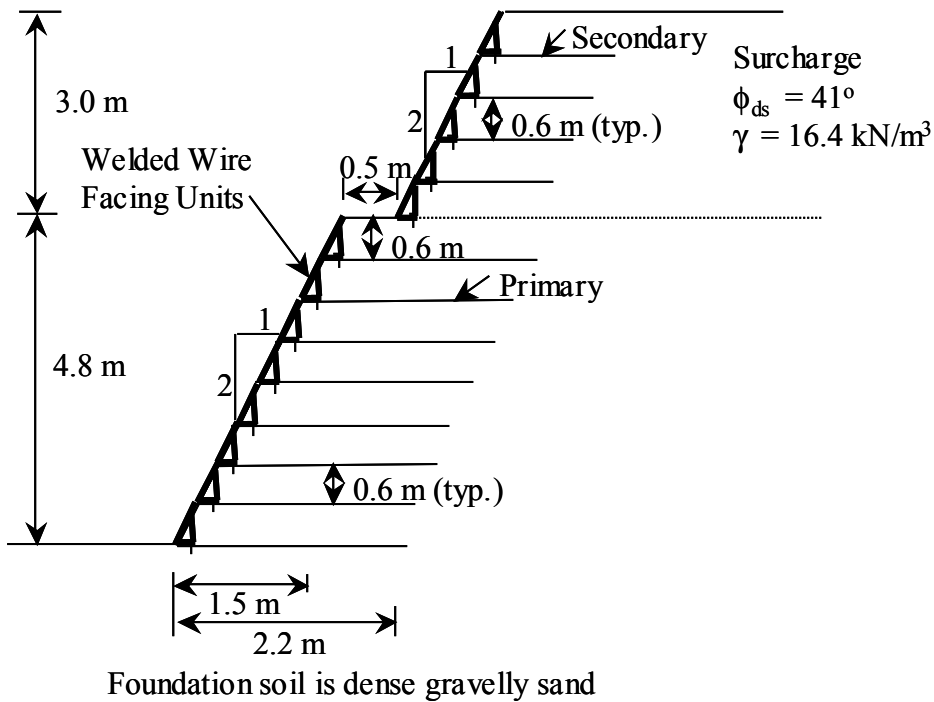
Figure 2.8. Cross-section for Oslo, Norway, (HDPE geogrid) wall, Section N.

2.2.8 Algonquin, HDPE Geogrid Concrete Panel Wall, 1988 (Case GW8, Figure 2.9)

A series of full-scale test walls were constructed in a gravel pit in Algonquin, Illinois, as part of a Federal Highway Administration (FHWA) study to investigate the behavior of mechanically stabilized earth (MSE) walls (Christopher 1993). Seven wall sections, 6.1 m high by 10 m long, were constructed with different reinforcement products but the same precast concrete facing panels. The section constructed with high density polyethylene (HDPE) geogrid reinforcement is reported here.

Measured maximum lateral movement of this wall was 35 mm, most of which occurred during construction. The wall was monitored for two years after construction. At that time the measured total strains were less than 1 percent, and lateral movements appeared to have stopped (Christopher 1998).
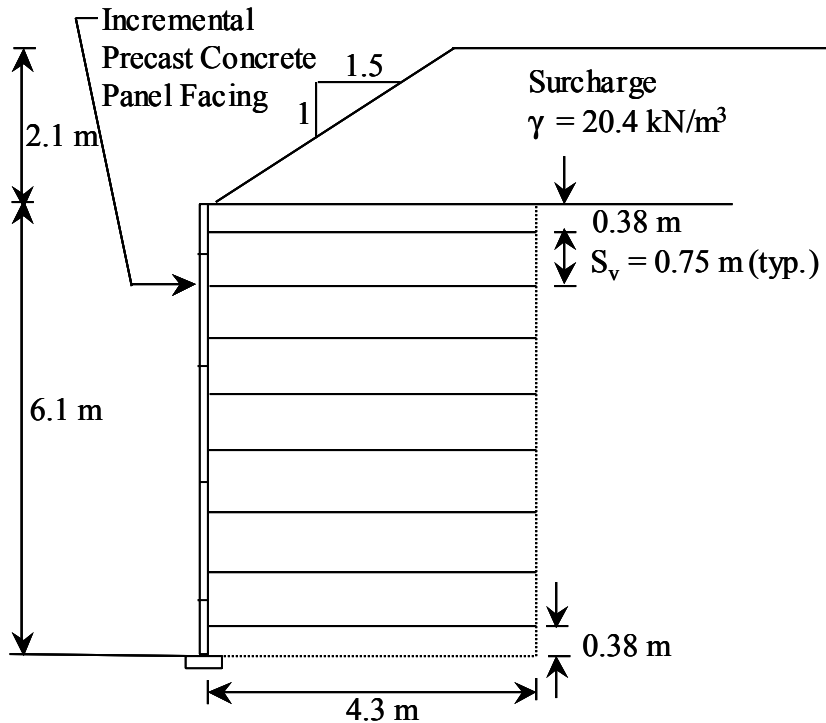
Foundation soil is 5 m of dense gravelly sand or fine to medium sand underlain by very dense sandy silt

Figure 2.9. Cross-section for Algonquin HDPE geogrid concrete panel wall.

2.2.9 Algonquin, Polyester (PET) Geogrid Modular Block Faced Wall, 1988 (Case GW9, Figure 2.10)

This wall was constructed at the Algonquin, Illinois, site described in the previous case study and was part of the same FHWA research program (Bathurst et al. 1993b). The geometry

of this wall was similar to other Algonquin walls, except that the wall was 15 m long and was constructed with a battered facing column of dry cast concrete modular blocks (segmental retaining wall).

The measured maximum lateral movement for this wall was about 150 mm, the majority of which occurred during construction. Measured maximum total strains were approximately 1.5 percent, and strains and deformations appeared to have stabilized one year after construction.
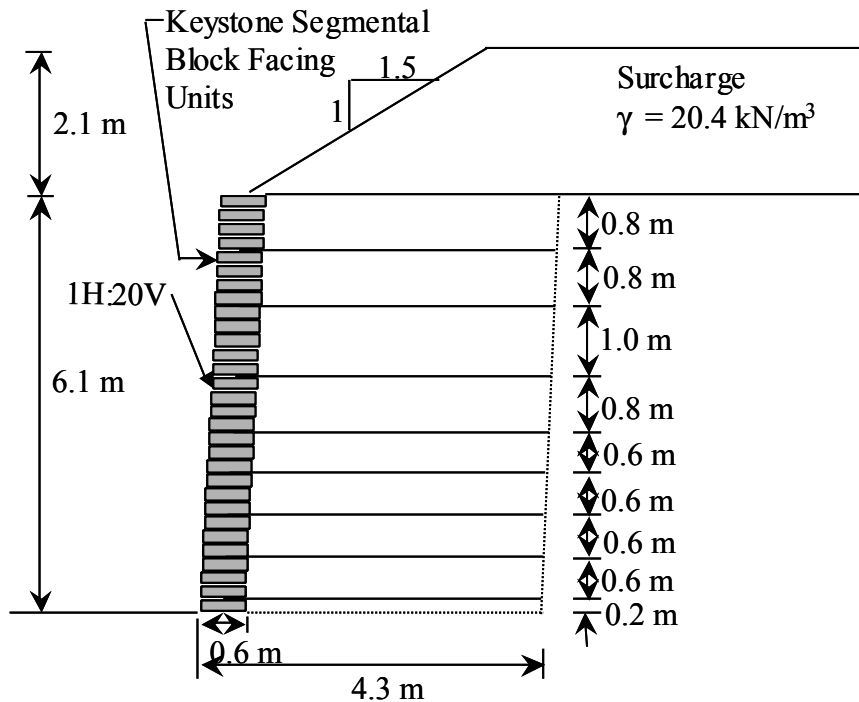
Figure 2.10. Cross-section for Algonquin PET geogrid modular block faced wall.

2.2.10 Algonquin, Geotextile Wrapped-Faced Wall, 1988 (Case GW10, Figure 2.11)

This wall was constructed at the Algonquin, Illinois, site described in the two previous case studies and was part of the same FHWA research program (Christopher 1993). A geotextile wrapped-face construction was used. In-soil confined tensile tests were also conducted on reinforcement layers in the wall backfill.

The wall was purposely under-designed to produce an internal stability failure. The wall was supported laterally over the bottom half of the structure during construction and for about four months thereafter by using a pond of water contained within a geomembrane. Total lateral wall deformations of approximately 150 mm were measured, as were maximum global reinforcement

strains of 2 to 3 percent at end-of-construction. The large strains were not unexpected since the wall was purposely under-designed using a very extensible, nonwoven geotextile. The soil did not exhibit cracking at this point, indicating that the geotextile remained in a confined state and that the soil had not reached a state of failure. Following release of the external support, the wall face deflected an additional 450 mm at the crest, and reinforcement strains exceeded the capacity of the strain gauges mounted directly on the geotextile (strains were likely in excess of 2 to 3 percent, given the last reliable measurement of reinforcement strain). The soil exhibited signs of failure (i.e., cracks in the backfill). The wall continued to strain with time, resulting in additional soil cracks. However, the strain rate appeared to decrease with time, and reinforcement rupture did not occur over the five years of post-construction observation (Christopher 1998).
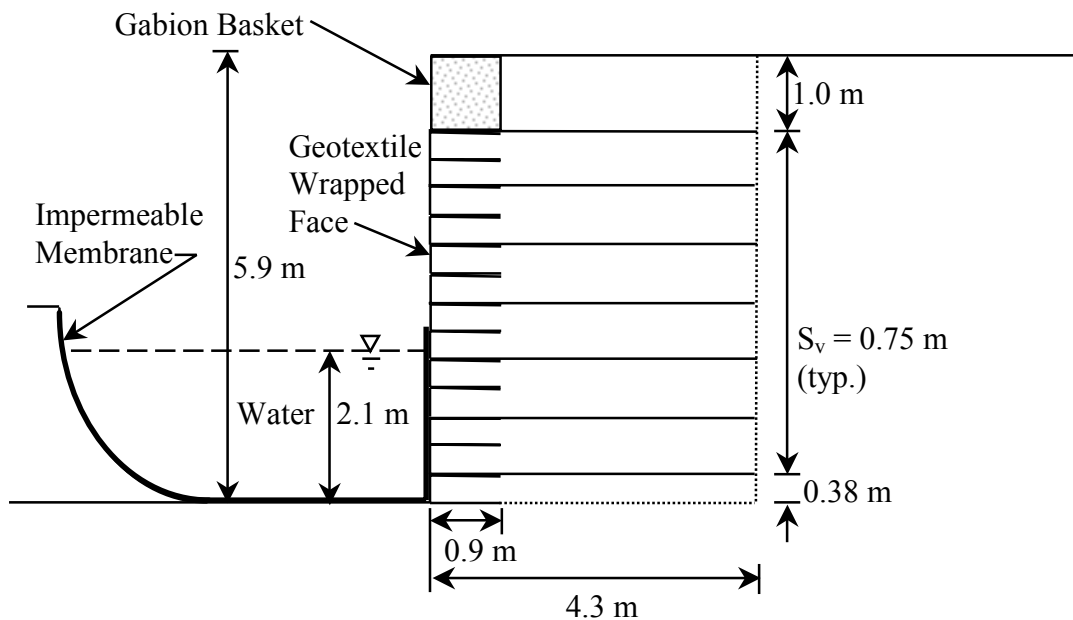
Foundation soil is 5 m of dense gravelly sand or fine to medium sand underlain by very dense sandy silt

Figure 2.11. Cross-section for Algonquin geotextile wrapped-face wall.

2.2.11 RMCC Geogrid Wrapped-Face Wall, 1986 (Case GW11, Figure 2.12)

A full-scale, geogrid, wrapped-faced test wall was constructed and monitored at the Royal Military College of Canada (RMCC) in Kingston, Ontario (Bathurst et al. 1988). The test wall was approximately 2.9 m high, 2.4 m wide, and retained a soil volume extending approximately 6 m behind the facing. Potential boundary effects of the full-scale test wall facility were quantified by carrying out a full-scale experiment in which the external support to an unreinforced full-height facing panel was slowly released to generate an active earth failure in

the soil. In addition, direct shear testing of the side wall friction-reducing interfaces (multiple layers of lubricated polyethylene sheeting) were carried out (Bathurst 1993). Fully mobilized side wall friction angles were calculated to be 10 to 15°.

The wall was purposely under-designed by using a weak biaxial geogrid oriented with the weakest direction in the direction of tensile loading and by using large vertical spacings. Strains measured during construction were as large as 2.6 percent, with additional creep strains after 600 hours of surcharging of up to 1.5 percent. Maximum facing deformations were 20 mm or less at the geogrid layer locations, with additional long-term deformations of 10 mm or less. Most wall deformations were confined to the front 0.6 m of the wall and were due to local failure of the soil in the slumped, wrapped-face portions. However, the geogrid reinforcement showed no signs of failure, and strain rates were observed to decrease with time. The geogrid reinforcement was excavated and tested for residual tensile strength. No signs of installation damage were observed, which was as expected since the soil was placed very carefully. No tensile strength loss was observed from index tensile wide-width strip tests on exhumed specimens of geogrid, indicating that long-term creep strains had not reduced the residual tensile strength of the geogrid reinforcement below virgin strength values (Bathurst et al. 1988).
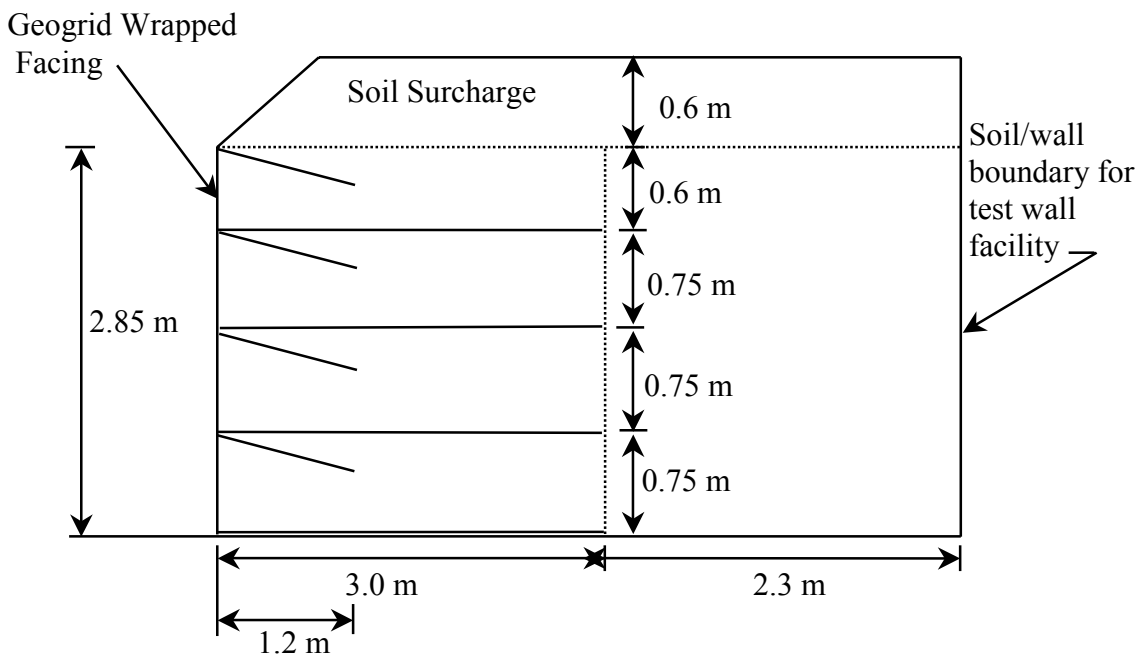
Foundation for wall is concrete floor.

Figure 2.12. Cross-section for RMCC polypropylene (PP) geogrid wrapped face wall.

2.2.12 RMCC Full-Height Propped Timber Panel Geogrid Test Wall (Case GW12, Figure 2.13a) and Incremental Timber Panel (Case GW13, Figure 2.13b) Geogrid Test Wall, 1987

Full-scale, instrumented, full-height, propped panel and incremental panel test walls were constructed and surcharged at RMCC (Bathurst et al. 1987). The test walls were 3 m high and 2.4 m wide, and they were constructed with timber and plywood bulkhead facings. See Case GW11 for additional details regarding backfill testing.

The full-height panel wall was braced externally for the duration of backfill placement. For the incremental panel wall, each row of panels was temporarily braced during backfilling behind the row, and the bracing was removed once the next row of facing panels was in place and backfilled.

The soil backfill in each test was uniform surcharge loaded in stages by using a system of airbags that covered the entire 6-m length of the RMCC Retaining Wall Test Facility. Friction reducing membranes were introduced between the airbags and soil surface. (The influence of side wall friction in the RMCC Retaining Wall Test Facility was discussed in the previous section (Case GW11).) A three-dimensional wedge analysis estimated that boundary effects in these tests contributed approximately 14 percent to wall capacity at collapse under surcharge loading (Bathurst and Benjamin 1990, Bathurst 1993).

Maximum lateral movement for the incremental panel wall was 18 mm, and reinforcement strains were 0.3 percent or less at the end of construction. For the companion full-height, propped panel wall, the maximum lateral movement during wall construction and before external prop removal was about 1 mm, and the maximum geogrid strain about 0.03 percent. The wall was stage surcharge loaded up to a maximum 50 kPa pressure (an effective surcharge pressure of 42 kPa after correction for boundary effects, according to Bathurst (1993)). At the end of the surcharging, the maximum outward face deformation and strain were approximately 40 mm and 0.9 percent, respectively, for the incremental panel wall, and approximately 12 mm and 0.88 percent, respectively, for the full-height propped panel wall. No strength reduction of the geogrid due to installation or time effects was apparent after wide-width tensile testing and constant load creep testing of exhumed reinforcement specimens (Bush and Swan 1987).

Foundation for wall is concrete floor.
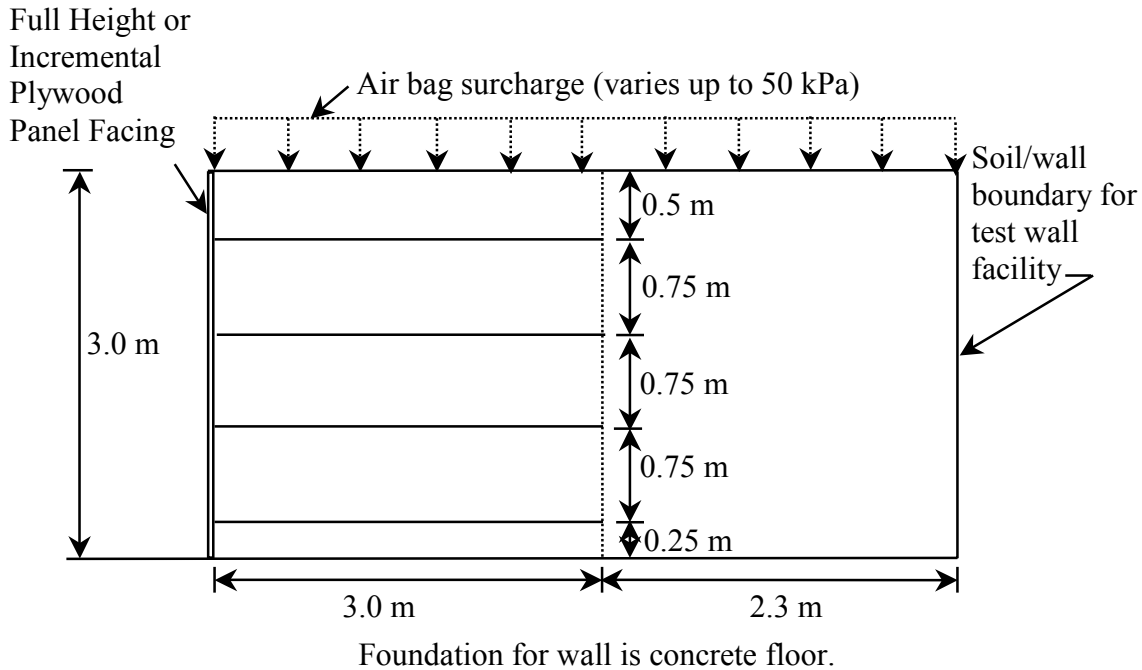
Figure 2.13. Cross-section for RMCC incremental and full-height plywood propped panel HDPE geogrid walls.

2.2.13 RMCC Full-Height Propped Aluminum Panel Geogrid Test Wall, 1989 (Case GW14, Figure 2.14)

A full-scale, instrumented, full-height propped panel wall was constructed and surcharged to failure at RMCC (Bathurst and Benjamin 1990). This wall differed from the previous case study (GW12) in the use of a stiffer aluminum panel for the facing, a pinned connection at the wall toe to measure toe forces (in Cases GW12 and GW13 the wall toe was only restrained by base friction), more instrumentation, and a weaker, more extensible geogrid reinforcement. In addition, the surcharge capacity of the RMCC Retaining Wall Facility was increased. Otherwise, the wall geometry and backfill soil were the same as in case GW12. After construction, the wall was stage uniform surcharge loaded to collapse by applying a maximum pressure of 80 kPa to the airbags located at the top of the soil surface.

Measured maximum lateral movement of this wall was about 10 mm, and reinforcement strains were 1 percent or less at the end of construction, immediately after external prop release construction (Bathurst and Benjamin 1990). The wall was stage surcharge loaded to a maximum load of 80 kPa, with each surcharge load increment maintained for a minimum of 100 hours to measure creep. The equivalent surcharge for an infinitely wide wall structure was estimated through back-analysis to be about 70 kPa because of the contribution of sidewall boundary

effects (Bathurst 1993). Approximately 250 hours after this last surcharge load had been applied, the soil in the reinforced zone exhibited signs of failure. Approximately 350 hours into the final load increment, the upper geogrid layer ruptured, and the wall was purposely unloaded to examine internal failure modes. At reinforcement failure, the maximum lateral deflection of the propped panel face was approximately 100 mm, and maximum reinforcement strains were approximately 10 to 12 percent at the facing connection and 7 to 8 percent near the soil failure surface.
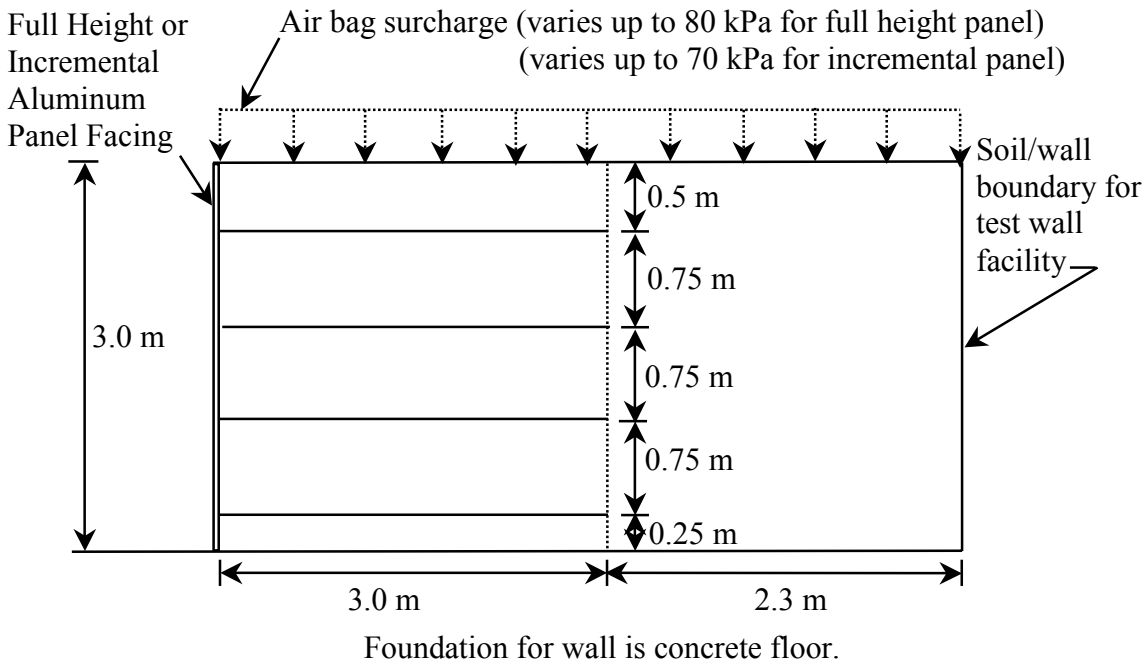
Figure 2.14. Cross-section for RMCC incremental and full-height propped panel geogrid test walls.

2.2.14 RMCC Incremental Aluminum Panel Geogrid Test Wall, 1989 (Case GW15, Figure 2.14)

This test wall was similar to the full-height, propped panel RMCC test wall presented in the previous case study, except that the aluminum facing panels were incremental rather than full-height (Bathurst et al. 1993a). The construction technique was the same as that described for case GW13.

Measured maximum lateral movement for this wall was 13 mm, and reinforcement strains were 1 percent or less at the end of construction but before surcharging. The wall was stage surcharge loaded to a maximum pressure of 70 kPa, with each surcharge load increment held for a minimum of 100 hours to measure creep. Three-dimensional stability calculations suggested

28

that approximately 10 kPa of the 70-kPa surcharge were carried by side wall friction (Bathurst 1993). Approximately 100 hours after the last surcharge load had been applied, the soil exhibited signs of failure, and approximately 380 hours later the upper geogrid layers ruptured and the wall failed catastrophically. At incipient collapse, the maximum lateral deflection was approximately 100 mm, and maximum reinforcement strains were approximately 10 percent.

2.2.15 WSDOT Rainier Avenue Wrapped-Face Geotextile Wall, 1989 (Case GW16, Figure 2.15)

Six geotextile walls were built to support a preload fill for the reconstruction of a major freeway interchange at Rainier Avenue in Seattle, Washington (Allen et al. 1992). Although the walls were intended to be temporary, they were in place long enough to assess long-term behavior. At the time of construction, the instrumented wall section at this interchange was the largest geotextile wall in the world. Soil shear strength was determined by using large-diameter (100-mm) triaxial tests and plane strain shear strength testing.

The measured maximum lateral movement of the instrumented section was 140 mm during construction, with an additional 30 mm of movement after construction. The wall was monitored for approximately one year after construction. Measured maximum total strains were on the order of 1 percent, and wall movement appeared to be stable after one year. Installation damage to the geotextile reinforcement was evaluated immediately after construction. Strength losses of approximately 10 to 30 percent due to installation damage were measured.
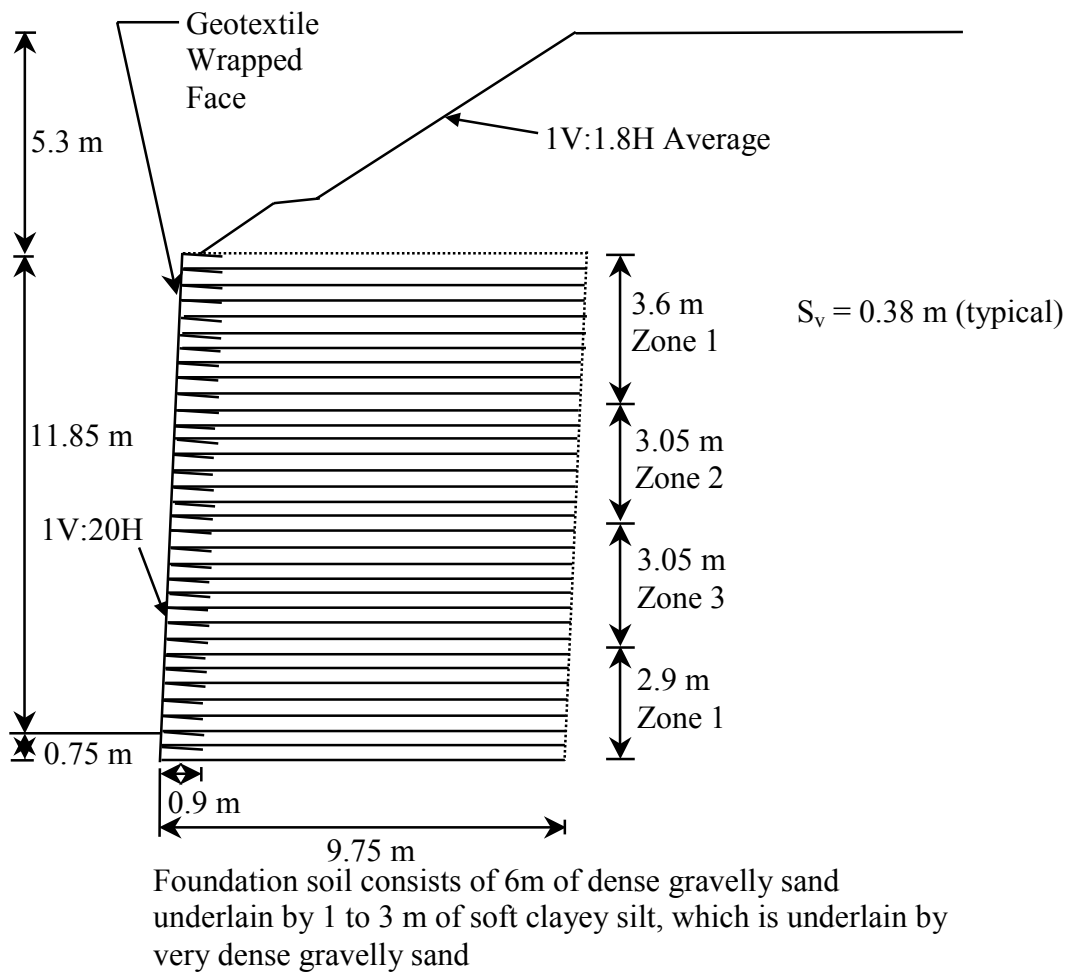
Figure 2.15. Cross-section for WSDOT Rainier Avenue wrapped face geotextile wall.

2.2.16 London, Ontario, Propped Panel Geogrid Wall, 1989 (Case GW17, Figure 2.16)

A geogrid reinforced, full-height, propped, precast concrete panel wall was constructed as part of the Highbury Avenue reconstruction and widening in London, Ontario (Bathurst 1992). The wall backfill used was a silty sand and gravel conforming to a Ministry of Transportation of Ontario Granular B specification.

Maximum wall deformations of 44 mm and geogrid strains of 3 to 3.5 percent, most of which occurred within 6 months after prop removal, were measured in the tallest (7.1-m-high) instrumented panel. The largest strains occurred near the wall face, which can be explained by downward soil movement behind the relatively stiff facing panel. No signs of distress have been observed in the wall since it was constructed.

Foundation soil is dense sandy till
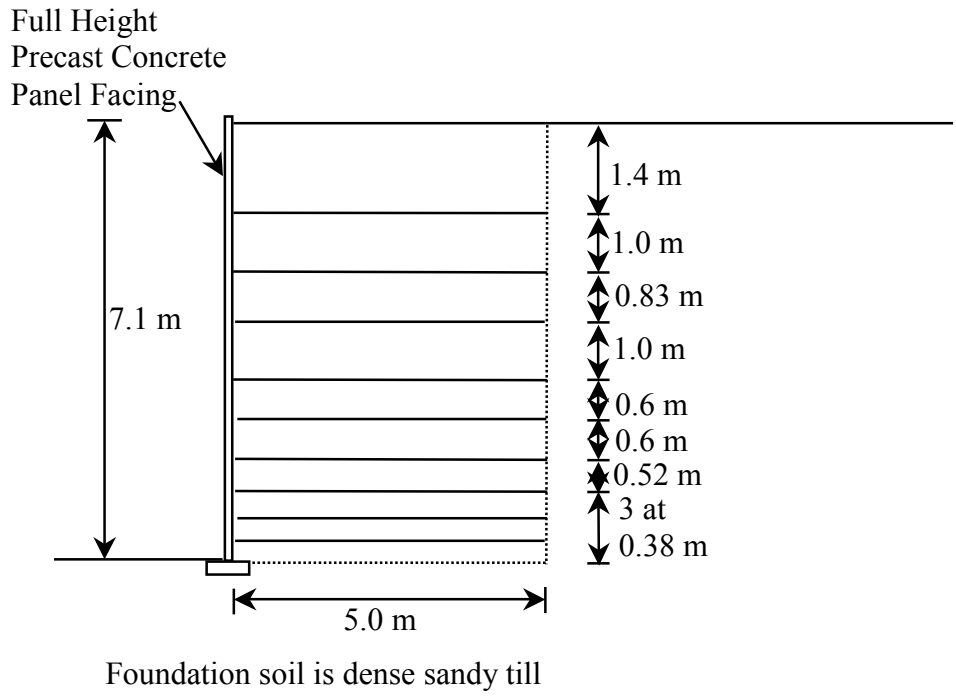
Figure 2.16. Cross-section for London, Ontario, propped panel (HDPE geogrid) wall.

2.2.17 Fredericton, New Brunswick, Propped Panel Geogrid Wall, 1990 (Case GW18, Figure 2.17)

A geogrid reinforced, full-height, propped, precast concrete panel wall was constructed in Fredericton, New Brunswick (Knight and Valsangkar 1993). Maximum wall deformations of 28 mm and geogrid strains of up to 2.1 percent, most of which occurred within 6 months after prop removal, were reported. No signs of distress have been observed in the wall since it was constructed.

Full Height
Precast Concrete
Panel Facing

Light weight
HDPE geogrid

6.1 m

1.22 m

1.22 m

1.22 m

1.22 m

1.22 m

All layers, except as noted,
use a medium weight
HDPE geogrid.
Intermediate, unconnected
layers spaced at
0.61 m (typical).

3.2 m

Foundation soil is sandstone
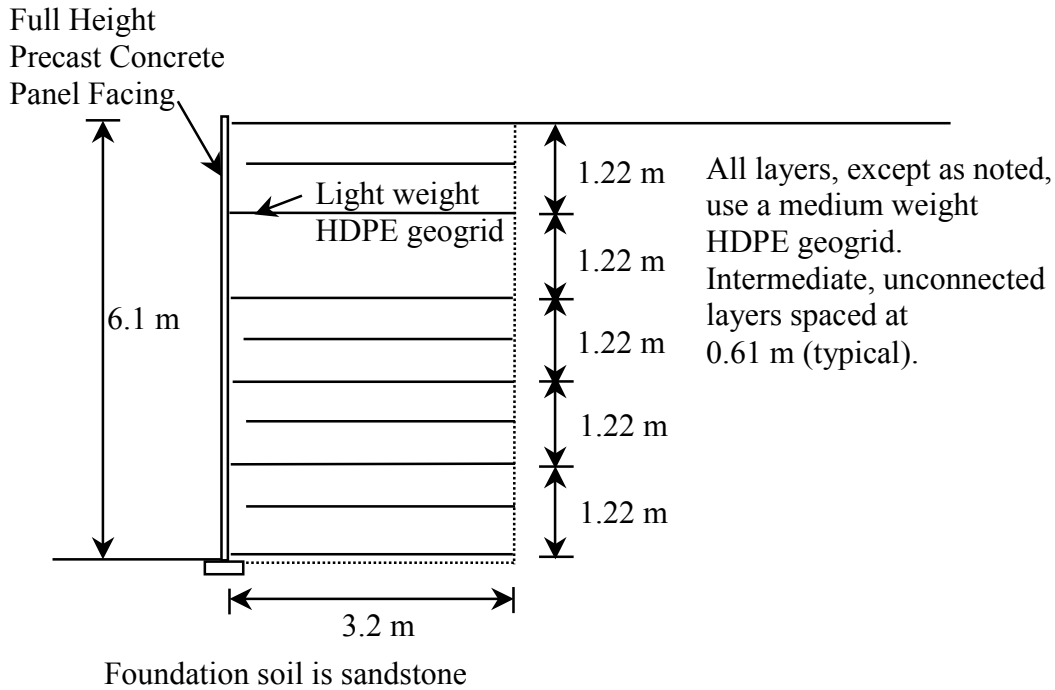
Figure 2.17. Cross-section for Fredericton, New Brunswick, propped panel (HDPE geogrid) wall.

2.2.18 Remy, France, Polyester Strap Concrete Panel Wall, 1993 (Case GW19, Figure 2.18)

A polyester strap, reinforced, incremental concrete panel wall 6.4 m high was constructed at the Centre Experimental du Batiment at St. Remy in 1993 (Schlosser et al. 1993). Total wall deformations were generally less than 50 mm, most of which occurred during construction.
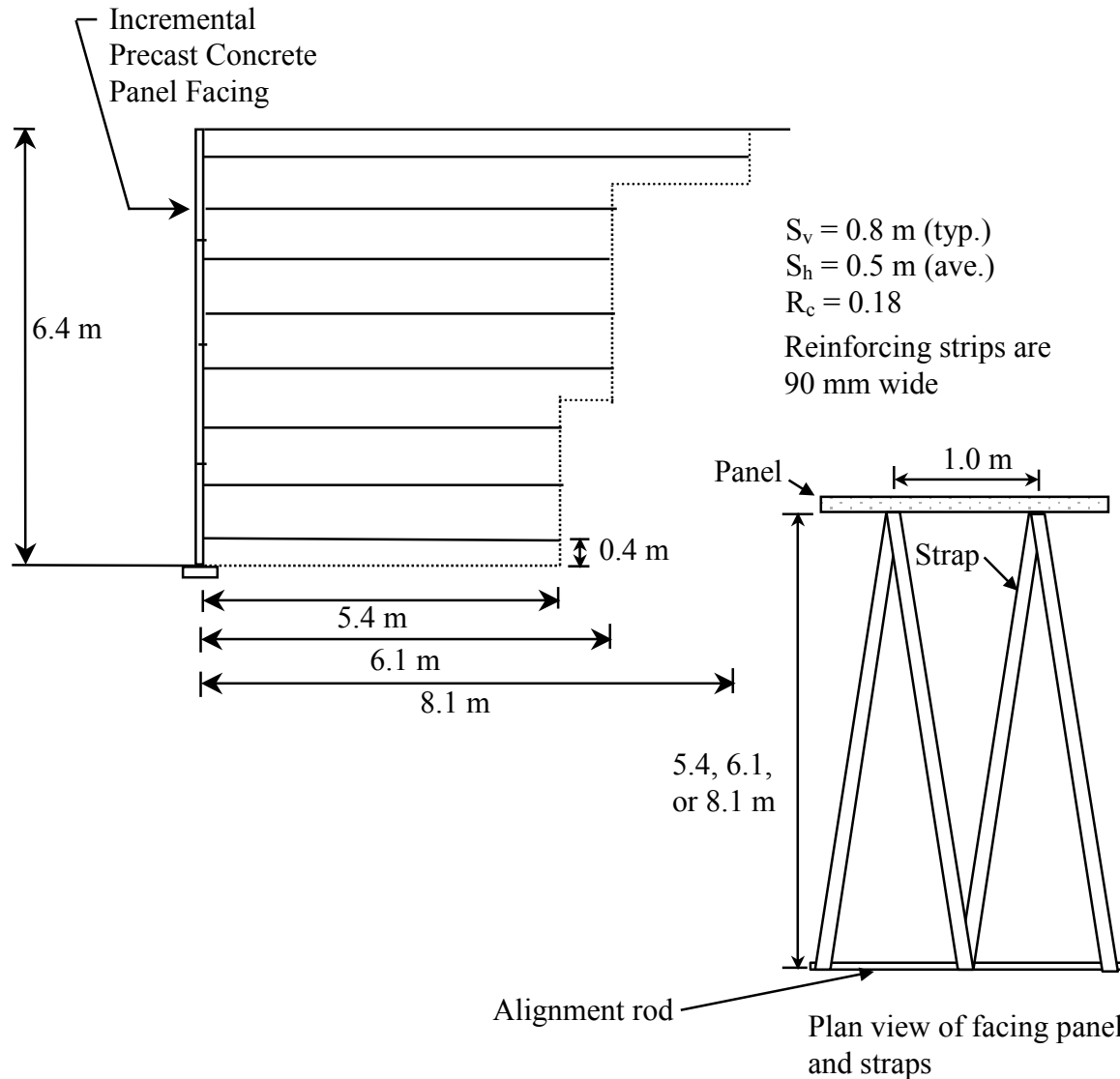
Figure 2.18. Cross-section for Freyssisol-Websol St. Remy test wall.

2.2.19 Vicenza, Italy, Geogrid Welded Wire Faced Wall, 1998 (Case GW20, Figures 2.19 and 2.20)

A 4-m-high welded wire faced geogrid wall near Vicenza, Italy, was constructed and surcharged in an attempt to produce an internal failure (Carruba et al. 1999). Large diameter (100 mm) triaxial tests were conducted to determine the shear strength of the soil. The wall consisted of two sections 5.0 m wide. One section was constructed with a uniaxial HDPE geogrid, and the other section with a biaxial PP geogrid. The foundation below the wall was rigid.

The wall was surcharged in three stages to a maximum surcharge height of 3.5 m. At the maximum surcharge, maximum strains in the reinforcement ranged up to 1.6 percent for the HDPE geogrid section and up to 4.2 percent for the PP geogrid section. Before surcharging, the maximum reinforcement strains were generally less than 0.5 percent. There was some indication that the HDPE section exhibited signs of pullout under the highest surcharge height (Montanelli 2000). However, 2,000 hours of creep data indicated that creep strains and strain rates were decreasing with time after the final surcharge was placed.
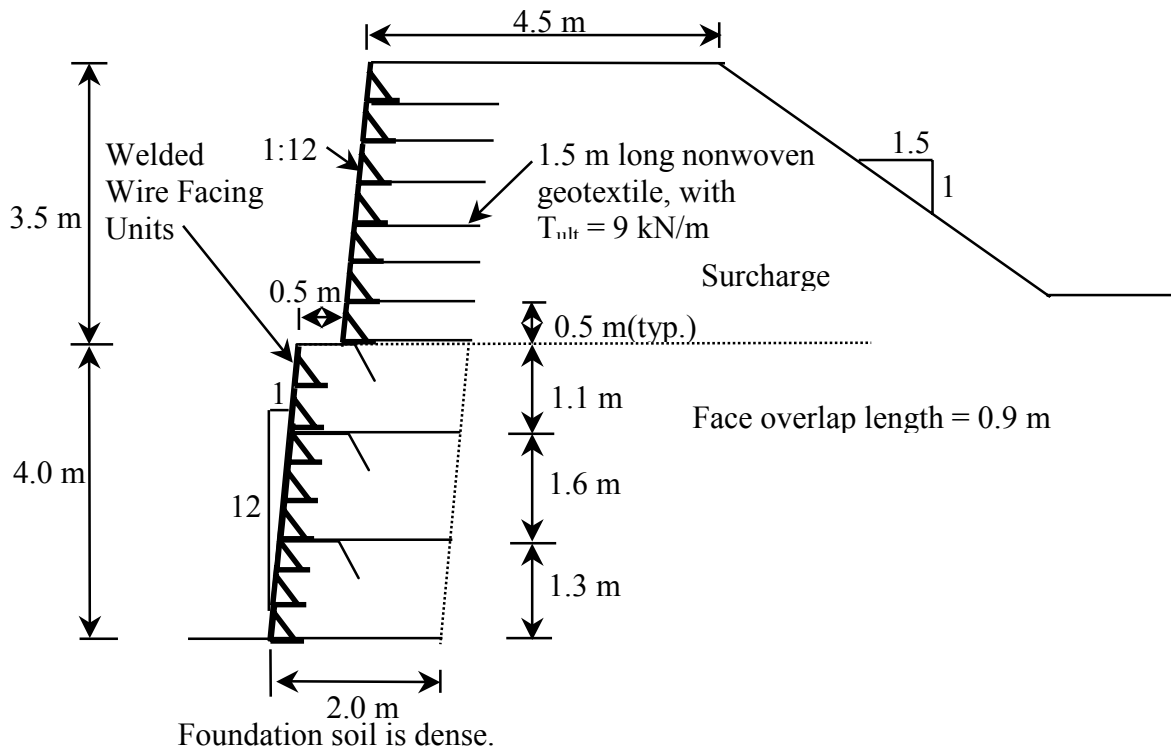
Figure 2.19. Cross-section for Vicenza, Italy, HDPE geogrid welded wire faced wall.
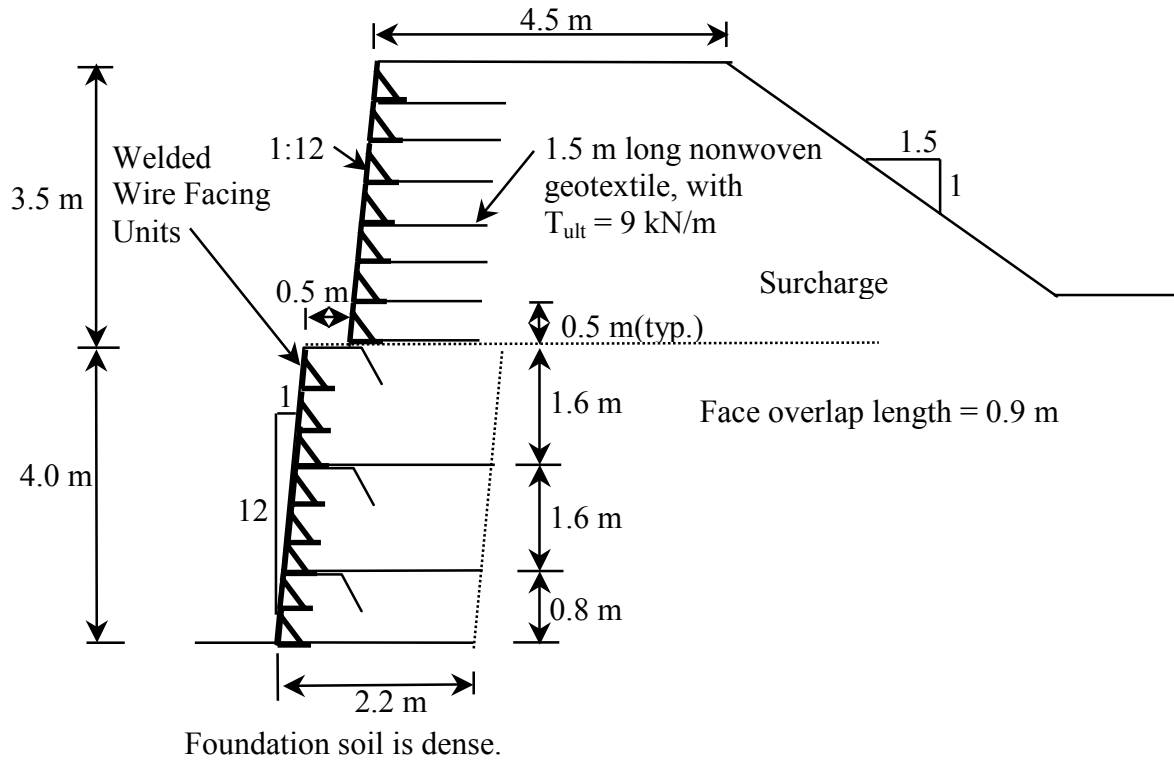
Figure 2.20. Cross-section for Vicenza, Italy, PP geogrid welded wire faced wall.

2.3 Determination of Resistance-Demand Ratio

2.3.1 General

In this chapter the resistance-demand (RD) ratio of a reinforced soil wall is described by expressions that have the following general form:

$$RD = \frac{R}{D} = \frac{\sum_{i=1}^{n} T_i}{D_{actual}} \tag{2.1}$$

Conceptually, R (resistance) = the total tensile capacity of the reinforcement layers in the structure and, D (demand) = the total horizontal earth force to be carried by the reinforcement layers. The resistance term is calculated as the sum of the tensile reinforcement capacities (T_i) of

n layers of reinforcement in the wall. The interpretation and computational details of the resistance term vary for different resistance-demand ratio expressions introduced below.

The denominator used to calculate the RD ratio, D_{actual}, is based on the measured shear strength of the soil. This is calculated from plane strain peak friction angles estimated from triaxial or direct shear data (Section 2.3.3) or directly measured in a plane strain test apparatus. D_{actual} is used in all RD ratio calculations that follow in order to provide a common basis of comparison.

Figure 2.21 illustrates resistance-demand concepts. The RD ratios shown in the figure are global parameters and therefore do not represent the RD ratio for individual layers within the structure. The quantities R_{index} and $R_{ultdesign}$ represent short-term resistance values, and R_{actual} and R_{design} represent long-term resistance values (i.e., at the end of the wall design life). D_{actual} is as defined previously, and D_{design} represents the magnitude of demand (total tensile load) on the reinforcement layers based on the design value of soil shear strength. Irrespective of how the demand term is calculated, the magnitude of this value is assumed to be constant over the design life of the structure. D_{design} is used only to estimate R_{design} in the RD calculations that follow. In practice, project-specific backfill shear strength tests are seldom conducted for wall design purposes, and if they are conducted for design, triaxial or direct shear strength tests are almost always used rather than plane strain testing. Hence, design values of soil shear strength are used to estimate D_{design} and R_{design} to determine the RD ratio that would be required if the wall were designed in accordance with the current design practice.

The short-term (index or ultimate) strength of the soil reinforcement (T_{ult}) is based on wide-width strip tensile test results and is the simplest and most consistent way to calculate the resistance term in Equation 2.1 (i.e., $R = R_{index} = \Sigma T_{ult}$). The *index* resistance-demand ratio RD_{index} (Equation 2.5) is illustrated in Figure 2.21a. At the very least this quantity provides a relative measure of how heavily reinforced a wall is.

Figure 2.21a represents the *idealized* case when the *actual* total available resistance at the end of design life is known (R_{actual}). This value can be calculated by carrying out wide-width strip tensile tests on retrieved samples of reinforcement materials at the design life of the structure. Alternatively, if the magnitude of index strength reduction due to installation damage, durability, and creep is known with certainty, then the predicted value of R_{actual} can be calculated as in Equation 2.11. The dashed line in the figure symbolizes that resistance values before the

end of design life are assumed to decrease with time, but the actual degradation rate is unknown. Regardless, the time history of reinforcement strength loss does not enter into the calculations reported in this chapter.
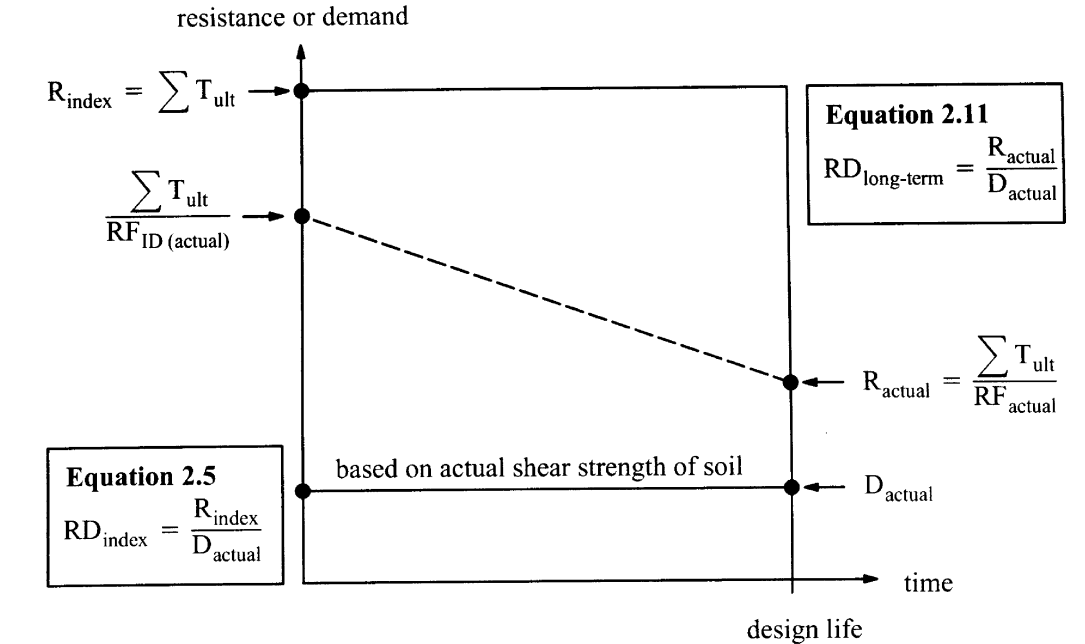
a) actual
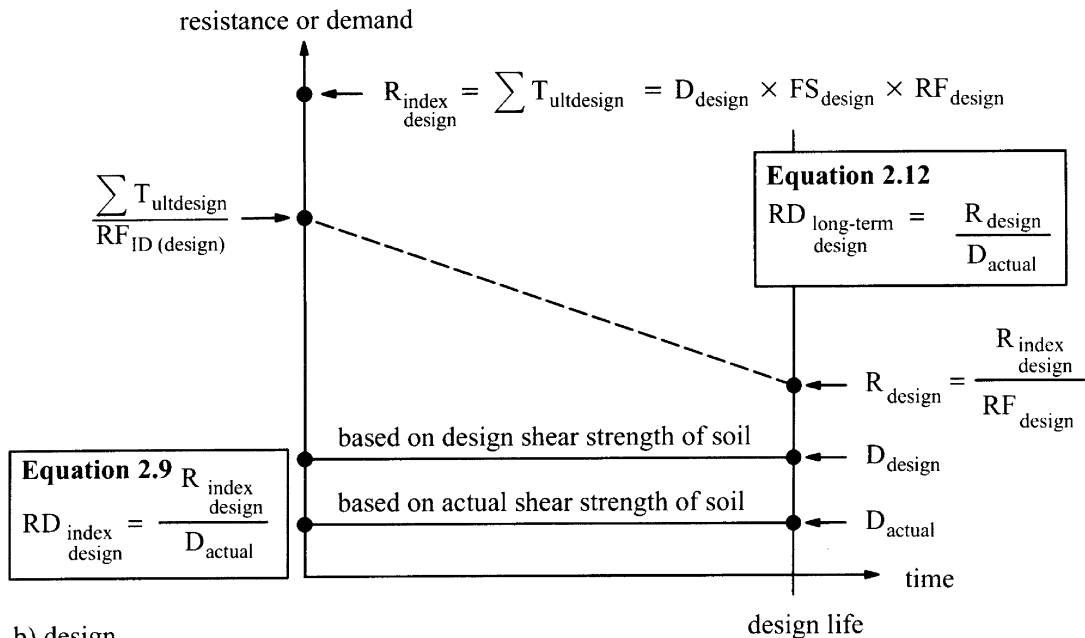
b) design

Figure 2.21. Resistance-demand concepts.

"Actual" strength reduction factors (RF_{actual}) were estimated on the basis of current knowledge of geosynthetic durability (Elias et al. 2001, Elias 2001, WSDOT 1998) and site conditions for the selected case histories. For some of the case histories, reduction factors were calculated from laboratory tests of recovered reinforcement specimens (Section 2.3.3).

Figure 2.21b illustrates the calculation of resistance-demand ratios on the basis of current design practice in North America. The demand term D_{design} is typically calculated by using shear strength values for the soil that are less than actual values, hence $D_{design} > D_{actual}$ in the figure. According to conventional AASHTO practice, the sum of the ultimate wide-width strip tensile strengths of the reinforcement layers ($\Sigma T_{ultdesign}$) must be at least equal to the product of the design demand load (D_{design}), a design global factor of safety (FS_{design}) to account for overall uncertainty, and a design reduction factor (RF_{design}) to account for the combined effect of installation damage, durability, and creep. Design values for the short-term and long-term resistance-demand ratios are calculated according to equations 2.9 and 2.12, respectively.

RF_{design} was calculated for each of the case histories. Current AASHTO requirements to estimate long-term geosynthetic strength reduction factors were used, and the calculations were based on what would have been known at the time of the wall case history regarding the aggressiveness of the backfill and the long-term geosynthetic properties. If little was known about the durability of the product used in the case history, the default reduction factor $RF = 7.0$ was used to calculate R_{design}.

RD ratio values should not be interpreted as a quantitative measure of the factor of safety against wall collapse because these values do not capture specific failure modes associated with geosynthetic reinforced soil walls (see also Section 2.3.2 regarding the potential accuracy of the method used to calculate demand). Rather, the global RD ratios introduced here are a convenient way to compare the *relative* short-term and long-term level of safety of different geosynthetic reinforced soil walls. They are also a way to quantify the degree of conservativeness between the best estimates of the resistance-demand ratio of actual geosynthetic reinforced soil walls based on measured or best estimates of actual properties, and resistance-demand values for the same structures, based on the assumption that they were designed to satisfy current AASHTO practice, using typical design properties.

For brevity in the following text, the term "global level of safety" or "level of safety" is understood to mean "resistance-demand ratio" as defined above. Both short-term levels of safety

and long-term levels of safety are calculated for each case study in Table 2.2 to provide insight into the global level of safety of geosynthetic walls built to date.

2.3.2 Calculation of Demand

The calculation method used to determine the value of demand (D) in Equation 2.1 is essentially the Simplified Method, which is specified in design practice for geosynthetic walls by AASHTO in the USA (AASHTO 1999, Elias et al. 2001). However, in the sections that follow, demand (D) is expressed as a total active force applied to the wall reinforcement rather than a force per reinforcement layer. For geosynthetic walls, the Simplified Method is essentially the same as the tieback wedge method that has been used to design geosynthetic walls for the past 20 years in North America (Allen and Holtz 1991). The total active earth force in the following sections was calculated by using the horizontal component of Coulomb earth force, since Coulomb theory explicitly includes the influence of wall batter. Interface friction, δ, between the wall facing and soil was assumed to be 0.0, and all soil volumes above the wall crest were treated as an equivalent uniform surcharge.

The Simplified Method is a limit equilibrium approach and contains two key assumptions for calculating reinforcement load:

1. The magnitude of tensile load in each reinforcement layer is proportional to the soil overburden stress. Hence, reinforcement load will increase linearly with increasing depth of soil below the crest of the wall.

2. Tensile load in the reinforcement is a direct indicator of the state of stress in the soil, since the reinforcement layer is assumed to carry the full-lateral active earth pressure in the soil near the layer (i.e., the contributory area approach).

Both the design demand, used only to calculate the amount of reinforcement required per the current AASHTO specifications (AASHTO 1999), and the "actual" demand were calculated with this method, but with different shear strength parameters as discussed previously. It should not be assumed that the actual demand accurately represents the stress levels that would be measured in geosynthetic reinforcement in actual walls. The two assumptions used by the Simplified Method listed above may not necessarily be correct (Rowe and Ho 1993, Zornberg et al. 1998a). The actual demand is simply the best estimate of demand the Simplified Method can provide.

Table 2.2. Summary of global resistance to demand and performance based on calculated reinforcement loads for geosynthetic walls.

Case Study	Height and Sur-charge	Sec-tion	Wall Perfor-mance to Date	K_{ah} Using Design ϕ	K_{ah} Using Plane Strain ϕ	Index RD Ratio for Actual Wall (Eq. 2.5)	Ultimate RD Ratio if Designed per AASHTO 1999 – Typical Practice (Eq. 2.9)	Ultimate RD Ratio if Designed per AASHTO 1999 – Perfect Match to Demand (Eq. 2.9)	Estimated Long-Term RD Ratio for Actual Wall (Eq. 2.11)	Long-Term RD Ratio if Designed per AASHTO 1999 – Typical Practice (Eq. 2.12)	Long-Term RD Ratio if Designed per AASHTO 1999 – Perfect Match to Demand (Eq. 2.12)
GW1	2.9 m plus 0.9 m soil surcharge	NA	Good	0.24	0.15	28.9	27.6	14.4	3.65	3.92	2.05
GW2	5.6 m	A	Good	0.17	0.085	12.8	22.6	19.1	2.21	3.21	2.71
	5.6 m	B	Good	0.17	0.085	12.4	22.6	19.1	1.10	3.21	2.71
GW3	4.8 m	1 & 9	Good	0.20	0.10	10.1	30.4	22.2	1.8	4.32	3.15
	4.8 m	2 & 10	Good	0.20	0.10	12.3	30.4	22.2	2.56	4.32	3.15
	4.8 m	3	Good	0.20	0.10	16.5	30.4	22.2	2.45	4.32	3.15
	4.8 m	4	Good	0.20	0.10	8.68	30.4	22.2	1.44	4.32	3.15
	4.8 m plus 2 m soil surcharge	5	Good	0.20	0.10	4.99	26.3	21.9	0.90	3.73	3.10
	4.8 m plus 2 m soil surcharge	6	Good	0.20	0.10	5.37	26.3	21.9	1.21	3.73	3.10
	4.8 m	7	Good	0.20	0.10	9.87	30.4	22.2	1.63	4.32	3.15
	4.8 m	8	Good	0.20	0.10	7.42	30.4	22.2	1.28	4.32	3.15
GW4	8.8 m	NA	Good	0.17	0.085	16.9	16.4	14.6	4.24	4.10	3.65
GW5	4.9 m	NA	Good	0.28	0.11	24.5	17.2	14.1	6.14	4.51	3.69
GW6	6.1 m	NA	Good	0.22	0.15	8.86	12.4	8.96	2.22	3.07	2.12
GW7	4.8 m plus 3 m soil surcharge	J	Good	0.14	0.04	21.4	30.2	24.9	4.78	7.05	5.98
		N	Good	0.14	0.04	26.2	30.2	24.9	6.38	7.05	5.98
GW8	6.1 m plus 2.1 m soil surcharge	2	Good	0.22	0.19	5.30	11.6	6.47	1.27	2.92	1.60

40

Table 2.2. Continued.

Case Study	Height and Surcharge	Section	Wall Performance to Date	K_{ah} Using Design ϕ	K_{ah} Using Plane Strain ϕ	Index RD Ratio for Actual Wall (Eq. 2.5)	Ultimate RD Ratio if Designed per AASHTO 1999 – Typical Practice (Eq. 2.9)	Ultimate RD Ratio if Designed per AASHTO 1999 – Perfect Match to Demand (Eq. 2.9)	Estimated Long-Term RD Ratio for Actual Wall (Eq. 2.11)	Long-Term RD Ratio if Designed per AASHTO 1999 – Typical Practice (Eq. 2.12)	Long-Term RD Ratio if Designed per AASHTO 1999 – Perfect Match to Demand (Eq. 2.12)
GW9	6.1 m plus 2.1 m soil surcharge	9	Good	0.20	0.17	3.38	6.64	5.21	1.08	2.12	1.67
GW10	5.9 m but supported by 2.1 m of water at base of wall	6	Fair to good	0.22	0.19	3.04	30.4	17.5	0.62	4.35	2.50
	5.9 m after water removed	6	Poor. Failed by excessive deformation	0.22	0.19	2.01	20.1	11.6	0.41	2.87	1.65
GW11	2.85 m plus 0.6 m soil surcharge	NA	Good, except for sagging at face	0.22	0.10	7.66	36.6	19.5	1.47	6.39	3.40
GW12	3 m plus effective surcharge of 42 kPa	NA	Good	0.22	0.10	13.0	16.6	11.9	3.76	4.35	3.13
GW 13	3 m plus effective surcharge of 42 kPa	NA	Good	0.22	0.10	13.0	16.6	11.9	3.76	4.35	3.13

Table 2.2. Continued.

Case Study	Height and Sur-charge	Sec-tion	Wall Perfor-mance to Date	K_{ah} Using Design ϕ	K_{ah} Using Plane Strain ϕ	Index RD Ratio for Actual Wall (Eq. 2.5)	Ultimate RD Ratio if Designed per AASHTO 1999 – Typical Practice (Eq. 2.9)	Ultimate RD Ratio if Designed per AASHTO 1999 – Perfect Match to Demand (Eq. 2.9)	Estimated Long-Term RD Ratio for Actual Wall (Eq. 2.11)	Long-Term RD Ratio if Designed per AASHTO 1999 – Typical Practice (Eq. 2.12)	Long-Term RD Ratio if Designed per AASHTO 1999 – Perfect Match to Demand (Eq. 2.12)
GW14	3 m		Good	0.22	0.10	5.96	34.4	17.7	1.15	6.01	3.10
	3 m plus effective surcharge of 70 kPa	NA	Failed by excessive deformation and rupture	0.22	0.10	1.66	23.1	17.9	0.32	4.04	3.13
GW15	3 m		Good	0.22	0.10	5.96	34.4	17.7	1.15	6.01	3.10
	3 m plus effective surcharge of 60 kPa	NA	Poor. Failed by excessive deformation and rupture	0.22	0.10	1.85	23.6	17.9	0.36	4.13	3.13
GW16	12.6 m plus 5.3 m soil surcharge	NA	Good	0.24	0.09	13.8	32.3	28.2	3.44	4.61	4.03
GW17	7.1 m	NA	Good	0.26	0.17	12.0	11.0	8.70	3.16	2.87	2.23
GW18	6.1 m	NA	Good	0.22	0.17	7.56	12.0	8.68	1.89	2.97	2.11
GW19	6.4 m	NA	Good	0.25	0.23	24.0	9.31	4.67	9.10	3.53	1.77
GW20 (HDPE)	4 m		Good	0.19	0.066	15.6	25.7	23.4	3.74	6.64	5.94
	4 m plus a 3.5 m soil surcharge	1	Good	0.19	0.066	7.61	47.1	27.9	1.71	10.4	5.89
GW20 (PP)	4 m		Good	0.19	0.066	8.47	36.9	33.0	1.25	6.44	5.76
	4 m plus a 3.5 m soil surcharge	2	Fair	0.19	0.066	3.71	55.5	34.3	0.53	8.83	5.58

2.3.3 Material Properties Used to Calculate Resistance-Demand Ratio

The reinforcement and soil properties used to calculate the resistance-demand (RD) ratio are based on measured properties rather than on design properties (sections 2.3.4 and 2.3.6). The exceptions are calculations performed to determine the resistance required for each case history wall with the current AASHTO design code (AASHTO 1999) (Sections 2.3.5 and 2.3.7).

Reinforcement strengths from wide-width strip tensile test results (ASTM D4595) on project-specific materials were used in many of the case histories to calculate the index and estimated long-term RD ratios (sections 2.3.4 and 2.3.6). In some cases, minimum average roll values (MARV) for wide-width tensile strength were used if lot-specific test data were not available. For the two oldest case studies (GW1 and GW2), lot-specific tensile test results were correlated to equivalent wide-width test results to estimate tensile strengths for analysis.

To calculate the long-term RD ratio (Section 2.3.6), reduction factors for installation damage, creep, and chemical durability were typically estimated on the basis of site-specific conditions. Unless specific information was available to the contrary, the soil condition at each case history site was assumed to be non-aggressive according to the AASHTO (1999) definition for geosynthetic walls. Installation damage reduction factors were based on the results of wide-width tensile testing of exhumed reinforcement samples. If these data were not available, the installation damage reduction factor for the geosynthetic was estimated on the basis of product-specific installation damage test results, backfill gradation, and other site characteristics. Product-specific stress rupture or creep data were used to estimate reinforcement creep reduction factors if available. For most of the geotextiles in the current study, product-specific creep data were not available. Hence, creep reduction factors were estimated on the basis of the polymer used in the geosynthetic and corresponding values reported in the literature (Jewell and Greenwood 1988, Elias et al. 2001, Allen 1991, Allen and Bathurst 1996). In general, a creep reduction factor of 4.5 was used for polypropylene geosynthetics and 1.8 for polyester geosynthetics, if product-specific data were not available. Durability reduction factors were estimated on the basis of the characteristics of the polymer used in the geosynthetic, the backfill environment, and typical long-term durability test results reported in the literature (Elias 2001, Elias et al. 1997, Salman et. al. 1997, 1998). Durability reduction factors for non-aggressive environments varied from 1.3 to 1.5 for polypropylene geosynthetics, 1.15 to 1.6 for polyester

geosynthetics, and 1.1 for high density polyethylene geosynthetics. None of the case histories had soil environments that would be considered chemically aggressive.

Soil shear strength values from triaxial compression or direct shear test results were generally available. Plane strain or equivalent shear strength results were available only for case studies GW11 through GW16. In two cases (GW5 and GW19), peak strengths from triaxial compression testing were converted by the writers from reported (c - ϕ) values to peak secant friction angle values that corresponded to a vertical pressure of γH, where γ is the bulk unit weight of the reinforced soil and H is the height of the wall.

Plane strain conditions were assumed to be applicable to all the walls in the current study. Furthermore, recent work indicates that the peak plane strain friction angle controls the internal capacity of geosynthetic structures, rather than the plane strain constant volume or critical state soil friction angle (Rowe and Ho 1993, Bathurst 1993, Zornberg et al. 1998a,b).

Peak plane strain peak friction angle values, ϕ_{ps}, for compacted granular fills are larger than values inferred from triaxial compression and direct shear results. To form a common basis of comparison, peak triaxial friction angles, ϕ_{tx}, were corrected to peak plane strain friction angles by using the following equation by Lade and Lee (1976):

$$\phi_{ps} = 1.5\phi_{tx} - 17 \text{ (in degrees)} \tag{2.2}$$

On the basis of data interpretation presented by Bolton (1986) and Jewell and Wroth (1987), for dense sands, peak plane strain friction angles, ϕ_{ps}, were calculated from peak direct shear friction angles, ϕ_{ds}, by using the following relationship:

$$\phi_{ps} = \tan^{-1} (1.2 \tan \phi_{ds}) \tag{2.3}$$

2.3.4 Index Resistance-Demand Ratio

Equation (2.1) can be used to calculate an *index* resistance-demand (RD) ratio. Term R is calculated as the sum of the ultimate tensile capacities of the reinforcement layers, given a standard laboratory (index) tensile strength value (T_{ult}) (e.g., ASTM 4595). The demand term D is equal to the *horizontal* component of earth force $P_{ah}(\phi_{ps})$ calculated by using classical earth pressure theory. Hence:

$$P_{ah}(\phi_{ps}) = 0.5\ K_{ah}\ \gamma\ H^2 + K_{ah}\ q\ H \tag{2.4}$$

where $K_{ah} = K_a(\phi_{ps}\ ,\ \delta,\ \omega) \times \cos(\delta - \omega)$; ϕ_{ps} = the peak plane strain friction angle of the soil; ω = wall batter; δ = interface shear angle between wall facing and backfill soil; H = total wall height measured from the toe of the wall to the soil surface immediately behind the wall facing; γ = the bulk unit weight of the soil and; q is the magnitude of any uniformly distributed surcharge load at the soil surface. For broken back surcharges, an equivalent uniform surcharge was calculated by using the total weight of the surcharge over the reinforced soil zone divided by the width of the reinforced soil zone. To simplify calculations and to make a common comparison between case studies, the interface friction angle was assumed to be $\delta = 0$, which is current AASHTO practice. The index RD ratio is as follows:

$$RD_{index} = \frac{\sum_{i=1}^{n} T_{ult}^i}{P_{ah}(\phi_{ps})} \tag{2.5}$$

Example 2.1. Calculate index resistance-demand ratio for Case Study GW9 with surcharge in place (Figure 2.10).

Soil properties: $\gamma = 20.4$ kN/m^3; $\phi = \phi_{ps} = 43°$

Number of reinforcement layers: 8

Reinforcement index tensile strength: $T_{ult} = 39.2$ kN/m (ASTM 4595)

Wall height and batter and interface friction: H = 6.10 m; $\omega = 3°$; $\delta = 0$

Equivalent surcharge load: $q = \gamma \times D_q = 20.4$ kN/m$^3 \times 1.30$ m $= 26.5$ kN/m^2

Coefficient of horizontal active earth pressure: $K_{ah} = K_a\ (\phi,\ \delta,\ \omega)\ \cos\ (\delta - \omega) = 0.171$

The total demand is equal to the horizontal component of earth force (Equation 2.4):

$$P_{ah} = 0.5K_{ah}\gamma H^2 + K_{ah}qH = 0.5 \times 0.171 \times 23.1\frac{kN}{m^3}(6.10)^2 m^2 + 0.171 \times 26.5\frac{kN}{m^2} \times 6.10\,m = 92.8\frac{kN}{m}$$

From Equation 2.5:

$$RD_{index} = \frac{\sum\limits_{i=1}^{n} T_{ult}^{i}}{P_{ah}(\varphi_{ps})} = \frac{8 \times 39.2 \frac{kN}{m}}{92.8 \frac{kN}{m}} = \frac{314}{92.8} = 3.38$$

<center>END OF EXAMPLE 2.1</center>

2.3.5 Ultimate Resistance-Demand Ratio Using AASHTO Design Method

In current design practice (AASHTO 1999) the maximum allowable design load T_{max}^{i} for a reinforcement layer is calculated as follows:

$$T_{max}^{i} = \frac{T_{al}^{i}}{FS} = \frac{T_{ult}^{i}}{FS \times RF_{design}} = \frac{T_{ult}^{i}}{FS \times RF_{ID} \times RF_{CR} \times RF_{D}} \qquad (2.6)$$

According to AASHTO terminology, the quantity T_{al} = long-term reinforcement strength, and FS is a factor of safety to account for overall uncertainty. The reduction factors used to account for other forms of degradation are RF_{ID} = installation damage, RF_{CR} = creep rupture and, RF_{D} = chemical and biological degradation. For brevity, the product of these terms for design using the AASHTO method can be expressed as $RF_{design} = RF_{ID} \times RF_{CR} \times RF_{D}$.

The maximum load to be carried by a reinforcement layer using the Simplified Method is:

$$T_i = S_i K_{ah}(\gamma z_i + q) \qquad (2.7)$$

The load in reinforcement layer i is calculated on the basis of the integrated lateral pressure acting over a contributory unit face area, S_i. The quantity K_{ah} is calculated by using the *design* friction angle for the soil ($\phi = \phi_{des}$), as reported in Table 2.1. Equating expressions 6 and 7 leads to the following:

$$T_{ultdesign}^{i} = FS \times RF_{design} \times T_i \qquad (2.8)$$

An *ultimate* design resistance-demand ratio can now be expressed as follows:

<center>46</center>

$$RD_{ultdesign} = \frac{\sum_{i=1}^{n} T_{ultdesign}^{i}}{P_{ah}(\varphi_{ps})} \qquad (2.9)$$

The numerator in the above expression can be understood to be the sum of the minimum index strengths required for the reinforcement layers in each case study to just satisfy the current AASHTO design method for calculating the maximum allowable design load T_{max}^{i}. The demand term in the denominator (total horizontal earth force) is calculated as before, using $\phi = \phi_{ps}$ to provide a common basis of comparison. The least conservative estimate of $RD_{ultdesign}$ can be obtained by matching the reinforcement strength required to the demand at each reinforcement layer level, termed "perfect match-to-demand" in Table 2.2. However, typical design practice is to determine the reinforcement strength required by using the calculated demand at the bottom of a constant reinforcement strength or vertical spacing zone within the wall cross-section, and using the strength calculated in this manner for the entire constant strength or vertical spacing zone. This is termed "typical practice" in Table 2.2. In all cases, this typical practice calculation will result in a higher $RD_{ultdesign}$ than will the perfect match-to-demand calculation.

Example 2.2. Calculate the ultimate design resistance-demand ratio using the AASHTO design method for Case Study GW9 with surcharge in place (Figure 2.10), for the perfect match-to-demand case. Additional parameter values from those in Example 2.1 are as follows:

Design friction angle: $\quad\quad\quad\quad\quad\quad\quad\quad \phi = \phi_{design} = 40°$

Coefficient of horizontal active earth pressure: $\quad K_{ah} = K_a(\phi_{design}, \delta, \omega) \times \cos(\delta-\omega) = 0.22$

Product-specific reduction factors: $\quad\quad\quad RF_{CR} = 1.85, RF_{ID} = 1.30, RD_D = 1.30$

Reinforcement spacing: $\quad S_8 = 1.2$ m; $S_7 = 0.9$ m; $S_6 = 0.9$ m; $S_5 = 0.7$ m; $S_4 = 0.6$ m; $S_3 = 0.6$ m; $S_2 = 0.6$ m; $S_1 = 0.4$ m

Depth of reinforcement layers: $\quad\quad z_8 = 0.8$ m; $z_7 = 1.6$ m; $z_6 = 2.6$ m; $z_5 = 3.4$ m; $z_4 = 4.0$ m; $z_3 = 4.6$ m; $z_2 = 5.2$ m; $z_1 = 5.8$ m

Example calculations for layers 4 and 1 using Equation 2.7:

$$T_4 = S_4 \times K_{ah} \times \left(\gamma z_4 + q\right) = 0.6 \text{ m} \times 0.199 \times \left(20.4 \ \frac{kN}{m^3} \times 4.0 \text{ m} + 26.5 \ \frac{kN}{m^2}\right) = 12.9 \ \frac{kN}{m}$$

$$T_1 = S_1 \times K_{ah} \times \left(\gamma z_1 + q\right) = 0.4 \text{ m} \times 0.199 \times \left(20.4 \ \frac{kN}{m^3} \times 5.8 \text{ m} + 26.5 \ \frac{kN}{m^2}\right) = 11.5 \ \frac{kN}{m}$$

The product of reduction factors is the following:

$$RF_{design} = RF_{ID} \times RF_{CR} \times RF_D = 1.85 \times 1.30 \times 1.30 = 3.13$$

Example calculations for the ultimate design strength for layers 4 and 1 using Equation 2.8 are:

$$T_{ultdesign}^4 = FS \times RF_{design} \times T_4 = \left(1.5 \times 3.13\right) \times 12.9 \ \frac{kN}{m} = 60.6 \frac{kN}{m}$$

$$T_{ultdesign}^1 = FS \times RF_{design} \times T_8 = \left(1.5 \times 3.13\right) \times 11.5 \ \frac{kN}{m} = 54.0 \frac{kN}{m}$$

The *ultimate* design resistance-demand ratio is calculated using Equation 2.9:

$$RD_{ultdesign} = \frac{\sum_{i=1}^{8} T_{ultdesign}^i}{P_{ah}(\varphi_{ps})} = \frac{\left(54.0 + 74.3 + 67.5 + 60.6 + 62.9 + 66.9 + 49.7 + 48.0\right)\frac{kN}{m}}{92.8 \ \frac{kN}{m}} = \frac{484}{92.8} = 5.21$$

<div align="center">END OF EXAMPLE 2.2</div>

2.3.6 Estimated Long-Term Resistance-Demand Ratio

The actual reinforcement strength available at the end of design life (long-term) is difficult to estimate given the current state of knowledge. However, the current AASHTO approach that uses "best estimate" values for degradation mechanisms, or actual measured losses from exhumation and testing of the reinforcement, if reported, can be used to calculate available long-term reinforcement strength for comparison purposes. The available reinforcement capacity T_i is:

$$T_i = \frac{T_{ult}^i}{RF_{actual}} = \frac{T_{ult}^i}{RF_{ID} \times RF_{CR} \times RF_D} \tag{2.10}$$

where RF_{actual} is calculated by using "best estimate" values for reduction factors RF_{ID}, RF_{CR}, and RF_D. The *estimated* long-term resistance-demand ratio can now be calculated as follows:

$$RD_{estimated} = \frac{\sum_{i=1}^{n} \frac{T_{ult}^i}{RF_{actual}}}{P_a(\phi_{ps})} \tag{2.11}$$

Example 2.3. Calculate the estimated long-term resistance-demand ratio for Case Study GW9 with surcharge in place (Figure 2.10).

"Best estimate" reduction factors: $RF_{CR} = 1.85$, $RF_{ID} = 1.30$, $RD_D = 1.30$

The product of estimated reduction factors is:

$RF_{actual} = RF_{ID} \times RF_{CR} \times RF_D = 1.85 \times 1.30 \times 1.30 = 3.13$

The estimated resistance-demand ratio is calculated using Equation (11):

$$RD_{estimated} = \frac{\sum_{i=1}^{8} \frac{T_{ult}^i}{RF_{actual}}}{P_a(\phi_{ps})} = \frac{8 \times \left(\frac{39.2}{3.13}\right) \frac{kN}{m}}{92.8 \frac{kN}{m}} = \frac{100}{92.8} = 1.08$$

END OF EXAMPLE 2.3

2.3.7 *Allowable Long-Term Resistance-Demand Ratio Using AASHTO Method*

The resistance-demand ratio for all case histories in the current study can be calculated by using long-term reinforcement strength values ($T_{aldesign}^i$). The *allowable* long-term design resistance-demand ratio using the AASHTO method can expressed as follows:

$$RD_{aldesign} = \frac{\sum_{i=1}^{n} T_{aldesign}^i}{P_a(\phi_{ps})} = \frac{\sum_{i=1}^{n} \frac{T_{ultdesign}^i}{RF_{design}}}{P_a(\phi_{ps})} \tag{2.12}$$

where $T_{ultdesign}^i$ is calculated with Equation 2.8, and RF_{design} is calculated with AASHTO-recommended values for reduction factors RF_{ID}, RF_{CR}, and RF_D, given what would have been known about the wall backfill and long-term properties of the reinforcement product at the time the wall was designed. As described in Section 2.3.5, $RD_{aldesign}$ can be obtained by matching the reinforcement strength required to the demand at each reinforcement layer level (termed "perfect match to demand" in Table 2.2), or it can be calculated in accordance with typical practice using constant zones of strength and spacing (termed "typical practice" in Table 2.2).

Example 2.4. Calculate the allowable long-term resistance-demand ratio using the AASHTO method for Case Study GW9 with surcharge in place (Figure 2.10), for the perfect match-to-demand case.

From Example 2:

$RF_{design} = RF_{ID} \times RF_{CR} \times RF_D = 1.85 \times 1.30 \times 1.30 = 3.13$

The *allowable* design resistance-demand ratio is calculated using Equation 2.12:

$$RD_{aldesign} = \frac{\sum_{i=1}^{8} T_{aldesign}^i}{P_a(\varphi_{ps})} = \frac{\sum_{i=1}^{8} \dfrac{T_{ultdesign}^i}{RF_{design}}}{P_a(\varphi_{ps})} = \frac{\dfrac{(54.0 + 74.3 + 67.5 + 60.6 + 62.9 + 66.9 + 49.7 + 48.0)}{3.13} \dfrac{kN}{m}}{92.8 \dfrac{kN}{m}} = \frac{156}{92.8} = 1.67$$

END OF EXAMPLE 2.4

2.4 Summary of Global Level of Safety and Performance for Case Histories

The calculated resistance to demand ratios, or level of safety, both short (equations 2.5 and 2.9) and long term (equations 2.11 and 2.12), for all case histories are summarized in Table 2.2. The table also compares the calculated level of safety for the case history to the level of safety that would be required by current AASHTO design specifications (AASHTO 1999). The long-term level of safety has been estimated at the end of a 75-year design life, which is a typical design life used for these types of walls.

Table 2.2 also records the observed long-term performance of each wall as "good" or "poor." The following definition for "good" long-term performance was used (see Chapter 6.0):

- Total reinforcement strains are small (typically less than 3 percent).

- Creep strains and strain rates decrease as time increases (i.e., only primary creep observed).

- The wall backfill soil does not exhibit signs of failure (cracking, slumping, etc.).

- Post-construction deformations, which are typically greatest at the wall top, are less than 30 mm within the first 10,000 hours.

Evidence of "poor" long-term performance included the following:

- The total reinforcement strains are relatively large (typically 5 percent or more).

- The creep strain rates are relatively constant or increase as a function of time.

- The wall backfill exhibits signs of failure (cracking, slumping, etc.)

- A reinforcement rupture occurs either at the connection or in the backfill (typically, the top reinforcement layer will fail first).

- Post-construction wall face deformations are greater than 35 mm in the first 10,000 hours after the end of wall construction, and increase at a constant or increasing rate.

In some cases, wall performance was described as fair, indicating a borderline case.

The average index RD ratios, based on measured properties, both short-term and long-term, and for walls that exhibited either good or poor performance, are compared in Table 2.3 to the RD ratios that would be required if the walls were designed in accordance with current AASHTO specifications. Additionally, figures 2.22 and 2.23 illustrate how the RD ratios are distributed statistically for the actual versus the AASHTO design RD ratio. Figure 2.24 illustrates the level of conservatism that current AASHTO design requirements would require relative to the actual RD ratio inherent in the wall case histories that exhibited good long-term performance. These figures and Table 2.3 clearly illustrate the difference in resistance-demand ratio between what has been built successfully in the past versus what is now required by current AASHTO specifications.

Table 2.3. Average global resistance to demand for all geosynthetic wall case histories.

Wall Performance	Number of Walls, Test Sections, or Load Cases	Average Resistance to Demand Ratio (RD)			Ratio: AASHTO to Actual RD	Conservatism due to Soil Strength Selection: Design K_{ah} / Plane Strain K_{ah}	Conservatism Due to Imperfect Match to Demand	Ratio of AASHTO RD, with Conservatism Due to Soil Strength Selection and Imperfect Demand matching Removed, to Actual RD
		Actual Wall	Designed per AASHTO (1999), Typical Practice, with Typical Soil Design Parameters	Designed per AASHTO (1999), Perfect Match to Demand, with Typical Soil Design Parameters				
good performance, short-term (index or ultimate)	30	12.4	24.9	18.1	2.8	2.11	1.38	0.9
fair or poor performance, short-term (index or ultimate)	5	2.45	30.5	19.8	11.5	1.92	1.54	4.5
good performance, long-term (estimated or allowable)	30	2.73	4.64	3.36	2.4	2.11	1.38	0.8
fair or poor performance, long-term (estimated or allowable)	5	0.45	4.84	3.2	9.9	1.92	1.51	3.8

*This "conservatism" is relative to the theoretical demand based on Coulomb theory, but with zero soil-wall interface friction, using measured soil strength parameters from which plane strain parameters were estimated. If the load calculation theory itself is conservative (i.e., measured reinforcement loads are below the theoretical reinforcement loads calculated), then additional conservatism will be present that is not shown in this table.
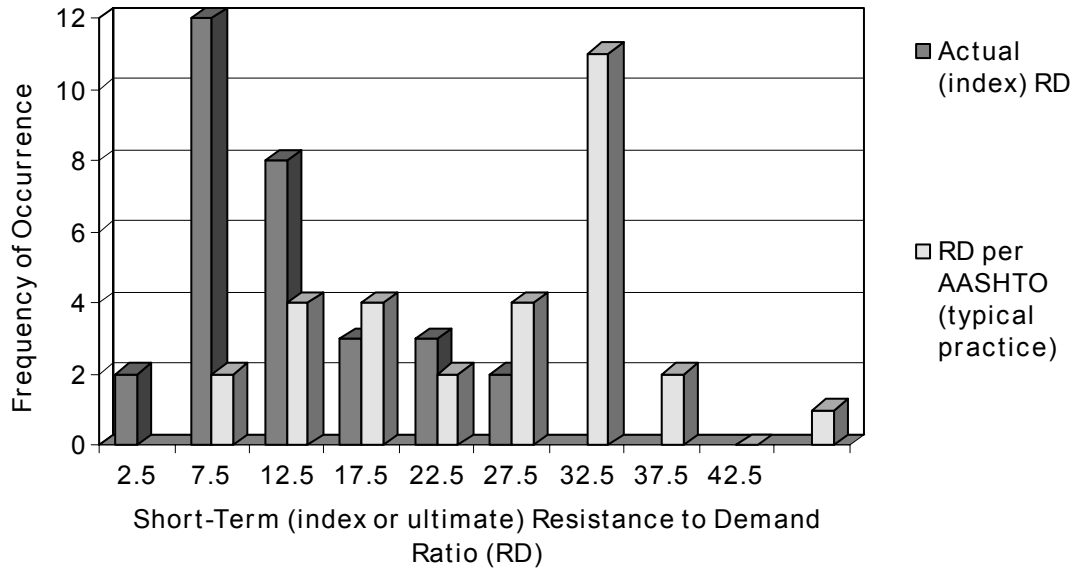
Figure 2.22. Comparison between the index (short-term) resistance-demand ratio for the actual walls and the ultimate resistance-demand ratio required by current AASHTO design specifications for geosynthetic wall case histories with good performance.
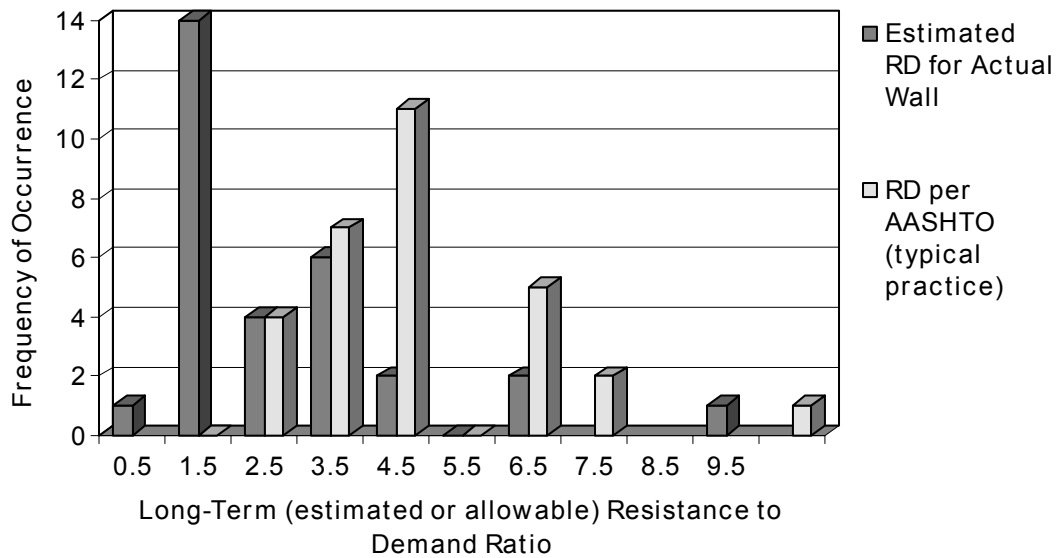
Figure 2.23. Comparison between the estimated long-term resistance-demand ratio for the actual walls and the allowable long-term resistance-demand ratio required by current AASHTO design specifications for geosynthetic wall case histories with good performance.
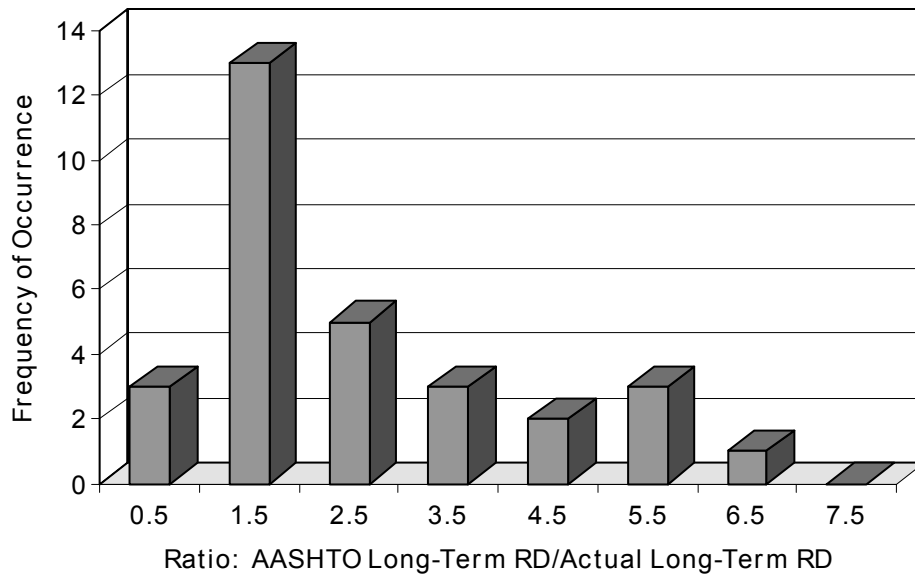
Figure 2.24. Degree of conservatism in long-term resistance-demand ratio when following current practice (AASHTO 1999) for case histories with good long-term performance.

2.5 Discussion of Wall Case History Performance and Level of Safety

The case histories summarized in tables 2.1 and 2.2 cover a variety of heights, surcharge conditions, foundation conditions, facing types and batter, reinforcement types and stiffness, and reinforcement spacings. The performance of these walls is considered to be representative of geosynthetic reinforced soil walls that are constructed with granular backfills.

Table 2.3 indicates that, for short-term strength, case study walls contain approximately one third of the reinforcement that would typically be required if the walls were designed in accordance with the current AASHTO specifications using typical soil design properties. For long-term level of safety, actual walls that exhibited good performance contain less than one half of the reinforcement that would typically be required if the walls were designed in accordance with the current AASHTO specifications. In some cases, only one-eighth of the reinforcement required by current AASHTO specifications was used.

As for the case study walls that exhibited poor performance, these walls contained only one tenth to one twelfth of the reinforcement that would typically be required if the walls were designed in accordance with the current AASHTO specifications for both short-term and long-term reinforcement strength. Given these observations, it appears that the reinforcement actually required to provide adequate internal strength for good long-term performance is somewhere

between one half and approximately one tenth of what current design practice, in particular the AASHTO specifications, would require. Clearly, there must be some significant sources of conservatism in current design practice. Possible sources of conservatism in internal stability design are discussed below.

In current design practice for walls with granular backfill, a design soil friction angle of 34 to 40 degrees is typically used, even for well-graded granular backfills with angular particles. It is generally not feasible to perform laboratory soil shear strength tests on project-specific backfill soils in advance of design, since the backfill source is typically not known at this stage. In those rare cases where measured backfill soil shear strength properties are available for design, the data are from direct shear box tests or triaxial tests, and peak friction angles are not converted to larger plane strain values.

The case histories reviewed here suggest that the use of a conservative soil shear strength value resulted in overestimation of reinforcement loads by a factor of 1.2 to 3.5, with an average value of about 2.0 (Table 2.3). Not considered here is potentially greater soil shear strength due to apparent soil cohesion (in general, 10 kPa or less) that could increase this overestimation factor even more. However, most designers are reluctant to rely on apparent cohesion over the long term.

Another source of conservatism, based on Table 2.3, is an imperfect match between the reinforcement strength available and the demand at each reinforcement level. An imperfect match may occur in design if the reinforcement strength used in calculations is determined at the base of a group (or zone) of reinforcement layers of the same strength, or of a group of layers with the same vertical spacing, and this strength is applied over the entire zone. As indicated in Table 2.3, this causes reinforcement loads, on average, to be overestimated by a factor of 1.4 to 1.5 for the case histories evaluated.

Combining both the soil shear strength and imperfect matching as sources of conservatism and applying them to reduce R_{design} for calculating $RD_{ultdesign}$ and $RD_{aldesign}$ (Table 2.3) indicates that the wall case histories, on average, have about the right amount of reinforcement relative to the theoretical minimum amount AASHTO would require for walls that performed well, and approximately one-fourth of the reinforcement for walls that performed fairly to poorly. Furthermore, for the walls that performed well, 13 of the wall case histories had less reinforcement than the theoretical minimum amount AASHTO would require (as low as one half

of the reinforcement required by AASHTO), as indicated in Figure 2.25, which summarizes the distribution of values for each case history used to develop the averages presented in the far right column of Table 2.3. This suggests that even after removing sources of conservatism such as soil strength parameter selection and imperfect matching of the reinforcement to the AASHTO demand, additional conservatism is still hidden in the current design methodology for walls that are known to perform well. It is likely that the magnitude of this hidden conservatism is somewhere between a factor of 1.5 and 4, with the larger value corresponding to walls with marginal to poor performance.
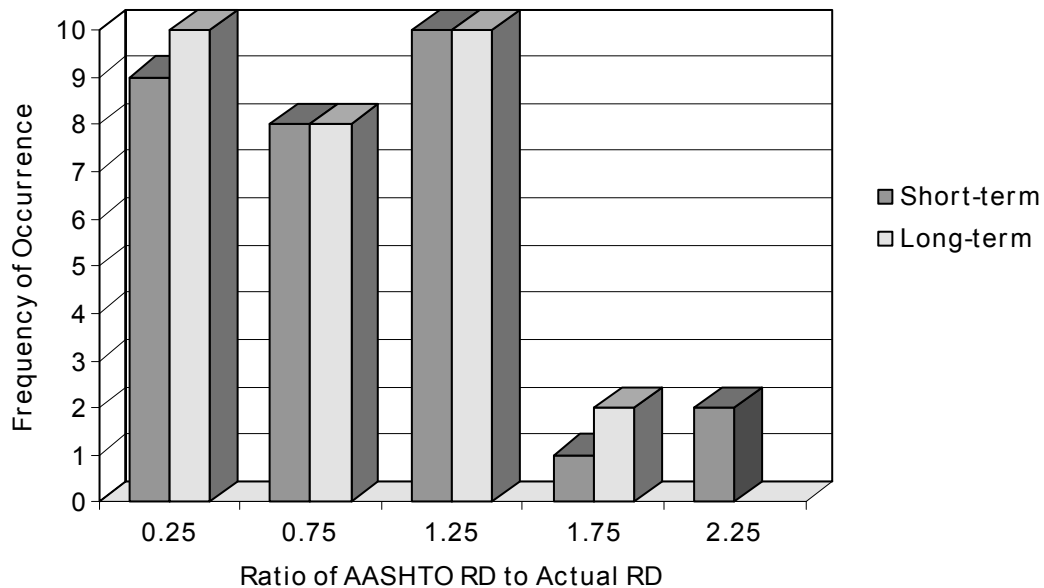
Figure 2.25. Ratio of the theoretical minimum AASHTO RD to the actual RD for walls with good long-term performance (conservatism due to soil strength selection and imperfect demand matching removed).

Even when measured soil properties are considered, loads interpreted from measured reinforcement strains in geosynthetic reinforced wall systems have consistently been observed to be significantly lower than the calculated load. Later chapters and other previous publications (e.g., Rowe and Ho 1993) provide detailed evidence of this observation.

Current methods of characterizing long-term geosynthetic reinforcement strength (e.g., Elias et al. 2001, Elias 2001, AASHTO 1999, WSDOT 1998) may also contribute to design conservatism. The paper by Allen and Elias (1996) contains a discussion of how current and

proposed durability laboratory test protocols are likely to produce a conservative estimate of geosynthetic polymer life. Chapter 6.0 discusses evidence that as long-term creep occurs, the remaining reinforcement tensile strength does not decrease until just before creep rupture is reached. Hence, the tensile strength of the reinforcement does not, in reality, decrease monotonically with the logarithm of elapsed time due to creep, as is often assumed in design. Furthermore, if the reinforcement layer stress is below the stress level required to cause creep rupture during the design lifetime, creep will never cause a reduction in reinforcement tensile strength during the wall design lifetime. Hence, creep becomes a non-issue, especially if conservative soil strength parameters are used, causing reinforcement resistance and the overall level of safety to be underestimated.

2.6 Summary and Conclusions

A summary of 19 geosynthetic wall case histories with a total of 35 analysis conditions has been presented. These case histories cover a variety of wall heights, surcharge conditions, foundation conditions, facing types and batter, reinforcement types and stiffness, and reinforcement spacings. All of the walls that were designed as production walls, including structures in place for 25 years, performed well with low strains and minimum deflections, both in the short term and long term. Some of the walls that were built for research rather than production were purposely under-designed so that failure could occur, providing an indication of the design limits of these types of wall systems. Some of these under-designed walls (e.g., Bell et al. 1983) could not be taken to failure even though they were intended to fail, indicating that the internal stability of geosynthetic walls has been greater than one could expect based on what is currently known.

Each of the walls was characterized globally with respect to internal level of safety, or resistance-demand (RD) ratio. The geosynthetic walls in these case histories that performed well appear to be significantly under-designed relative to the design that would result from using current design codes and practices. Even when sources of conservatism are considered, such as soil parameter selection and imperfect matching of the reinforcement strengths to the demand (Simplified Method), the Simplified Method still appears to require approximately 1.5 to 4 times as much geosynthetic reinforcement as would to be needed to achieve acceptable performance based on the actual long-term performance of many walls.

This analysis indicates that there would be significant benefit in reevaluating the current approach used to design geosynthetic walls for internal reinforcement rupture. Furthermore, designers who use the Simplified Method should consider the "hidden" conservatism that results from current design practices applied to geosynthetic walls. For example, a more aggressive approach to the selection of soil design parameters and matching of the reinforcement strength to demand should be considered.

3.0 SHORT-TERM STRAIN AND DEFORMATION BEHAVIOR OF GEOSYNTHETIC WALLS AT WORKING STRESS CONDITIONS

3.1 Introduction

The previous chapter summarized a number of geosynthetic wall case histories and evaluated the internal stability of those case histories from a global perspective. That global analysis revealed substantial design conservatism exists in how design parameters are selected, how the design procedures are applied, and in the design procedure itself. It is possible that the conservatism in the design procedure alone could produce 1.5 to 4 times the amount of reinforcement needed to obtain good, long-term performance.

To better understand the generally good performance of geosynthetic reinforced walls (in some cases after 25 years in service) and to quantify this performance in a way that can be used to develop improved design procedures, it is valuable to review available data on the loads and strains that have been recorded in carefully instrumented and monitored structures. Measured strains and loads can then be used to guide the development of improved design methods that will result in less conservative designs while ensuring satisfactory long-term performance.

To determine actual geosynthetic reinforcement loads, the strain in the reinforcement must be measured and strain readings correctly interpreted. This chapter focuses on the case histories reported in Chapter 2.0 for which high quality reinforcement strain measurements are available. This chapter reviews the strain measurement techniques that were used, how measurements were interpreted, accuracy of reinforcement strain measurements, and some advantages and disadvantages of different reinforcement strain instrumentation techniques. In addition, the relationship between measured wall facing deflections and reinforcement strains is examined.

The strain data reported in this study are used in a later chapter to estimate loads in reinforcement layers and finally to support a new geosynthetic wall design methodology.

3.2 Geosynthetic Wall Case Histories

Only the case histories reported in Chapter 2.0 that have good quality reinforcement and displacement strain data are considered. The key characteristics of each of these case histories are summarized in tables 3.1 and 3.2. Additional details of each wall can be found in Chapter

2.0. Table 3.3 summarizes the instruments used to measure the strains in the walls. The case histories in the tables span the past 17 years and include a range of wall heights (3 to 12.6 m), surcharge conditions, reinforcement types, and arrangement. Most of the walls used geogrid reinforcement products, although some employed woven geotextiles and one a nonwoven geotextile.

Table 3.1. Summary of geometry for selected case histories.

Wall Case No.	Case History	Date Built	Wall Height (m)	Surcharge Conditions
GW5	Tanque Verde Tensar Concrete Panel Wall	1984	4.9	None
GW7	Oslo, Norway (Tensar) Walls (Sections J and N)	1987	4.8	3 m steeply sloping soil surcharge
GW8	Algonquin Tensar Concrete Panel Wall	1988	6.1	2.1 m sloping surcharge
GW9	Algonquin Miragrid Modular Block faced Wall	1988	6.1	2.1 m sloping surcharge
GW10	Algonquin Geotextile Wrapped Face Wall	1988	6.1	None
GW11	RMCC Geogrid Wrapped Face Full Scale Test Wall	1986	3	0.7 m soil surcharge
GW12	RMCC Full Height Propped Plywood Panel full Scale test wall	1987	3	Full test wall top coverage with air bag loading system, up to effective pressure of 42 kPa
GW13	RMCC Incremental plywood Panel full Scale test wall	1987	3	Full test wall top coverage with air bag loading system, up to effective pressure of 42 kPa
GW14	RMCC Full Height Propped Panel Full Scale (Tensar) Test Wall	1989	3	Full test wall top coverage with air bag loading system, up to effective pressure of 70 kPa
GW15	RMCC Incremental Panel Full Scale (Tensar) Test Wall	1989	3	Full test wall top coverage with air bag loading system, up to effective pressure of 60 kPa
GW16	WSDOT Rainier Avenue Wrapped Face Geotextile Wall	1989	12.6	5.3 m sloping surcharge
GW17	London, Ontario Propped Panel (Tensar) Wall	1989	7.1	None
GW18	Fredericton, New Brunswick Propped Panel (Tensar) Wall	1990	6.1	None
GW20	Vicenza, Italy Welded Wire Faced Geosynthetic Walls (HDPE test section)	1998	4	3.5 m steeply sloping soil surcharge
GW20	Vicenza, Italy Welded Wire Faced Geosynthetic Walls (PP test section)	1998	4	3.5 m steeply sloping soil surcharge

Table 3.2. Summary of materials and design for selected case histories.

Wall Case No.	Geosynthetic Type	Geosynthetic Polymer	Long-Term Global Resistance to Demand Ratio for Actual Wall, per Chapter 2.0	Long-Term Global Resistance to Demand Ratio if Designed per AASHTO '98, per Chapter 2.0 (perfect match to demand)
GW5	Extruded uniaxial geogrid	HDPE	6.14	3.69
GW7	Extruded uniaxial geogrid	HDPE	Section J – 4.78 Section N – 6.38	5.98 for both sections
GW8	Extruded uniaxial geogrid	HDPE	1.27	1.60
GW9	Woven geogrid	PET	1.08	1.67
GW10	NP NW geotextile	PET	0.6 before water restraint removed, 0.4 after water removed	2.50 before water removed, 1.65 after water removed
GW11	Extruded biaxial geogrid	PP	1.47	3.40
GW12	Extruded uniaxial geogrid	HDPE	3.76	3.13
GW13	Extruded uniaxial geogrid	HDPE	3.76	3.13
GW14	Extruded biaxial geogrid	PP	1.15 end of constr. 0.32 with full surcharge	3.1
GW15	Extruded biaxial geogrid	PP	1.15 end of constr. 0.36 with full surcharge	3.1
GW16	Woven geotextile	PP for upper 75% of wall, PET for lower 25% of wall	3.44	4.03
GW17	Extruded uniaxial geogrid	HDPE	3.16	2.23
GW18	Extruded uniaxial geogrid	HDPE	1.89	2.11
GW20, with surcharge	Extruded uniaxial geogrid	HDPE	1.71	5.89
GW20, with surcharge	Biaxial geogrid	PP	0.53	5.58

Table 3.3. Summary of instrumentation details for measuring strain for each case history.

Wall Case No.	Strain Measurement Method	Gauge Type	Number of Measurement Points	Number of Gauges Per Point	Method used to Attach Gauges to Geosynthetic	Gauge Length (mm)	Gauge Calibration Method	Strain Gauge Calibration Factor	Reference for Details
GW5	Strain gauges (local reinforcement strain)	Bonded Resistance Strain Gauges: Micro Measurements Type CAE-06-25OUT-350	50 points distributed among two wall sections	2 (top and bottom)	AE-10 adhesive beneath entire gauge. Gauge was attached to the rib	6.3	In-isolation wide width test on specimens with gauge attached	1.0	Desert Earth 1987
GW7	Inductance coils (global strain)	Bison inductance coils, 54 mm in diameter and 7 mm thick	23 points Section J, 37 points Section N	2 (one at each end of the rib)	Bolted through small hole drilled through rib nodes	Length of rib between nodes (156 mm)	Laboratory calibration using physical measurements of distance in comparison to readings	1.0	Fannin 1998
GW8	Strain gauges (local strain)	Hottinger-Baldwin gauge 6/120 LY61	28 points	2 (top and bottom)	Micro Measurements M Bond 200 adhesive; attached to rib	60 mm	In-isolation wide width test on specimens with gauge attached	1.0	Christopher 1993
GW9	Strain gauges (local reinforcement strain)	Kyowa Dengyo high elongation foil gauge type KFE-5-C1	42 points	2 (top and bottom)	Tokyo Sokki Kenyujo Type CN cynoacrylate adhesive	5 mm	In-isolation wide width test on specimens with gauge attached	1.75	Bathurst et al. 1993
	Extensometers (global reinforcement strain)	Gloetzl extensometers	13 points	1	Not reported, but likely similar to method used for GW15 extensometers	Varies	N/A	1.0	Bathurst et al. 1993

Table 3.3. Continued.

Wall Case No.	Strain Measurement Method	Gauge Type	Number of Measurement Points	Number of Gauges Per Point	Method used to Attach Gauges to Geosynthetic	Gauge Length (mm)	Gauge Calibration Method	Strain Gauge Calibration Factor	Reference for Details
GW10	Strain gauges (local strain)	Hottinger-Baldwin gauge 10/120 LD20	28 points	2 (top and bottom)	Micro Measurements AE15 adhesive; attached only at ends of gauge	10 mm	In-isolation wide width test and in-soil tests on specimens with gauge attached	Approx. 1.5	Christopher 1993
GW11	Strain gauges (local strain)	Bonded resistance gauges: Showa Measuring Instruments Type Y11-FA-5-120	14 points	3 gauges on different ribs but at nominally identical distances from wall face	RTC epoxy beneath entire gauge	5 mm	In-isolation wide width test on specimens with gauge attached	1.33	Benjamin 1989, Lescoutre 1986, Bathurst et al. 1988
GW12 and GW13	Strain gauges (local strain)	Bonded resistance gauges: Showa Measuring Instruments Type Y11-FA-5-120	20 points	3 gauges on different ribs but at nominally identical distances from wall face	RTC epoxy beneath entire gauge	5 mm	In-isolation wide width test on specimens with gauge attached	1.05	Benjamin 1989

Table 3.3. Continued.

Wall Case No.	Strain Measurement Method	Gauge Type	Number of Measurement Points	Number of Gauges Per Point	Method used to Attach Gauges to Geosynthetic	Gauge Length (mm)	Gauge Calibration Method	Strain Gauge Calibration Factor	Reference for Details
GW14 and GW15	Strain gauges (local strain)	Bonded resistance gauges: Showa Measuring Instruments Type Y11-FA-5-120	24 points	3 gauges on different ribs but at nominally identical distances from wall face	RTC epoxy beneath entire gauge	5 mm	In-isolation wide width test on specimens with gauge attached	1.05	Benjamin 1989
	Extensometers (global strain)	Wire extensometers	16 points	1	Bolted to grid node with very small set screw	varies	N/A	1.0	Benjamin 1989
GW16	Strain gauges (local reinforcement strain)	Bonded resistance gauges: BLH, Inc., SR-4 type PA3 gauges for the PET geosynthetic, Tokyo Lokki Kenkyojo Ltd. YL-20 Gauges for the PP geosynthetics	45 installed (69% survived throughout wall life)	2 (top and bottom)	High elongation, low creep adhesive beneath entire gauge	50 mm for PA3 gauge, 31 mm for YL-20 gauge	In-isolation wide width test on specimens with gauge attached, tested at a strain rate of 1% and 10% per minute,	1.4 for PET geosynthetics, 2.0 for PP geosynthetics	Allen et al. 1992, Boyle and Holtz 1998
	Extensometers (global reinforcement strain)	Glotzl Instrument Co. mechanical extensometer, with a fiberglass rod	14 (11 survived wall construction)	1	Wire placed through geosynthetic layer and glue at anchor head	varies	N/A	N/A	Allen et al. 1992

Table 3.3. Continued.

Wall Case No.	Strain Measurement Method	Gauge Type	Number of Measurement Points	Number of Gauges Per Point	Method used to Attach Gauges to Geosynthetic	Gauge Length (mm)	Gauge Calibration Method	Strain Gauge Calibration Factor	Reference for Details
GW17	Strain gauges (local reinforcement strain)	High elongation bonded resistance gauges: Kyowa Electronic Instruments Type KFE	20 points	1	RTC epoxy beneath entire gauge, mounted to rib	5 mm	In-isolation wide width test on specimens with gauge attached, tested at a strain rate of 2% per minute	1.25	Bathurst 1992
GW18	Strain gauges (local reinforcement strain)	Bonded Resistance Strain Gauges: Micro Measurements Type AE-13-125BT-120	12 (50% of the gauges survived construction)	2 (top and bottom)	Not reported	Not reported	Correction to gross strain was estimated based on similar work by Bathurst, 1992	1.25	Knight and Valsangkar 1993
GW20	Strain gauges (local reinforcement strain)	Bonded Resistance Strain Gauges: Tokyo Sokki KenkyujoType TFLA-5	63 points (62 gauges survived construction)	1	Gauge mounted to rib, near junction with cross rib, using cynoacrylate adhesive	5 mm	In-isolation wide width test on specimens with gauge attached, tested at various strain rates	1.05 for HDPE geogrid, 1.1 for PP geogrid	Carrubba et al. 1999

Although other wall case histories in the literature reported reinforcement strain readings, they are not listed in the tables. These case histories were deficient with respect to soil shear strength and/or reinforcement load-strain properties. Other walls used nonwoven geotextiles and lack site- and product-specific in-soil modulus data. Walls with unusual or complicated boundary conditions were also omitted in this study.

Most of the case histories used redundant instrumentation schemes either in terms of multiple gauges at a given point and/or an independent measurement technique to verify measured strains (e.g., strain gauges and extensometers). In many of the cases, the strain gauge response was compared to global strains in the reinforcement by using in-isolation tensile tests. The comparison was used to quantify under-registration of average strain in the reinforcement as a result of gauge attachment method, gauge-reinforcement interaction, or variation of geosynthetic properties with location (e.g., integral drawn polyolefin geogrids). Where these data were available, correction factors (if required) could be applied to strain gauge readings to estimate global strains in the reinforcement. Global strain values are required to estimate loads in polymeric reinforcement materials from in-isolation isochronous tensile load-strain data.

Finally, many of the case histories reported wall face deformation measurements. These deformations were used to check the reasonableness of the reinforcement strain measurements.

3.3 Interpretation of Strain Measurements

Interpretation of strain or displacement readings from devices attached to geosynthetic reinforcement layers depends on the type of device (Perkins and Lapeyre 1997). The most common types of devices are strain gauges bonded directly to the surface of the geosynthetic reinforcement material and extensometers. Displacements recorded by pairs of extensometers are used to calculate global strains assumed to be constant over the distance between the monitoring points.

3.3.1 Strain Gauges

Small, high elongation strain gauges glued to the reinforcement material must be calibrated against the "true" global strain in the reinforcement. Strain gauges bonded to woven geogrids or geotextiles typically generate a local "hard spot," causing under-registration of global tensile strains. Strain gauges bonded to integral drawn polypropylene (PP) and high density

polyethylene (HDPE) geogrids will record the local strain at the attachment point, which may vary from point to point on the reinforcement material because of product geometry (cross-sectional area) and polymer modulus (a result of the drawing process during manufacture). The calibration factor for a particular combination of gauge, bonding technique, reinforcement type, and location of gauge is typically established from constant rate of strain, in-isolation, wide-width strip tensile testing (ASTM D 4595). Strain gauges may be mounted on one or both sides of the geosynthetic specimen during in-isolation tensile testing. Examples of in-isolation strain gauge calibration tests on four different products are illustrated in figures 3.1 to 3.4.
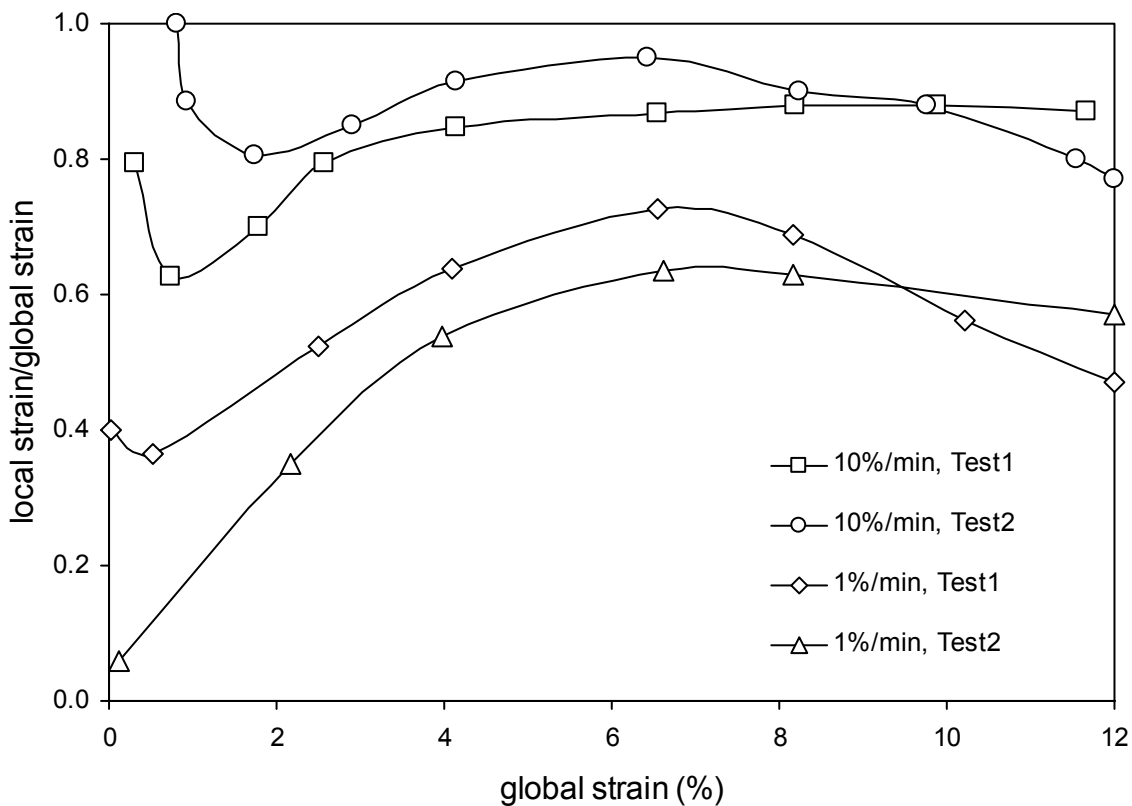
Figure 3.1. Ratio of local strain from strain gauges to global strain versus global strain for polypropylene woven slit film geotextile (after Boyle and Holtz 1998)
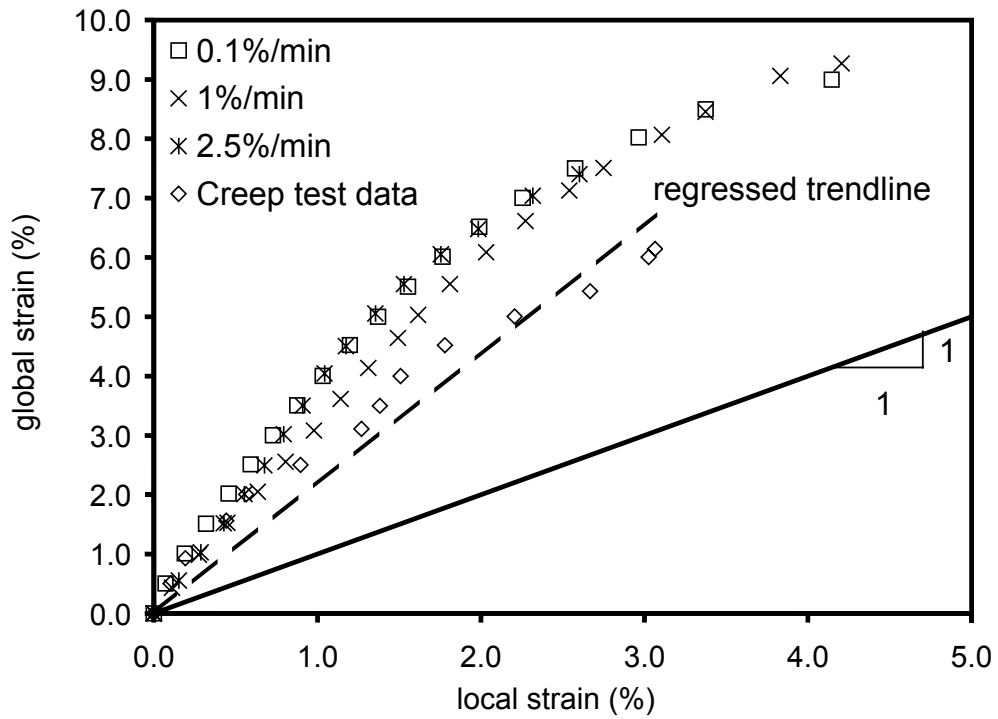
Figure 3.2. Example of in-isolation strain gauge response versus global strain for woven polyester (PET) geogrid (after Saunders 2001).
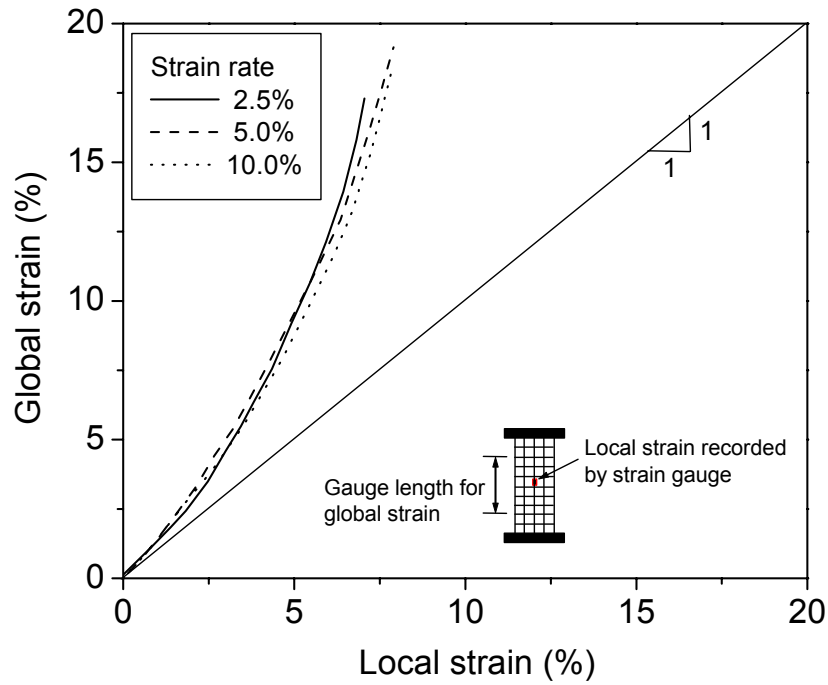
Figure 3.3. Example of in-isolation global strain versus strain gauge response for PP biaxial geogrid (after Bathurst et al. 2001).
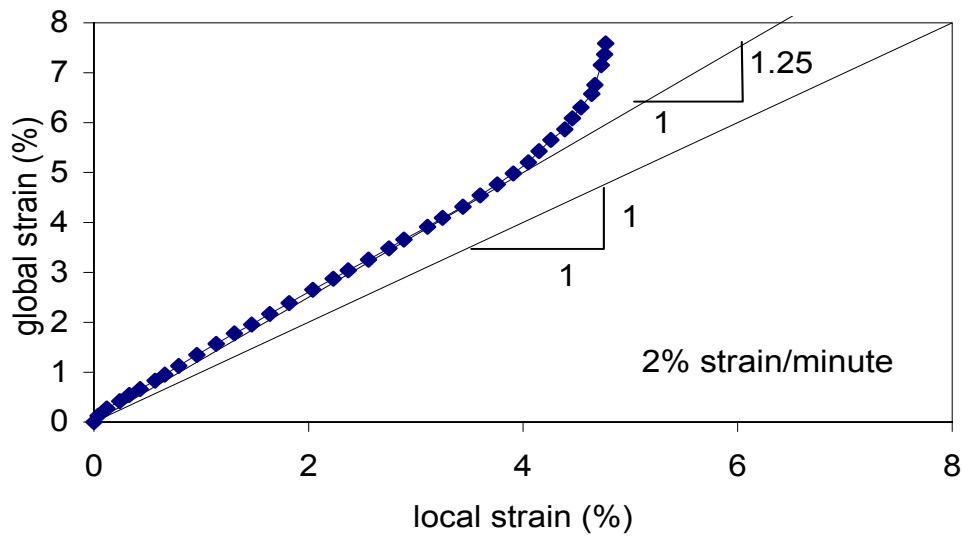
Figure 3.4. Example of in-isolation global strain versus strain gauge response for HDPE uniaxial geogrid (after Bathurst 1993).

Figure 3.1 reports data for a polypropylene woven slit film geotextile that was used in the Rainer Avenue wall (GW16). Strain gauges 30 mm long were centered over an instrumented 75 mm length of specimen (Boyle and Holtz 1998). The data show the ratio of strain gauge reading to global strain reading as a function of global strain. A ratio of 1.0 represents perfect correspondence between strain gauge readings and global strain. The data show that the magnitude of under-registration varied widely with rate of loading and magnitude of global strain, and that the registration (calibration) factor varied between nominally identical tests. A single-value calibration factor from these data over a range of 4 percent strain is about 2. In other words, the strain gauge values must be doubled to represent "true" global strains. Clearly, interpretation of strain gauge readings can be problematic for woven geotextiles, and any strain gauge readings should be corroborated by extensometer or inductance coil readings in the field, or at least multiple strain gauges at nominally identical locations to provide adequate redundancy. For the Rainier Avenue wall, a calibration factor CF = 1.4 to 2.0 was used to convert measured strain gauge strains to true global strains after in-isolation strain data had been reviewed and measured strain gauge readings in-situ had been compared with corresponding extensometer readings.

Figure 3.2 shows similar data for a knitted polyester (PET) geogrid (Saunders 2001). The response curves for constant rate of strain tensile loading fall within a relatively narrow band. The significant under-registration of global strains is considered to be the result of the impregnation of the longitudinal polyester fiber bundles by gauge epoxy glue, which creates a locally stiff region in the longitudinal member (a "hard spot"). Also shown on the figure are data from a constant load (creep) test. The calibration factor for the constant rate of loading test is about CF = 2.2 and is a lower bound on the constant rate of strain calibration curves. It can be argued that the actual loading history of a reinforcement layer during construction falls between the two idealized loading conditions performed in the laboratory. Case study GW9 describes a wall with a woven PET geogrid as the reinforcement. The calibration factor from a single constant rate of tension test gave CF = 1.75.

Figure 3.3 shows strain calibration data for an extruded, drawn PP geogrid that is very similar to the material used in Royal Military College of Canada (RMCC) test walls GW14 and GW15 (Bathurst et al. 2001). The local strain gauge readings were independent of rate of strain testing, but the magnitude of calibration factor increased with the magnitude of global strain.

70

Nevertheless, at very low strains (< 2 percent) the value of CF is close to unity and has been adopted as CF = 1.05 for the RMCC walls.

Finally, in Figure 3.4 the strain registration response of a typical calibration tensile test on an extruded, drawn uniaxial HDPE geogrid is presented (Bathurst 1993). The gauges in this case study were mounted directly on longitudinal members at the mid-point between cross-members. These data show a reasonably constant calibration factor of CF = 1.25 up to a global strain of 5 percent. The non-linearity in the response thereafter may be related to debonding of the gauge from the geogrid surface.

On the basis of a review of available in-isolation tensile strain gauge calibration test data the following observations can be made:

1. The magnitude of strain gauge under-registration (and hence magnitude of calibration factor CF) is greatest for woven geotextiles or knitted geogrids and least for extruded, drawn HDPE geogrids.

2. Variability in strain gauge response is greatest for woven geotextiles.

3. Non-linearity in CF values with magnitude of global strain is greatest for woven geotextiles and geogrids and least for uniaxial HDPE geogrids.

4. In all cases reviewed the magnitude of the calibration factor was 1.0 or better (i.e., CF ≥ 1).

The experience of the writers with strain gauge installation techniques and the interpretation of strain readings from actual field monitoring has led to several important observations. Flexure of reinforcement longitudinal members in the direction of loading may cause additional strain at the gauge location or may attenuate strains, depending on the direction of flexure. For example, local bending may occur as the longitudinal members of stiff, extruded geogrids are compressed flat under soil lifts. In addition, local contact with gravel or cobble particles can cause a local increase or attenuation of strain gauge readings. Flexure of the reinforcement at the connections with hard facings may tend to reduce strain readings because of convex-down reinforcement geometry or may increase strain readings near the wrapped-face for flexible geosynthetic-faced walls because of convex-up geometry. A strategy to avoid flexure-induced strain readings is to attach bonded gauges in pairs on opposite sides of the reinforcement and to arrange the two gauges in a bridge completion that gives a pure tension strain (Gnanendran and Selvadurai 2001). The majority of the case studies included in this investigation in which strains were

71

measured with strain gauges utilized pairs of gauges to account for bending. Other case histories reported herein did use single gauges, but additional gauges were placed in the wall at nominally identical locations for redundancy.

Finally, it is also possible that strain gauges can malfunction because of electronic problems resulting from exposure to moisture, damage during the reinforcement installation and backfilling process, or debonding of the gauge from the reinforcement because of glue failure. Allen et al. (1992) provided a detailed assessment of these issues as they were applied to Wall GW16. Such problems can be identified so that bad readings are not used in the final analysis.

3.3.2 In-situ Global Strains from Extensometer Readings

A correction factor is not needed if extensometers are mounted to the geosynthetic. Nevertheless, strains inferred from extensometers may overestimate geosynthetic yarn or rib strains because of initial surface wrinkles or warps in the geosynthetic that occur during placement.

3.3.3 Other Devices

In one case study (GW7), inductance coil pairs attached to and in the same plane as the geogrid reinforcement were used to infer strains. Global strains as great as 0.9 percent were recorded by these devices at the end of surcharging (Fannin 1988). These devices are calibrated in-isolation and do not require a correction factor. However, the signal from inductance coil pairs is sensitive to the magnitude of out-of-plane movements that may be generated under the conditions described earlier regarding sources of flexure-induced strain gauge readings.

3.3.4 Redundancy of Reinforcement Measurements

In several case studies, multiple strain gauges were placed at nominally identical locations from the wall facing. This approach allows readings to be averaged across the width of the wall and also provides redundancy in the event of failure of an individual gauge in a set of two or more gauges. Data showing variation in strain gauge response for nominally identical gauges are not reported for the case studies considered herein. However, data from recent full-scale polypropylene geogrid reinforced soil walls reported by Bathurst et al. (2000) do give a quantitative indication of the variation in strain gauge response that may be expected *in-situ*

under carefully controlled laboratory conditions corresponding to the RMCC test walls in the current study. Figure 3.5 shows that the uncorrected response of a pair of strain gauges mounted on a PP geogrid may vary by about ±15 percent of the mean reading of 2 percent strain at a confidence level of 95 percent.
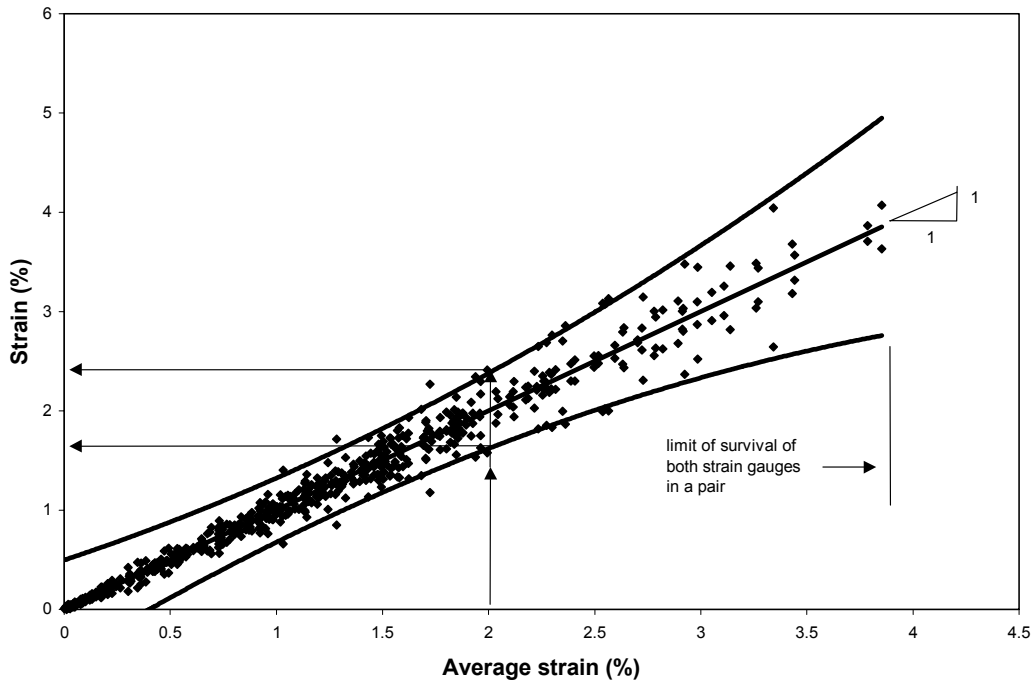
Figure 3.5. Variation in strain gauge response versus average of strain gauge pair mounted at nominally identical positions on a PP geogrid (error curves represent 95 percent confidence level) (Burgess 1999).

The best strategy for providing a check on strain gauge readings is to use strain gauges *and* extensometers. After the strain gauge readings have been adjusted with an appropriate calibration factor established from in-isolation testing of the type described earlier, the corrected strain gauge reading can be compared to strains determined from adjacent extensometer monitoring points that span the strain gauge location.

An example of the variation between uncorrected strain gauge readings for the same full-scale wall described above (Bathurst et al. 2000) is shown in Figure 3.6. The data show that in this carefully controlled experiment there is a linear correspondence between extensometer strains and gauge strains measured *in-situ*. Correcting the strain readings by using a calibration factor CF = 1.05 from in-isolation testing of the PP geogrid for true global strains of less than 2

percent strain (Figure 3.3) results in a corrected strain gauge reading that varies by ±30 percent of the 2 percent extensometer strain reading at a 95 percent confidence level.
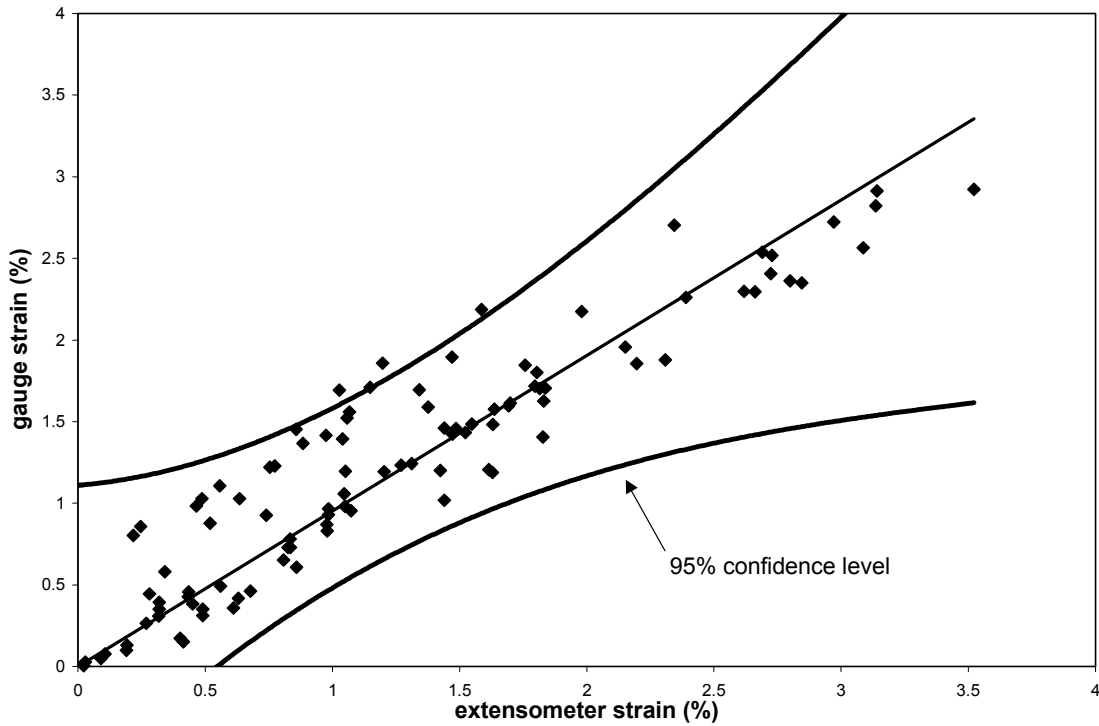
Figure 3.6. Average response of strain gauge pair versus strain calculated from extensometer measurements at the same location on PP geogrid (error curves represent 95 percent confidence level) (Burgess 1999).

Corrected strain gauge readings in the current case studies were compared to extensometer strain measurements (if available). In cases where significant discrepancies occurred in strain values, the calibration factor from in-isolation testing was adjusted and re-applied to all strain gauges in the data set for the case study. Figure 3.7 shows a direct comparison between extensometer and calibrated strain gauge strains. The figure illustrates generally good agreement between the two types of strain measurement, though the strain gauge strains appear to be too high at a few points. These high readings are likely due to out-of-plane movement.
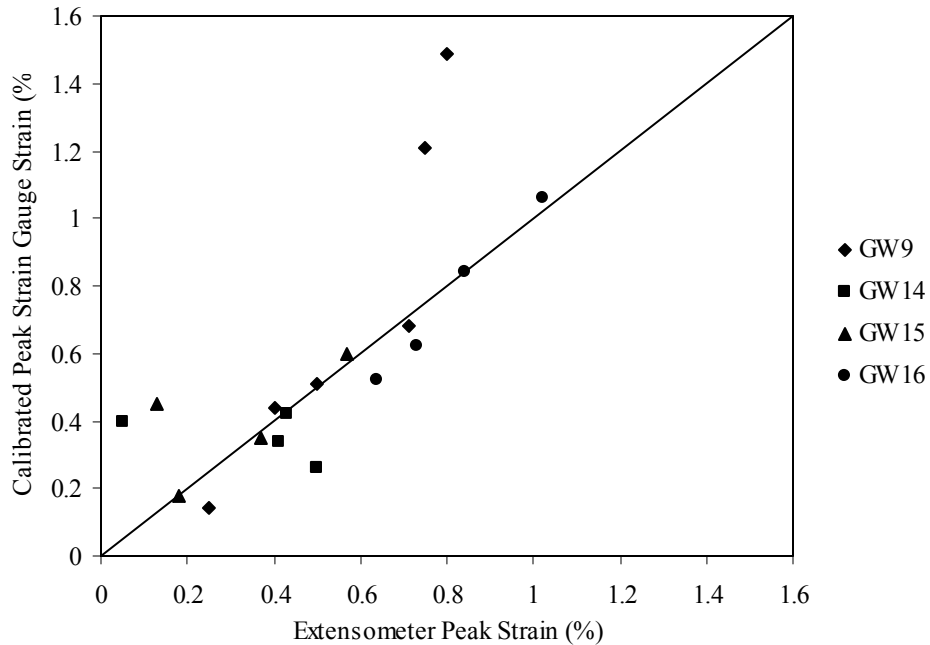
Figure 3.7. Comparison of corrected strain gauge values with extensometer strains.

In case history GW7, inductance coils were used to measure strains rather than strain gauges or extensometers. The data provided by Fannin (1988) suggest that the variability in strain measurements was in the range of 0.1 to 0.25 percent strain, based on multiple coil installations at nominally identical positions on the reinforcement.

3.3.5 Distribution of Strains at the End of Construction

For all walls the peak (maximum) strain readings were determined from inspection of strain readings along the length of the reinforcement layer, with the exception of strains in the immediate vicinity of the facings (i.e., near the connections) or at locations where the facing slumped for wrapped face walls. Hence, the possibility of reinforcement curvature effects on the magnitude of strain gauge readings was minimized.

Examples of strain distributions are shown in figures 3.8 to 3.10. Figure 3.8 is from case study GW16 – the Rainier Avenue wrapped-face geotextile wall. The strain gauge readings in the figure are uncorrected and are generally lower than those reported from interpretation of extensometer readings, which is consistent with the results of the in-isolation testing of woven geotextiles discussed in Section 3.3.1. However, the focus here is on the distribution of strains,

which in this case study were generally coincident with a potential log-spiral internal failure surface through the reinforced soil zone. Note that for the second instrumented layer in case study GW16, the maximum strain locations indicated by extensometers and strain gauges were different. However, the strain gauge readings that caused this difference were identified as questionable, which is explained in detail by Allen et al. (1992). In the summary data to follow, peak strains for this particular wall have been taken from the internal locations roughly coincident with the hatched area in the figure. This wall provides an example of the need for correct interpretation of strain data, based on redundant strain measurement systems, analysis of gauge behavior, and overall development of strain patterns within the wall.

Figure 3.9 shows strain distributions recorded under a uniform 50 kPa surcharge (working stress level) for nominally identical walls constructed with a propped panel face and an incremental panel face (Case studies GW14 and GW15, respectively). The data illustrate the influence of facing type on the distribution of strains in the reinforcement. For the propped panel wall the strains were largest at the connections as a result of downward movement of the soil behind the connections as the wall facing rotates outward. The incremental panel wall was constructed with panels that had some vertical compressibility, and as a result, peak strains no longer occurred at the connections in the top two layers.

Figure 3.10 shows strain distributions from uncorrected strain gauge readings for a modular block-faced wall (Case study GW9) taken immediately after surcharge loading. The data show distinct peaks. One peak is at the facing and the other peaks are within the soil mass. There was no systematic change in the magnitude of strains with the exception of the facing, where connection strains decreased, perhaps as a result of reinforcement stress relaxation with time and possible redistribution of load between reinforcement layers.

In the chapters to follow, a distinction is made between strains generated in the reinforcement layers because of lateral earth pressures and those generated as a result of local facing effects (e.g., down-drag forces as the reinforced fill moves down with respect to the facing). Peak strain readings that occurred immediately at the facing were generally disregarded in favor of peak strain readings within the soil reinforced zone in order to correlate peak strain levels in the reinforcement to reinforced soil properties.
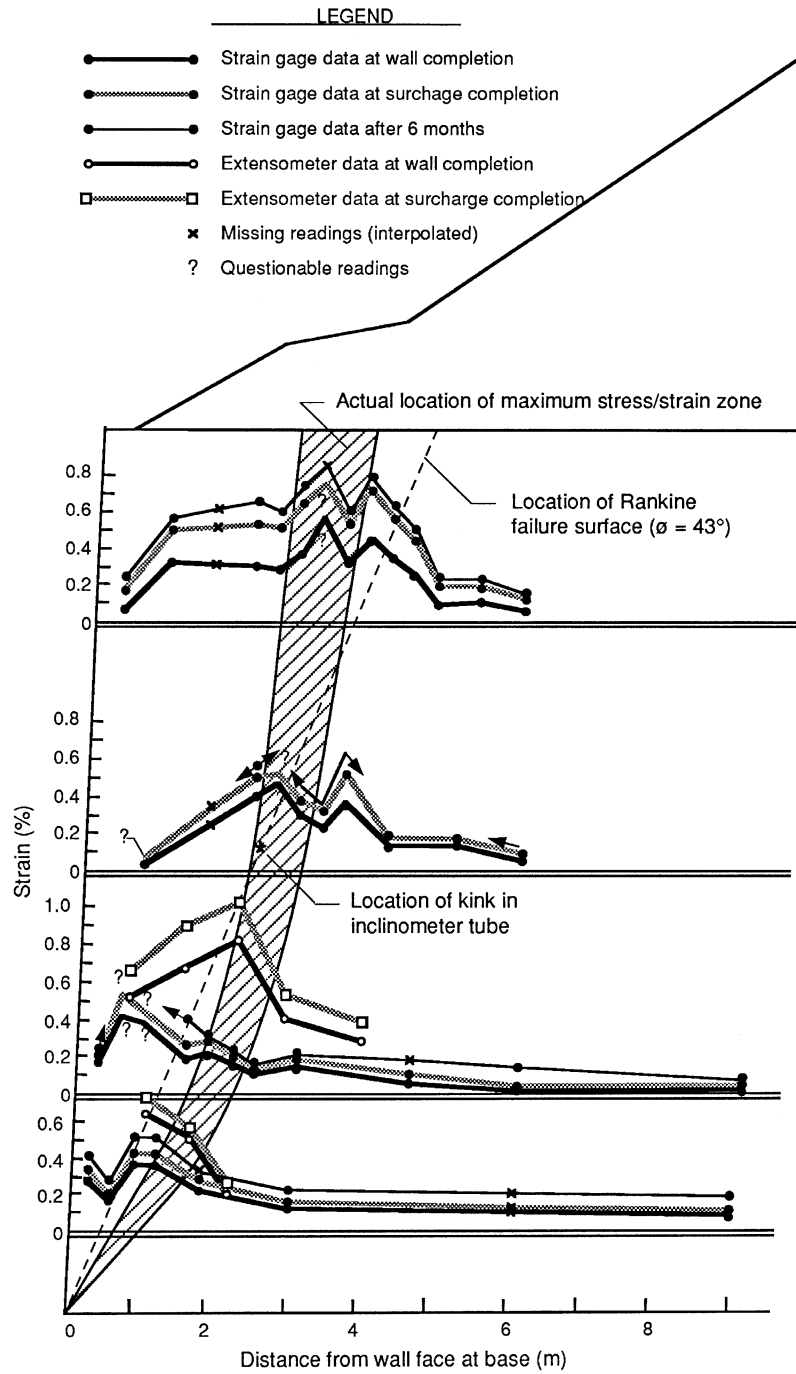
Figure 3.8. Strain distributions (strain gauge readings as plotted are uncorrected) recorded for Rainier Avenue Wall (Allen et al. 1992).

77
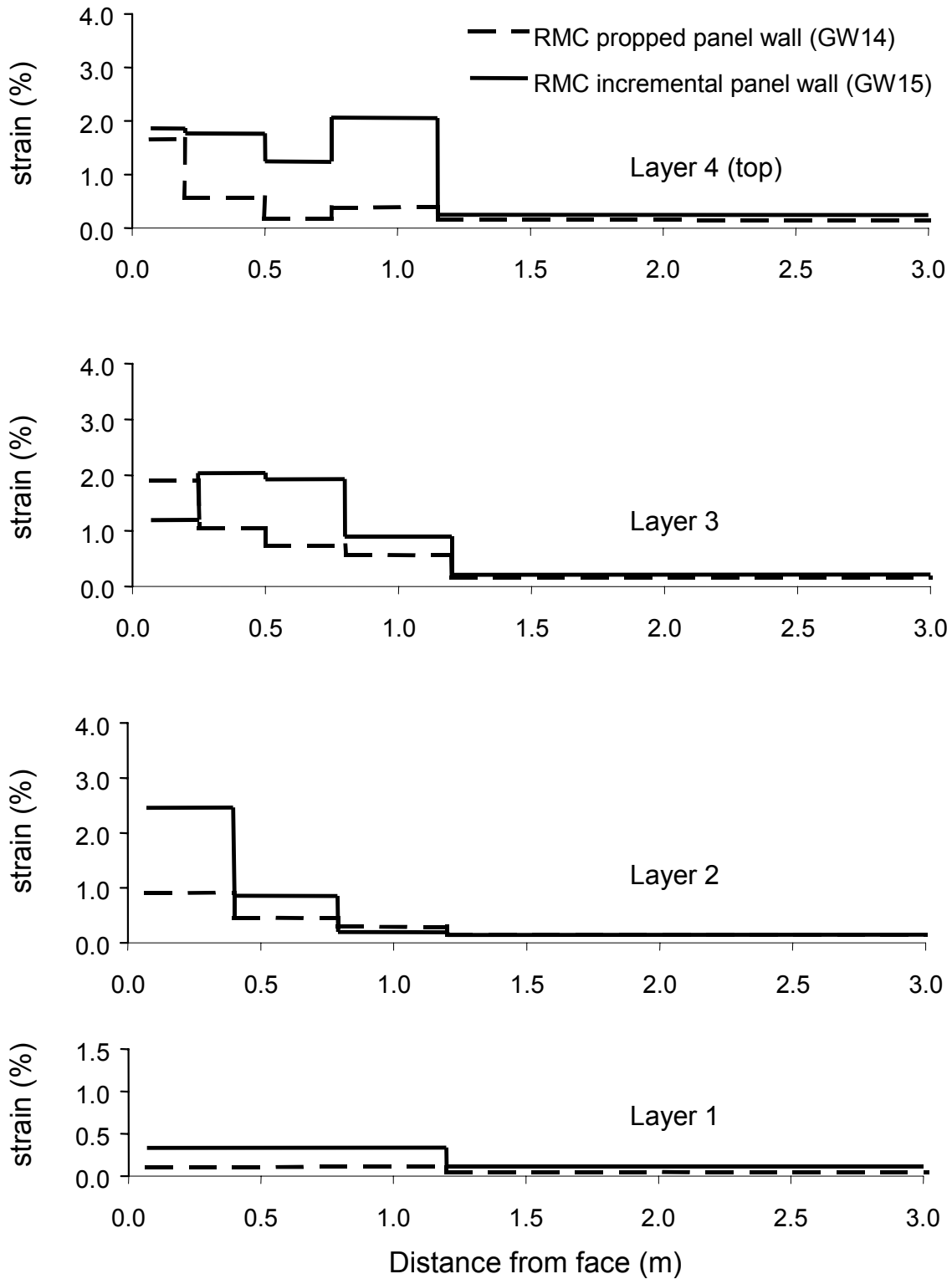
Figure 3.9. Summary of reinforcement strains at 50 kPa surcharge load for the RMCC propped panel and incremental panel walls (after Benjamin 1989).
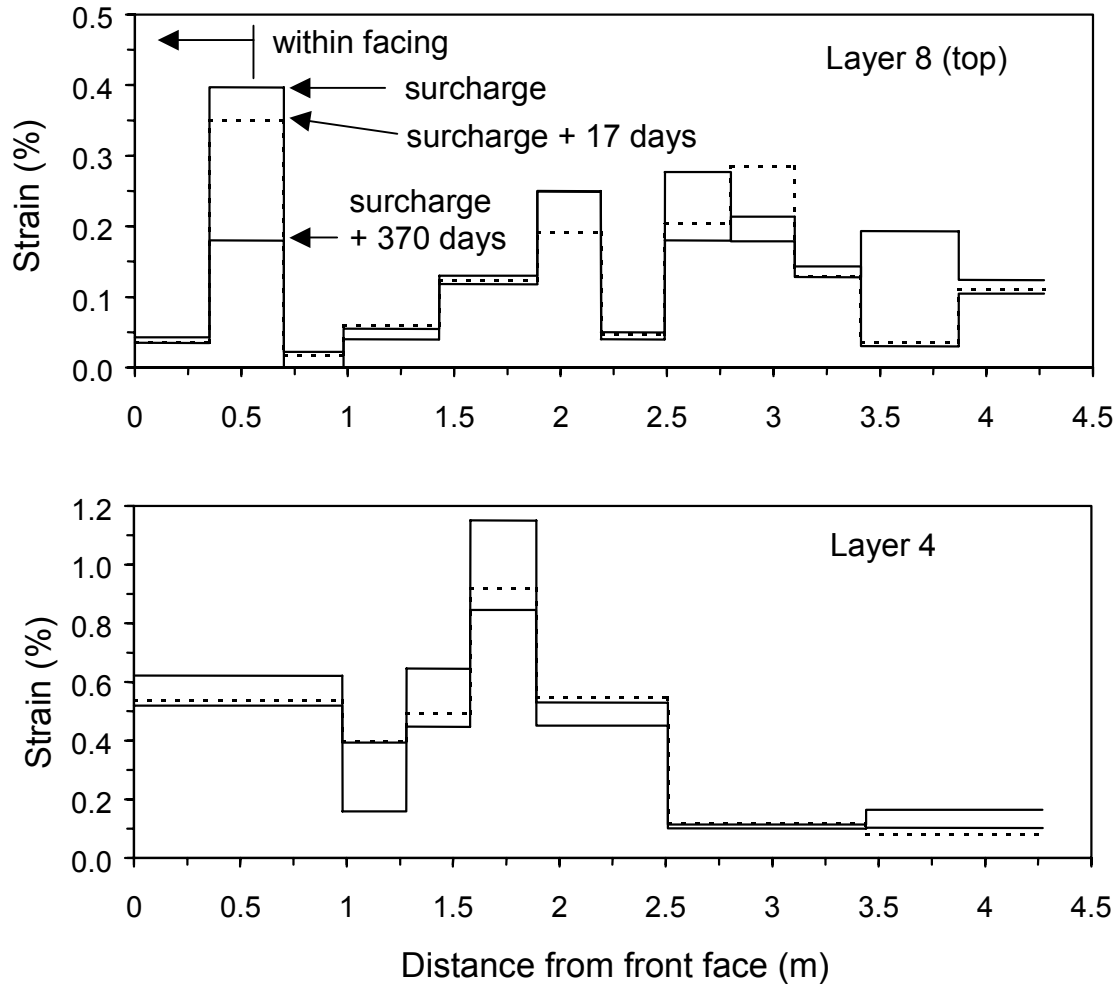
Figure 3.10. Summary of reinforcement strains for modular block-faced wall after end of construction with 2.1-m sloped surcharge (Case study GW9, uncorrected strains) (after Bathurst et al. 1993b).

3.3.6 Summary of Short-Term Peak Strains from Case Studies

Tables 3.4 through 3.18 summarize global strains from extensometers, inductance coils, and corrected local strain measurements (if applicable) for the case studies identified earlier. The readings correspond to end of construction (which in some case studies included a surcharge). The data in the tables show that where comparisons could be made between corrected strain gauge readings and extensometer strains, the difference between the local strain measurements (i.e., from strain gauges) and the global strain measurements was ±0.4 percent strain or less for all but one data point. The majority of the reading pairs are within 0.1 percent strain, which is below the accuracy of most strain gauges mounted on geosynthetic materials.

Table 3.4. Measured peak strains in the geosynthetic reinforcement for the Tanque Verde wall (GW5).

Event	Depth Below Wall Top (m)	Measured Strain from Strain Gauges (%)	Strain Gauge Calibration Factor from Lab Testing	Calibrated Strain from Strain Gauges (%)
End of wall construction	1.14	0.18	1.0	0.18
	3.28	0.33	1.0	0.33
	4.2	0.25	1.0	0.25

Table 3.5. Measured peak strains in the geosynthetic reinforcement for the Oslo Wall, Section J (GW7).

Event	Depth Below Wall Top (m)	Global Strain from Inductance Coils (%)
End of wall construction	1.2	0.37
	2.4	0.42
	3.6	0.26
	4.2	0.28
	4.8	0.08
Completion of Surcharge	1.2	0.52
	2.4	0.70
	3.6	0.28
	4.2	0.79
	4.8	0.10

Table 3.6. Measured peak strains in the geosynthetic reinforcement for the Oslo Wall, Section N (GW7).

Event	Depth Below Wall Top (m)	Global Strain from Inductance Coils (%)
End of wall construction	0.6	0.66
	1.2	0.56
	1.8	0.37
	2.4	0.52
	3.0	0.63
	3.6	0.43
	4.2	0.43
	4.8	0.30
Completion of Surcharge	0.6	0.92
	1.2	0.82
	1.8	0.78
	2.4	0.79
	3.0	0.80
	3.6	0.79
	4.2	0.70
	4.8	0.31

Table 3.7. Measured peak strains in the geosynthetic reinforcement for the Algonquin HDPE geogrid wall (GW8).

Event	Depth Below Wall Top (m)	Measured Strain from Strain Gauges (%)	Strain Gauge Calibration Factor from Lab Testing	Calibrated Strain from Strain Gauges (%)
End of wall construction	1.2	0.35	1.0	0.35
	2.5	0.71	1.0	0.71
	4.2	0.76	1.0	0.76
	5.0	0.74	1.0	0.74
	5.7	0.18	1.0	0.18

Table 3.8. Measured peak strains in the geosynthetic reinforcement for the Algonquin PET geogrid wall (GW9).

Event	Depth Below Wall Top (m)	Measured Strain from Strain Gauges (%)	Strain Gauge Calibration Factor from Lab Testing	Calibrated Strain from Strain Gauges (%)	Global Strain from Extensometers (%)
End of wall construction	0.8	0.08	1.75	0.14	0.25
	2.6	0.29	1.75	0.51	
	4.0	0.29	1.75	0.51	0.50
	5.2	0.39	1.75	0.68	0.71
	5.8	0.11	1.75	0.19	
Completion of Surcharge	0.8	0.25	1.75	0.44	0.40
	2.6	0.0.65	1.75	1.14	
	4.0	0.85	1.75	1.49	0.80
	5.2	0.69	1.75	1.21	0.75
	5.8	0.19	1.75	0.33	

Table 3.9. Measured peak strains in the geosynthetic reinforcement for the Algonquin geotextile wall (GW10).

Event	Depth Below Wall Top (m)	Measured Strain from Strain Gauges (%)	Strain Gauge Calibration Factor from Lab Testing	Calibrated Strain from Strain Gauges (%)
End of wall construction, before water at wall face released	1.0	1.4	1.5	2.1
	2.6	1.2	1.5	1.8
	4.2	1.25	1.5	1.9
	4.9	0.95	1.5	1.4
	5.65	0.75	1.5	1.1
End of wall construction, after water at wall face released	1.0	2.0+	1.5	3.0+
	2.6	2.0+	1.5	3.0+
	4.2	1.35	1.5	2.0
	4.9	1.05	1.5	1.6
	5.65	0.75	1.5	1.1

Table 3.10. Measured peak strains in the geosynthetic reinforcement for the RMCC geogrid, wrapped–face, full-scale test wall (GW11).

Event	Depth Below Wall Top (m)	Measured Strain from Strain Gauges (%)	Strain Gauge Calibration Factor from Lab Testing	Calibrated Strain from Strain Gauges (%)
End of wall construction	0.6	1.48	1.33	1.97
	1.35	2.00	1.33	2.66
	2.1	0.94	1.33	1.25
	2.85	0.15	1.33	0.20

Table 3.11. Measured peak strains in the geosynthetic reinforcement for the RMCC full height, plywood panel, full-scale test wall (GW12).

Event	Depth Below Wall Top (m)	Measured Strain from Strain Gauges (%)	Strain Gauge Calibration Factor from Lab Testing	Calibrated Strain from Strain Gauges (%)
End of wall construction (no surcharge)	0.5	0.038	1.05	0.040
	1.25	0.019	1.05	0.020
	2	0.018	1.05	0.02
	2.75	0.008	1.05	0.01
With 50 kPa surcharge	0.5	0.66	1.05	0.50
	1.25	0.47	1.05	0.49
	2	0.31	1.05	0.33
	2.75	0.21	1.05	0.22

Table 3.12. Measured peak strains in the geosynthetic reinforcement for the RMCC incremental plywood panel, full-scale test wall (GW13).

Event	Depth Below Wall Top (m)	Measured Strain from Strain Gauges (%)	Strain Gauge Calibration Factor from Lab Testing	Calibrated Strain from Strain Gauges (%)
End of wall construction (no surcharge)	0.5	0.034	1.05	0.036
	1.25	0.26	1.05	0.27
	2	0.30	1.05	0.32
	2.75	0.32	1.05	0.34
With 50 kPa surcharge	0.5	0.76	1.05	0.8
	1.25	0.76	1.05	0.79
	2	0.57	1.05	0.6
	2.75	0.48	1.05	0.53

Table 3.13. Measured peak strains in the geosynthetic reinforcement for the RMCC full height, propped aluminum panel, full-scale test wall (GW14).

Event	Depth Below Wall Top (m)	Measured Strain from Strain Gauges Located at Extensometer Peak Strain (%)	Strain Gauge Calibration Factor from Lab Testing	Calibrated Strain from Strain Gauges Located at Extensometer Peak Strain (%)	Global Strain from Extensometers (%)
End of wall construction (no surcharge)	0.5	0.38	1.05	0.40	0.05
	1.25	0.32	1.05	0.34	0.41
	2	0.25	1.05	0.26	0.50
	2.75	0.40	1.05	0.42	0.43
With effective 70 kPa surcharge	0.5				2.93
	1.25				3.47
	2				2.00
	2.75				1.45

Table 3.14. Measured peak strains in the geosynthetic reinforcement for the RMCC incremental, aluminum panel, full-scale test wall (GW15).

Event	Depth Below Wall Top (m)	Measured Strain from Strain Gauges Located at Extensometer Peak Strain (%)	Strain Gauge Calibration Factor from Lab Testing	Calibrated Strain from Strain Gauges Located at Extensometer Peak Strain (%)	Global Strain from Extensometers (%)
End of wall construction (no surcharge)	0.5	0.17	1.05	0.18	0.18
	1.25	0.57	1.05	0.60	0.57
	2	0.33	1.05	0.35	0.37
	2.75	0.42	1.05	0.45	0.13
With effective 60 kPa surcharge	0.5				4.0
	1.25				4.15
	2				1.20
	2.75				0.42

Table 3.15. Measured peak strains in the geosynthetic reinforcement for the Rainier Avenue wall (GW16).

Event	Depth Below Wall Top (m)	Measured Strain from Strain Gauges (%)	Strain Gauge Calibration Factor from Lab Testing	Calibrated Strain from Strain Gauges (%)	Global Strain from Extensometers (%)
End of wall construction	3.1	0.57	2	1.14	
	6.5	0.46	2	0.92	
	9.6	0.42	2	0.84	0.84
	11.5	0.37	1.4	0.52	0.64
Completion of Surcharge	3.1	0.75	2	1.50	
	6.5	0.53	2	1.06	
	9.6	0.53	2	1.06	1.02
	11.5	0.44	1.4	0.62	0.73

Table 3.16. Measured peak strains in the geosynthetic reinforcement for the London, Ontario, propped panel, HDPE geogrid wall (GW17).

Event	Depth Below Wall Top (m)	[+]Measured Strain from Strain Gauges (%)	Strain Gauge Calibration Factor from Lab Testing	Calibrated Strain from Strain Gauges (%)	*Global Strain from Inclinometers (%)
End of wall construction	2.4	2.42	1.25	3.02	0.7
	4.23	1.58	1.25	1.97	0.5
	5.4	1.30	1.25	1.62	0.35
	6.33	0.70	1.25	0.87	0.3

*Obtained from differential movement between two inclinometers, one at face and one 1.5 m behind face. Because the strain in the wall was restricted by the prop restraint during wall construction, all movement recorded by the inclinometers should reflect movement that occurred in the reinforcement. Note that this is an average strain, yet it is known from the nature of propped panel walls that the highest strains will occur at the face, dropping rapidly with distance from the face. The available strain gauge data, though erratic, appear to indicate this type of strain pattern. It is estimated that the peak strains within this 1.5-m zone could be on the order of 50 to 70 percent higher than the average strain.

+Obtained at a point in time when the equilibrium condition was judged to occur after prop release. Because the soil behind the wall was frozen during the initial months of wall life after prop release, equilibrium was not reached until the following summer after construction. Note that the gauges were highly erratic, and some judgment was required to establish peak strains from the strain gauges.

Table 3.17. Measured peak strains in the geosynthetic reinforcement for the Fredericton, New Brunswick, full height, propped panel, HDPE geogrid wall (GW18).

Event	Depth Below Wall Top (m)	Measured Strain from Strain Gauges (%)	Strain Gauge Calibration Factor from Lab Testing	Calibrated Strain from Strain Gauges (%)
End of wall construction	2.44	0.33	1.3	0.43
	4.88	0.38	1.3	0.50

Table 3.18. Measured peak strains in the geosynthetic reinforcement for the Vicenza, Italy, welded wire faced geosynthetic wall (GW20).

Wall Section	Event	Depth Below Wall Top (m)	Measured Strain from Strain Gauges (%)	Strain Gauge Calibration Factor from Lab Testing	Calibrated Strain from Strain Gauges (%)
1 (HDPE geogrid)	With soil surcharge	1.1	0.87	1.05	0.91
		2.7	1.42	1.05	1.49
2 (PP geogrid)	With soil surcharge	1.6	2.85	1.1	3.13
		3.2	1.84	1.1	2.02

3.4 Comparison of Wall Deformations with Strain Measurements

A strategy to check the interpretation of reinforcement strains is to integrate reinforcement strains over the length of the reinforcement and to compare the result with wall deformations recorded at each reinforcement elevation during construction. Allen et al. (1992) attempted to make such a comparison for the Rainier Avenue Geotextile Wall (Wall GW16). An updated comparison is presented in Figure 3.11 with calibrated strain gauge data that were not available in 1992. Integration was accomplished by using the average values of the measured strain over the length segments, and the product of the average strain and the segment length summed to estimate the total extension of the reinforcement layer. This approach assumes that there is no deformation at the free end of the reinforcement layer. The cumulative deformation from integration of the strains is compared to the lateral deflection measured at the wall face at the same elevation as the reinforcement layer and with respect to the time the reinforcement layer was installed. Hence, the curves in the figure are not wall deformation profiles but rather curves representing deflections measured (or estimated) from the time of installation of the reinforcement layer.

Figure 3.11 shows that there are significant differences between predicted wall deflections based on integrated strain measurements and surveyed deflections. Some of the discrepancy may be attributed to the accuracy of the wall face survey deflection measurements, which are typically on the order of $\pm$ 10 mm. It should also be recognized that overall face deflection is affected by mass lateral movements of the soil behind and below the wall that can occur during construction. Consequently, strain gauges and extensometers may have under-estimated the

horizontal facing deflections in comparison to measurements obtained by optical survey methods.

Similar data for the RMCC geogrid, wrapped-face wall (GW11) are presented in Figure 3.12. A large vertical spacing (0.75 m) was used between reinforcement layers in this wall that resulted in vertical sagging of the wrappedface when each layer facing form was removed (Bathurst et al. 1988). This resulted in observations of additional deflection at the wall face that were not reflected by the reinforcement strain measurements.

Figure 3.13 shows a comparison of measured lateral wall facing deflections versus estimated deflections from integrated strains for case study GW8, which was constructed with concrete panels (incremental panel construction). In this case, the facing deflections are approximately the same as the deformations estimated from integrated strain gauge measurements.

Taken together the results of this comparison suggest that integration of reinforcement strains can be expected to underestimate peak wall deflections during construction, especially for flexible-faced wall systems.
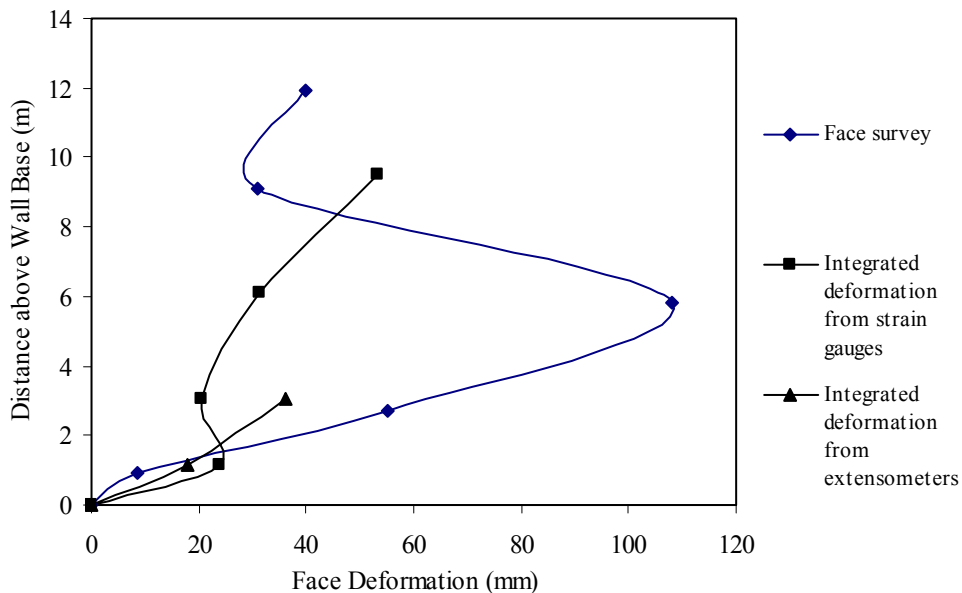
Figure 3.11. Comparison of measured wall facing deflections with estimated values from integration of reinforcement strains (Case study GW16 – wrapped face).

86
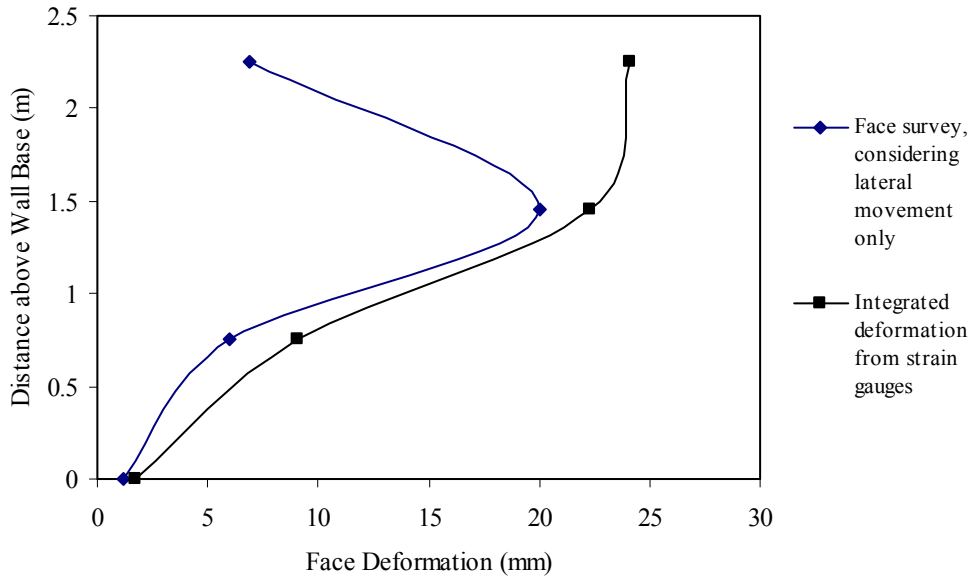
Figure 3.12. Comparison of measured wall facing deflections with estimated values from integration of reinforcement strains (Case study GW11 – wrapped face).
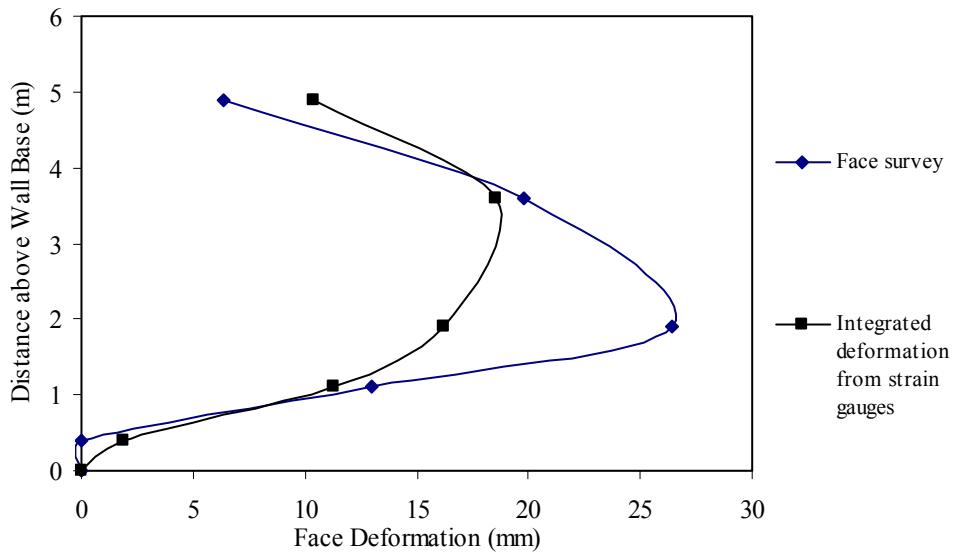
Figure 3.13. Comparison of measured wall facing deflections with estimated values from integration of reinforcement strains (Case study GW8 – incremental concrete panel face).

Finally, it is useful to normalize the surveyed lateral facing deflection curves for the three walls investigated in this section to provide empirical guidance on the magnitude of end-of-

construction deflection that may be anticipated in the field. They were normalized in the following manner:

- The location of each lateral deformation measurement was normalized by the wall height (a geometrical normalization).
- The lateral deformation was normalized by the wall height plus average surcharge height to approximate the difference in total loading applied in each wall case.

This is done in Figure 3.14, and the data show that peak lateral movements recorded between the time a reinforcement layer was installed and the end of construction ranged from 0.4 to 0.8 percent of the height of the structures. As may be expected, the wall with a hard facing (GW8) and a stiffer reinforcement deformed less than the two wrapped-face walls. In all cases the largest relative deformations occurred at heights above the base of the wall corresponding to 30 to 50 percent of the height of the facing.
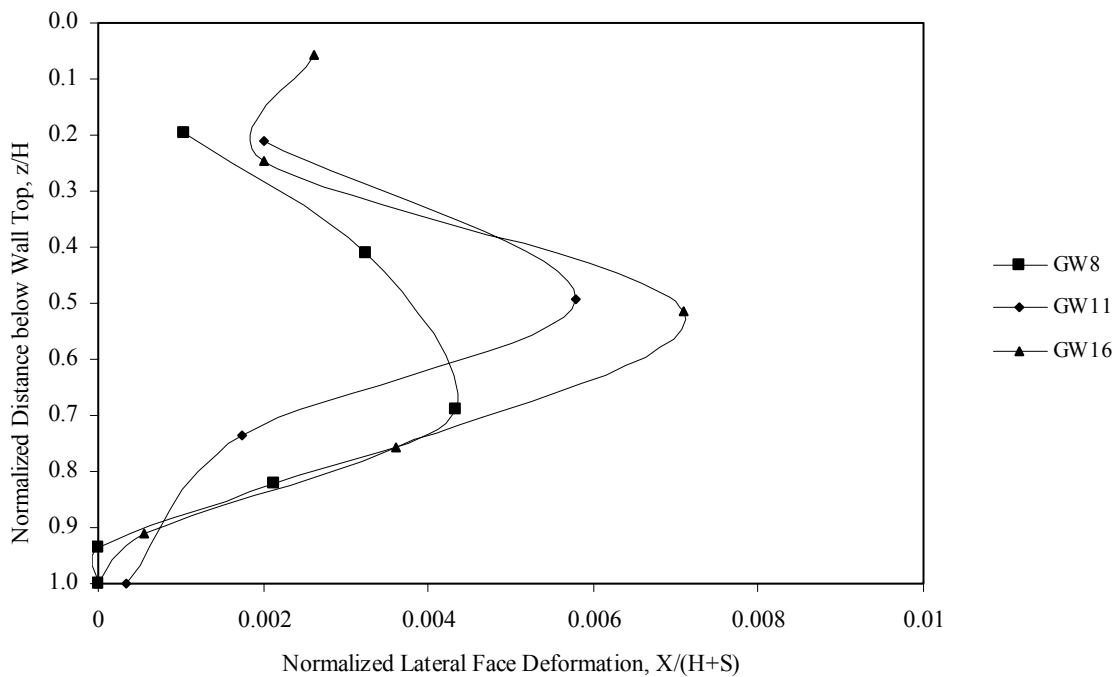
Figure 3.14. Normalized lateral facing deflections from wall facing survey measurements taken with respect to initial reading (Case study GW8 – incremental concrete panel face; Case study GW11 and GW16 – wrapped face).

3.5 Summary and Conclusions

This chapter focuses on the interpretation of strain readings from instruments used in well-documented case studies of geosynthetic reinforced soil walls. The major conclusions from this review regarding the determination of reinforcement strains are as follows:

- Strain gauge readings in the field must be corrected to true global strains by using in-isolation tensile tests of instrumented reinforcement products. Under-registration of global strains was shown to vary from a factor of 1 to as high as 2.2 at strain levels of 2 percent or less.

- In general, under-registration of global strains by strain gauges increases with global strain level.

- Local strain readings at nominally identical locations on a reinforcement layer can be expected to vary because of variation in load transfer across reinforcement layers, reinforcement type and possible local bending of the reinforcement.

- A strategy to improve confidence in interpretation of strain readings is to use both strain gauges and extensometers in the field, and to adjust strain gauge calibration factors (if required) on the basis of in-situ measurements from both types of devices.

- In general, strain gauges have proved useful for estimating reinforcement strains at low strain levels ($\leq$ 2 to 3 percent). Extensometers and inductance coils provide marginal accuracy for very low strains (< 0.5 to 1.0 percent). The limit of their accuracy is on the order of 0.1 percent to 0.25 percent strain, as defined by the experience of the writers and the data provided herein. At higher strain levels global strains must be calculated from displacements recorded from tandem extensometer points.

- In general, wall face deformations tend to be under-estimated when reinforcement strain readings are integrated, as integrated strain gauge readings do not account for global movements of the soil mass.

The methodologies described above have been applied to a number of case studies to summarize the best estimates of peak strains in reinforcement layers at the end of construction. The data are used in later chapters to estimate reinforcement loads and to compare reinforcement loads to values predicted with current and proposed methods for designing the internal stability of geosynthetic reinforced soil walls.

4.0 CONVERSION OF GEOSYNTHETIC WALL STRAINS TO LOAD BY USING IN-SOIL REINFORCEMENT MODULUS

4.1 Introduction

A knowledge of both soil reinforcement strains and loads is required to fully understand the internal stability behavior of mechanically stabilized earth (MSE) walls so that design procedures can be improved. Measurements indicative of the internal behavior of full-scale walls typically consist of reinforcement strains and overall deformations, since it is difficult to directly measure reinforcement loads. Chapter 3.0 summarizes the strain measurements obtained in several geosynthetic wall case histories to provide a baseline for analysis.

For steel reinforced MSE walls, the conversion of reinforcement strain to load is relatively straightforward, since the modulus of the steel reinforcement is affected by neither soil confinement nor time. For geosynthetic reinforcement on the other hand, the reinforcement modulus, which must be known to convert measured strains to reinforcement loads, may be affected by both soil confinement and time under load. Given that the time dependent properties and response to load for the soil are much different than those of the geosynthetic reinforcement, the determination of the correct modulus of the geosynthetic has the potential to be complex, and the factors that affect the confined modulus and the rate at which the geosynthetic modulus changes over time must be carefully understood.

The focus of this chapter is the development of a methodology that can be used to convert measured strains reported for full-scale, geosynthetic reinforced structures to load. To accomplish this, the intrinsic visco-elastic-plastic behavior of the geosynthetic, which is dependent on the polymer type and macro-structure of the geosynthetic, must be characterized. In-isolation and in-soil test data are summarized for a variety of products to demonstrate this behavior. Furthermore, the interaction between the soil and the geosynthetic in full-scale structures, and the effect that this interaction has on the boundary conditions applied to the reinforcement in soil, must be understood, characterized, and related to the visco-elastic-plastic behavior of the geosynthetic reinforcement. The scope of this paper is limited to geogrids and woven geotextiles in granular backfill soils.

There are a few case histories where the load in the reinforcement was measured directly. These cases will be used to verify the methodology developed for converting geosynthetic reinforcement strain to load.

4.2 The Development of Reinforcement Load and Strain in Geosynthetic Walls—Concepts

To assess the development of load and strain in geosynthetic MSE wall reinforcement, given time and rate effects, the creep and load-strain behavior of both the geosynthetic and the soil must be considered. Geosynthetics are visco-elastic-plastic materials, which means that the geosynthetic polymer will undergo time dependent rearrangement of molecules within the polymer when placed under load, regardless of the loading mechanism and load level. Granular soils also exhibit viscous creep effects under conditions of constant stress or load (Kuhn and Mitchell 1993). If the soil is for practical purposes perfectly bonded to the geosynthetic (i.e., no relative slippage), the soil and the geosynthetic must move together. This means that if the geosynthetic strains under constant load due to creep, the soil must also strain. If the soil has not reached its peak shear capacity, which is typically the case at working stress conditions, the soil must take on more load or must creep under constant load to strain with the geosynthetic. The time dependent equilibrium between these two very different materials will likely cause the geosynthetic reinforcement to exhibit behavior between that of pure creep and pure stress relaxation, if the soil creep rate is less than the geosynthetic creep rate. Kuhn and Mitchell (1993) showed that the creep of sands, even at typical working stresses, can be significant. Therefore, whether or not stress relaxation or creep occurs will depend on the stress-strain-time properties of the geosynthetic and soil backfill.

The concepts provided above only apply at working stress conditions, where the soil has not strained beyond its peak shear capacity. Beyond peak strength, the soil can no longer take on additional load with larger geosynthetic strains. At post-failure the soil creep rate can exceed the geosynthetic creep rate. Under these conditions the geosynthetic reinforcement will continue to creep rather than undergo stress relaxation. Since the soil strength and stiffness drop off significantly after reaching peak strength, the geosynthetic may also take on additional load to maintain equilibrium, further accelerating the creep process. However, once the soil has reached this state behind a reinforced soil wall, the wall has for all practical purposes failed, and it would not be prudent or necessary to attempt to design the wall reinforcement to have a long design life

in this condition. Rather, one should design the wall reinforcement to prevent the soil from reaching a failure state in the first place.

Since the relationship between load and strain is a function of time for geosynthetics, the geosynthetic modulus will be affected by the magnitude, sequence, and rate at which load is applied to a wall. To determine the appropriate modulus with which to convert strain to load in the geosynthetic reinforcement, the reinforcement loading history must be known. In most geosynthetic walls, the peak strain has been on the order of 2 percent or less at the end of construction (see Chapter 3.0). In a typical index tensile strength test carried out at a strain rate of 10 percent/minute (ASTM D4595), the test specimen takes 12 seconds to reach a strain of 2 percent. Figure 4.1 gives example construction histories reported in the literature for geosynthetic reinforced soil walls. The construction times ranged from 8 to 70 days (200 to 1700 hours). Assuming that a maximum reinforcement strain of 2 percent was achieved at the end of construction, then the rate of loading of the reinforcement is four to five orders of magnitude less than the conventional (ASTM D4595) tensile test. Furthermore, the loading sequence in geosynthetic walls is not continuous but, rather, a series of step-wise load increases. In many cases, the steps are small enough that, for practical purposes, the loading rate is continuous. In some of the full-scale instrumented walls referenced in Chapter 2.0, post-construction surcharge load steps were large in relation to the time it took to build the wall. In such cases, the selection of an appropriate geosynthetic modulus with which to convert measured strains to loads may be influenced by the magnitude and duration of each surcharge increment.

4.3 Laboratory Simulation of Geosynthetic Reinforcement Loading in Walls—Concepts

Laboratory testing must be conducted to assess the properties of geosynthetic reinforcement needed for design and analysis, and to convert measured reinforcement strains to loads in full-scale walls. Laboratory tests in general do not perfectly simulate the loading and response of geosynthetic reinforcement in the field. The suitability of the laboratory test results for analyzing the structure and for converting strain to load depends on how accurately the laboratory test simulates the loading of the geosynthetic in the structure and the boundary conditions on the geosynthetic.
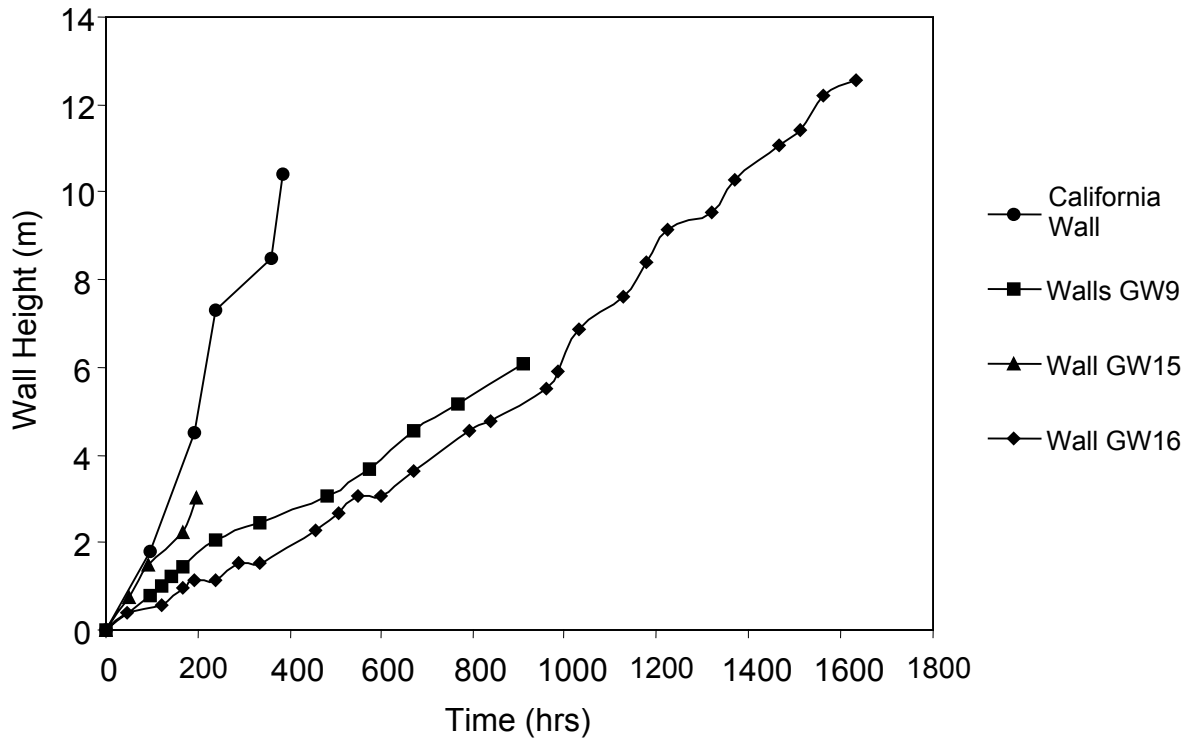
Figure 4.1. Wall construction rates observed for some geosynthetic reinforced soil walls (from Bathurst et al. 1995, Bathurst et al. 1993b, Benjamin 1989, and Allen et al. 1992).

Laboratory in-isolation tests include standard wide-width tensile tests in which a constant rate of strain (CRS) is applied to the specimen, creep tests in which a constant load is applied to the specimen (ASTM D5262), and stress relaxation tests in which a constant strain level is applied to the specimen (ASTM E328-86). For creep and stress relaxation tests, a series of specimens is tested at different load levels or different initial strain levels to produce a family of curves. For CRS wide-width tensile tests, a series of specimens is loaded at different strain rates to produce a family of curves.

In-soil characterization of geosynthetic reinforcement load-strain-time behavior has been accomplished in the laboratory with one of two broad classes of devices:

1. devices that apply the load directly to the geosynthetic
2. devices that apply the load to the geosynthetic through the surrounding soil.

Examples of these devices and their relationship to in-situ soil-geosynthetic reinforcement interaction are illustrated conceptually in Figure 4.2. Detailed descriptions and evaluations of devices that have been used to quantify the in-soil behavior of geosynthetic reinforcement were

provided by Elias et al. (1998b). In-soil laboratory testing devices can be used to apply tensile loads through the soil or directly to the geosynthetic using constant strain rate, constant loading rate, or constant load boundary conditions.

In a reinforced soil structure, the soil applies load to the geosynthetic reinforcement, as illustrated in Figure 4.2. Therefore, a laboratory test apparatus with plane strain boundary conditions that allows loads to be applied to the geosynthetic through the soil is desirable for modeling the working stress load-strain-time response of the geosynthetic *in-situ*. If a soil with less creep potential than the geosynthetic is used (e.g., a sand, depending on the amount of stress carried by the soil), the soil will restrict time dependent movement of the geosynthetic. Then stress relaxation will occur in the geosynthetic, either between load increments (analogous to wall construction) or under constant load (analogous to end of wall construction).

For a device in which a tensile load is applied to the geosynthetic directly, the surrounding soil may reduce the creep rate in the geosynthetic, but stress relaxation cannot occur. The geosynthetic is gripped and pulled from both ends (or one end could be fixed) in the test. This type of test may be a reasonable simulation of a geosynthetic reinforcement layer intersected by a soil shear surface in a wall that has reached a failure state. The grips in the laboratory device are analogous to the two sides of the soil shear zone and provide a constant tensile load to the reinforcement. In this loading scenario, pure creep is likely.

While an in-soil test in which the load is applied to the geosynthetic through the soil best simulates the loading and boundary conditions in full-scale structures, this does not mean that the other types of laboratory tests cannot be used to obtain geosynthetic properties, including the geosynthetic modulus. The key is to understand the limitations of the laboratory testing method, how those limitations affect the properties measured, and how to apply those properties to actual field conditions. The following section examines the results from various laboratory tests and how the test results can be interpreted to determine the time dependent modulus of the reinforcement.
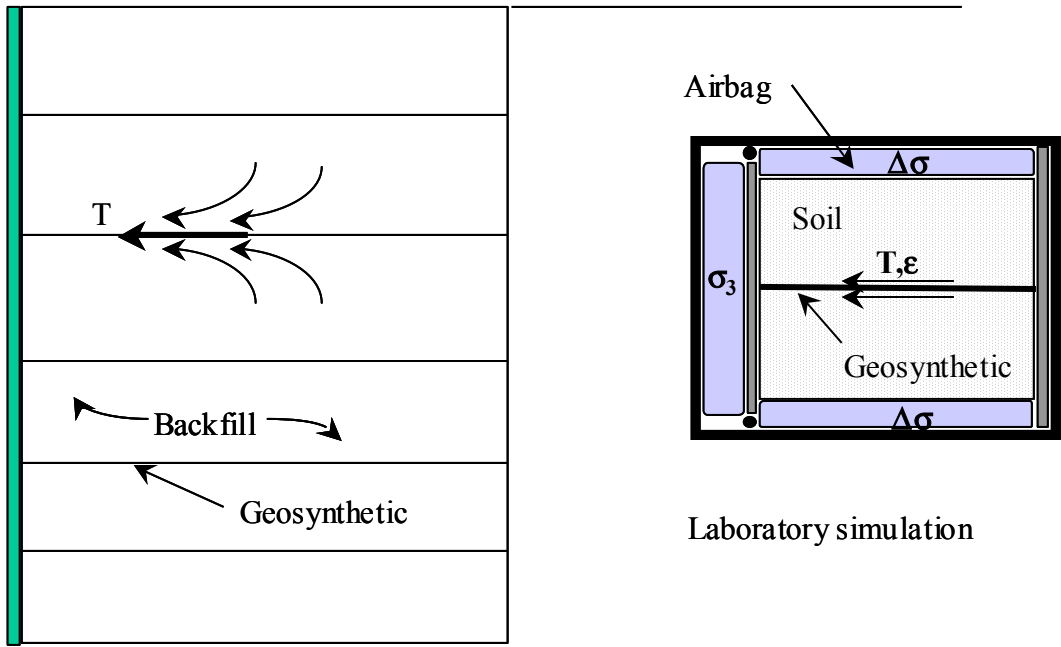
a. At working stresses
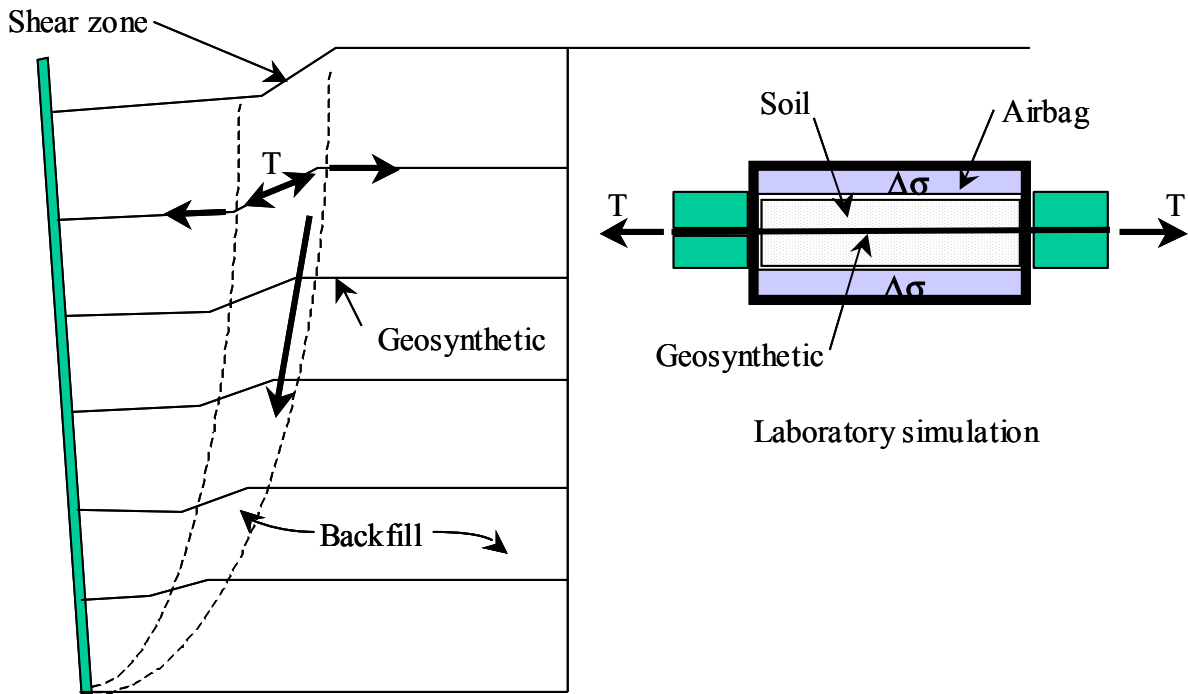
b. At failure

Figure 4.2. Conceptual relationship between the behavior of geosynthetic reinforcement in full-scale structures and confined in-soil laboratory tensile/creep tests.

4.4 Geosynthetic Modulus from Laboratory Tests

The modulus of a geosynthetic is essentially the slope of a load-strain curve from a tensile test, or the slope of an isochronous curve from either a creep test or stress relaxation test. A secant slope is used to define the modulus for the data presented herein. The modulus obtained from a family of creep curves is typically called the creep modulus or creep stiffness. If the modulus value is obtained from a family of stress relaxation curves it is called a relaxation modulus. The creep modulus, J_c, is expressed as follows:

$$J_c = \frac{T_i}{\varepsilon_i} \qquad\qquad\qquad (Eq.\,4.1)$$

where T_i is the load and ε_i is the strain at any time. The same equation can be used for the relaxation modulus, although the creep modulus is not necessarily equal to the relaxation modulus. Figure 4.3 illustrates how the modulus of a geosynthetic reinforcement product can be determined from constant rate of strain tensile tests, constant load (creep) tests, and stress relaxation tests.

The following variables must be considered to determine the appropriate modulus of the geosynthetic reinforcement (Bush 1990, Rimoldi and Montanelli 1993, Allen and Bathurst, 1994, Boyle et al. 1996, Yuan et al. 1998):

1. loading sequence
2. rate of loading or time after application of the load
3. installation damage
4. soil confinement.

The loading sequence is a function of the type of test conducted. The effect of each of these variables on the modulus value is a function of the constituent polymer and macro-structure of the geosynthetic product. Note that temperature will also affect the modulus value, with increasing temperature resulting in lower moduli, especially for polyolefin materials (e.g., Bush 1990). The effect of temperature is not specifically addressed herein. In practice, the modulus used to estimate load from strain measurements must be determined at the temperature in the wall. The data in this report were obtained at a temperature of 20° C unless otherwise noted.
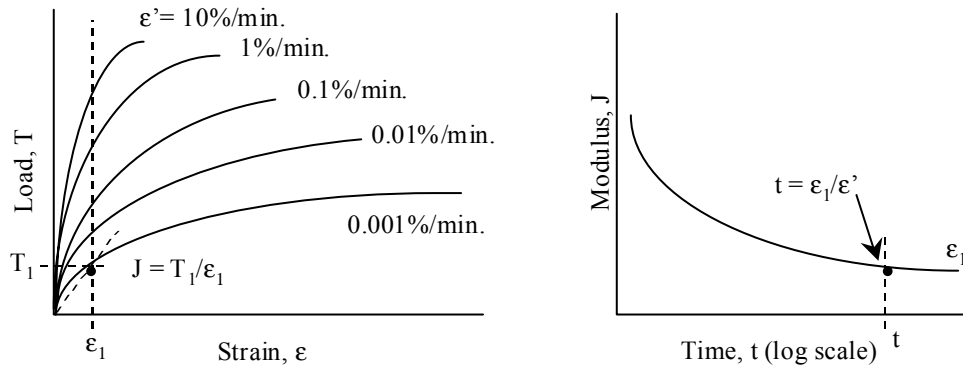
a. Constant rate of strain tensile test
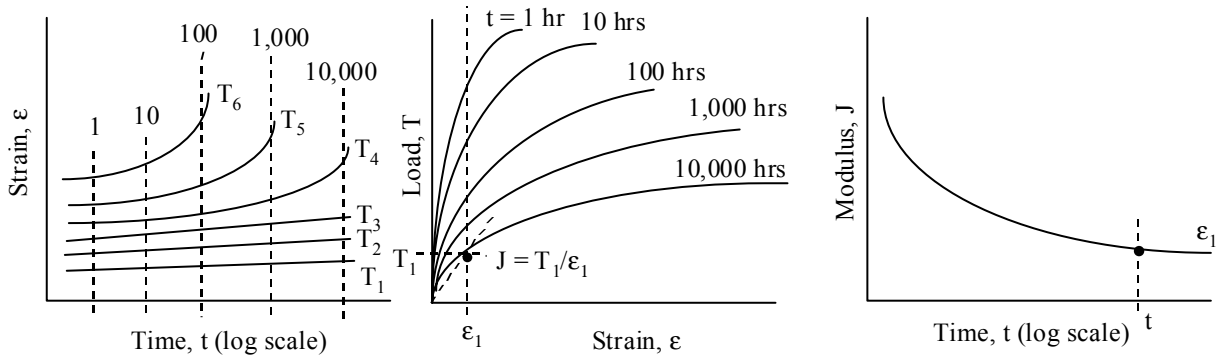
b. Constant load (creep) test
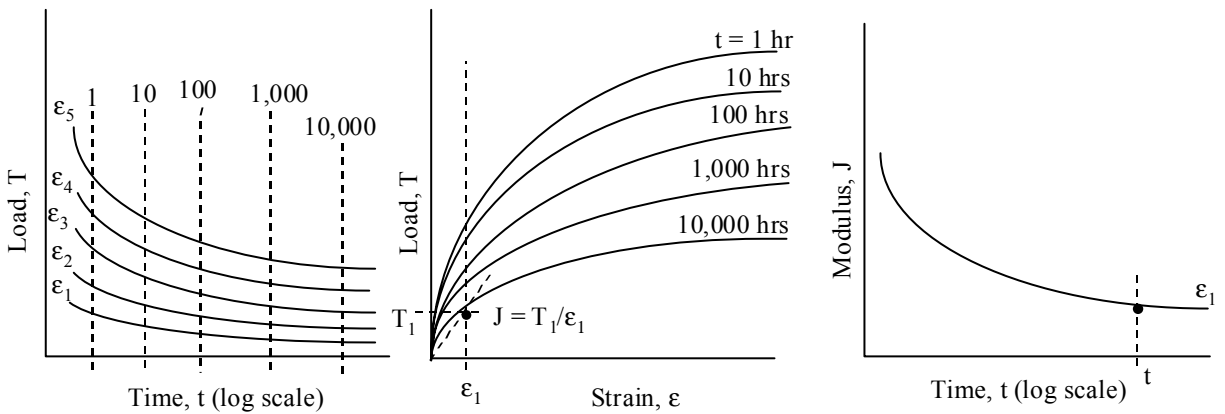
c. Constant strain (stress relaxation) test

Figure 4.3. Determination of modulus (stiffness) from various types of laboratory tests.

97

Data from previous studies in which comparisons between creep, stress relaxation, and/or constant rate of strain (CRS) could be made for the same geosynthetic product were evaluated to assess what effect the test type had on the short- and long-term modulus of geosynthetics. The geosynthetic materials analyzed and compared in the sections that follow are summarized in Table 4.1. Note that geosynthetics EGG-3 and EGG-4 were taken from the same roll of material but were tested by two independent sets of researchers in different locations with different equipment (Burgess 1999, and Kaliakin et al., 2000). The two designations are given to differentiate between the results obtained from these two independent studies.

4.4.1 In-Isolation Data from Previous Studies

Example test results from previous studies are summarized in figures 4.4 through 4.10. All of the data in these figures are presented as modulus as a function of time based on the approach illustrated in Figure 4.3. The following observations can be made:

1. The modulus of polyester (PET) products is less affected by time than polypropylene (PP) and high density polyethylene (HDPE) geosynthetics (at least for strains up to 2 percent).

2. In general, the relaxation modulus has a lower value than the creep modulus.

3. The modulus values obtained from the CRS tests as a function of time for HDPE and PP geosynthetics are roughly the same or slightly lower than the modulus values obtained from creep testing, especially at longer times.

4. The modulus values obtained from the different test methods tend to converge at longer times.

5. The modulus becomes less sensitive to time after approximately 500 to 1,000 hours, which is the typical time it takes to build a geosynthetic wall.

Table 4.1. Geosynthetic materials used in previous and current studies.

Designation	Product Name	Type	Polymer	Index Tensile Strength, T_{ult} (kN/m)	Reference
WGT-1	Exxon GTF375	Woven geotextile	PP	62.0	Boyle 1995
EGG-1	Tensar SS1	Extruded biaxial geogrid	PP	12.0	Yeo 1985, and Benjamin 1989
EGG-2	Tensar SR-2	Extruded uniaxial geogrid	HDPE	70.5	Yeo 1985
EGG-3	Tensar BX1100	Extruded biaxial geogrid	PP	13.0	Burgess 1999
EGG-4	Tensar BX1100	Extruded biaxial geogrid	PP	13.0	Kaliakin et al. 2000
EGG-5	Tensar UX1000 SB	Extruded uniaxial geogrid	HDPE	38.0	Kaliakin et al. 2000
EGG-6	Tensar UX1500 SB	Extruded uniaxial geogrid	HDPE	72.0	Kaliakin et al. 2000
WGG-1	Fortrac 35/20-20	Woven biaxial geogrid with PVC coating	PET	36.0	Kaliakin et al. 2000
WGG-2	Miragrid 5T	Woven biaxial geogrid with acrylic coating	PET	41.0	Kaliakin et al. 2000
WGG-3	Stratagrid 100	Woven biaxial geogrid with PVC coating	PET	15.8	Saunders 2001
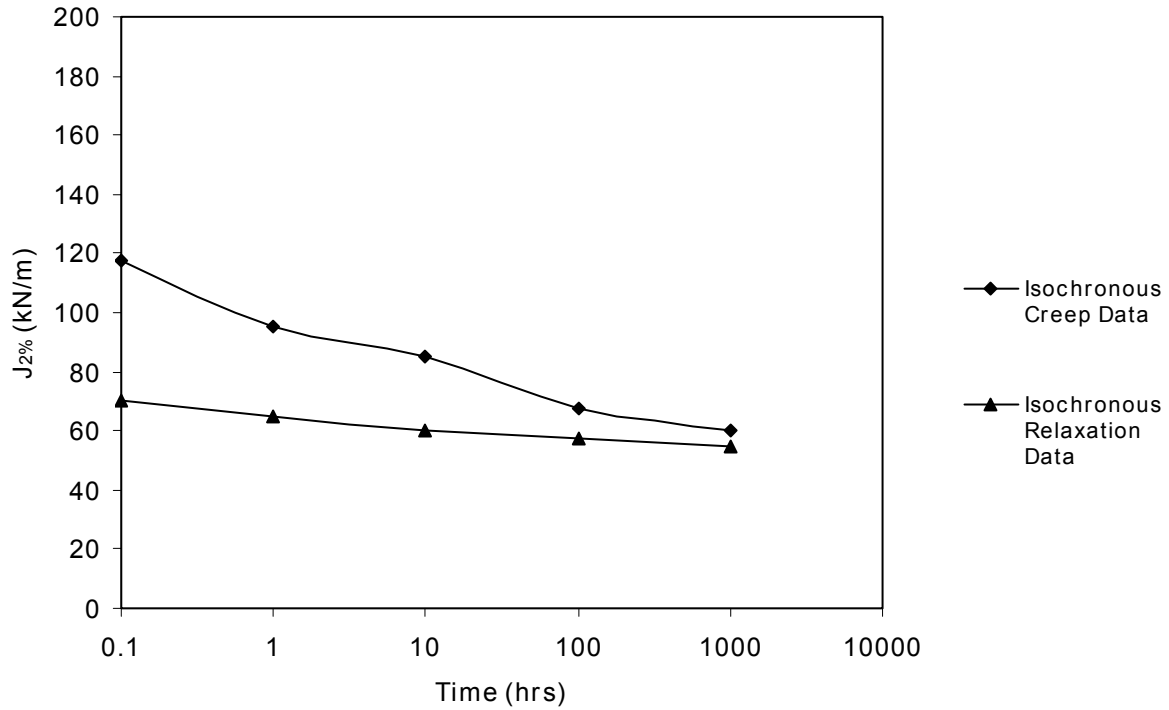
Figure 4.4. Comparison of in-isolation isochronous relaxation and isochronous creep $J_{2\%}$ values for woven PET geogrid WGG-2 (data from Kaliakin et al. 2000).
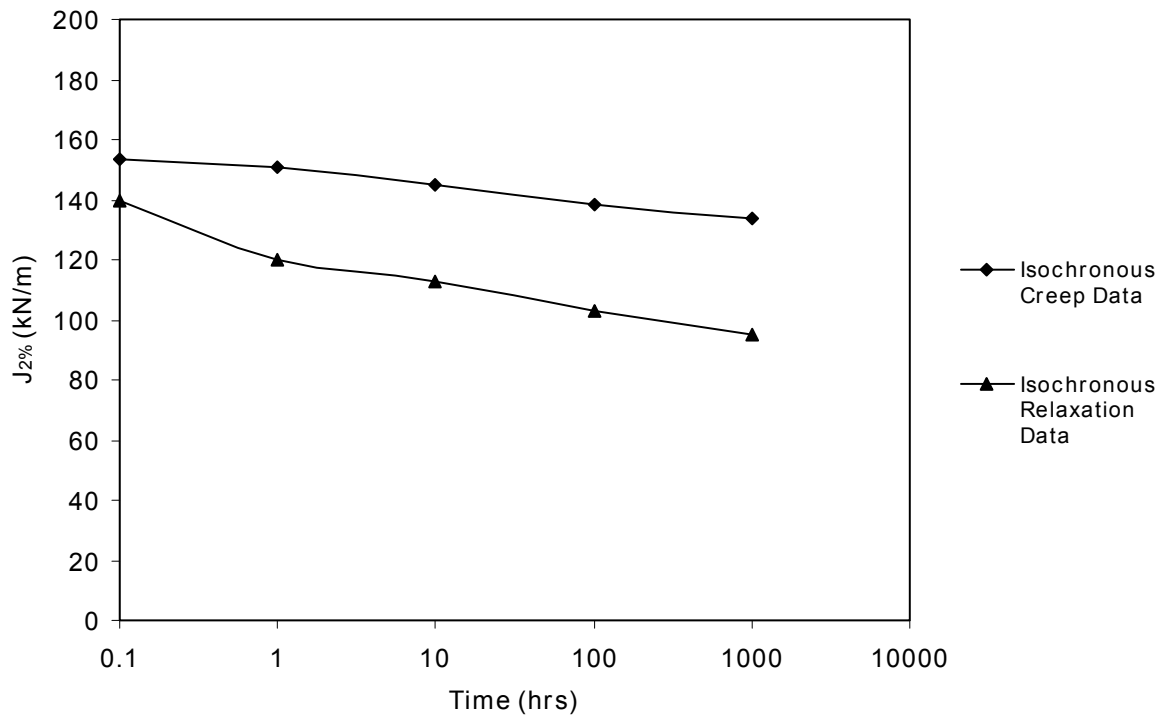
Figure 4.5. Comparison of in-isolation isochronous relaxation and isochronous creep $J_{2\%}$ values for woven PET geogrid WGG-1 (data from Kaliakin et al. 2000).

100
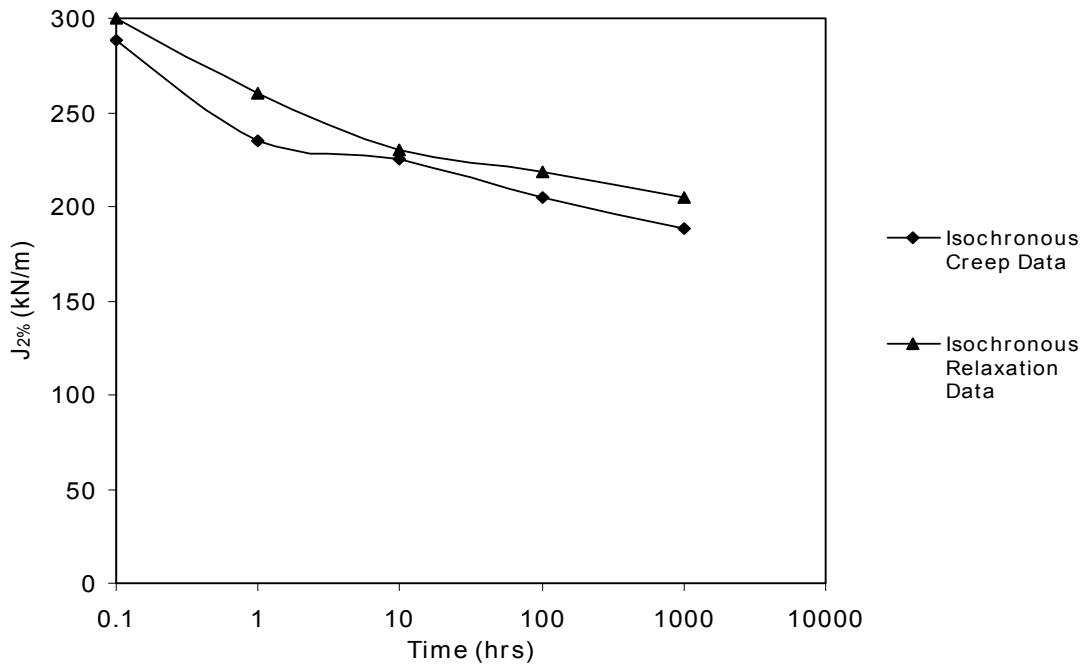
Figure 4.6. Comparison of in-isolation isochronous relaxation and isochronous creep $J_{2\%}$ values for uniaxial HDPE geogrid EGG-5 (data from Kaliakin et al. 2000).
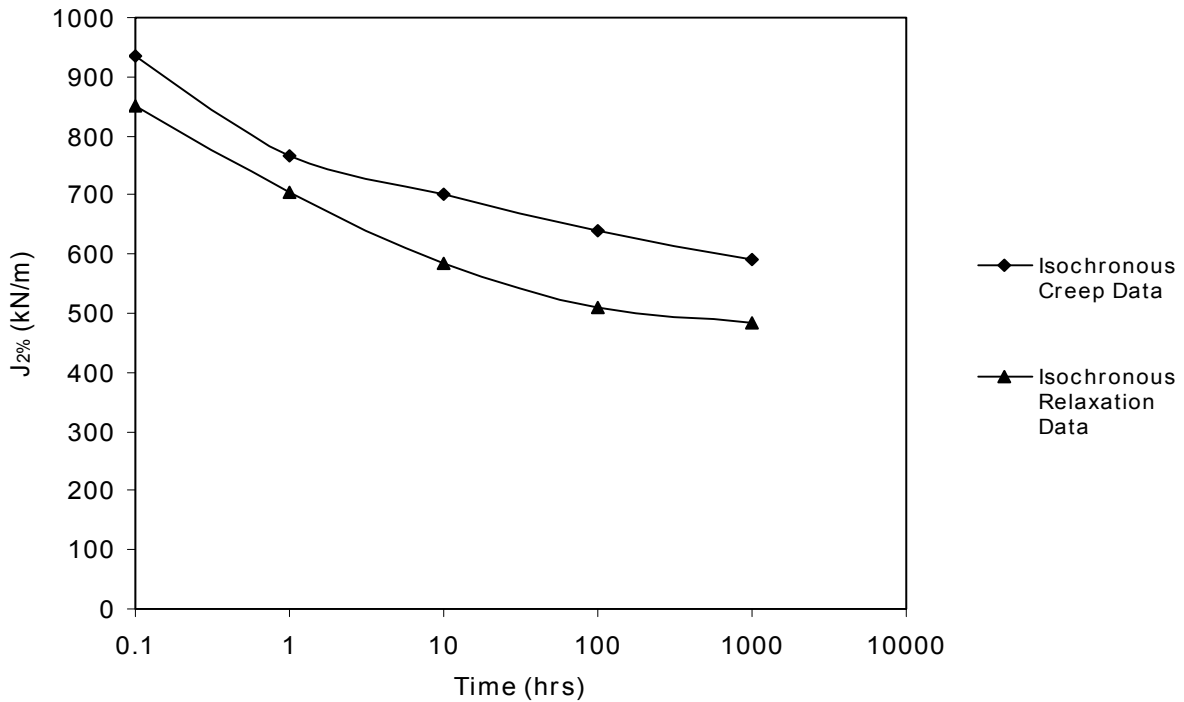
Figure 4.7. Comparison of in-isolation isochronous relaxation and isochronous creep $J_{2\%}$ values for uniaxial HDPE geogrid EGG-6 (data from Kaliakin et al. 2000).
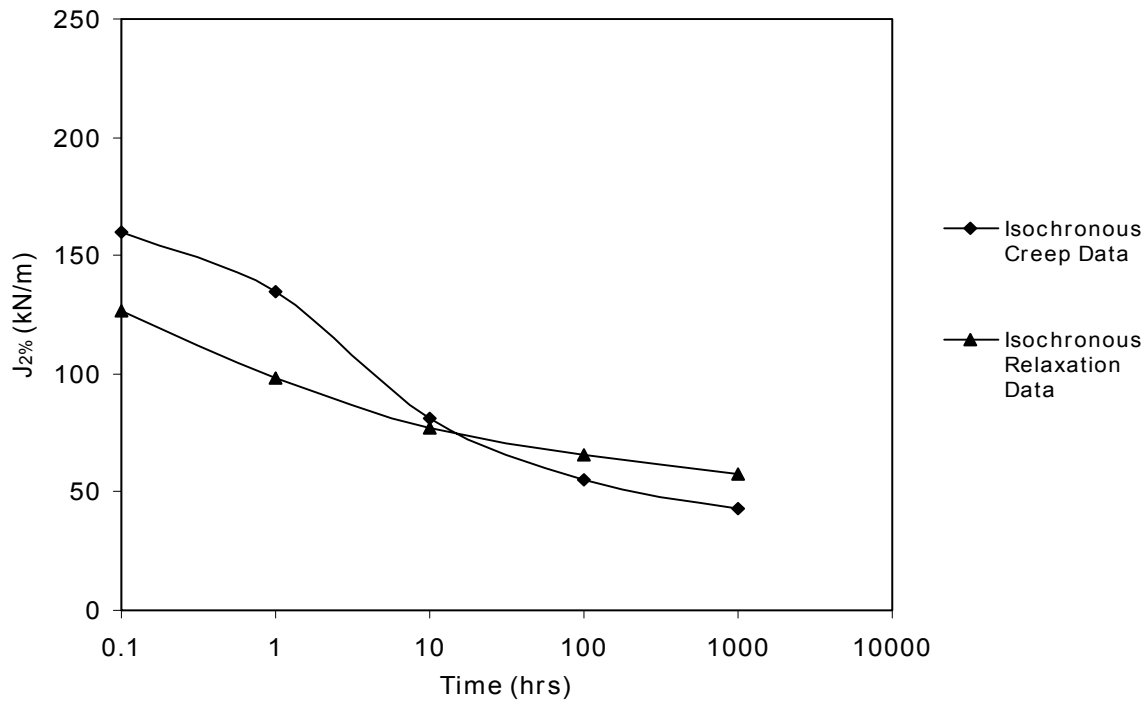
Figure 4.8. Comparison of in-isolation isochronous relaxation and isochronous creep $J_{2\%}$ values for biaxial PP geogrid EGG-4 (data from Kaliakin et al. 2000).
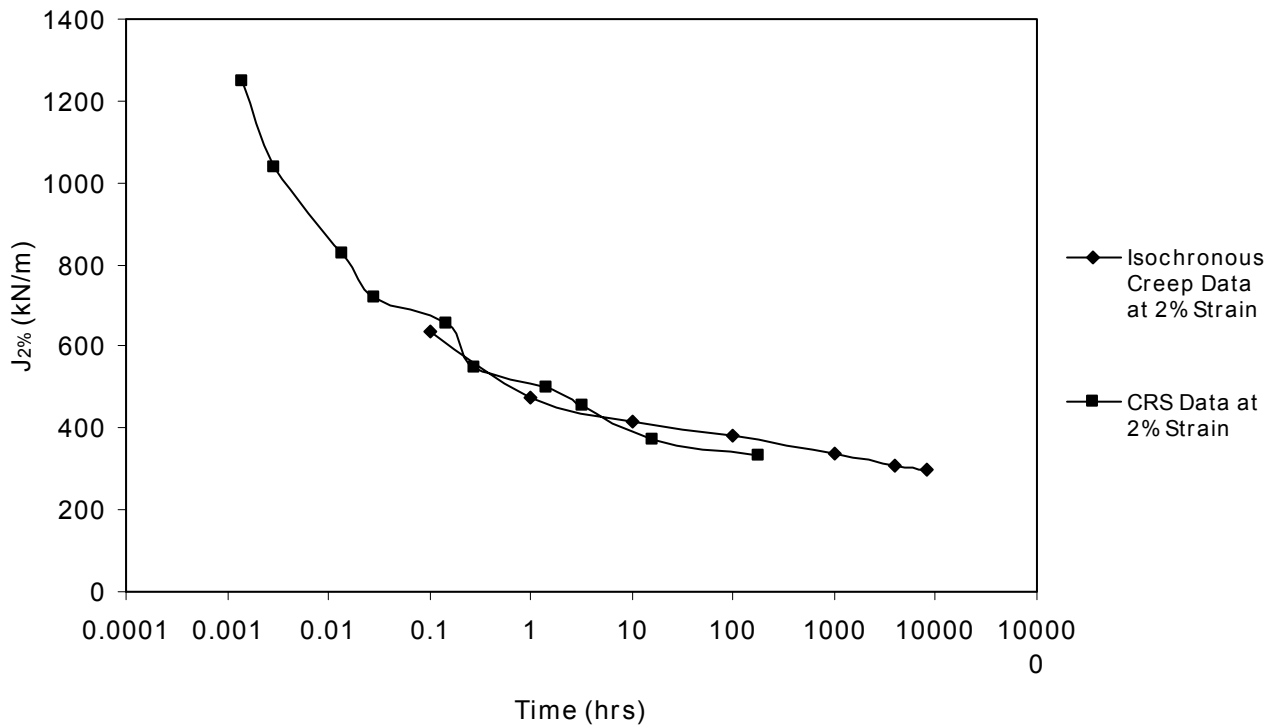
Figure 4.9. Comparison of in-isolation constant rate of strain (CRS) and isochronous creep $J_{2\%}$ values for uniaxial HDPE geogrid EGG-2 (data from Yeo 1985).
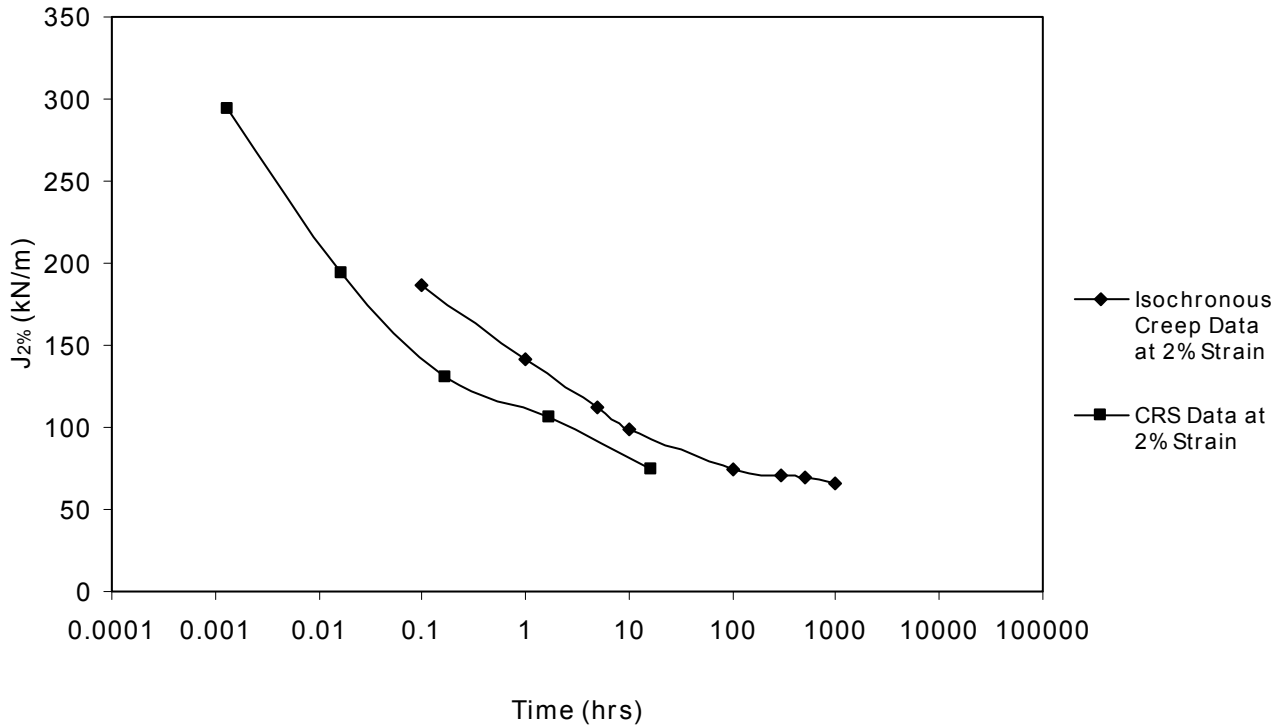
Figure 4.10. Comparison of in-isolation CRS and isochronous creep $J_{2\%}$ values for biaxial PP geogrid EGG-1 loaded in weak direction (data from Benjamin 1989, and Yeo 1985).

Figures 4.11 through 4.15 show comparisons between creep and stress relaxation data at all strain levels rather than just 2 percent strain. If the isochronous curves for both creep and stress relaxation are very close together, this indicates that the moduli obtained from both types of tests are approximately the same. On the basis of these figures, the PET geosynthetic moduli from both types of tests are approximately the same at all but the highest load and strain levels. The HDPE geosynthetic modulus values from both types of tests are about the same at low strain levels only and tend to diverge at higher strain levels. For the PP geogrid, the modulus values from both types of tests are reasonably close at low strains. Note that Kaliakin et al. (2000) came to similar conclusions regarding the tendency of creep and relaxation data to match better at lower strain levels.

103
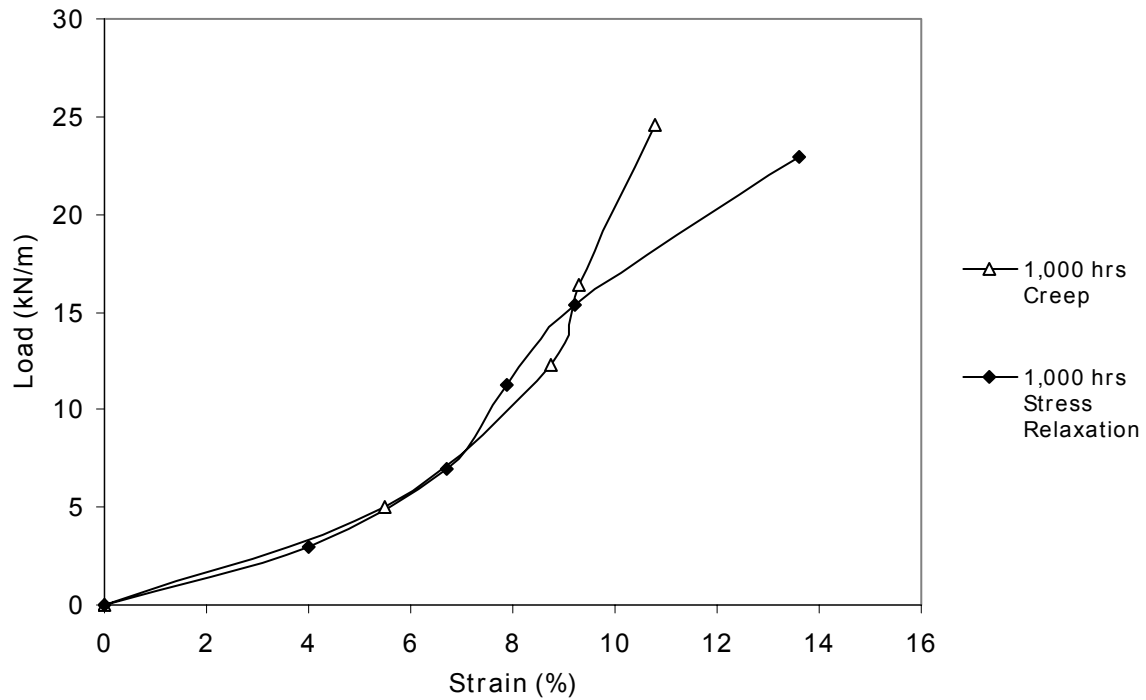
Figure 4.11. In-isolation 1000-hour isochronous curves for woven PET geogrid WGG-2 from stress relaxation and creep data (data from Kaliakin et al. 2000).
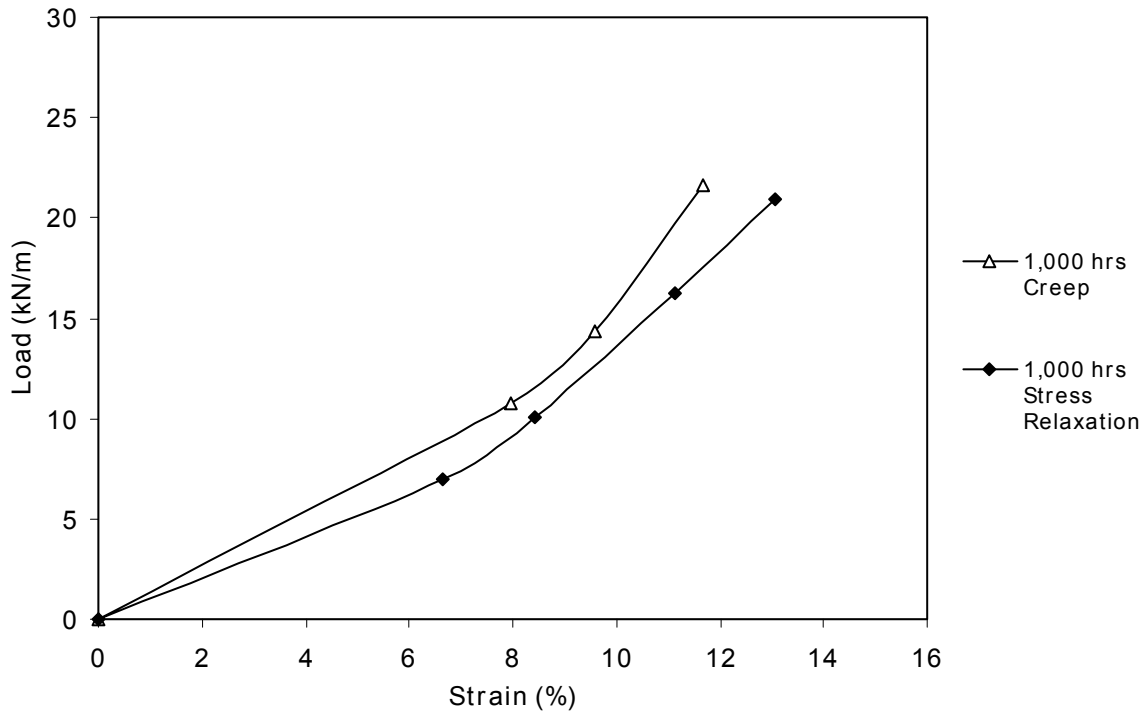
Figure 4.12. In-isolation 1000-hour isochronous curves for woven PET geogrid WGG-1 from stress relaxation and creep data (data from Kaliakin et al. 2000).
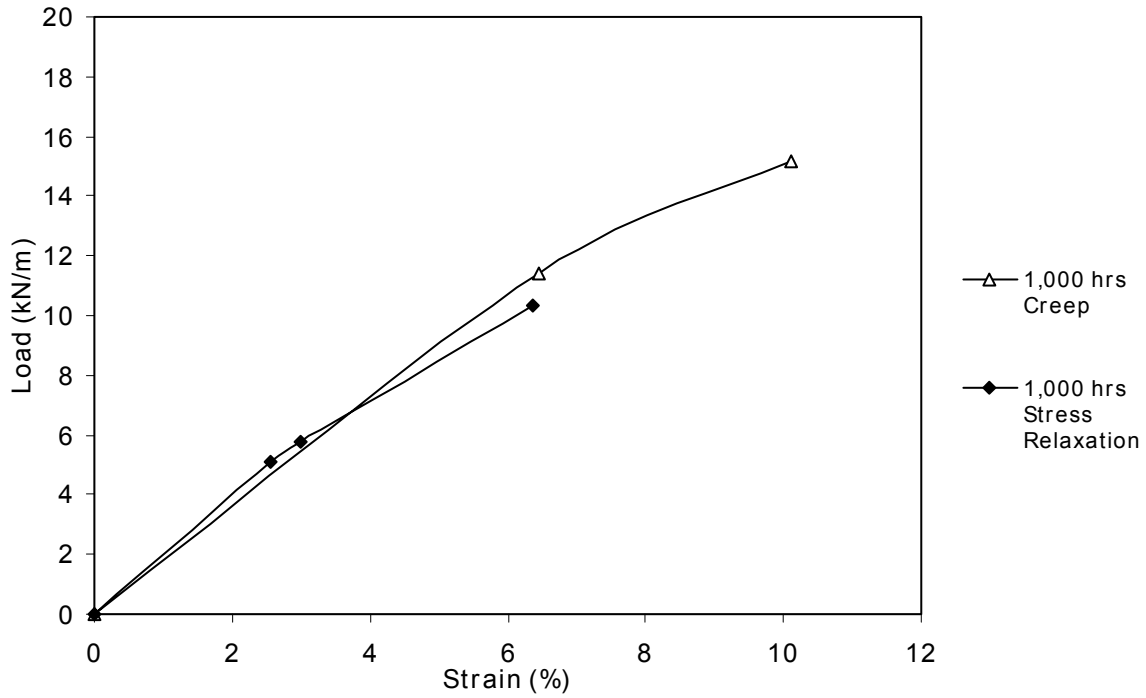
Figure 4.13. In-isolation 1000-hour isochronous curves for uniaxial HDPE geogrid EGG-5 from stress relaxation and creep data (data from Kaliakin et al. 2000).
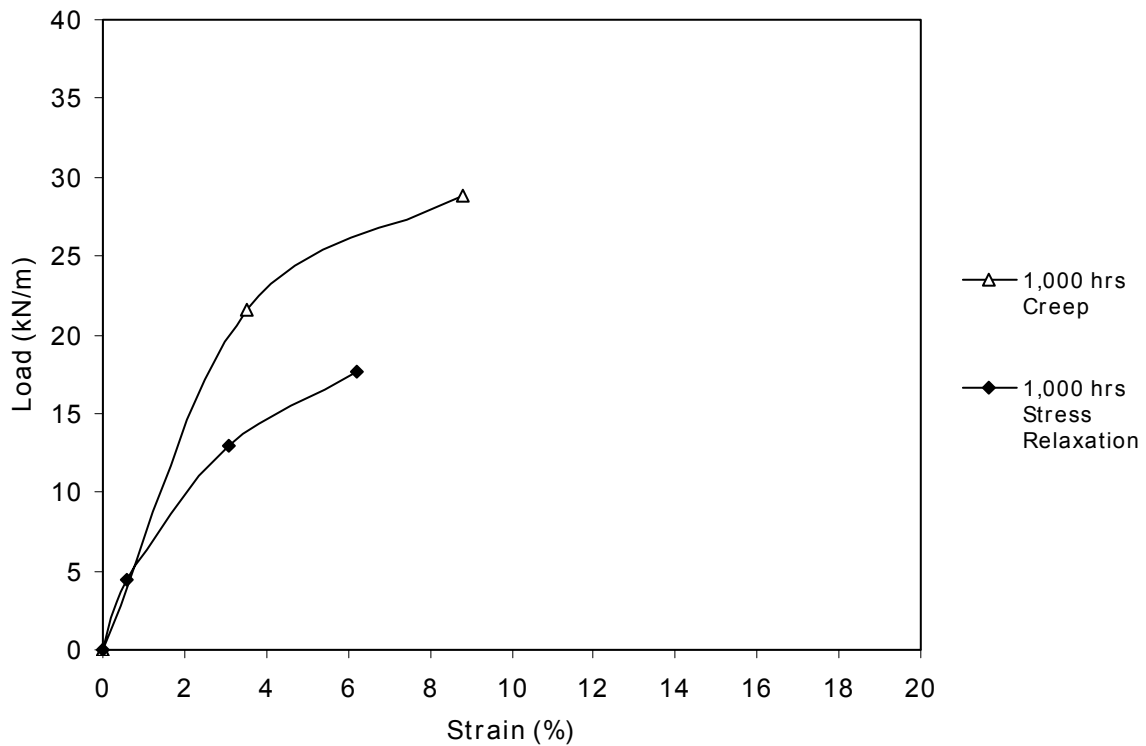
Figure 4.14. In-isolation 1000-hour isochronous curves for uniaxial HDPE geogrid EGG-6 from stress relaxation and creep data (data from Kaliakin et al. 2000).
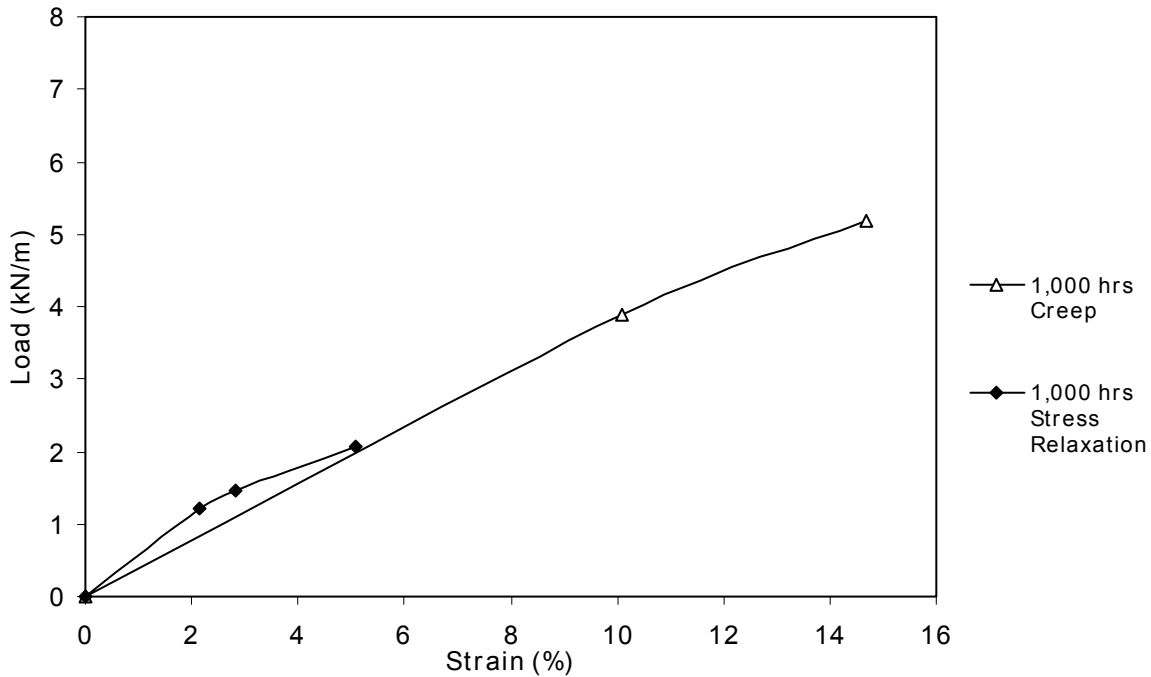
Figure 4.15. In-isolation 1000-hour isochronous curves for biaxial PP geogrid EGG-4 from stress relaxation and creep data (data from Kaliakin et al. 2000).

Creep and stress relaxation test data were obtained by Thornton (2001) to characterize the low load time-dependent behavior of PP biaxial geogrid EGG-3 (samples of material from the same roll of geogrid that was used by Burgess (1999), and Kaliakin et al. (2000). These data revealed that at small load levels, the creep modulus was almost equal to the stress relaxation modulus, although the creep modulus was slightly greater. However, in the non-linear range, where increases in the applied loads or strains resulted in changes in the molecular structure of the polymer, a more complex relationship between the creep and stress relaxation modulus developed. The creep modulus determined in this non-linear range can be greater than, equal to, or less than the relaxation modulus.

Thornton (2001) also conducted rapid loading tensile tests (CRS tests on single rib specimens) to determine the ultimate strength of the reinforcement. These tests revealed a high coefficient of variation in the strain at maximum load, thus suggesting the potential for material variability to affect the modulus determined from any loading sequence.

106

4.4.2 In-Isolation Data from the Current Study

In none of the studies reported previously were creep, stress relaxation, and constant rate of strain tests conducted on the same sample of material. Hence, a direct comparison of results from all these different types of tests could not be made. Therefore, all three types of tests were conducted at the Royal Military College of Canada (RMCC) (Walters 2001) on a light-weight PP biaxial geogrid (EGG-3) and a light-weight PET woven biaxial geogrid (WGG-3). Figures 4.16 and 4.17 show modulus values determined from creep, relaxation, and constant rate of strain (CRS) tests on these materials. These geosynthetics are very weak (T_{ult} = 13 to 17 kN/m) and were specifically chosen to generate large strains in instrumented, full-scale, reinforced-soil retaining wall structures (Bathurst et al. 2000).

The in-isolation creep and constant rate of strain (CRS) tests of the EGG-3 (HDPE) geogrid were conducted with 200-mm-wide specimens, while the creep and CRS tests of WGG-3 (PET) geogrid were conducted on single rib specimens. However, the stress relaxation tests were conducted on single rib specimens for both EGG-3 and WGG-3 using a modified standard laboratory tensometer (Walters 2001). A preliminary set of tests on the PET specimens showed that the 200-mm-wide specimens subjected to creep and CRS testing were susceptible to nonuniform loading, resulting in lower strengths than the single rib tests (Saunders 2001). This was not a problem for the PP geogrid. Therefore, to make sure that the results from all three types of tests could be directly compared for the WGG-3 geogrid material, all tests were conducted on single rib specimens.

Creep testing of the EGG-3 geogrid was conducted in accordance with ASTM D5262, with the exception that the load was applied quickly but smoothly to the specimens. In-isolation creep testing of the WGG-3 reinforcement was conducted on the single rib specimens in accordance with GRI GG3(b). The gauge length of the test specimens was 500 mm, and creep strains were measured with displacement-type potentiometers clamped to the specimens (Burgess 1999, Saunders 2001). The test specimens from each geosynthetic product were taken from the same roll and loaded for 1000 hours or until creep rupture of the specimen, whichever occurred first.
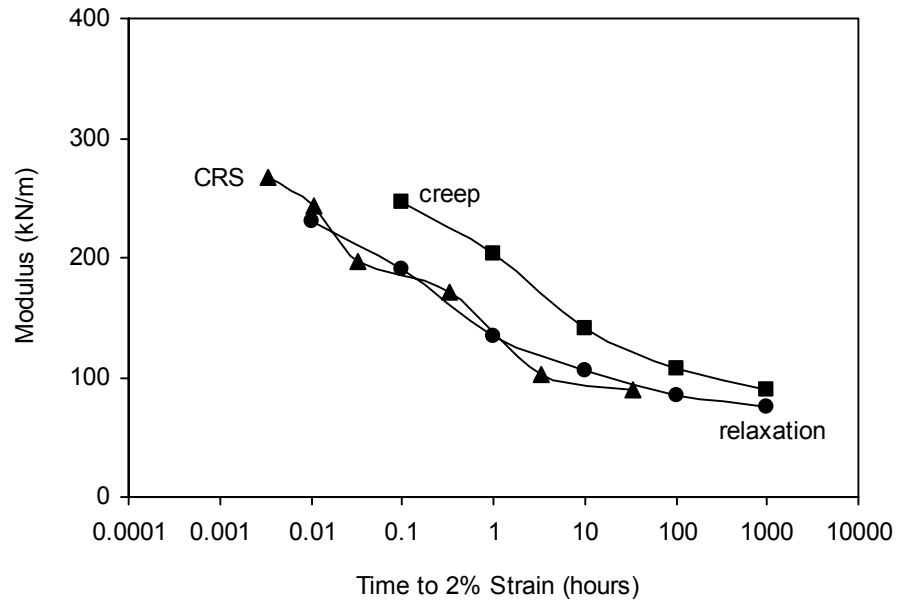
Figure 4.16. Comparison of in-isolation constant rate of strain (CRS) modulus, isochronous $J_{2\%}$ creep modulus, and $J_{2\%}$ stress relaxation modulus for biaxial PP geogrid EGG-3.
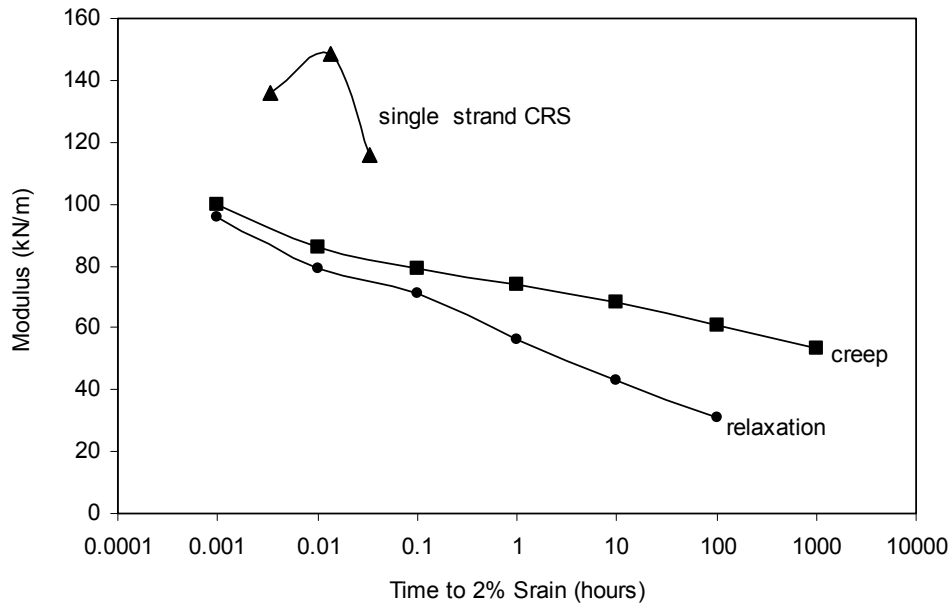
Figure 4.17. Comparison of in-isolation constant rate of strain (CRS) modulus, isochronous $J_{2\%}$ creep modulus, and $J_{2\%}$ stress relaxation modulus for woven PET geogrid WGG-3.

Relaxation testing of EGG-3 and WGG-3 specimens generally adhered to the recommendations in ASTM E328-86 and used single rib specimens taken from the same roll. The ends of the specimens were cast in a cylindrical mold of molten Ostalloy (Saunders 2001) and gripped by the spring loaded tensometer jaws. Specimens were about 320 mm long, and a series of tests was conducted at different initial strain magnitudes. The initial strain was applied at a rate of 110 percent per minute, and each test was monitored for a minimum of 100 hours.

CRS testing to determine the index strength of EGG-3 specimens was conducted in accordance with ASTM D4595. The 200-mm-wide specimens were held by split roller clamps and tested at a strain rate of 10 percent per minute. CRS tests were also conducted at strain rates of 1, 0.1, 0.01 and 0.001 percent per minute. CRS tests to determine the index strength of the WGG-3 product were also conducted on single rib specimens at a strain rate of 10 percent per minute. Additional CRS tests were conducted at strain rates of 3 and 1 percent per minute. The specimens had an overall length of approximately 200 mm and a gauge length of 100 mm. Displacement-type potentiometers were attached to the specimens to measure the strain during testing. All tests described here were carried out at a temperature of $20^o \pm 2^o$ C.

The following observations can be made from the data presented in figures 4.16 and 4.17 based on the test methods described above:

- The creep modulus of the geosynthetics is greater than the relaxation modulus at the 2 percent strain level.
- For the PP geogrid, the relaxation modulus and the CRS modulus are almost identical, with all three moduli (creep, relaxation, and CRS) appearing to converge at long times.
- The CRS modulus for PET is greater than the creep modulus at the times shown.
- During the observation time of 1,000 hours, the moduli for the PET geogrid do not converge.

The data presented show that the PP geogrid behaved in a manner similar to the other polyolefin (HDPE and PP) geosynthetics summarized in Section 4.4.1. Similar agreement was not observed for the PET geogrid.

4.4.3 In-Soil Data

Soil confinement can affect both the short- and long-term modulus of the geosynthetic. Yuan et al. (1998) performed in-soil tests of the type shown conceptually in Figure 4.2b, at a

constant strain rate of 10 percent/minute. The soil was a beach sand. The results of these tests on one nonwoven geotextile, three woven geotextiles, and one geogrid are provided in Figure 4.18. The test results show that soil confinement has only a minor effect, if any, on the modulus values of woven geotextiles and geogrids (an increase of 5 to 30 percent over the in-isolation value) but has a large effect on the modulus values of nonwoven geotextiles (an increase on the order of up to 500 percent, depending on the confining pressure and soil type).
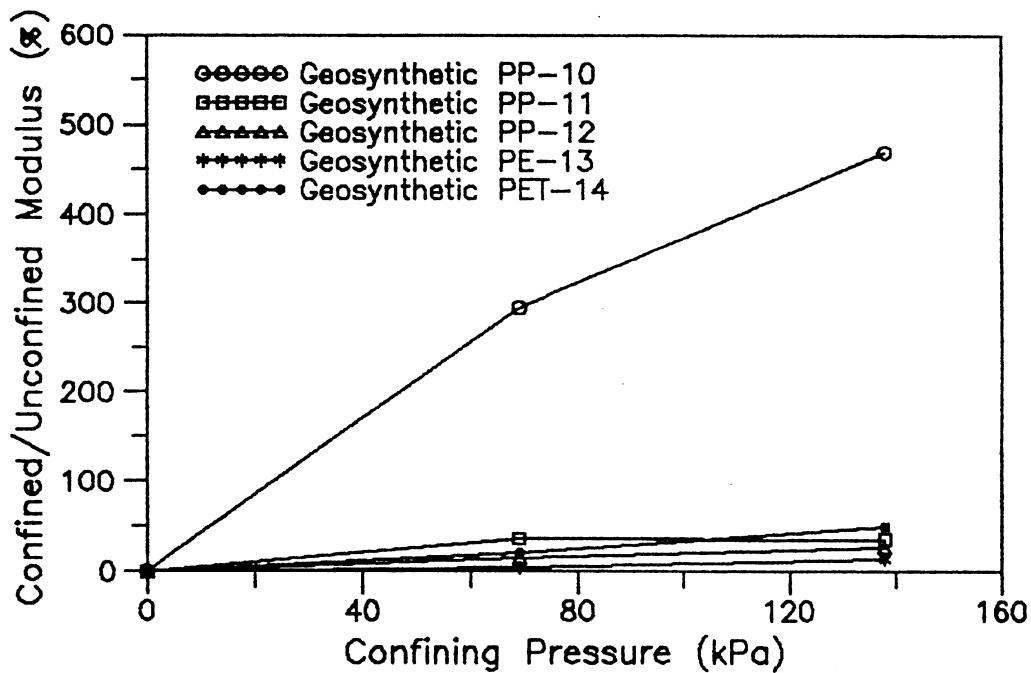
Figure 4.18. Soil confinement effect on the secant stiffness modulus at 5 percent strain for selected geosynthetic materials confined in beach sand (from Yuan et al. 1998).

A similar study was conducted by Wilson-Fahmy et al. (1993) on woven and nonwoven geotextiles using a similar device. Figure 4.19 shows the test results from this study for a woven calendared, monofilament geotextile confined in sand. The results show that soil confinement up to 138 kPa had a negligible effect on the modulus for the woven geotextile. However, for the nonwoven geotextiles tested, the modulus increased 180 to 480 percent, depending on the confining stress, because of soil confinement. The researchers concluded that load-strain response from in-isolation tests can be used to estimate the short-term modulus of woven geotextiles under soil confinement but not of nonwoven geotextiles.
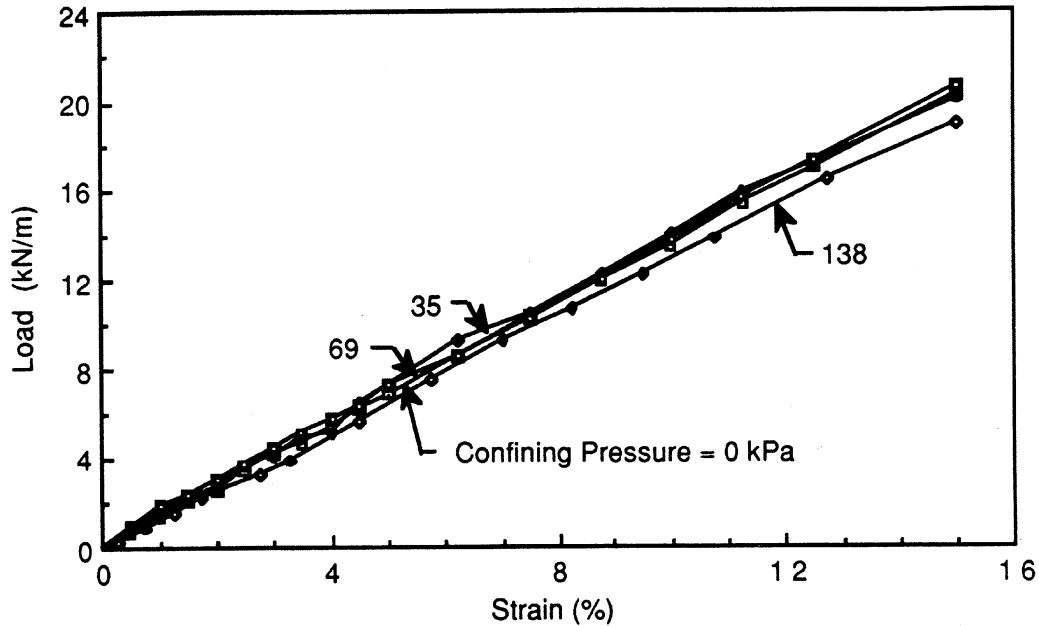
Figure 4.19. Load-extension behavior of Geotextile A confined in soil (from Wilson-Fahmy et al. 1993).

Boyle et al. (1996) conducted in-soil load-strain tests with a unit cell device (see Figure 4.2a and Figure 4.20), which allowed the geosynthetic response to a constant deviator stress ($\sigma_1 - \sigma_3$) applied to the soil to be monitored through direct measurement of both load and strain in the reinforcement. As discussed previously, this type of device can be used to better simulate the way geosynthetic reinforcement is loaded in actual structures (i.e., the soil loads the geosynthetic rather than the geosynthetic being loaded directly). For the simulation to be perfect, the device must produce true unit cell conditions. To produce these conditions, the friction on the inside surface of the cell must be negligible. Friction was reduced on all sides of the cell through a low viscosity silicon grease and a 0.3-mm-thick latex membrane. The measured friction angle for the silicon grease was approximately 4°, as indicated by direct shear interface tests. As shown in Figure 4.21, the strain distribution along the specimen length was not uniform but at least exhibited an approximately linear distribution along the length of the specimen. Boyle (1995) concluded that although some non-uniformity in the strain distribution did exist in some of the tests, indicating some deviation from true unit cell conditions (i.e., in a true unit cell, strains should be fairly uniform within the cell), analysis of test results showed that the error caused by this deviation was small. He concluded that, from a practical point of view, the device appeared to adequately simulate unit cell conditions and could be treated as such. Additional insights into

how well this test simulated true in-soil conditions in reinforced soil walls, and to what degree stress relaxation occurs, are provided in Chapter 6.0.
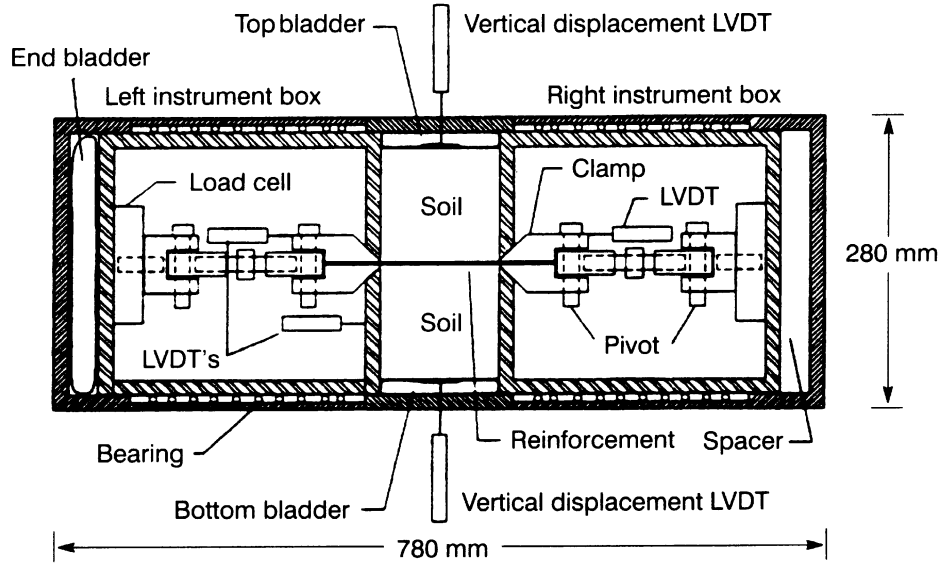
Figure 4.20. Cross-section of unit cell in-soil geosynthetic testing device (from Boyle et al. 1996).
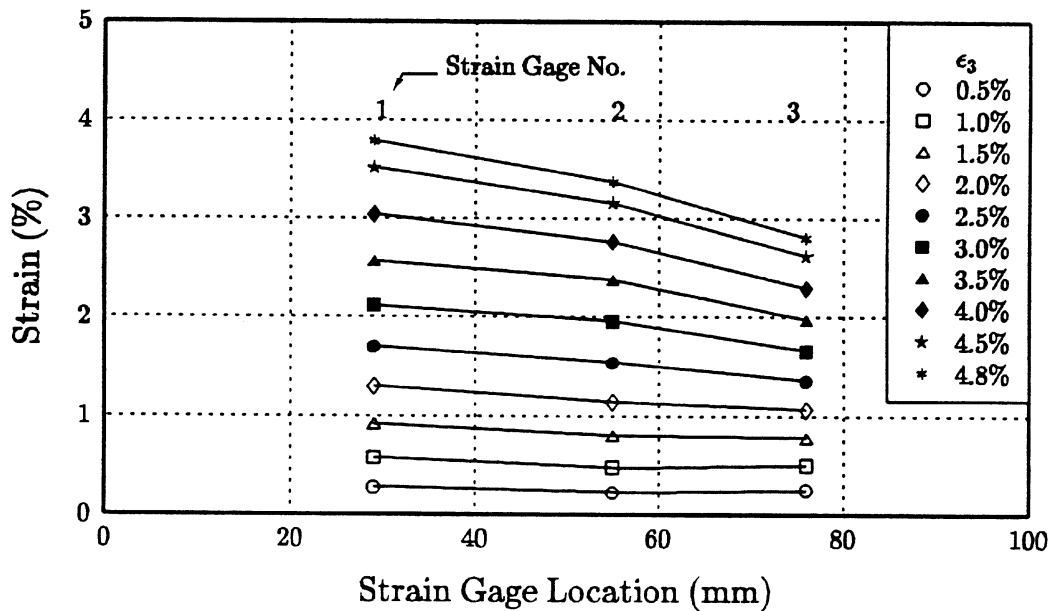
Figure 4.21. Strain distribution in polypropylene woven geosynthetic specimen confined in gravelly sand in unit cell device (from Boyle 1995).
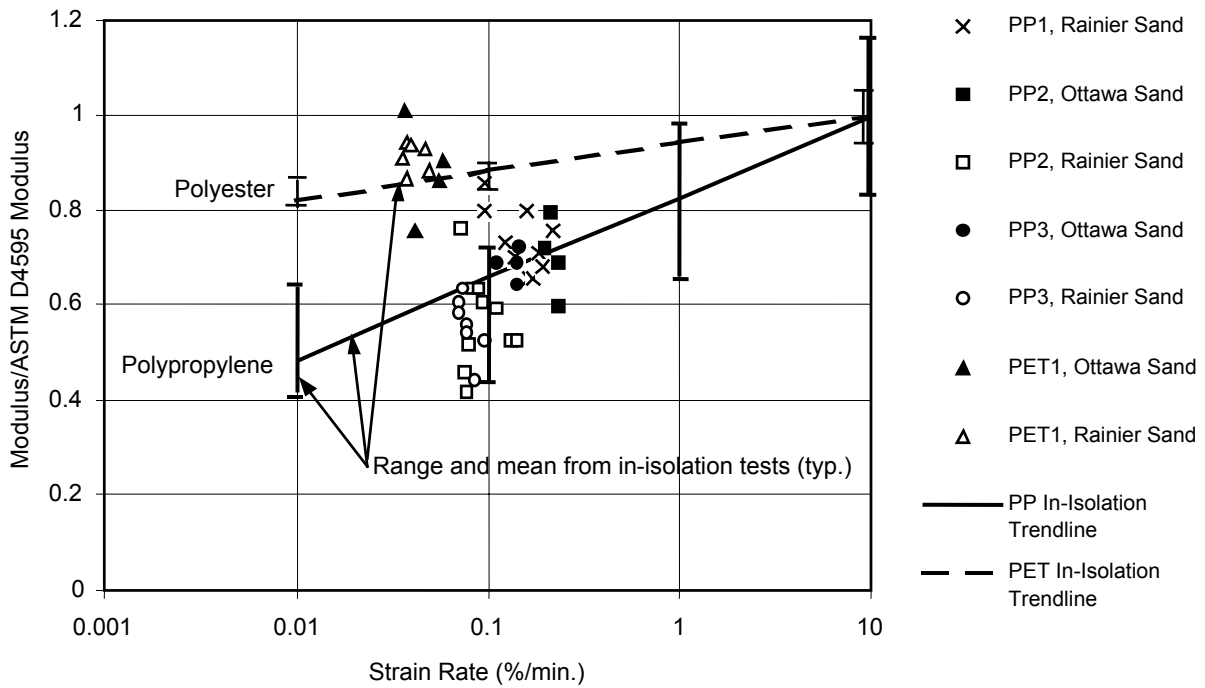
Figure 4.22. Five percent secant modulus versus strain rate from in-soil and in-isolation tests on woven PP and PET geotextiles (adapted from Boyle et al. 1996).

Measurements of short-term in-soil geosynthetic modulus from the unit cell device are summarized in Figure 4.22. This figure also shows the modulus obtained from in-isolation tests on the same geosynthetics. Note that the in-soil unit cell test is conducted as a constant rate of soil loading test, rather than as a constant rate of strain test, to better simulate how a soil/geosynthetic composite is loaded in real structures. If there is a confinement effect, because the normal confining stress on the geosynthetic is not held constant, the effect of confining stress can only be determined approximately. This issue is only significant for nonwoven geotextiles, as the effect of confining stress on woven geotextiles is minimal. Because the test is controlled by the soil loading rate, the in-soil strain rates reported in Figure 4.22 are average rates determined over the duration of the test.

The first observation that can be made from Figure 4.22 is that the log-linear curve describing the trend in data for the ratio of in-isolation modulus to index modulus versus strain rate passes through the data sets for the in-soil PET and PP results. It may be argued that the in-soil moduli measured for the PET geotextile are, on average, slightly above the in-isolation trend line for the PET geotextile data points. This observation is consistent with the data provided in

113

Figure 4.18, which showed a slight improvement in modulus of PET geotextiles because of soil confinement. The second observation is that the in-soil modulus values for the geosynthetic products tested at an average rate of 0.1 percent strain/minute were less than the in-isolation modulus at 10 percent strain rate/minute. It is reasonable to assume that the log-linear trend for the in-isolation tests is preserved and, therefore, that the in-soil modulus of geosynthetics can be expected to also decrease with a decreasing logarithm of strain rate.

Boyle (1995) and Boyle and Holtz (1996) also evaluated the creep behavior of the PP woven geotextiles confined in soil with the unit cell device described previously. Figure 4.23 provides the test results for a woven PP geotextile (WGT-1 in Table 1) confined in a gravelly sand tested in the device under constant deviator stress, σ_1. The test was conducted at a confining pressure of $\sigma_3 = 20$ kPa. This figure shows that both creep and stress relaxation occurred in this unit cell simulation of geosynthetic reinforcement confined in soil in a wall or reinforced slope.

Helwany and Shih (1998) performed similar experiments with a heatbonded geotextile confined in sand with $\sigma_1 = 70$ kPa and $\sigma_3 = 3.5$ kPa. They also found that both stress relaxation and creep occurred when the soil applied the load to the geosynthetic through a deviator stress. However, as shown in Figure 4.24, the stress relaxation did not occur immediately but was delayed approximately 20 hours after the initial application of the vertical deviator stress. Although Helwany and Shih indicated that side wall friction in the device was low, the actual sidewall interface friction was not reported, nor was an overall evaluation of whether unit cell conditions existed in the device reported. A plausible explanation for the unusual shape of the stress relaxation curve obtained from the test was that it took time, possibly because of soil creep, for the load to transfer along the geosynthetic back to the end of the geosynthetic where the load was measured. This delayed load transfer could have caused the load as measured by the load cell to increase during the first 20 hours of loading. Work by Boyle (1995) suggests that the maximum load in the reinforcement occurred at the moveable end of the specimen. Load transfer to the back (fixed) end of the geosynthetic specimen occurred as strain in the reinforcement developed in Boyle's (1995) tests. In any case, once full load transfer occurred, stress relaxation did occur, as it did in the tests by Boyle (1995), confirming that stress relaxation is a potential time dependent mechanism in geosynthetic reinforced structures, at least at working stress conditions. The results from these two tests certainly point to the importance of

114

considering the effect of the boundary conditions, as well as how reinforcement loads and strains are measured, when results from such tests are interpreted.
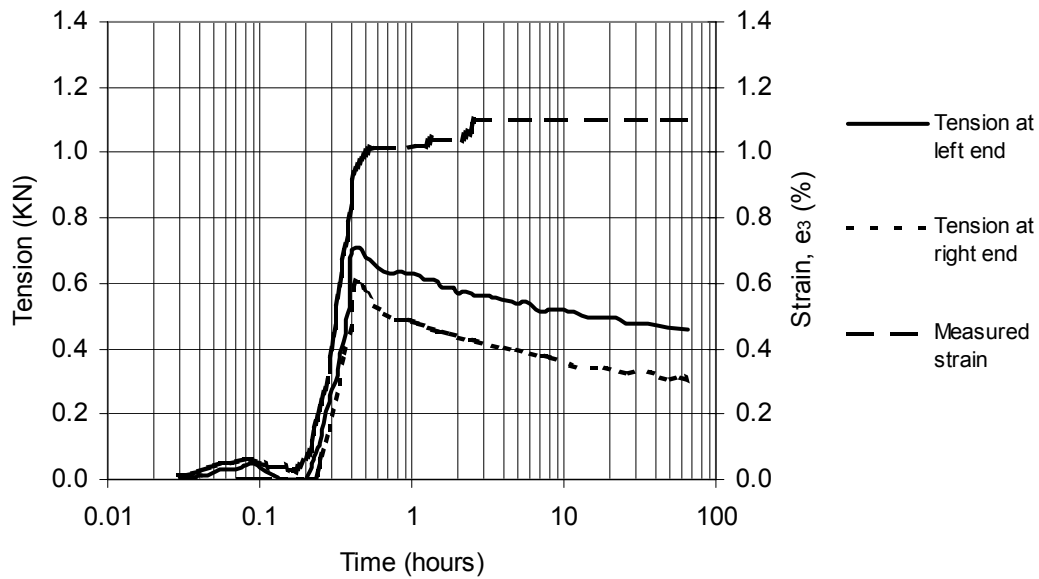
Figure 4.23. Confined creep and stress relaxation response of woven PP geotextile WGT-1 in Rainier Avenue gravelly sand at 20 kPa confining pressure (adapted from Boyle and Holtz 1996).
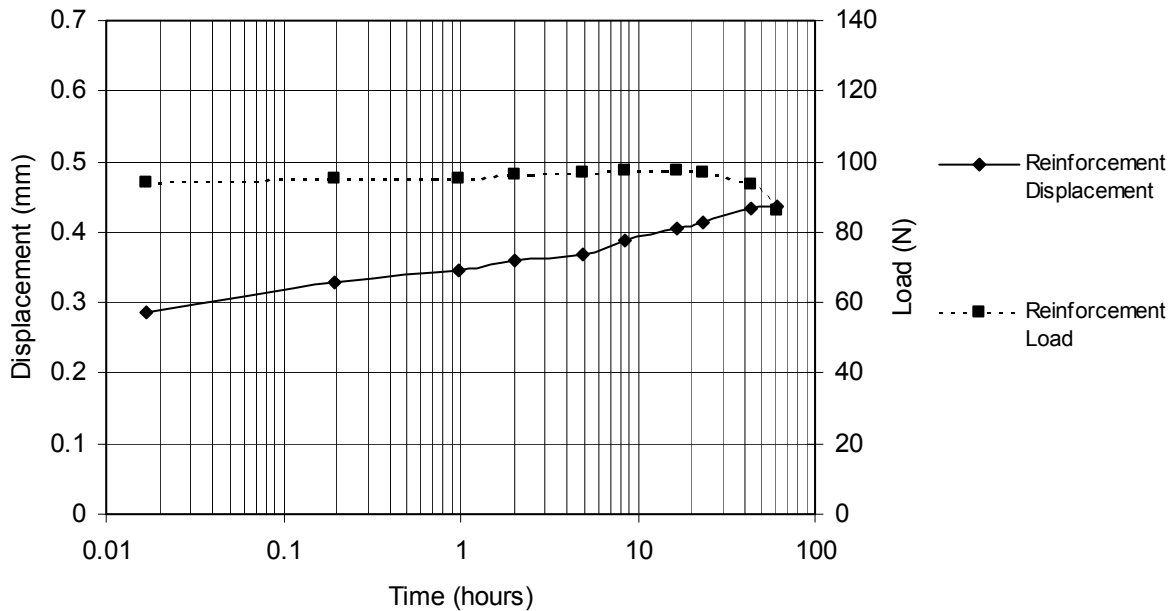
Figure 4.24. Confined creep of a PP heatbonded nonwoven geotextile at a confining stress of 3.5 kPa (adapted from Helwany and Shih, 1998).

Figure 4.25 provides a comparison of the moduli obtained from the in-isolation and in-soil constant rate of strain and creep tests conducted by Boyle (1995) and Boyle et al. (1996) on a woven PP geotextile. The moduli reported in this figure were determined at 1 percent strain rather than at the 2 percent strain used for the data presented elsewhere in this chapter. The creep test data at higher strain values were insufficient to develop isochronous curves at all times of interest. In general, modulus values appear to converge in all of the test results at longer times, both in-isolation and in-soil.

In Chapter 6.0, the in-isolation and in-soil data in figures 4.23 and 4.25 are compared to the long-term measurements obtained from the full-scale walls the laboratory tests were set up to simulate. Chapter 6.0 concludes, on the basis of the measured creep rates from the reinforcement in Wall GW16, that the unit cell device may have led to more stress relaxation than occurred in the actual wall. However, some stress relaxation still appears to have occurred, given the creep rates measured in the unit cell and in-isolation creep tests in comparison to measured values obtained from the full-scale wall reinforcement.
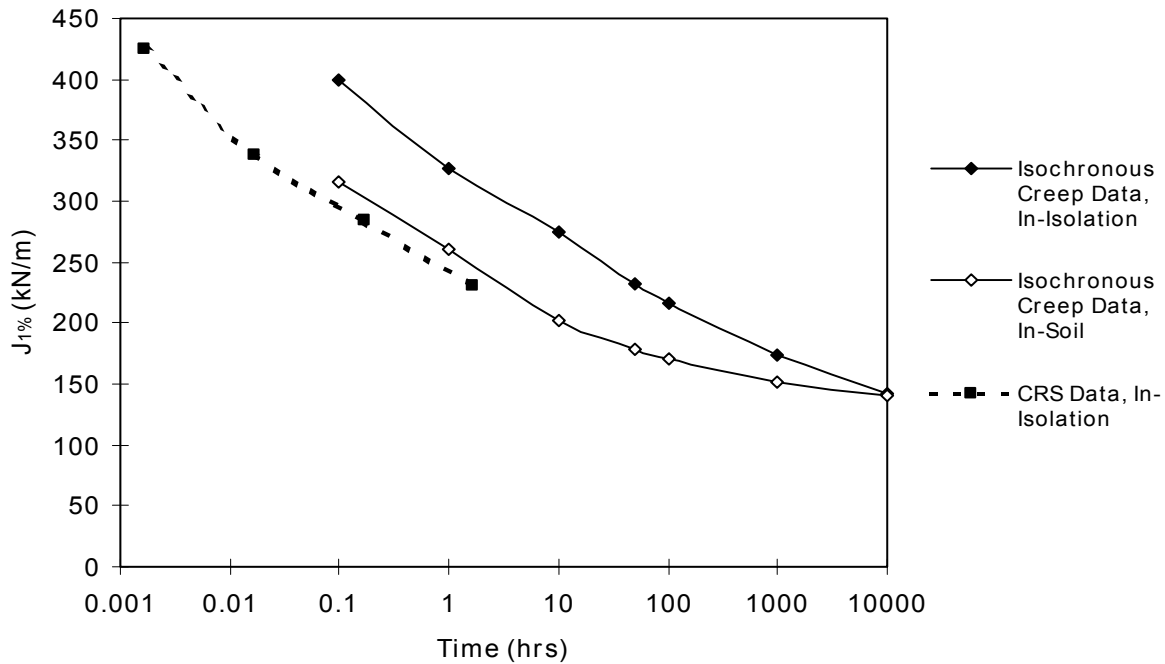
Figure 4.25. Comparison of CRS and isochronous creep $J_{1\%}$ values from in-isolation and in-soil tests on woven PP geotextile WGT-1 (data from Boyle 1995).

116

4.4.4 Installation Damage Effects on Geosynthetic Modulus

Allen and Bathurst (1994) investigated the effect of installation damage on the modulus of different types of geosynthetic reinforcement. Figure 4.26 provides an example of how installation damage affects the short-term modulus (as determined from constant rate of strain tensile tests) of geosynthetics. For woven geotextiles, the decrease in modulus with increasing levels of damage is minor for damage that results in a loss of peak tensile strength of less than 40 percent. For geogrids, the modulus loss is insignificant until very high levels of damage occur.

Allen and Bathurst (1996) also investigated and summarized the combined effect of installation damage and creep on the strain response to load of various geosynthetics. As shown in Figure 4.27, the creep strain response is the same before and after installation damage, which indicates that the creep modulus will also be the same before and after damage. However, they noted that if the installation damage is great enough to cause a significant modulus reduction, as indicated by short-term tensile tests, the creep strain response before damage may be different than the creep strain response after damage.
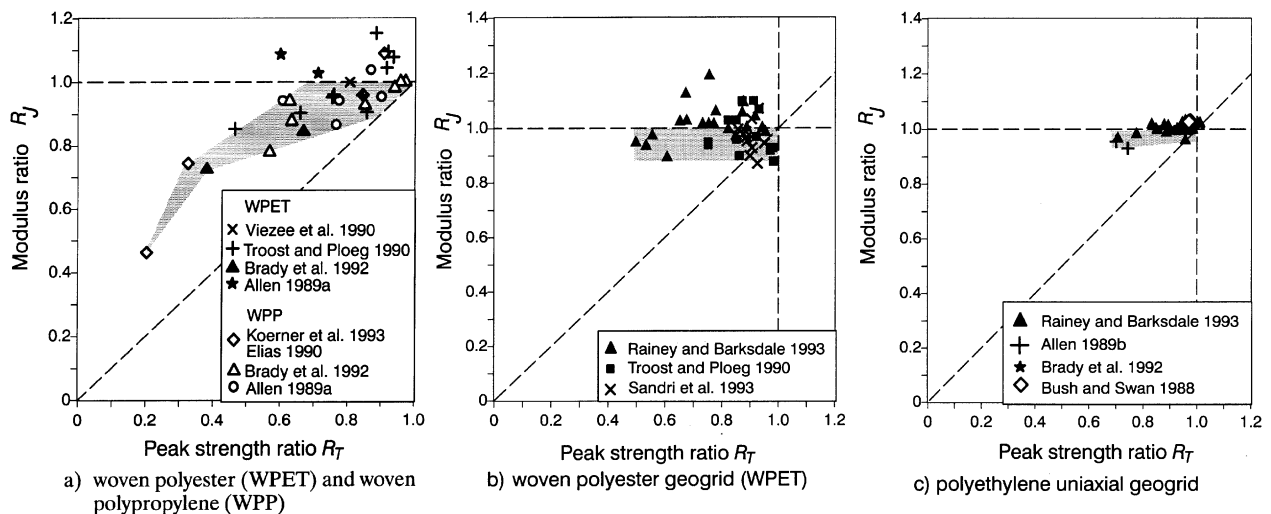
Figure 4.26. Summary of secant modulus ratio versus peak strength ratio for various geosynthetics (from Allen and Bathurst 1994).

117
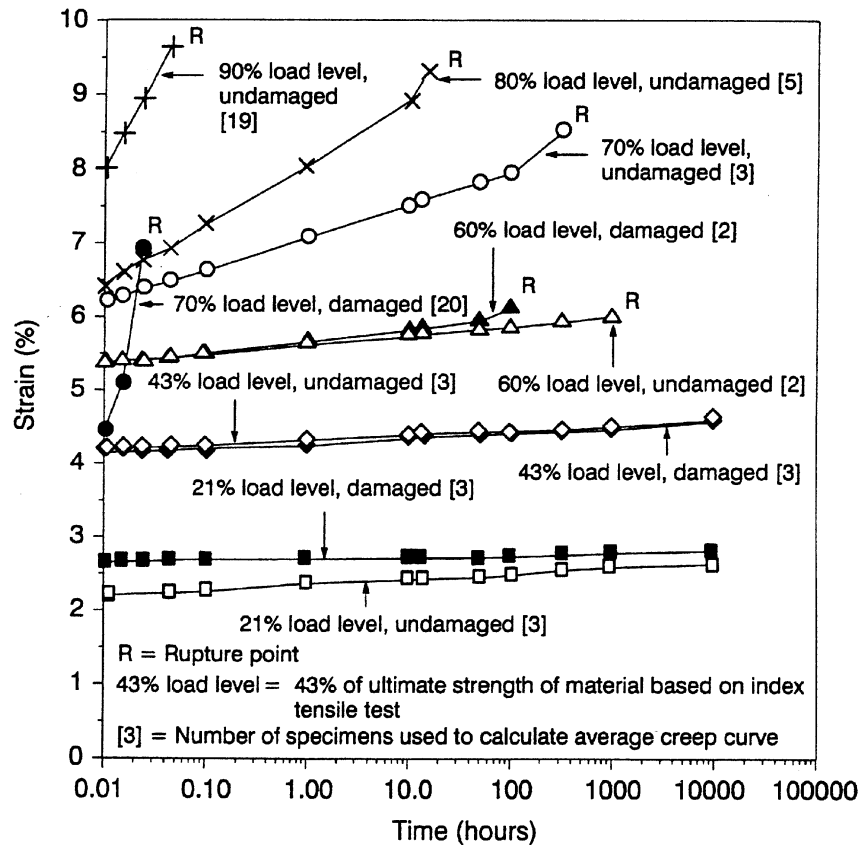
Figure 4.27. Constant load creep curves for undamaged and damaged PET yarns (from Allen and Bathurst 1996).

4.5 Analysis of Laboratory Geosynthetic Modulus Assessment

Geosynthetic modulus trends, as a function of time, have been presented for CRS, creep, and stress relaxation laboratory tests, both in-isolation and in-soil. The next step is to assess which type(s) of test best represents the true modulus of the geosynthetic, both experientially and theoretically, as well as to assess the amount of error that could be incurred if a simpler test were used to determine the modulus.

4.5.1 Effect of Test Type on Geosynthetic Modulus Determination (Laboratory Test Results Analysis)

As mentioned previously, the most accurate laboratory method for simulating how geosynthetic reinforcements are loaded in full-scale structures is to use an in-soil testing device such as the unit cell device developed by Boyle (1995) and Boyle and Holtz (1996). However,

118

this type of test is difficult to run and limits the range of conditions that can be simulated, particularly in terms of maximum strains and time of loading.

The first question that must be asked is whether a simpler in-isolation test can provide an adequate measure of the in-situ modulus of geosynthetic reinforcement. In figures 4.22 and 4.25 the modulus values measured for most times of interest were approximately the same in-soil or in-isolation. Elias et al. (1998b) concluded that soil confinement, without consideration of time effects, will increase the modulus of a geosynthetic if the following is true:

- The fibers/yarns in the geosynthetic are not completely oriented in the direction of loading or

- The tortuosity of the fibers oriented in the direction of loading, as they go over or under the cross-direction fibers/yarns, is significant

    and

- Either the internal friction between fibers is great enough under soil confinement to prevent or significantly reduce fiber/yarn/rib reorientation, or the soil particles can penetrate through the geosynthetic, preventing fiber/yarn reorientation.

If the fibers/yarns/ribs cannot reorient or straighten significantly under tensile load in-isolation, which is the case with most woven geotextiles and all geogrids, soil confinement will have little effect on the in-situ modulus. The average of 10 to 15 percent modulus increase for woven geotextiles and 5 percent or less increase for geogrids observed when under confinement is likely statistically insignificant, given the other sources of variability in the modulus determination. Therefore, in-isolation modulus determinations are probably accurate enough for the purpose of converting strains to loads for most woven geotextiles and all geogrids, without consideration of time effects.

In-isolation modulus values also appear to be adequate even when time effects are considered. Although the soil may tend to restrict creep deformation, soil confinement does not change the visco-elastic or visco-plastic properties of the geosynthetic material. Therefore, if the geosynthetic cannot creep, then it will stress relax instead, as illustrated in figures 4.21 and 4.22. Either way, the modulus is reduced because of time effects. This is why the effect of strain rate on geosynthetic modulus is the same in-soil and in-isolation, as demonstrated in figure 4.24. The question that remains regarding time effects on the modulus in-soil versus in-isolation is whether the effect of being in a stress relaxation mode versus a creep mode is significant to the modulus

119

determination. Furthermore, if the load is applied to the geosynthetic during the construction of the full-scale structure in a fairly continuous manner, is a slow, constant rate of strain test a better simulation of how the geosynthetic is loaded than a creep or stress relaxation test?

With the test data available, the moduli determined with CRS tests for HDPE and PP geogrids were slightly lower than the moduli determined with creep tests at a given time. As shown in Table 4.2, the average ratio of the CRS modulus (J_{crs}) to the creep modulus (J_c) at 100 hours or more was approximately 0.8 to 0.9. Some convergence of the moduli obtained from the two types of tests did occur at longer times, resulting in an average ratio of 0.92, although this trend was not always consistent. This observation of convergence is supported by figures 4.28 and 4.29, which show that at longer times, the strain response tended to be the same whether the load was applied rapidly, slowly, or in steps, for the HDPE geogrids tested. That is, the stress history is partially or fully erased as strain or time dependent molecular rearrangement continues to occur. The figures support the conclusion of Thornton et al. (1997), based on visco-elastic theory, that the creep or relaxation rate becomes independent of the loading ramp rate (i.e., stress history) at greater than 3 to 10 times the loading ramp time.

Table 4.2. Ratio of moduli at a given time and strain from different test methods.

Material Designation	Polymer	At 2% Strain, at 100 hrs		At 2% Strain, at 1000 hrs	
		J_{crs}/J_c	J_r/J_c	J_{crs}/J_c	J_r/J_c
WGT-1	PP	0.82		0.89	
EGG-1	PP	0.84		0.86	
EGG-2	HDPE	0.9		0.93	
EGG-3	PP	0.84		1.0	
WGG-3	PET	1.1		1.1	
EGG-4	PP		1.193		1.3
EGG-5	HDPE		1.07		1.08
EGG-6	HDPE		0.80		0.82
WGG-1	PET		0.74		0.71
WGG-2	PET		0.83		0.89
Average		0.9	0.93	0.96	0.96
COV (%)		12.9	19.4	10.0	23.3

J_{crs} = modulus from CRS test; J_c = modulus from constant load creep test; J_r = modulus from stress relaxation test;; COV = coefficient of variation = (standard deviation of ratio of modulus values/mean of ratio of modulus values) x 100%.

The modulus determined from the CRS test for the PET geogrid in Figure 4.17 was about 10 percent greater than the creep modulus, conflicting with the trend in the difference between creep and CRS tests described above. This exceptional but relatively small difference should not detract from the overwhelming trends reported for the other geosynthetics. However, this does point to the fact that the load-strain response of PET geosynthetics at low load levels can be quite complex and difficult to model.

For stress relaxation versus creep, there are also some differences in the moduli, as shown in Table 4.2. The ratio of the relaxation modulus to the creep modulus varied from 0.7 to 1.3, with an average of about 0.93 at 100 hours to 0.96 at 1,000 hours. Thornton et al. (1997) indicated that the relaxation modulus should be lower than the creep modulus, since during stress relaxation the material will tend to reach equilibrium sooner than during creep. The differences between the creep and relaxation moduli observed in tests conducted by Thornton et al. (1997) were generally on the order of 10 percent or less. Greenwood (1990) also conducted stress relaxation tests, compared the results to creep tests, and found that the difference in the moduli was within approximately 10 percent.
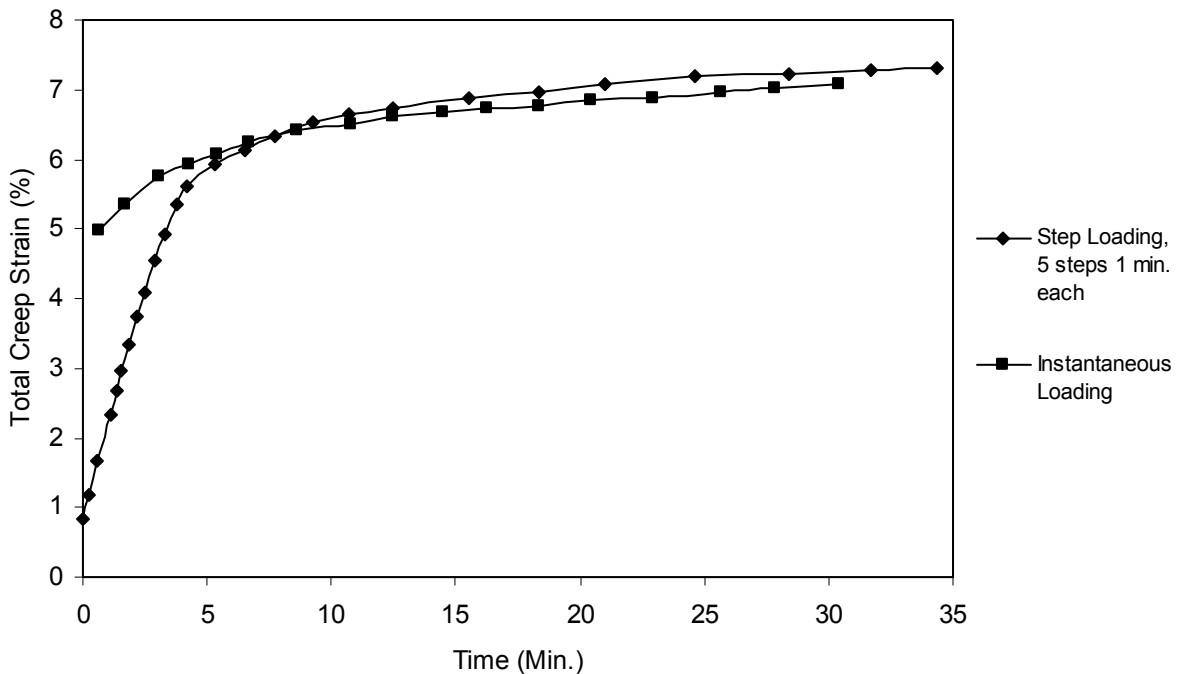
Figure 4.28. Effect of load application rate for polyolefin geogrid creep test (adapted from Yeo 1985).
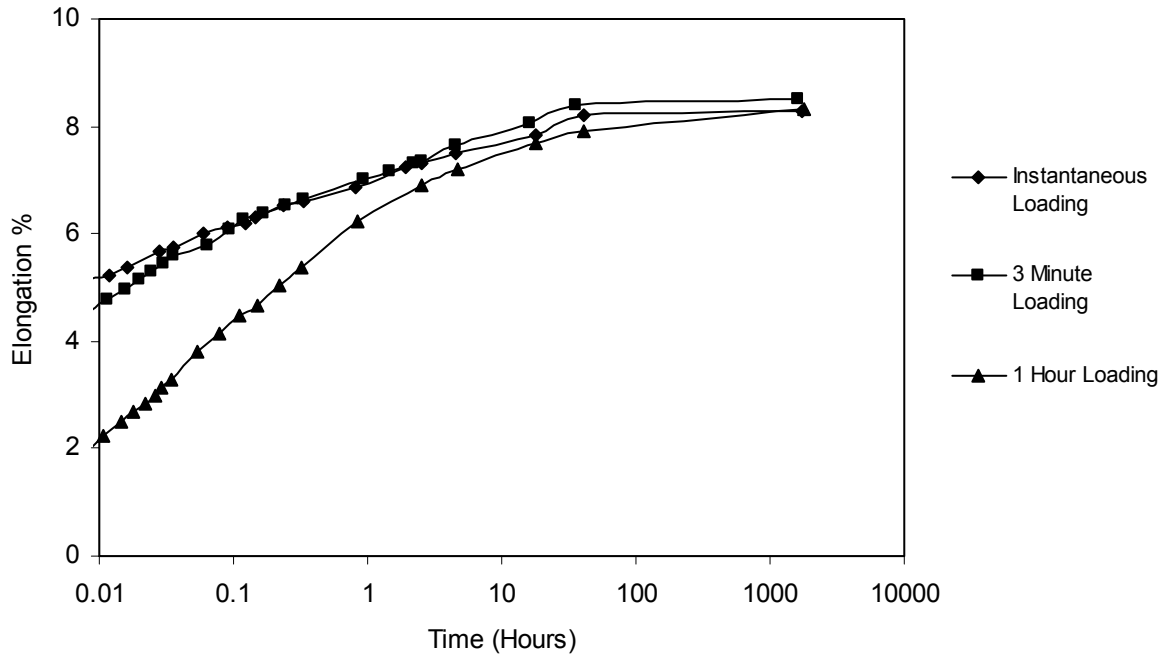
Figure 4.29. Effect of load application rate on creep response of HDPE geogrid (adapted from Rimoldi and Montanelli 1993).

4.5.2 Effect of Test Type on Geosynthetic Modulus Determination (Theoretical Analysis)

A simple rheological model can be used to illustrate the effect of test type on geosynthetic modulus determination. Rheological models offer several advantages related to the ease with which they can be conceptualized and implemented in numerical codes. The simplest model that can simulate the viscoelastic behavior of geosynthetics is the Standard Linear Solid (SLS) Model (Williams 1980). Sawicki (1999) showed that this model is capable of predicting the actual behavior of geosynthetic reinforcement at small strains (i.e., in the linear visco-elastic range).

Figure 4.30a presents a schematic of the SLS model, where T is the load per unit width and ε is the total strain. J_1 represents the modulus of the independent spring and J_2 is the modulus of the second spring, which is placed in parallel with the viscous element with a viscosity of η. The relationship between the viscosity of the viscous element and the modulus of the second spring is referred to as a retardation time τ, where $\tau = \eta/J$.

During a creep or stress relaxation test, the application of a load or strain on the geosynthetic reinforcement will result in an immediate elongation of the test specimen. The simulated response from the model is controlled by only the modulus of the independent spring (J_1), since

the elongation of the second spring is temporarily frozen because of the inability of the viscous element to respond instantaneously to the application of the load or strain. Therefore, at the start of both tests and for a short time thereafter, the modulus of the reinforcement will be approximately equal to J_1, as shown in Figure 4.30b. The slight separation between the curves is shown to aid the reader in following the history of both plots.

The sustained application of the load or the strain will result in the flow of the viscous element and, hence, continuous elongation of the second spring until the system reaches equilibrium. At equilibrium, the modulus of the reinforcement will be a combination of the elongation of both springs. This condition represents the delayed elastic modulus (J_{EQ}) of the model and indicates that at long times the modulus determined from both tests should converge, as shown in Figure 4.30b. The delayed elastic modulus is given by:

$$J_{EQ} = \frac{J_1 J_2}{J_1 + J_2}$$
(Eq. 4.2)

The load-strain-time behavior of the SLS model can be defined by the following differential equation (Williams 1980):

$$\dot{\varepsilon} + \frac{J_2}{\eta} = \frac{J_1 + J_2}{\eta} \frac{T}{J_1} + \frac{\dot{T}}{J_1}$$
(Eq. 4.3)

During a creep test in which the load is constant, $\dot{T}$ becomes 0 and the solution to Equation 4.3 can be rewritten as follows:

$$J_{cr} = \frac{J_1 J_2}{J_1 + J_2} \frac{1}{\left[1 - \frac{J_1}{J_1 + J_2} \exp\left(-\frac{t}{\tau_2}\right)\right]}$$
(Eq. 4.4)

For the stress relaxation test in which $\dot{\varepsilon}$ is 0, the solution to Equation 3 can be rewritten as follows:

$$J_r = \frac{J_1 J_2}{J_1 + J_2} \left[1 + \frac{J_1}{J_2} \exp\left(-\frac{t}{\tau_1}\right)\right]$$
(Eq. 4.5)
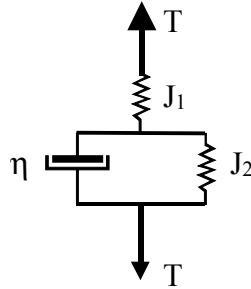
a) Schematic of standard linear solid model
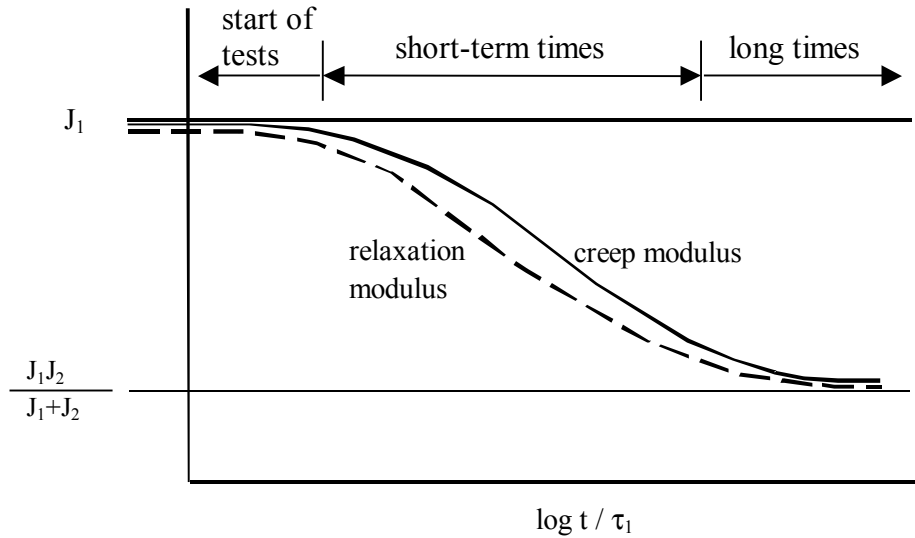
b) Modulus as function of time

Figure 4.30. Creep and relaxation using the Standard Linear Solid (SLS) Model (from Williams 1980).

where retardation times are $\tau_2 = \eta/J_2$ and $\tau_1 = \eta/(J_1+J_2)$.

Using Equations 4.4 and 4.5, Williams (1980) showed that at any time between the commencement of both tests and long times corresponding to equilibrium of the model, the creep modulus is about 10 percent greater than the relaxation modulus. Figure 4.30b shows a schematic of the history of the creep modulus determined from Equation 4.4 and the relaxation modulus determined from Equation 4.5.

In general, the experimental data summarized in this report support this theoretical conclusion. Williams' hypothesis was based on linear visco-elastic theory, in which the loads and strains are very small. This theory provides a plausible explanation for the better match shown between the experimentally determined moduli from both types of tests at lower load

levels. For practical purposes, the creep and relaxation moduli determined for HDPE geosynthetics WGG-5 and WGG-6 may be considered equal, at least at low strain levels. Only two geosynthetics did not behave according to linear visco-elastic theory. One was the very weak biaxial PP geogrid (EGG-4), which had a relaxation modulus that was higher than the creep modulus at low strains. The second was the PET woven geogrids, which tended to have larger differences between the relaxation and creep moduli than would be expected from theory and did not converge consistently at longer times. Note that the same PP biaxial geogrid material as EGG-4 was tested in the current study and found to behave consistently with the theory by Williams (1980). The apparent deviation in the behavior of EGG-4 from William's theory could be due to the large extrapolation required to extend the creep data down to strains of 2 percent, so that the 2 percent creep modulus could be determined, or could possibly be due to some differences in the test protocol used by the two research groups.

The other modulus of interest is that determined from the CRS test. By integrating the relaxation modulus using the convolution integral approach, McCrum et al. (1988) showed that the load at time t in the test is as follows:

$$T(t) = \varepsilon(t)\bar{J}(t) \tag{Eq.4.4}$$

where $\bar{J}(t)$ is the mean value of the modulus averaged over the interval of time from 0 to t in a stress relaxation test. This expression describes the relaxation of load in a CRS test at longer times, which results in nonlinear stress-strain curves for polymeric materials. Therefore, if the creep modulus is always greater than the relaxation modulus, even at the 2 percent strain level, then the creep modulus should also be greater than the modulus determined from the CRS test.

The theoretical conclusion that the creep modulus is greater (though typically less than 10 percent greater) than the relaxation and CRS moduli holds true for the data presented for the HDPE and PP geosynthetics. The PET geogrids exhibited behavior that was not always consistent with this theoretical conclusion. The differences in the creep, stress relaxation, and CRS behavior observed for the PET geogrids may be the result of the complex nonlinear load-strain behavior of PET at low strains. In most cases, the differences observed for the PET are potentially within the range of variability for the material and may therefore not be significant.

4.5.3 Effect of Test Type and Material Variability on the Reliability of the Geosynthetic Modulus Determination

Biases or errors in the estimate of the modulus may depend on the type of test that is used to characterize the modulus as a function of time, as well as material variability. It is not practical to conduct CRS tests at a strain rate that is slow enough to match conditions in full-scale structures (see Figure 4.1). The experience of the writers suggests that relaxation tests can also be very difficult to conduct. Fortunately, the differences in the moduli obtained from the various test types at the times of interest (100 to 1,000 hours or more) are relatively small. These differences may in fact be statistically insignificant, although theoretically some small differences should be expected as discussed previously. It is also fortunate that the test from which it is easiest to obtain long-term modulus values, the creep test, tends to provide the highest estimate of the long-term modulus, which is conservative for the estimation of reinforcement loads in design. Therefore, bias in the modulus determination due to test type appears to be relatively insignificant.
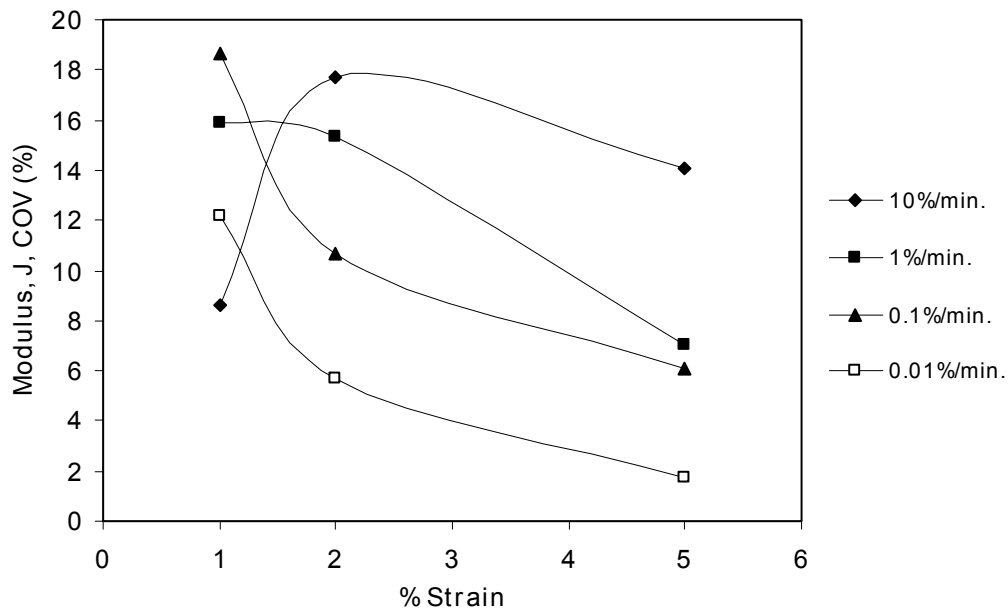
Figure 4.31. Coefficient of variation for moduli at various strains for a woven PP geotextile tested at various strain rates.
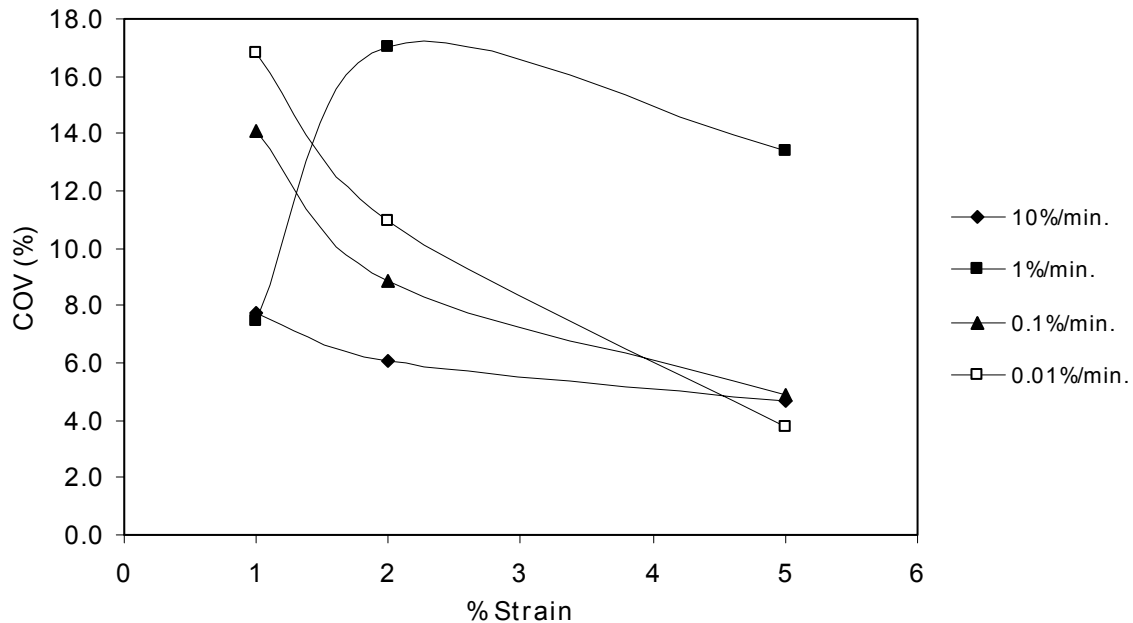
Figure 4.32. Coefficient of variation for moduli at various strains for a woven PET geotextile tested at various strain rates.

Material variability and uncertainty in test interpretation can become a significant issue for the determination of modulus at very low strains. Data obtained by Gallagher (1995) for virgin specimens of geotextiles and summarized in figures 4.31 and 4.32 show a general trend of increasing coefficient of variation (COV) as the modulus is determined at lower and lower strains. However, no trend is apparent in regard to the effect of strain rate or time on the coefficient of variation for the modulus.

Table 4.3. Coefficient of variation of reinforcement modulus at 5 percent strain for various geosynthetics in both virgin and damaged conditions.

Product Type	Condition	10% Strain/min., 5% Modulus COV (%)	% Increase in COV Due to Damage
Geotextile	Virgin	10.3	
	Damaged	15.2	47.6
HDPE Geogrid	Virgin	2.6	
	Damaged	3.1	19.2
PET Geogrid	Virgin	6.4	
	Damaged	7.1	10.9
PP Geogrid	Virgin	8.2	
	Damaged	10.3	25.6

Table 4.3 uses data presented by Allen and Bathurst (1994) on installation damage effects to quantify variability in modulus values caused by installation damage. These data suggest that installation damage increases the COV by a factor of 1.1 to almost 1.5, depending on the type of geosynthetic. Geotextiles showed the largest increases in COV as a result of damage. This table also shows the magnitude of COV values that are typical for different geosynthetics. Geosynthetic modulus variability can be summarized as follows:

- At 5 percent strain, the short-term CRS modulus had a COV of 3 to 10 percent. Calculating the modulus at lower strains, say 2 percent, caused the COV to increase by a factor of approximately 1.7 relative to the COV measured at 5 percent strain. Furthermore, installation damage caused the COV to increase by a factor of 1.2 for geogrids (on average) and 1.5 for woven geotextiles.

- The COV did not appear to consistently be affected by time effects. Therefore, the short-term modulus COV is assumed to be approximately the same as the long-term COV.

These data lead to the conclusion that the COV of the modulus at 2 percent strain, given the effects of significant installation damage and time, can be expected to vary from 5 percent to 18 percent for geogrids to approximately 26 percent for woven geotextiles. If installation damage is light (say, strength losses of less than 20 percent), the COV values will be approximately two-thirds to four-fifths of these values.

4.6 Approach to Determine the Correct Modulus for Converting Strain to Load

The empirical data presented in the earlier sections have shown that, in general, both the relaxation modulus and the CRS modulus are slightly lower than the creep modulus and that the difference is on the order of 5 to 10 percent. Given the arguments presented in the previous sections, a practical approach for calculating the in-soil reinforcement modulus is to use the modulus from in-isolation creep tests, at least for geogrids and woven geotextiles.

If in-isolation creep data are used, the modulus of the geosynthetic can be estimated as follows:

1. Determine the total length of time necessary to complete construction of the wall at a given section (i.e., the time after which no additional loading will occur).

2. Using an in-isolation creep modulus versus time curve, select the creep modulus on the basis of time at the end of wall construction. For most walls, this time is on the order of

128

500 hours to 1,500 hours. For design purposes a modulus at 1,000 hours is likely reasonable. Select the modulus at the anticipated maximum working strains for the wall, as the modulus is likely to be dependent on strain level.

3. Correct the modulus obtained in step 2 for soil confinement effects if the reinforcement is not a geogrid or slit film woven geotextile. For multi-filament woven geotextiles, the modulus may need to be increased by a factor of 1.1 to 1.2. In-soil load-strain tests are highly recommended for nonwoven geotextiles. For preliminary design purposes the creep-based modulus should be increased by a factor of 2 to 5 for nonwoven geotextiles.

For typical geosynthetics in wall applications, the ratio of the modulus value at typical working conditions (i.e., strains on the order of 2 percent and loading times of approximately 1,000 hours) to the modulus in a CRS wide-width test (at 10 percent strain per minute) can be estimated from Table 4.4. The data in the table show that the ASTM D4595 wide-width modulus at 10 percent strain per minute can greatly overestimate the modulus of the material in soil reinforcement applications.

Table 4.4. Ratio of typical working stress modulus (at 1,000 hours) to the modulus obtained in a CRS test at 10 percent/minute, per ASTM D4595.

Geosynthetic Polymer	$J_{1000 \, hrs}/J_{D4595}$
PP	0.25 to 0.35
HDPE	0.25 to 0.35
PET	0.75 to 0.85

4.7 Case Histories in Which Measured Loads Can Be Compared to Measured Strains in Full-Scale Geosynthetic Walls

Direct measurements of both the reinforcement load and strain have been obtained in only one full-scale field case history (a welded wire faced, steep reinforced slope) and in only a few full-scale laboratory geosynthetic walls.

4.7.1 Wall GW7

This "wall" is technically a steep reinforced slope with a facing batter of 2V:1H. Details of this case history are reported in Chapter 2.0. This wall consists of two different reinforcement

sections. Figure 4.33, developed from data provided by Fannin and Hermann (1990), provides a comparison of loads measured by load cells placed directly in the reinforcement layers and loads estimated from the nearest location of a Bison inductance coil strain reading, for both wall sections. Reinforcement moduli of 365 kN/m at 960 hours (end of construction) and 353 kN/m at 2600 hours (surcharge in place) were used to convert strains to load, with long-term creep data (from the manufacturer but not lot specific) for the product used in the wall. This modulus was determined from isochronous creep data at a strain of 2 percent, estimated at a temperature based on soil temperature data of 6° C.

As shown in the figure, the loads estimated from strain gauges with the procedures discussed herein were approximately 10 to 50 percent lower than the loads measured by the load cells for Section J, and about the same for Section N. It should be recognized that loads measured by load cells are not without uncertainty, as is true of any in-situ measurement. Furthermore, load cells may attract additional load as a result of soil-load cell interaction and do not have the ability to creep or relax as does the reinforcement. As soil creep occurs, the load cells tend to gain load, whereas the geosynthetic reinforcement stiffness continues to soften (see Chapter 6.0 for additional discussion on this issue). However, the range of loads predicted from an interpretation of strain readings based on the long-term modulus of the reinforcement is considered to be reasonable, given that the load cell readings are likely over-estimated.

4.7.2 Propped Panel Wall GW14

A propped panel faced geogrid wall built to full scale in the laboratory (maximum height of 3.0 m) was reported by Benjamin (1989). Reinforcement forces were measured directly by load cells at the connection with the facing and by strain gauges and extensometers attached to the reinforcement just beyond the load cells. The distance between the load cells and the strain gauges on the reinforcement was 0.07 m or less. Chapter 2.0 provides a cross section of this wall. Figure 4.34, developed from data provided by Benjamin, compares loads measured by load cells at the facing connection and loads estimated from the nearest location of a strain gauge strain reading. Isochronous creep data were used to determine the modulus on the basis of construction time, duration of surcharging, and the strain level in the reinforcement.
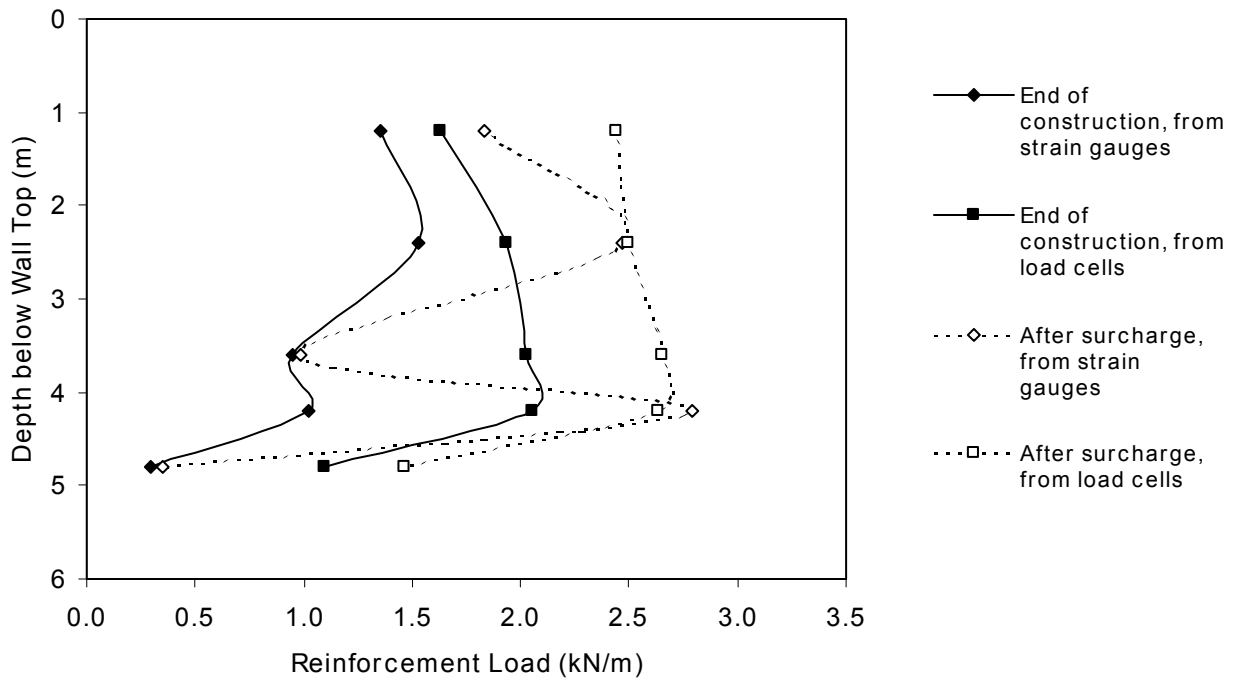
a) Wall Section J
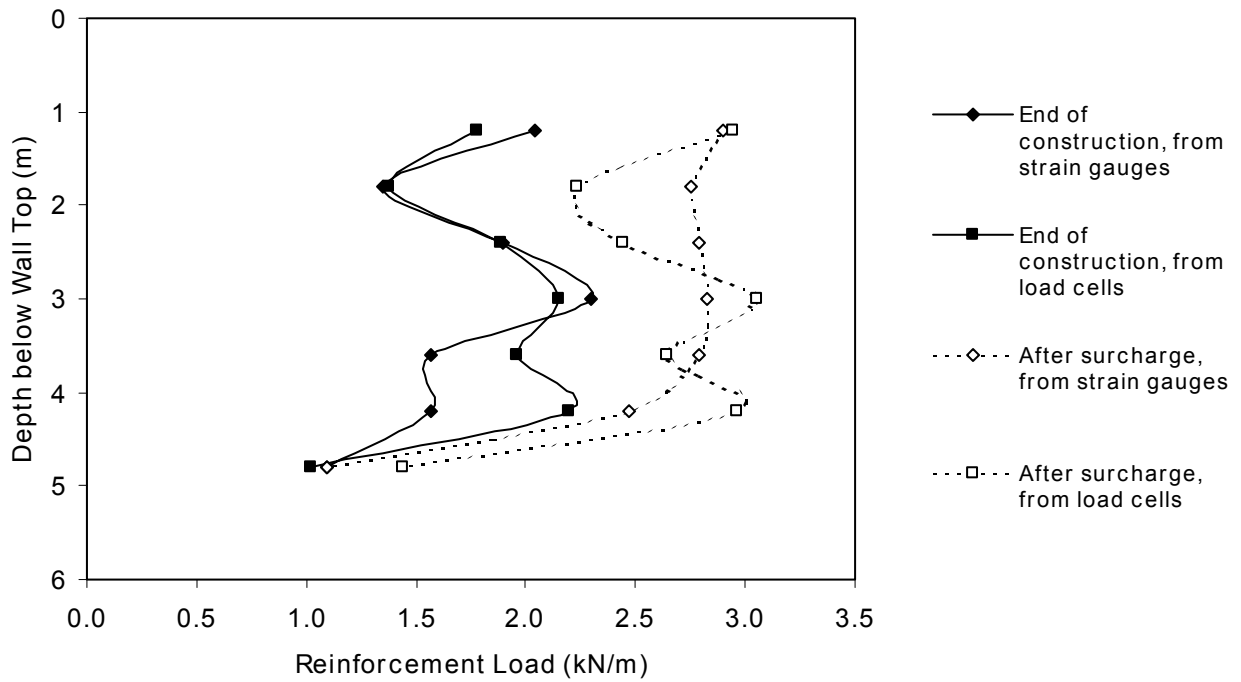
b) Wall Section N

Figure 4.33. Measured reinforcement loads and loads predicted from strain gauge measurements for Wall GW7.

The load levels from the load cells at the connection are slightly lower than those estimated from the strain gauge readings. The high value of the load estimated with the strain gauge in the top reinforcement layer relative to the load measured by the load cell is thought to be due to vertical settlement of the soil directly behind the facing, which can lead to the generation of additional downdrag strains. The strain gauges are able to record additional strains because of changes in the reinforcement out-of-plane geometry, whereas the load cells were configured to record only the in-plane horizontal load in the reinforcement. Notwithstanding the complications noted above, the measured loads and loads estimated from interpretation of reinforcement strains are considered to be in reasonable agreement.
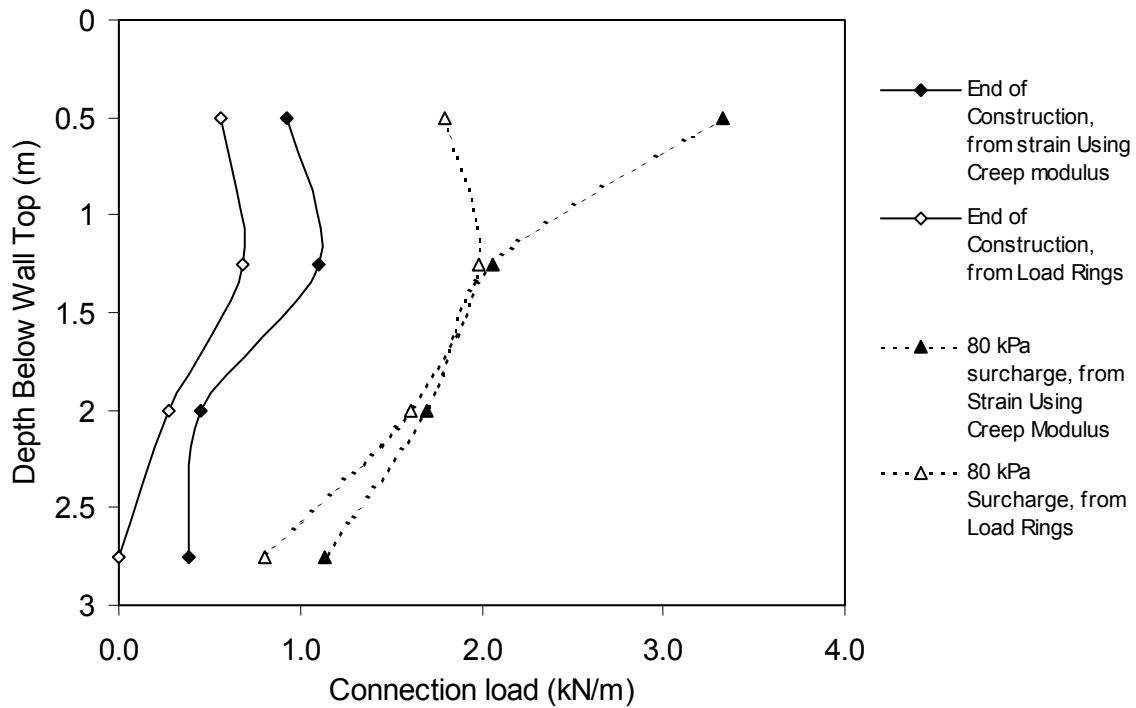
Figure 4.34. Measured reinforcement connection loads and connection loads predicted from strain gauge measurements, for Wall GW14.

4.7.3 RMCC Segmental Block Faced Walls

Three segmental block faced geogrid walls built to full scale in the laboratory (maximum height of 3.6 m) were reported by Burgess (1999), Vlachopoulos (2000) and Bathurst et al. (2000). Reinforcement forces were measured directly by load cells at the connection with the facing and by strain gauges and extensometers attached directly to the reinforcement close to the load cells.

The distance between the load cells and the strain gauges on the reinforcement was 0.13 m or less. Figure 4.35 provides a cross section of Wall 1 as an example of the typical configuration and instrumentation of these test walls. Figures 4.36, and 4.37, developed from data provided by Burgess (1999), and Figure 4.38, developed from data by Vlachopoulos (2000), provide a comparison of loads measured by connection load cells and loads estimated from the nearest location of a strain gauge or extensometer point. Again, isochronous creep data were used to estimate the modulus on the basis of the duration of construction time, surcharging, and measured strains.
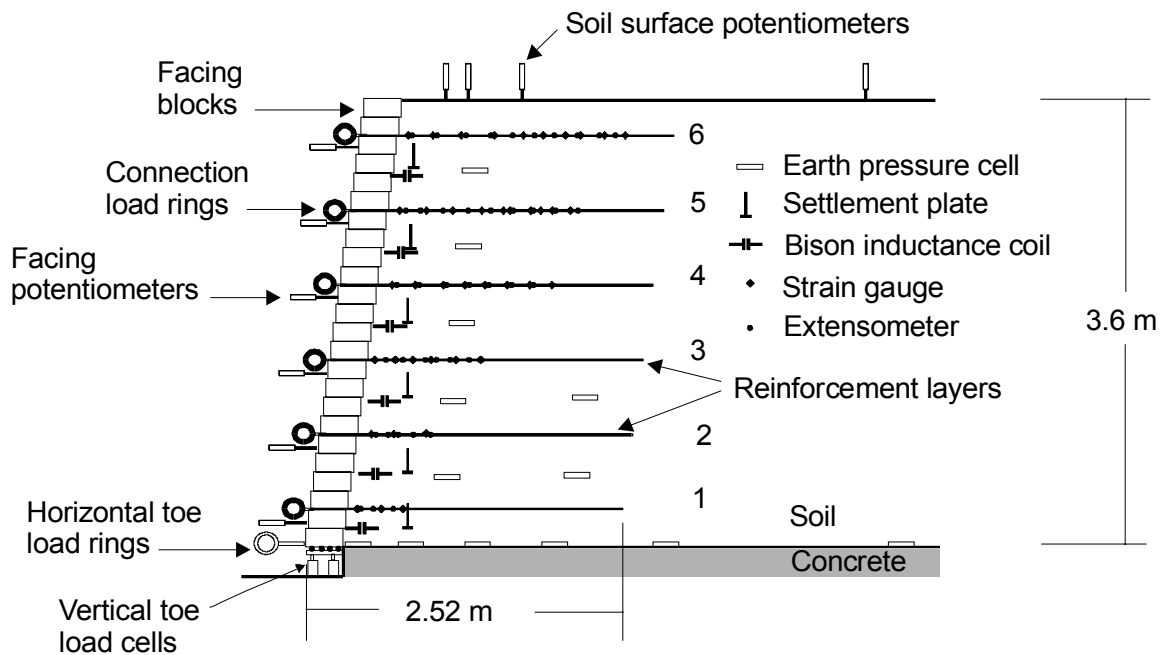
Figure 4.35. Typical cross-section for RMC Walls 1 and 2 (after Bathurst et al. 2000).

133
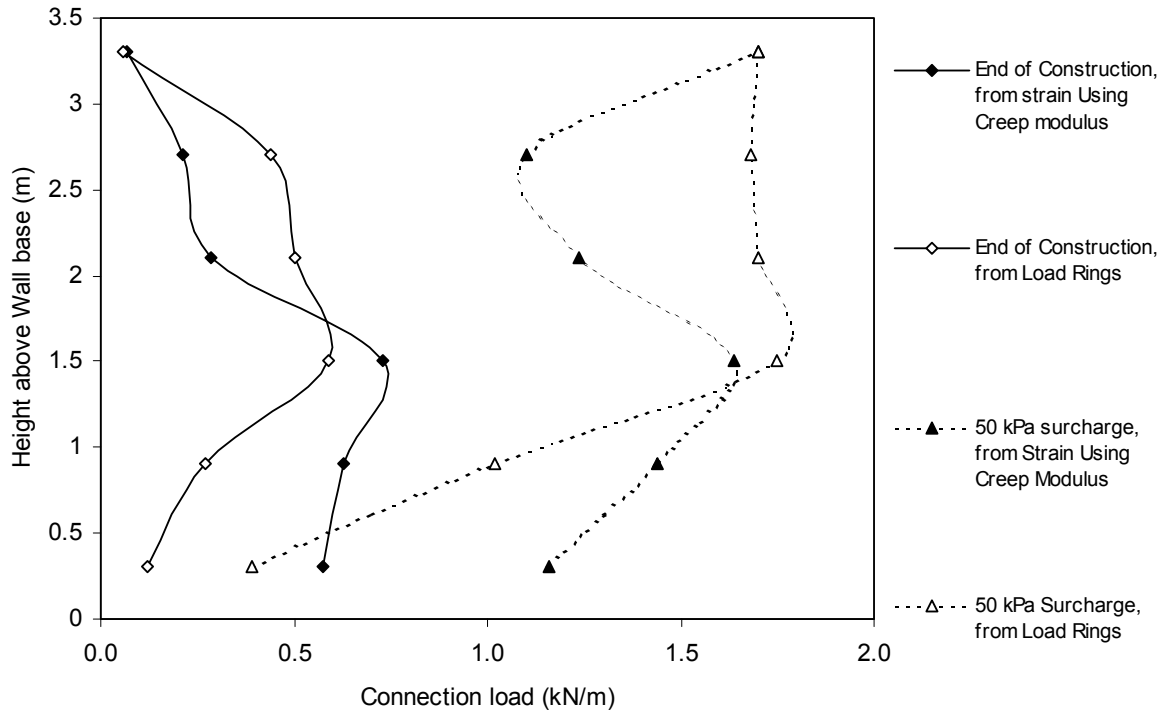
Figure 4.36. Measured reinforcement connection loads and connection loads predicted from strain gauge measurements for RMCC Wall 1.
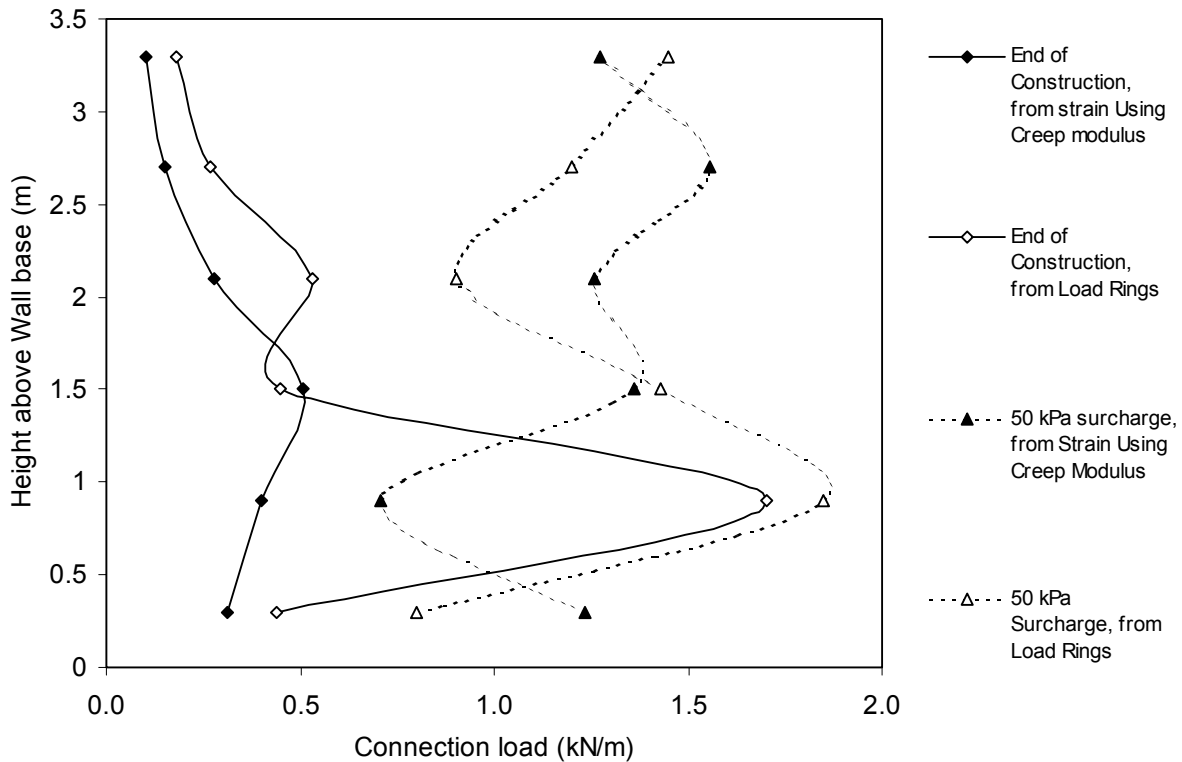
Figure 4.37. Measured reinforcement connection loads and connection loads predicted from strain gauge measurements for RMCC Wall 2.

134
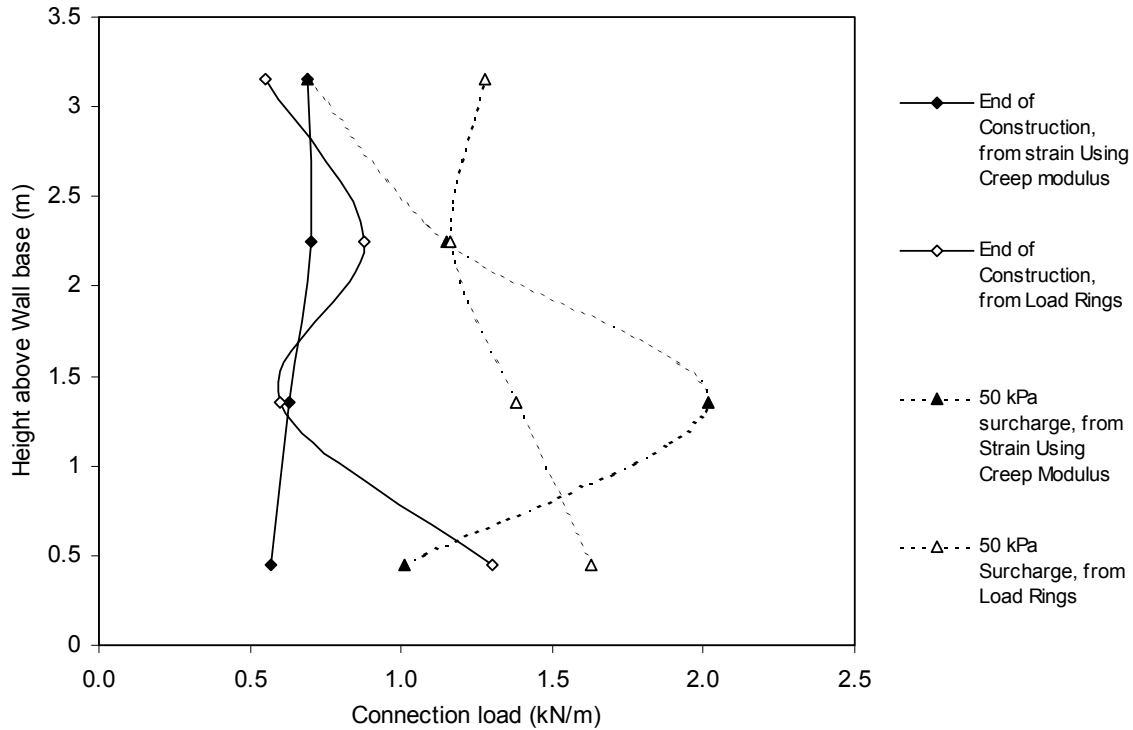
Figure 4.38. Measured reinforcement connection loads and connection loads predicted from strain gauge measurements for RMCC Wall 3.

As shown in the figures, the loads estimated from strain gauges with the procedures described herein were within 10 to 50 percent of the loads measured by the load cells, and they generally overlapped the range of measured loads. Possible sources of local differences in measured loads and loads inferred from strain readings are noted in the previous section. An exception to the generally good agreement are the data for the second from the bottom layer in RMCC Wall 2 (Figure 4.37). Both the strain gauge/extensometer strains converted to load and the load cell readings were well outside of the pattern of load and strain developed at other elevations in the wall. This result may be due to excessive bending of the reinforcement that caused strain gauges bonded to the top of the reinforcement to under-register tensile load in the reinforcement location. At all other layers the measured and inferred loads based on the long-term modulus of the reinforcement are considered to be in reasonable agreement.

4.8 Summary and Conclusions

The primary means of assessing the load level in geosynthetic reinforcement in full-scale geosynthetic walls is to convert reinforcement strain measurements to load through the

reinforcement modulus. Because the geosynthetic modulus is a function of time, and to some extent loading history, the reinforcement modulus must be determined with consideration for the time over which the load is applied. The typical method of obtaining the modulus of a geosynthetic has been to use a short-term index test such as ASTM D4595. However, it has been shown that the loading rate in this test is approximately five orders of magnitude larger than the loading rate of the reinforcement in full-scale walls. This difference in loading rate makes a large difference in the modulus value.

Both stress relaxation and creep can occur in geosynthetic reinforcement embedded in soil in full-scale structures. The loading of the geosynthetic in full-scale walls can be simulated with laboratory tests. Creep, relaxation, and constant rate of strain test results were evaluated and compared to see what effect test type might have on the modulus at a given time and strain level. The evaluation found that although minor differences occur in the results among the various types, they are not large enough to be significant, given the natural variation in the material properties. The subsequent conclusion is that the use of the in-isolation creep stiffness data, determined for the time required to reach the end of wall construction, the reinforcement temperature, and the strain in the reinforcement, is sufficiently accurate for estimating reinforcement loads from strain measurements, at least for geogrids and most woven geotextiles. This assumes that strain measuring devices are properly calibrated. However, for nonwoven geotextiles, the effects of soil confinement are significant, and confined creep tests are necessary to accurately determine the modulus needed for converting strains to load.

The general approach has been validated by using data from carefully instrumented wall case histories in which reinforcement loads were measured directly and compared to reinforcement loads estimated from measured reinforcement strain data.

5.0   SOIL REINFORCEMENT LOADS IN GEOSYNTHETIC REINFORCED MSE WALLS AT WORKING STRESS CONDITIONS

5.1 Introduction

Knowing the load in geosynthetic reinforcements in full-scale mechanically stabilized earth (MSE) walls is an important step toward improving the procedures for designing the internal stability of MSE walls. The internal design of MSE walls is based on the reinforcement load, which helps to assess the reinforcement strength and spacing required, as well as on the length of the reinforcement for pullout design. The study of such empirical reinforcement load data enables analytical models to be properly calibrated, and the empirical data also provide a baseline upon which any new design methods can be compared to assess their accuracy.

In general, loads in MSE wall soil reinforcements must be estimated from strain measurements and converted to load through the modulus of the reinforcement material. Two requirements to estimate reinforcement load are as follows:

1. accurate determination of the strain in the reinforcement that accounts for sources of strain measurement error through proper gauge location, calibration, and redundancy in the measurements

2. accurate determination of the modulus of the reinforcement that accounts for the time dependence of the modulus, the effect of soil confinement, the effect of installation damage, and the various sources of modulus measurement error.

The first issue is addressed in Chapter 3.0, where a summary of measured strains in actual geosynthetic walls and an assessment of the accuracy and reliability of the strain measurements are provided. The second issue is addressed in Chapter 4.0, where a detailed assessment of the time dependence of the modulus of geosynthetics and an assessment of the accuracy and reliability of the modulus values are provided.

The purpose of this chapter is to use the data and principles developed in the previous chapters to determine the "measured" peak loads in the reinforcement layers in several well documented geosynthetic wall case histories. Once the correct reinforcement loads have been determined and summarized, general trends in the data are compared to predictions from current design practice. The scope of this chapter is limited to walls with non-cohesive backfill.

5.2 Geosynthetic Modulus Assessment for Geosynthetic Wall Case Histories

Chapter 4.0 provides a protocol that can be used to determine the best geosynthetic modulus for converting measured strain from strain gauges or extensometers to estimated reinforcement loads. The modulus of geosynthetics is typically time dependent, tending to decrease with the amount of time over which the load is applied. The processes that result in time dependent changes in the modulus may include both creep and stress relaxation in granular soils before soil failure. The soil may restrict the time dependent deformation of the geosynthetic, forcing it to exhibit some stress relaxation. In some respects, the loading of the reinforcement is best simulated by a constant rate of loading or constant rate of strain test, since the load and strain levels within a wall during construction typically increase with the height of the wall. Test results provided in Chapter 4.0 show that the modulus determined from creep tests is not necessarily the same as the modulus obtained from stress relaxation tests or constant rate of strain tests. Fortunately, the differences are not large, especially at the times of interest for assessing the modulus of geosynthetic reinforcement during wall construction. Chapter 4.0 concludes that the use of in-isolation creep data to assess the time dependent modulus of geosynthetic reinforcements in walls is sufficiently accurate for the purpose of converting strains to loads in reinforced walls, given other sources of variability in the geosynthetic material properties, such as the effect of soil confinement, variability in the reinforcement properties, and variability in the strain measurements. Comparison of reinforcement loads determined with this approach to loads measured in the reinforcement directly by load cells for those case histories in which these data were available verifies this conclusion.

Another key parameter that affects the modulus of geosynthetics is the strain level since the load-strain curve, especially for polyolefin geosynthetics, can be very non-linear. Therefore, the correct modulus for determining reinforcement load from strain measurements must account for both the strain level and time.

Key properties and parameters for each of the case histories for which reinforcement loads are determined and analyzed in this chapter are summarized in Table 5.1. Details for each of these case histories, including wall and reinforcement geometry, reinforcement type, soil properties, and construction history, are provided in Chapter 2.0. Using the strain measurements from Chapter 3.0 and the modulus assessment approach provided in Chapter 4.0, the reinforcement loads for each of the wall case histories can be determined.

For each case history, the determination of the recommended modulus is provided in the sections that follow. This determination starts with the wide-width tensile test modulus, comparing it to the modulus from in-isolation creep data at the time corresponding to the end of construction. This value is then adjusted for the average temperature within the wall and any soil confinement and installation damage effects. Note that in most cases, soil confinement effects are minor (nonwoven geotextiles are the exception). The modulus is also adjusted for the strain level as needed, especially if the strain level is greater than 2 percent. For walls in which strains vary widely, and if detailed isochronous creep data are available, the modulus is obtained directly from the isochronous creep curves at the desired time and is adjusted for temperature, installation damage effects, and soil confinement effects as required.

In addition, the reliability and accuracy of the modulus determination is discussed. Because of the complexity of the factors that affect the accuracy of the modulus, a strict statistical determination of the variability in the modulus is not possible. However, the combined potential variation in the modulus caused by factors such as material variability, installation damage effects, lack of lot-specific test data, and time effects can be roughly estimated.

5.2.1 Tanque Verde HDPE Geogrid Wall (GW5)

The long-term modulus for the product used in this wall was determined from 8000 hours of in-isolation creep data and 180 hours of in-isolation CRS data from Yeo (1985). Both types of data produced the same modulus value at 2 percent strain at the times of interest (see Chapter 4.0). The normalized modulus reduction relative to a standard wide width test was approximately 38 percent at 350 hours, the time necessary to construct the wall to full height. The index wide-width modulus (i.e., at 10 percent strain/minute test rate) obtained by Yeo (1985) was 980 kN/m at 2 percent strain, although for this particular product the modulus was relatively constant in the range of 1 to 2percent strain. It is not known whether the data were lot specific for the wall, but they were at least of a similar vintage. The temperature correction factor from Yeo to get the modulus at 27° C relative to 20° C was approximately 0.9. Therefore, the final temperature and time dependent modulus was approximately 34 percent of the wide-width modulus obtained at a strain rate of 10 percent strain/minute. Installation damage was not great enough to cause significant reductions in modulus (Allen and Bathurst 1994; see also Chapter 2.0).

Table 5.1. Summary of properties and parameters used to calculate geosynthetic modulus for each case history.

Wall Case History	Time for Wall Construction (hours)	Wall Temperature (^{o}C)	Depth Range Below Wall Top (m)	Geosynthetic	$J_{2\%}$, kN/m (10%/min. Strain rate, 20° C)	$J_{2\%}$, kN/m (at end of wall construction)	Global Wall Stiffness at End of Wall Construction (kN/m^2)
Tanque Verde HDPE Geogrid Wall (GW5)	350	27° C	All	Tensar SR-2	980	335	720
Oslo, Norway Wall, Sections J and N (GW7)	960 to top of wall, 2600 to surcharge completion	6° C	All	Tensar SR-55	670 at 20° C, 770 at 6° C	363 at EOC, 353 at surcharge completion	368 for Section J, 588 for Section N
Algonquin Tensar Geogrid Wall (GW8)	920	17° C	All	Tensar SR-2	2040	750	984
Algonquin Miragrid Wall (GW9)	920	17° C	All	Miragrid 5T	500	420	551
Algonquin Geotextile Wall (GW10)	8000 for wall construction, then 10 hours to remove water supporting bottom part of wall face	17° C	All	Quline 160	175 confined in soil	Approximately 175	208
RMCC Geogrid Wrapped Face Wall (GW11)	65	20° C	All	Tensar SS2, weak direction	430	105	147
RMCC Full Height Plywood Panel Faced Wall (GW12)	100 hrs after prop release	20° C	All	Tensar SR-2	980	540 at EOC, 450 at surcharge completion	720 at EOC, 600 at surcharge completion
RMCC Incremental Plywood Panel Faced Wall (GW13)	220	20° C	All	Tensar SR-2	980	490 at EOC, 450 at surcharge completion	653 at EOC, 600 at surcharge completion
RMCC Full Height (GW14) Aluminium Panel and Incremental Panel (GW15) Faced Wall	200 hours for incremental panel wall, 100 hrs	20° C	All	Tensar SS1, weak direction	250	87 to 93 at EOC, 45 to 90 at end of surcharging	120 at EOC, 81 to 86 at end of surcharging
Rainier Ave. Wall (GW16)	1650	14° C	0 to 3.1	GTF 200	206	90	1087
			3.2 to 6.5	GTF 375	408	174	
			6.6 to 9.6	GTF 500	713	311	
			9.7 to 12.5	GTF 1225T	1407	1126	

Table 5.1. Continued.

Wall Case History	Time for Wall Construction (hours)	Wall Temper-ature (^{o}C)	Depth Range Below Wall Top (m)	Geosynthetic	$J_{2\%}$, kN/m (10%/min. Strain rate, 20° C)	$J_{2\%}$, kN/m (at end of wall construction)	Global Wall Stiffness at End of Wall Construction (kN/m^2)
Fredericton, New Brunswick Wall (GW18)	100 hrs after prop release	10° C	All	Tensar SR-2	980	500	738
St Remy PET Strip Test Wall (GW19)	Estimate 500 to 1,000 hours	20° C (assumed)	All	Parweb 2S Strip	9504	7603	9504
Vicenza, Italy HDPE Wall (GW20)	150	20° C (assumed)	All		900	380	285
Vicenza, Italy PP Wall (GW20)	150	20° C (assumed)	All		500	125	94

On the basis of 17 sets of wide-width tensile tests on installation-damaged, high density polyethylene (HDPE) geogrid specimens that are not project specific, the coefficient of variation (COV) was estimated to be approximately 3.1 percent at 5 percent strain, and to increase by a factor of 1.4 on average at a strain of about 2 percent, resulting in a COV of 4.3 percent (see Chapter 4.0). Additional uncertainty is caused by a lack of lot-specific data for the tensile strength and creep. Therefore, the total variance in the modulus may be slightly higher than 4.3 percent, and could be on the order of 5 to 6 percent.

5.2.2 *Oslo, Norway, Geogrid Steep Slope (GW7)*

Geogrid 1000-hour creep data supplied by the manufacturer (probably not lot specific to the wall) were used (Fannin 1991) in this investigation. The wide width modulus at 2 percent strain, 20° C, and a strain rate of 2 percent/minute was 565 kN/m. Given the results of Yeo (1985) for a similar HDPE geogrid, correcting this wide-width modulus to the ASTM D4595 strain rate of 10 percent/minute yielded 670 kN/m. The temperature correction factor from Yeo to get the modulus at 6° C relative to 20° C was approximately 1.14. This resulted in a wide-width modulus of 770 kN/m. The creep modulus at 2 percent strain and 6° C was extrapolated from creep data at 10° C and 20° C, resulting in a modulus of 363 kN/m at 960 hours and 353 kN/m at 2600 hours, which were approximately 54 percent of the wide-width strength at 20° C.

The uncertainty in the modulus would be similar to the uncertainty for the Tanque Verde wall as discussed above (on the order of 5 to 6 percent).

5.2.3 *Algonquin HDPE Geogrid Wall (GW8)*

The long-term modulus for the product used in this wall was determined from 8000 hours of in-isolation creep data and 180 hours of in-isolation CRS data Yeo (1985). Both types of data produced the same modulus value at 2 percent strain at the times of interest (see Chapter 4.0). The normalized modulus reduction relative to the modulus from a standard wide-width test at 2 percent strain was approximately 35 percent at 920 hours. The wide-width modulus of 2040 kN/m was obtained from lot-specific specimens at what was assumed to be 2 percent strain (Christopher 1993), although for this particular product, the modulus was relatively constant in the range of 1 to 5 percent strain. The temperature correction factor for this HDPE geogrid product from Yeo (1985) to get the modulus at 17° C relative to 20° C was approximately 1.05.

The uncertainty in the modulus was considered to be similar to the uncertainty for the Tanque Verde wall as discussed above (on the order of 5 to 6 percent).

5.2.4 *Algonquin PET Geogrid Modular Block Wall (GW9)*

The long-term modulus for the PET geogrid used in this wall was determined from 2000 hours of in-isolation creep data from the same lot of material used in the wall, log-linearly interpolated to 920 hours from Bathurst et al. (1993). These data were normalized with lot-specific, wide-width modulus data to determine the modulus reduction at 4 percent strain (multiple load levels were not available at lower strains). This approach resulted in a "long-term" modulus that was 84 percent of the wide-width modulus. However, the modulus at 1 percent strain was needed for conversion of strains to load. The final modulus used to convert strains to loads was determined by using 84 percent of the 1 percent strain wide-width modulus from lot specific tests on the PET geogrid used in the wall. From Bathurst et al. (1993), the wide-width modulus at 1 percent strain was 500 kN/m. No temperature correction was required.

On the basis of 40 sets of wide-width tensile tests on installation damaged, acrylic coated PET geogrid specimens that were not project specific, the coefficient of variation (COV) was estimated to be approximately 7.1 percent at 5 percent strain and to increase by a factor of 1.7 on average at a strain of about 2 percent, resulting in a COV of approximately 12 percent (see Chapter 4.0). Since the wide-width modulus and creep modulus were determined from lot-specific tests, no additional uncertainty about the tensile strength is likely.

5.2.5 *Algonquin PET Geotextile Wrapped Face Wall (GW10)*

Only in-isolation, wide-width (ASTM D4595) data and confined wide-width data from zero span (Christopher, et al. 1986) and pullout testing on lot specific material were available. The modulus values at 5 percent strain were approximately 35 kN/m unconfined and 175 kN/m under a soil confining pressure equal to the pressure at the mid-height of the wall (Christopher 1993, 1999). Because the material was a polyester, time dependent modulus reductions would be minimal (approximately 15 percent or less), and because of the approximate nature of the modulus values, no additional reduction was applied. It was assumed that the modulus was approximately linear in the range of 1 to 5 percent strain. The temperature correction for the modulus to reflect a temperature of 17° C was not significant. The reduction in modulus due to

143

installation damage was minor up to peak tensile strength losses of 40 percent, which was the amount of loss estimated to occur at this site (Allen and Bathurst 1994; see also Chapter 2.0). Therefore, no additional reduction in modulus was applied to account for installation damage effects.

On the basis of 13 sets of wide-width tensile tests on installation damaged, PET nonwoven geotextile specimens that were not project specific, the coefficient of variation (COV) was estimated to be approximately 26 percent (see Chapter 4.0). Because the number of specimens tested was very limited and only short-term, significant additional uncertainty is likely. Because of this, the uncertainty could be twice as high as the COV resulting from material variability after installation damage (i.e., on the order of 50 percent).

5.2.6 RMCC Geogrid Wrapped Face Wall (GW11)

Wide-width data for the product used in the wall, but at a strain rate of 2 percent/minute, and confirmation, lot-specific, wide-width testing at a strain rate of 2 percent/minute resulted in a modulus of 360 kN/m from tests reported by Yeo (1985) and 350 kN/m for tests carried out on the lot used in the wall (Bathurst et. al. 1988). On the basis of the Yeo data, the standard wide-width modulus (10 percent strain per minute) was estimated to be 430 kN/m at 2 percent strain. On the basis of 120 hours of CRS data on the product used in the wall and interpreted from data by Yeo (1985), a modulus reduction factor of 0.25 was used to reflect the modulus at the end of wall construction relative to the wide-width test data at 10 percent/minute (this was consistent with data from a similar product reported by Benjamin (1989)). Creep data from Yeo (1985) out to 3000 hours, interpolated to the wall construction time of 65 hours, produced a slightly higher modulus. This was consistent with other available data for PP geogrids, but the difference between the creep and CRS data was small enough to be attributable to specimen variability.

On the basis of 22 sets of wide-width tensile tests on installation-damaged, polypropylene (PP) geogrid specimens that were not project specific, the coefficient of variation (COV) was estimated to be approximately 10.3 percent at 5 percent strain and to increase by a factor of 1.4 on average at a strain of about 2 percent, resulting in a COV of approximately 15 percent (see Chapter 4.0). Because the wide-width modulus was determined from lot-specific tests, no additional uncertainty would be caused by a lack of lot-specific data for the tensile strength; however, some uncertainty was caused by the unavailability of lot-specific slow strain rate CRS

or creep data. Because of this, the total uncertainty was probably a little higher and was estimated to be on the order of 16 to 17 percent.

5.2.7 RMCC Full Height Plywood Panel Face Wall (GW12)

Roll specific samples were used to obtain the short- and long-term properties of the HDPE geogrid used in the wall. The in-isolation modulus at 2 percent strain at a strain rate of 2 percent/minute was 840 kN/m. Given the data by Yeo (1985) for this product, this was equivalent to a wide-width modulus at 10 percent/minute strain rate of 980 kN/m. On the basis of up to 1000 hours of roll specific, in-isolation creep data (Bathurst et. al. 1987), a modulus reduction factor at 100 hours of approximately 0.56 relative to the wide width modulus at a strain rate of 10 percent/minute was used.

On the basis of 17 sets of wide-width tensile tests on installation-damaged, HDPE geogrid specimens that were not project specific, the coefficient of variation (COV) for the modulus at 2 percent strain was estimated to be approximately 4.3 percent, as discussed previously for the Tanque Verde Wall (see Chapter 4.0). Because roll specific tensile and creep test data were used for this wall, this COV value adequately reflects the uncertainty in the modulus for this wall.

5.2.8 RMCC Incremental Plywood Panel Face Wall (GW13)

The assessment of the modulus was similar to that of the full height, plywood panel faced test wall, since the same product was used. However, a modulus reduction factor at 220 hours of 0.53 relative to the wide-width modulus at a strain rate of 10 percent/minute was used.

5.2.9 RMCC Full Height and Incremental Aluminum Panel Face Wall (GW14 and GW15)

Lot-specific, PP geogrid, 1000-hour creep data from Benjamin (1989) were available, as were slow strain rate CRS data from Yeo (1985). Wide-width index test results reported by Benjamin (1989) were very similar to index test results by Yeo (1985), resulting in a wide-width modulus (10 percent strain per minute) of 250 kN/m at 2 percent strain. On the basis of 100 hours of CRS data from Yeo (1985) on the PP geogrid product used in the wall, a modulus reduction factor of 0.25 was used to account for wall construction time at this strain. The lot-specific, 1000-hour creep data (Benjamin 1989) produced a slightly higher modulus, which was consistent with other available data (see Chapter 4.0, for a plot comparing creep and CRS data). The moduli from the two different types of tests were close enough in magnitude that the

145

difference could be attributed to specimen variability. Note that the modulus decreased very little for times longer than 100 hours in this case. Also note that the modulus for this geogrid was highly dependent on the strain level, especially once strains exceeded 2 percent. Isochronous creep curves were used to adjust the modulus for the strain level.

On the basis of 22 sets of wide-width tensile tests on installation-damaged, PP geogrid specimens that were not project specific, the coefficient of variation (COV) for the modulus at 2 percent strain was estimated to be approximately 15 percent, as discussed previously for the RMCC Geogrid Wrapped Face Test Wall. Because lot-specific tensile and creep test data were used for this wall, the COV value adequately reflects the uncertainty in the modulus for this wall.

5.2.10 Rainier Avenue Geotextile Wrapped Face Wall (GW16)

Approximately 70 hours of in-soil creep/relaxation data, 70 hours of in-isolation creep data, and 2 hours of in-isolation CRS data from the same roll of one of the PP woven geotextiles used in the wall were available. These data were log-linearly extrapolated to 1650 hours to allow the modulus at the end of wall construction to be estimated. Modulus values were calculated at a strain of 1 percent since there was not enough data available at 2 percent strain. Note that the in-isolation creep modulus was higher than in-soil creep-relaxation modulus, especially at short times, whereas the in-soil creep-relaxation modulus was about the same as the in-isolation CRS modulus (see Chapter 4.0). At longer times, all these modulus values converged. In-isolation creep data were limited, and specimen variability may have contributed to the differences observed. The in-soil creep-relaxation modulus was used to convert measured strain to load. These data were normalized with the wide-width modulus (ASTM D4595) and applied to the other PP geotextiles used in the wall. The other two PP geotextiles only differed from the one tested regarding the number of stitch-bonded layers. This resulted in using 40 percent of the 1 percent strain modulus ($J_{1\%}$) from standard wide-width tests for all three woven PP geotextiles used in the wall to convert strains to load. For the woven PET geotextile used in the wall, only 2 hours of in-isolation CRS data were available (Boyle et al. 1996; Boyle and Holtz 1996; see also Chapter 4.0). Application of these data, as well as general knowledge of PET creep behavior, resulted in use of 80 percent of the 2 percent strain modulus ($J_{2\%}$) from a standard wide-width test. Wide-width tests were conducted on material taken from the wall. To correct 20° C data to 14° C values, the 20° C PP geotextile data were multiplied by 1.09 on the basis of data reported

by Yeo (1985) for PP geogrids, but the PET geotextile modulus was not affected significantly by the temperature and was therefore not corrected for temperature.

Given the results of wide-width tensile tests on installation-damaged, PP geotextile specimens taken from the wall, the coefficient of variation (COV) was approximately 18 percent. Since long-term modulus data were obtained for roll specific specimens tested under in-soil conditions, no additional uncertainty resulted from the test method and source of the material tested. However, considerable extrapolation was required, resulting in an additional 7 percent potential variance, as recommended in the WSDOT (1998) creep extrapolation protocol. Therefore, the total potential variance in the modulus was estimated to be 25 percent.

5.2.11 Fredericton Propped Panel Geogrid Wall (GW18)

The long-term modulus for the product used in this wall was based on data reported by Yeo (1985) comprising 8000 hours of in-isolation creep data and 180 hours of in-isolation CRS data. Both types of data produced the same modulus value at 2 percent strain at the times of interest (see Chapter 4.0). The normalized modulus reduction relative to a standard wide-width test was approximately 45 percent at 100 hours, the time necessary to construct the wall to full height. The 10 percent strain/minute wide-width modulus of 980 kN/m was also obtained from the Yeo data at 2 percent strain, although for this particular product, the modulus was relatively constant in the range of 1 to 2 percent strain. The temperature correction factor from Yeo (1985) to get the modulus at 10° C relative to 20° C was approximately 1.14 for the product used in the wall. Therefore, the final temperature and time dependent modulus was approximately 51 percent of the 10 percent/minute wide-width modulus. Installation damage was not great enough to cause significant reductions in modulus (Allen and Bathurst 1994; see also Chapter 2.0).

The uncertainty in the modulus value of the HDPE geogrid used in this wall was similar to that for the Tanque Verde Wall (5 to 6 percent).

5.2.12 St. Remy PET Strap Wall (GW19)

Isochronous creep data for the reinforcement reported by Schlosser et al. (1993) were used. "Instantaneous" tensile test results indicated a modulus of 9,504 kN/m. It was not clear whether these data were lot specific. For an estimated 500- to 1,000-hour wall construction time, the typical modulus reduction for polyester (PET) l is approximately 80 percent of the short-term

tensile test modulus. The isochronous data indicated a larger drop in the modulus for that period of time, and the reduction could be as low as 60 percent of the original short-term modulus from the tensile test. The data on this issue from Schlosser et al. (1993) were not clear enough to be sure on this point, and a modulus reduction factor of 80 percent was used to conservatively estimate the modulus at the end of wall construction and to correct the reported loads. (The loads were determined from the measured strains by using the instantaneous, short-term modulus, as reported by Schlosser et al. (1993). The modulus used to convert strains to loads was considered to be an upper bound value.

5.2.13 Vicenza, Italy, HDPE Wall (GW20)

The wide-width modulus at 2 percent strain, based on lot-specific tensile test data, was approximately 900 kN/m for the HDPE geogrid, with an ultimate tensile strength of approximately 58 kN/m (Alberto 1998). Product specific, but not lot-specific, creep data were available for this material (Cazzuffi and Sacchetti 1999). These product specific creep data yielded a modulus of 343 kN/m at 150 hours, although the product tested for creep was weaker (an ultimate strength of 52.7 kN/m) than the lot specific test results indicated. However, given data for similar HDPE geogrids (see Chapter 4.0), the long-term modulus at 150 hours would be approximately 45 percent of the wide-width modulus, resulting in an end-of-construction, lot-specific modulus of 405 kN/m. This would be higher than the modulus obtained from the creep tests on the weaker material. Splitting the difference, a modulus of 380 kN/m was used to convert strains to load.

The uncertainty in the modulus value for the HDPE geogrid used in this wall was similar to that for the Tanque Verde Wall (5 to 6 percent).

5.2.14 Vicenza, Italy, PP Wall (GW20)

On the basis of lot-specific data, the wide-width 2 percent modulus was approximately 500 kN/m for the PP geogrid used in this wall (Alberto 1998). No creep data were available for this material. However, given data from similar PP geogrids (see Chapter 4.0), the long-term modulus at 1,000 hours would be approximately 25 percent of the wide-width modulus. This approach was used here.

On the basis of 22 sets of wide-width tensile tests on installation-damaged, PP geogrid specimens from a similar product, the coefficient of variation (COV) for the modulus at 2 percent strain was estimated to be on the order of 15 percent, as discussed previously for the RMCC Geogrid Wrapped Face Wall. Because the wide-width modulus was determined from lot-specific tests, no additional uncertainty about the tensile strength was likely. However, lot-specific, slow strain rate CRS or creep data were not available. Because of this, the total uncertainty was probably a little higher and was estimated to be on the order of 16 to 17 percent.

5.3 Estimated Reinforcement Loads for Geosynthetic Wall Case Histories

The previous section provided details on how the reinforcement modulus was selected, accounting for factors such as wall construction time, temperature, soil confinement, and installation damage effects. In general, a 2 percent secant modulus was reported in this section. However, the modulus is also strain dependent, and where possible, the modulus was adjusted to reflect the strain level measured in the wall reinforcement to estimate the reinforcement load as accurately as possible.

Uncertainty in the reinforcement loads is the result of uncertainty in both the strain measurements and the modulus determination. An attempt was made in the previous section to estimate the uncertainty in the modulus determination for each wall case history. Attempts were also made in Chapter 3.0 to estimate the reliability and uncertainty in the strain measurements. The accuracy of the strain readings is dependent on the type of instrumentation used. At low strains (i.e., approximately 0.5 to 1 percent strain or less), extensometers generally have marginal accuracy, and strain gauges calibrated in the laboratory to global strain are typically used. Bathurst and Allen (2001) reviewed data by Burgess (1999) that showed that under uniform loading conditions in the direction of the wall length, the variation in the strain measurements from multiple strain gauges near a given point is on the order of 15 percent of the mean measurement for a typical PP geogrid. This variation is the result of variation in the calibration factor to relate strain gauge strain to global strain, as well as of other factors such as gauge bending and local variations in strain. Because this variation was measured in a test wall where conditions were carefully controlled, variation in strain readings might be expected to be greater (possibly almost twice as high – on the order of 25 percent) in full-scale production walls where conditions are not as well controlled. Bathurst and Allen also indicated that for higher strains

where extensometers or other global strain measuring devices are used, the maximum accuracy that can be expected is on the order of ±0.10 to ±0.25 percent strain. For each of the wall case histories, if project specific strain measurement accuracy data were not available, the strain measurement uncertainties reported above were used. Note that in some cases the strain measurement systems were redundant. Redundancy in strain measurement devices can be expected to improve the accuracy of strain measurements (see Chapter 3.0), but this is difficult to quantify.

In one of the case histories (GW 7), inductance coils were used to measure strains rather than strain gauges or extensometers. Sources of error for these devices are discussed in Chapter 3.0, but they are believed to have an accuracy that is similar to that of extensometers.

Uncertainty in strain measurements (COV_1) and modulus values (COV_2) are uncorrelated (i.e., independent). Therefore, total uncertainty in estimated strain readings can be quantified by a coefficient of variation (COV_{total}) value calculated as follows (Ang and Tang 1975):

$$COV_{total} = \sqrt{COV_1^2 + COV_2^2} \qquad\qquad (5.1)$$

The measured strains, estimated uncertainty in the strain, estimated modulus, estimated uncertainty in the modulus, the reinforcement load, and the total estimated uncertainty in the load for each wall case history are summarized in Table 5.2. The strains shown in Table 5.2 represent the highest measured strain in each layer, as reported in Chapter 3.0. In some cases, strains were obtained from more than one strain measurement method (i.e., strain gauges and extensometers). In general, strain gauge readings were used for small reinforcement strains. In some cases, however, as noted in the table and shown in Chapter 3.0, there were significant differences between the extensometer and strain gauge readings. In such cases, a strain level was selected that best reflected readings from both sources. In almost all of those cases, the differences were well within the strain measuring variances mentioned above.

5.4 Analysis of Reinforcement Loads

Once reinforcement loads and their uncertainty have been defined, general trends in the loads can be evaluated. Understanding trends in reinforcement load can be helpful in assessing the accuracy of current methods for designing the internal stability of geosynthetic MSE walls. This understanding can also provide strategies for improving the methods available for

estimating reinforcement loads, as reinforcement load estimation is a key step in all aspects of internal wall stability design.

5.4.1 Current Design Methods for Estimating Reinforcement Loads

Three primary methods can be found in recent North American design codes and design guidelines to estimate loads in geosynthetic reinforced soil walls – a) the Tieback Wedge Method (AASHTO 1996), b) the FHWA Structure Stiffness Method (Christopher et al. 1990), and c) the Simplified Method (AASHTO 1999, Elias et al. 2001). Note that all of these methods are semi-empirical in nature. All three methods produce similar load predictions, with the exception of the Structure Stiffness Method for geogrid reinforced walls. All three methods use limit equilibrium concepts to develop the design model but use working stress observations to adjust the models to fit what has been observed in full-scale structures. Small-scale models taken to failure have also been used to evaluate these design models at true limit equilibrium conditions (e.g., Adib 1988).

5.4.1.1 Tieback Wedge Method

Originally developed by Bell et al. (1975) and the US Forest Service (Steward et al. 1977), the Tieback Wedge Method has been applied mainly to geosynthetic walls and not to steel reinforced MSE wall systems. This method was developed as an adaptation of the earliest work by Lee et al. (1973), which summarized the basis for steel strip reinforced MSE wall design. Reduced-scale laboratory model walls (Bell et al. 1975) were used to validate the model developed by Lee et al., and some early attempts were made to verify design assumptions with full-scale walls (Steward et al. 1977, Bell et al. 1983).

In the Tieback Wedge Method, the wall is assumed for internal design to be flexible. Therefore, the lateral soil stresses behind the reinforced zone have no influence on the vertical stresses within the reinforced wall zone. Vertical stress within the wall is simply equal to γz, where γ is the unit weight of the reinforced soil and z is the depth below the backfill surface. Because the method has been applied primarily to extensible geosynthetic reinforcement, enough deformation is assumed to occur to generate an active state of stress. Hence, the lateral earth pressure coefficient K_a is used to convert vertical stress to lateral stress. Although initially K_o was recommended for use with these walls (Bell et al. 1975), Bell et al. (1983) found that this

was likely too conservative given full-scale wall performance, and K_a was recommended instead. K_a is determined in this method by assuming a horizontal backslope and no wall interface friction in all cases. These assumptions are based on an active zone defined by the Rankine failure plane. The reinforcement is assumed to resist the lateral stress occurring within the wall, with each reinforcement layer designed to resist the lateral stress over a tributary area. The Rankine failure wedge is held in horizontal equilibrium by the reinforcement layers that act as tiebacks.

The maximum tensile load in a reinforcement layer, T_{max} (in units of force per running unit length of wall) is calculated as follows:

$$T_{max} = S_v K_a \left(\gamma \left[z + S \right] + q \right) \tag{5.2}$$

where S_v is the tributary area (assumed equivalent to the vertical spacing of the reinforcement when analyses are carried out per unit length of wall), K_a is the active lateral earth pressure coefficient, γ is the soil unit weight, z is the depth to the reinforcement level relative to the wall top at the wall face, S is the average soil surcharge depth above the wall top, and q is the vertical stress due to traffic surcharge.

5.4.1.2 FHWA Structure Stiffness Method

The Structure Stiffness Method was developed as the result of a major FHWA research project in which a number of full-scale MSE walls were constructed and monitored (Christopher et al. 1990, Christopher 1993). Model walls were also constructed and numerical modelling carried out (Adib 1988). This method is similar to the Tieback Wedge Method, but the lateral earth pressure coefficient is determined as a function of depth below the wall crest, reinforcement type, and global wall stiffness, rather than by using K_a directly. The design methodology is summarized in equations 5.3, 5.4, and 5.5. Note that for geosynthetic walls, K_r is very nearly equal to the Rankine value of K_a for sheet-type reinforcements (geotextiles) and is approximately $1.5K_a$ at the wall crest for geogrid reinforcements, decreasing to approximately K_a at 6 m below the wall top. The maximum load in the reinforcement is expressed as follows:

$$T_{max} = S_v K_r \left(\gamma \left[z + S \right] + q \right) \tag{5.3}$$

where

$$K_r = K_a \left(\Omega_1 \left(1 + 0.4 \frac{S_r}{47880} \right) \left(1 - \frac{z}{6} \right) + \Omega_2 \frac{z}{6} \right) \qquad \text{if } z \le 6 \text{ m} \tag{5.4a}$$

$$K_r = K_a \Omega_2 \qquad \text{if } z > 6 \text{ m} \tag{5.4b}$$

and

$$S_r = \frac{J}{(H/n)} \tag{5.5}$$

Here, K_r = lateral earth pressure coefficient, S_r = global reinforcement stiffness for the wall (i.e., the average reinforcement stiffness over the wall face area), Ω_1 = dimensionless coefficient equal to 1.0 for strip and sheet reinforcements or equal to 1.5 for geogrids and welded wire mats, Ω_2 = dimensionless coefficient equal to 1.0 if $S_r \le$ 47880 kPa (1000 ksf) or $\Omega_2 = \Omega_1$ if $S_r >$ 47880 kPa, J = average reinforcement modulus for the wall (in units of force per running unit length of wall), and H/n = average vertical spacing of the reinforcement, where n = total number of reinforcement layers.

5.4.1.3 Simplified Method

For geosynthetic walls, the design methodology for the Simplified Method (AASHTO 1999) is identical to the Tieback Wedge Method. A distinction can be made between the two methods in that only the former is used for steel reinforcement.

5.4.2 Comparison of "Measured" Reinforcement Loads to Loads Estimated from Current Procedures

A total of 16 geosynthetic wall cases (the same wall with and without a surcharge is considered to be one case) were analyzed (see tables 5.1 and 5.2), and the results were compared to predictions made with current design methodologies. Eleven walls were full-scale field structures, and five were instrumented, full-scale walls built in an in-door laboratory environment. The cases included a variety of wall geometries and facing types, surcharge conditions, and a range of granular backfills. Wall reinforcement included geotextiles and geogrids, a variety of polymers—including PP, HDPE, and PET—strip and continuous

reinforcements, a wide range of index tensile strengths from 12 to 200 kN/m (see Chapter 2.0), and reinforcement stiffness values from 65 to 7,603 kN/m. Reinforcement vertical spacings varied from 0.3 to 1.6 m. Wall facing batter angles varied from 0° (vertical) to 27°, although most of the walls had facing batter angles of 8° or less. Wall heights varied from 3.0 m to 12.6 m, with surcharge heights of up to 5.3 m of soil. Facing types included geosynthetic wrapped-face, welded wire, pre-cast concrete panels, and modular concrete blocks. Measured plane strain peak soil shear strengths varied from 42° to 57°. Although in general it is not possible to make direct comparisons to isolate the effect of a specific variable, most of the conditions that are likely to be encountered in practice were included in these case histories.

Figure 5.1 provides an overall view of how well the Tieback Wedge/Simplified Method predicts reinforcement loads in geosynthetic walls built in the field. The error bars in the figure show the potential variance (± one standard deviation) in the "best estimate of measured" reinforcement loads, given the estimate of variance in strain and reinforcement modulus measurement reported in Section 5.3. Note that plane strain peak soil friction angles and unit weights estimated from measured data were used to estimate loads with the current load prediction methods, which means that there is no conservatism in the reinforcement load predictions as a result of conservatism in the selection of soil parameters (see Chapter 2.0). Figure 5.2 is similar to Figure 5.1 but shows results for full-scale walls built in the laboratory. Table 5.3 summarizes how well the Tieback Wedge/Simplified Method and the FHWA Structure Stiffness Method predict the measured loads with the coefficient of variation of the ratio of predicted to best estimate of measured load. The effects of assuming no wall interface friction, which is the case for the Tieback Wedge/Simplified methods, and of accounting for full wall face interface friction (the Tieback Wedge/Simplified methods modified to use the horizontal component of Coulomb active earth pressure coefficient) can also be observed in Table 5.3. This shows that even accounting for full interface friction, the two methods are generally conservative for design.

Table 5.2. Summary of measured peak strains and loads estimated from those strains, including their uncertainty, for geosynthetic reinforcement in walls.

Wall	Depth Below Wall Top, z (m)	Measured Peak Strain (%)	Estimated Strain COV (%)	Reinforcement Modulus (kN/m)	Estimated Modulus COV (%)	Reinforcement Load (kN/m)	Estimated Total COV for Reinforcement Load (%)
Tanque Verde HDPE Geogrid Wall (GW5)	1.14	0.18	25	335	6	0.59	25.7
	3.28	0.33	25	335	6	1.09	25.7
	4.2	0.25	25	335	6	0.84	25.7
Oslo, Norway, Geogrid Steep Slope, Section J (GW7) (with soil surcharge)	1.2	0.52	38	353	6	1.84	38.5
	2.4	0.7	29	353	6	2.47	29.6
	3.6	0.28	36	353	6	0.99	36.5
	4.2	0.79	32	353	6	2.79	32.6
	4.8	0.1	50	353	6	0.35	50.4
Oslo, Norway, Geogrid Steep Slope, Section N (GW7) (with soil surcharge)	0.6	0.92	27	353	6	3.25	27.7
	1.2	0.82	30	353	6	2.89	30.6
	1.8	0.78	32	353	6	2.75	32.6
	2.4	0.79	32	353	6	2.79	32.6
	3	0.8	31	353	6	2.82	31.6
	3.6	0.79	32	353	6	2.79	32.6
	4.2	0.7	36	353	6	2.47	36.5
	4.8	0.31	31	353	6	1.09	31.6
Algonquin HDPE Geogrid Wall (GW8)	1.2	0.35	25	750	6	2.63	25.7
	2.5	0.71	25	750	6	5.33	25.7
	4.2	0.76	25	750	6	5.7	25.7
	5	0.74	25	750	6	5.55	25.7
	5.7	0.18	25	750	6	1.35	25.7
Algonquin PET Geogrid Wall, no surcharge (GW9)	0.8	*0.20	25	420	12	0.84	27.7
	2.6	*0.45	25	420	12	1.89	27.7
	4	*0.51	25	420	12	2.14	27.7
	5.2	*0.70	25	420	12	2.94	27.7
	5.8	*0.19	25	420	12	0.80	27.7

Table 5.2. Continued.

Wall	Depth Below Wall Top, z (m)	Measured Peak Strain (%)	Estimated Strain COV (%)	Reinforcement Modulus (kN/m)	Estimated Modulus COV (%)	Reinforcement Load (kN/m)	Estimated Total COV for Reinforcement Load (%)
Algonquin PET Geogrid Wall, with surcharge (GW9)	0.8	*0.42	25	420	12	1.76	27.7
	2.6	*0.95	25	420	12	3.99	27.7
	4	*1.10	25	420	12	4.62	27.7
	5.2	*0.95	25	420	12	3.99	27.7
	5.8	*0.25	25	420	12	1.05	27.7
Algonquin Geotextile Wall (GW10)	1.0	+3.0	30	175	50	5.25	58.3
	2.6	+3.0	30	175	50	5.25	58.3
	4.2	2.0	30	175	50	3.5	58.3
	4.9	1.6	30	175	50	2.8	58.3
	5.65	1.1	30	175	50	1.93	58.3
RMCC Geogrid Wrapped Face Wall (GW11)	0.6	1.97	13	105	17	2.07	21.4
	1.35	2.66	13	105	17	2.79	21.4
	2.1	1.25	13	105	17	1.31	21.4
	2.85	0.2	13	105	17	0.21	21.4
RMCC Full Height Plywood Panel Faced Wall (GW12) (no surcharge)	0.5	0.04	13	540	4.3	0.22	13.7
	1.25	0.02	13	540	4.3	0.11	13.7
	2.0	0.02	13	540	4.3	0.10	13.7
	2.75	0.01	13	540	4.3	0.04	13.7
RMCC Full Height Plywood Panel Faced Wall (GW12) (50 kPa surcharge)	0.5	0.50	13	450	4.3	2.25	13.7
	1.25	0.49	13	450	4.3	2.21	13.7
	2.0	0.33	13	450	4.3	1.49	13.7
	2.75	0.22	13	450	4.3	0.99	13.7
RMCC Incremental Plywood Panel Faced Wall (GW13) (no surcharge)	0.5	0.036	13	490	4.3	0.18	13.7
	1.25	0.27	13	490	4.3	1.32	13.7
	2.0	0.32	13	490	4.3	1.57	13.7
	2.75	0.34	13	490	4.3	1.67	13.7

Table 5.2. Continued.

Wall	Depth Below Wall Top, z (m)	Measured Peak Strain (%)	Estimated Strain COV (%)	Reinforcement Modulus (kN/m)	Estimated Modulus COV (%)	Reinforcement Load (kN/m)	Estimated Total COV for Reinforcement Load (%)
RMCC Incremental Plywood Panel Faced Wall (GW13) (50 kPa surcharge)	0.5	0.8	13	450	4.3	3.6	13.7
	1.25	0.79	13	450	4.3	3.56	13.7
	2.0	0.6	13	450	4.3	2.7	13.7
	2.75	0.53	13	450	4.3	2.39	13.7
RMCC Full Height Aluminium Panel (GW14) (no surcharge)	0.5	0.40	13	90	15	0.36	19.8
	1.25	0.34	13	90	15	0.31	19.8
	2.0	0.26	13	90	15	0.23	19.8
	2.75	0.42	13	90	15	0.38	19.8
RMCC Full Height Aluminium Panel (GW14) (80 kPa surcharge)	0.5	2.93	4.3	53.4	10.3	1.67	11.2
	1.25	3.47	4.2	48	10.3	1.34	11.1
	2.0	2.00	11.5	67	15	1.34	18.9
	2.75	1.45	13	73.8	15	1.07	19.8
Incremental Aluminium Panel Faced Wall (GW15) (no surcharge)	0.5	0.18	13	93	15	0.17	19.8
	1.25	0.60	13	89	15	0.53	19.8
	2.0	0.35	13	87	15	0.30	19.8
	2.75	0.45	13	90	15	0.41	19.8
Incremental Aluminium Panel Faced Wall (GW15) (70 kPa surcharge)	0.5	4.0	6.6	45	10.3	1.80	12.2
	1.25	4.15	6.1	45	10.3	1.87	12.0
	2.0	1.20	6.9	80	10.3	0.96	12.4
	2.75	0.42	13	90	15	0.38	19.8
Rainier Ave. Wall (GW16) (no surcharge)	3.1	1.14	30	90	25	1.03	39.1
	6.5	0.92	30	174	25	1.6	39.1
	9.6	0.84	30	311	25	2.61	39.1
	11.5	0.52	30	1126	25	5.86	39.1
Rainier Ave. Wall (GW16) (with soil surcharge)	3.1	1.5	30	90	25	1.35	39.1
	6.5	1.06	30	174	25	1.84	39.1
	9.6	1.06	30	311	25	3.3	39.1
	11.5	0.62	30	1126	25	6.98	39.1
Fredericton, New Brunswick, Wall (GW18)	2.44	0.43	25	500	6	2.15	25.7
	4.88	0.5	25	500	6	2.5	25.7

Table 5.2. Continued.

Wall	Depth Below Wall Top, z (m)	Measured Peak Strain (%)	Estimated Strain COV (%)	Reinforcement Modulus (kN/m)	Estimated Modulus COV (%)	Reinforcement Load (kN/m)	Estimated Total COV for Reinforcement Load (%)
St Remy PET Strip Test Wall (GW19)	0.4			7603	20	3.09	20.0
	1.2			7603	20	7.66	20.0
	2			7603	20	9.35	20.0
	2.8			7603	20	11.14	20.0
	3.6			7603	20	11.44	20.0
	4.4			7603	20	12.74	20.0
	5.2			7603	20	13.34	20.0
	6			7603	20	6.17	20.0
Vicenza, Italy, HDPE Wall (GW20)	1.1	0.91	25	380	6	3.46	25.7
	2.7	1.49	25	380	6	5.66	25.7
Vicenza, Italy, PP Wall (GW20)	1.6	3.13	25	125	17	3.91	30.2
	3.2	2.02	25	125	17	2.53	30.2

*Based on extensometer and calibrated strain gauge readings.

+Gauges failed at this strain. Therefore, it is possible that the true strains are greater for this loading condition.

COV = coefficient of variation = (standard deviation of values/mean of values) x 100%

These graphics show that the loads estimated with the various prediction methods are quite conservative in relation to the "measured" loads, despite the potential variance in those loads, with the exception of a few specific walls. For example, the reinforcement loads in Wall GW7 (Section N) and Wall GW19 were under-predicted by the Tieback Wedge and Simplified methods, and Wall GW10 loads were under-predicted near the top of the wall where loads are expected to be lower, and significantly over-predicted near the bottom of the wall where loads are expected to be higher. However, the unusual features of these particular walls may shed some light on why they did not behave like the majority of the walls regarding reinforcement loads. For example, the face of Wall GW7 was heavily battered and may be classified as a reinforced slope. Wall GW19 is the only wall reinforced with PET strips rather than continuous sheets. Wall GW10 is the only wall reported here that was reinforced with a nonwoven geotextile and was so lightly reinforced in terms of reinforcement stiffness and vertical spacing that strains were quite high. Soil cracking was observed in the wall along with measured high strain values consistent with incipient soil failure (Christopher 1993). There is also large uncertainty in the Wall GW10 reinforcement loads, as depicted by the rather large error bars.
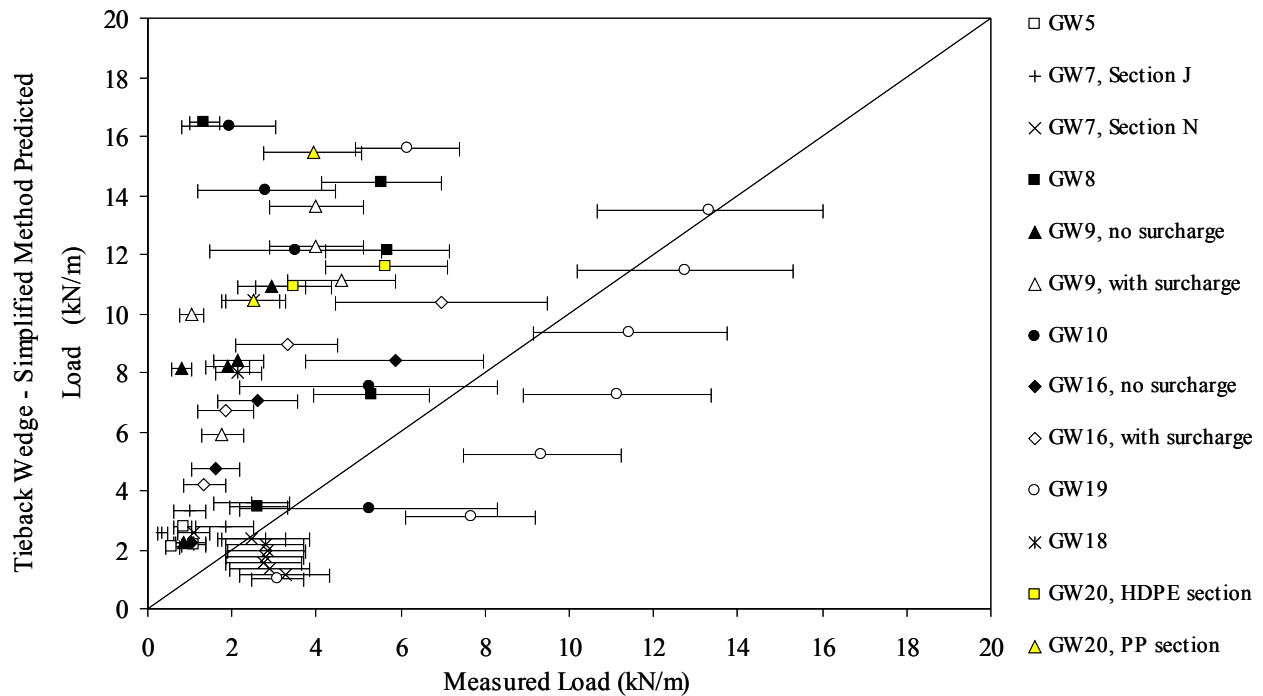
Figure 5.1. Measured reinforcement loads for full-scale field geosynthetic walls versus loads predicted with the Tieback Wedge/Simplified methods. Note: Error bars represent best estimate of measured load ± 1 standard deviation.
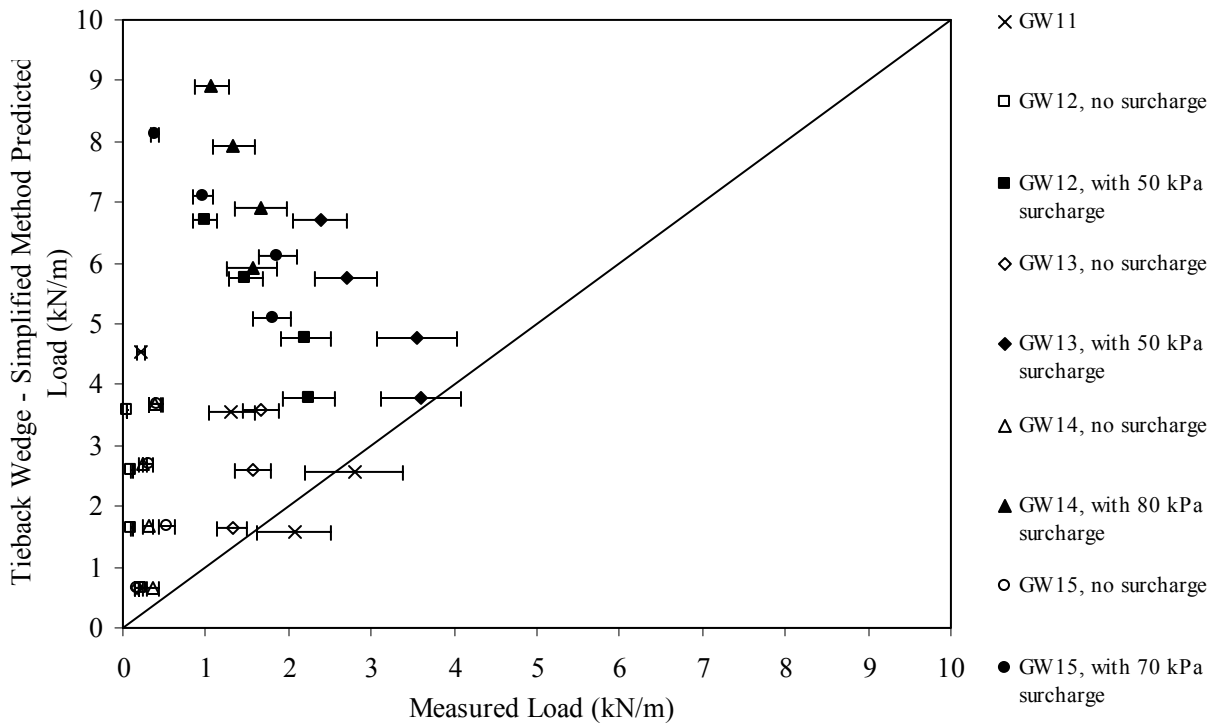
Figure 5.2. Measured reinforcement loads for full-scale laboratory RMCC geosynthetic walls versus loads predicted with the Tieback Wedge/Simplified methods.

There is also a tremendous amount of scatter in the predicted loads, and overall, the correlation of measured values to those predicted with current design methodology is poor. A comparison plot for the FHWA Structure Stiffness method results versus measured results is not presented here for brevity, but the visual impression of the data is the same as in figures 5.1 and 5.2. However, Table 5.3 shows that the FHWA Structure Stiffness method is more conservative (for design) than the Tieback Wedge and Simplified methods and therefore offers no significant advantage, at least for geosynthetic walls.

Note that Table 5.3 shows that the measured reinforcement loads from full-scale laboratory walls deviate even more from predicted loads than do the results for full-scale field walls. The boundary conditions in the test walls, in particular the combination of facing stiffness and degree of toe restraint, appear to have much to do with the poorer match to the predictions from the Tieback Wedge/Simplified methods. The influence of the restrained toe in these laboratory tests is more pronounced for short walls (3 m high) than for the hard-faced walls in the field case histories (typically 4 m or higher). Although detailed analytical modelling can address these boundary issues and extend the test wall data to typical field walls, such modelling is beyond the

Table 5.3. Summary of the ratio of predicted to best estimate of measured reinforcement load for geosynthetic walls.

Prediction Method	Data Subset	No. of Data Points	Average Value of Ratio: Predicted/Measured Reinforcement Load	COV of Ratio (%)
Simplified/Tieback Wedge	All full-scale field walls	58	2.89	85.9
	All RMCC full-scale lab walls prior to 1990 which had full toe restraint and/or stiff facing	16	11.8	169.6
	RMCC full-scale lab walls prior to 1990 which had minimal wall facing stiffness/toe restraint	12	4.0	145.2
	RMCC lab walls prior to 1990 with toe restraint, near failure	8	7.1	85.7
FHWA Structure Stiffness	All full-scale field walls	58	3.3	80.6
	All RMCC full-scale lab walls prior to 1990 which had full toe restraint and/or stiff facing	16	15.6	163.9
	RMCC full-scale lab walls prior to 1990 which had minimal wall facing stiffness/toe restraint	12	5.2	139.4
	RMCC lab walls prior to 1990 with toe restraint, near failure	8	9.5	80.3
Simplified/Tieback Wedge, but using Coulomb K_a and full interface friction	All full-scale field walls	58	2.2	84.6
	All RMCC full-scale lab walls prior to 1990 which had full toe restraint and/or stiff facing	16	8.4	169.6
	RMCC full-scale lab walls prior to 1990 which had minimal wall facing stiffness/toe restraint	12	2.8	145.2
	RMCC lab walls prior to 1990 with toe restraint, near failure	8	5.1	85.7

scope of this report. The full-scale laboratory test wall data are presented here to demonstrate the general effect of certain variables on the behavior of geosynthetic walls (e.g., wall toe restraint, facing type, etc.) that cannot be easily isolated in the full-scale field wall data.

The combined effect of toe restraint and facing stiffness can be observed in figures 5.3 and 5.4. For all of these test walls, except wall GW11, and to some extent GW12 and GW13, the facing at the wall toe was pinned and prevented from moving in vertical and horizontal directions. Wall GW11 had a very flexible face and very extensible reinforcement. Walls GW12 and GW13 had a moderately flexible plywood panel facing combined with relatively stiff soil reinforcement (although during wall construction the Wall GW12 facing was fully restrained with props, in effect making the facing behave as if it were very stiff). Walls GW14 and GW15 had a relatively stiff aluminium facing combined with very extensible soil reinforcement. Note for Wall GW12 that the wall facing was free to move during the surcharge loading period following prop release, resulting in reinforcement loads that were similar in magnitude to Wall GW13 (see Figure 5.2). Figures 5.3 and 5.4 show that the combined effect of increasing facing stiffness and greater toe restraint, especially for relatively extensible soil reinforcement, do significantly reduce the loads in the reinforcement layers.
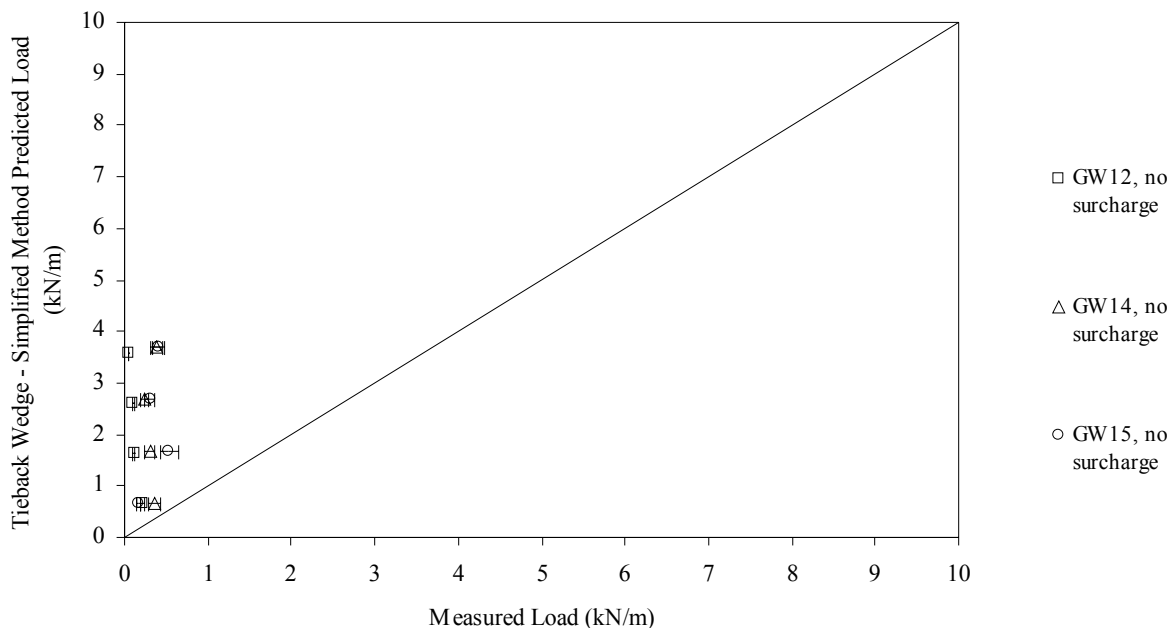
Figure 5.3. Predicted versus measured reinforcement load for full-scale laboratory RMCC geosynthetic walls with high toe restraint and/or facing stiffness.

162
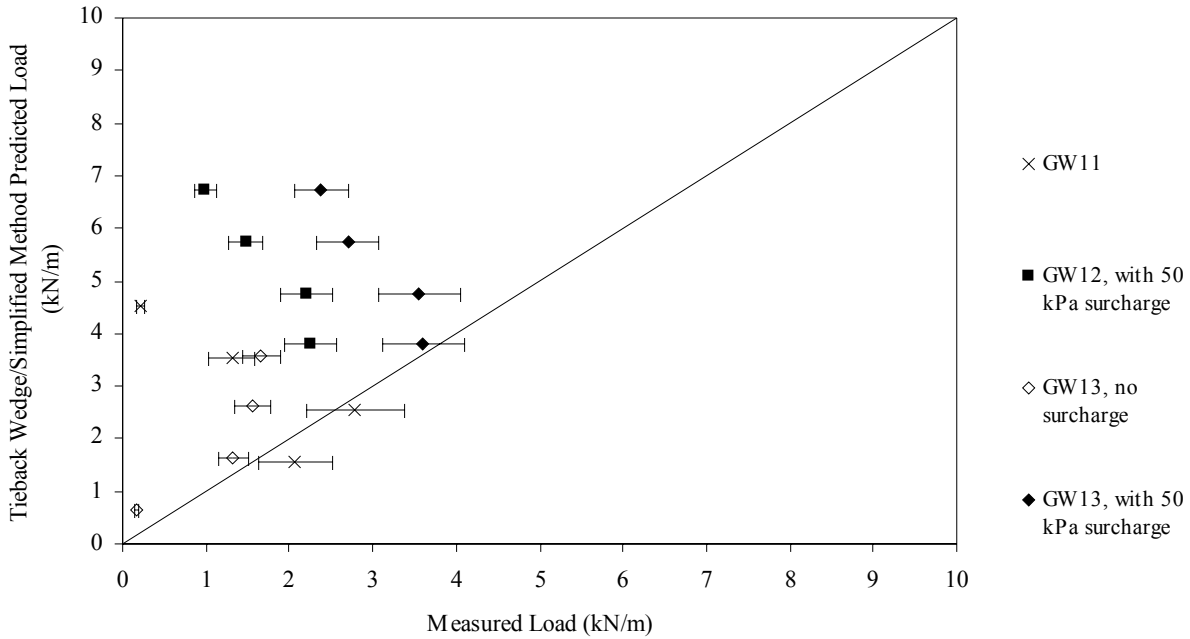
Figure 5.4. Predicted versus measured reinforcement load for full-scale laboratory RMCC geosynthetic walls with low toe restraint and/or facing stiffness.

The uniform surcharge loading of these laboratory test walls was carried out to generate catastrophic failure of the soil-geosynthetic system to effectively achieve limit equilibrium conditions. For walls GW14 and GW15 under surcharge loading, the reinforcement strains were high enough (on the order of 4 percent or more) to allow soil failure, as reported by Bathurst et al. (1993a) and Bathurst and Benjamin (1990).

5.4.3 Load Distribution with Depth

Figures 5.5 through 5.12 show the distribution of the best estimate of "measured" reinforcement load and predicted values as a function of depth below the wall top for several selected case histories. These figures support the observation made previously that the current design methods may significantly over-estimate the reinforcement loads in geosynthetic walls, particularly over the bottom half of the wall. Note that each figure contains a curve representing the Tieback Wedge/Simplified methods, as well as a curve representing the use of the Coulomb method to calculate K_a (wall interface friction angle equal to the soil backfill friction angle, using only the horizontal component of the Coulomb earth pressure). Full interface friction was assumed for the Coulomb method because continuous or nearly continuous reinforcement layers attached to a facing will restrict downward movement of the backfill soil against the face,

163

resulting in a fully mobilized interface friction angle at the back of the wall face equal to the backfill soil friction angle. The exception is wall GW19 because the reinforcement was placed in discrete strips and likely generated much less shear transfer to the back of the facing than that calculated by assuming fully mobilized facing panel-soil interface friction. For this wall, an interface friction angle of two-thirds of the soil backfill friction angle was used to calculate the Coulomb K_a value, which is a typical concrete-soil interface friction angle.

Figure 5.13 shows the distribution of reinforcement loads, T_{max}, as measured in the full-scale field walls, normalized to the maximum reinforcement load within the wall, T_{mxmx}. The load distribution is not triangular, as is currently assumed for design, but rather is trapezoidal in shape. A proposed envelope for the reinforcement load distribution in the wall is superimposed on the measured data in the figure.
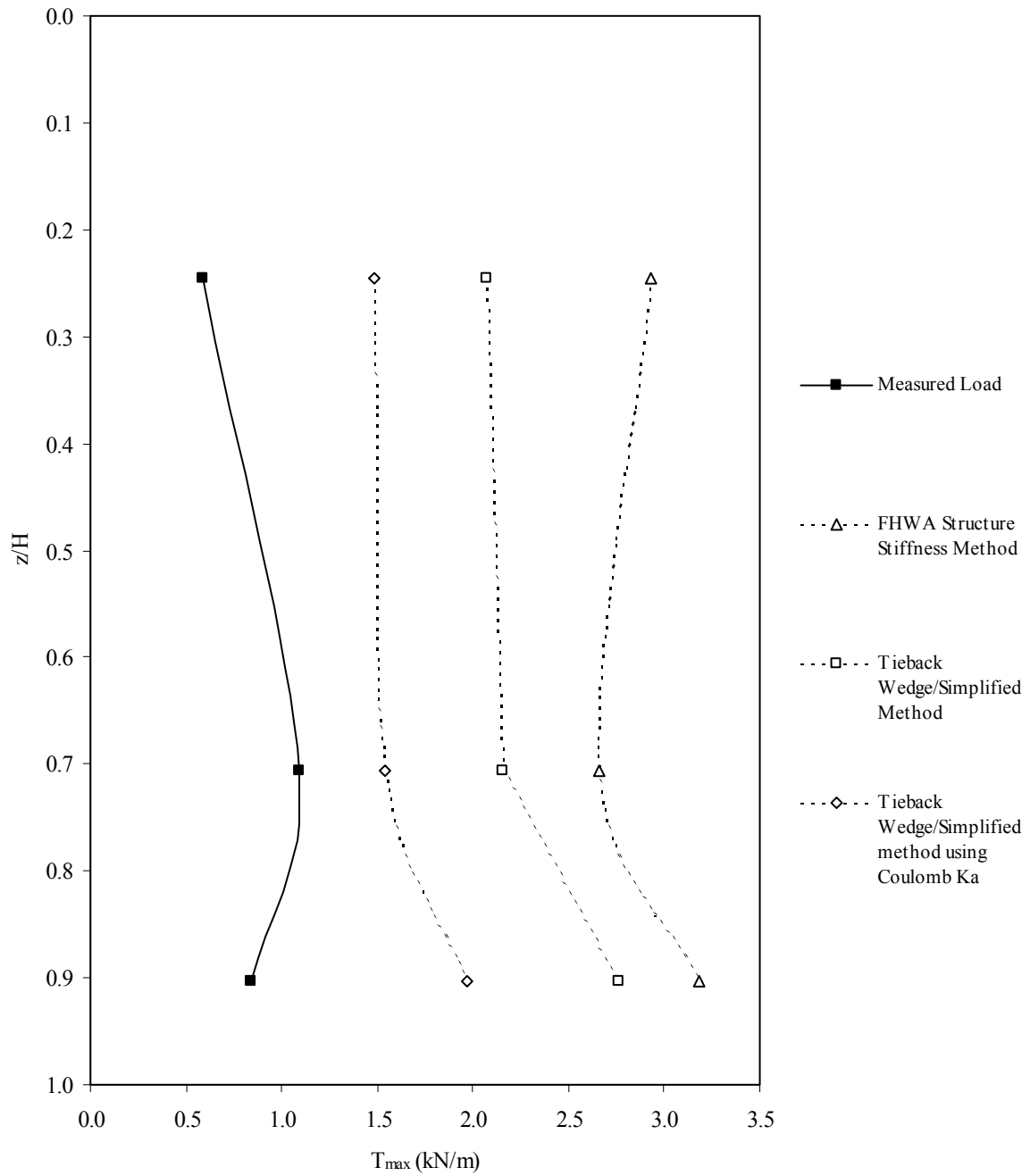
Figure 5.5. Predicted and measured reinforcement peak loads for Wall GW5.
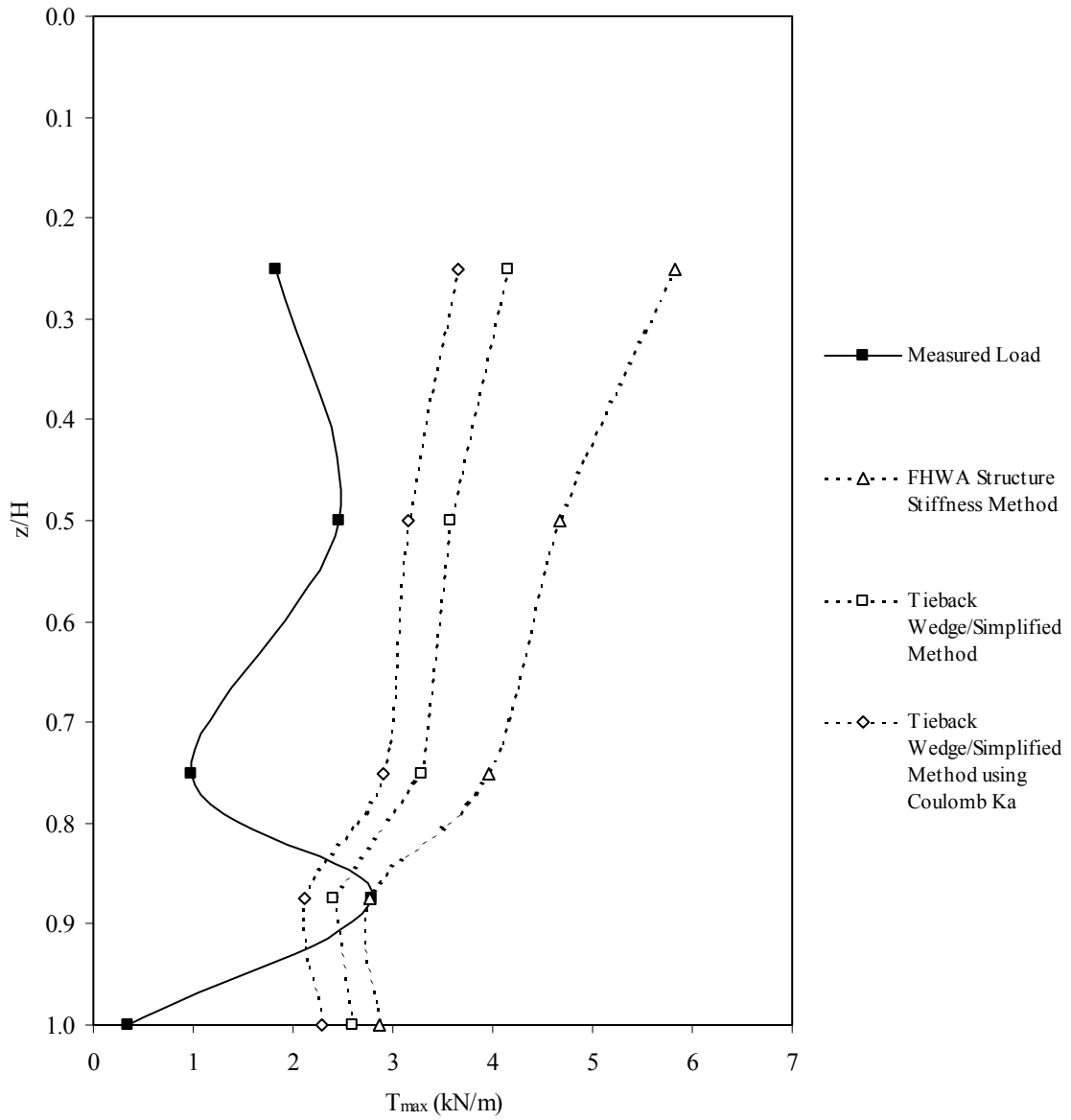
Figure 5.6. Predicted and measured reinforcement peak loads for Wall GW7, Section J.
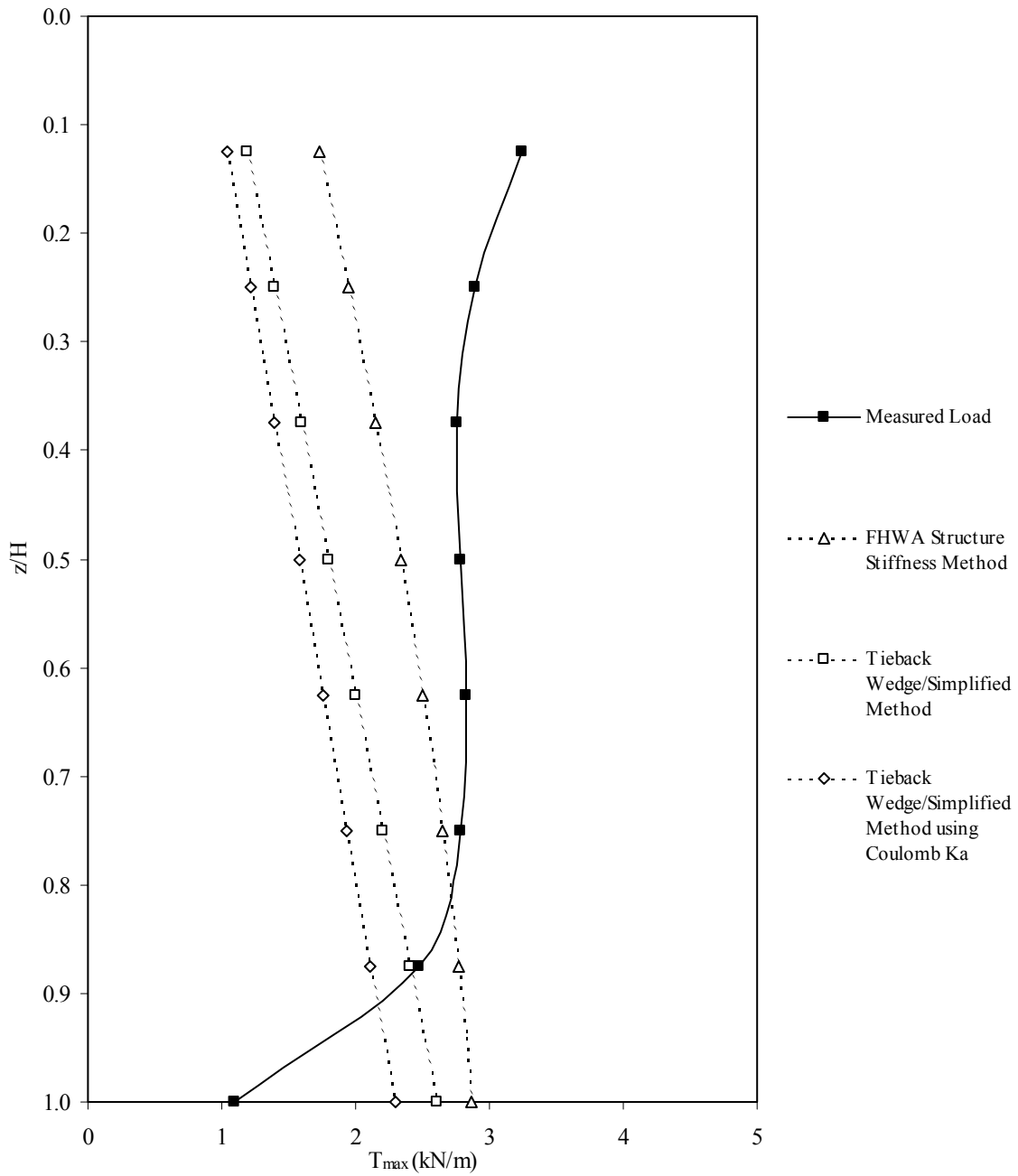
Figure 5.7. Predicted and measured reinforcement peak loads for Wall GW7, Section N.
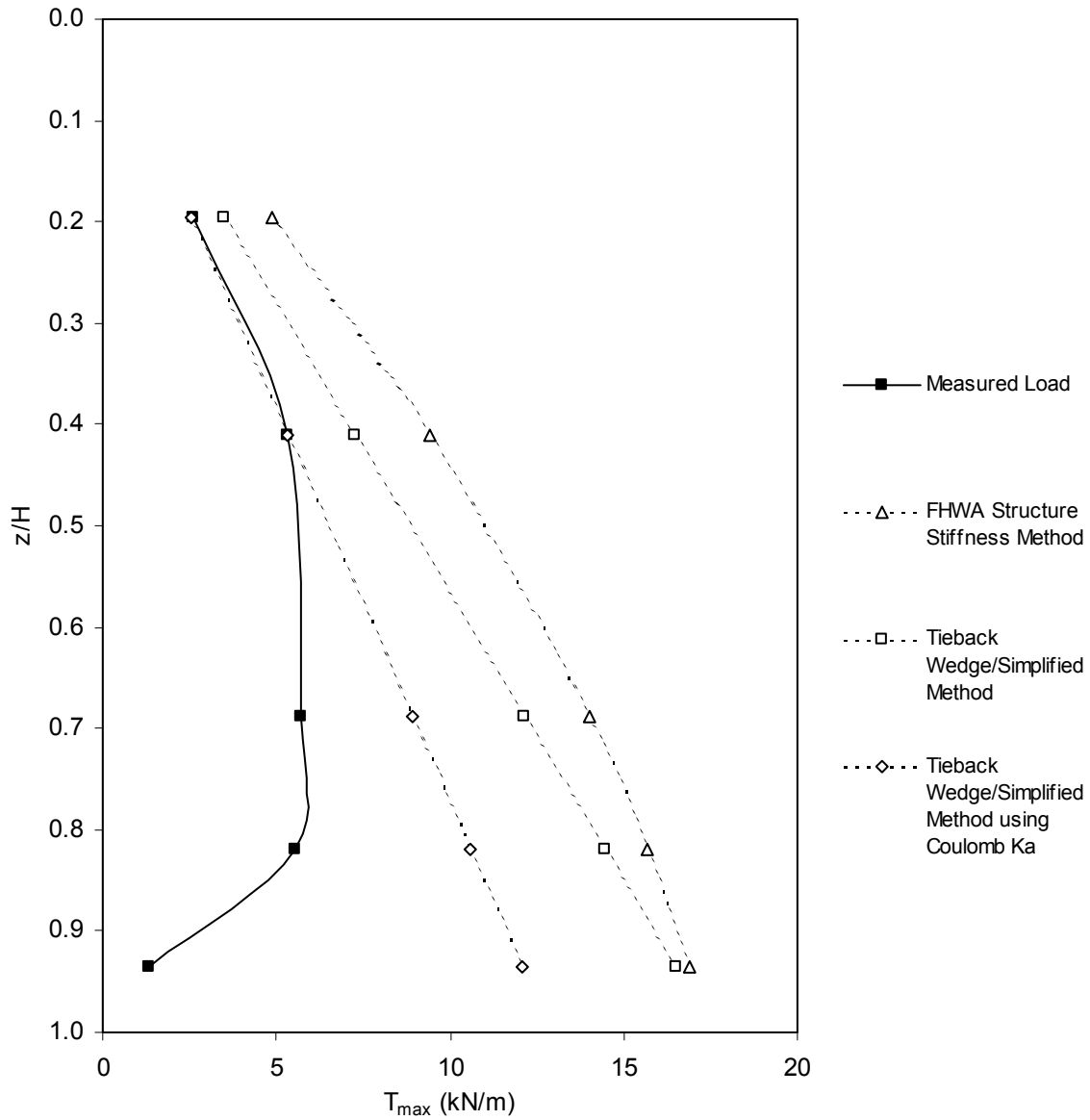
Figure 5.8. Predicted and measured reinforcement peak loads for Algonquin Wall GW8.
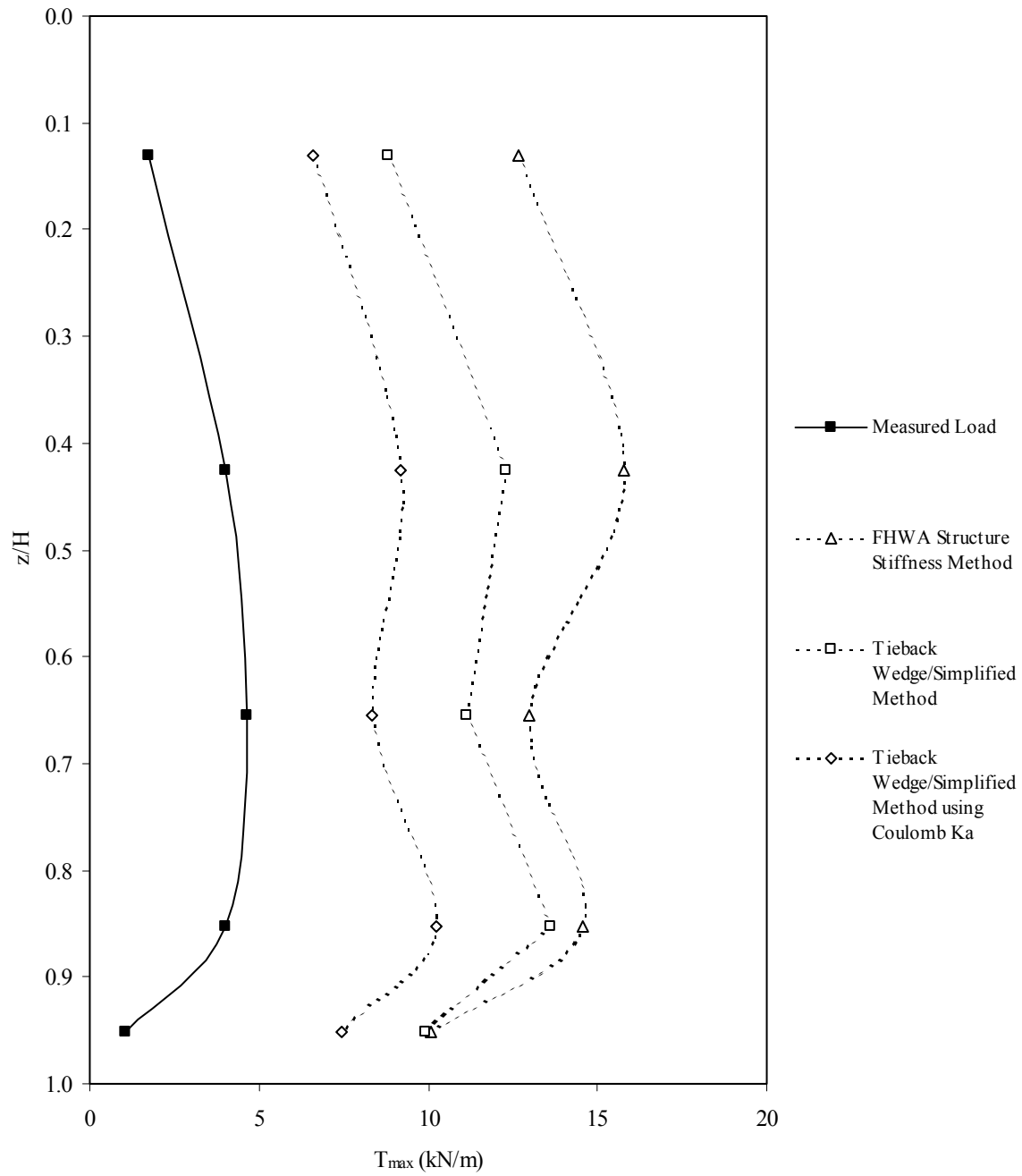
Figure 5.9. Predicted and measured reinforcement peak loads for Algonquin Wall GW9, with surcharge.

169
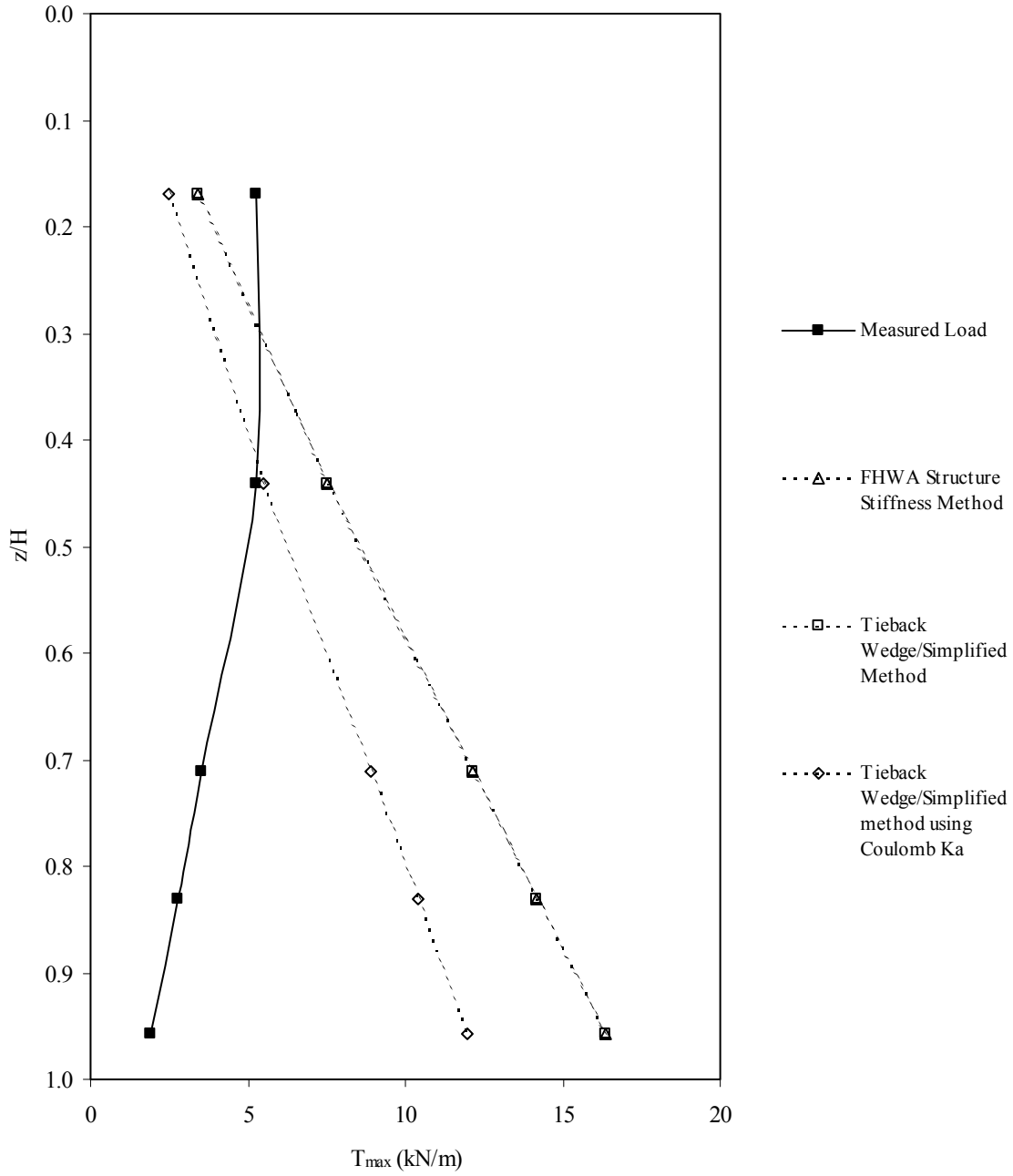
Figure 5.10. Predicted and measured reinforcement peak loads for Wall GW10, after water pressure restraint in front of wall was removed.

170
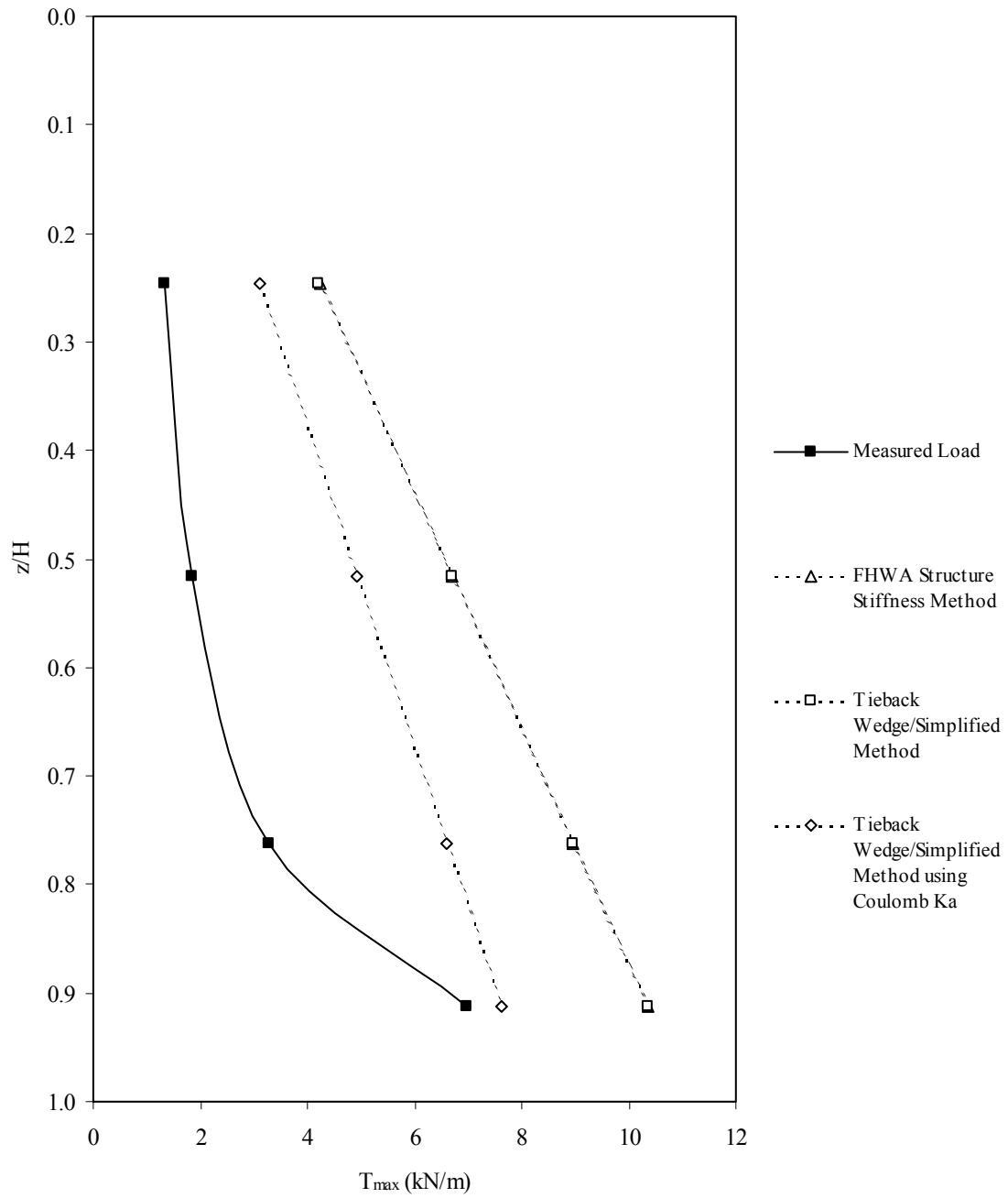
Figure 5.11. Predicted and measured reinforcement peak loads for Wall GW16, with surcharge.

171
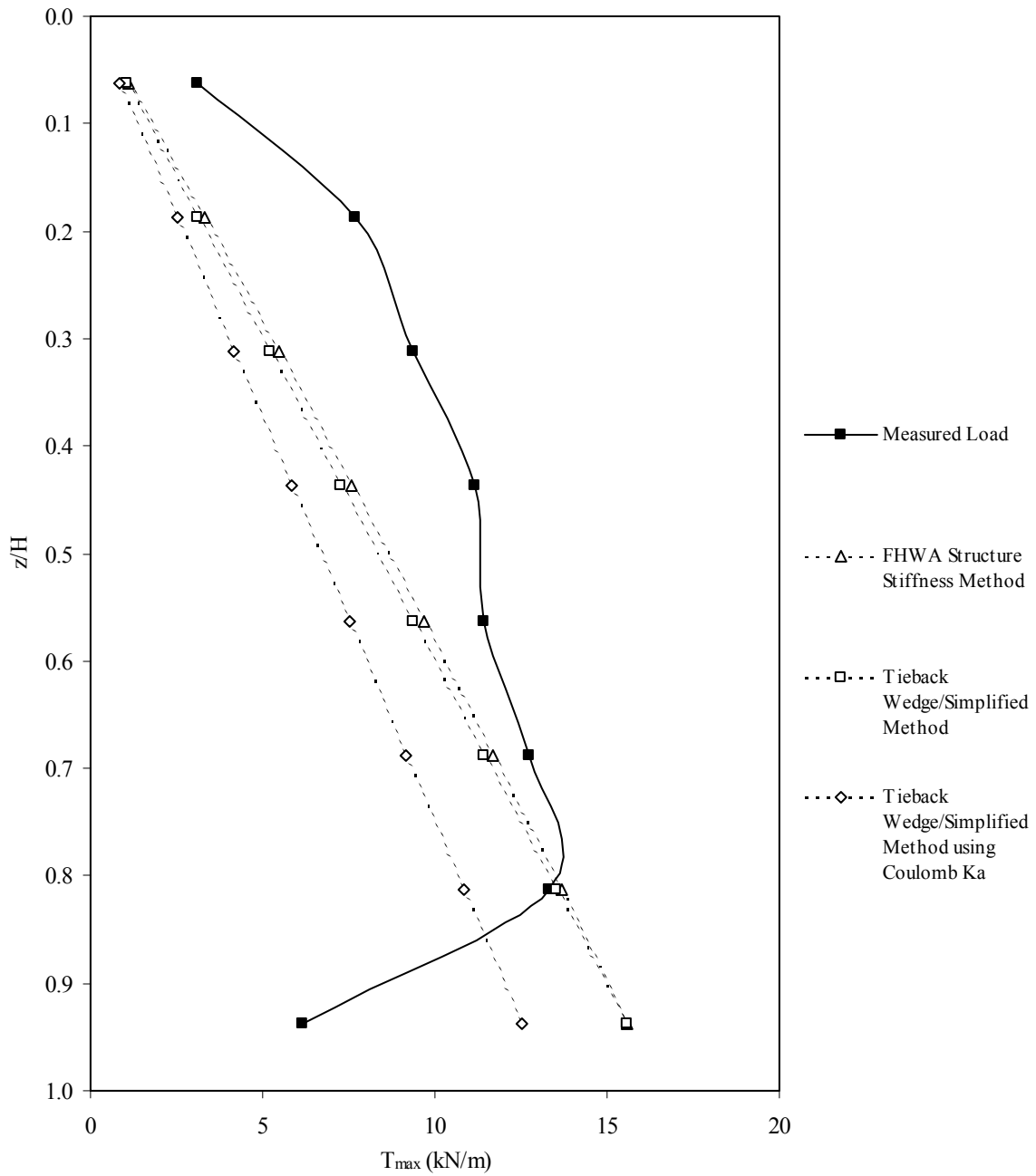
Figure 5.12. Predicted and measured reinforcement peak loads for Wall GW19.

172
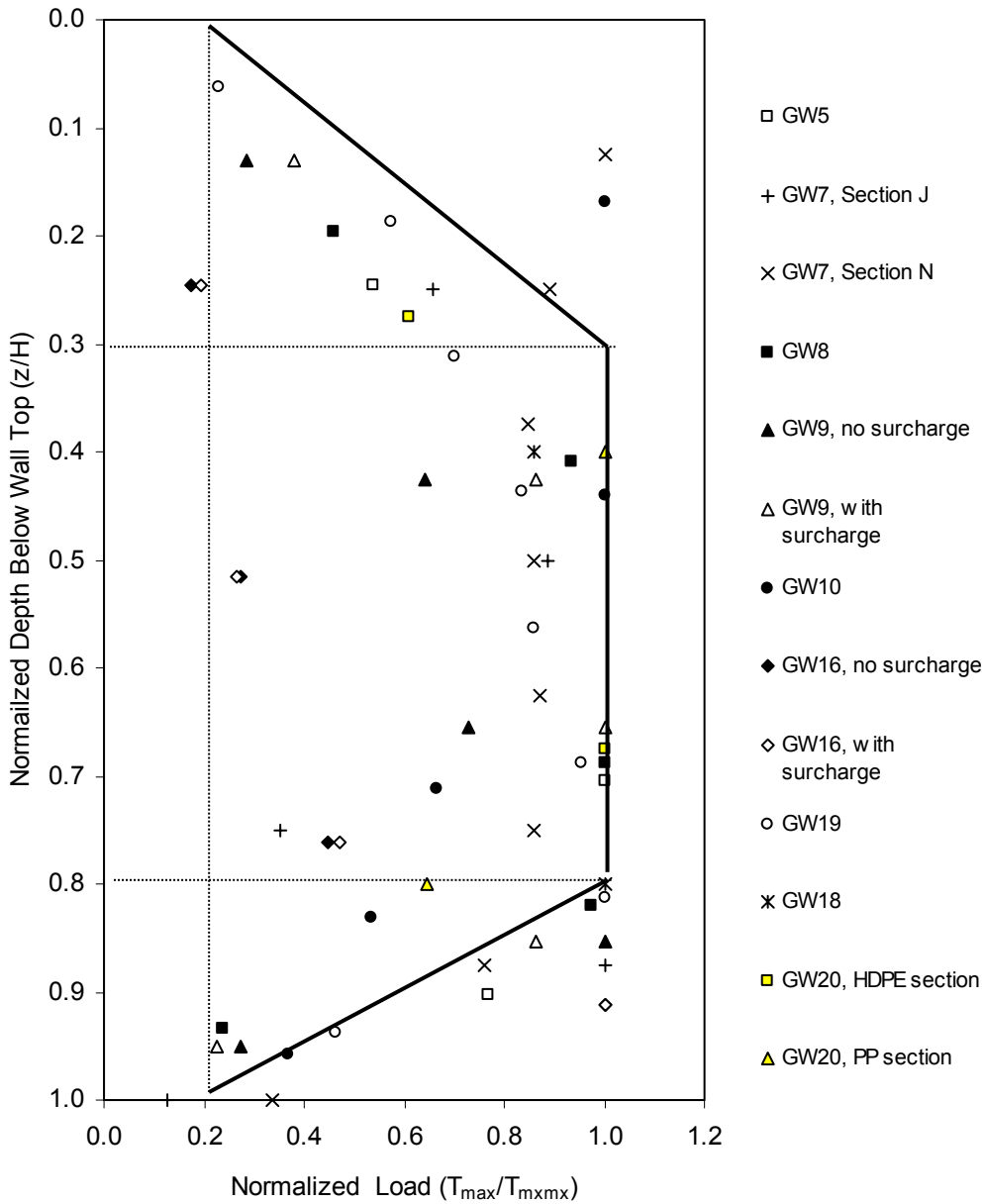
Figure 5.13. Normalized measured load as a function of normalized depth below wall top.

5.5 Discussion

The empirical evidence reviewed herein suggests that conservative predictions of reinforcement loads can be expected even when fully mobilized peak plane strain soil shear strength parameters are used in reinforcement load calculations. Using the constant volume shear strength for the soil can be expected to lead to even more conservative designs. For most geosynthetic walls built to date, the reinforcement strains have been at or below the strains

required to mobilize peak soil shear strength. Furthermore, it is undesirable to allow the soil to strain beyond peak shear strength since the load carrying capacity of the soil at post peak strength may be very much less, and this would lead to over-stressing of the reinforcement. This condition was observed for the RMCC test walls (GW14 and GW15) subjected to high surcharge loads, as well as the Algonquin wrapped face geotextile wall (GW10) (see Chapter 2.0 and Bathurst 1993). Fortunately, even after the soil reaches failure, the geosynthetic reinforcement can be expected to continue to strain with time (see Chapter 2.0 regarding wall GW10). This points to the built-in safety of geosynthetic systems because of their inherent flexibility and large rupture strains. Other test wall studies appear to confirm that the peak soil shear strength is a key parameter that is closely related to observed wall loads and predictions of failure (Zornberg et al. 1998).

Note that relative to the peak plane strain soil shear strength derived from backfill-specific soil shear strength tests, design soil friction angles typically used for geosynthetic wall design result in a built-in additional factor of safety that is on average approximately 2.0. This is simply due to the choice of soil strength parameters alone (see Chapter 2.0). Therefore, the selection of soil strength parameters is a major source of design conservatism for geosynthetic walls.

A key assumption in current design methodologies is that internally the wall is at a state of limit equilibrium. That is, the strength of the soil and the reinforcement is fully mobilized everywhere, and all components of the wall system are at a state of incipient collapse. However, most of the measurements that have been used to estimate actual reinforcement loads have been taken at working stress conditions. Are the mechanisms of load development and distribution in geosynthetic soil reinforcement under conditions of limit equilibrium the same as those at working stress conditions? Related to this question is the validity of the assumption that the load in the reinforcement, distributed over the reinforcement tributary area, is representative of the soil state of stress. Rowe and Ho (1993) suggested that the reinforcement loads do not represent the soil state of stress for two reasons:

1. The force in the reinforcement depends solely on the strain and the stiffness of the reinforcement.

2. Equating the soil stress (K_a or K_o) to the reinforcement load distributed over the tributary area implicitly assumes that principle stress directions remain vertical and horizontal, which further implies that there is no shear stress at the soil/reinforcement interface. Yet

shear stress is known to occur at the soil/reinforcement interface, and principle stress directions do rotate in a reinforced soil mass by 20° to 40° (Murray and Farrar 1990).

Given that the current limit equilibrium methods correlate very poorly to the actual loads in the reinforcement layers and also tend to over-predict those loads, the empirical evidence suggests that the distribution of load within a reinforced soil system based on limit equilibrium assumptions does not satisfactorily predict reinforcement loads at working stress conditions. Furthermore, the empirical data provided in figure 5.1 support the view that the soil state of stress is not represented by the lateral stress calculated from the reinforcement force distributed over the tributary area, as the lateral earth pressure determined from the measured reinforcement force is significantly less than the active or at rest state earth pressure. Although Table 5.3 and figures 5.5 through 5.12 do suggest that using the Coulomb active earth pressure coefficient (reduced to consider only the horizontal component), which accounts for full wall interface friction, does help to move the predicted load closer to the measured load, it does not completely remove the difference; and other factors must be contributing to the reduced load measured in the reinforcement. Note that the Coulomb analysis results presented in Table 5.3 and figures 5.5 through 5.12 do account for the rotation of principle stresses by assuming full interface friction and by taking only the horizontal component of the active force. Therefore, the rotation of principle stresses does not fully account for the conservatism illustrated in the table and figures. Figure 5.13 also shows that the distribution of load to each reinforcement layer is much different than what is derived from limit equilibrium concepts and is a major contributor to the poor correlation between measured and predicted loads.

So what then governs the development and distribution of load in geosynthetic soil reinforcement layers at working stress conditions, and why are measured reinforcement loads in general so much smaller than the loads predicted by limit equilibrium methods? The first point made above provides part of the key to answering this question. Figures 5.3 and 5.4 show that the stiffness of the facing system and degree of wall toe restraint relative to the stiffness of the reinforcement significantly affect how much load is carried by the reinforcement. Since stresses are not fully mobilized in each of the load carrying components of a wall at working stress conditions, the distribution of loads will be governed by the relative stiffness of each component. Furthermore, the component that has the greatest stiffness will tend to carry the largest portion of the load. The data provided herein, especially in figures 5.3 and 5.4, demonstrate that all wall

175

components are involved in carrying the load: the soil reinforcement, the soil, the wall facing, the wall toe, and the wall foundation soil. Note that current limit equilibrium methods used in the Tieback Wedge/Simplified methods and the FHWA Structure Stiffness Method do not consider the effect of the wall facing and toe resistance, nor the wall foundation soil, on wall load capacity. Bathurst (1993) also came to this conclusion as a result of back analysis of two of the full-scale RMCC test walls reported herein and comparison between measured reinforcement loads and wall toe loads. The distribution of maximum reinforcement loads versus depth below the wall top (figures 5.5 through 5.13) shows that the foundation soil below the wall may also carry a portion of the lateral load, as the reinforcement stress tends to decrease substantially near the bottom of the wall.

Comparison of figures 5.6 and 5.7 also provides some insights into the role of the facing on the development of loads in soil reinforcement. The predicted loads are conservative relative to the measured loads in Figure 5.6, but they are about the same or non-conservative in Figure 5.7. The wall (technically a very steep, reinforced slope) represented in Figure 5.6 contains secondary facing reinforcement, and more widely spaced reinforcement layers, than the wall represented in Figure 5.7. Both walls are sections within the same test wall. The presence of the secondary reinforcement appears to reduce the loads carried by the reinforcement, which means that in effect, the facing system is carrying part of the lateral load.

Because the stiffness of the wall components greatly affects the magnitude and distribution of load in the reinforcement, the Structure Stiffness Method should at least conceptually have some advantages. However, the equation for this method was developed so that the load in the reinforcement distributed over the tributary area of the reinforcement would never be less than K_a, regardless of how low the stiffness is. This, in effect, maintains the assumption that the force in the reinforcement directly reflects the state of stress in the soil for geosynthetic reinforced systems. Furthermore, more is known regarding the conversion of measured geosynthetic reinforcement strains to load in walls (see Chapter 4.0). The empirical adjustments made to develop this method were based on reinforcement loads that were derived from measured strains and then converted to load with a short-term geosynthetic modulus, rather than with a longer term modulus, causing the loads in the empirical database to be too high. Therefore, at least for geosynthetic reinforcement, the Structure Stiffness Method does not provide an advantage

regarding the issue of stiffness for geosynthetic reinforced walls because of the assumptions and database used to develop it.

Of the methods currently available for estimating reinforcement loads in geosynthetic walls, all characterize the soil response by using the active earth pressure coefficient. However, at working stress conditions, the amount of load carried by the reinforcement depends on the stiffness of the reinforcement relative to the soil stiffness, as well as the stiffness of the other wall components, if the soil shear strength is not fully mobilized. The stiffer the reinforcement relative to the soil modulus, the more load the reinforcement will attract. However, accurately estimating the soil modulus is not a simple task, and currently the soil modulus value is restricted to numerical modelling exercises of wall performance, for example, finite element modelling of MSE walls. This is the reason that a semi-empirical approach based on measurements from full-scale walls has been taken to modify the limit equilibrium approach. The intent is to more accurately reflect working stress conditions by using soil parameters such as the peak soil friction angle that are readily available to designers. The authors believe that a fundamental property of reinforced soil walls is the soil stiffness, as demonstrated in numerical modelling (e.g., Bathurst and Hatami 1998, Rowe and Ho 1993). However, more work is required to establish explicit relationships between soil stiffness and conventional soil properties such as peak soil strength and lateral earth pressure coefficient.

Figure 5.7 demonstrates that for the steep reinforced slope, the Tieback Wedge/Simplified methods and the Structure Stiffness Method under-predict the reinforcement loads when the face is significantly battered. This appears to be another indication that the assumption that the reinforcement load directly reflects the soil state of stress is not correct, and that the limit equilibrium approach is inaccurate for predicting reinforcement loads at working stress conditions.

The PET strip reinforced wall data (Figure 5.12) show that the Tieback Wedge/Simplified methods, and even the FHWA Structure Stiffness Method, which could account for the unusually high stiffness of the reinforcement, tend to under-predict loads in this case. This may indicate that there is a benefit in full soil confinement produced by the lateral restraint imparted by the reinforcement. This may increase the strength of the system beyond the sum of the contributions of the soil and reinforcement separately. This would result in an equivalent increase in soil shear

177

strength and, therefore, a decrease in the load demand that the reinforcement must resist. The discontinuous strips may not be adequate to provide this confinement effect.

For the walls that were subjected to loadings great enough to fail the soil, which should cause the walls to approach a true limit equilibrium condition, the measured reinforcement loads were slightly to considerably below the loads predicted by the current design methods (see figures 5.2 and 5.10). For the full-scale test walls with aluminium panel facings, the combination of toe restraint and facing stiffness may account for the majority of this difference. For the wrapped face field wall, some of the load may be carried by the additional reinforcement because of overlaps at the face, but this is not likely to account for all of the differences. Base restraint due to good foundation soil conditions may also partially contribute to the difference. However, the current design methodology assumes no wall friction when active earth pressure coefficients are calculated, resulting in a Rankine earth pressure. When the current limit equilibrium approaches for design are considered in relation to the data presented in figure 5.10, thus comparing the Rankine earth pressure with the Coulomb earth pressure, the assumption that there is no wall interface friction appears to be too conservative even when true limit equilibrium conditions are approached.

5.6 Summary and Conclusions

The principles of estimating the geosynthetic reinforcement modulus as a function of time, as described in Chapter 4.0, was applied to 16 full-scale geosynthetic wall case histories to calculate a best-estimate of the load levels in geosynthetic reinforcement in walls. Uncertainties in those measurements were also determined and considered in a comparison of the "measured" loads to loads predicted by current design methodologies. This evaluation determined that the difference between the measured and predicted values was significant, both in terms of consistency of the prediction and the tendency of the current design methods to substantially over-estimate reinforcement loads. This warrants re-evaluation of the current methods for predicting reinforcement loads in walls.

On the basis of the evaluation of the geosynthetic wall reinforcement loads derived from strain measurements, the following conclusions are made:

1. Reinforcement loads derived from strain measurements at working stress conditions are in general much lower than would be predicted by current design methods based on limit equilibrium approaches that use Rankine earth pressure, even with best estimates of the peak plane strain shear strength of the backfill soil. Variability in the strain measurements and the modulus used to convert strains to loads does not account for this difference between "measured" and predicted reinforcement loads.

2. The current limit equilibrium design methods provide a very poor correlation with measured reinforcement loads. Possible reasons for the poor correlation include the following:

   - The mechanism of load distribution within the wall is different at working stress conditions than at limit equilibrium (i.e., incipient collapse of the wall). The differences in the stiffness of the various wall components appear to dictate how load is distributed to the reinforcement layers. Therefore, the measured reinforcement loads do not necessarily represent the soil state of stress.

   - The combination of the wall face and the wall toe restraint carries a significant portion of the internal load for geosynthetic walls, thereby reducing the load the reinforcement must carry. The stiffer the wall face/wall toe restraint, the less load the reinforcement must carry.

   - The foundation soil may also provide some restraint to strain development within the reinforced wall mass, acting as a boundary condition not considered in current design methodologies.

   - Because of the factors mentioned above, the distribution of forces to each of the reinforcement layers is not triangular, as is currently assumed, but is instead trapezoidal, contributing to the poor correlation between measured and predicted values.

3. Neither Rankine nor Coulomb earth pressure coefficients properly account for the effect of wall face batter on geosynthetic wall reinforcement loads. This results in under-prediction of load for heavily battered walls. This may be further evidence that the wall reinforcement loads do not directly correlate with the soil state of stress.

4. If current limit equilibrium-based design methodologies are used, assuming the wall interface friction to be zero will be conservative. Assuming full interface friction, except where noted above, will produce safe estimates of reinforcement load.

5. Although evidence is very limited, the continuity of the reinforcement layer appears to affect the amount of load carried by the reinforcement. This suggests that there may be benefits to continuous (sheet) reinforcement for confining the soil and the synergy it creates to improve the strength of the system.

The low reinforcement strains and loads measured to date in geosynthetic walls point to the desirability of using peak soil shear strengths rather than constant volume shear strengths for design purposes. Doing so will help keep design conservatism more reasonable and will be consistent with the philosophy of preventing failure of a major component of the reinforced soil system, the soil. However, at working stress conditions, the modulus of the soil may be a more important parameter than soil shear strength for estimating reinforcement loads. Because it is difficult to estimate the soil modulus and to implement this parameter into close-formed design analyses, the use of a soil shear strength parameter is still desirable. Furthermore, because the geosynthetic reinforcement can reach much higher strains than can the soil without failure, as was observed for the RMCC test walls GW14 and GW15 and the Algonquin geotextile wall GW10, the current focus of design, which is to prevent failure of the reinforcement, may need to be changed. The focus instead should be to prevent reinforcement strains from becoming high enough at any time during the design life of the structure to allow failure of the soil, defined as allowing the soil to strain beyond peak shear strength. Once the soil has failed, for all practical purposes the wall has failed too.

6.0   OBSERVED LONG-TERM PERFORMANCE OF GEOSYNTHETIC WALLS, AND IMPLICATIONS FOR DESIGN

6.1 Introduction

In recent years, considerable work has focused on establishing the long-term performance of geosynthetic reinforcement as a material, addressing such issues as installation damage, creep, and durability.   However, only limited effort has been expended to establish the long-term performance of geosynthetic walls as a whole. Geosynthetic walls have been viewed by the civil engineering profession, in general, as a new technology whose performance has yet to be established. Nevertheless, geosynthetic walls have been used for almost 25 years. Is enough case history data available, and has the science of geosynthetic material degradation prediction advanced enough, to demonstrate the long-term performance of geosynthetic walls? Furthermore, what are the likely reasons for the generally good long-term behavior of geosynthetic walls observed to date? In light of proven good performance, are current design procedures for internal stability of geosynthetic walls too conservative, and if so, what is the source of this conservatism? In Chapter 2.0, back-analysis of global load and resistance of available wall case histories demonstrated that geosynthetic reinforcement load levels appear to be significantly lower than values estimated with the current North American design methodology (e.g., AASHTO 1999). Several sources for this conservatism were identified. This earlier work has led the authors to investigate whether long-term deformation and strain measurements are consistent with the hypothesis that operational load levels are lower than design values, and whether geosynthetic reinforced soil walls, other than those specifically identified as having poor performance, can be expected to be stable over their target design lifetime.

This chapter uses long-term performance data to examine whether reinforcement load levels predicted with the current design methodology are indeed conservative, given observed long-term wall performance. Estimated long-term loads are also compared to the lower load levels reported for the same structures in Chapter 5.0. The objectives of this chapter are as follows:

1. Identify and analyze the long-term behavior observed in well-documented, full-scale wall case studies and to determine their long-term stability.

2. Provide at least an approximate verification of the load levels identified in a number of full-scale wall case histories reported in Chapters 2.0 and 5.0. Accomplish this by comparing the measured creep data from these walls to laboratory in-isolation creep data for the same geosynthetic material.

3. Establish some quantitative guidelines to distinguish between walls that can be expected to exhibit good long-term performance and those that can be expected to exhibit marginal or poor performance.

Only case histories in which granular soil was used as backfill are considered in this investigation (see Chapter 2.0).

6.2 Long-Term Performance Factors and Design

Current North American geosynthetic reinforcement design procedures recognize the potential for loss of reinforcement strength as a result of installation damage, creep, and durability. This is represented in equation form as follows:

$$T_a = \frac{T_{ult}}{RF \times FS} = \frac{T_{ult}}{RF_{ID} \times RF_{CR} \times RF_D \times FS} \tag{6.1}$$

Here, T_{ult} is the ultimate wide-width strip tensile strength of the geosynthetic. RF is a combined factor to account for geosynthetic strength loss during the wall design life and is equal to RF_{ID} x RF_{CR} x RF_D, where RF_{ID} is a reduction factor that accounts for strength loss due to installation damage, RF_{CR} is a reduction factor for strength loss due to creep, and RF_D is a reduction factor for strength loss due to chemical and biological degradation.

The reduction factors RF_{ID} (installation damage—a short-term strength loss), RF_{CR} (creep—a long-term strength loss), and RF_D (chemical and biological degradation—a long-term strength loss) are not uncertainty factors but are reduction factors used to calculate the long-term strength remaining in the geosynthetic reinforcement after a given period of time. These reduction factors are analogous to the reduction in steel area used to account for corrosion losses in steel reinforcement products. Material strength variation is taken into account during the selection of T_{ult} and is based on standardized quality control and quality assurance procedures used by geosynthetics manufacturers. The Minimum Average Roll Value (MARV), which is defined as

the strength that is two standard deviations below the mean tensile strength, is used for design rather than the mean tensile strength.

In past years, in particular before 1990, protocols for determining these reduction factors, to some extent creep and especially chemical durability factors, were either nonexistent or practically unusable. The long-term geosynthetic strength data that were available at that time were either inconsistent or extremely conservative because of the use of laboratory procedures that did not simulate in-situ conditions. This resulted in unrealistically conservative assessments of potential strength degradation. Because of this, geosynthetic walls at that time were considered too unreliable to use for long-term permanent applications in most cases. Simply too much was unknown, and not enough long-term performance history was available for geosynthetic walls. A detailed description of durability issues is provided by Allen (1991) and Allen and Elias (1996).

At present, protocols for determining the long-term strength and behavior of geosynthetic reinforcement are much better developed. Examples of these protocols are now included in design codes through the AASHTO Bridge Specifications (AASHTO 1999), FHWA manuals (Elias et al. 2001, Elias 2001a), and in one state department of transportation test method (WSDOT 1998).

6.3 Overview of Case Histories

Only case histories with enough deformation and strain data to determine long-term creep rates are considered herein. However, comparison of the long-term performance of these selected case histories to the overall long-term performance of all the case histories provided in Chapter 2.0 can be used to extrapolate the lessons learned from these selected case histories to geosynthetic walls in general. The key characteristics of each of these case histories are summarized in tables 6.1 and 6.2. The type of long-term data available for each case history is summarized in Table 6.3. Instrumentation details can be found in Chapter 3.0 for each case history. Table 6.2 provides best estimates of the actual long-term resistance to demand ratio for the case histories that had long-term deformation and strain data available, as well as the global resistance to demand ratio that would be obtained if the current AASHTO specifications were used for design (a total of 10 case histories and 12 wall sections). In Chapter 2.0, this comparison was made for all of the case histories in which some indication of long-term

183

performance was available (35 wall sections). Table 6.4 compares the average long-term resistance to demand ratio for the 12 wall sections that had detailed long-term deformation data to the average long-term global level of safety for all of the case histories. As shown in the table, the average global resistance to demand ratio for the 12 selected wall sections with good long-term performance data is similar to the average resistance to demand ratio for the entire database of walls. Furthermore, as shown in tables 6.1 and 6.2, the range of wall heights, surcharge conditions, and reinforcement types and polymers span the range of what is typical today for geosynthetic walls. Therefore, the long-term deformation data reported herein for these 12 selected wall sections can be considered representative of the larger database of geosynthetic walls, especially given the similarities in observed long-term performance between this subset and the entire database. Note that most of these case histories were designed less conservatively than would be required by the current AASHTO design specifications (AASHTO 1999), in some cases much less conservatively.

Recent work by Elias (2001b), in which 24 geosynthetics from 12 retrieval sites were evaluated, confirms that little, if any, chemical degradation has occurred to date in geosynthetics in reinforcement applications in full-scale structures up to 25 years old. Elias concluded that observed strength losses could be largely or wholly attributed to installation damage for polypropylene (PP) and high density polyethylene (HDPE) geosynthetics, as well as for high tenacity–high viscosity polyester (PET) products. Some measurable strength losses due to chemical degradation were observed in low tenacity–low molecular weight PET geotextiles. These strength losses were on the order of 0.25 to 0.5 percent per year, which is consistent with the laboratory studies reported by Elias et al. (1998). Note that all of the case histories evaluated herein constructed with PET geosynthetic reinforcement products used high tenacity–high viscosity PET, although some of the additional case histories reported in Chapter 2.0 did utilize lower viscosity PET geotextiles. For the PP and HDPE products, some antioxidant consumption appeared to have occurred during the 20- to 25-year observation period, but not enough to allow degradation of the polymer to occur. This is consistent with the laboratory studies reported by Salman et al. (1998).

Table 6.1. Summary of geometry, observation period, and data source for selected case histories.

Case History	Date Built	Wall Height (m)	Surcharge Conditions	Time for Wall Construction (hrs)	Wall Temperature (^{o}C)	Years of Monitoring Available	Source of Data Used for Analysis
Tanque Verde GeogridConcrete Panel Wall, GW5	1984	4.9	None	350	27° C	11 years	Desert Earth Engineering, 1987; McMahahon and Mann Consulting Engineers, 1996
Oslo, Norway Geogrid Walls (Sections J and N), GW7	1987	4.8	3 m steeply sloping soil surcharge	960 to top of wall, 2600 to surcharge completion	6° C	11 years	Fannin 1988; Fannin and Hermann 1991; Fannin 2001
Algonquin GeogridConcrete Panel Wall, GW8	1988	6.1	2.1 m sloping surcharge	920	17° C	1 year	Christopher, 1993; Christopher, 1998
Algonquin Geogrid Modular Block faced Wall, GW9	1988	6.1	2.1 m sloping surcharge	920	17° C	1 year	Bathurst et al. 1993
RMC Geogrid Wrapped Face Full-scale Test Wall, GW11	1986	3	0.7 m soil surcharge	65	20° C	1 month	Bathurst, et al. 1988
RMC Full Height Propped Panel Full-scale (Geogrid) Test Wall, GW14	1989	3	Full test wall top coverage with air bag loading system, up to 70 kPa	100 after prop release	20° C	2 months	Benjamin, 1989
RMC Incremental Panel Full-scale (Geogrid) Test Wall, GW15	1989	3	Full test wall top coverage with air bag loading system, up to 70 kPa	200	20° C	2 months	Benjamin, 1989
WSDOT Rainier Avenue Wrapped Face Geotextile Wall, GW16	1989	12.6	5.3 m sloping surcharge	1650	14° C	1 year	Allen, et al. 1992
Fredericton, New Brunswick Propped Panel Geogrid Wall, GW18	1990	6.1	None	100 after prop release	10° C	1.2 years	Knight and Valsangkar, 1993
Vicenza, Italy Welded Wire Faced Geosynthetic Walls (HDPE and PP test sections with final surcharge), GW20	1998	4	3.5 m steeply sloping soil surcharge	150	20° C, assumed	1 year	Carrubba, et al. 1999; Alberto, 1998

Table 6.2. Summary of materials and design for selected case histories.

Case History	Geosynthetic Type	Geosynthetic Polymer	Long-Term Global Resistance to Demand Ratio for Actual Wall, (Chapter 2.0)	Long-Term Global Resistance to Demand Ratio if Designed per AASHTO '99 and Typical Practice, (Chapter 2.0)
GW5	Extruded uniaxial geogrid	HDPE	6.14	4.51
GW7	Extruded uniaxial geogrid	HDPE	Section J - 4.78 Section N - 6.38	7.05 for both sections
GW8	Extruded uniaxial geogrid	HDPE	1.27	2.92
GW9	Woven geogrid	PET	1.08	2.12
GW11	Extruded biaxial geogrid	PP	1.47	6.39
GW14	Extruded biaxial geogrid	PP	1.15 end of construction with full surcharge	6.01 end of construction, 4.04 with full surcharge
GW15	Extruded biaxial geogrid	PP	1.15 end of construction, 0.36 with full surcharge	6.01 end of construction, 4.13 with full surcharge
GW16	Woven geotextile	PP for upper 75% of wall, PET for lower 25% of wall	3.44	4.61
GW18	Extruded uniaxial geogrid	HDPE	1.89	2.97
GW20	Extruded uniaxial geogrid	HDPE	1.71	10.4
GW20	Biaxial geogrid	PP	0.53	8.83

Table 6.3. Summary of the type of measurements that are available for each case history.

Case History	Strain	Deformation	Load
GW5	Resistance strain gauges, Bison coils for soil and geogrid strain	--	Lateral and vertical earth pressure cells
GW7	Bison coils attached to geogrid	--	Load cells attached to geogrid; vertical earth pressure
GW8	Resistance Strain Gauges, Bison coils near geogrid	Inclinometers, survey measurement of facing panels	Lateral earth pressure behind face
GW9	Resistance strain gauges, extensometers on geogrid	Inclinometers	Lateral and vertical earth pressure cells
GW11	Resistance strain gauges, extensometers on geogrid	Survey measurement of facing	Vertical earth pressure cells
GW14	Resistance strain gauges, extensometers on geogrid	Survey measurement of facing	Load cells at geogrid connection to facing; vertical earth pressure; load cells at wall toe
GW15	Resistance strain gauges, extensometers on geogrid	Survey measurement of facing	Load cells at geogrid connection to facing; vertical earth pressure; load cells at wall toe
GW16	Resistance strain gauges, extensometers; Bison coils for soil strain	Inclinometers, face survey measurements	Lateral and vertical earth pressure cells
GW18	Strain gauges	Survey measurement of facing	Lateral earth pressure cells
GW20	Strain gauges	Wall base lateral deformation only	Vertical earth pressure; load cells attached to geogrid

Table 6.4. Average global resistance to demand ratio for all wall case histories (a total of 35) vs. the 12 case histories with detailed long-term creep/deformation data.

Wall Type/Performance	Average Resistance to Demand Ratio (RD)	
	Actual Wall	Designed per AASHTO (1999) with Typical Design Practice and Soil Design Parameters
Geosynthetic walls with good performance; all case histories	2.73	4.64
Geosynthetic walls with poor performance; all case histories	0.45	4.84
Geosynthetic walls with good performance; case histories with detailed long-term creep data	2.77	5.46
Geosynthetic walls with poor performance; case histories with detailed long-term creep data	0.40	5.66

6.4 Geosynthetic Load-Strain-Time Behavior Overview – Use of Laboratory Data to Evaluate Field Performance

In general, the largest contributors to strength loss and reduced wall performance for the geosynthetic reinforcement products in use today are installation damage and possibly creep. Chemical degradation plays a minor role in wall performance because chemical degradation has so far been found to be limited in typical soil environments. Installation damage also has limited impact on the initial working stress performance of geosynthetic walls. This is because for most geosynthetics used as reinforcement (i.e., woven geotextiles and geogrids), the load-strain-time behavior of the geosynthetic is not significantly affected by installation damage at typical or even relatively high working strains (Allen and Bathurst 1994) for the typical levels of installation damage observed in full-scale walls. Allen and Bathurst (1996) also provided strong evidence that installation damage has little, if any, effect on creep strains and rates for the typical levels of installation damage in full-scale structures. For the case histories evaluated herein (and the geosynthetics used in those case histories), this is certainly the case. As a result of the observations summarized above, an accurate assessment of long-term performance can be obtained through measurement and extrapolation of the creep deformations and strains recorded in the wall case histories. Hence, the sections that follow focus on the available creep strain and deformation data for each case history to assess long-term wall performance.

Creep is simply the visco-elastoplastic response of the geosynthetic to sustained load. Creep results in time-dependent deformation that may continue to occur as long as the reinforcement is loaded. At low to intermediate load levels, depending on the polymer type, the creep rate will continue to decrease with time and may eventually stabilize, at least within the accuracy of the measurements. At higher load levels, creep will continue until rupture occurs.

In general, up to three stages of creep are observed in polymeric materials. These include primary, secondary or steady-state, and tertiary creep. Primary creep strains are characteristically linear when plotted against a logarithmic time scale and increase at a decreasing rate on an arithmetic time scale. Secondary creep strains are typically linear when plotted against an arithmetic time scale. Tertiary creep is the rupture phase of creep and is characterized by a rapidly increasing creep rate with time. Geosynthetic structure tends to dominate primary creep (at least for nonwoven geotextiles, but much less so for woven geotextiles and not at all for geogrids), and the polymer characteristics tend to dominate

188

secondary and tertiary creep mechanisms (Allen 1991). Polyolefins (HDPE and PP) tend to exhibit all three stages of creep, whereas PET tends to exhibit only primary and tertiary creep.

6.4.1 Long-Term Wall Stability Evaluation

To meet the objectives of this chapter it is necessary to a) define what is meant by good long-term behavior, b) determine whether the existing wall case histories are exhibiting good long-term behavior, and c) determine whether the walls will be stable throughout their design lifetime. This can be accomplished by establishing whether the wall reinforcements are exhibiting only primary creep, or better yet, determining whether logarithmic strain rates are decreasing and thus approaching complete stabilization within the observation period. Establishing whether the measured creep strains are well below what would be observed for the material from laboratory in-isolation data near the creep limit can also help.

6.4.2 Verification of Reinforcement Loads

Another objective of this chapter is to at least approximately verify the load levels identified in the available wall case histories. This will be accomplished by comparing the measured creep data from these walls to laboratory in-isolation creep data for the same geosynthetic material at actual load levels in the wall. In Chapter 5.0, measured strains at the end of wall construction, and an estimated geosynthetic modulus value that correctly accounted for the loading rate that occurred during wall construction, were used to determine a best-estimate of the reinforcement load level in each of the case histories reported herein. A summary of the load levels estimated for each wall case history in Chapter 5.0 is provided in Table 6.5.

The observed creep strains and rates are strongly influenced by the load level applied (Wilding and Ward 1981, Allen 1983, Yeo 1985, Koutsourais 1995, among others). PP and HDPE materials are in general more sensitive to load level than PET materials, except near the rupture limit, where PET creep is very sensitive to load level. Because of this sensitivity, it should be possible to provide an approximate verification of the load levels determined in Chapter 5.0. The creep rates and strains determined from laboratory in-isolation tests, at least for geogrids and woven geotextiles, can be compared to the creep rates and strains observed for the reinforcement in the full-scale walls. This comparison should be possible whether or not the geosynthetic in the wall has experienced significant installation damage, since installation

189

Table 6.5. Reinforcement load levels estimated from strain measurements for selected case histories.

Wall Case	Depth Below Wall Top, z (m)	Load Level (% of T_{ult})	Wall Case	Depth Below Wall Top, z (m)	Load Level (% of T_{ult})
GW5	1.14	0.8	GW11	0.6	12.9
	3.28	1.5		1.35	17.5
	4.2	1.1		2.1	8.2
GW7 (Section J)	1.2	3.9		2.85	1.3
	2.4	5.3	GW14, with 80 kPa surcharge, at connection	0.5	26
	3.6	2.1		1.25	16.4
	4.2	5.9		2	14.8
	4.8	0.8		2.75	8.9
GW7 (Section N)	0.6	6.9	GW15, with 70 kPa surcharge, at connection	0.5	16.2
	1.2	6.2		1.25	22.5
	1.8	5.9		2	20.0
	2.4	5.9		2.75	12.9
	3.0	6.0	GW16, with surcharge	3.1	4.4
	3.6	5.9		6.5	3.0
	4.2	5.3		9.6	3.6
	4.8	2.3		11.5	3.8
GW8	1.2	3.9	GW18	2.44	2.9
	2.5	7.9		4.88	3.4
	4.2	8.4	GW20 (HDPE Section)	1.1	6.0
	5.0	8.2		2.7	9.8
	5.7	2.0	GW20 (PP Section)	1.6	16.5
GW9 (with surcharge)	0.8	4.5		3.2	10.7
	2.6	10.2			
	4.0	11.8			
	5.2	10.2			
	5.8	2.7			

damage has little effect on creep strains and rates, provided that the load level is below the creep rupture limit for the reinforcement (Allen and Bathurst 1996).

If the strain level is held constant and the stress level in the reinforcement is allowed to decrease with time, stress relaxation occurs. The stress relaxation process has similarities to creep, in that molecules within the polymer must slip past one another in response to load. Both stress relaxation and creep can occur in the reinforcement, depending on the creep rate of the soil relative to the creep rate of the geosynthetic.

The writers reviewed typical sand creep data from triaxial compression tests presented by Kuhn and Mitchell (1993) that show that the creep of sands can be significant. After triaxial strain rates were adjusted to account for plane strain boundary conditions (i.e., plane strain

values are about 2 to 2.5 times less than comparable triaxial test values, according to Lee (2000), it was apparent that sand strain rates can be of the same order of magnitude, or slightly less than, tensile creep rates observed in-situ for geosynthetic reinforcement materials under working stress conditions.

An implication of this comparison is that the soil, provided it has not reached its peak shear stress, can restrict the creep deformation of the geosynthetic, but only if the creep rate of the backfill soil is less than the creep rate of the geosynthetic reinforcement. If the soil controls the creep rate of the composite system, the molecules within the geosynthetic polymer can still slip past one another because of the load applied to the polymer, resulting in stress relaxation. Note that if stress relaxation does occur and composite creep strain levels are restricted by the soil, measured creep rates for reinforcement in granular backfill soil can be expected to be lower than values measured during in-isolation laboratory creep tests.

For geosynthetics that have significant macro-structure complexity (e.g., nonwoven geotextiles), reduced time-dependent macrostructure rearrangements should be expected in soil relative to creep behavior of the same geosynthetics tested under in-isolation laboratory conditions (Elias et al. 1998b). However, reduced macro-structure creep will not be a significant factor for most geogrids and woven geotextiles.

There is a significant difference between the way the geosynthetic is loaded in the laboratory and the way it is loaded in full-scale walls. Laboratory creep specimens are brought up to the creep load rapidly (on the order of seconds), whereas in the field the loading of the geosynthetic up to its final load is very slow (on the order of 1,000 hours). This large difference in loading rate does have a significant influence on the short-term creep rates observed in the wall versus what is observed in the laboratory. The difference is illustrated in Figure 6.1 for an HDPE geogrid taken from work by Rimoldi and Montanelli (1993). However, in the long term the strains in the specimen are not influenced by the initial loading condition. Yeo (1985) also observed a similar effect due to loading rate. In the current investigation, time zero was adjusted to the beginning of wall construction to provide a meaningful evaluation of creep strain rates from both in-isolation and in-wall data (Figure 6.2).

Temperature can also affect the creep rates observed, especially for polyolefins. Temperature needs to be considered when creep data from laboratory testing are compared with creep measurements from full-scale field structures.
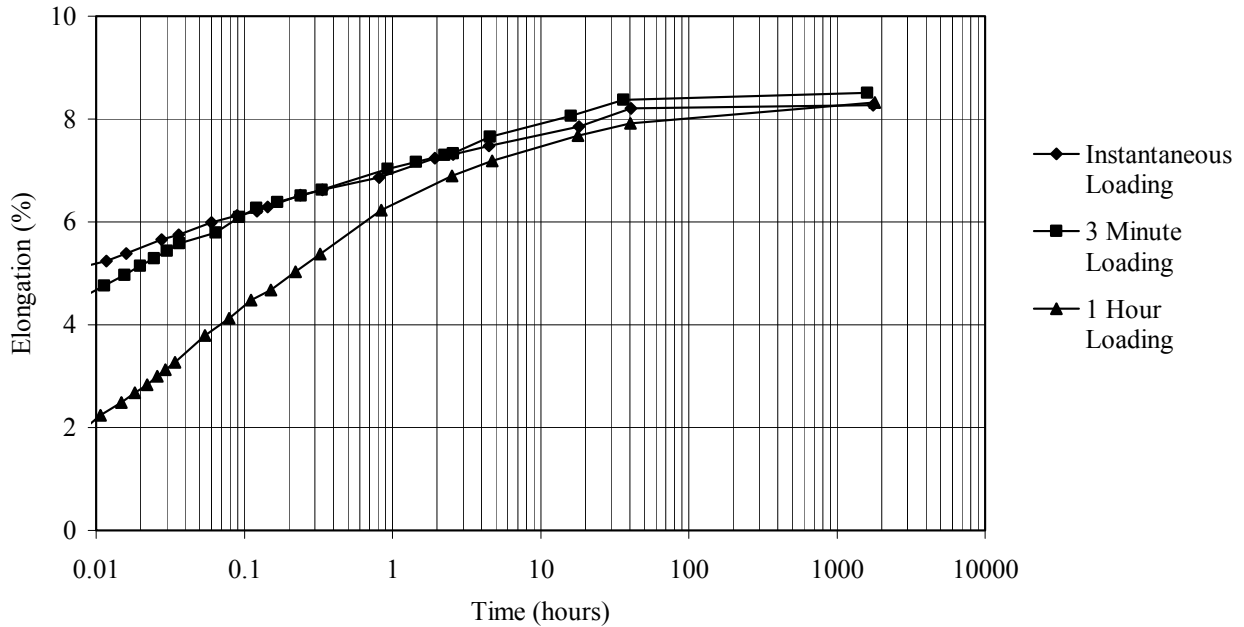
Figure 6.1. Effect of loading rate on measured creep strains for an HDPE geogrid (after Rimoldi and Montanelli 1993).
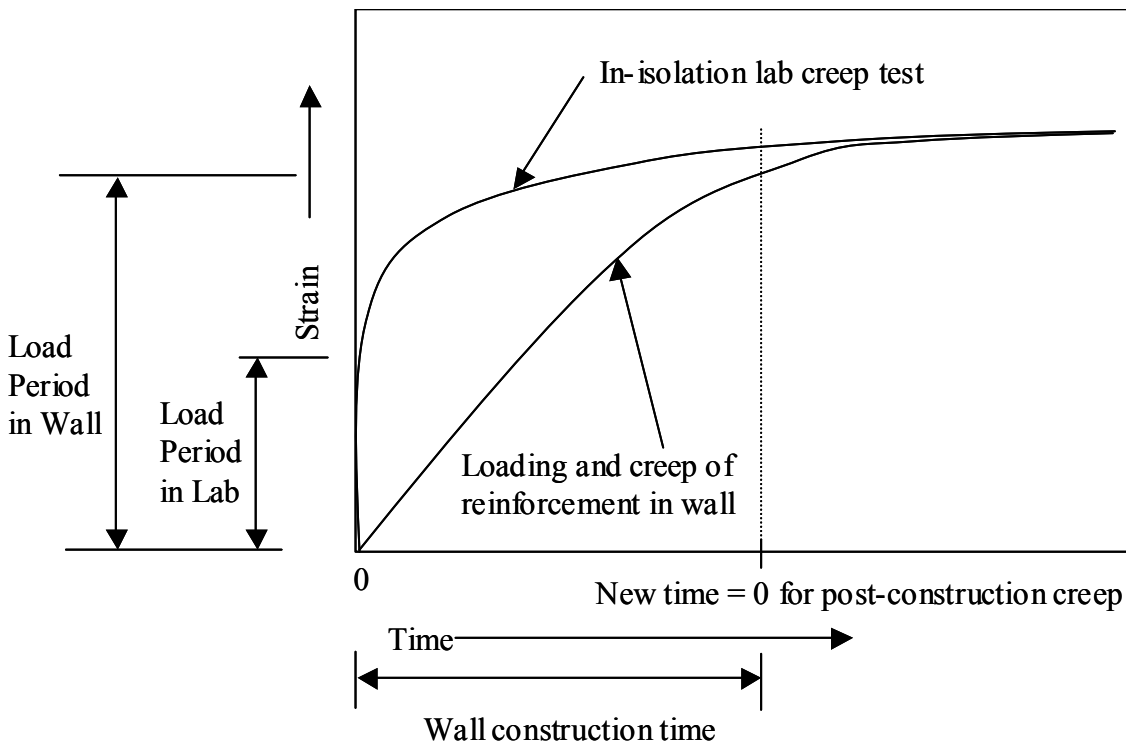
Figure 6.2. Conceptual illustration for comparing the creep measured in walls to in-isolation laboratory creep data.

6.5 Long-Term Creep and Deformation Observations and Background

Long-term measurements of creep strains, creep strain rates, and lateral wall deformations are provided in figures 6.3 through 6.32. Additional data from the other case studies reviewed can be found in Appendix B. The sources for all of the long-term creep strain and deformation data used to produce these figures are identified in Table 6.1. Note that for strain gauges, the strain reported herein has been corrected with strain gauge calibration data (see Chapter 3.0). In all cases, the creep strains presented are from locations with the largest strains in a given layer, which were typically located near the boundary between the active and resistant zones but in some cases near the connection with the face. Therefore, the measured creep strains are representative of the maximum load levels in the reinforcement layers.

In all cases, except for the highest surcharge loading for the full-scale test walls GW14 and GW15, the creep strains increased at a decreasing rate with time, indicating that only primary creep occurred. The last strain readings for GW5 and GW7 indicate that strain was actually decreasing.

6.5.1 Comparison of Strain and Deformation Data

Figures 6.3 and 6.4 provide a comparison of strains and deformations measured as a function of time for walls GW9 and GW16. Note that for these walls creep strains were generally less than 0.4 percent, and at some locations less than 0.1 percent strain. Creep deformations at the wall face were also small, on the order of 20 mm or less. Similar comparisons can be made for Walls GW11 and GW18 (see Appendix B). What can be observed from these comparisons is that the patterns of creep deformation and creep strain show similar trends of decreasing creep strains and deformations.
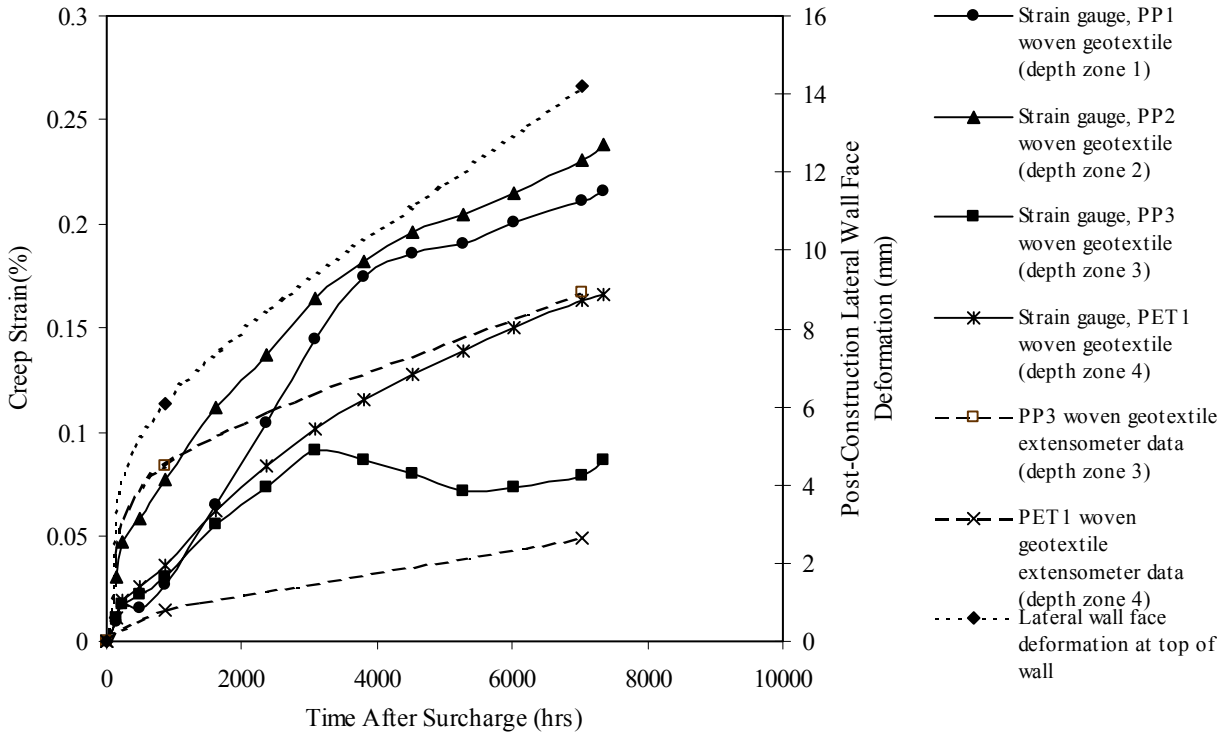
Figure 6.3. Measured creep strains and deformations for Wall GW16.
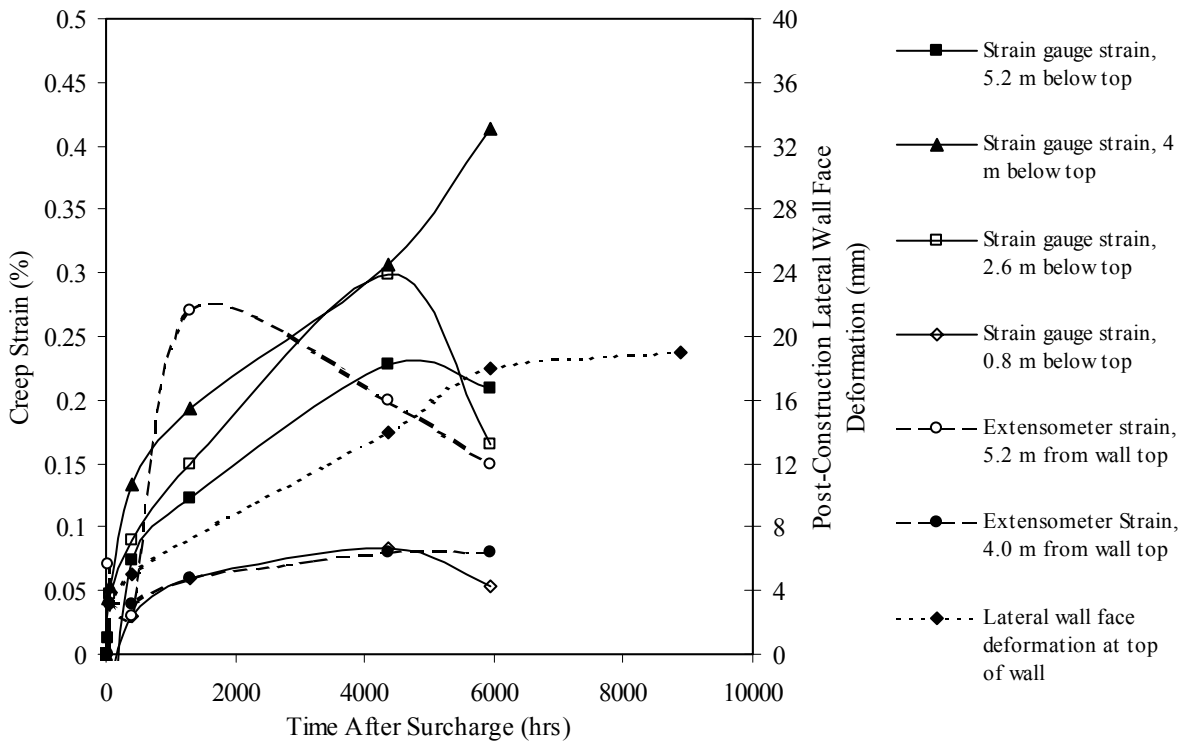
Figure 6.4. Measured creep strains and deformations for Wall GW9.

6.5.2 Creep Strain Data

Figures 6.5 through 6.13 provide examples of plots of total creep strain as a function of time from the beginning of wall construction or laboratory creep test loading. The in-isolation laboratory creep strains correspond to load levels in the wall reinforcement estimated from in-situ strain measurements at the end of wall construction. The in-isolation creep curves for load levels estimated from current design methods using measured soil shear strength values and soil unit weights (Simplified Method) are also plotted in figures 6.5 through 6.11.

In general, the creep strains estimated from in-isolation data at the load level observed in the wall reinforcement were greater than the creep strains measured in the wall reinforcement, indicating that either the load estimated from measured wall reinforcement strain at the end of wall construction was too large, or that in-isolation creep strains and rates were greater than in-soil creep strains and rates at the same load level.
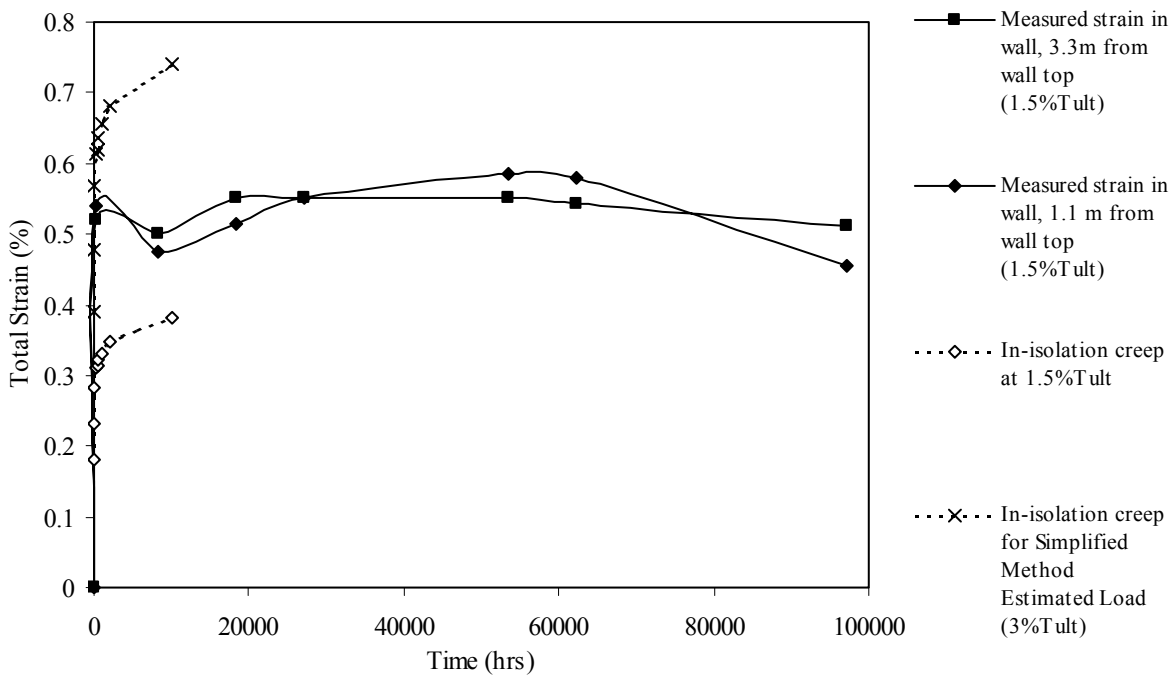
Figure 6.5. Long-term strain for Wall GW5.
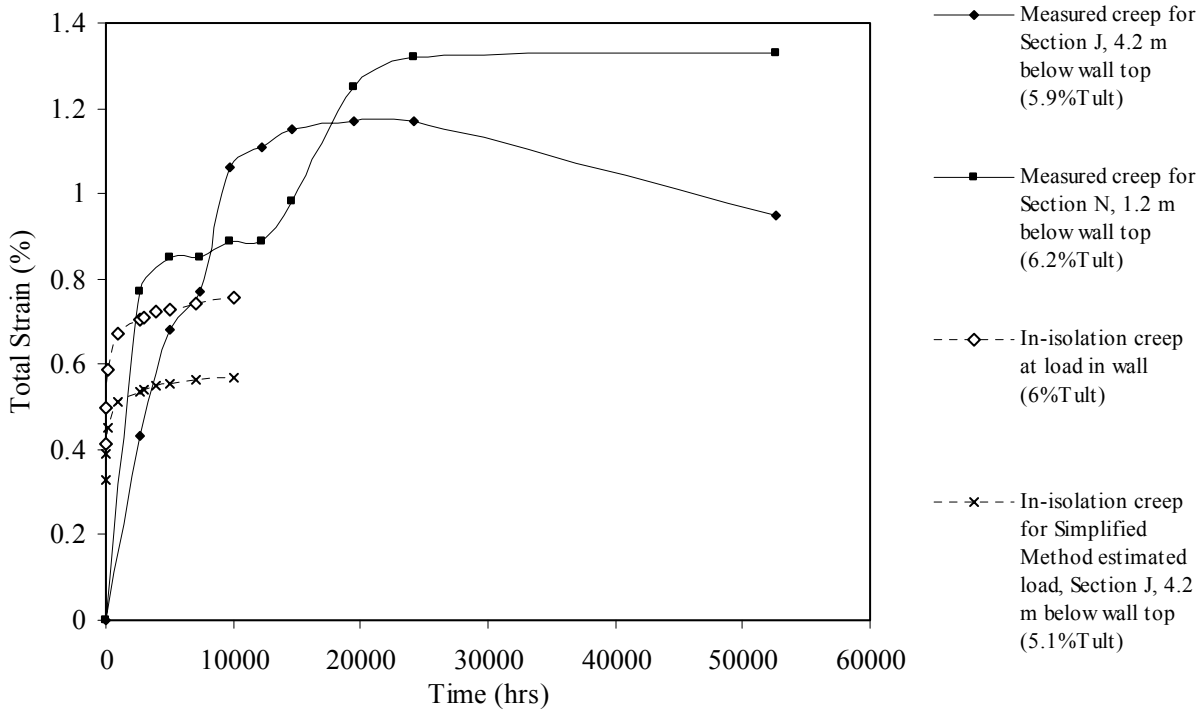
Figure 6.6. Wall GW7 long-term strains.
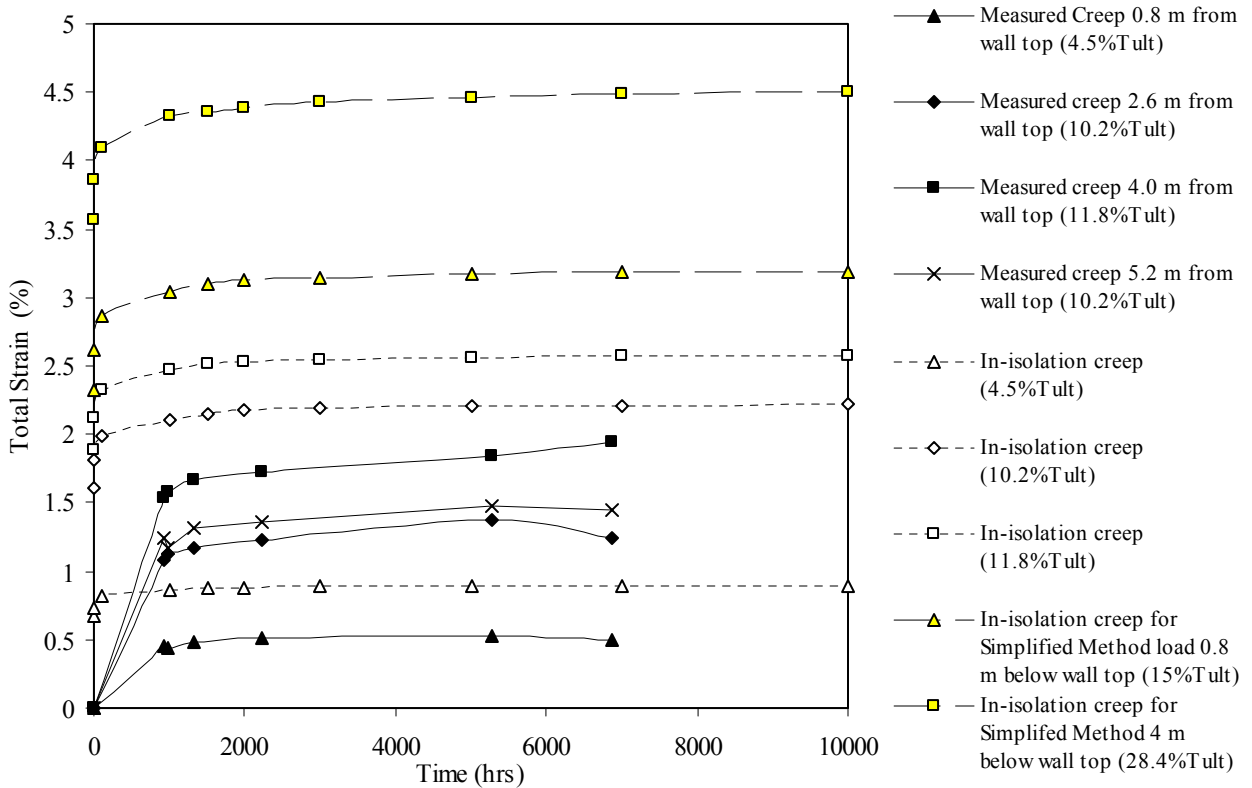
Figure 6.7. Long-term strains for Wall GW9.
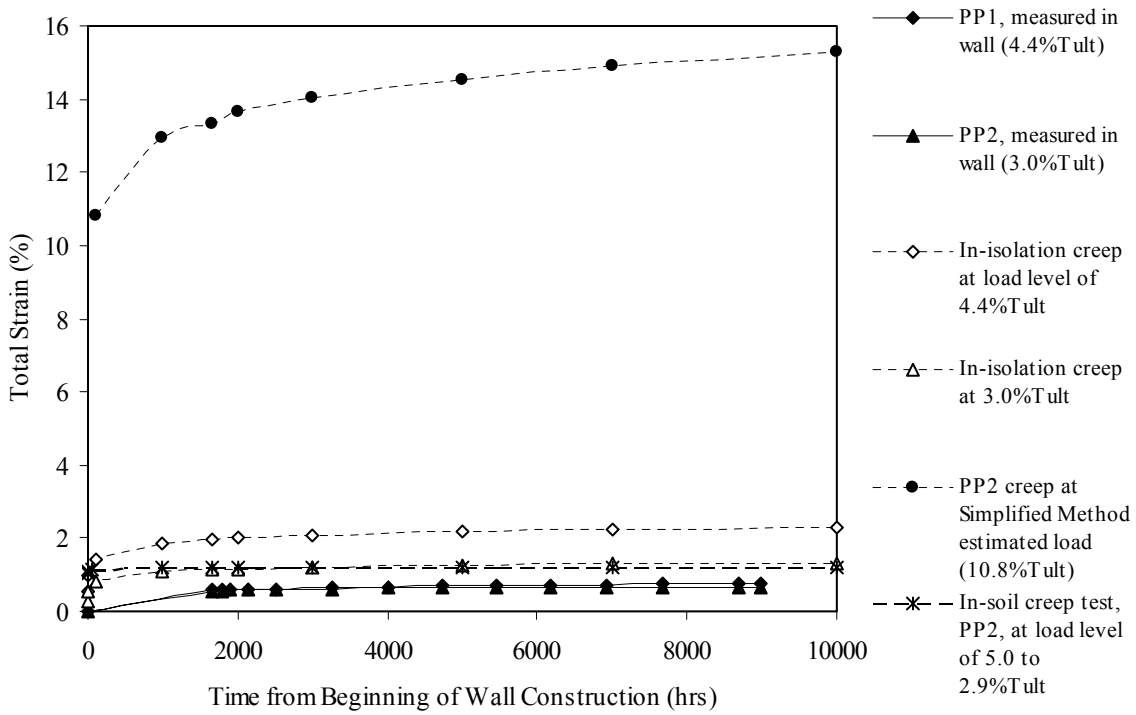
Figure 6.8. Wall GW16 long-term strains.
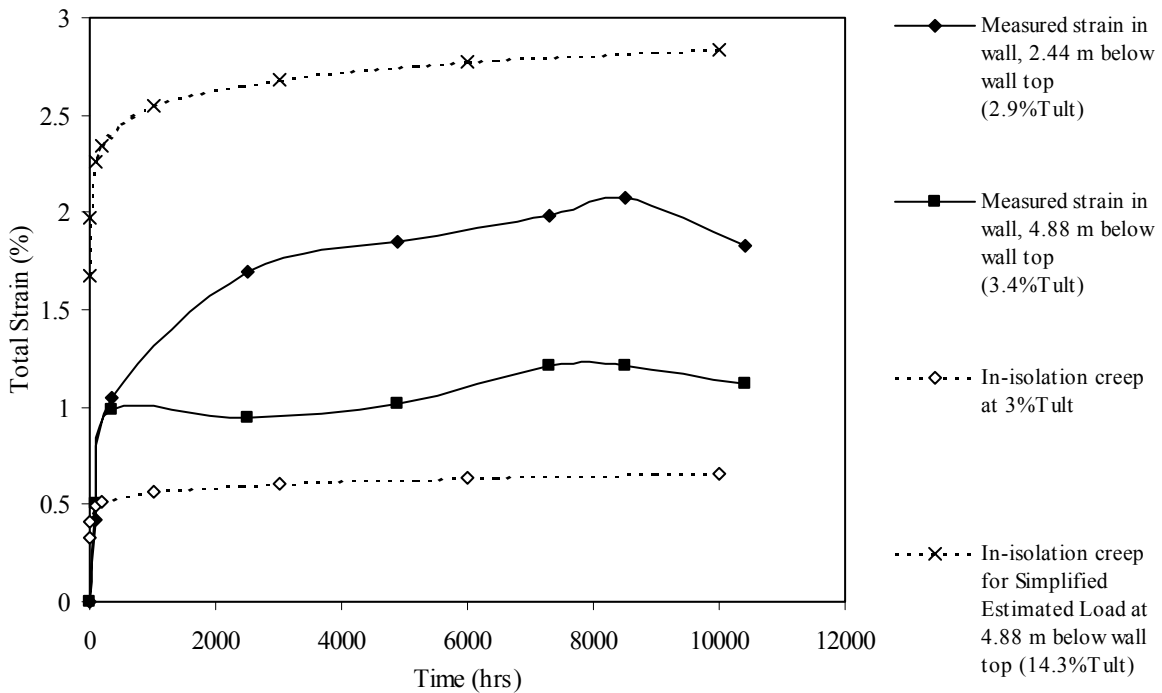
Figure 6.9. Long-term strain for Wall GW18.
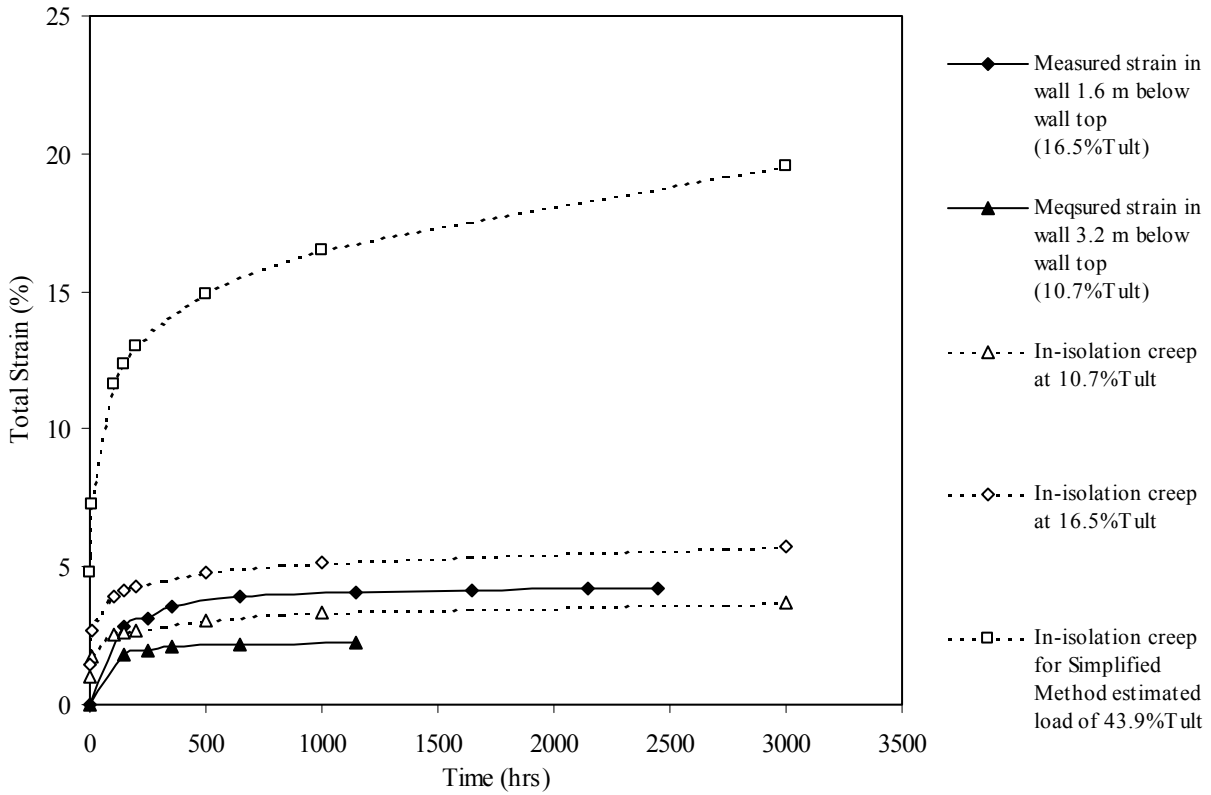
Figure 6.10. Long-term strain for Wall GW20, PP section.
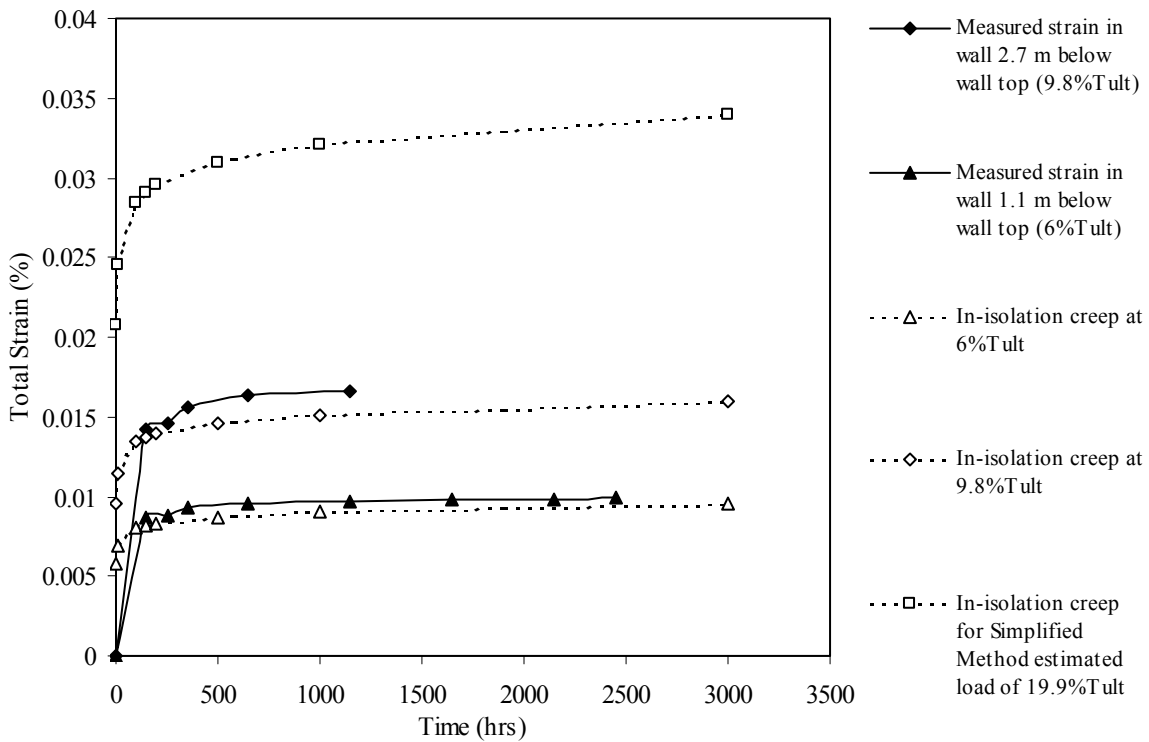
Figure 6.11. Long-term strain for Wall GW20, HDPE section.
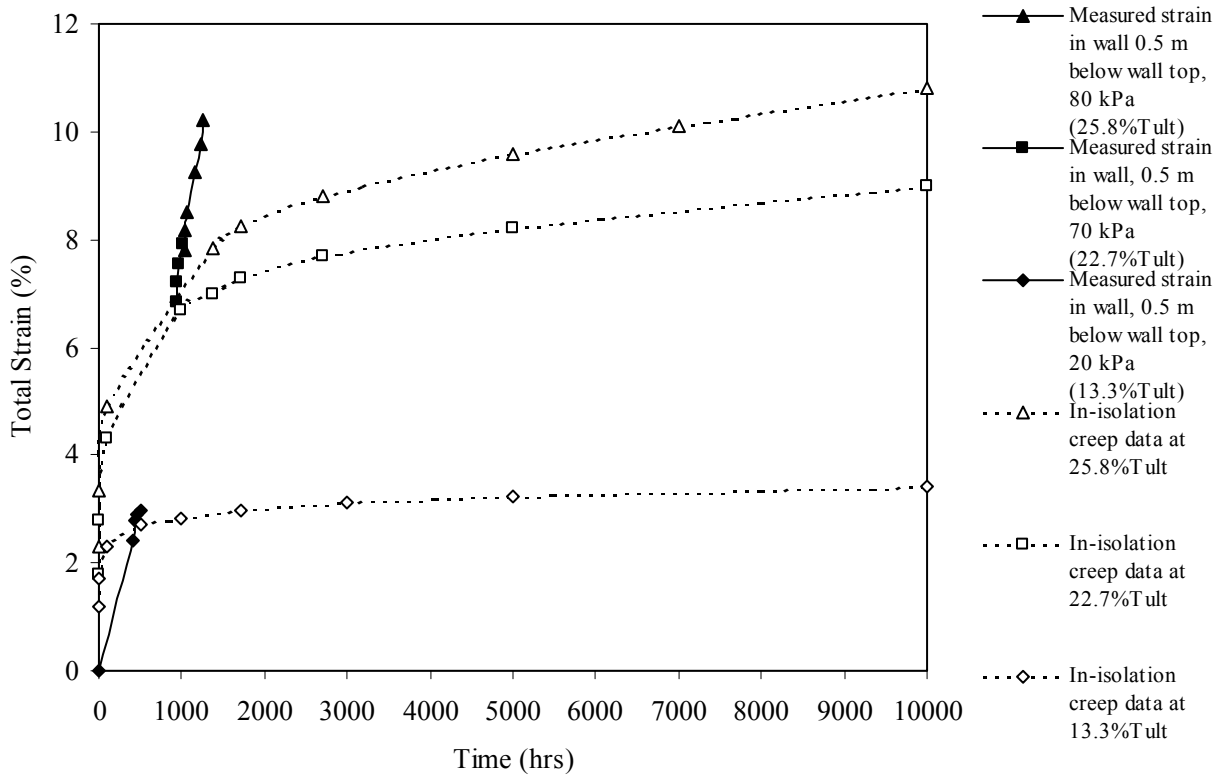
Figure 6.12. Total long-term strain for Wall GW14.
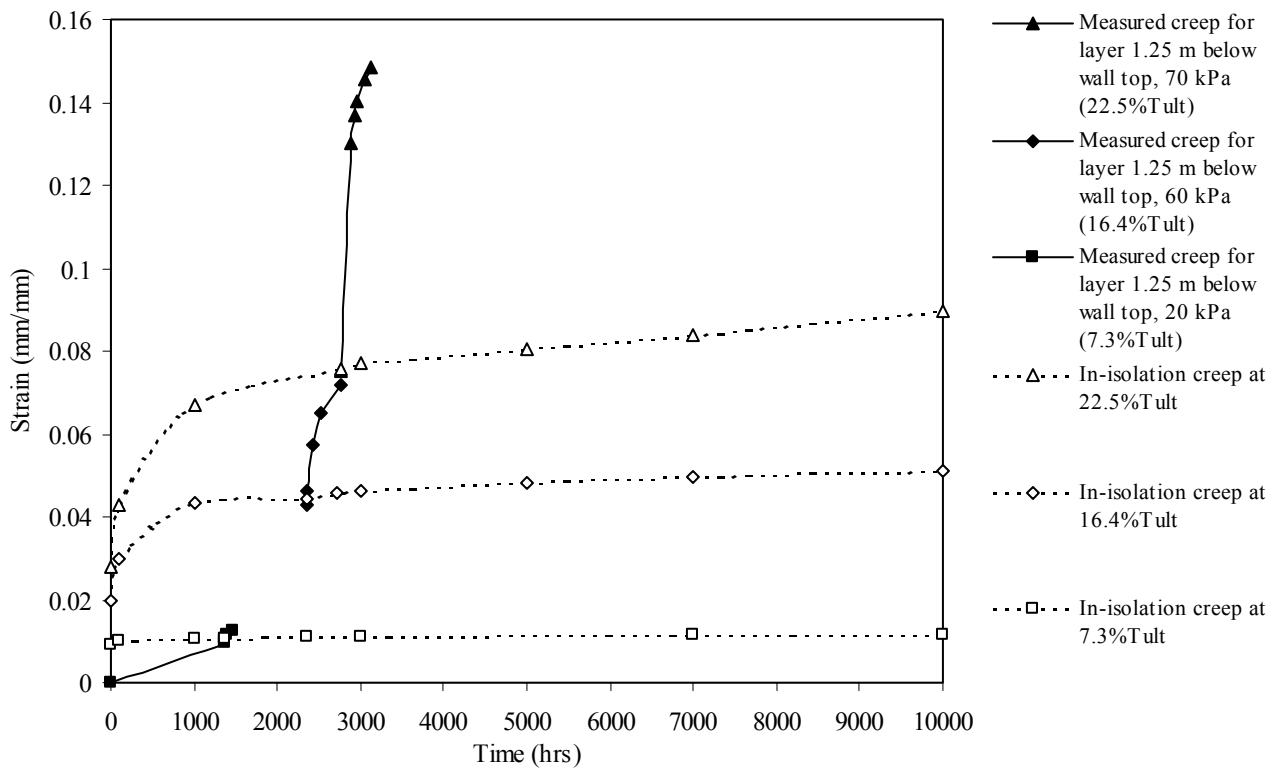
Figure 6.13. Total long-term strain for Wall GW15.

199

6.5.3 Creep Strain Rate Data

Insights into the long-term creep behavior of wall reinforcement can be gained by evaluating the creep strain rates measured in the wall reinforcement layers. Figures 6.14 through 31 provide comparisons of strain rates determined from in-isolation creep tests at the load level estimated in the wall reinforcement from measured strain data, and strain rates determined from as-measured post-construction strains in the walls. The in-isolation laboratory creep rate data at the load level estimated for the reinforcement layer with the Simplified Method are also shown.

Two types of plots are provided: Sherby-Dorn plots, and log strain rate versus log time plots. A Sherby-Dorn plot is a well known plotting technique used in polymer science (McGown 1984, WSDOT 1998). Each curve represents a specific geosynthetic layer in a wall or a specific geosynthetic specimen tested at a specific load level. Creep strain rates observed under constant load are plotted against the total strain in the specimen or layer measured at the time the creep strain rate was calculated. The creep strain rate is simply the slope of the creep strain curve at a given point in time. Curves that are linear or concave downward indicate that only primary creep is occurring and that stabilization (no rupture) is likely. Curves that are concave upward indicate that secondary or tertiary creep is occurring and that rupture is likely. The closer the curves are located to the bottom left corner of the plot, the better the creep performance of the material. The closer the curves are to the upper right corner, the more likely creep rupture will occur. For the log strain rate versus log time plots, curves that decrease linearly with time, or are concave downward, indicate that only primary creep is occurring and that stabilization will eventually occur. Curves that are horizontal or concave upward indicate that secondary or tertiary creep is occurring, which will potentially result in rupture at some time.

Note that some interpretation of the creep curves through curve fitting is required to determine strain rates, since local jumps in the measured creep strain curves can cause wide variations in calculated creep strain rates. The jumps in the curves are typically the result of the short increments of time used in the calculations and the small magnitude of changes in strain readings that may be at the limit of the resolution of the measuring devices. Hence, the slope of the measured creep curves must be taken over fairly long increments of time to be meaningful. Such an approach was taken to determine the creep rates for this study.
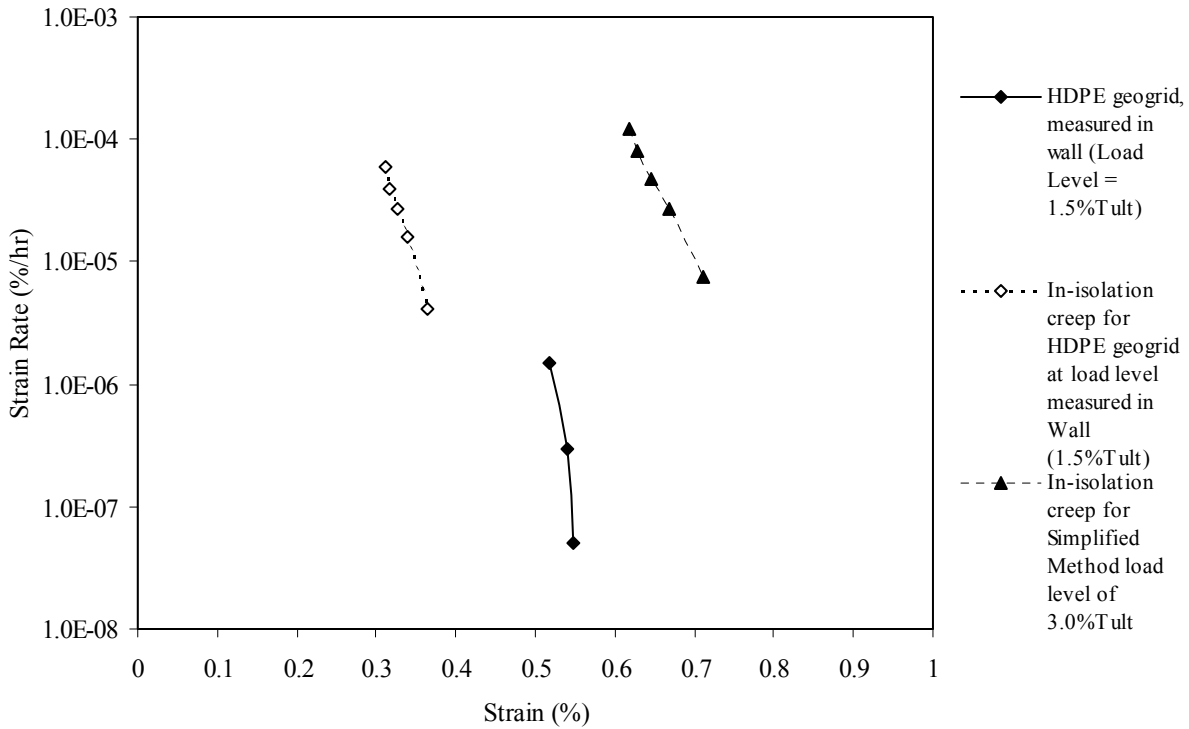
Figure 6.14. Sherby-Dorn plots for Tanque Verde HDPE geogrid walls (GW5) using in-isolation and measured strain data.
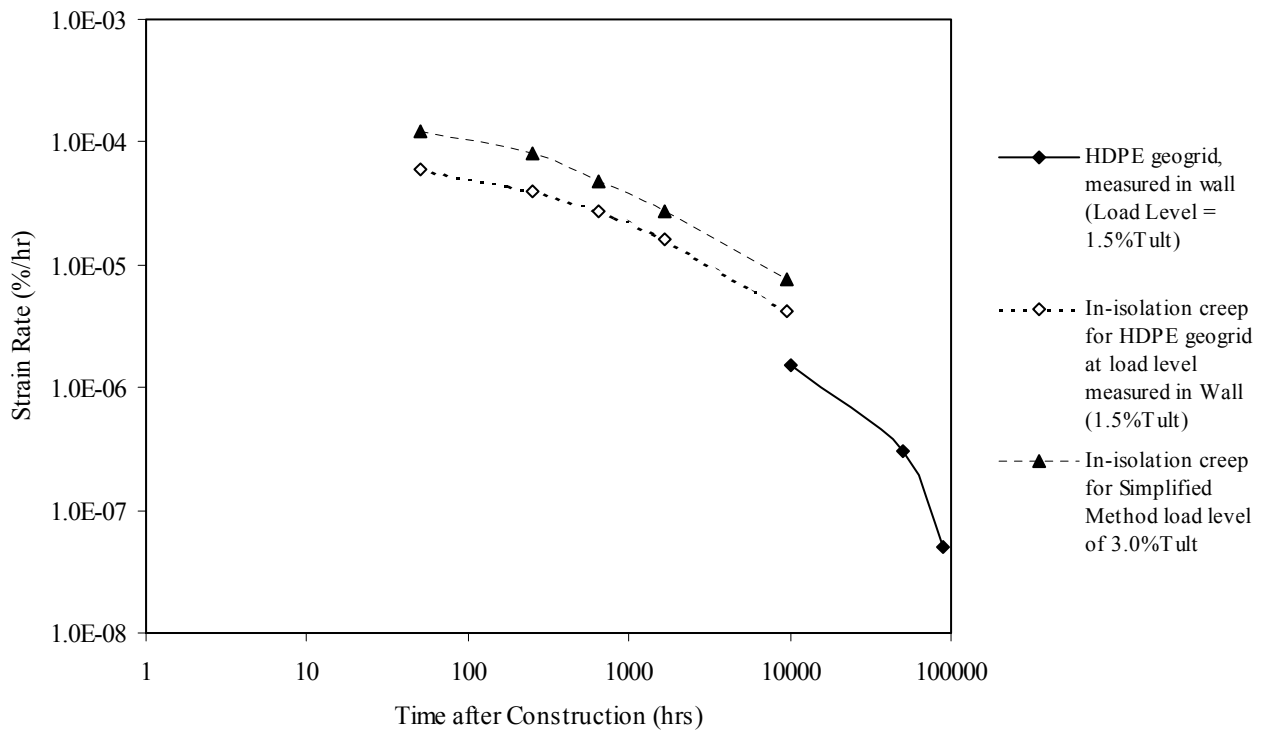
Figure 6.15. Strain rate versus time for Tanque Verde HDPE geogrid walls (GW5) using in-isolation and measured strain data.
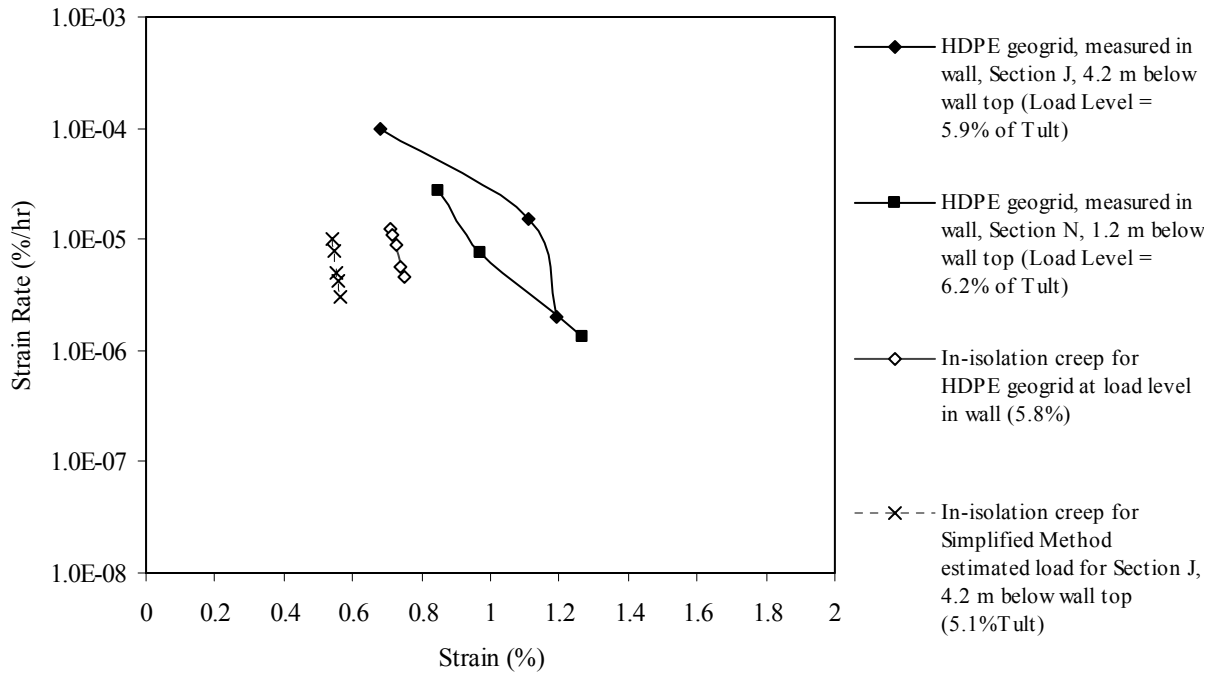
Figure 6.16. Sherby-Dorn plot for Oslo, Norway, HDPE geogrid walls (GW7)— in-isolation vs. measured in wall.
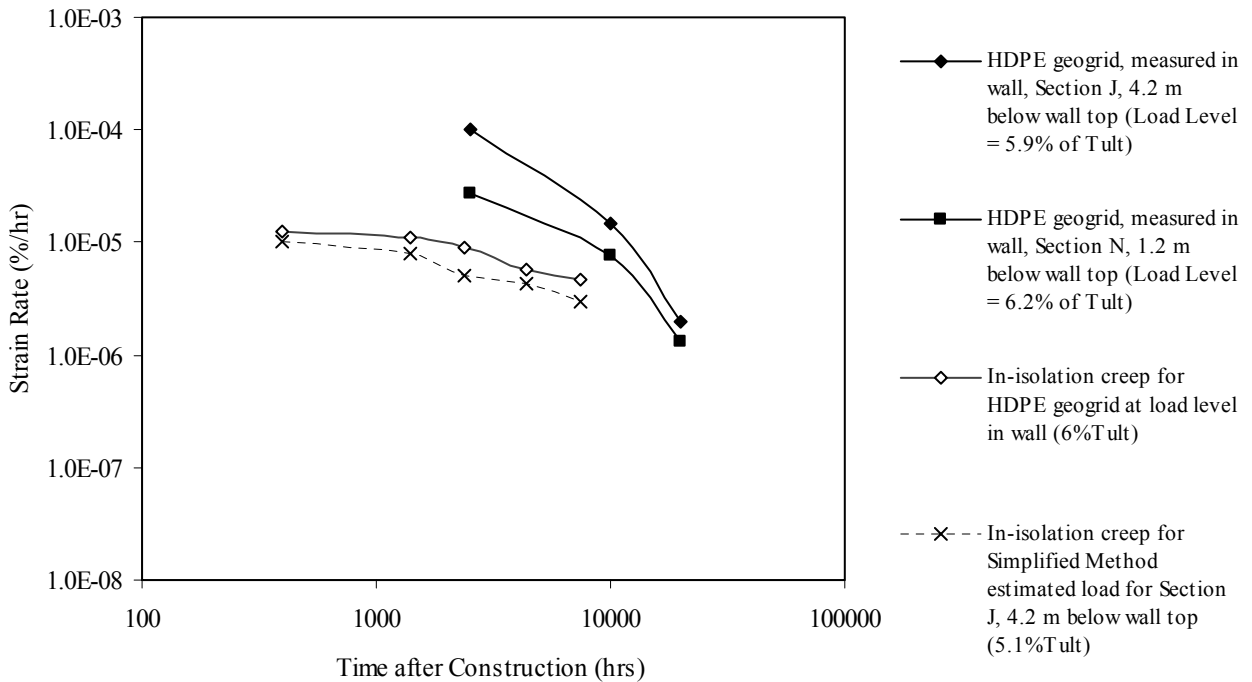
Figure 6.17. Strain rate vs. time for Oslo, Norway, HDPE geogrid walls (GW7)—in-isolation vs. measured in wall.

202
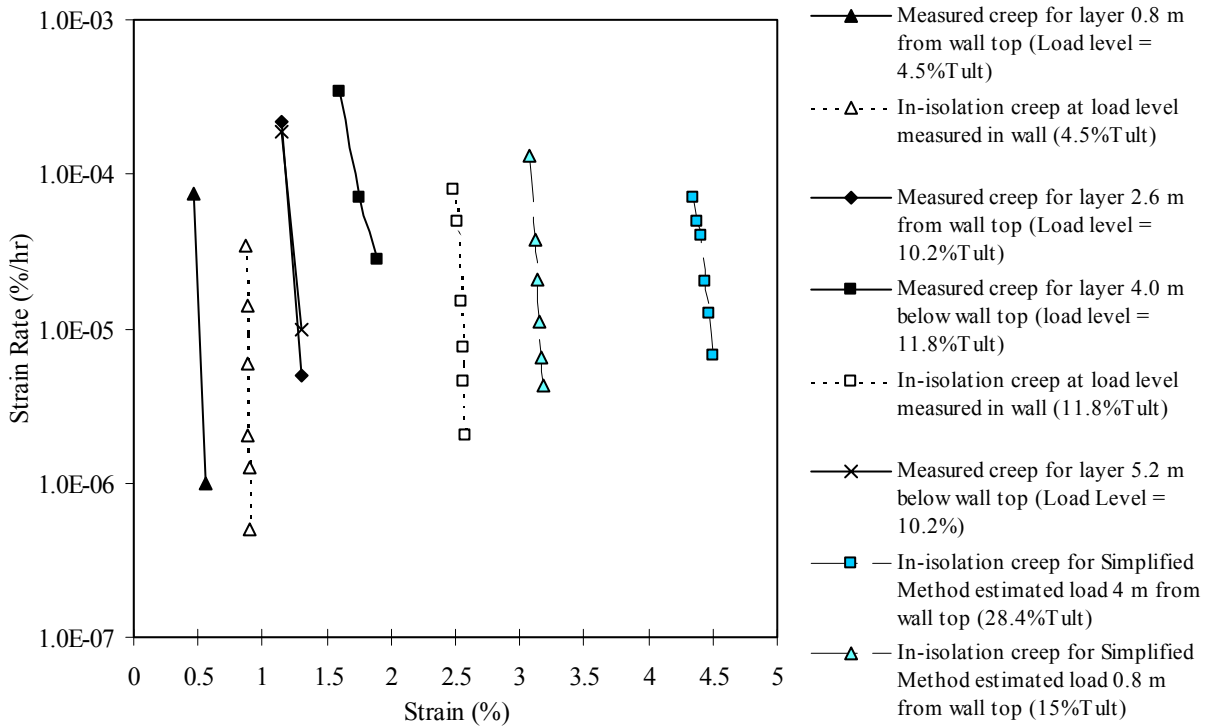
Figure 6.18. Sherby-Dorn plot for Algonquin PET geogrid wall (GW9)—in-isolation vs. measured in wall.
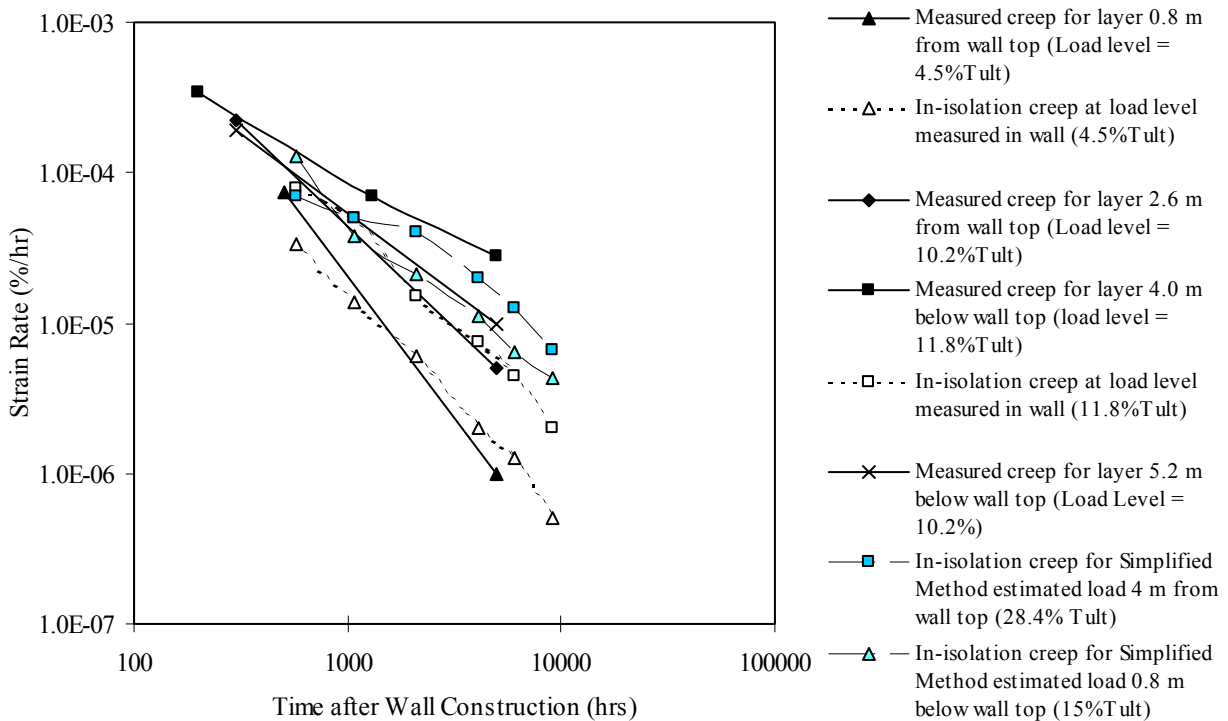
Figure 6.19. Strain rate vs. time for Algonquin PET geogrid wall (GW9)—in-isolation vs. measured in wall.
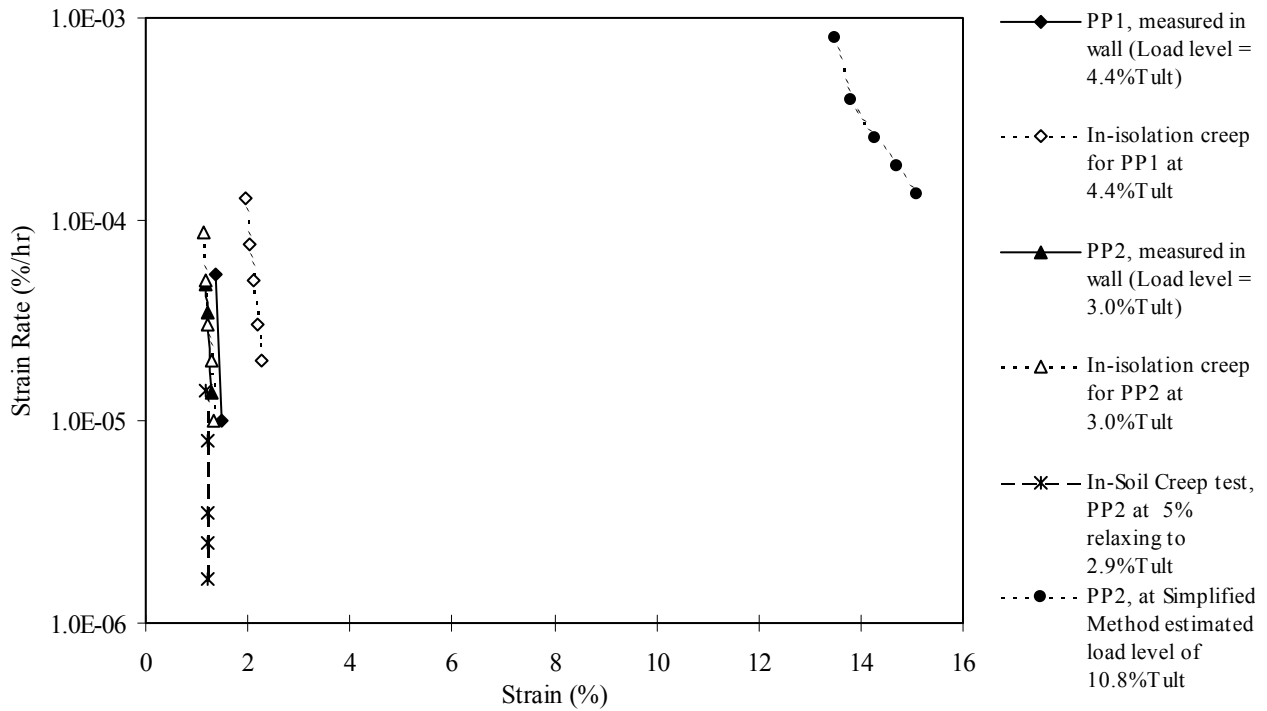
Figure 6.20. Sherby-Dorn plot for Rainier Ave. PP geotextiles (GW16)—in-isolation vs. measured in wall.
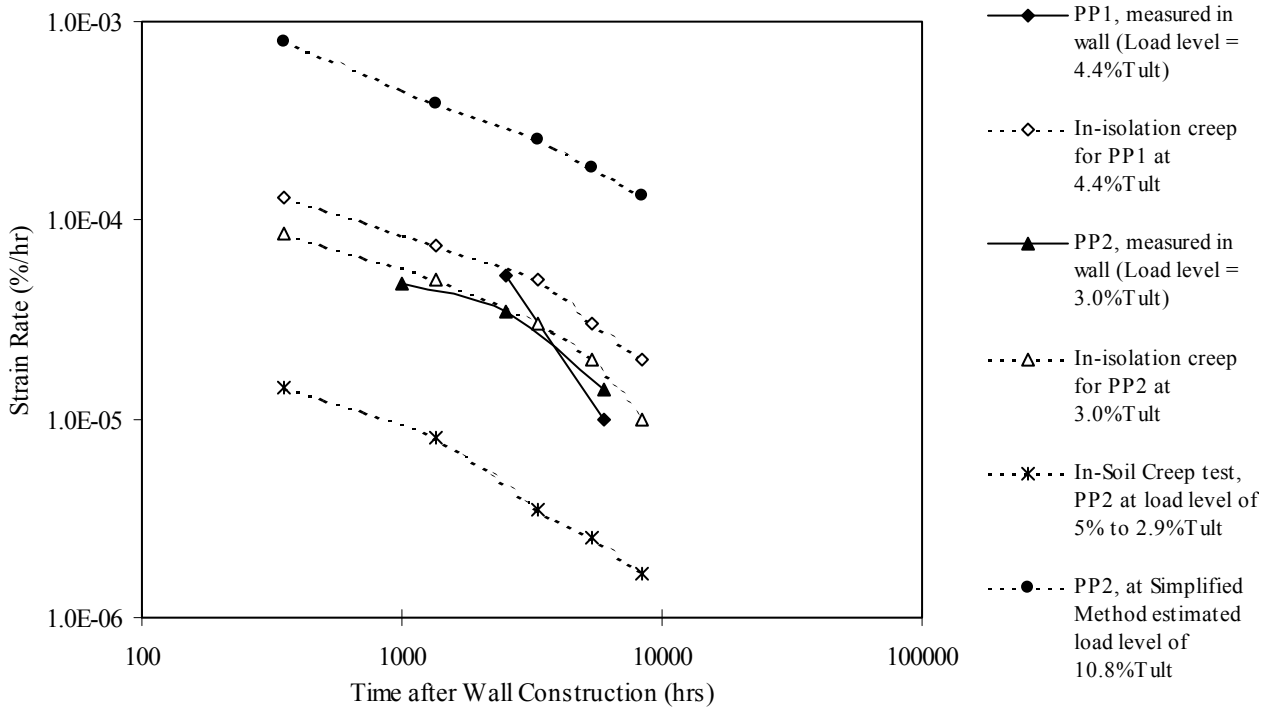
Figure 6.21. Creep rates as a function of time for Rainier Ave. PP geotextiles (GW16)—in-isolation vs. measured in wall.

204
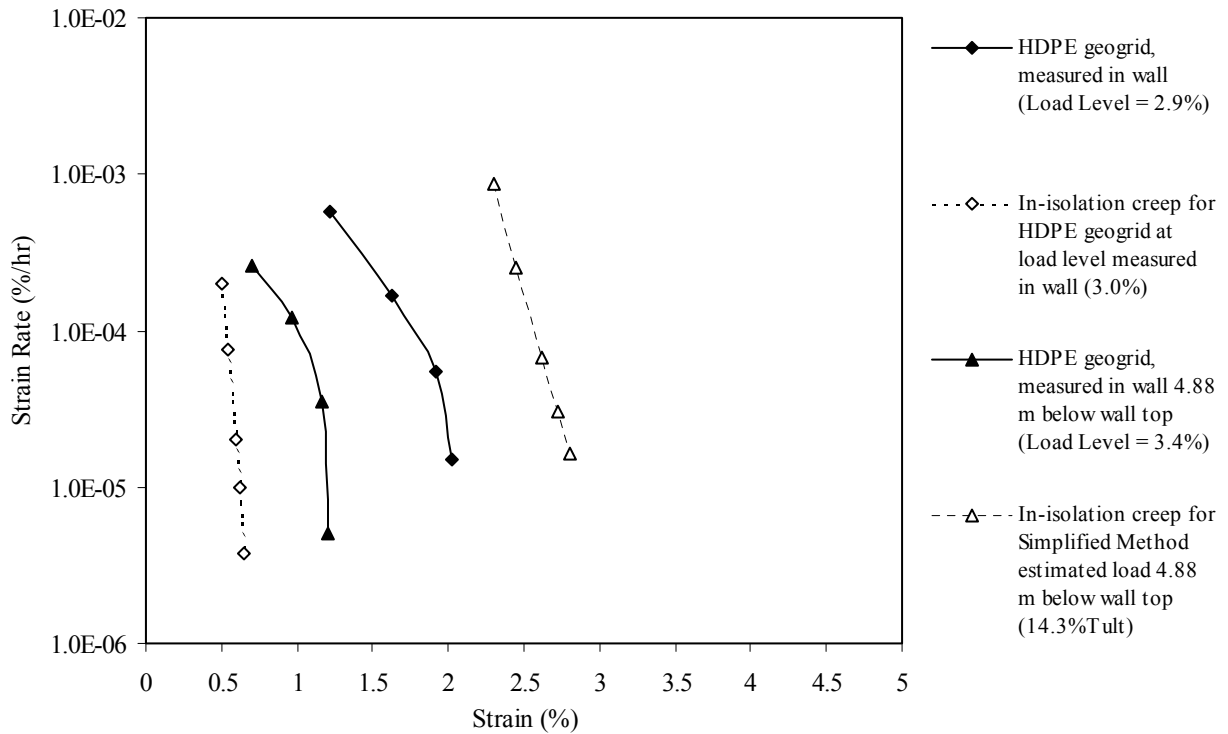
Figure 6.22. Sherby-Dorn plot for Fredericton HDPE geogrid walls (GW18)—in-isolation vs. measured in wall.
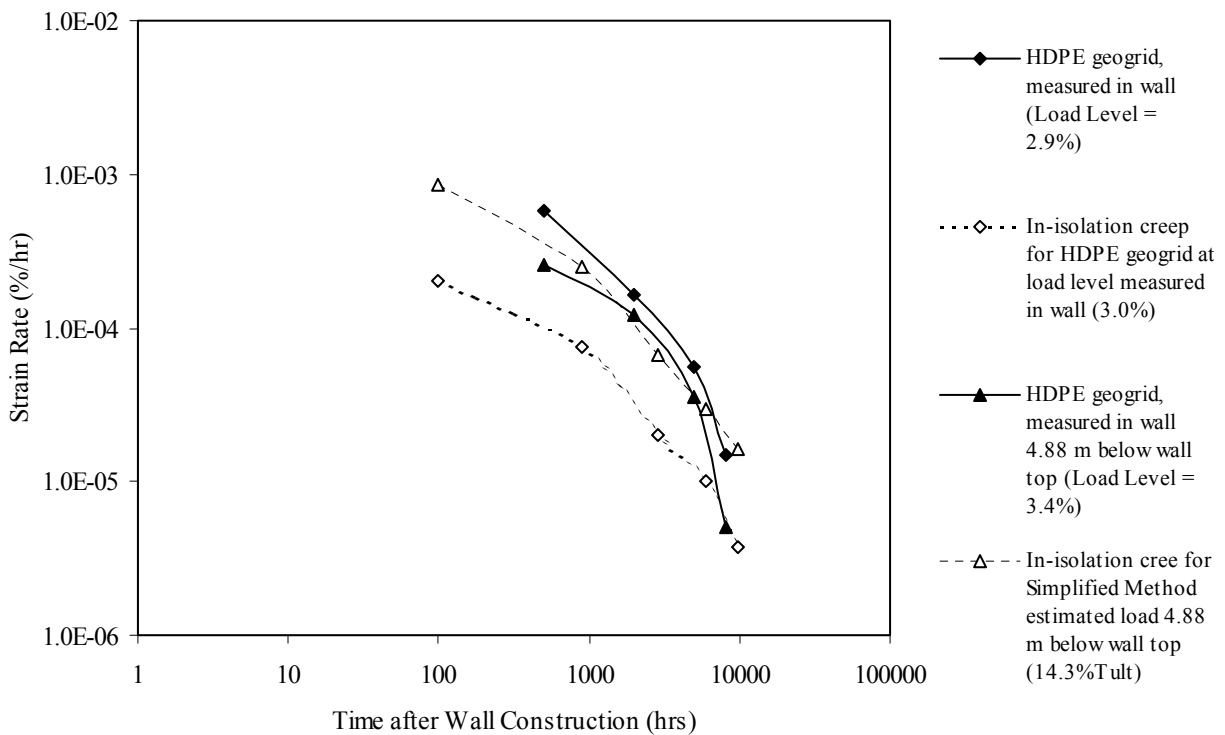
Figure 6.23. Strain rate vs time for Fredericton HDPE geogrid walls (GW18)—in-isolation vs. measured in wall.
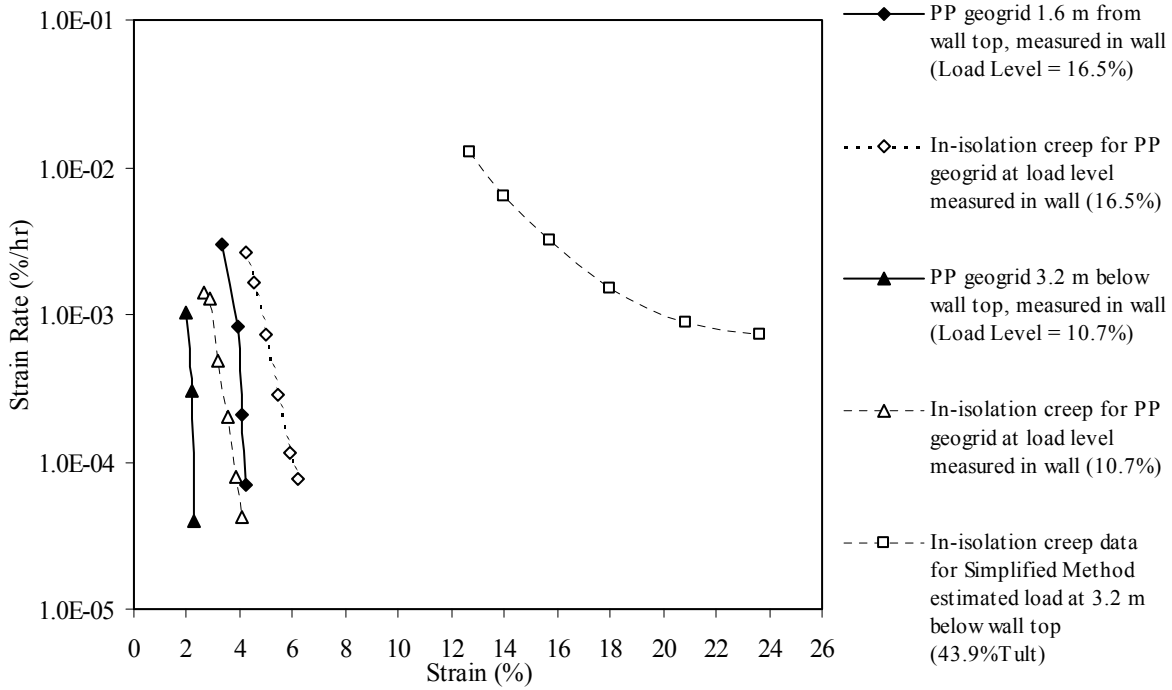
Figure 6.24. Sherby-Dorn plot for Vicenza, Italy, PP geogrid wall (GW20)—in-isolation vs. measured in wall.
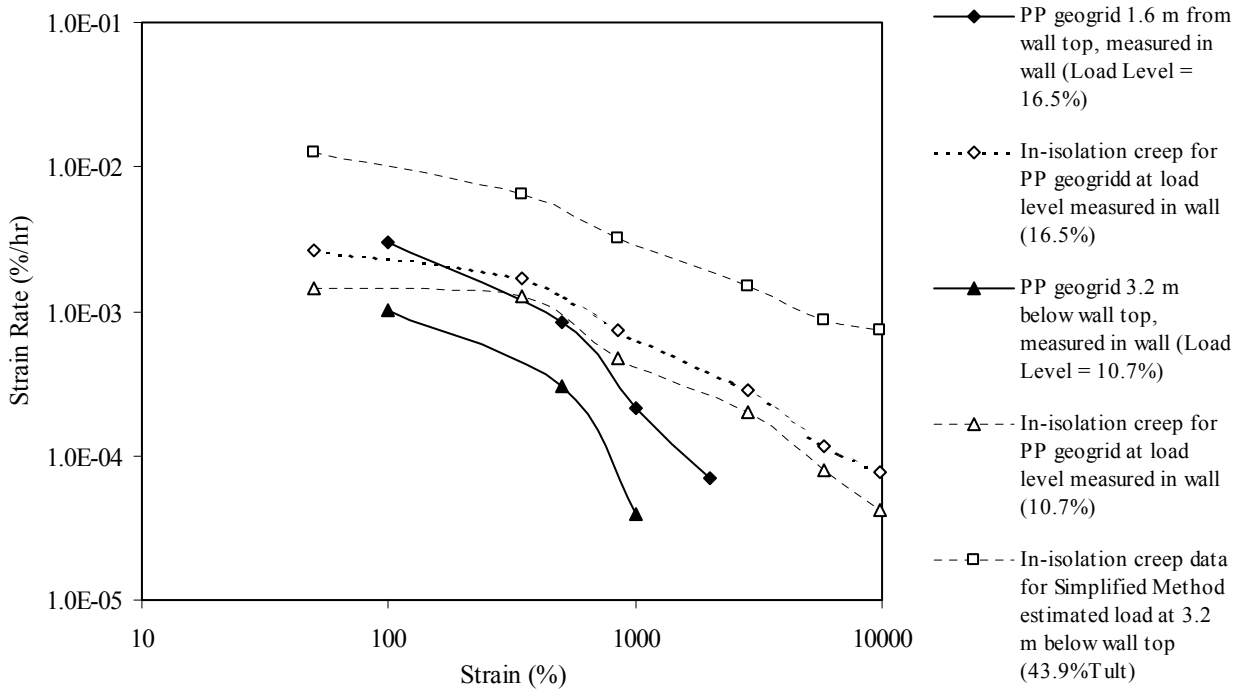
Figure 6.25. Strain rate vs. time for Vicenza, Italy, PP geogrid wall (GW20)—in-isolation vs. measured in wall.

206
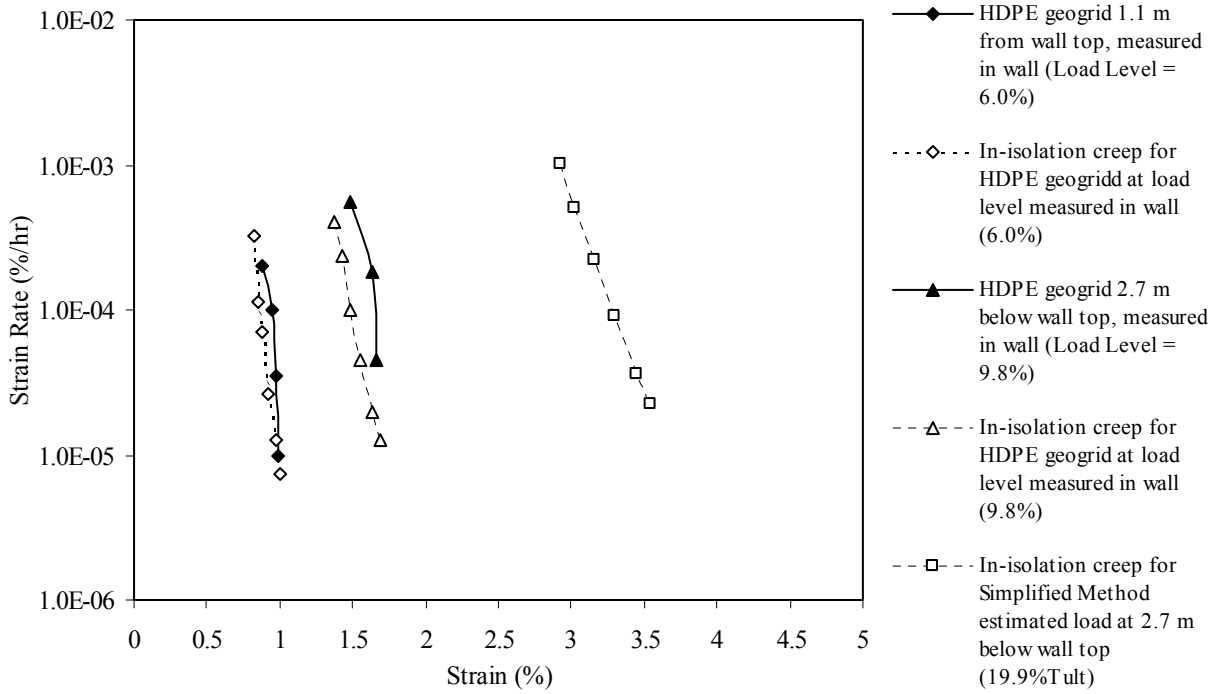
Figure 6.26. Sherby-Dorn plot for Vicenza, Italy, HDPE geogrid wall (GW20)—in-isolation vs. measured in wall.
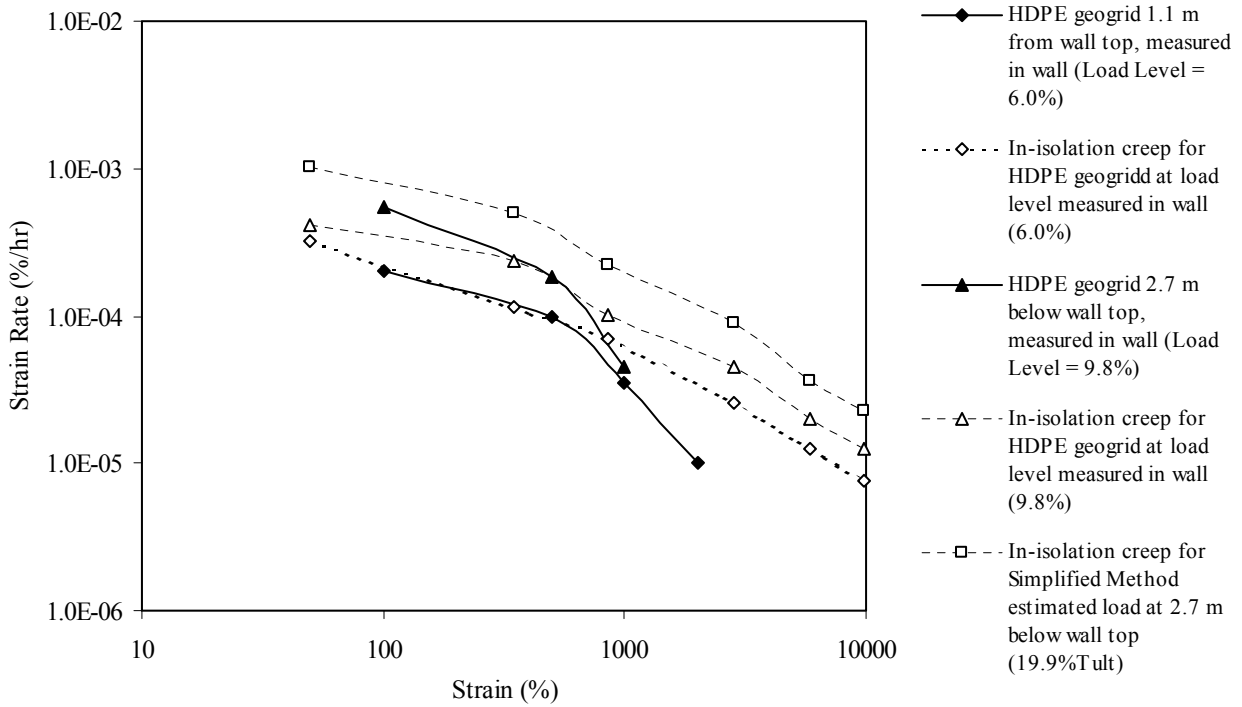
Figure 6.27. Strain rate vs. time for Vicenza, Italy, HDPE geogrid wall (GW20)—in-isolation vs. measured in wall.

207
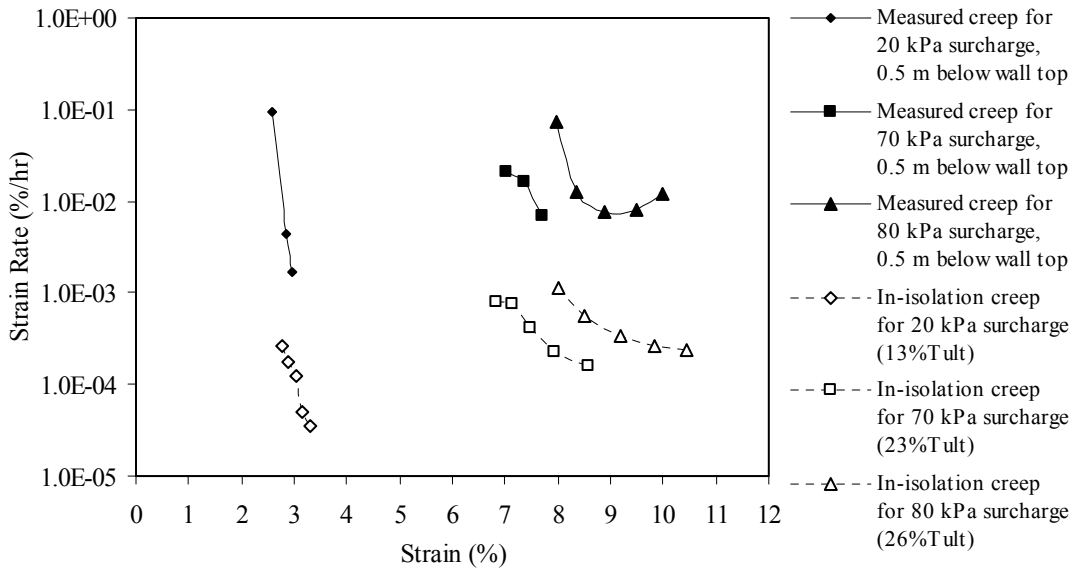
Figure 6.28. Sherby-Dorn plot for wall GW14 propped panel, PP, geogrid full-scale test wall—in-isolation vs. measured in wall.
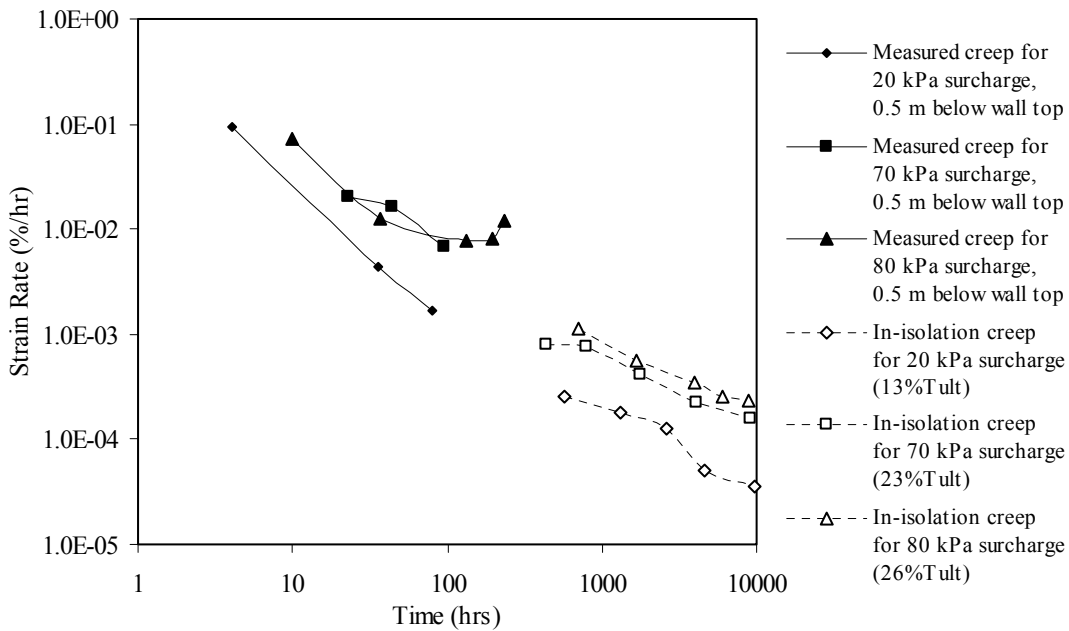
Figure 6.29. Strain rate vs. time for wall GW14 propped panel, PP, geogrid full-scale test wall—in-isolation vs. measured in wall.

208
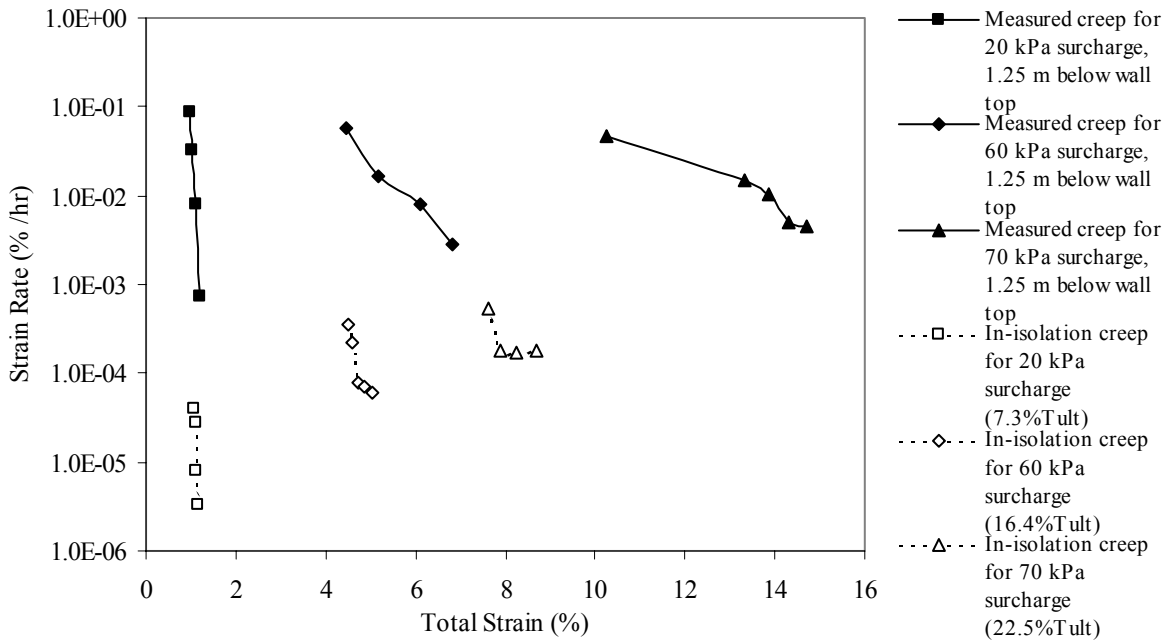
Figure 6.30. Sherby-Dorn plot for wall GW15 incremental panel, PP, geogrid full-scale test wall—in-isolation vs. measured in wall.
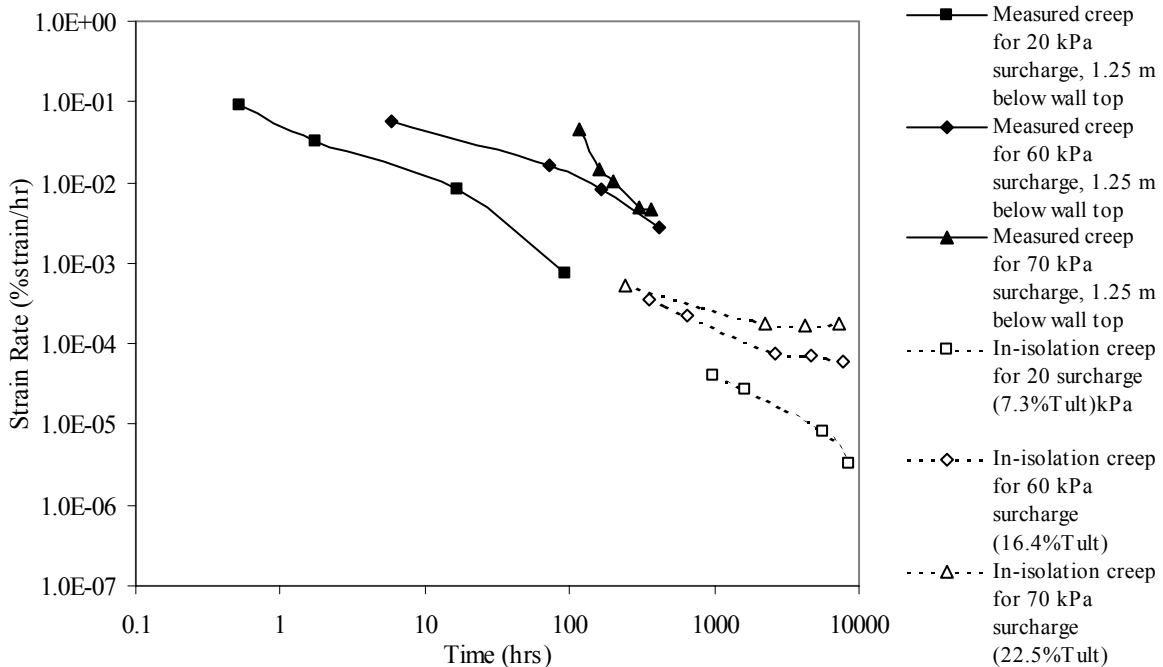
Figure 6.31. Strain rate vs. time for Wall GW15 incremental panel, PP, geogrid full-scale test wall—in-isolation vs. measured in wall.

6.6 Analysis of Case History Creep and Deformation Measurements

6.6.1 Creep Strains and Rates

Table 6.6 summarizes of the average values of the ratios of creep strains and rates measured in-isolation in the laboratory and measured in full-scale walls.

Table 6.6. Comparison of in-isolation to measured creep strains and rates for full-scale walls.

Wall	Reinforcement Type	Depth Below Wall Top (m)	Average Ratio – In-Isolation to Measured Total Creep Strain at EOC	Time Increment After EOC (hrs)	Average Ratio – In-Isolation to Measured Creep Rate
GW5	HDPE geogrid	1.14 and 3.28	0.6	all	23
GW7	HDPE geogrid	1.2 and 4.2	0.9	0 to 10,000	0.12 to 0.25
				10,000 to 100,000	2.6
GW8	HDPE geogrid	1.2	2.0	all	0.013
		2.5 to 5	2.2	all	0.9
GW9	PET geogrid	0.8	2.0	all	1.0
		4.0	1.5	all	0.36
		2.6 and 5.2	1.7	all	**0.6**
GW11	PP Geogrid	0.6	1.4	0 to 300	1.2
				300 to 500	3.7
		0.6, in slump zone	1.1	0 to 300	0.7
				300 to 500	2.5
		1.35	1.3	0 to 300	2.0
				300 to 500	7.2
		2.1	1.0	all	1.9
GW14	PP Geogrid	0.5 m, 20 kPa surcharge	1.1	all	0.7
		0.5 m, 80 kPa surcharge	0.9	0 to 100	0.6
			.	100 to 200	0.15
GW15	PP Geogrid	1.25 m, 20 kPa surcharge	1.05	all	0.43
		1.25 m, 70 kPa surcharge	0.9	all	0.12
GW16	PP Woven Geotextile	3.1	3.0	0 to 3000	1.1
				3000 to 7000	2.7
		6.5	2.1	All	1.1
GW18	HDPE geogrid	2.44	0.5	0 to 2000	0.3
				2000 to 10,000	0.55
GW20	HDPE geogrid	1.1	1.05	0 to 500	1.0
			1.05	500 to 1500	3.5
		2.7	1.1	0 to 500	0.75
				500 to 1500	2.7
GW20	PP Geogrid	1.6	1.4	0 to 500	1.1
				500 to 1500	4.5
		3.2	1.4	0 to 500	1.9
				500 to 1500	10.3

For six out of eleven walls, the in-isolation creep data estimated at the measured load levels in the walls exhibited greater total creep strains than the strains measured in the actual walls. The in-isolation creep data also predicted greater long-term creep strain rates relative to the strain rates measured in the actual walls for all walls except GW8, GW9, GW14, GW15, and GW18. Note that the creep strain rates for GW7 were under-predicted by the in-isolation data in the short term after wall construction.

In general, for the PP and HDPE geosynthetics, the in-isolation strain rates were greater than the measured creep strain rates in the full-scale walls at longer times after construction. This appears to be the result of a "knee" in the log strain rate versus log time curves for the measured strain rate data from these walls. A "knee" in the plots for the PET geosynthetics (Wall GW9) was not detectable from the available data. In the short term after wall construction (i.e., depending on the specific case history, approximately 200 to 10,000 hours after the end of wall construction or surcharging), walls GW11 and GW16, and both sections of Wall GW20 had measured creep rates that were very close to the creep rates predicted by in-isolation laboratory creep data. However, at longer times, because of the "knee" in the strain rate plots, the measured creep rates from these walls were lower than the in-isolation laboratory creep rates. Walls GW5 and GW7 also exhibited a "knee" in the data, although initially the wall creep rates were not as close to the in-isolation creep rates.

Assuming that in-situ strain and strain rates can be expected to be lower than comparable in-isolation values, the exceptions in the data may be explained by the following observations:

- **Wall GW5:** Estimated in-soil reinforcement strains were lower but creep rates higher than values predicted from the laboratory in-isolation data. This project site was subject to elevated temperature (average temperature of 27° C). It is possible that temperature had a greater effect on the in-isolation creep rates than on comparable material in-situ. Furthermore, the creep data were not lot specific to the wall reinforcement.

- **Wall GW7 (actually, a steep, reinforced slope):** Reinforcement strains were less than the in-isolation laboratory creep data would predict, and, at least initially, the creep rate was higher than the in-isolation laboratory creep data would predict. As shown in Chapter 4.0, the load cells in the reinforcement in the backfill reported slightly higher loads than would be predicted by the strain gauges combined with an appropriate creep

modulus at the end of construction. As with Wall GW5, lot-specific creep data were not available for this wall. Therefore, the differences could be due to variance in the material properties, resulting in an underestimation of the true load in the wall reinforcement. The available data suggest that the underestimation of the end of construction loads for this case study is likely to be less than 10 to 20 percent.

- **Wall GW9:** This is the only exclusively PET reinforced wall in the database. The in-isolation creep data over-predicted the total strains but under-predicted the creep rates in the wall. Though lot specific creep data were available for this wall, the data were limited at the lower load levels observed in the wall. This possibly contributed to the observed differences in creep rates. The differences were not great and could easily be explained by variability in the creep data, so for practical purposes the prediction could be considered to be reasonably close. Given that PET reinforcement has less tendency to creep than does HDPE or PP, the PET creep may be more compatible with the ability of the soil to creep, allowing the PET to creep with less tendency to stress relax because of the soil confinement. Therefore, the in-isolation creep and the measured wall reinforcement creep would tend to match better than they would for PP or HDPE geosynthetics.

- **Walls GW14 and GW15:** These structures were taken to high surcharge loads, and the reinforcement creep response represents wall behavior at incipient collapse. At the highest surcharge levels, the in-isolation creep rates under-estimated the creep rates observed in walls GW14 and GW15, both in magnitude and time for onset of tertiary creep. However, at lower surcharge levels, the in-isolation laboratory creep rates were similar to those observed in-situ. Because the soil had failed at the highest surcharge loads, the soil was less able to restrict the creep of the geosynthetic. As more strain occurs, the soil becomes weaker and less stiff, and it approaches a residual strength value. This in turn requires that the soil reinforcement carry additional load. Therefore, if soil failure is allowed to occur, the reinforcement will have to carry a greater load, resulting in greater creep strain and creep strain rates. This hypothesis explains the reinforcement strain response observed for these two walls at the higher surcharge levels. For Wall GW15 at 70 kPa surcharge, a significant jump in strain occurred approximately 90 hours after surcharge loading because of the rupture of the

reinforcement layer above the layer for which data are shown (figures 6.30 and 6.31). This resulted in additional load transfer to the next lower layer (Benjamin 1989). This increase in load may be the cause of the greater under-prediction of strain and strain rate based on the in-isolation creep data relative to what was observed for Wall GW14. Wall GW14 failed more catastrophically because of a wall face connection failure in the highest reinforcement layer (Benjamin 1989).

- **<u>Wall GW18</u>:** This structure is a propped panel wall, and wall deformation was not allowed to occur until the wall was completely built and the props released. To estimate the end of construction loads in the reinforcement, the strain in the reinforcement at 100 hours after prop release was assumed to be representative of the reinforcement load levels, and all strain that occurred thereafter was due to creep at constant load. If the time required to reach load equilibrium were closer to, say, 1,000 hours, the upper layers in the wall would experience less than a 10 percent increase in load over what had been determined previously, and the layers in the lower half of the wall would exhibit no load increase. This could contribute to some of the under-prediction with the in-isolation creep data of both the creep strain and creep rate values. Part of the difference could also be due to the fact that lot specific creep data were not available for the reinforcement used in this wall. Therefore, variability in the creep data could contribute to the differences observed.

Ideally, the creep strain level from in-isolation creep curves at a time corresponding to the end of wall construction should be about the same as the creep strains measured in the wall reinforcements if in-isolation isochronous curves are used to convert measured strains in the wall reinforcement to loads. However, the writers considered other factors to select an appropriate modulus value to convert measured strains to loads. For example, adjustments were made in the estimate of the end of wall construction modulus to account for, in some cases, lack of lot specific creep data (walls GW5, GW7, GW8, GW18, and GW20), to make approximate adjustments in the modulus for site temperature (walls GW5, GW7, and GW16), or to ensure that reductions in modulus relative to the wide-width (index) tensile modulus for a given polymer and geosynthetic type were the same. Furthermore, the modulus values are strain level dependent, and some rounding to the nearest percentage of strain was done to determine representative

modulus values. These adjustments likely contributed to some scatter in the comparisons between in-soil and laboratory measured creep strains, as well as the creep rates.

Note that estimating the in-isolation creep curves at the load levels in the wall reinforcement also required interpolation between the load levels used to generate the isochronous curves, or extrapolation to load levels below the lowest load levels tested. As for time, because the load levels were quite low in most of the case histories, it was usually feasible to extrapolate log linearly beyond the available data while maintaining the desired accuracy. In some cases, more sophisticated extrapolation techniques were needed (Yeo 1985, WSDOT 1998). The extrapolation of the creep data was likely not a significant source of error in these comparisons. Curve fitting was applied to some data to provide both smooth and consistent isochronous curve sets. Clearly, curve fitting can reduce the variability in the results, but it can also introduce error. Such error could contribute to the differences between the creep rates observed in the wall and the in-isolation creep rates estimated from the laboratory data. However, the error should not be greater than the coefficient of variation in the creep data, which, the writers' experience indicates, is typically about the same as the coefficient of variation in the wide-width strength (ASTM D4595) for the geosynthetic. Therefore, the error will not be great enough to mask the trends in the data observed and discussed in later sections.

Given all of these issues, the writers attempted to estimate the modulus of the reinforcement materials conservatively to partially account for these sources of variability. Hence, the creep strains from the in-isolation data tend to be approximately the same as or greater than the measured creep strains in the walls.

6.6.2 Creep Deformations at the Wall Face

Wall face post-construction lateral deformations as a function of normalized depth below the wall top are summarized in Figure 6.32. Two observations can be made from the data:

1. The post-construction face deformations increase linearly with increasing height above the wall base for four out of the five walls shown, with the maximum deformation near the wall top.

2. The post-construction face deformations do not appear to be a function of total wall height, nor do they appear to be a function of wall facing type.

The linear increase in wall face deformation with distance above the wall base for most of the structures appears to be the result of the wall facing rotating outward from the wall toe. The soil at the wall base is largely confined by the rigid foundation (in these case studies), as the restrained toe has little, if any, ability to creep outward over time. As distance above the wall base increases, the reinforcement layers are less constrained by the toe of the wall, allowing more long-term deformation to occur.

The walls included in Figure 6.32 have total heights that range from 3 to 12.6 m, yet the normalized deformation curves fall within a narrow band. Furthermore, these walls encompass a variety of facing types, including a geosynthetic wrapped face, a precast panel face, a full-height propped panel facing, and a modular block facing. The one exception to the linear trend in wall deformations is the data for Wall GW9, which is a modular block faced wall. Note that the data for all of the walls summarized in this figure were obtained from either an optical facing survey or extensometers/potentiometers, whereas the data for Wall GW9 were obtained from an inclinometer attached to the face. Allen et al. (1992) discussed the difference between deformation measurements obtained from optical survey/potentiometers and inclinometers and noted that inclinometers represent total deformation relative to the beginning of wall construction, whereas optical facing survey measurements represent movement relative to the time at which the specific layer was installed. Nevertheless, taken together the data for all five case studies fall within a reasonably narrow band.
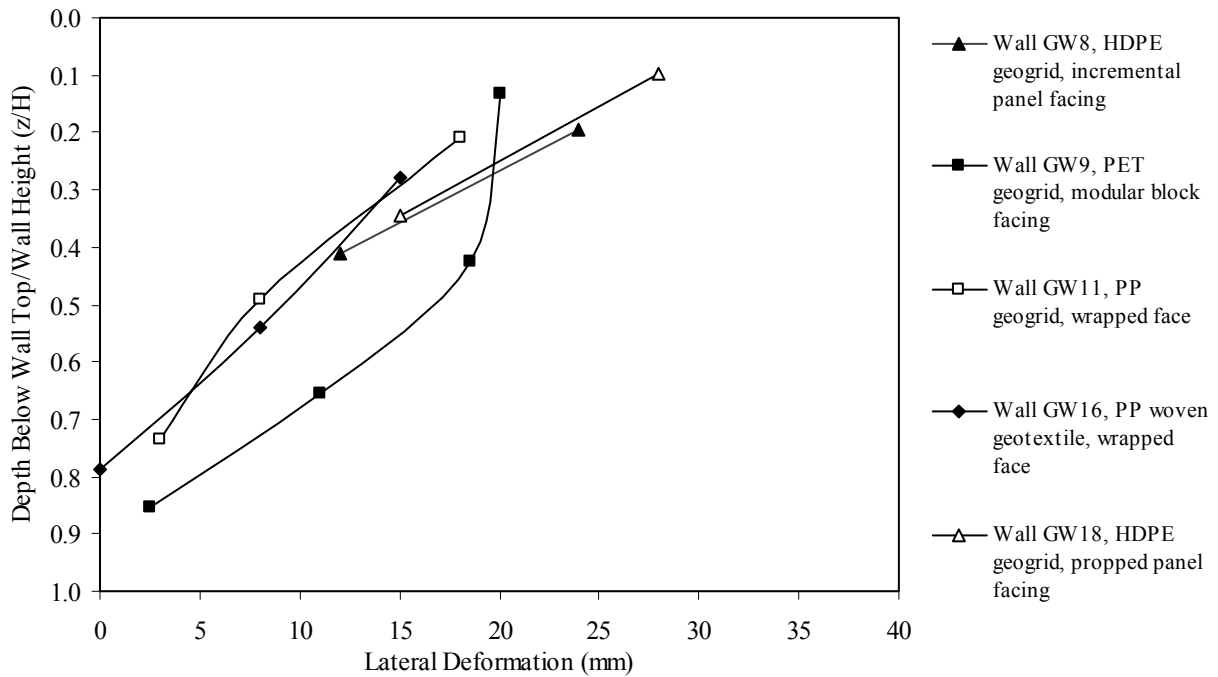
(a) from end of wall construction to 10,000 hrs after wall construction
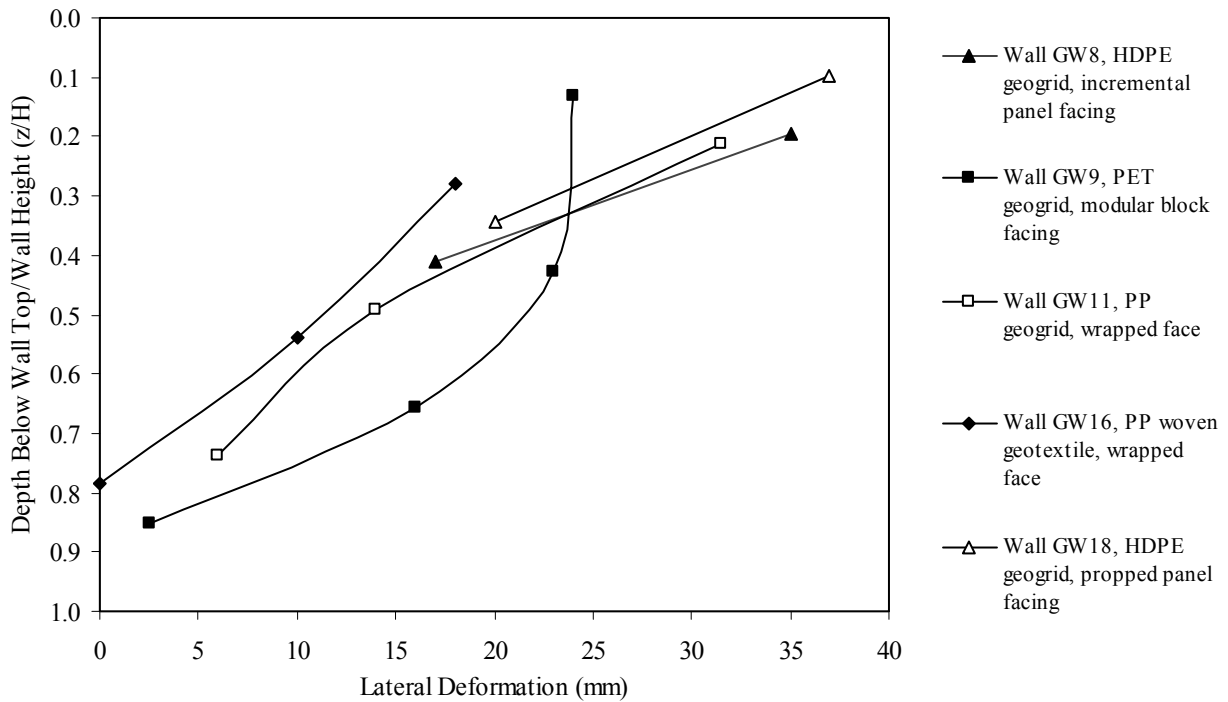
(b) from end of wall construction to 75 years after wall construction (estimated)

Figure 6.32. Lateral post-construction long-term wall face deflection versus normalized depth of reinforcement z/H.

6.7 Discussion

6.7.1 Long-Term Wall Performance

The creep data for all the walls (figures 6.5 through 6.31), except GW14 at the higher surcharge levels, GW15 at the higher surcharge levels, and possibly the PP section for GW20, strongly indicate that only primary creep occurred in the reinforcement. In addition, for some of the walls creep had virtually stopped within the observation period available. The creep behavior observed is consistent with the low load levels determined in Chapter 5.0, which are well below the load levels required to cause creep strains and rates that would lead to rupture within the design lifetime of these walls. Given that these results already include any installation damage effects, and that chemical degradation has been shown to be minimal for all of the case histories observed to date, it can be concluded, with the exception of the walls specifically mentioned above, that the full-scale geosynthetic walls evaluated herein are stable and are not expected to become unstable over their design lifetime.

Furthermore, Greenwood (1997), Bernardi and Paulson (1997), and Orsat et al. (1998) provided evidence that demonstrates that as long-term creep occurs, the remaining reinforcement tensile strength does not decrease until the tertiary creep phase (i.e., the creep rupture phase) has been reached. This concept is illustrated in Figure 6.33. A theoretical explanation for this behavior is that very few molecular chains within the polymer break during the creep process; rather, they slide past one another until the molecular chains achieve their maximum orientation. Only when the polymeric reinforcement reaches a state of tertiary creep (the creep rupture phase) do significant numbers of polymer molecular chains break. The strength of the polymeric reinforcement is directly related to the number of polymer molecular breaks. Hence, the tensile strength of the reinforcement does not decrease monotonically as creep progresses, as assumed in design. Furthermore, if the reinforcement layer stress is below the stress level required to cause creep rupture during the design lifetime, creep will never cause a reduction in reinforcement tensile strength during the wall design lifetime. This means, as far as reinforcement strength is concerned, that the factor of safety against reinforcement rupture is significantly higher than current design protocols would indicate for working stress conditions, even without consideration for the fact that reinforcement load levels are much lower than those based on current design methodology.

217
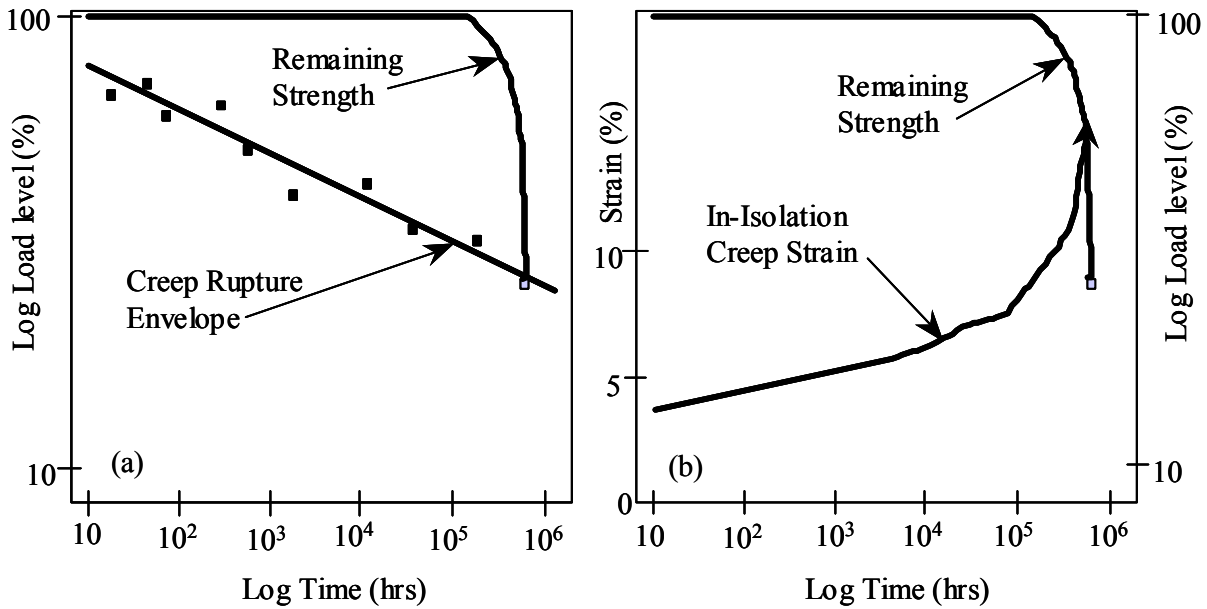
Figure 6.33. Creep rupture, creep strain, and residual strength concepts: (a) stress rupture envelope plus curve for remaining strength vs. time for rupture point at longest time, and (b) creep strain curve and remaining strength curve for rupture test at longest time in part (a).

Poor long-term performance (walls GW14 and GW15 at the highest surcharge load) was always accompanied by signs of soil failure within the wall backfill. Typically, reinforcement strains were less than 3 percent for most of the walls that performed well, and no signs of soil backfill failure were observed. Furthermore, post-construction lateral deformations of the wall face within the first 10,000 hours after the completion of wall construction were generally less than 25 to 30 mm for the walls that were considered to perform well.

The example data presented here were selected to span the larger database of results reported in Chapter 2.0. The general observations presented below are considered by the writers to be true for a wide range of geosynthetic-reinforced walls constructed with granular backfill soils up to a wall height of approximately 13 m. In general, a geosynthetic wall can be considered to be performing well and have adequate long-term stability if all of the following are true:

- Total reinforcement strains are small (typically less than 3 percent).
- Creep strains and strain rates are decreasing with time (i.e., only primary creep is observed).
- The wall backfill soil is not exhibiting signs of failure (cracking, slumping, etc.).

218

- Post-construction deformations, which are typically greatest at the wall top, are less than 30 mm within the first 10,000 hours for walls 13 m or shorter.

A geosynthetic wall can be considered to be performing poorly or be potentially unstable during the wall design lifetime if any one of the following is true:

- The total reinforcement strains are relatively large (typically 5 percent or more).

- The creep strain rates are relatively constant or increasing with time.

- The wall backfill is exhibiting signs of failure (cracking, slumping, etc.)

- A reinforcement rupture occurs either at the connection or in the backfill (typically, the top reinforcement layer will fail first).

- Post-construction wall face deformations are greater than 35 mm in the first 10,000 hours after the end of wall construction and are growing at a constant or increasing rate (for walls 13 m or shorter).

Implicit in these recommendations is the assumption that lifetime boundary loads and ground conditions for the structures do not change from those present at the end of construction. A more exact determination of the threshold reinforcement strain that results in a transition to poor wall performance is reserved for future study as a more complete database of poorly performing walls accumulates in the literature. The reinforcement strain at which this transition to poorer performance occurred in the case histories for which high strain data were available appears to be between 3 and 5 percent. This magnitude of reinforcement strain is about the same as or slightly greater than the magnitude of peak soil shear strain for granular soils under plane strain conditions.

6.7.2 *Comparison of Measured to In-Isolation Creep Behavior, and Implications Regarding the Actual Load Level in the Reinforcement*

The creep strain and creep strain rate data presented in this report provide at least an approximate verification of the load levels determined in Chapter 5.0 with isochronous creep stiffness data, given the time required to construct the wall and to achieve a constant load in the reinforcement. In most cases, the creep strains and creep strain rates determined from in-isolation data at the load levels summarized in Table 6.5 were greater than corresponding values in the field, indicating that these load levels are reasonably accurate or slightly conservative. For those cases in which the in-isolation creep strains and rates were less than field values, it appears

that the load levels were greater than those estimated at the end of wall construction. The reasons for this increased load after end of wall construction appear to be as follows:

- The wall backfill reached a failure state, causing the soil to become more plastic. Therefore, the stiffness of the soil decreased significantly, resulting in more load being shed to the reinforcement. If reinforcement failure occurred in the upper layer(s), the load originally carried by that reinforcement was shed to the adjacent lower layer, causing the load in the lower layer to increase.

- For propped panel walls, the measured strain response to prop release is the result of load being transferred to the reinforcement from the props in addition to creep. It may take longer than 100 hours (the time assumed for end of construction in this study) for the load in the reinforcement to reach equilibrium with the soil in this type of wall. Wall GW18 (Figure 6.9) suggests that it takes approximately 1,000 hours or more for the wall reinforcement loads to reach equilibrium after prop release, meaning that load increase stops and pure creep begins.

- Figures 6.1 and 6.2 suggest that some additional time beyond the end of construction is required for the soil and reinforcement to reach equilibrium, given all of the time dependent processes involved. However, this source of increased load after the end of wall construction is likely to be small.

- Other sources may contribute to load after the end of wall construction, such as snow load, water buildup in the backfill, or load from undocumented sources. Wall GW7 may be a case in point, given the significant jump in strain that occurred after the end of wall construction. This behavior appears similar to the strain jump that occurred for wall GW18 (a propped panel wall) and Wall GW15 (a wall that failed).

Fannin (2001) observed load increase in the reinforcements (indicated by measurements from load cells embedded in the reinforcement) throughout most of the period of observation for Wall GW7. He concluded that the load increase was due to long-term soil creep, which induced strain and, therefore, load in the reinforcement. Given the observed strain increases in the reinforcement layers, it appears that most of the strain that occurred was interpreted as load by the load cells in the reinforcement. This indicates that the load cells were recording too much post-construction load increase, as it is not reasonable that all of the strain increase measured in the reinforcement was due to load increase. Because a load cell does not have the ability to

creep while the reinforcement does, the deformation in the soil-geosynthetic system allowed by the time dependent movements of the reinforcement will be translated to load by the load cell. The load cell responds elastically, creating a local "hard spot" in the composite soil-reinforcement system. However, the unusual strain increases observed in the first 10,000 to 20,000 hours after the surcharge was in place may be due to some type of load increase as described above, although the specific cause of the increased loading may never be known with certainty.

Another hypothesis for these load increases is that some other mechanism is transferring load between reinforcement layers as time dependent deformation of the soil-geosynthetic system occurs, causing the reinforcement loads to become more uniform with depth and over time after the end of construction. For example, the greatest creep strains, at least in some of the walls, occurred near the wall top where the reinforcement loads were lowest. This is partly due to typical boundary conditions at the wall base that limit time dependent movements (unless large vertical settlements occur). These larger creep strains near the wall top could be partly due to load transfer from the more heavily loaded reinforcement layers in the middle of the wall. But for this load transfer to occur, the loads in the middle reinforcement layers would need to decrease (stress relax).

In about 50 percent of the walls, the largest creep strains occurred where the loads in the wall were highest (in the middle third of the wall). Furthermore, there was no evidence that loads were in fact decreasing for the layers in the middle third of the wall as a result of load transfer to the upper layers. In Wall GW7, the load increases measured by the load cells were greatest in the middle third of the wall, where the reinforcement loads were already highest. Furthermore, in walls GW14 and GW15, connection loads were not observed to decrease with time anywhere in the wall. Instead, shortly after loading at all reinforcement levels, connection loads increased very slightly, in most cases becoming virtually constant after the first 50 hours after surcharge loading (Benjamin 1989). Nevertheless, Wall GW17 (Highbury Wall), reported in Chapter 2.0, for which connection strains were recorded over 1.5 years, may present evidence of stress relaxation at the connections as the system reached long-term equilibrium (Bathurst 1992).

Vertical earth pressures in walls GW14 and GW15 also remained constant or even decreased slightly after load application at all levels, another indicator that loads do not increase as a

function of time. The same is true of full-scale field walls in which vertical earth pressures were measured: no time dependent increases have been observed.

Vertical settlements were observed to increase at a decreasing rate over time after surcharge load application in walls GW14 and GW15. In full-scale walls, some time dependent vertical settlements were observed within the wall backfill (e.g., Wall GW16). If these settlements occur differentially, they could be the source for time dependent increases in reinforcement loads. However, no time dependent shifts in reinforcement strains along the length of the reinforcement layers were observed in any of the case histories, so the effects of vertical settlements within the wall backfill have apparently not been significant. All this points to minimal load transfer occurring between or along layers.

If soil creep toward the wall face is a mechanism that increases reinforcement loads over time, the reinforcement (at least PP and HDPE geosynthetics) would in general need to be less susceptible to creep than the soil. However, as discussed previously, the reinforcement typically has similar or greater ability to creep than does the granular backfill. Because of this, any creep that occurs in the soil after the end of construction will be offset by a decrease in the reinforcement modulus that occurs during that time. Furthermore, if soil creep contributes to a time dependent increase in reinforcement load, steel reinforcement loads should theoretically increase as a function of time, as the steel has much less ability to creep than does the soil. However, the experience of the writers is that time-dependent increases in steel reinforcement loads are generally not observed in granular backfills.

This additional long-term load, due to an unknown source in the case of Wall GW7, due to time dependent load transfer from the props to the reinforcement in the case of Wall GW18, or due to post peak soil shear strength behavior or rupture of the upper layer of soil reinforcement in the case of walls GW14 and GW15, may explain why the measured strain rates are greater than the in-isolation laboratory test strain rates in these walls and, thus, are the exceptions to the trends reported here. Because the strain at the end of wall construction was used to estimate load, these other time-dependent load increases were not considered in the calculation of loads summarized in Table 6.5. In spite of these long-term load increases, the under-estimation of load in the case of walls GW7 and GW18 is still on the order of 10 to 20 percent or less, as stated previously.

Chapter 4.0 provides an analysis of the plane strain in-soil creep tests conducted by Boyle (1995). The geosynthetic creep rate in these tests was controlled by the soil creep rate, as evidenced by the stress relaxation that occurred in the geosynthetic. The in-soil creep rates obtained by Boyle were an order of magnitude less than the in-isolation creep rates for the same geosynthetic at the same load level (see Figure 6.21). Yet the measured creep rates in the wall (GW16) were much closer to the in-isolation creep rate than the creep rate measured from the in-soil creep tests. The strain magnitudes measured in the wall were also very close to those measured for the in-isolation and the in-soil tests, indicating that the load level determined for the GW16 wall reinforcement was reasonably accurate (see Figure 6.8). These observations indicate that little, if any, stress relaxation occurred during the one-year observation period after the end of wall construction. The in-soil tests by Boyle appear to have under-estimated the geosynthetic and soil creep relative to what was observed in the wall and to have over-estimated the amount of stress relaxation that likely occurred. Side wall friction in the test device may have also contributed to this difference in creep rates. The dense, angular sand used in the tests conducted by Boyle would be expected to be much less susceptible to creep than the full range of granular materials that could be used as wall backfill. Therefore, if a looser, weaker sand was used in the tests conducted by Boyle, it is possible that less stress relaxation, if any, would be observed.

Therefore, at least in the short-term after wall construction, significant stress relaxation must not have occurred in the reinforcement for Wall GW16. For the rest of the walls (other than GW7, GW14, GW15, and GW18), given that the measured creep rates were about the same as or less than the in-isolation creep rates, the time dependent response to load appears to be primarily due to creep. However, as mentioned previously, the log creep rate versus log time plots for these walls tend to exhibit a "knee" in the curve, indicating some type of change in the ability of the soil to creep. In most cases, the in-isolation creep rate versus log time curve did not exhibit the same drop in creep rate as that measured in the corresponding wall. Such a decrease in the ability of the soil to creep at longer times can force the geosynthetic to exhibit more stress relaxation at longer times.

The main point here is that at the end of construction, and for a time beyond the end of construction, the geosynthetic appears to primarily exhibit creep. Therefore, the correct modulus for converting strain to load can be determined directly from the isochronous creep stiffness of

the material. For geogrids and most woven geotextiles (which is the case for all of the case histories evaluated herein), the in-isolation creep data appear to be adequate for this purpose. For geosynthetics with greater macro-structure influence on load-strain-time response, confined creep data are required.

6.8 Summary and Conclusions

Long-term creep data from ten full-scale geosynthetic wall case histories (12 wall sections) have been presented and analyzed. These case histories span a wide range of geometries, geosynthetics, and granular soil properties, and they include observations at both working stress conditions and near failure. With extrapolation of the data, including due consideration for potential chemical degradation (which was minimal in all cases) and installation damage, wall strain levels and trends were identified that are characteristic of walls that will be stable for typical design lifetimes of 75 to 100 years or more. The difference between good and poor wall performance appears to be linked to whether reinforcement strain levels are large enough to allow the soil to reach peak strain. That is, if the reinforcement strains are low enough to prevent the soil from reaching failure, reinforcement creep will be minimal and the wall will remain stable. Specific criteria have been provided to identify the potential for the wall to exhibit good or poor long-term performance.

The creep strains measured in the full-scale walls were compared to the creep that would be expected on the basis of laboratory creep tests conducted in-isolation (unconfined), and in one case on the basis of laboratory in-soil creep tests. The creep measured in the walls should be comparable to the laboratory creep rates if the load levels determined from the measured strains in the wall, converted to load through a creep modulus, have been determined correctly, if the laboratory creep curves are accurate, and if pure creep, rather than a combination of stress relaxation and creep, is occurring. Though there were some notable exceptions, in the majority of cases, the laboratory in-isolation creep rates were the same as or greater than the measured geosynthetic reinforcement creep rates in full-scale walls, providing an approximate corroboration of the reinforcement load levels for these walls determined in Chapter 5.0. This also indicates that in-isolation laboratory creep data, in general, produce a conservative estimation of creep in walls.

Whether or not significant stress relaxation occurred in the reinforcement near the end of construction for each of the wall case histories could not be determined with certainty from the available case study data. It appears that the effect of any stress relaxation that is occurring at the end of wall construction is sufficiently small that that creep rates measured in the walls and during laboratory in-isolation tests are approximately equivalent, at least within the first 200 to 10,000 hours after the end of construction. However, at longer times, the creep rate measured in the wall reinforcement layers dropped off more quickly with time than did the laboratory in-isolation creep rates. This indicates that the ability of the soil to creep decreased more rapidly than the ability of the geosynthetic to creep, forcing the geosynthetic to exhibit a greater percentage of stress relaxation at longer times after construction, eventually resulting in the complete cessation of creep in the geosynthetic wall.

In some cases, reinforcement load increased after the end of wall construction, which may have been due to the following:

1. time dependent load transfer from the props to the reinforcement in the case of Wall GW18 during the first 1,000 hours

2. post peak soil shear strength behavior, resulting in a decrease in the soil stiffness and an increase in the load carried by the soil reinforcement as failure of the soil-geosynthetic system progresses, in the case of Walls GW14 and GW15

3. an unknown source in the case of Wall GW7.

In these cases, the measured creep strain rates were greater than the in-isolation laboratory creep strain rates. These load increases appear to be less than 10 to 20 percent of the load measured at the end of wall construction. Note that load increase due to post peak soil shear strength behavior should be avoided through proper design, as for all practical purposes, the wall has failed when this condition occurs.

Post-construction, long-term wall face deformation data show that geosynthetic wall face deformations, if the wall is properly designed, will generally be less than 25 to 30 mm during the first year of service and less than 35 mm during the design lifetime for walls shorter than 13 m. This long-term face deformation is generally greatest at the wall top, decreasing linearly to zero at the base of the wall, and it appears to be independent of wall height or facing type for the range of conditions available in the database. This long-term deformation can easily be taken

into account through selection of a wall face pre-batter and by designing the facing system to be tolerant of this movement.

A substantial body of long-term evidence demonstrates that geosynthetic walls can be used reliably for permanent applications. Current procedures provided in design codes for geosynthetic walls are conservative, and new design methodologies that can reduce the level of conservatism in geosynthetic wall designs could provide significant economic benefits without compromising long-term reliability.

7.0   A NEW WORKING STRESS METHOD FOR PREDICTING REINFORCEMENT LOADS IN GEOSYNTHETIC MSE WALLS

7.1 Introduction

Accurate prediction of loads and their distribution in mechanically stabilised earth (MSE) wall backfill reinforcement is necessary to produce cost effective, internally stable reinforced soil wall designs. The predicted reinforcement loads affect the strength and spacing required for the reinforcement, as well as the reinforcement length required to resist pullout.

The three primary methods identified in the most recent design codes and design guidelines in North America for estimating loads in geosynthetic reinforced MSE walls include the Coherent Gravity Method (AASHTO 1996), the FHWA Structure Stiffness Method (Christopher et al. 1990), and the Simplified Method (AASHTO 1999, Elias et al. 2001). Chapter 5.0 provides an assessment of the predictive accuracy of these methods for geosynthetic walls, and Allen et al. (2001) evaluated the predictive accuracy of these methods for steel reinforced structures. These approaches have worked reasonably well for typical steel reinforced MSE walls (Allen et al. 2001), but they have worked poorly for predicting loads in geosynthetic reinforced structures (Bell et al. 1983, Rowe and Ho 1993; see also Chapter 5.0).

All of these methods are semi-empirical in nature, using limit equilibrium concepts to develop the design model, but they use working stress observations to adjust the models to fit what has been observed in full-scale structures. The development of these methods assumed that reinforcement loads can be equated directly to the soil state of stress and that limit equilibrium concepts are applicable. Because measured reinforcement loads in steel reinforced structures have been found to be equal to or greater than the load that would result from integration of active or at-rest lateral earth pressures over the tributary area of the reinforcement, designers have not hesitated to adjust the load predictions to match the empirical data. Such an adjustment would be more conservative for design than simply using the unmodified lateral earth pressure coefficient. However, for geosynthetic reinforced walls, measured strains converted to load with a reinforcement modulus that properly accounted for the time required to build the wall showed that reinforcement loads are less than those predicted by integrating the active earth pressure over the tributary area. To maintain the assumption that the reinforcement loads should directly

reflect the soil state of stress, the data that appeared to support lower reinforcement load levels were ignored, and the design reinforcement load was maintained at active earth pressure levels.

Uncertainties about the effects of time (creep or stress relaxation) and soil confinement on the determination of the geosynthetic modulus has hindered acceptance of the lower reinforcement loads inferred from strain measurements. Fannin and Hermann (1991), Bathurst (1990) and Bathurst and Benjamin (1990) suggested that the in-isolation isochronous creep stiffness be used to convert measured geosynthetic strains to load for geogrid reinforcement products rather than the modulus from an index tensile test such as ASTM D4595. Chapter 4.0 investigates this issue in detail. It confirms that for geogrids and woven geotextiles, the in-isolation isochronous creep stiffness, with consideration of the time necessary to construct the wall and apply any surcharges, provides a reasonably accurate modulus for converting measured reinforcement strains to load. It also confirms that the short-term, wide-width tensile modulus is much too high for this purpose.

The proper estimation of the geosynthetic modulus needed to convert measured strain to load is a major source of uncertainty in determining actual load levels in geosynthetic reinforcement layers. This uncertainty is compounded by the need to correctly interpret measured strains. However, through proper strain gauge calibration and redundancy in monitoring points and strain measurement type, reasonable estimates of in-soil reinforcement strain are possible. Chapters 3.0, 4.0, and 5.0 address and quantify these sources of uncertainty and their effect on the "measured" reinforcement loads in instrumented, full-scale structures. Notwithstanding these uncertainties, Chapter 5.0 shows that current design approaches greatly over-estimate geosynthetic reinforcement loads, even when plane strain soil strength parameters are used.

The past performance of geosynthetic reinforced MSE walls has also provided strong evidence that current design methodologies for internal stability, in particular the prediction of reinforcement loads, are very conservative. Chapter 2.0 shows that a number of well-documented geosynthetic walls that have demonstrated good long-term performance for up to 25 years were designed with significantly lower global resistance to demand ratios than would be required by current practice. Furthermore, Chapter 6.0 demonstrates that the measured long-term creep rates in full-scale geosynthetic structures corroborate reinforcement load levels that are much lower than previously thought.

In this chapter a new working stress methodology, termed the K_0-Stiffness Method, is proposed. The method has been calibrated against measurements of strain and load in the monitored, full-scale walls reported in the previous chapters. The proposed design methodology, in addition to being relatively easy to apply, provides a seamless transition between geosynthetic and steel reinforced MSE walls.

The scope of this chapter and the proposed design methodology are limited to walls with granular (non-cohesive) backfills.

7.2 Summary of Case Histories Evaluated

The key properties and parameters for each of the case histories referenced in this report are summarized in Table 7.1. Additional details for each of these case histories, including wall type, reinforcement geometry, reinforcement type, soil properties, and construction history, are provided in chapters 2.0, 3.0, and 5.0.

A total of 16 geosynthetic wall cases from Table 7.1 were analyzed (the same wall with and without a surcharge was considered to be one case). Of these, eleven were walls built to full scale in the field and five were full-scale walls built in an in-door laboratory environment. These wall cases included a variety of wall geometries and materials, surcharge conditions, and granular backfill. Wall reinforcement products included geotextiles and geogrids, different polymers—polypropylene (PP), high density polyethylene (HDPE) and polyester (PET), strip and continuous reinforcements, a range of tensile strengths from 12 to 200 kN/m (See Chapter 2.0), and a range of reinforcement stiffnesses from 65 to 7,603 kN/m. Reinforcement vertical spacing varied from 0.3 to 1.6 m. Wall facing batter angles varied from 0° (vertical) to 27°, although most of the walls had facing batter angles of 8° or less. Wall heights varied from 3.0 m to 12.6 m, with surcharge heights of up to 5.3 m of soil. Facing types included geosynthetic wrapped-face, welded wire, pre-cast concrete panels, and modular concrete blocks. Estimated plane strain peak soil friction angles varied from 42° to 57°.

Although it is not possible to isolate the effect of a specific variable, most of the conditions that are likely to be encountered in the field were included within the database of case histories described above.

Table 7.1. Summary of geosynthetic wall case histories.

Wall Case History (Case History No.)	Date Wall Built	Wall Height (m)	Surcharge Conditions	Face Batter Angle from Vert. ω (º)	Backfill Plane Strain Soil ϕ (º)	Geosynthetic	$J_{2\%}$, for Layer (at end of wall construction, considering creep, kN/m)	Global Wall Stiffness at End of Wall Construction (kN/m²)
Tanque Verde HDPE Geogrid Wall (GW5)	1984	4.9	None	0	53	Tensar SR-2 (HDPE geogrid)	335	720
Oslo, Norway Wall, Sections J and N (GW7)	1987	4.8	3 m steeply sloping soil surcharge	26.6	46	Tensar SR-55 (HDPE geogrid)	363 at EOC, 353 at surcharge completion	368 for Section J, 588 for Section N
Algonquin Tensar Geogrid Wall (GW8)	1988	6.1	2.1 m sloping surcharge	0	43	Tensar SR-2 (HDPE geogrid)	750	984
Algonquin Miragrid Wall (GW9)	1988	6.1	2.1 m sloping surcharge	2.9	43	Miragrid 5T (PET geogrid)	420	551
Algonquin Geotextile Wall (GW10)	1988	6.1	None	0	43	Quline 160 (PET nonwoven geotextile)	Approximately 175	208
RMCC Geogrid Wrapped Face Wall (GW11)	1986	3	0.7 m soil surcharge	0	55	Tensar SS2, weak direction (PP geogrid)	105	147
RMCC Full Height Plywood Panel Faced Wall (GW12)	1987	3	Full test wall top coverage with air bag loading system, up to effective pressure of 42 kPa	0	55	Tensar SR-2 (HDPE geogrid)	540 at EOC, 450 at surcharge completion	720 at EOC, 600 at surcharge completion
RMCC Incremental Plywood Panel Faced Wall (GW13)	1987	3	Full test wall top coverage with air bag loading system, up to effective pressure of 42 kPa	0	55	Tensar SR-2 (HDPE geogrid)	490 at EOC, 450 at surcharge completion	653 at EOC, 600 at surcharge completion

Table 7.1, Cont.

| Wall Case History (Case History No.)	Date Wall Built	Wall Height (m)	Surcharge Conditions	Face Batter Angle from Vert. $\omega(^o)$	Backfill Plane Strain Soil ϕ $(^o)$	Geosynthetic	$J_{2\%}$, for Layer (at end of wall construction, considering creep, kN/m)	Global Wall Stiffness at End of Wall Construction (kN/m^2)
RMCC Full Height (GW14) Aluminium Panel and Incremental Panel (GW15) Faced Wall	1989	3	Full test wall top coverage with air bag loading system, up to effective pressure of 70 kPa for GW14 and 60 kPa for GW15	0	55	Tensar SS1, weak direction (PP geogrid)	87 to 93 at EOC, 45 to 90 at end of surcharging	120 at EOC, 81 to 86 at end of surcharging
Rainier Ave. Wall (GW16)	1989	12.6	5.3 m sloping surcharge	2.9	54	GTF 200 (PP woven geotextile)	90	1087
						GTF 375(PP woven geotextile)	174	
						GTF 500(PP woven geotextile)	311	
						GTF 1225T (PET woven geotextile)	1126	
Fredericton, New Brunswick Wall (GW18)	1990	6.1	None	0	45	Tensar SR-2 (HDPE geogrid)	500	738
St Remy PET Strip Test Wall (GW19)	1993	6.4	None	0	42	Parweb 2S Strip (PET)	7603	9504
Vicenza, Italy HDPE Wall (GW20)	1998	4	3.5 m steeply sloping soil surcharge	4.8	57	Tenax TT201 SAMP (HDPE geogrid)	380	285
Vicenza, Italy PP Wall (GW20)	1998	4	3.5 m steeply sloping soil surcharge	4.8	57	Tenax LBO220 SAMP (PP geogrid)	125	94

231

Note that the plane strain friction angle was used to characterize soil shear strength in Table 7.1 case histories. Plane strain conditions typically exist in MSE walls, and recent work indicates that the plane strain soil friction angle correlates best to reinforcement loads, at least for geosynthetic walls (Rowe and Ho 1993, Zornberg et al. 1998a,b; see also Chapter 5.0).

7.3 Analysis of Reinforcement Loads

In Chapter 5.0, current North American methods for predicting reinforcement loads were investigated. The conclusion was that the AASHTO Simplified Method produces results similar to those of the other methods, yet it has the advantage of being simpler to use and more broadly applicable. Therefore, the Simplified Method will be used herein as the baseline of comparison for reinforcement loads predicted with the new working stress method.

Figure 7.1 summarizes how well the Simplified Method predicts reinforcement loads in geosynthetic walls built in the field (see Chapter 5.0 for additional details). Note that measured plane strain peak soil friction angles and unit weights were used to estimate loads with the Simplified Method, which means that there is no conservatism in the reinforcement load predictions as a result of conservatism in the selection of soil parameters (see Chapter 2.0).

The loads predicted for geosynthetic walls with the Simplified Method are generally very conservative in relation to the "measured" loads. The only exceptions are walls GW7 (Section N), GW10, and GW19. The reinforcement loads in Wall GW7 (Section N) and GW19 were under-predicted by the Simplified Method, and GW10 was under-predicted near the top of the wall where loads are expected to be lower and significantly over-predicted near the bottom of the wall where loads are expected to be higher. However, the unusual features of those walls may have contributed to their unusual behavior with respect to reinforcement loads (i.e., GW7 was heavily battered, GW19 was reinforced with discontinuous strips and had high stiffness, and GW10 was so lightly reinforced that the soil failed – see Chapter 5.0 for additional details). The figure also shows a large amount of scatter in the predicted loads and, overall, a poor correlation of measured to predicted values with the current design methodology.
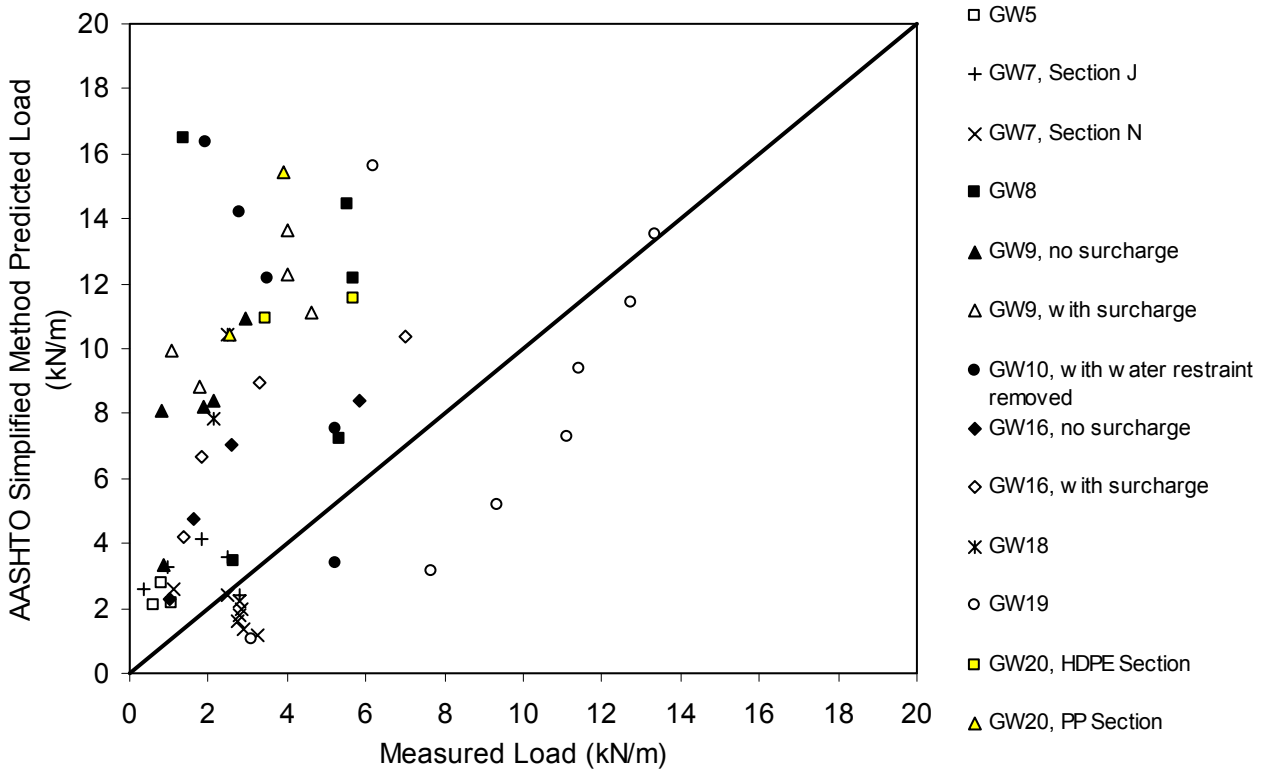
Figure 7.1. Measured values of T_{max} in reinforcement layers for geosynthetic walls versus values predicted with the AASHTO Simplified Method.

7.4 Development of a New Approach for Predicting Maximum Reinforcement Loads

7.4.1 General

The following key factors influence the magnitude of maximum reinforcement load, T_{max}:

- height of the wall and any surcharge loads
- global and local stiffness of the soil reinforcement
- resistance to lateral movement caused by the stiffness of the facing and restraint at the wall toe
- face batter
- shear strength and modulus of the soil
- unit weight of the soil
- vertical spacing of the reinforcement.

These factors are introduced analytically in the following general expression for the maximum load per running unit length of wall in reinforcement layer i:

$$T_{max}^i = S_v^i \, \sigma_h \, D_{tmax} \, \Phi \tag{7.1}$$

where S_v^i = tributary area (equivalent to the average vertical spacing of the reinforcement near each layer when analyses are carried out per unit length of wall); σ_h = lateral earth pressure acting over the tributary area; D_{tmax} = load distribution factor that modifies the reinforcement load on the basis of layer location; and Φ = influence factor that is the product of factors that account for the influence of local and global reinforcement stiffness, facing stiffness, and face batter.

The lateral earth pressure is calculated as the average value acting over the height of the wall, H, according to conventional earth pressure theory, hence:

$$\sigma_h = \frac{1}{2} K \gamma (H + S) \tag{7.2}$$

Here K = lateral earth pressure coefficient, γ = unit weight of the soil, H = height of the wall, and S = equivalent height of uniform surcharge pressure q (i.e., S = q/γ). The coefficient of lateral earth pressure, K, is calculated with the Jaky equation (Holtz and Kovacs 1981):

$$K = K_o = 1 - \sin \phi_{ps} \tag{7.3}$$

where ϕ_{ps} is the peak plane strain friction angle.

Substitution of equations 7.2 and 7.3 into Equation 7.1 leads to:

$$T_{max}^i = \frac{1}{2} K \gamma (H + S) \, S_v^i \, D_{tmax} \, \Phi \tag{7.4}$$

Equation 7.4 contains the conventional expression for calculating reinforcement loads in current limit equilibrium methods of analysis. The modifiers D_{tmax} and Φ are empirically determined parameters, or functions, that reflect actual mechanisms. They are used to improve the correspondence between measured and predicted reinforcement loads at working stress conditions on the basis of a large number of case studies. Parameter D_{tmax} is a load distribution factor that modifies the reinforcement load as a function of normalized depth below the top of the wall (z/H), and it varies over the range $0 \leq D_{tmax} \leq 1$. For brevity in Equation 7.4 the influence factor, Φ, is used to represent the product of four factors as follows:

$$\Phi = \Phi_g \times \Phi_{local} \times \Phi_{fs} \times \Phi_{fb} \tag{7.5}$$

Parameter Φ_g is a global stiffness factor that accounts for the influence of the stiffness and spacing of the reinforcement layers over the entire wall height. It has the following general form:

$$\Phi_g = \alpha \left(\frac{S_{global}}{p_a} \right)^{\beta} \tag{7.6}$$

Here, S_{global} is the global reinforcement stiffness and α and β are constant coefficients. The non-dimensionality of the expression is preserved by dividing the global reinforcement stiffness by p_a = 101 kPa (atmospheric pressure). The global reinforcement stiffness value for a wall is calculated as follows:

$$S_{global} = \frac{J_{ave}}{(H/n)} = \frac{\sum_{i=1}^{n} J_i}{H} \tag{7.7}$$

Here, J_{ave} is the average tensile modulus of all "n" reinforcement layers over the wall height, and J_i is the tensile modulus of an individual reinforcement layer expressed in units of force per unit length of wall.

Parameter Φ_{local} is a local stiffness factor that accounts for relative stiffness of the reinforcement layer with respect to the average stiffness of all reinforcement layers. It is expressed as follows:

$$\Phi_{local} = \left(\frac{S_{local}}{S_{global}} \right)^{a} \tag{7.8}$$

The coefficient term "a" is taken as a = 0 for steel reinforcement and a = 1 for geosynthetic reinforced soil walls. S_{local} is the local reinforcement stiffness for reinforcement layer i, calculated as:

$$S_{local} = \left(\frac{J}{S_v} \right)_i \tag{7.9}$$

It is used to quantify the local combined influence of the individual layer stiffness and spacing on reinforcement load.

Parameters Φ_{fs} (facing stiffness factor) and Φ_{fb} (facing batter factor) in Equation 7.5 are factors that account for the influence of the facing stiffness (Section 7.4.5) and facing batter (Section 7.4.6), respectively, and are constant values for a given wall.

Equations 7.1 and 7.5 show that the maximum load in a reinforcement layer is the product of eight terms, many of which are non-linear. It is assumed *a priori* that the factors are, for practical purposes, uncorrelated. This assumption allows the influence of each factor on predicted reinforcement loads to be examined separately while keeping other parameters at baseline values. The baseline values for coefficient terms in expressions for Φ_g , Φ_{local} , Φ_{fs} and Φ_{fb} are identified in the following sections. For example, the constant in Equation 7.8 is taken as a = 1, corresponding to the case of geosynthetic reinforced soil walls unless noted otherwise.

The accuracy of the K_0-stiffness method when different expressions for the influence factors and associated constant coefficient values identified above are used is evaluated in the following sections in two ways:

1. direct comparison of predicted and measured reinforcement values for selected walls
2. comparison of the mean and variation of the ratio of predicted reinforcement loads to measured values for all case studies (Table 7.2).

Clearly, values of the mean of the ratio of reinforcement loads close to but greater than unity are desirable while the coefficient of variation of this ratio is maintained at a minimum value.

7.4.2 Load Distribution Factor, D_{tmax}

Current design methodologies assume a triangular distribution of T_{max} with depth below the wall top for geosynthetic walls (Figure 7.2a). They assume a modified triangular distribution with depth for steel reinforced MSE walls (Figure 7.2b). The lateral earth pressure coefficient, K, varies as a function of depth. Other types of reinforced soil structures, such as anchored walls, have used trapezoidal distributions for T_{max} versus depth (Figure 7.2c). Data presented in Chapter 5.0 showed that measured values for the ratio of maximum reinforcement load in a layer, T_{max}, to the maximum reinforcement load for all layers, T_{mxmx}, plotted against normalized depth of layer fell within a trapezoidal envelope (see Figure 5.13 in Chapter 5.0). Over the normalized depth range z/H = 0.3 to 0.8, the normalized reinforcement loads match the

Table 7.2. Summary of the ratio of predicted to measured reinforcement load for MSE walls.

Geosynthetics	No. of Data Points	AASHTO Simplified Method (plane strain ϕ)	Ratio of Predicted/Measured T_{max} or T_{mxmx}									
						K_0-Stiffness Method						
			Coefficient of Earth Pressure			Influence of Selected Values on Ratio of Predicted/Measured Loads						
			Proposed Approach: K_0 (and a=1 in Eq. 8, d=0.5 in Eq. 11)	K_{ah}	K = 0.3 for all Soils	γ = 18 kN/m³ for all Walls	Local Stiffness Factor Φ_{local} (Eq. 8)		Facing Stiffness Factor Φ_{fs} =1 for all Walls	Facing Batter Factor		S_v = 0.6 m for all Walls
							a=0 (Φ_{local}=1)	a=0.5		Φ_{fb} =1 (d=0 in Eq. 11)	Φ_{fb} (d= 1 in Eq. 11)	
Mean T_{max}	58	2.89	1.12	1.12	1.27	1.06	1.29	1.17	1.40	1.41	0.97	1.03
COV T_{max} (%)	58	85.9	40.8	45.0	45.4	42.2	62.4	44.9	53.9	60.6	46.5	51.2
Mean T_{mxmx}	13	2.25	0.97	0.98	1.22	0.89	0.99	0.97	1.24	1.17	0.86	1.02
COV T_{mxmx} (%)	13	52.9	19.7	27.6	37.2	17.1	40.6	27.2	37.7	33.6	31.7	58.1

Note: T_{max} = maximum load in reinforcement layer; T_{mxmx} = maximum reinforcement load in the wall; COV = coefficient of variation = (standard deviation of ratio of reinforcement load values/mean of ratio of reinforcement load values) x 100%; K_{ah} is based on Coulomb analysis, assuming full wall friction ($\delta = \phi$) and wall batter ψ.

maximum reinforcement load value (T_{mxmx}) taken from all reinforcement layers, while at the top and bottom of the wall the predicted reinforcement loads tend to reach small but finite values representing 20 percent of the maximum reinforcement load. The coordinates for this distribution are approximate only and have been selected to capture the majority of the data while simplifying the envelope geometry.

Lee (2000) carried out a numerical investigation of geosynthetic reinforced soil walls. The numerical model was calibrated against some of the case studies referenced in this report, and the study extended to a wider range of wall geometry, reinforcement stiffness, and soil properties. Calculated, normalized reinforcement loads from his parametric analyses fell on or within the trapezoidal envelope shown in Figure 5.13 of Chapter 5.0.
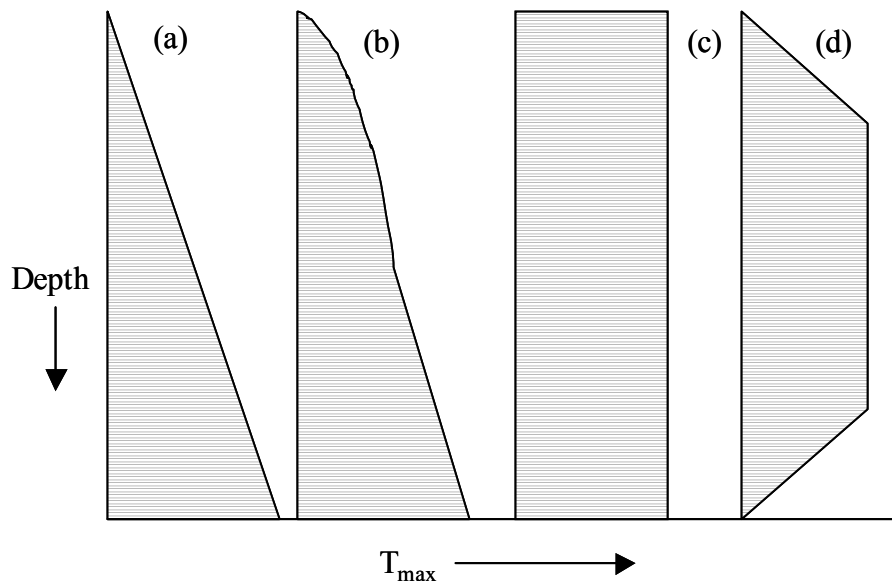
Figure 7.2. Typical distributions of T_{max} with depth below the wall top for MSE walls: (a) triangular distribution used in Tieback Wedge Method, (b) modified triangular distribution used in Coherent Gravity and Simplified methods, (c) rectangular distribution proposed by Broms (1978) for geosynthetic walls, and (d) trapezoidal distribution recommended by Sabatini et al. (1999) for anchored walls.

Numerical simulation results of geosynthetic reinforced soil walls reported by Lee (2000) and Rowe and Ho (1993) also predicted that load in the reinforcement layers near the bottom of the wall tend to be less than the reinforcement loads within the middle third of the wall height. Rowe and Ho (1993) provided a summary of physical data from reduced scale and full-scale

walls that confirms this observation for walls with a pinned toe. Bathurst and Hatami (1998) demonstrated the same effect through numerical parametric analyses of an idealized, full height panel, reinforced soil wall with a toe that was free to rotate. However, they also showed that attenuation of reinforcement loads at the base of the wall did not occur if the toe was free to slide. Given the observations made here, it is clear that the stiffness of the foundation and the degree of fixity of the wall facing toe influence the distribution of reinforcement loads at the base of a geosynthetic reinforced soil wall. However, most walls have a fixed toe condition due to wall embedment, and hence the attenuation of reinforcement load in proximity to the foundation predicted by a trapezoidal distribution is reasonable for walls constructed on stiff competent foundations.

7.4.3 Global Reinforcement Stiffness Factor, Φ_g

As discussed in Chapter 5.0, the stiffness of the various internal components of the wall directly affects the distribution of loads to each of the wall components at working stress conditions. This is true of any composite material in which the components of the system have different stiffness values and in which the components are perfectly bonded together (e.g., steel or fiber reinforced concrete). To account for the effect of stiffness, the relationship between reinforcement load and reinforcement stiffness must be quantified. The influence of reinforcement stiffness on reinforcement loads can be assessed from both a global perspective (i.e., the influence of all reinforcement layers in the wall section - Equation 7.7) and a local perspective (i.e., individual reinforcement layer – Equation 7.9). Christopher (1993) showed that maximum reinforcement loads increase with increasing magnitude of global reinforcement stiffness value, S_{global}. In other words, as the average stiffness of the reinforcement layers increases, the reinforcement loads increase. Equation 7.1 is rewritten below to enable back-calculation of global stiffness factor values, Φ_g (measured), from measured maximum reinforcement load (T_{mxmx}) values:

$$\Phi_g \text{ (measured)} = \frac{T_{mxmx}}{S_v^i \, \sigma_h \, D_{tmax} \, \Phi_{local} \, \Phi_{fs} \, \Phi_{fb}} \qquad (7.10)$$

Data for Φ_g (measured) versus (S_{global}/p_a) are plotted in Figure 7.3 for all of the geosynthetic wall case histories in Table 7.1 plus the steel wall case histories identified in Chapter 8.0.

239
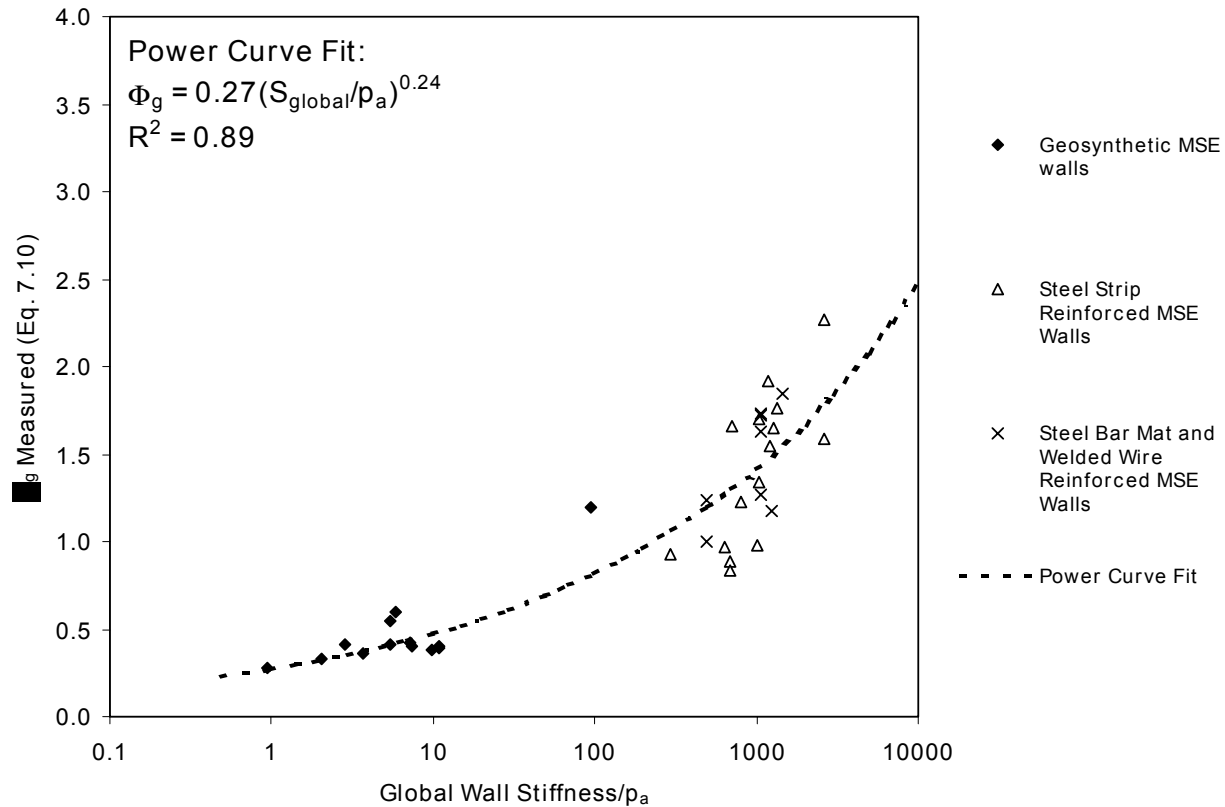
Figure 7.3. Measured Φ_g (Equation 7.10) versus normalized global reinforcement stiffness value (S_{global}/p_a).

The data in Figure 5.13 (Chapter 5.0) show that the maximum reinforcement load in the wall corresponds to the case with $D_{tmax} = 1$. Hence, D_{tmax} was set equal to 1.0. The constant for the local stiffness factor, Φ_{local}, in these calculations (Equation 7.8) has been taken as a = 1 for geosynthetic reinforced soil walls and a = 0 for steel reinforced soil walls (Section 7.4.1). Values for Φ_{fs} (facing stiffness factor) and Φ_{fb} (facing batter factor) can be found in Section 7.4.5 and Section 7.4.6, respectively. Superimposed on Figure 7.3 is a regressed approximation to the trend in data for the geosynthetic case histories in Table 7.1 *and* for steel reinforced wall case studies reported by Allen et al. (2001) using the power function for the global stiffness factor with constants $\alpha = 0.27$ and $\beta = 0.24$. The data for steel reinforced MSE walls were used in the regression analysis to extend the predicted relationship to reinforcement stiffness values beyond those available for the geosynthetic reinforced soil walls in Table 7.1, so that the regression equation would be applicable to both the geosynthetic and steel datasets. The power curve fit to the physical data is reasonably accurate, although there is some scatter in the steel reinforced

240

MSE walls data. This may be due to factors unique to steel MSE walls (see Chapter 8.0 and Allen et al. 2001). In the parametric analyses to follow, coefficient terms $\alpha = 0.27$ and $\beta = 0.24$ are used.
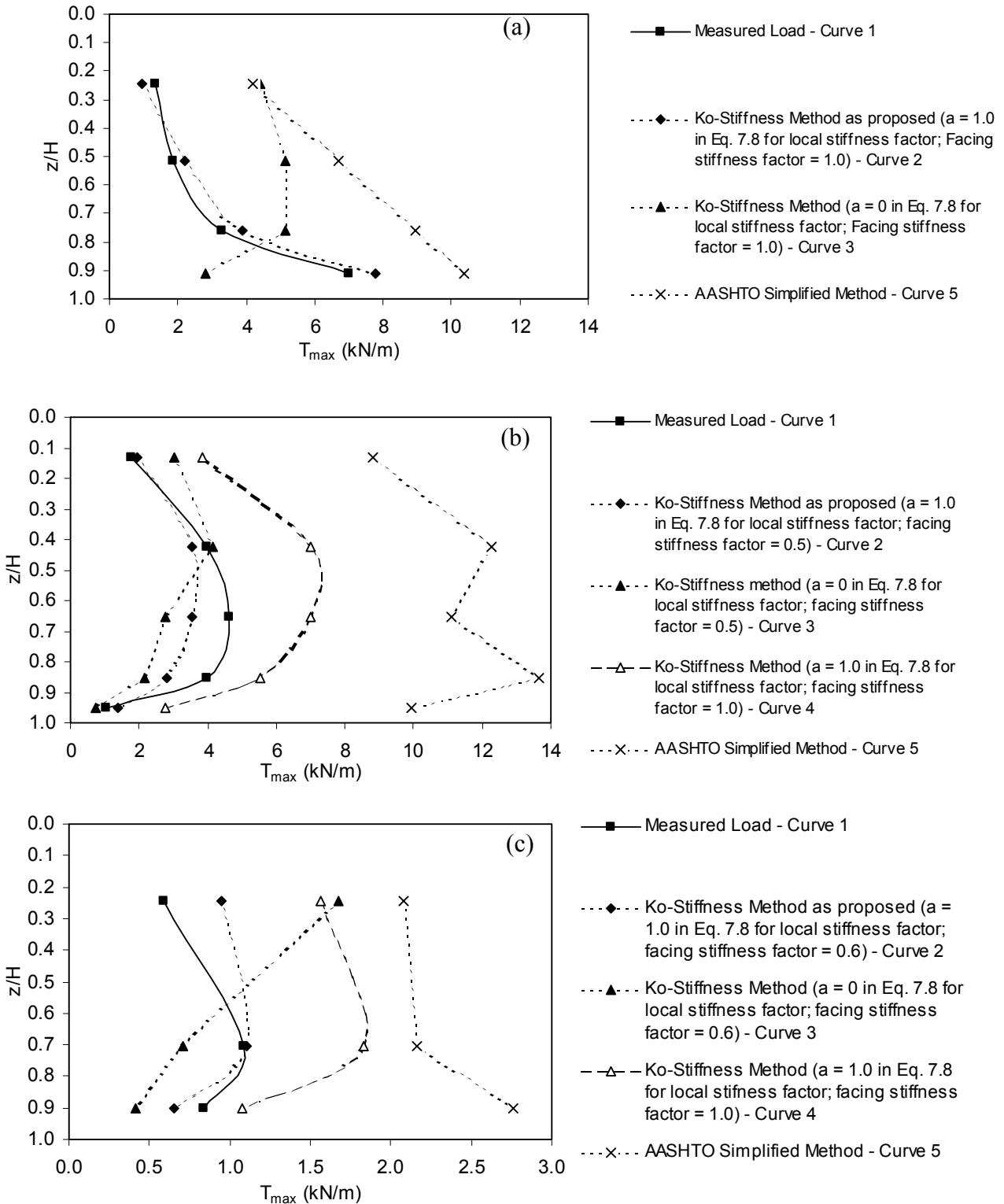
7.4.4 Local Stiffness Factor, Φ_{local}

Local deviations from overall trends in reinforcement loads can be expected when the reinforcement stiffness and/or spacing of the reinforcement change from average values over the height of the wall (i.e., $S_{local}/S_{global} \neq 1$). This effect is captured by a local stiffness factor, Φ_l, expressed by Equation 7.8. Figure 7.4 shows the best predictions for maximum load in the geosynthetic reinforcement layers for three different case studies. The predictions were calculated with the working stress method and correspond to local stiffness factor calculations with a = 1. A value of a = 1 was selected as a preliminary estimate in the working stress method for structures built with geosynthetic reinforcement layers.

A parametric investigation, similar to what was done in Section 7.4.3 for the global reinforcement stiffness factor, was conducted for the local stiffness factor. Equation 7.1 is rewritten below to back-calculate values of local stiffness factor, Φ_{local} (measured), from measured maximum reinforcement load (T_{mxmx}) values:

$$\Phi_{local} \ (measured) = \frac{T_{mxmx}}{S_v^i \ \sigma_h \ D_{tmax} \ \Phi_g \ \Phi_{fs} \ \Phi_{fb}} \tag{7.11}$$

The values of these variables are as described in Section 7.4.3. Values of Φ_{local} (measured) versus (S_{local}/S_{global}) are plotted in Figure 7.5 for the geosynthetic wall case histories in Table 7.1. As shown in the figure, an exponent "a" that is approximately equal to 1.0 provides the best fit for geosynthetic walls.

A similar parametric investigation in Chapter 8.0 shows that for steel reinforced soil walls a value of a = 0 for the constant coefficient in the local stiffness factor equation is more accurate. An explanation for the difference in values is that steel reinforcement is much stiffer than the soil, and hence local variations in stiffness may have little effect on the redistribution of reinforcement loads. Table 7.2 shows the influence of assigning values of a = 0 ($\Phi_{local} = 1$, i.e., ignoring any possible local reinforcement stiffness effects) and a = 0.5 on predicted

Figure 7.4. Influence of magnitude of facing stiffness factor and local stiffness factor on magnitude and distribution of reinforcement load T_{max} (a) GW16 (wrapped face wall) with soil surcharge, (b) GW9 (modular block wall) with soil surcharge, and (c) GW5 (incremental precast panel wall).

242
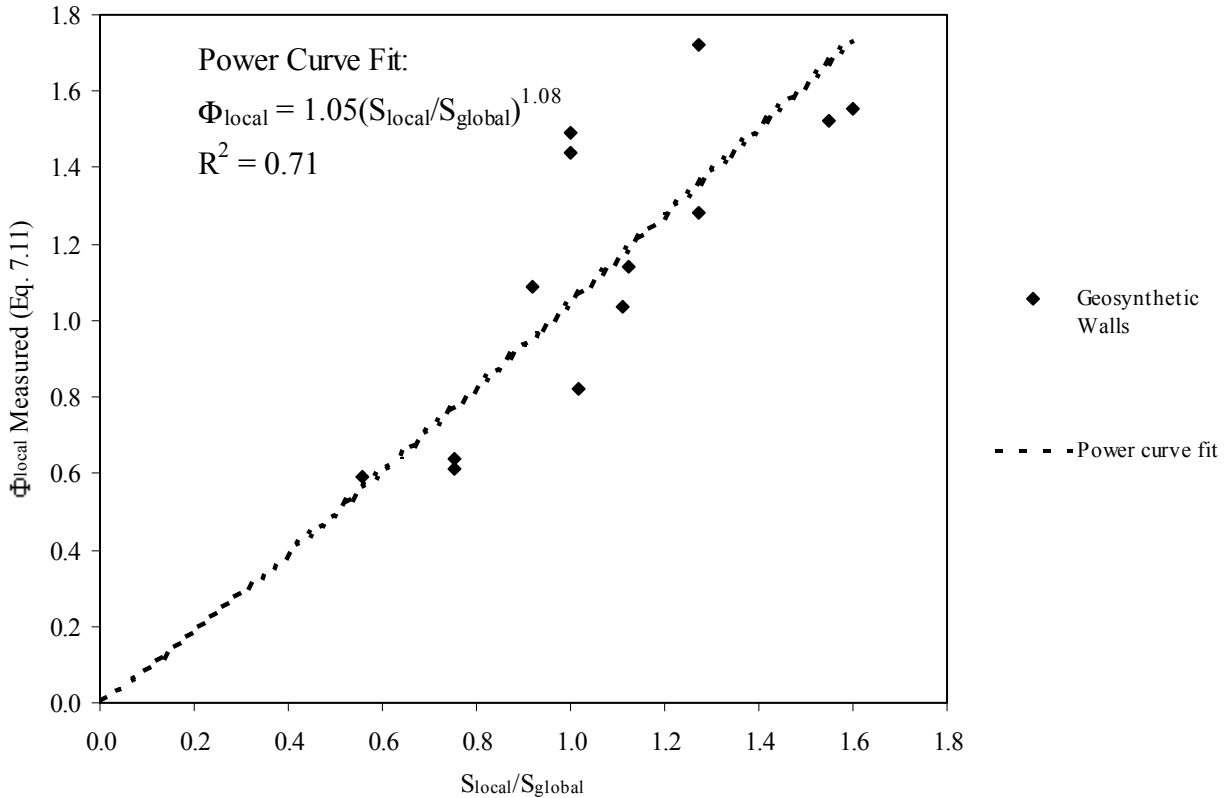
Figure 7.5. Measured Φ_{local} (Equation 7.11) versus S_{local}/S_{global}.

reinforcement loads in Stiffness Method calculations for geosynthetic walls. (See also figures 7.4a, 7.4b, and 7.4c, in particular comparing curves 2 and 3 in each case study.)

7.4.5 Facing Stiffness Factor, Φ_{fs}

Research reported in the literature has indicated that the stiffness of the facing and the lateral restraint of the wall facing at the wall toe can significantly influence the loads carried by the soil reinforcement, at least for geosynthetic walls. Tatsuoka (1993) overviewed facing stiffness effects on MSE wall reinforcement loads. He attempted to categorize facings on the basis of their stiffness characteristics, with facing types A and B being very flexible, wrapped geosynthetic, gabion, or steel skin facings; Type C facings being articulating concrete panels; Type D facings being full-height, precast concrete panels; and Type E being concrete gravity structures. Facing rigidity was defined in terms of local, axial, shear, and bending rigidity, and overall mass as a gravity structure. Tatsuoka concluded that soil reinforcement strains tend to decrease as facing rigidity increases because of the increase in soil confinement caused by a very stiff facing,

thereby reducing reinforcement loads. Loads carried axially by the facing to the toe may also contribute to the increased stability that occurs in stiffer facings. If the wall facing is massive enough to behave as a gravity structure, the loads in the reinforcement may be reduced to very low values.

Rowe and Ho (1993) concluded that both the facing and foundation stiffness affect the overall stiffness of the system, as well as the portion of horizontal load carried by the reinforcement and the footing. In fact, for stiff facings (e.g., full-height panel walls), force equilibrium cannot be satisfied without considering the toe forces transferred to the bottom of a facing with a restrained toe (Rowe and Ho 1993, Bathurst et al. 1989). Bathurst (1993) investigated the issue of facing stiffness/toe restraint for two full-scale test walls (walls GW14 and GW15 in Table 7.1) with full-height propped and incremental aluminum panel facings. For these two walls, he found that 25 percent of the total lateral load at collapse due to surcharging was carried by the wall toe. In more recent work with 3.6-m-high modular block-faced systems, Bathurst et al. (2000) found that the wall toe carried approximately 40 percent of the lateral load when the wall was loaded to near collapse. This more recent work appears to indicate, however, that as wall lateral deformations develop, the reinforcement layers carry a greater proportion of the total lateral load. Chapter 5.0 indicates that propping the wall facing while backfilling (for example, wall GW12) caused the wall facing to behave as if it were very stiff, even after final equilibrium had been reached following prop release. However, after surcharge loading of the wall, reinforcement loads approached values recorded for the companion wall with an incremental panel facing that was not externally supported during wall construction.

The numerical parametric studies conducted by Lee (2000) also investigated the effect of facing stiffness on reinforcement loads. Lee used two categories of facings: 1) flexible face (e.g., wrapped-face walls) and 2) stiff faced walls (e.g., precast incremental concrete panel and modular block faced walls). Lee found that the reinforcement loads in the stiff faced walls were approximately 50 percent of the reinforcement loads in the flexible faced walls. Note that the concrete panel faced walls were modelled with a very stiff interface between adjacent panels to prevent potential numerical instability problems. This stiff interface, in effect, caused the incremental panels to behave as if they were a single panel (i.e., a full-height panel). Therefore, in the analytical model, the concrete panel facing likely behaved more rigidly than the actual walls they were intended to model.

The empirical data, provided herein, available from the full-scale wall case histories with stiff facings versus those with flexible facings were compared to determine the effect of facing stiffness on reinforcement loads. As suggested by the data reviewed here, the effect of facing type on reinforcement loads is captured by a facing stiffness factor with the following values:

- $\Phi_{fs} = 0.5$ for modular block and propped concrete panel faced walls (stiff facings)
- $\Phi_{fs} = 1.0$ for all other types of wall facings (flexible facings, e.g., wrapped-face, welded wire or gabion faced, and incremental precast concrete facings).

Structures may be constructed that fall between the categories identified above, and hence facing stiffness factors with values between 0.5 and 1.0 may be appropriate. For example, in case history GW5, the full-height panel was externally braced during the initial two-thirds of backfilling and was free to move thereafter. For this special case a facing stiffness factor of 0.6 was used.

Figures 7.4b and 7.4c demonstrate the improvement in predicted maximum reinforcement loads for modular block and incremental concrete panel faced walls by using $\Phi_{fs} = 0.5$ or 0.6 (curve 2) in comparison to the value of $\Phi_{fs} = 1.0$ (curve 4) used for flexible faced structures. Curve fitting exercises to select coefficient values for influence factors in Equation 7.1 were dominated by geosynthetic reinforced soil walls with wrapped face construction and geosynthetic and steel reinforced soil walls with precast, concrete panel facings. The empirical data indicated that precast, incremental panel faced wall facings should be considered flexible, as there was no difference in reinforcement loads for these two categories of wall facing, all other conditions being equal. Hence, both types of wall facings were grouped together with the same facing stiffness factor. However, the reinforcement loads in the walls with relatively rigid concrete facings, such as modular block and propped panel concrete facings, were consistently half of the loads in walls with flexible facings, as defined herein. The incremental panel walls in this study can be argued to have behaved as walls with flexible facings because of the mobility of the panel joints, and the wrapped-face walls may have developed additional facing stiffness because of reinforcement overlaps at the face in combination with the relatively high strength granular backfills. Greenway et al. (1999) attributed part of the good long-term stability of the first geosynthetic wall built in the United States to the reinforcement overlaps at the face. Zornberg et al. (1998a,b) also believed that the facing overlaps in their model walls contributed to the stability of the walls. Similarly, secondary reinforcement, which is generally not

245

considered as tensile resistance in internal wall stability calculations, contributes to the overall internal wall stability, thereby reducing loads in the primary reinforcements (see next section). Table 7.2 also shows the result of assuming that $\Phi_{fs} = 1.0$ for all case studies while using the baseline values for all the other factors.

Although Φ_{fs} is set equal to 1.0 for "flexible" wall facings, this does not mean that the facing has no effect on the reinforcement loads for these relatively flexible facings. Equation 7.1 empirically already accounts for the effect of the facing on the reinforcement loads for these flexible wall facings. It is possible that facings of even greater flexibility could require a facing stiffness factor of slightly more than 1.0.

In summary, the baseline facing stiffness factor values introduced here should be considered approximate values that may need refinement as the database of wall case studies is expanded. For example, the facing stiffness factor is assumed to apply through the entire height of the wall. However, the influence of toe restraint on walls with stiff facings can be expected to increase with decreasing wall height. Conversely, values of $\Phi_{fs} > 0.5$ may be applicable for walls with stiff facings and a height greater than 6 m, given that the maximum height of structures for which comparisons could be made was 6 m. The influence of toe restraint and wall height is discussed further in Section 7.5.

7.4.6 Facing Batter Factor, Φ_{fb}

In current practice, wall face batter (i.e., inclination from the vertical) is taken into account explicitly with Coulomb earth pressure theory. While calculations with the new working stress method described up to this point in this chapter improved reinforcement load predictions, significant discrepancies remained for the battered walls in Case Study GW 7 (see Figure 7.6). Limit equilibrium methodologies attempt to capture this effect through the Coulomb earth pressure coefficient. However, as demonstrated in Chapter 5.0 and as will be shown later, the Coulomb earth pressure coefficient tends to reduce reinforcement loads excessively for heavily battered walls. The influence of reduced confining pressure near the wall face cannot be captured explicitly by limit equilibrium methods.

The influence of wall facing batter on maximum reinforcement loads is adjusted in the proposed working stress method by using an empirical facing batter factor expressed as:

$$\Phi_{fb} = \left(\frac{K_{abh}}{K_{avh}}\right)^{d} \tag{7.12}$$

where K_{abh} is the horizontal component of the active earth pressure coefficient accounting for wall face batter, and K_{avh} is the horizontal component of active earth pressure coefficient, assuming the wall is vertical and d is a constant coefficient. The form of the equation shows that as the wall face batter angle $\omega \to 0$ (i.e., the wall facing batter approaches the vertical), the facing batter factor $\Phi_{fb} \to 1$. With the exception of case study GW7, the structures in Table 7.1 correspond to values of Φ_{fb} that are greater than 0.85. Different values of the constant coefficient "d" in Equation 7.12 were examined to improve the fit between measured and predicted values of reinforcement loads for the case studies with wall batter, especially case study GW7 (facing batter angle $\omega = 27$ degrees from vertical).

A parametric investigation, similar to what was done in Section 7.4.3 for the global reinforcement stiffness factor, was conducted for the facing batter factor. Equation 7.1 is rewritten below to back-calculate values of facing batter factor, Φ_{fb} (measured), from measured maximum reinforcement load (T_{mxmx}) values:

$$\Phi_{fb} \; (\text{measured}) = \frac{T_{mxmx}(\text{measured})}{S_v^i \; \sigma_h \; D_{tmax} \; \Phi_g \; \Phi_{local} \; \Phi_{fs}} \tag{7.13}$$

The values of these variables are as described in Section 7.4.3. Values of Φ_{fb} (measured) versus (K_{abh}/K_{avh}) are plotted in Figure 7.7 for the geosynthetic wall case histories in Table 7.1. The regression analysis for the data in the figure yielded an exponent "d' of approximately 0.4. Note that the data are limited at lower ratios of (K_{abh}/K_{avh}), and the R^2 value is rather low. The scatter in the data indicates that improvement in the formulation of the batter factor proposed herein may be needed, though the writers believe that the proposed facing batter factor is an improvement over the Coulomb earth pressure coefficient to account for facing batter effects.
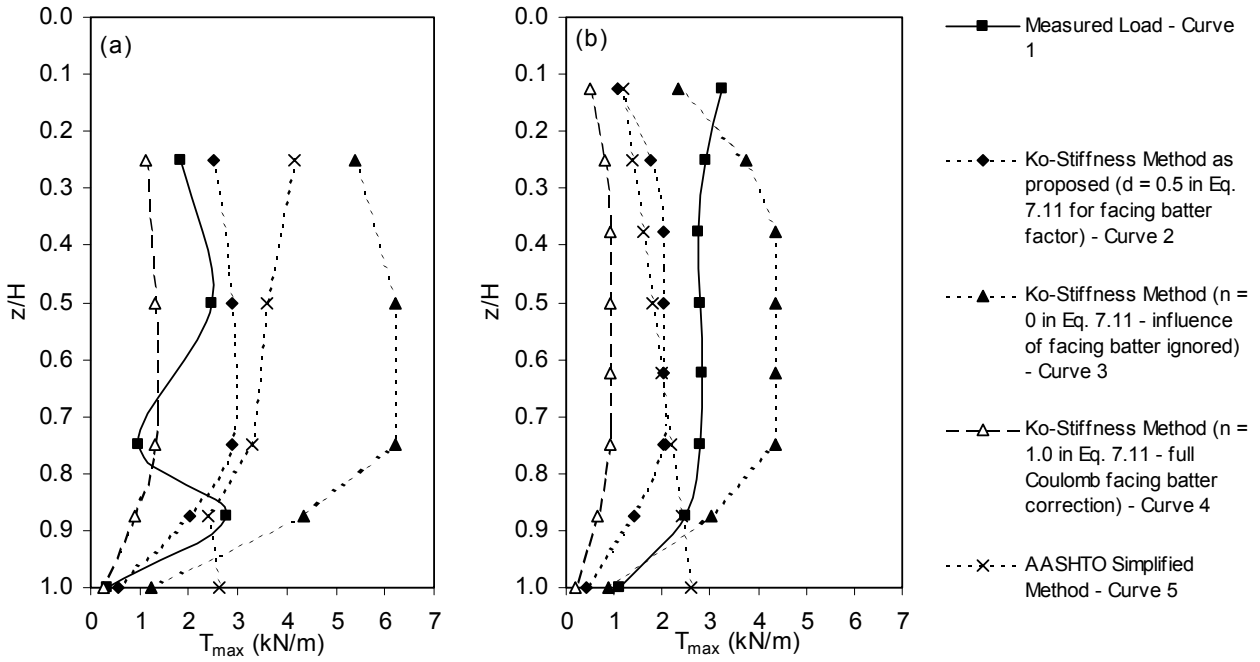
Figure 7.6. T_{max} distribution versus normalized depth for GW7 (a) Section J, and (b) Section N, showing effect of secondary reinforcement and facing batter on T_{max} prediction.
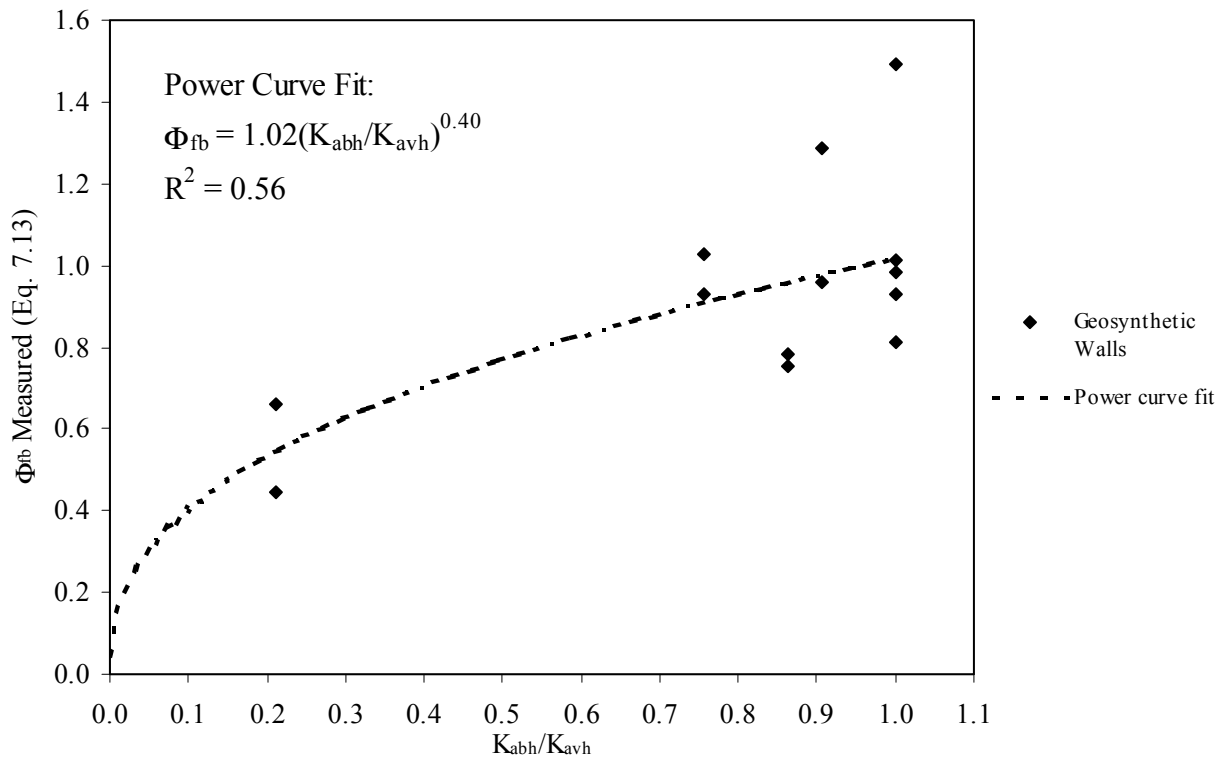
Figure 7.7. Measured Φ_{fb} (Equation 7.13) versus K_{abh}/K_{avh}.

Figure 7.6 shows plots of predicted reinforcement loads using equations 7.1 and 7.12 with d = 0 (curve 3), 1 (curve 4) and 0.5 (curve 2). Predictions calculated with the Simplified Method (AASHTO 1999) are also provided for comparison. For Section J of case GW7 in Figure 7.6a, the loads predicted with Equation 7.1 and Equation 7.12 with d = 0.5 (curve 2) are reasonably close to, but generally greater than, measured values (curve 1). The same factor applied to Section N of the structure (GW7) under-predicts the measured loads in Figure 7.6b. Nevertheless, the K_0-Stress Method with d = 0.5 (curve 2) produces values that are, on average, closer to measured values than the Simplified Method (curve 5). Section N of this case study was constructed without overlapping of the reinforcement layers at the face and hence may have been more flexible than other "flexible-wall" cases used to establish baseline coefficient values in the parametric analyses (see discussion on the facing stiffness issue in Section 7.4.5). This may explain why the proposed K_0-Stiffness Method provided in Equation 7.1 (see curve 2 in Figure 7.6b) slightly under-predicts the loads measured in the reinforcement.

Table 7.2 compares the spread (represented by the coefficient of variation, or COV) in the ratios of predicted to measured reinforcement loads for the proposed method by ignoring the facing batter effect (d = 0), using d = 0.5, or assigning a constant coefficient d = 1 (which in effect yields the full effect of the facing batter in the Coulomb equation) in Equation 7.12 for all cases. A d = 0.4, as determined from Figure 7.7, provides a slightly poorer fit when T_{max} is considered rather than just T_{mxmx}. The proposed value of d = 0.5 yields the best fit given the available T_{max} data and is recommended as the default value in the proposed K_0-Stiffness method.

7.4.7 Influence of Soil Strength on Reinforcement Loads

For working stress conditions in MSE walls, the soil property that most likely affects the distribution of load to the reinforcement layers in the wall is the soil modulus. This is because of the relatively low strain levels and the fact that limit equilibrium conditions have not been reached. However, the soil modulus is difficult to determine, and for most of the case histories reported herein, a measured soil modulus was not available. The peak soil friction angle is routinely available, familiar to designers, and is relatively easy to measure or estimate. In general, as peak friction angle for a granular soil increases, the soil modulus also increases

(Duncan et al. 1980). Hence, peak friction angle can be interpreted as an indicator of relative soil modulus value between soil types.

In the development of the stiffness method proposed herein, values of $K = K_o$ (Equation 7.3) and $K = K_{ah}$ were examined to investigate the relative accuracy of predicted values of T_{max} and T_{mxmx}. K_0 was considered because of it is simple to calculate and is calculated independent of wall face batter (face batter is handled by a separate factor—see Section 7.4.6). K_{ah} (the horizontal component of active earth pressure) was determined by using the Coulomb method, assuming full interface friction for all walls (i.e., $\delta = \phi$), and assuming continuous or nearly continuous reinforcement layers. For these structures the reinforcement-facing connections will restrict downward movement of the backfill soil against the face, effectively resulting in an interface friction angle at the back of the wall face equal to the backfill soil friction angle. In wall GW19, the reinforcement comprised discrete strips, and hence full mobilization of soil shear strength behind the wall facing panels might not be expected. For this wall, an interface friction angle of two-thirds of the soil backfill friction angle was used to calculate the Coulomb K_{ah} value, which is typical of concrete-soil interface friction angles. The data in Table 7.2 show less spread in the ratios of predicted to measured reinforcement loads when K_0 was used rather than K_{ah}. Interestingly, setting K_0 equal to a constant value of 0.3 for all soil friction angles yielded a value of spread in the ratios that was similar to the values produced by using K_{ah}. Some of this spread using K_{ah} was likely due to an inaccurate accounting of wall face batter on T_{max} (see Section 7.4.6).

A parametric investigation, similar to that reported in Section 7.4.3 for the global reinforcement stiffness factor, was conducted to back-calculate K in the K_0-Stiffness Method from measured maximum reinforcement load (T_{mxmx}) values normalized as shown below:

$$K \text{ (measured)} = \frac{T_{mxmx}}{S_v^i \left(0.5\gamma(H+S)\right) D_{tmax} \, \Phi_g \, \Phi_{local} \Phi_{fb} \, \Phi_{fs}}$$
(7.14)

The values of the variables are as described in Section 7.4.3. The back-calculated values of K determined from the measured values of T_{mxmx} versus K_0 (Equation 7.3) are plotted in Figure 7.8 for the geosynthetic wall case histories in Table 7.1. This figure indicates that the load in the reinforcement is influenced by the soil response to load, as characterized by K_0 in this plot. However, the scatter suggests that other factors may also influence this relationship. Until these

250

other unknown factors are more specifically evaluated, the use of K_0 to characterize the soil is considered to be a reasonable approximation.
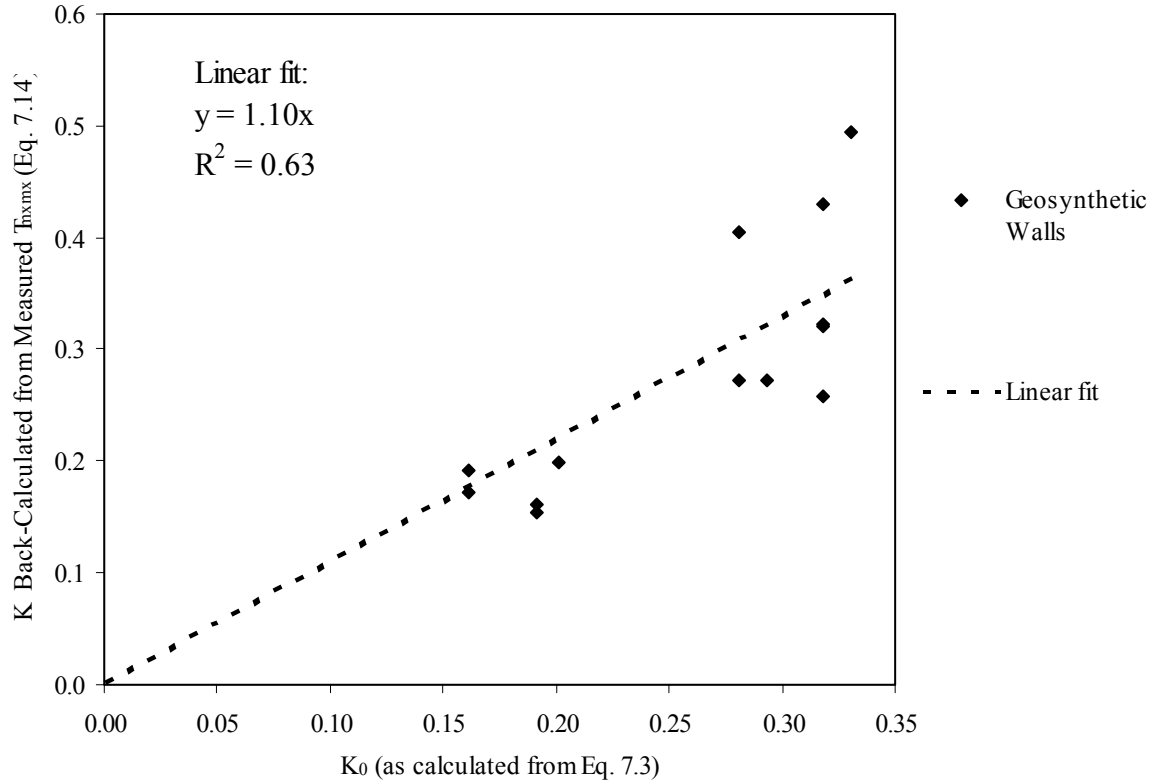
Figure 7.8. Back-calculated K (Equation 7.14) versus K_0 calculated from Equation 7.3.

7.4.8 Effect of Soil Unit Weight on Soil Reinforcement Loads

The soil unit weight recorded for each case study was typically within 10 percent of the mean value for all of the walls ($\gamma_{mean} = 18$ kN/m^3) and ranged from 16.4 to 21.1 kN/m^3. This variation was considered to be small in comparison to the uncertainty associated with other parameter values in this investigation, including estimated reinforcement loads. However, the fundamental expression for reinforcement loads (Equation 7.4) using the Stiffness Method shows that loads (and hence strains) should vary linearly with soil unit weight. To investigate the influence of soil unit weight on predicted reinforcement loads, calculations for T_{max} and T_{mxmx} were done while using a constant value for γ of 18 kN/m^3. Table 7.2 shows that there was only a minor difference in the accuracy of predicted reinforcement loads with a default constant unit

251

weight of 18 kN/m^3 in the calculations rather than project-specific values. This minor difference was consistent with the variation in the measured value of this parameter.

7.4.9 Effect of Reinforcement Layer Spacing on Soil Reinforcement Loads

The vertical distance between reinforcement layers in the case studies for this investigation varied from 0.3 to 1.6 m. Note that this is not necessarily the same as the vertical zone in the wall that contributes to load in a given reinforcement layer (i.e., the tributary area). S_v is representative of the tributary area when loads are calculated on the basis of load per unit of wall length and the spacing between layers is uniform. When the spacing is not uniform, this parameter is representative of the average distance between the layers that are adjacent to the layer in question. At the top of a wall, S_v includes the full distance between the top layer and the top of the wall, plus the distance to the mid-point between the top layer and the next layer below.

The magnitude of reinforcement loads (and strains) can be expected to vary linearly with S_v, as assumed in the Stiffness Method and conventional design methods. Calculations were redone with a default value of $S_v = 0.6$ m, which is the approximate average of the vertical spacing for all of the walls. Table 7.2 shows that S_v has a significant effect on reinforcement loads for all of the case histories.

A parametric investigation, similar to what was done in Section 7.4.3 for the global reinforcement stiffness factor, was conducted to evaluate S_v. Equation 7.1 is rewritten below to back-calculate values of S_v from measured maximum reinforcement load (T_{mxmx}) values:

$$S_v \text{ (back-calculated)} = \frac{T_{mxmx}}{\sigma_h \, D_{tmax} \, \Phi_g \, \Phi_{local} \, \Phi_{fs} \, \Phi_{fb}} \tag{7.15}$$

The values of the variables are as described in Section 7.4.3. Values of S_v, back-calculated from the measured values of T_{mxmx}, versus S_v, as determined directly from the spacing of the reinforcement in the wall, are plotted in Figure 7.9 for the geosynthetic wall case histories in Table 7.1. The regressed data demonstrate a linear relationship between reinforcement load and S_v, as predicted by both the proposed method and current design methods. This correlation appears to hold reasonably well even to large values of S_v.
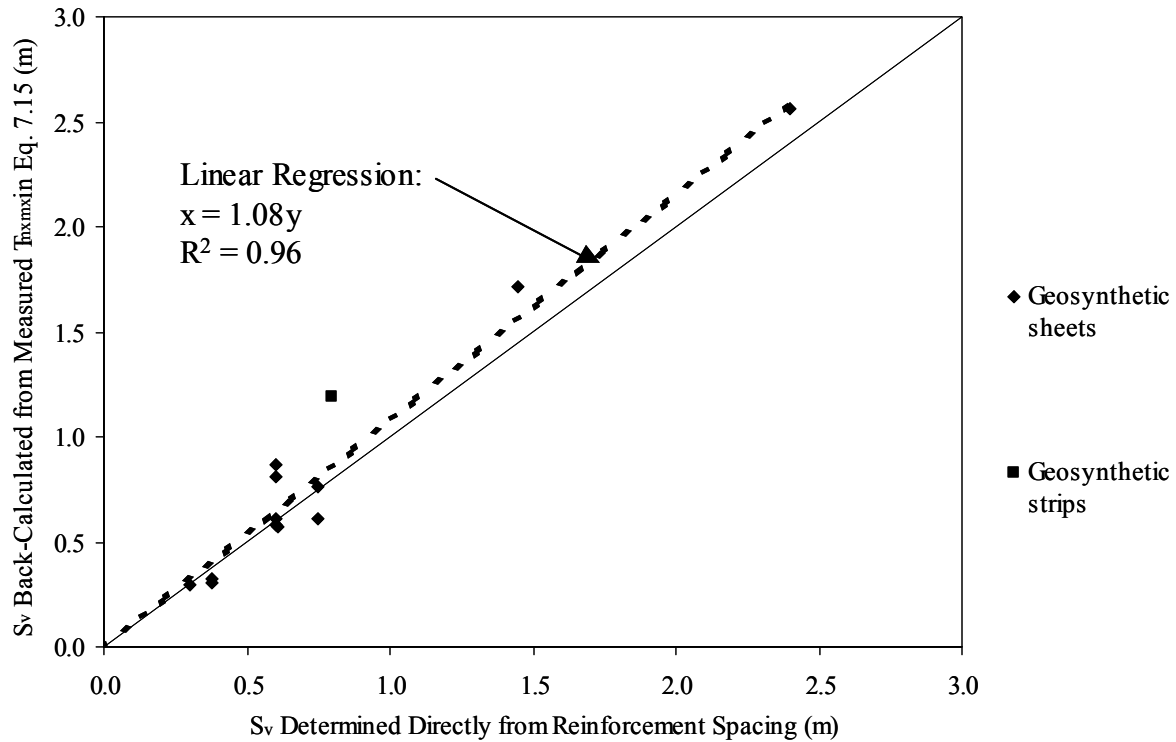
Figure 7.9. Back-calculated S_v from measured T_{mxmx} (Equation 7.15) versus S_v determined directly from the spacing of reinforcement in the wall.

7.5 Overall Performance of the K_0-Stiffness Method

The accuracy of the proposed K_0-Stiffness Method (Equation 7.4) for geosynthetic walls is illustrated in Figure 7.10 for all of the full-scale field wall case histories in Table 7.1. The improvement in predicted loads versus measured values when the proposed stiffness method is used in comparison to when the AASHTO Simplified Method is used is apparent when Figure 7.10 is compared to Figure 7.1. The same conclusion is reached by examination of values for the mean and spread (COV) of the ratio of predicted to measured reinforcement loads for the two methods in Table 7.2.
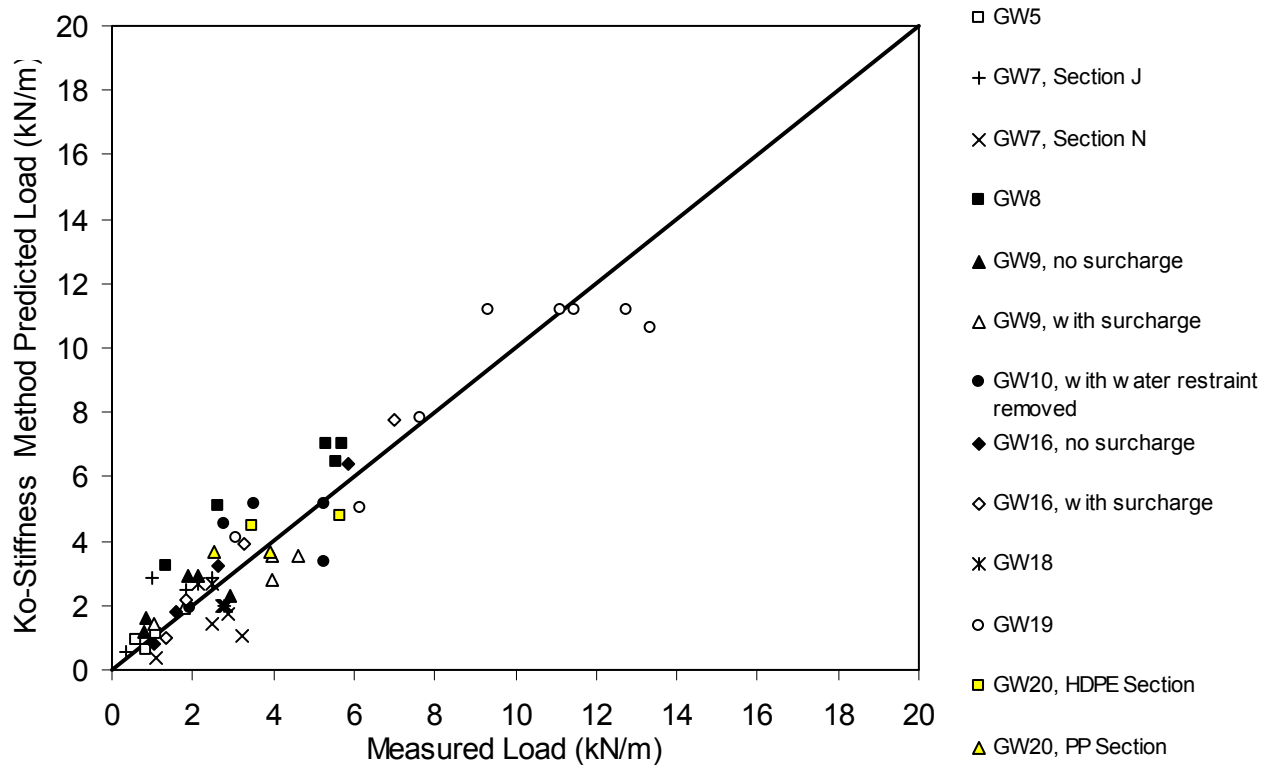
Figure 7.10. Measured values of T_{max} in reinforcement layers for geosynthetic walls versus values predicted with the K_0-Stiffness Method.

The data in Table 7.2 indicate that there is twice as much variation in the prediction of reinforcement load T_{max}, given all reinforcement layers, than in the prediction of the maximum reinforcement load, T_{mxmx} (compare the COV for T_{max} with the COV for T_{mxmx}). Therefore, better prediction of the distribution of T_{max} versus depth could greatly improve the prediction accuracy of the K_0-Stiffness Method.

The strain level in the reinforcement also appears to have a significant effect on the prediction accuracy of the K_0-Stiffness Method. Figure 7.11 shows strains, based on T_{mxmx}, predicted by the K_0-Stiffness Method plotted against the measured reinforcement strains for geosynthetic walls. The predicted strains were calculated by dividing T_{mxmx} by the reinforcement layer secant modulus, J. Once reinforcement strains exceed approximately 3 to 5 percent for the available case histories, the K_0-Stiffness Method appears to consistently under-predict the measured strain. Note that all of the strains greater than 3 percent were measured in full-scale test walls that were surcharged to loads well in excess of working stress conditions (see Bathurst et al. 1990, 1993; Burgess, 1999; and Vlachopoulos 2000 for details regarding these full-scale

254

test walls). Bathurst et al. (1993), Burgess (1999), and Vlachopoulos (2000) noted that in these tests, soil failure occurred before reinforcement rupture. Evidence of soil failure included a sudden and large outward movement of the wall face, soil settlement directly behind the wall face and a concurrent increase in reinforcement strains. None of the full-scale field walls recorded reinforcement strains that were consistent with soil failure, except Wall GW10, which exhibited signs of soil failure but only after the strain gauges had ceased to function.

Note in Figure 7.11 that at high strains the walls with stiff facings plot consistently below the walls with flexible facings. This may be an indicator that the facing stiffness correction factor used in the K_0-Stiffness method is not a constant, as proposed in that method, but increases toward 1.0 (i.e., less effect of facing stiffness) as the facing is unable to carry additional load.

Geosynthetic reinforcement can reach much higher strains without failure than can the soil. Therefore, prevention of reinforcement failure, the current focus of internal stability design, does not address the more likely mode of failure for geosynthetic walls, which is failure of the backfill soil. Prevention of reinforcement strains high enough at any time during the design life of the structure to allow failure of the soil must also be considered. Soil failure is defined, on the basis of observed behavior of heavily surcharged test walls, as soil strains in excess of the strain at peak strength. Once the soil has failed, for all practical purposes the wall has failed, too, and has reached an internal strength limit state.

All of the geosynthetic wall case histories reported herein used relatively clean high-shear strength sands and gravels as backfill. In general, the peak shear strain for these types of soils is in the range of 3 percent to 6 percent (Bathurst and Jones 2001). Plane strain shear strength data for the backfill used in Wall GW16 indicated that the soil had peak strains about 2 to 3 percent (Boyle, 1995). Since the backfill used for that wall had a shear strength that was at the upper end of those for the case histories considered, these peak strains are likely at the lower end of the typical range for granular soils. Plane strain shear strength data for the soil used in the full scale RMCC test walls also indicated that the peak strains for the soil used were about 2 to 3 percent (Lee 2000). This indicates that the reinforcement strains may need to be slightly greater than the soil peak shear strain before the soil begins to fail and the K_0-Stiffness Method begins to under-predict reinforcement loads. Figure 7.11 shows that for the available data the K_0-Stiffness Method provides an accurate prediction of reinforcement strains up to reinforcement strain levels that are at or slightly above the soil peak shear strain (i.e., reinforcement strain levels of

approximately 3 to 5 percent appear to correspond to soil peak shear strains of 2 to 3 percent). The relationship between reinforcement strain and the shear strain required to reach the soil peak strength needs to be better developed, so that the objective of designing to prevent soil failure within the reinforced soil zone of MSE walls can be obtained. However, it appears that preventing the reinforcement strain from exceeding 3 to 5 percent will be adequate or even conservative to prevent the failure of most granular backfill soils.

7.6 Summary and Conclusions

A new approach, termed the K_0-Stiffness Method, is proposed to predict reinforcement loads and strains for designing the internal stability of MSE walls. The working stress methodology has been developed and calibrated by using a database of MSE wall reinforcement strain and load data. This new methodology considers the stiffness of the various wall components and their influence on reinforcement loads. An objective of the method is to design the wall reinforcement so that the soil within the wall backfill is prevented from reaching a state of failure consistent with the notion of working stress conditions. This soil failure limit state is not considered in the MSE wall internal stability design methods currently available, yet, based on the research results presented herein, is likely to be a controlling limit state for geosynthetic structures. This new approach is largely empirical, based on back-analysis and curve fitting of measured data from full-scale MSE walls. The database used is extensive and captures a variety of wall geometries and materials. This gives confidence that the new method is applicable to most typical geosynthetic reinforced soil walls constructed with granular backfill soils.
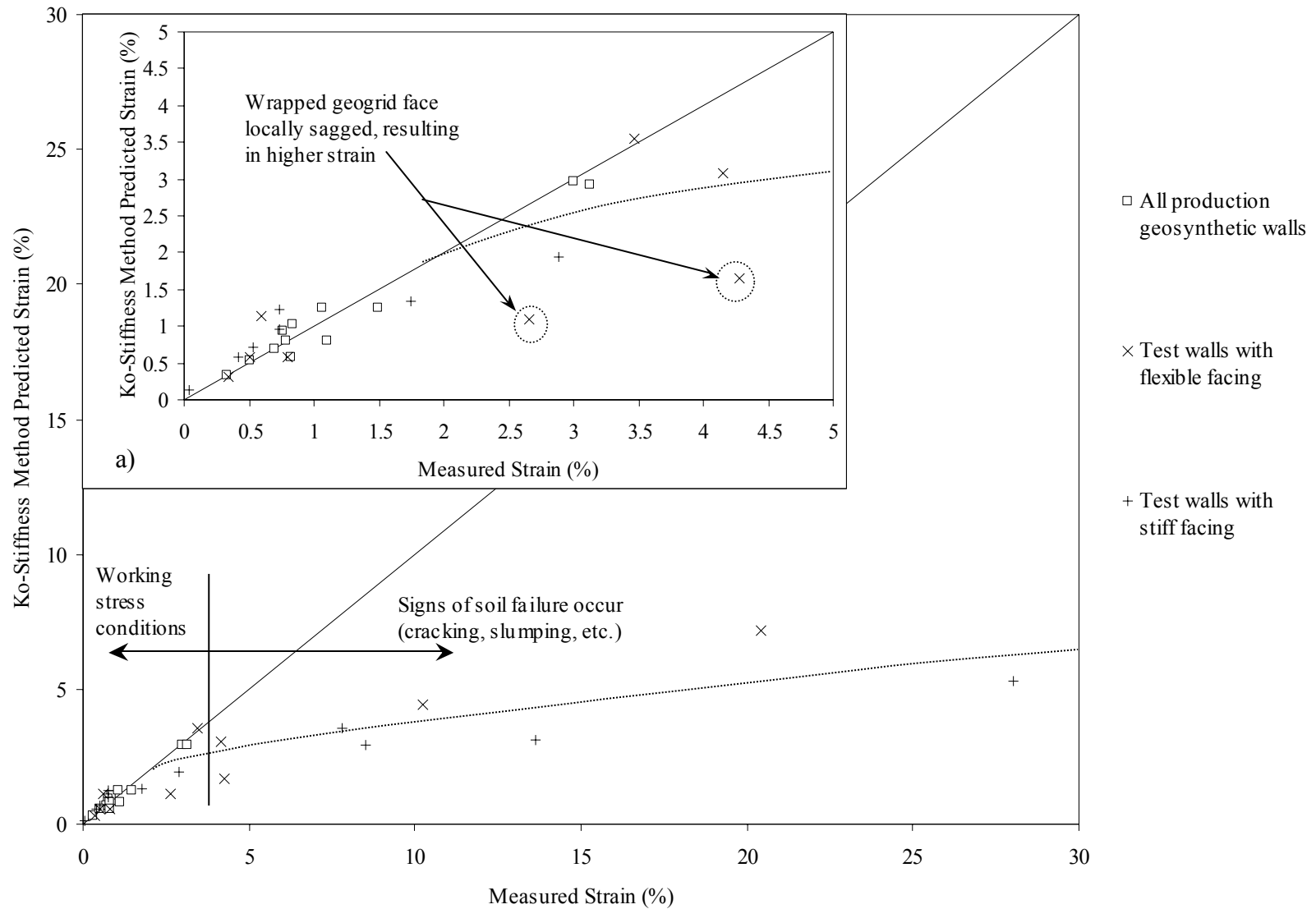
Figure 7.11. Predicted versus measured strain using the K₀-Stiffness Method for full-scale production (field) and full-scale laboratory geosynthetic walls, a) enlargement showing first 5 percent strain.

8.0   DEVELOPMENT OF THE K_0-STIFFNESS METHOD FOR STEEL REINFORCED MSE WALLS

8.1 Introduction

In Chapter 7.0, a new working stress method, called the K_0-Stiffness Method, is developed for geosynthetic walls. A desirable feature of any new methodology for designing MSE wall internal stability is a seamless transition between geosynthetic and steel reinforced MSE walls. Doing so will keep the design approach for MSE walls simpler, allow different reinforcement options to be evaluated within a common framework, and provide the designer confidence that the approach can be applied to a wide range of geosynthetic and metallic soil reinforcement products.

This chapter demonstrates how the K_0-Stiffness Method proposed by the writers for geosynthetic reinforced soil walls can be extended to steel reinforced MSE walls. As is true in Chapter 7.0, the scope of this chapter is limited to MSE walls with granular (non-cohesive) backfill.

8.2   Summary of Case Histories Evaluated

The key properties and parameters for each of the case histories referred to in this chapter are summarized in tables 8.1 and 8.2 for steel reinforced MSE walls. Additional details for each of these case histories, including wall and reinforcement geometry, reinforcement type, soil properties, and construction history are provided by Allen et al. (2001).

The database of steel reinforced MSE walls includes 19 case histories of walls that were built to full scale in the field. These case histories include walls with steel strip, bar mat, and welded wire reinforcement (reinforcement stiffness values varied from 18,000 to 166,000 kN/m), walls with precast concrete panel and welded wire facings, walls with and without significant soil surcharges, narrow base- and wide base-width walls, walls with trapezoidal cross-sections, very tall walls up to 18 m high, walls with a wide range of reinforcement coverage ratios varying from $R_c = 0.053$ to 1.0, and walls with a range of plane strain peak friction angles ($\phi_{ps} = 35^o$ to

Table 8.1. Summary of steel strip MSE wall case histories.

Wall Case History (Case History No.)	Date Wall Built	Wall Height (m)	Surcharge Conditions	Backfill Plane Strain Friction Angle ϕ_{ps} (°)	Reinforcement Type and Geometry (mm)	Reinforcement Stiffness J (kN/m)	Global Wall Stiffness S_{global} (kN/m²)
Lille, France Steel Strip Wall (SS1)	1972	6.0	None	49	1.5 x 80 (smooth steel strip)	48,000	64,000
UCLA Steel Strip Test Wall (SS2)	1974	6.1	None	40	80 x 3 (smooth steel strip)	63,158	103,538
WES Steel Strip Test Wall (SS3)	1976	3.66	Uniform lead weight surcharge of up to 90 kPa over entire wall	40	101.6 x 0.635 (smooth steel strip)	17,981	29,477
Fremersdorf Steel Strip Wall (SS4)	1980	7.3	None	40	60 x 5 (ribbed steel strip)	78,987	102,791
Waltham Cross Steel Strip Wall (SS5)	1981	8.2	None	56	40 x 5 (ribbed steel strip)	52,658 to 105,315	105,274
Guildford Bypass Steel Strip Walls, Sections A & B (SS6)	1981	6.0	None	53	75 x 5 (smooth steel strip)	83,375	264,021
Asahigaoka, Japan Steel Strip MSE Wall (SS7)	1982	12.0	Sloping soil surcharge 1 m thick	40	100 x 3.2 (smooth steel strip)	80,533 to 120,800	127,511
Ngauranga Steel Strip Wall (SS10)	1985	12.6	5° negative slope	50	60 x 5 (ribbed steel strip)	78,987 to 117,706	121,935
Algonquin Steel Strip Wall (SS11)	1988	6.1	None	43	50 x 4 (ribbed steel strip)	54,822	71,898
Gjovik (Norway) Steel Strip Wall (SS12)	1990	12.0	1.5:1 sloping soil surcharge up to 3 m thick	41	40 x 5 (ribbed steel strip)	52,658	70,211
Bourron Marlotte Steel Strip Rectangular Test Wall (SS13)	1993	10.5	None	40	60 x 5 (ribbed steel strip)	78,987 to 117,706	136,667
Bourron Marlotte Steel Strip Trapezoidal Test Wall (SS14)	1993	10.5	None	40	60 x 5 (ribbed steel strip)	78,987 to 117,706	118,228
INDOT Minnow Creek Steel Strip Wall (SS15)	2001	16.9	None	40	50 x 4 (ribbed strip)	38,095 to 105,263	81,359

Table 8.2. Summary of bar mat and welded wire MSE wall case histories.

Wall Case History (Case History No.)	Date Wall Built	Wall Height (m)	Surcharge Conditions	Backfill Plane Strain Friction Angle $\phi_{ps}(^o)$	Reinforcement Type and Geometry (mm)	Reinforcement Stiffness J (kN/m)	Global Wall Stiffness S_{global} (kN/m²)
Hayward Bar Mat Wall, Section 1 (BM1)	1981	6.1	2:1 continuous sloping soil surcharge	44	Five W11 bars spaced at 150 mm c-c	66,388	108,833
Hayward Bar Mat Wall, Section 2 (BM2)	1981	4.3	2:1 continuous sloping soil surcharge	44	Five W11 bars spaced at 150 mm c-c	66,388	108,073
Algonquin Bar Mat Wall (sand) (BM3)	1988	6.1	None	43	Four W11 bars spaced at 150 mm c-c	37,886	49,687
Algonquin Bar Mat Wall (silt) (BM4)	1988	6.1	None	35	Four W11 bars spaced at 150 mm c-c	37,886	49,687
Cloverdale Bar Mat Wall (BM5)	1988	18.2	None	43	Four W11 bars for top 5 layers, six W11 bars for next 5 layers, four W20 bars for next 5 layers, six W20 bars for next 6 layers, and eight W20 bars for bottom 3 layers, all spaced at 150 mm c-c	57,287 to 166,486	126,119
Rainier Ave. Welded Wire Wall (WW1)	1985	16.8	0.3 m soil sourcharge	48	W4.5xW3.5 for top 13 layers, W7xW3.5 for next 7 layers, W9.5xW3.5 for next 11 layers, and W12xW5 for bottom 7 layers, with all longitudinal wires spaced at 150 mm c-c	38,619 to 103,252	146,535

56°). Vertical spacing of reinforcement layers varied from 0.3 to 0.75 m. The facing batter for all of the steel reinforced MSE walls was near vertical.

Although it is generally not possible to isolate the effect of a specific variable, most of the conditions that are likely to be encountered in the field are included within the database of case histories described above.

Note that the plane strain friction angle was used to characterize soil shear strength in the case histories. Plane strain conditions typically exist in MSE walls, and recent work indicates that the plane strain soil friction angle correlates best to reinforcement loads, at least for geosynthetic walls (Rowe and Ho 1993, Zornberg et al. 1998a,b).

8.3 Analysis of Reinforcement Loads

Allen et al. (2001) investigated North American methods for predicting reinforcement loads and concluded that the AASHTO Simplified Method produces results similar to those of the other methods in use today, yet has the advantage of being simpler to use and more broadly applicable. Therefore, the Simplified Method will be used herein as the baseline of comparison for reinforcement loads predicted with the new working stress method.

Figures 8.1 and 8.2 summarize how well the Simplified Method predicts reinforcement loads in steel reinforced MSE walls built in the field. Figure 8.3 shows the same data plotted together with results of Simplified Method calculations and measured loads for geosynthetic walls (see Chapter 7.0). A log-log scale has been selected to better display the geosynthetic data that have generally lower load levels than steel reinforced wall structures. The reinforcement load T_{max} in the figures is the maximum load in the reinforcement layer. Note that measured plane strain peak soil friction angles and unit weights were used to estimate loads with the Simplified Method, which means that there is no conservatism in the reinforcement load predictions as a result of conservatism in the selection of soil parameters (see Chapter 2.0).

The data in Figure 8.3 show that the Simplified Method is more likely to overestimate reinforcement loads for geosynthetic reinforced soil walls than for steel reinforced soil walls. The data provided in Chapter 5.0 demonstrate that predicted loads for geosynthetic reinforced soil walls are approximately three times greater than observed values. For steel reinforced MSE walls, the Simplified Method predictions are more accurate, with maximum reinforcement loads (on average) about 90 percent of measured values. This better agreement may not be surprising

since the Simplified Method was largely developed and calibrated against the results of steel reinforced structures (Allen et al. 2001). Nevertheless, the Simplified Method does slightly under-predict the reinforcement loads for steel reinforced MSE walls. A possible explanation is that during the original development of the Simplified Method, peak friction angles were interpreted as peak triaxial or peak direct shear soil friction angles, and these values were not corrected for plane strain field conditions. If the Simplified Method is evaluated with triaxial or direct shear data, the ratio of predicted to measured maximum reinforcement load values is close to 1.0 on average (Allen et al. 2001).
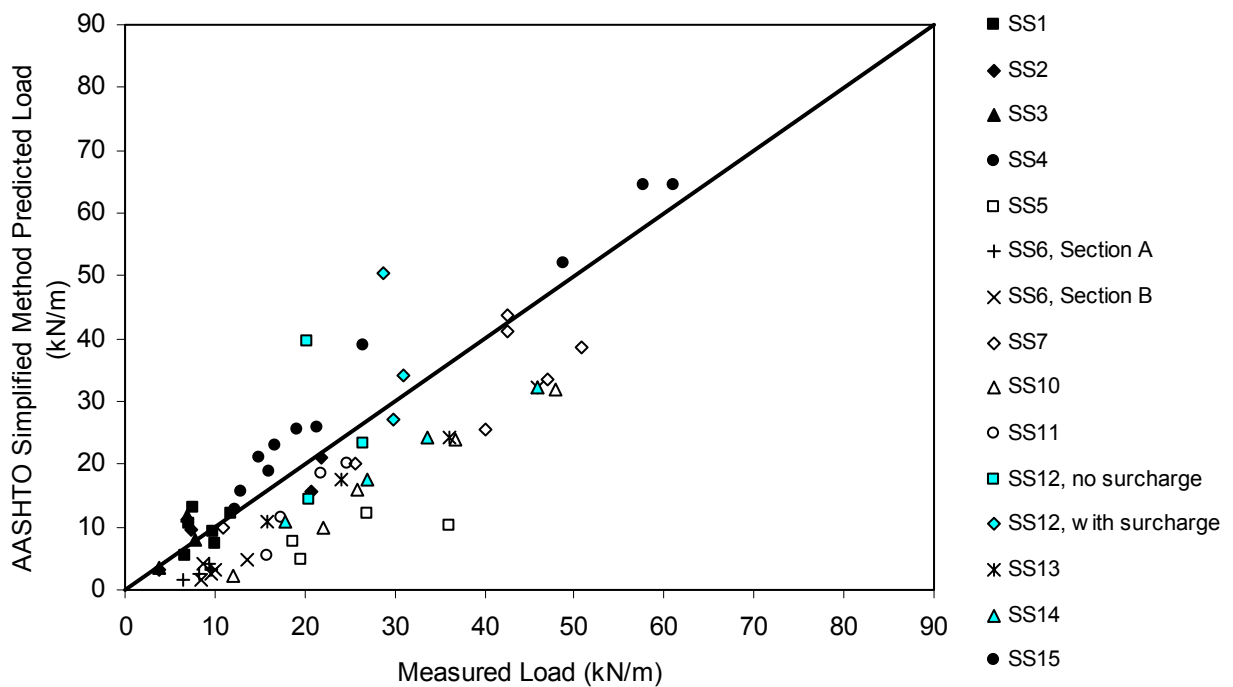
Figure 8.1. Measured values of T_{max} in the reinforcement for steel strip reinforced MSE walls versus values predicted with the AASHTO Simplified Method with plane strain ϕ.
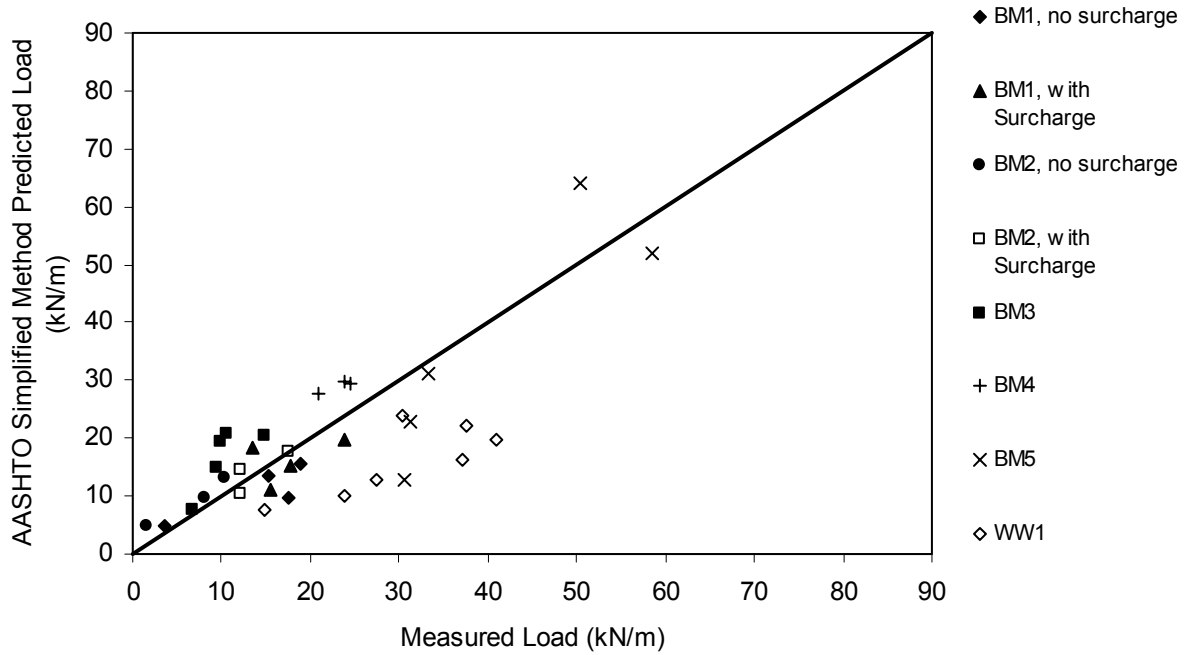
Figure 8.2. Measured values of T_{max} in the reinforcement for steel bar mat and welded wire MSE walls versus values predicted with the AASHTO Simplified Method with plane strain ϕ.
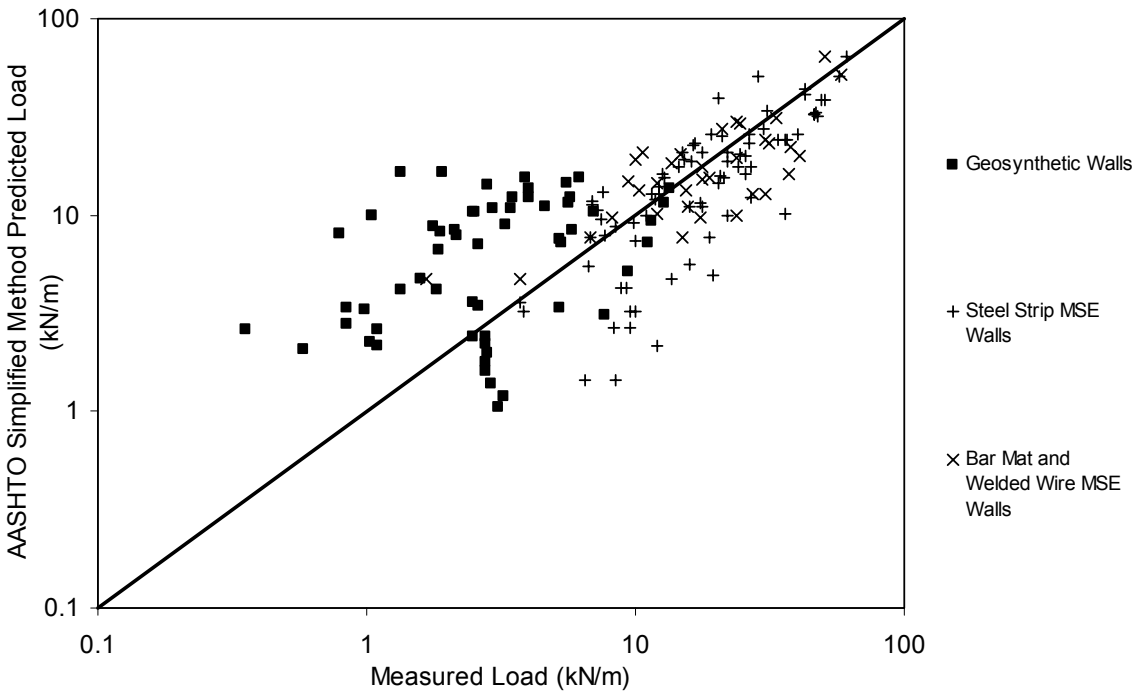
Figure 8.3. Measured values of T_{max} in the reinforcement for all MSE walls versus values predicted with the AASHTO Simplified Method with peak plane strain friction angles (ϕ_{ps}).

263

8.4 Development of The K_0-Stiffness Method to Predict T_{max} for Steel Reinforced Systems

8.4.1 General

As discussed in Chapter 7.0, the following key factors influence the magnitude of maximum reinforcement load, T_{max} in MSE walls:

- height of the wall and any surcharge loads
- global and local stiffness of the soil reinforcement
- resistance to lateral movement caused by the stiffness of the facing and restraint at the wall toe
- face batter
- shear strength and modulus of the soil
- unit weight of the soil
- vertical spacing of the reinforcement.

Chapter 7.0 addresses each of these factors in the development of the K_0-Stiffness Method for geosynthetic walls. Each of these factors must also be addressed to develop the K_0-Stiffness Method for steel reinforced systems. Details of the derivation of the K_0-Stiffness Method are provided in Chapter 7.0. For convenience, the method is summarized below.

T_{max} is calculated with the following general expression, per running unit length of wall in reinforcement layer i:

$$T_{max}^i = \frac{1}{2} K \gamma (H + S)\, S_v^i\, D_{tmax}\, \Phi_g \Phi_{local}\, \Phi_{fs} \Phi_{fb} \tag{8.1}$$

where S_v^i = tributary area (equivalent to the vertical spacing of the reinforcement near each layer location when analyses are carried out per unit length of wall); D_{tmax} = load distribution factor that modifies the reinforcement load on the basis of layer location; K = lateral earth pressure coefficient; γ = unit weight of the soil; H = height of the wall; S = equivalent height of uniform surcharge pressure q (i.e., S = q/γ); and Φ_g, Φ_{local}, Φ_{fs}, and Φ_{fb} are influence factors that individually account for the influence of local and global reinforcement stiffness, facing stiffness, and face batter.

The coefficient of lateral earth pressure, K, is calculated by using the Jaky equation for "at rest" earth pressure (Holtz and Kovacs 1981):

$$K = K_0 = \left(1 - \sin \phi_{ps}\right) \text{ and } K_0 \geq 0.3 \tag{8.2}$$

where ϕ_{ps} is the peak plane strain friction angle. The limitation on the minimum value of K_o is explained in Section 4.7.

Equation 8.2 contains the conventional expression for the calculation of reinforcement loads in current limit equilibrium methods of analysis. Parameter D_{tmax} is a load distribution factor that modifies the reinforcement load as a function of normalized depth below the top of the wall (z/H). It varies over the range $0 \leq D_{tmax} \leq 1$.

Parameter Φ_g is a global stiffness factor that accounts for the influence of the stiffness and spacing of the reinforcement layers over the entire wall height. It has the following general form:

$$\Phi_g = \alpha \left(\frac{S_{global}}{p_a} \right)^{\beta} \tag{8.3}$$

Here, S_{global} is the global reinforcement stiffness, and α and β are constant coefficients. The non-dimensionality of the expression is preserved by dividing the global reinforcement stiffness by p_a = 101 kPa (atmospheric pressure). The global reinforcement stiffness value for a wall is calculated as shown in Chapter 7.0.

Parameter Φ_{local} is a local stiffness factor that accounts for relative stiffness of the reinforcement layer with respect to the average stiffness of all reinforcement layers. It is expressed as follows:

$$\Phi_{local} = \left(\frac{S_{local}}{S_{global}} \right)^{a} \tag{8.4}$$

Here, parameter S_{local} is the local reinforcement stiffness for reinforcement layer i, calculated as shown in Chapter 7.0. It is used to quantify the local combined influence of the individual layer stiffness and spacing on reinforcement load. The coefficient term "a" in Equation 8.4 is taken as a = 0 for steel reinforcement and a =1 for geosynthetic reinforced soil walls.

Parameters Φ_{fs} (facing stiffness factor) and Φ_{fb} (facing batter factor) in Equation 8.1 account for the influence of the facing stiffness (Section 4.5) and facing batter (Section 4.6), respectively, and are constant values for a given wall.

Examination of Equation 8.1 shows that the maximum load in a reinforcement layer is the product of eight terms, many of which are non-linear. As is true in Chapter 7.0, it is assumed *a priori* for analysis of the steel reinforced MSE wall data that the factors are for practical purposes uncorrelated. This assumption allows the influence of each factor on predicted reinforcement loads to be examined separately while keeping other parameters at baseline values. The baseline values for coefficient terms in the expressions for Φ_g , Φ_{local}, Φ_{fs} and Φ_{fb} are identified in the following sections. For example, the constant in Equation 8.4 is taken as a = 0, corresponding to the case of steel reinforced soil walls.

The accuracy of the K_0-stiffness method when different expressions for the influence factors and associated constant coefficient values identified above are used is evaluated in the following sections in two ways:

1. direct comparison of predicted and measured reinforcement values for selected walls
2. comparison of the mean and coefficient of variation (COV) of the ratio of predicted reinforcement loads to measured values for all case studies.

Clearly, values of the mean of the ratio of reinforcement loads close to but greater than unity are desirable while the coefficient of variation of this ratio is maintained at a minimum value.

8.4.2 Load Distribution Factor, D_{tmax}

Chapter 5.0 demonstrated that the distribution of T_{max} from measured geosynthetic reinforcement loads versus normalized depth below the top of the wall is trapezoidal. The results of numerical modelling of geosynthetic reinforced soil walls have also shown that a trapezoidal distribution of geosynthetic reinforcement loads with depth is typical for this class of structure (Rowe and Ho 1993, Lee 2000). A similar empirical approach was applied here to generate a normalized reinforcement load distribution envelope for the steel reinforced soil wall case histories in tables 8.1 and 8.2. The results are plotted in figures 8.4a and 8.4b.
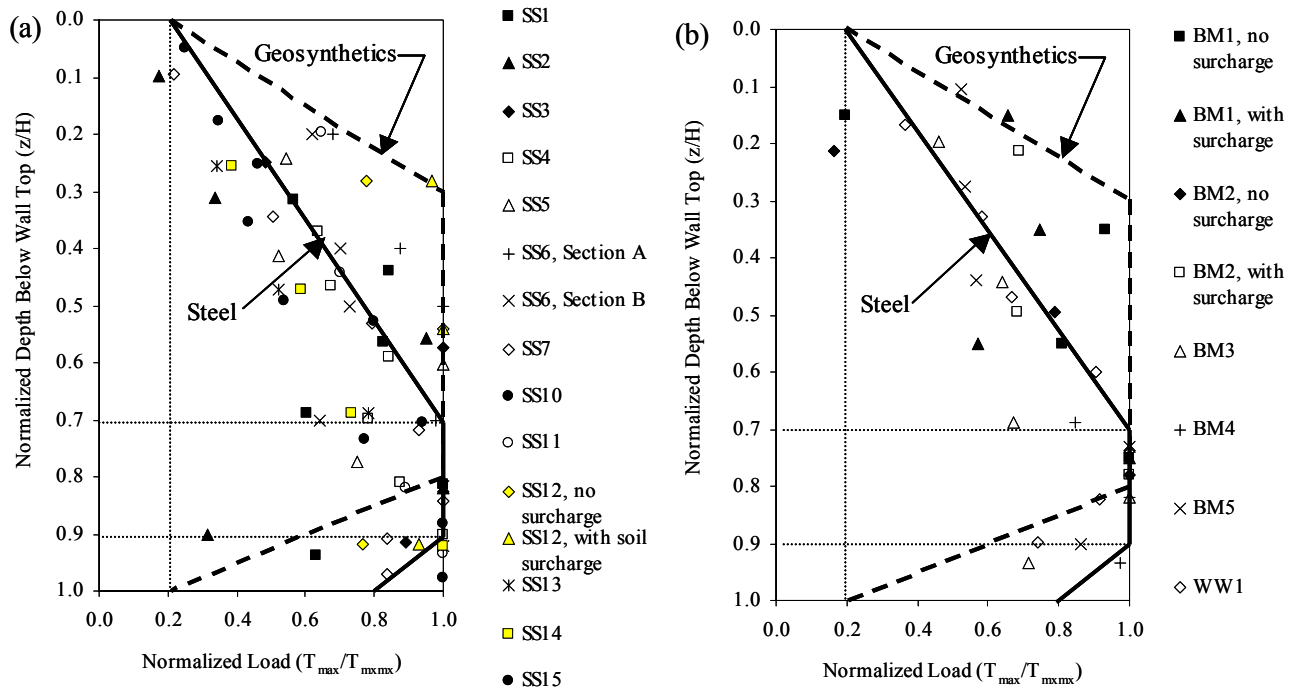
Figure 8.4. Normalized distribution of measured values of T_{max}: (a) steel strip reinforced MSE walls, and (b) steel bar mat and welded wire reinforced MSE walls. Note: T_{max} = maximum load in reinforcement layer; T_{mxmx} = maximum reinforcement load in the wall.. The dashed line envelopes in the figures are the proposed distributions for geosynthetic reinforced soil walls (see chapters 5.0 and 7.0).

The normalized reinforcement load is calculated as the ratio of the maximum load in a reinforcement layer (T_{max}) divided by the maximum reinforcement load in the wall (T_{mxmx}). The load distribution factor, D_{tmax}, is assumed to be coincident with the envelope traced on the figures. Over the normalized depth from $z/H = 0.7$ to 0.9, normalized reinforcement loads are roughly coincident with the maximum reinforcement load value (T_{mxmx}) taken from all reinforcement layers. However, at the top and bottom of the wall the predicted reinforcement loads tend to be finite values representing 20 percent and 80 percent of the maximum reinforcement load, respectively. The coordinates for this distribution are approximate only and have been selected to capture the majority of the data while simplifying the envelope geometry for all classes of steel reinforced wall structures. Superimposed on the figures is the trapezoidal distribution that was used to develop the empirical load distribution factor for geosynthetic reinforced soil walls (see Chapter 5.0). The approximately triangular envelope used for the steel reinforced soil wall data is visually a better predictor of the measured data than the trapezoidal

267

distribution recommended for geosynthetic reinforced soil walls. The difference between the load distribution envelopes for steel and geosynthetic reinforced systems is likely due to differences in the ability of the two types of reinforcements to deform and redistribute load. Steel reinforcement has less ability to deform, and therefore, the reinforcement load distribution tends to more closely follow the increase in earth pressure with depth than it does in geosynthetic walls.

Bathurst and Hatami (1998) reported on the numerical simulation of propped panel walls with a range of soil reinforcement stiffness values corresponding to both typical geosynthetic and steel reinforced walls. They showed that the distribution of reinforcement loads is triangular for stiffness values associated with steel reinforcement products. For both steel and geosynthetic reinforced walls, the loads in the reinforcement layers near the bottom of the wall tend to be less than the loads observed in the layers within the middle third of the wall height. Rowe and Ho (1993) provided a summary of data from reduced-scale model and full-scale walls that is consistent with the trends in Figure 8.4. The results of numerical work by Rowe and Ho (1993) and Bathurst and Hatami (1998) showed that the stiffness of the foundation and the degree of fixity of the wall facing toe influence the distribution of reinforcement loads at the base of geosynthetic and steel reinforced soil walls. However, most walls have a fixed toe condition as a result of wall embedment. Therefore, the attenuation of reinforcement load in proximity to the foundation predicted by both distributions in Figure 8.4 is reasonable for walls constructed on stiff, competent foundations.

8.4.3 Global Reinforcement Stiffness Factor, Φ_g

As discussed in chapters 5.0 and 7.0, the stiffness of the various internal components of the wall directly affects the distribution of loads to each of the wall components at working stress conditions. In other words, as the average stiffness of the reinforcement layers increases, the reinforcement loads increase. Chapter 7.0 develops and applies this concept to MSE walls by rewriting Equation 8.1 to back-calculate values of global stiffness factor, Φ_g (measured), from measured maximum reinforcement load (T_{mxmx}) values:

$$\Phi_g \text{ (measured)} = \frac{T_{mxmx}}{S_v^i \, \sigma_h \, D_{Tmax} \, \Phi_{local} \, \Phi_{fs} \, \Phi_{fb}} \qquad (8.5)$$

Data for Φ_g (measured) versus (S_{global}/p_a) are plotted in Figure 7.3 (Chapter 7.0) for all of the steel reinforced wall case histories in tables 8.1 and 8.2 and the geosynthetic wall case histories summarized in Chapter 7.0. Since the regression between the measured Φ_g and the normalized global stiffness included both the geosynthetic and steel reinforced MSE wall case histories, no additional adaptation is needed to determine Φ_g for steel reinforced systems. As noted in Chapter 7.0, the regression of these data results in values of $\alpha = 0.27$ and $\beta = 0.24$ for the global stiffness power function constants. The power curve fit to the physical data is reasonably accurate, although there is some scatter for the steel reinforced MSE walls data. This may be due to factors unique to steel MSE walls (see below). In the parametric analyses to follow, coefficient terms $\alpha = 0.27$ and $\beta = 0.24$ are used.

8.4.4 Local Stiffness Factor, Φ_{local}

Local deviations from overall trends in reinforcement loads can be expected when the reinforcement stiffness and/or spacing of the reinforcement change from average values over the height of the wall (i.e., $S_{local}/S_{global} \neq 1$). This effect has been shown to be captured for geosynthetic reinforced soil walls by introducing a local stiffness factor, Φ_{local}, expressed by Equation 8.4 and by setting the coefficient term to $a = 1$. A range of parameter values corresponding to $a = 1$, 0.5, and 0 were assumed in Equation 8.1, together with baseline values for the other factors described in the previous and following sections. The results, summarized in Table 8.3, show that the improvement between measured values of T_{max} and T_{mxmx} and predicted values is marginally better for $a = 0$ (i.e., compare K_o - Proposed Method column with Local Stiffness Factor columns in Table 8.3). In other words, ignoring the local stiffness factor previously introduced for geosynthetic reinforced soil walls provides the best prediction of reinforcement loads. An explanation for the difference in values is that steel reinforcement is much stiffer than reinforced soil, and hence local variations in reinforcement stiffness are likely have little effect on the redistribution of reinforcement loads.

269

Table 8.3. Summary of the ratio of predicted to measured reinforcement loads for steel reinforced MSE walls.

Steel	No. of Data Points	AASHTO Simplified Method		Ratio of Predicted/Measured T_{max} or T_{mxmx} — K_0-Stiffness Method (Equation 4)							
				Coefficient of Earth Pressure				Influence of Selected Values on Ratio of Predicted/Measured Loads			
		Triaxial/ Direct Shear ϕ	Plane Strain ϕ	Proposed Method: K_o, Capped to Min. Value of 0.3 (a=0 in Eq. 8, d=0.5 in Eq. 11)	K_{ah}	K = 0.3 for all Soils	K_0	$\gamma = 18$ kN/m³ for all Walls	Local Stiffness Factor Φ_{local} (Eq. 8)		$S_v = 0.6$ m for all Walls
									a = 0.5	a = 1	
Mean T_{max}	111	1.04	0.90	1.12	1.11	1.03	1.04	1.02	1.12	1.14	1.06
COV T_{max} (%)	111	50.7	50.6	35.1	41.8	36.0	40.2	36.2	36.3	40.6	41.7
Mean T_{mxmx}	22	0.99	0.87	1.05	1.05	0.95	0.98	0.95	1.09	1.14	0.99
COV T_{mxmx} (%)	22	35.1	36.2	22.7	33.1	23.2	29.4	24.8	22.7	26.1	36.3

Note: T_{max} = maximum load in reinforcement layer; T_{mxmx} = maximum reinforcement load in the wall; COV = coefficient of variation = (standard deviation of ratio of reinforcement load values/mean of ratio of reinforcement load values) x 100%; K_{ah} is based on Coulomb analysis, assuming full wall friction ($\delta = \phi$) and wall batter $\omega = 0$.

It is possible that a steel reinforced soil wall with a very low global stiffness value (for example, gabion hexagonal wire mesh) could require an exponent value of "a" between 0 and 1. As additional case studies become available, and/or calibrated numerical models are developed, the magnitude of this coefficient term may need to be adjusted to reflect a wider range of metallic reinforcement products and spacing.

8.4.5 Facing Stiffness Factor, Φ_{fs}

Chapter 7.0 examines the influence of wall facing stiffness and toe restraint on the load levels observed in geosynthetic reinforced walls. It was found that very stiff facings could reduce the reinforcement loads by a factor of two relative to the loads in geosynthetic reinforced walls with a more flexible facing. This effect could not be evaluated for steel reinforced walls because not enough different wall facing types are in the database. In fact, all of the steel walls in Table 8.1 and all but one of the walls in Table 8.2 were built with incremental, precast concrete facings. However, it may be reasonable to assume that the high global stiffness of steel reinforced walls in relation to that of geosynthetic reinforced walls minimizes the influence of the stiffness of the facing and wall toe on reinforcement loads. In the absence of available data to the contrary, the facing stiffness factor for all steel reinforced soil walls is recommended to be $\Phi_{fs} = 1.0$. This value is consistent with the same value recommended for geosynthetic reinforced soil walls constructed with incremental, precast concrete facings (see Chapter 7.0).

8.4.6 Facing Batter Factor, Φ_{fb}

In current practice, wall face batter (i.e., ω = inclination from the vertical) is taken into account explicitly with Coulomb earth pressure theory. Limit equilibrium methods include the facing batter in the calculation of the Coulomb earth pressure coefficient. However, as demonstrated in Chapter 7.0, the Coulomb earth pressure coefficient tends to reduce reinforcement loads excessively for heavily battered walls. The influence of reduced confining pressure near the wall face cannot be captured explicitly by limit equilibrium methods. The influence of wall facing batter on maximum reinforcement loads is adjusted in the proposed working stress method for geosynthetics by using an empirical facing batter factor expressed as follows:

$$\Phi_{fb} = \left(\frac{K_{abh}}{K_{avh}} \right)^{d}$$

(8.6)

where K_{abh} is the horizontal component of active earth pressure coefficient accounting for wall face batter, and K_{avh} is the horizontal component of active earth pressure coefficient, assuming the wall is vertical and d is a constant coefficient. A value of d = 0.5 was demonstrated in Chapter 7.0 to be a convenient numerical value for matching measured reinforcement loads for geosynthetic-reinforced soil walls with a range of facing batters. No data are available in the literature for instrumented battered steel reinforced soil walls (i.e., for $\omega > 0$) However, a value of d = 0.5 may be reasonable for steel reinforced soil walls as well as for geosynthetic reinforced soil walls and is recommended until more data are available.

8.4.7 Soil Strength Effects on Soil Reinforcement Loads

As discussed in Chapter 7.0, though the soil modulus is likely the best property to use for modelling the soil in working stress conditions, the soil modulus is difficult to determine. Furthermore, for the case histories reported herein, a measured soil modulus was not available. The peak soil friction angle is routinely available, familiar to designers, and is relatively easy to measure or estimate. In general, as peak friction angle for a granular soil increases, the soil modulus also increases (Duncan et al. 1980). Hence peak friction angle can be interpreted as an indicator of relative soil modulus value between soil types.

In the development of the stiffness method proposed herein, values of $K = K_o$ (Equation 8.2) and $K = K_{ah}$ were examined to investigate the relative accuracy of predicted values of T_{max} and T_{mxmx}. K_0 was considered because it is simple to calculate and is calculated independent of wall face batter (face batter is being handled by a separate factor—see Section 8.4.6). K_{ah} was determined with the Coulomb method and the assumption that the wall interface friction angle is equal to the soil backfill friction angle (i.e., $\delta = \phi_{ps}$) for coverage ratios $R_c \geq 0.7$ and decreases linearly with coverage ratios between 0.7 and 0.0 to a minimum value of $\delta = 0.65\phi$ for concrete faced walls. Full interface friction was assumed for coverage ratios greater than 0.7 because the continuous or nearly continuous reinforcement layers will restrict downward movement of the backfill soil against the face and effectively generate an interface friction angle at the back of the wall face that is equal to the backfill soil friction angle. The data in Table 8.3 show that

reinforcement load ratios were closer to unity with K_0 (see the columns in the table for K_{ah} and K_0) than with K_{ah} in Equation 8.1, and the spread in ratio values was slightly less.

Allen et al. (2001) observed that current methods in use (e.g. the Simplified and Coherent Gravity methods) tend to under-predict reinforcement loads in steel reinforced MSE walls when triaxial or direct shear peak soil friction angles (ϕ) greater than 40° are used. (The peak friction angle from these test methods can be used to estimate a peak plane strain friction angle value of approximately $\phi_{ps} = 44^o$.) The influence of friction angle and the choice of K_o value were explored further by dividing the case study set for steel reinforced soil walls into projects with $\phi_{ps} < 44^o$ and $\phi_{ps} \geq 44^o$. For plane strain soil friction angles of 44° or more, the mean and COV of the ratio of predicted to measured T_{max} using K_0 was 0.87 and 53.0%, respectively. Using a constant $K_o = 0.3$ for walls with $\phi_{ps} \geq 44^o$ improved the calculated ratios for mean ratio and COV of ratio values to 1.04 and 43.5 percent, respectively (i.e., the predicted values are close to but greater than unity and the spread in values is reduced). For steel reinforced MSE walls with a plane strain friction angle $\phi_{ps} < 44^o$, the average and COV of the ratio of predicted to measured T_{max} using K_0 was 1.18 and 28.0 percent, respectively. The same analyses for walls with $\phi_{ps} < 44^o$ but using a constant $K_o = 0.3$ produced mean and COV values of 1.02 and 29.2 percent, indicating that using a constant $K_0 = 0.3$ did not improve the prediction for walls with $\phi_{ps} < 44^o$.

Taken together, the results of this investigation lead to the recommendation that the value of K_o should be calculated according to Equation 8.2 but should not be less than 0.3. This approach preserves the current practice of accounting for the soil response on the basis of the peak soil friction angle. At the same time, it reduces the spread in the predicted load by accounting for the lack of correlation between soil friction angle and peak reinforcement load at higher soil friction angles through the utilization a constant value of K_0.

For geosynthetic reinforced systems, the correlation between T_{max} and the peak soil friction angle throughout the range of values was stronger than it was for steel reinforced systems (see Chapter 7.0). The influence of soil strength and stiffness on T_{max} appears, on the basis of this observation, to be affected by the global wall stiffness value. That is, the higher the global wall stiffness value, the less that changes in soil strength affect the magnitude of T_{max}, especially for very high soil strengths.

8.4.8 Effect of Soil Unit Weight on Soil Reinforcement Loads

The soil unit weight recorded for each case study was typically within 10 percent of the mean value for all of the walls (γ_{mean} = 18 kN/m^3) and ranged from 16.8 to 22.6 kN/m^3. This variation was considered to be small in comparison to the uncertainty associated with other parameter values in this investigation, including estimated reinforcement loads. However, the fundamental expression for reinforcement loads (Equation 8.1) calculated with the Stiffness Method shows that loads (and hence strains) should vary linearly with soil unit weight. To investigate the influence of soil unit weight on predicted reinforcement loads, calculations for T_{max} and T_{mxmx} were redone with a constant value for γ of 18 kN/m^3. Table 8.3 shows that there was only a minor difference in the accuracy of predicted reinforcement loads when a default constant unit weight of 18 kN/m^3 was used in the calculations rather than project-specific values. This minor difference was consistent with the variation in the measured value of this parameter.

8.4.9 Effect of Reinforcement Layer Spacing on Soil Reinforcement Loads

The vertical distance between reinforcement layers in the case studies investigated varied from 0.3 to 0.75 m. Note that this is not necessarily the same as the vertical zone in the wall that contributes to load in a given reinforcement layer (i.e., the tributary area). S_v is representative of the tributary area when loads are calculated on the basis of load per unit of wall length and the spacing between layers is uniform. When the spacing is not uniform, this parameter is representative of the average distance between layers that are adjacent to the layer in question. At the top of a wall, S_v includes the full distance between the top layer and the top of the wall, plus the distance to the mid-point between the top layer and the next layer below.

The magnitude of reinforcement loads (and strains) can be expected to vary linearly with S_v, as assumed in the stiffness method proposed here and conventional design methods. Calculations were redone with a default value of S_v = 0.6 m, which was an average value from the steel MSE case studies in Table 8.1. Table 8.3 shows that reinforcement spacing does influence calculated results, particularly the spread in the ratios of predicted to measured reinforcement loads in comparison to values calculated with the full procedure.

A parametric investigation, similar to what was done in Section 8.4.3 for the global reinforcement stiffness factor, was conducted to evaluate S_v. Equation 8.1 is rewritten below to back-calculate values of S_v from measured maximum reinforcement load (T_{mxmx}) values:

$$S_v \text{ (back-calculated)} = \frac{T_{mxmx}}{\sigma_h \, D_{tmax} \, \Phi_g \, \Phi_{local} \Phi_{fs} \, \Phi_{fb}} \qquad (8.7)$$

The values of the variables are as described in Section 4.3. Data for S_v, back-calculated from the measured values of T_{mxmx}, versus S_v as determined directly from the spacing of the reinforcement in the wall are plotted in Figure 8.5 for both steel and geosynthetic reinforced wall systems (the case histories used are provided in tables 8.1 and 8.2, and in Allen et al., 2001). The regressed data demonstrate a linear relationship between reinforcement load and S_v, as predicted by both the proposed method and current design methods. This correlation appears to hold reasonably well even for large values of S_v.
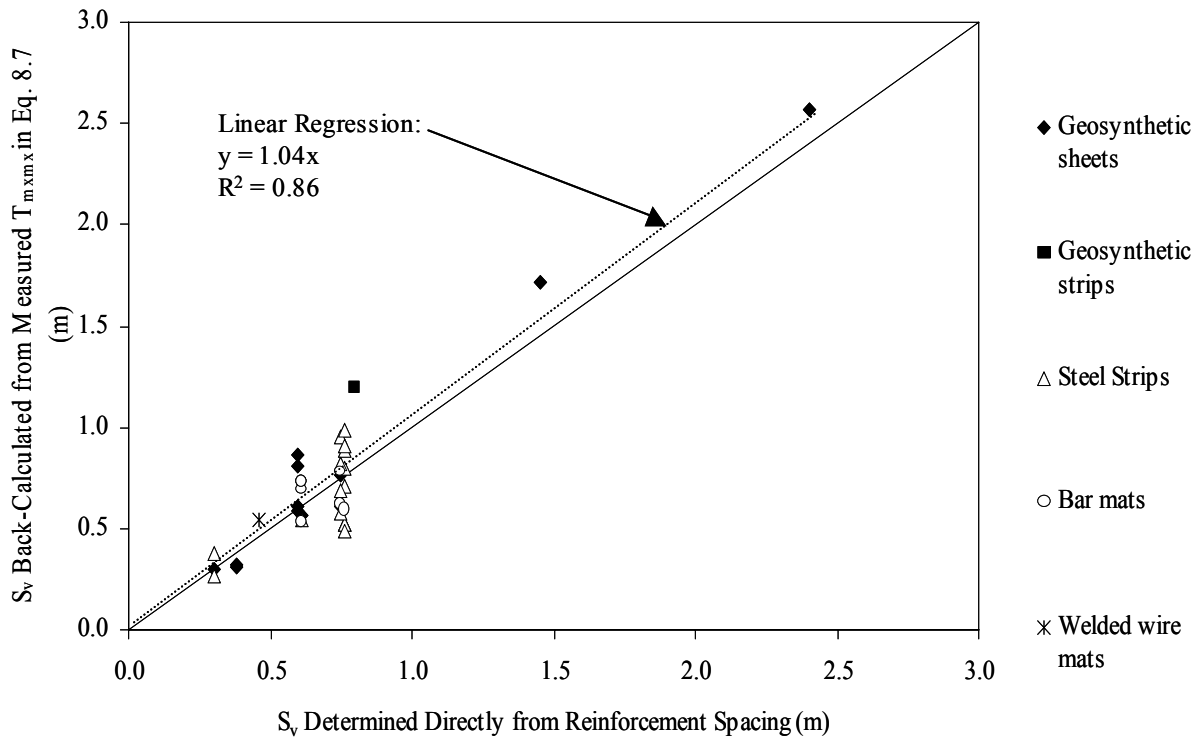
Figure 8.5. Back-calculated S_v from measured T_{mxmx} (Equation 8.7) versus S_v determined directly from spacing of reinforcement in wall.

8.4.10 Overall Performance of the K_0-Stiffness Method Applied to Steel Reinforced Soil Walls

Examples of measured values of T_{max} as a function of depth for several wall case histories are presented in figures 8.6 through 8.9. Superimposed on the figures are values predicted with the

275

AASHTO Simplified Method and the K_0-Stiffness Method. The following observations can be made:

1. Both the AASHTO Simplified Method and the proposed K_0-Stiffness Method capture the general trend in reinforcement loads, which can be seen to increase with depth below the top of the wall.

2. The proposed K_0-Stiffness Method matches the measured data more consistently than does the AASHTO Simplified Method, although both methods produce an average ratio of predicted to measured T_{max} that is slightly over 1.0, provided that triaxial or direct shear soil friction angles are used with the Simplified Method.

Comparisons of measured loads and loads predicted with the K_0-Stiffness Method for steel reinforced MSE walls are illustrated in figures 8.10 and 8.11 for all of the full-scale field case histories listed in tables 8.1 and 8.2. The K_0-Stiffness Method has been developed to work for both geosynthetic and steel reinforced soil walls. Data reported in chapters 5.0 and 7.0 for 16 different geosynthetic reinforced soil walls are plotted with the steel reinforced wall data points in Figure 8.12. Comparison with figures 8.1, 8.2, and 8.3 presented earlier shows that the K_0-Stiffness Method greatly improves prediction accuracy for geosynthetic walls. The improved prediction accuracy for steel reinforced MSE walls over that of the Simplified Method is relatively small but is nevertheless visually apparent in the figures. Quantitative support for the improvement in reinforcement loads predicted with the proposed method can be found in Table 8.3. Specifically, the COV of the ratio of predicted to measured T_{max} is 50.7 percent for the AASHTO Simplified Method, and 35.1 percent for the K_0-Stiffness Method—a significant improvement.

For both steel and geosynthetic reinforced systems, Table 8.3 and similar data reported in Chapter 7.0 suggest that approximately 50 percent of the coefficient of variation for the data set is due to variations in the distribution of T_{max} with depth (compare the COV for T_{max} with the COV for T_{mxmx}). Therefore, better prediction of the distribution of T_{max} versus depth could greatly improve the prediction accuracy of the K_0-Stiffness Method.
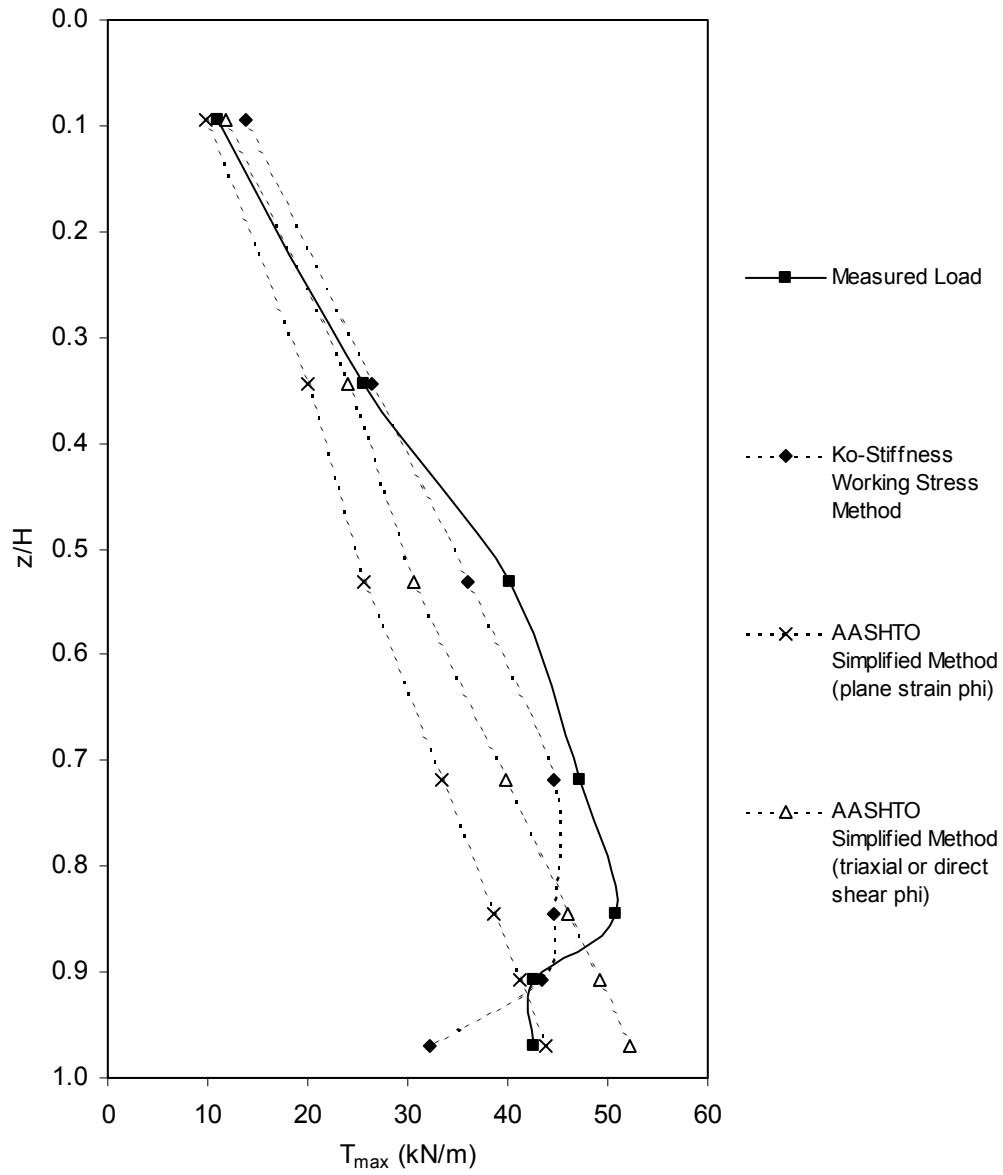
Figure 8.6. T_{max} distribution versus normalized depth for steel strip reinforced MSE wall (SS7).

277
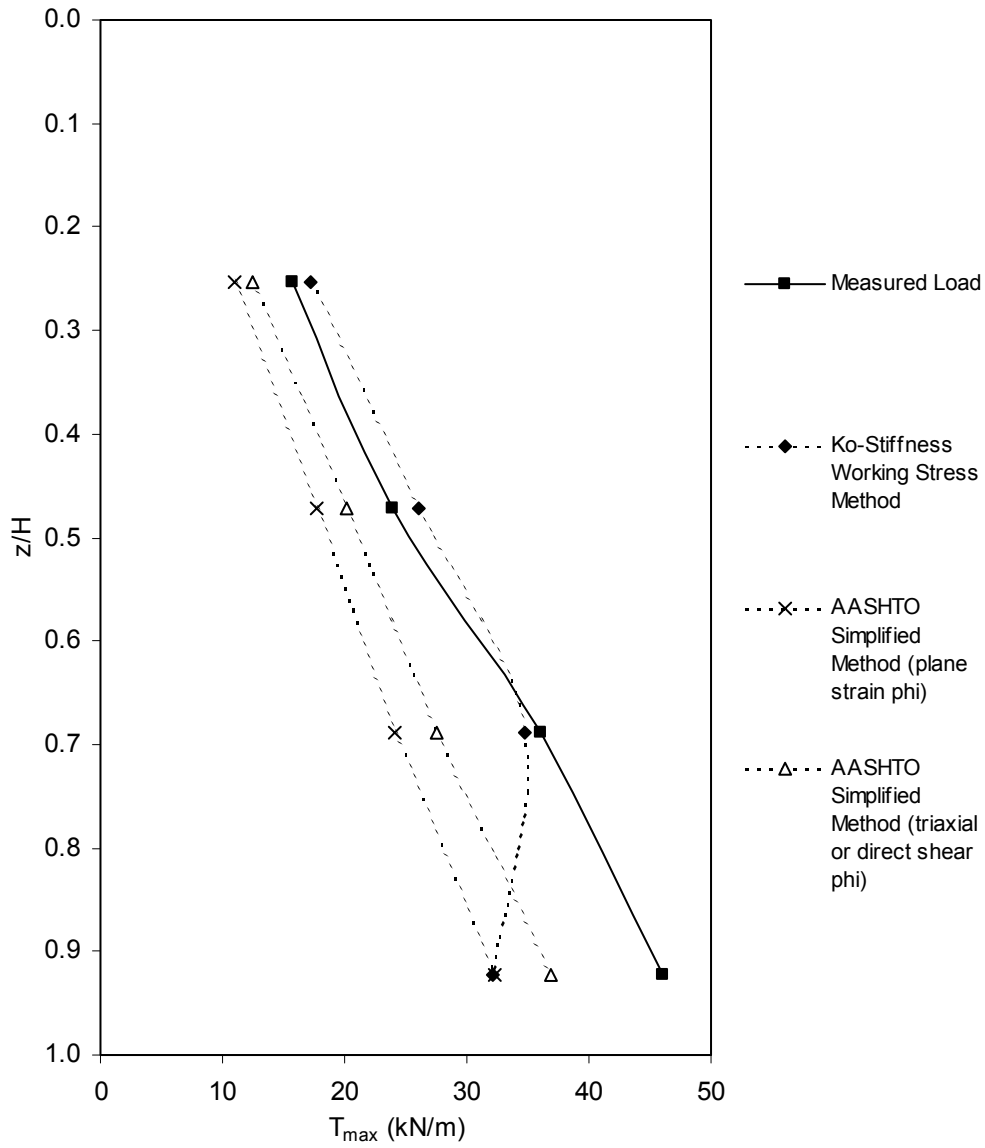
Figure 8.7. T_{max} distribution versus normalized depth for steel strip reinforced MSE wall (SS13).

278
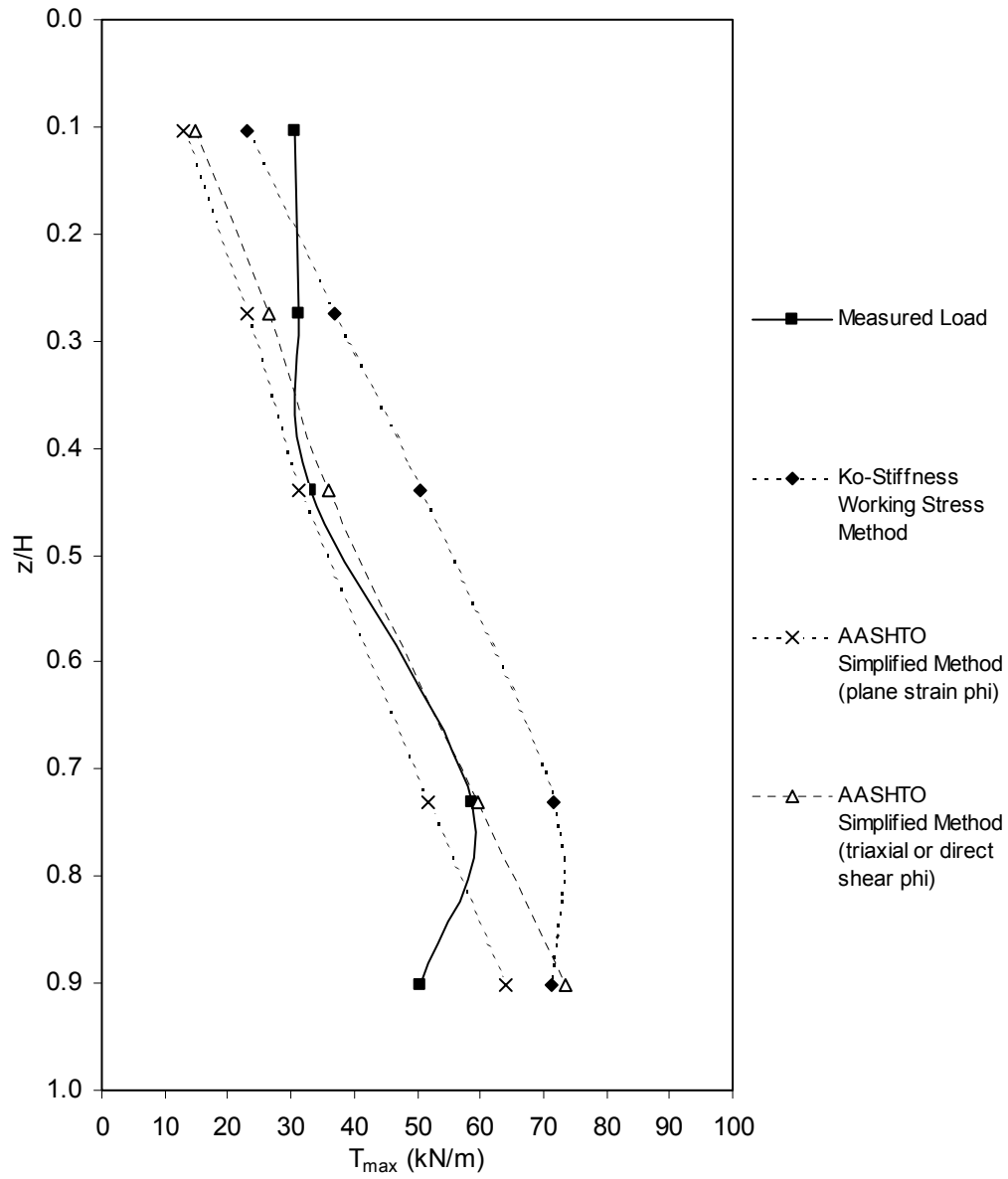
Figure 8.8. T_{max} distribution versus normalized depth for bar mat reinforced MSE wall (BM5).

279
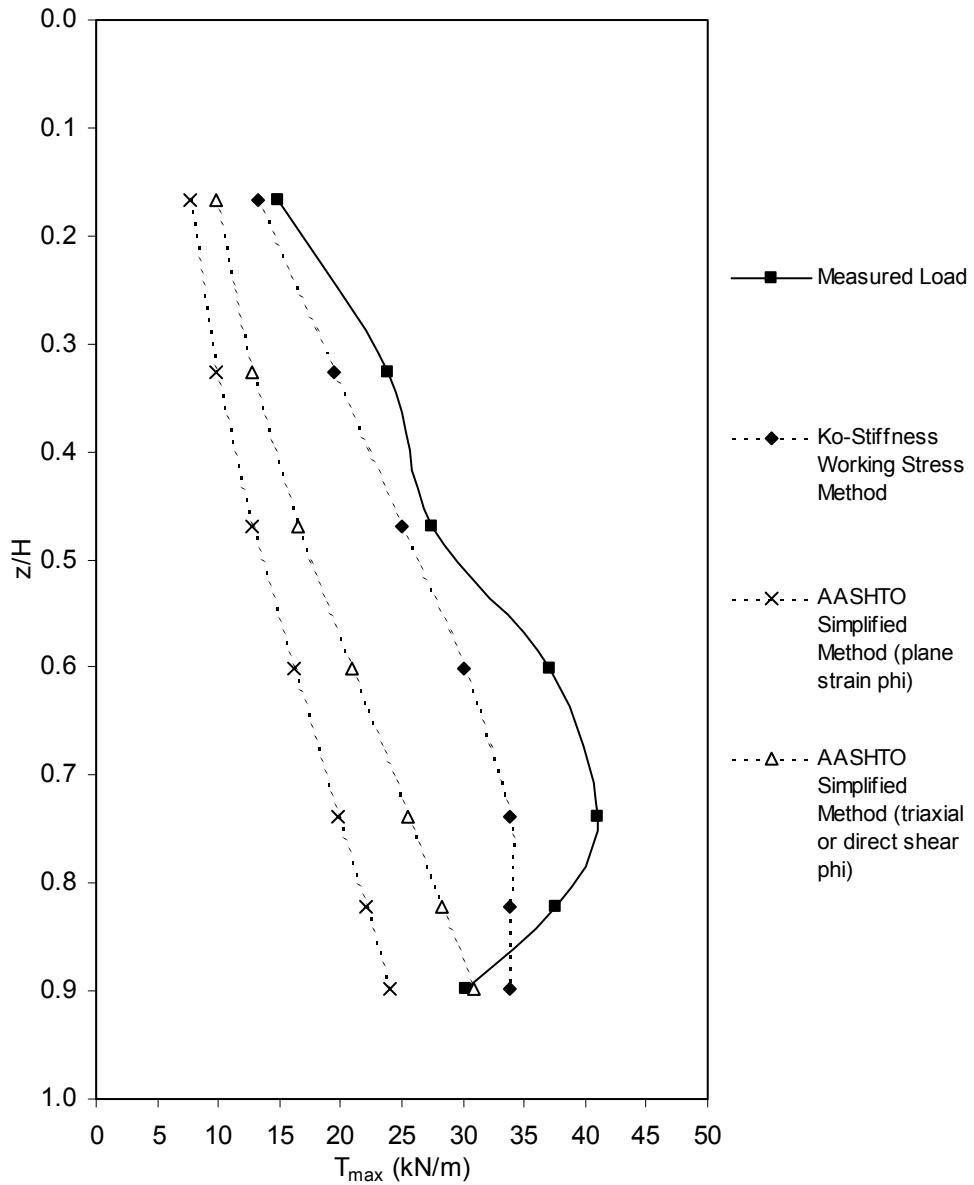
Figure 8.9. T_{max} distribution versus normalized depth for welded wire reinforced MSE wall (WW1).
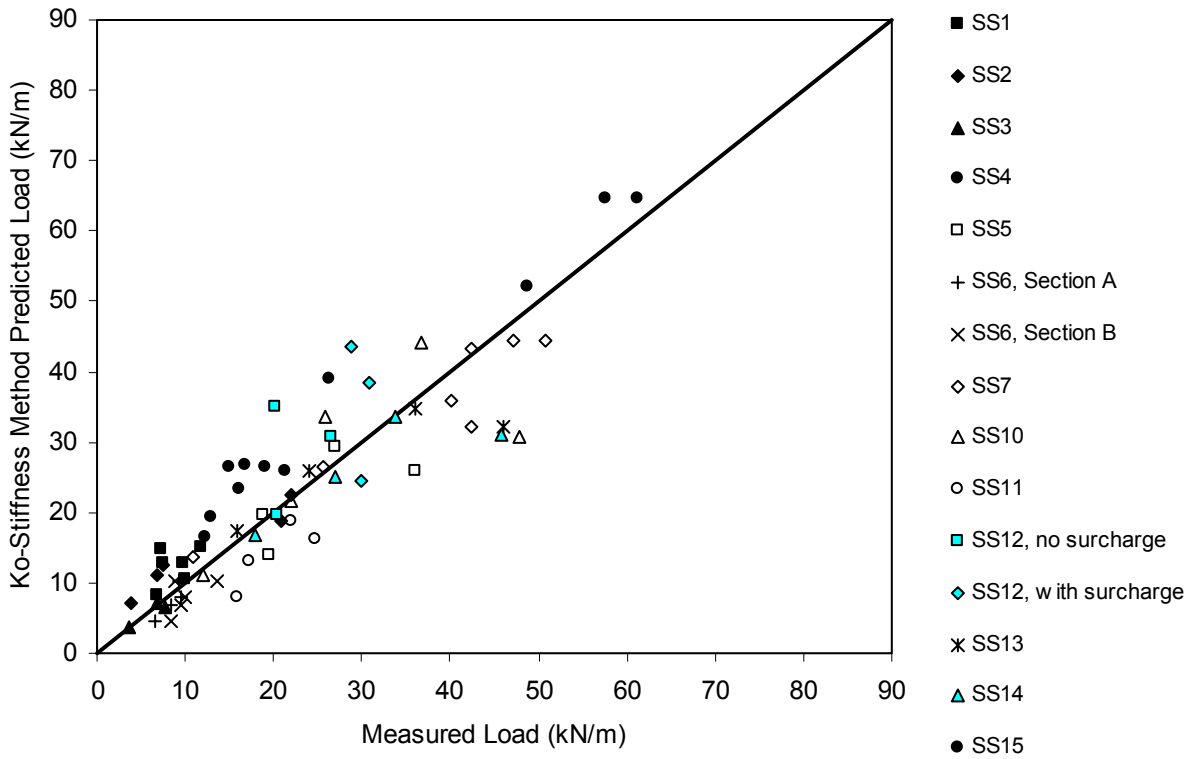
Figure 8.10. Measured values of T_{max} in the reinforcement for steel strip reinforced MSE walls versus values predicted with the K_0-Stiffness method.
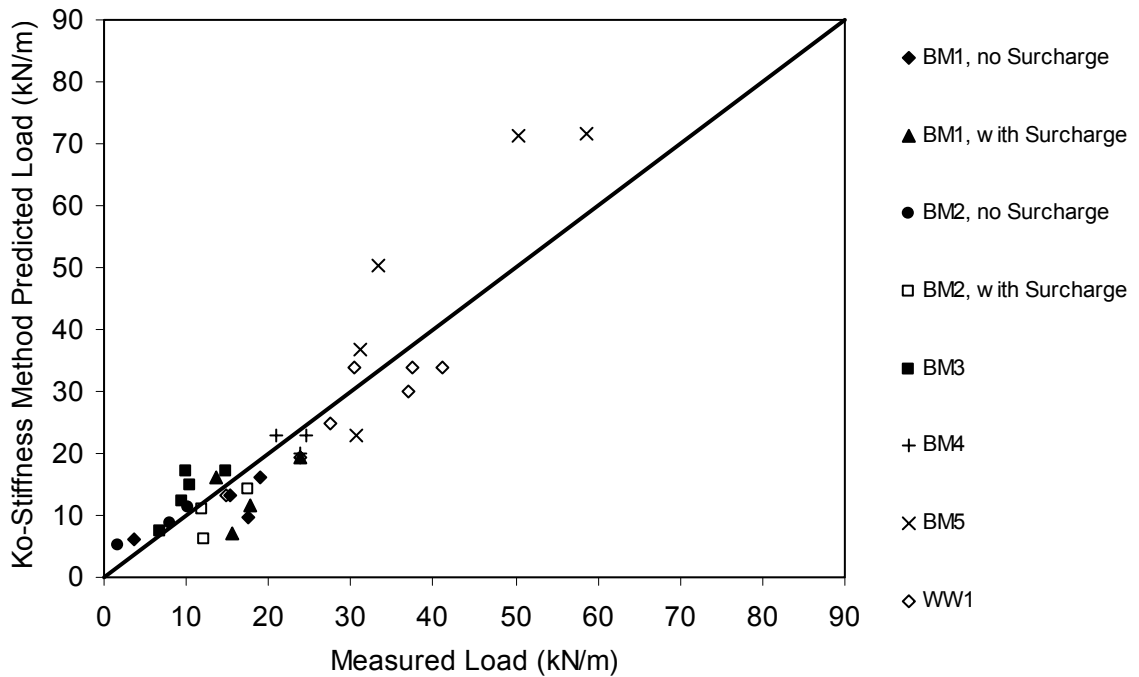
Figure 8.11. Measured values of T_{max} in the reinforcement for steel bar mat and welded wire reinforced MSE walls versus values predicted with the K_0-Stiffness Method.
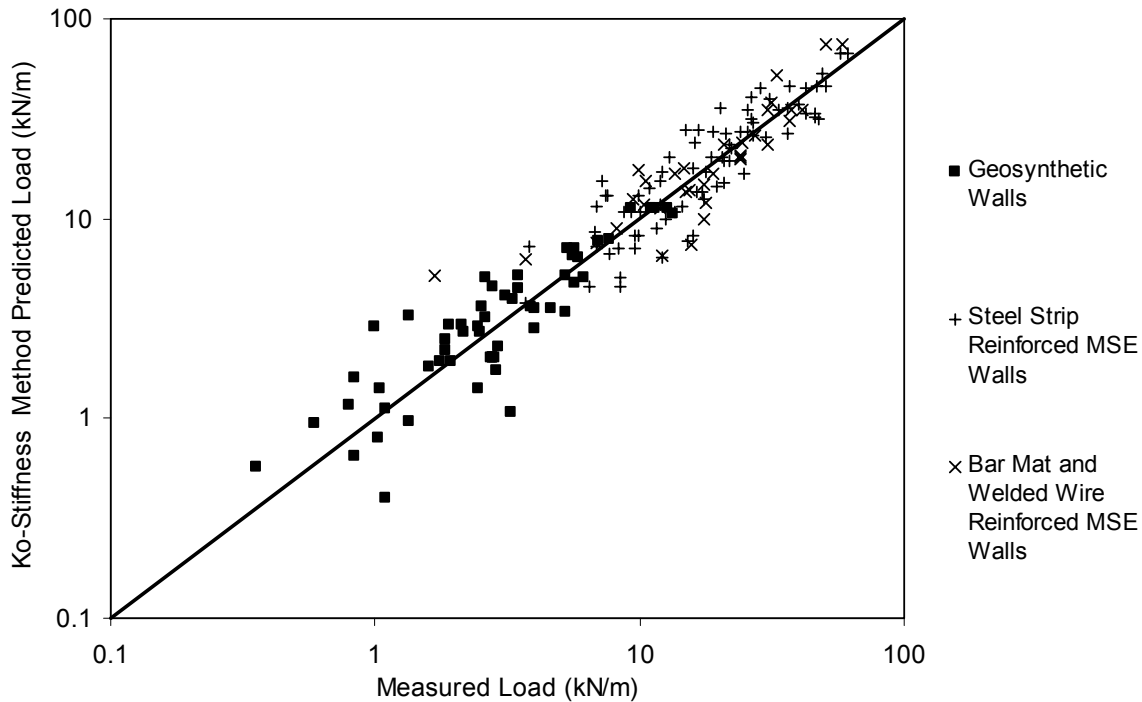
Figure 8.12. Measured values of T_{max} in the reinforcement for all MSE walls versus values predicted with the K_0-Stiffness Method.

Another potential contributing factor to the spread in the ratios of predicted to measured steel reinforcement loads for both the K_0-Stiffness Method and the Simplified Method are compaction stresses, which have not specifically been taken into account by these methods. On the basis of a global comparison of the empirical reinforcement load data, Allen et al. (2001) found that, at least for the Simplified Method, the degree of compaction did not appear to have a significant effect on the reinforcement load levels in the completed walls. Theoretically, it is possible that the degree of compaction may temporarily affect reinforcement loads during wall construction (Ehrlich and Mitchell 1994). As the wall is constructed, the stress history imparted to the soil during the compaction process is overcome by the increased vertical stress resulting from the weight of soil above. However, in the upper portion of the wall, the overburden stress present at end of wall construction may not be great enough to overcome the stress history imparted to the soil by the compaction process. This could cause reinforcement stresses in the upper portion of the wall to be elevated above values anticipated from overburden stresses alone. The amount of increased reinforcement load is likely to be dependent on the location of the reinforcement relative to the wall top, the proximity of the location of T_{max} relative to the wall

282

face, the rigidity of the wall facing, the size of the compaction equipment and amount of compaction effort, and the ability of the soil to lock in compaction stresses.

To further investigate the influence of compaction effects on steel reinforcement loads, case histories SS2, SS3, SS13, and SS14 with light compaction (typical of test walls) were compared to case histories SS4, SS7, SS11, SS12, SS15 with typical field compaction. In general, typical field compaction is defined here as the use of full-size compaction equipment and the application of sufficient compaction effort to meet contract specification requirements. The case histories selected for this comparison had plane strain soil friction angles that ranged from 40 to 43$^{\mathrm{o}}$, to minimize the influence of friction angle on the interpretation of compaction effects. The mean of the ratio of predicted to measured T_{max} was 1.12 for the light compaction group and 1.18 for the heavy compaction group, while the corresponding COV values were 31.4 percent and 28.9 percent, respectively. Because the K_0-Stiffness method is empirically derived on the basis of the average value of input parameters, one can conclude that compaction effects may have a slight effect on predicted reinforcement loads.

Figure 8.12 provides plots of the ratio T_{max}/T_{mxmx} from measured data for walls known to have been compacted with typical field compaction and for structures known to have been lightly compacted. Superimposed on the figure is the distribution for the load distribution factor D_{tmax} introduced in Section 8.4.2. The data in this figure show that if compaction is light, the T_{max} distribution tends to be linear (triangular shaped), whereas if a more typical level of compaction is used, the distribution tends to become trapezoidal. The trapezoidal shape of the T_{max} distribution appears to be the result of elevated reinforcement stresses remaining from the compaction process rather than mechanisms associated with geosynthetic reinforced soil walls, which also have a trapezoidal distribution for D_{tmax}. Because the recommended envelope shown in Figures 8.4a and 8.4b captures the distribution of T_{max} for the walls with typical compaction, the K_0-Stiffness Method can be argued to take into account the influence of compaction stresses on reinforcement loads. However, this recommended envelope only accounts for an approximate average degree of "typical" compaction, and reinforcement load increases due to compaction could be greater if backfill soils are heavily compacted and are able to lock in compaction stresses. This observed apparent compaction stress effect may explain a number of other data points in figures 8.4a and 8.4b that fall well above the proposed envelope at the top of the walls.
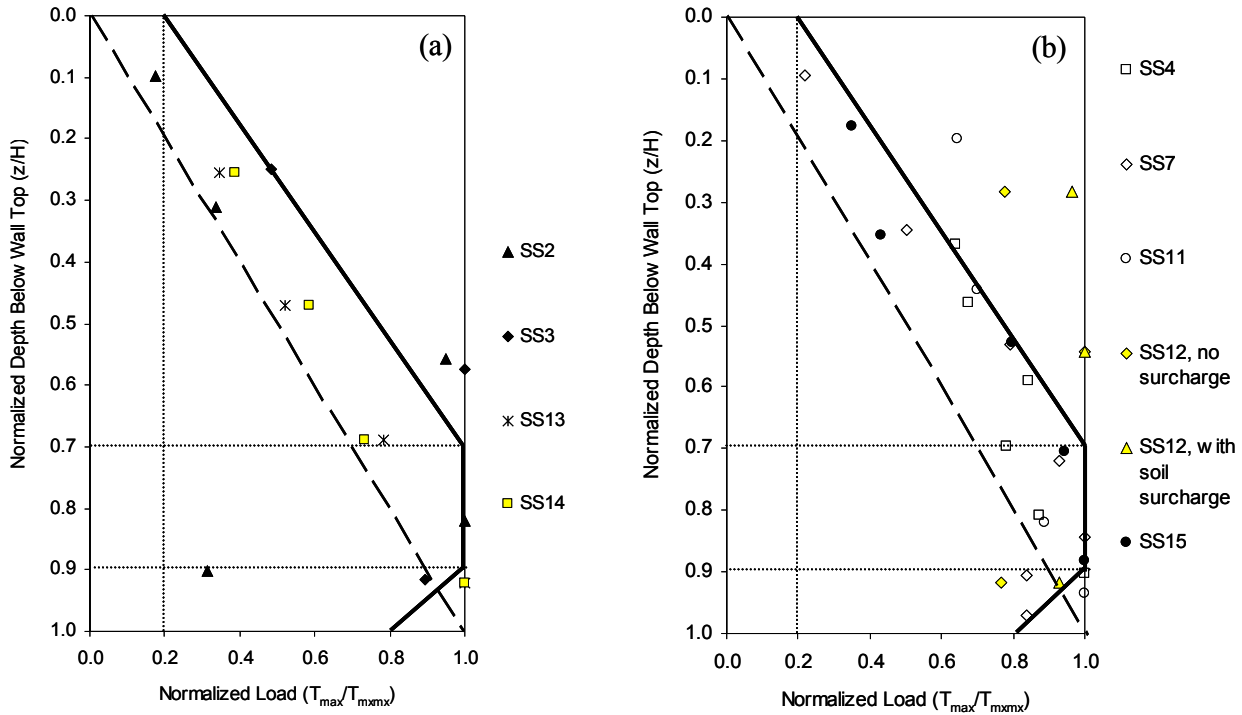
Figure 8.13. Normalized T_{max} as a function of relative depth below the wall top for steel strip reinforced MSE walls with $\phi_{ps} \leq 44^{\circ}$: (a) light compaction (typically the case for test walls), and (b) typical field compaction. Note: The triangular distribution in the figures corresponds to the distribution of normalized load assumed in the current Simplified Method of design.

8.5. Concluding Remarks

The K_o-Stiffness Method proposed in Chapter 7.0 for geosynthetic reinforced soil walls constructed with granular soils has been extended to steel reinforced MSE walls. The methodology is largely empirical, but it retains the familiar concepts of Coulomb earth pressure theory and the tributary area approach found in current limit-equilibrium based design methods. A fundamental feature of the new approach is the use of reinforcement stiffness to predict wall reinforcement loads and strains for internal stability design under working stress conditions.

The K_0-Stiffness Method has been shown to improve the accuracy of predicted reinforcement loads in comparison to the Simplified Method. The improvement in the prediction of reinforcement loads relative to predictions produced by the Simplified Method can be judged to be modest for steel reinforced systems. However, an additional benefit of the method is that it provides a seamless transition between MSE walls constructed with steel reinforcement and nominally identical walls constructed with geosynthetic reinforcement.

For geosynthetic walls, the focus of the method is to design the wall reinforcement so that the soil within the wall backfill is prevented from reaching a state of failure, preserving working stress conditions (see Chapter 7.0). This soil failure limit state is not considered in the MSE wall internal stability design methods currently available, yet, given the research results presented herein, is likely to be a controlling limit state for geosynthetic structures. For steel reinforced walls, soil failure is only an issue if the reinforcement is allowed to yield. Since the proposed method should prevent the steel reinforcement from reaching its yield strength, the prevention of soil failure will generally not be a controlling limit state for steel reinforced walls.

9.0 CONCLUDING REMARKS AND RECOMMENDATIONS FOR FUTURE RESEARCH

A large database of case histories has been used to calibrate the empirical-based model proposed herein. The proposed K_0-Stiffness Method represents a first step in the development of an empirically based working stress design method. This proposed method significantly improves the accuracy of reinforcement load prediction in relation to current design protocols, especially for geosynthetic walls, and provides a consistent approach for both geosynthetic and steel reinforced MSE wall systems. However, refinement of the methodology, including formulations for influence factor expressions and associated constant coefficient values that are a primary feature of the method, is warranted. Specific areas of research needed to accomplish this refinement are summarized below for each variable or influence factor:

9.1 Reinforcement Spacing

Conventional design practice and back-analyses of the full-scale field wall data indicate that the value of T_{max} is directly proportional to the vertical spacing of the reinforcement, S_v. However, very small vertical spacing or very large vertical spacing could result in a deviation from this linear relationship. For example, at small spacing, it may be possible to derive additional benefit (i.e., reduced reinforcement loads) as a result of improved confinement of the soil. At some larger spacing, it is reasonable to assume that the reinforced backfill will cease to function as a coherent mass and will thus require refinement of the methodology presented in this report. Analysis of full-scale structures and analytical models calibrated against full-scale data where S_v is the primary variable is needed to more clearly establish this relationship.

The horizontal distribution of the reinforcement, as represented by the coverage ratio, R_c, is currently considered in the methodology as a modifier to the available reinforcement tensile strength expressed as a force per unit width of wall. However, the use of R_c in this manner may not account for the possible effect of the reinforcement to confine the soil. The proposed methodology is based on continuous reinforcement layers for geosynthetic-reinforced systems but on discontinuous strip reinforced systems for steel MSE walls because of the available database of case histories. What effect, if any, does R_c have on reinforcement stresses other than what has already been assumed? Furthermore, what effect does reinforcement continuity have

on downdrag forces that develop on the back of the wall facing, and what effect does downdrag have on reinforcement stresses, both in the backfill and at the connection?

9.2 Lateral Earth Pressure Coefficient, K_0

The correlation between lateral earth pressure/peak soil friction angle and the value of T_{max} is not as obvious as it is for other variables such as S_v, at least from the standpoint of load prediction accuracy. For geosynthetic-reinforced systems, the correlation between the earth pressure coefficient based on peak soil strength parameters (K_0 as proposed herein) and the reinforcement load is fairly strong. However, for steel reinforced systems, this correlation appears to be very poor, especially for high shear strength soils. The difference in this correlation for steel and geosynthetic-reinforced systems may be related to the relative stiffness between the soil and the reinforcement. As the reinforcement becomes much stiffer than the soil (e.g., steel), the influence of the soil stiffness on the reinforcement load may become less, possibly to the point of having no influence at all. Additional research is needed to determine how to best incorporate the soil properties into the design method, with particular emphasis on the relative stiffness of the soil and the reinforcement. Furthermore, very few data are available for walls that use lower quality (i.e., very silty) backfills. The availability of high quality backfill is the exception rather than the rule in much of North America. Significant cost reductions can be obtained by using poorer quality backfills.

9.3 Soil Unit Weight, γ

Only minor variations in the magnitude of reinforcement load with soil unit weight were observed. This variation was considered to be very small in comparison to the uncertainty associated with other parameter values in the current investigation, including estimated reinforcement loads. However, the fundamental expression for reinforcement loads with the stiffness method shows that loads should vary linearly with soil unit weight. This linearity is preserved in the back-analyses resulting from the available database of case histories. Therefore, specific research regarding the influence of soil weight on reinforcement loads is not warranted at this time.

9.4 Wall Height Plus Surcharge (H + S)

This variable is used to characterize the overall wall geometry by an equivalent height. The fundamental expression for the stiffness method shows that reinforcement loads vary linearly with this quantity. The surcharge (S) is currently defined as the average equivalent height of soil over the reinforced backfill zone. Investigation is warranted to better understand the depth of influence of surcharge loads below the top of the wall for different wall heights (H) and the overall effect of the surcharge on the distribution of reinforcement loads within the wall. Full-scale wall reinforcement data for very tall walls are also needed to extrapolate the K_0-Stiffness Method to large values of H.

9,5 Load Distribution Factor, D_{tmax}

The load distribution with depth shown in Chapter 5.0 is likely to be influenced by foundation conditions (soft versus hard, for example). Better quantification of the load distribution with depth shown in Figure 5.13 is needed to determine the effect of various foundation soil conditions and various facing types on the distribution. The shape of the load distribution envelope is trapezoidal for extensible reinforcement (geosynthetics) but becomes more triangular for stiff reinforcement (steel). This indicates the possible influence of reinforcement stiffness on the distribution of reinforcement loads. Variation in the load distribution with depth appears to account for approximately 50 percent of the total variation in the loads predicted by the K_0-Stiffness Method relative to the measured reinforcement loads. Additional research to refine the load distribution factor is considered to be a major requirement to improve reinforcement load prediction accuracy within the framework of the new design methodology.

9.6 Local Stiffness Factor, Φ_{local}

This factor is related to the distribution factor, in that the local stiffness affects how load is distributed among reinforcement layers with different stiffness and spacing values. The effect of local stiffness appears to be significant for geosynthetic reinforcement, but the available data suggest that it has little effect on steel reinforced wall systems. On the basis of this observation, the exponent "a" has been set to 1.0 for geosynthetics and 0.0 for steel reinforcements. Additional study is needed to determine why there is a difference in the effect of this local

stiffness factor for geosynthetic and steel reinforcements and whether the preliminary values of "a" assigned for this factor are accurate.

9.7 Wall Face Batter Factor, Φ_{fb}

The proposed batter factor is an approximation based on limited empirical evidence. To date, only two wall sections within the database of geosynthetic structures with facing batters are large enough to fully investigate this issue, and no steel reinforced MSE walls are available with significant facing batters. Batter affects the loads in the reinforcement in the backfill, connection loads, and for frictional modular block systems, the connection strength. The analysis provided herein indicates that use of the Coulomb method to account for facing batter excessively reduces reinforcement loads. For frictional modular block faced systems, the hinge height concept also appears to cause too severe a reduction in the connection strength available for the typical range of facing batters used today. The influence of the magnitude of facing batter on reinforcement loads, connection loads, and connection strength in MSE walls is an important area of further research.

9.8 Facing Stiffness Factor, Φ_{fs}

The empirical evidence suggests a strong influence of facing stiffness on reinforcement loads for walls with modular block facings and full-height propped panel facings (see Chapter 7.0). The proposed values for this factor are approximate only and assume that the same reduction in reinforcement tensile loads would occur if a wall were 10 ft high or 40 ft high. However, preliminary results from full-scale laboratory test walls (see chapters 5.0 and 7.0) indicate that the facing may have a finite capacity to carry load, and only after that capacity is reached is geosynthetic reinforcement load capacity mobilized. The distribution of load capacity between the facing and reinforcement layers is likely a function of wall height. For example, the reduction in maximum reinforcement tensile forces due to a modular block or full-height, propped panel structure may not be as great for tall walls. Furthermore, no empirical evidence is currently available to validate this effect for steel reinforced walls. Because steel is much stiffer than geosynthetic reinforcement, the effect of facing stiffness observed for geosynthetic-reinforced walls may not be as strong for steel reinforced wall systems. Improved quantification

of how facing stiffness and wall toe restraint affect reinforcement loads, especially for steel reinforced MSE walls, is needed.

9.9 Global Reinforcement Stiffness, S_{global}

All of the variables discussed previously affect the correlation between global stiffness and maximum reinforcement loads, as shown by the regression analyses performed to obtain the power function relationship between global stiffness and maximum reinforcement stress within the K_0-Stiffness method. Hence, the form and magnitude of coefficients that relate the global stiffness parameter to reinforcement loads will need to be reevaluated if other fundamental variable values are refined.

9.10 Application of the K_0 - Stiffness Method to MSE Wall Internal Stability Design

Because the new method for estimating reinforcement loads must be in Load and Resistance Factor Design (LRFD) format (i.e., a limit states approach) to be implemented in current public sector design specifications (e.g., AASHTO), multiple full-scale laboratory test walls and field walls are needed to assess the variability in key parameters so that both load and resistance factors can be determined at each of the appropriate limit states. The accuracy of load and resistance factor values can be expected to increase as the database of monitored and instrumented wall structures grows.

Though the proposed design method can accurately predict reinforcement strains, these values need to be better linked to global wall deformations so that serviceability limit state deformations can be accurately predicted and reasonable design criteria can be developed. Some relevant data have been gleaned from full-scale field walls, but at the time of this writing, a strategy for predicting both short-term and long-term deformations is needed.

The development of the K_0-Stiffness Method has primarily focused on predicting peak reinforcement loads within the wall backfill. Prediction of loads at the connection between the facing and soil reinforcement is also a necessary part of a complete MSE wall design procedure. Internal reinforcement failures that have occurred in full-scale field walls to date may have been, at least in part, the result of poor connections with the facing. How many of these failures can be assigned to fundamental flaws in design and how many to other factors such as poor construction is a topic of debate in the industry. The influence of connection design on wall performance

requires further study if the risk of failure is to be properly quantified. Load factors for connection design must also be determined.

One of the limit states that must be evaluated to implement the new method is the strength limit state to prevent soil failure within the reinforced backfill. To accomplish this, data are needed to assess how much strain can be allowed in the reinforcement without causing the soil to reach a state of failure. This limit reinforcement strain is likely related to the plane strain peak soil shear strain for the backfill. Very few field walls have been taken to a high enough load level to assess this limit state. Necessarily, only an approximate quantification of the limit reinforcement strain has been provided herein. More research is needed to better quantify this limit strain for a range of backfill soils.

A systematic program of monitoring full-scale walls should be carried out in which one key parameter is varied in each test (e.g., reinforcement spacing, facing stiffness/toe restraint, soil modulus and shear strength, soil compaction, foundation stiffness, and reinforcement stiffness). Finally, additional analytical modeling, properly calibrated to match the existing case history data, must be conducted to provide some theoretical verification of the trends observed herein, and to extrapolate the available case history data to a wider range of wall geometry, reinforcement type, and soil materials.

ACKNOWLEDGMENTS

REFERENCES

AASHTO, 1996, *Standard Specifications for Highway Bridges, with 1999 Interims*, American Association of State Highway and Transportation Officials, Sixteenth Edition, Washington, D.C., USA, 686 p.

Adib, M. E., 1988, *Internal Lateral Earth Pressure in Earth Walls*, Doctoral Thesis Submitted to the University of California, Berkeley, California, 376 pp.

Alberto, L. V., 1998, *Studio Teorico E Sperimentale Del Comportamento Statico Di Un Rilevato in Terra Rinforzata*, Dissertation, Universita' Degli Studi di Padova, 285 pp.

Allen, T. M., 1983, *Properties of Geotextiles in Cold Regions Applications*, Transportation Research Report 83-6, Oregon State University.

Allen, T. M., 1991, "Determination of Long-Term Strength of Geosynthetics: a State-of-the-Art Review", *Proceedings of Geosynthetics '91*, Atlanta, GA, USA, Vol. 1, pp. 351-379.

Allen, T. M., 1997, "Viscoelastic Behavior of Geosynthetics in MSB Systems," *Mechanically Stabilized Backfill,* J. T. H. Wu, ed., Balkema, Rotterdam, pp. 401-406.

Allen, T. M., and Bathurst, R. J., 1994, "Characterization of Geosynthetic Load-Strain Behavior After Installation Damage," *Geosynthetics International*, Vol. 1, No. 2, pp. 181-199.

Allen, T. M., and Bathurst, R. J., 1996, "Combined Allowable Strength Reduction Factor for Geosynthetic Creep and Installation Damage," *Geosynthetics International,* Vol. 3, No. 3, pp. 407-439.

Allen, T. M., and Bathurst, R. J., 2001, *Application of the K_0-Stiffness Method to MSE Wall Limit States Design*, WSDOT Research Report.

Allen, T. M., and Elias, V., 1996, *Durability of Geosynthetics for Highway Applications - Interim Report,* FHWA-RD-95-016, Washington, D.C.

Allen, T. M., and Holtz, R. D., 1991, "Design of Retaining Walls Reinforced with Geosynthetics," *ASCE Geotechnical Engineering Congress*, Vol. II, Geotechnical Special Publication No. 27, Boulder, CO, pp. 970-987.

Allen, T. M., Christopher, B. R., Elias, V., and DiMaggio, J. D., 2001, *Development of the Simplified Method for Internal Stability Design of Mechanically Stabilized Earth (MSE) Walls*, WSDOT Research Report WA-RD 513.1, 108 pp.

Allen, T. M., Christopher, B.R., and Holtz, R.D., 1992, "Performance of a 12.6 m High Geotextile Wall in Seattle, Washington", *Geosynthetic Reinforced Soil Retaining Walls*, J. T. H. Wu (editor), Balkema, Rotterdam, pp. 81-100.

Ang, A. H-S., and Tang, W.H., 1975, *Probability Concepts in Engineering Planning and Design: Volume 1 – Basic Principles*, John Wiley and Sons, New York, NY, USA, 409 pp.

ASTM D4595. *Standard Test Method for Tensile Properties of Geotextiles by the Wide-Width Strip Method. American Society for Testing and Materials*, West Conshohocken, PA, USA.

ASTM D5262. *Standard Test Method for Evaluating the Unconfined Tension Creep Behavior of Geosynthetics*. American Society for Testing and Materials, West Conshohocken, PA, USA.

ASTM E328-86. *Standard Test Method for Stress Relaxation for Materials and Structures. American Society for Testing and Materials*, West Conshohocken, PA, USA.

Bathurst, R. J., 1990, "Intrumentation of Geogrid-Reinforced Soil Walls," Transportation Research Record 1277, Washington, DC, pp. 102-111.

Bathurst, R. J., 1992, "Case Study of a Monitored Propped Panel Wall," Proceedings of the International Symposium on Geosynthetic-Reinforced Soil Retaining Walls, Denver, Colorado, pp. 159-166.

Bathurst, R. J., 1993, "Investigation of Footing Restraint on Stability of Large-Scale Reinforced Soil Wall Tests," 46'th Annual Canadian Geotechnical Conference, Saskatoon, Saskatuan, pp. 389-398.

Bathurst, R. J., and Benjamin, D. J., 1990, "Failure of a Geogrid-Reinforced Soil Wall," Transportation Research Record 1288, Washington, D.C., pp. 109-116.

Bathurst, R.J. and Hatami, K., 1998, "Seismic Response Analysis of a Geosynthetic Reinforced Soil Retaining Wall," *Geosynthetics International*, Vol. 5, Nos. 1&2, pp. 127-166.

Bathurst, R. J., Jarrett, P.M., and Lescoutre, S. R., 1988, "An Instrumented Wrap-Around Geogrid Reinforced Soil Wall," Third Canadian Symposium on Geosynthetics, Kitchener, Ontario, pp. 71-78.

Bathurst, R. J., Benjamin, D. J., and Jarrett, P.M., 1989, "An Instrumented Geogrid Reinforced Soil Wall," Proceedings of the 12th International Conference on Soil Mechanics and Foundation Engineering, Rio de Janerio, Brazil, pp. 1223-1226.

Bathurst, R. J., Jarrett, P.M., and Benjamin, D. J., 1993a, "A Database of Results from an Incrementally Constructed Geogrid-Reinforced Soil Wall Test," Reinforcement Des Sols: Experimentations en Vraie Grandeur des Annees 80, Paris, pp. 401-430.

Bathurst, R. J., Simac, M. R., Christopher, B. R., and Bonczkiewicz, C., 1993b, "A Database of Results from a Geosynthetic Reinforced Modular Block Soil Retaining Wall," Renforcement Des Sols: Experimentations en Vraie Grandeur des Annees 80, Paris, pp. 341-365.

Bathurst, R. J., Wawrychuk, W. F., and Jarrett, P. M., 1987, "Laboratory Investigation of Two Large-Scale geogrid Reinforced Soil Walls," *The Application of Polymeric Reinforcement in Soil Retaining Structures*, NATO Advanced Study Institutes Series, Kluwer Academic Publishers, pp. 75-125.

Bathurst, R.J., and Jones, C.J.F.P., 2001, "Chapter 17: Earth Retaining Structures and Reinforced Slopes," *Geotechnical and Geoenvironmental Engineering Handbook*, Kluwer Academic Publishing, Norwell, MA, U.S.A. (R.K. Rowe, Editor) 1088p.

Bathurst, R.J., Blatz, J., and Burger, M.H., 2001, "Performance of Full-Scale Reinforced Embankments Loaded to Failure," submitted to *Canadian Geotechnical Journal*.

Bathurst, R.J., Simac, M.R., and Sandri, D., 1995, "Lessons Learned from the Construction Performance of a 14m High Segmental Retaining Wall," *Proceedings of Geosynthetics: Lessons Learned from Failures*, Nashville, Tennessee, pp. 15.

Bathurst, R.J., Walters, D., Vlachopoulos, N., Burgess, P., and Allen, T.M., 2000, "Full Scale Testing of Geosynthetic Reinforced Walls", Keynote paper, *ASCE Special Publication No. 103, Advances in Transportation and Geoenvironmental Systems using Geosynthetics, Proceedings of GeoDenver 2000*, Denver, Colorado, pp. 201-217.

Bell, J. R., 1998, personal communication.

Bell, J. R., and Barrett, R. K., 1995, "Survivability and Durability of Geotextiles Buried in Glenwood Canyon Wall," *Transportation Research Record 1474*, Washington, DC, pp. 55-63.

Bell, J. R., and Steward, J. E., 1977, "Construction and Observations of Fabric Soil Walls," Proceedings International Conference on Use of Fabrics in Geotechniques, Paris, Vol. 1, pp. 123-128.

Bell, J. R., Barrett, R. K., and Ruckman, A. C., 1983, "Geotextile Earth-Reinforced Retaining Wall Tests: Glenwood Canyon, Colorado," Transportation Research Record 916, Washington, DC, pp. 59-69.

Bell, J. R., Stilley, A. N., and Vandre, B., 1975, "Fabric Retained Earth Walls," Proceedings of the Thirteenth Annual Engineering Geology and Soils Engineering Symposium, University of Idaho, Moscow, Idaho, pp. 271-287.

Bell, J.R., Szymoniak, T. and Thommen, G.R., 1985, "Construction of a Steep Sided Geogrid Retaining Wall for an Oregon Coastal Highway," *Proceedings of the Polymer Grid Reinforcement Conference,* London England, March 22-23, 1984, Thomas Telford, London, pp 198-202.

Benjamin, J. R. S., 1989, *Performance of Full Scale Geogrid Reinforced Soil Retaining Walls*, MEng Thesis, Royal Military College, Kingston, Ontario, 256 pp.

Berg, R. R., Allen, T. M., and Bell, J. R., 1998, "Design Procedures for Reinforced Soil Walls - A Historical Perspective," *Proceedings of the Sixth International Conference on Geosynthetics,* Atlanta, GA, Vol. 2, pp. 491-496.

Berg, R.R., Bonaparte, R., Anderson, R. P., and Chouery, V.E., 1986, "Design, Construction, and Performance of Two Geogrid Reinforced Soil Retaining Walls," *Proceedings of the Third International Conference on Geotextiles*, Vienna, pp. 401-406.

Bernardi, M., and Paulson, J., 1997, "Is Creep a Degradation Phenomenon?," Mechanically Stabilized Backfill, J. T. H. Wu, ed., Balkema, Rotterdam, pp. 289-294.

Bolton, M.D. 1986, "The Strength and Dilatancy of Sands," Geotechnique, Vol. 36, No. 1, pp. 65-78.

Boyle, S. R., 1995, *Deformation Prediction of Geosynthetic Reinforced Soil Retaining Walls*, Ph.D. Dissertation, University of Washington, 391 pp.

Boyle, S. R., and Holtz, R. D. 1996, "Discussion of 'A Performance Test for Assessment of Long-Term Creep Behavior of Soil-Geosynthetic Composites' by Wu, J. T. H., and Helwany, S. M. B.", *Geosynthetics International*, Vol. 3, No. 4, pp. 551-557.

Boyle, S. R., Gallager, M. and Holtz, R. D., 1996, "Influence of Strain Rate, Specimen, Length and Confinement on Measured Geotextile Properties*," Geosynthetics International*, Vol. 3, No. 2, pp. 205-225.

Boyle, S.R, and Holtz, R.D. 1998, "Measuring Geotextile Strains with Strain Gauges", *Proceedings of the Sixth International Conference on Geosynthetics*, Atlanta, Georgia, Vol 1. pp.517-522.

Bright, D. G., Collin, J. G., and Berg, R. R., 1994, "Durability of Geosynthetic Soil Reinforcement Elements in Tanque Verde Retaining Wall Structures," Transportation Research Record 1439, Washington, DC, pp. 46-54.

Broms, B. B., 1978, "Design of Fabric Reinforced Retaining Structures," Proceedings ASCE Symposium on Earth Reinforcement, Pittsburgh, pp. 282-303.

Burgess, G. P., 1999, *Performance of Two Full-Scale Model Geosynthetic-Reinforced Segmental Walls*, M. S. Thesis, Royal Military College of Canada, Kingston, Ontario, 206 pp.

Bush, D.I. and Swan, D.B.G., 1987, "An Assessment of the Resistance of Tensar SR-2 to Physical Damage during Construction and Testing of a Reinforced Soil Wall," *The Application of Polymeric Reinforcement in Soil Retaining Structures*, NATO Advanced Study Institutes Series, Kluwer Academic Publishers, pp. 173-180.

Bush, D.I., 1990, "Variation of Long-Term Design Strength of Geosynthetics in Temperatures up to 40^OC," *Proceedings of the Fourth International. Conference on Geotextiles, Geomembranes, and Related Products*, The Hague, Netherlands, pp. 673-676.

Carrubba, P., Moraci, N., and Montanelli, F., 1999, "Instrumented Soil Reinforced Retaining Wall: Analysis of Measurements," *Geosynthetics '99 Conference Proceedings*, Boston, MA, pp. 921-934.

Cazzuffi, D., and Sacchetti, M., 1999, "Temperature Effects on Tensile-Creep Behaviour of High Strength Geosynthetics," *Geosynthetics '99*, Boston, Vol. 2, pp. 723-734.

Christopher, B. R., 1993, *Deformation Response and Wall Stiffness in Relation to Reinforced Soil Wall Design,* Ph.D. Dissertation, Purdue University, 352 pp.

Christopher, B. R., 1998, Personal Communication.

Christopher, B. R., Holtz, R. D., and Bell, W. D., 1986, "New Test for Determining the In-Soil-Stress-Strain Properties of Geotextiles," *Proceedings of the Third International Conference on Geotextiles*, Vol. 2, Vienna, Austria, pp. 683-686.

Christopher, B. R., Gill, S. A., Giroud, J.-P., Juran, I., Mitchell, J. K., Schlosser, F., and Dunnicliff, J., 1990, *Reinforced Soil Structures, Vol. 1 Design and Construction Guidelines*, FHWA Report FHWA-RD-89-043, 285 pp.

Delmas, Ph., Blivet, J.C. and Matichard, Y., 1987, "Geotextile-Reinforced Retaining Structures: A few Instrumented Examples," *The Application of Polymeric Reinforcement in Soil Retaining Structures*, NATO Advanced Study Institutes Series, Kluwer Academic Publishers, pp. 285-311.

Desert Earth Engineering, 1987, *Final Report on Tensar Earth-Reinforced Wall Monitoring at Tanque Verde-Wrightstown-Pantano Road*.

Duncan J.M., Byrne, P., Wong, K.S. and Mabry, P., 1980, "Strength, Stress-Strain and Bulk Modulus Parameters for Finite Element Analyses of Stresses and Movements in Soil Masses", Geotechnical Engineering Report No. UCB/GT/80-01, University if California, Berkeley, 70p.

Ehrlich, M., and Mitchell, J. K., 1994, "Working Stress Design Method for Reinforced Earth Soil Walls," *ASCE Journal of Geotechnical Engineering*, Vol. 120, No. 4, pp. 625-645.

Elias, V., 2001a, *Corrosion/Degradation of Soil Reinforcements for Mechanically Stabilized Earth Walls and Reinforced Soil Slopes*, FHWA-NHI-00-044, Federal Highway Administration, Washington, D.C.

Elias, V., 2001b, *Long-Term Durability of Geosynthetics Based on Exhumed Samples from Construction Projects*, FHWA Report FHWA RD-00-157, 53 pp.

Elias, V., and Christopher, B.R., and Berg, R. R., 2001, *Mechanically Stabilized Earth Walls and Reinforced Soil Slopes - Design and Construction Guidelines*, No. FHWA-NHI-00-043, Federal Highway Administration.

Elias, V., Salman, A., and Goulias, D., 1998, "The Effect of pH, Resin Properties, and Manufacturing Process on Laboratory Degradation of Polyester Geosynthetics," *Geosynthetics International*, Vol. 5, No. 5, pp. 459-490.

Elias, V., Yuan, Z., Swan, R. H., and Bachus, R. C., 1998b, *Development of Protocols for Confined Extension/Creep Testing of Geosynthetics in Highway Applications*, Federal Highway Administration, No. FHWA-SA-97-143.

Fannin, R. J., 1988, *Soil Reinforcement for Norwegian Conditions - An Instrumented Field Study of the Analysis and Design of Geogrid Reinforced Slopes,* Report to the Norwegian Geotechnical Institute.

Fannin, R. J., 1994, "Field Observations on the Load-Strain-Time Behavior of Geogrid Reinforcement," *Canadian Geotechnical Journal*, No. 31, pp. 564-569.

Fannin, R. J., 2001, "Long-Term Variations of Force and Strain in a Steep Geogrid-Reinforced Soil Slope," *Geosynthetics International*, Vol. 8, No. 1, pp. 81-96.

Fannin, R. J., and Hermann, S., 1990, "Performance Data for a Sloped Reinforced Soil Wall," *Canadian Geotechnical Journal*, No. 27, pp. 676-686.

Fannin, R. J., and Hermann, S., 1991, "Creep Measurements on Polymeric Reinforcement," *Geosynthetics '91 Conference*, Atlanta, pp. 561-573.

Gallagher, M. D., 1995, *In-Isolation Wide Width Tests on Geotextiles*, MS Thesis, University of Washington, Seattle, 132 pp.

Gnanendran, C.T., and Selvadurai, A.P.S., 2001. "Strain Measurement and Interpretation of Stabilizing Force in Geogrid Reinforcement", Geotextiles and Geomembranes 19: pp. 177-194.

Gourc, J.-P., and Matichard, Y., 1992, "Development of Geotextile Reinforcement Techniques in France," *Geosynthetic Reinforced Soil Retaining Walls*, J. T. H. Wu (editor), Balkema, Rotterdam, pp. 131-152.

Greenway, D., Bell, J. R., and Vandre, B.,1999, "Snailback Wall - First Fabric Wall Revisited at 25 Year Milestone," *Geosynthetics '99 Conference Proceedings*, Boston, MA, pp. 905-919.

Greenwood, J. H., 1990, "The Creep of Geotextiles," *Proceedings of the Fourth International. Conference on Geotextiles, Geomembranes, and Related Products*, The Hague, Netherlands, pp. 645-650.

Greenwood, J. H., 1997, "Designing to Residual Strength of Geosynthetics Instead of Stress-Rupture," *Geosynthetic International,* Vol. 4, No. 1, pp. 1-10.

Helwany, S. M. B., and Shih, S., 1998, "Creep and Stress Relaxation of Geotextile Reinforced Soils," *Geosynthetics International*, Vol. 5, No. 4, pp. 425-434.

Holtz, R. D., and Kovacs, W. D., 1981, *An Introduction to Geotechnical Engineering*, Printice-Hall, Inc., New Jersey, 733 pp.

Jewell, R. A., and Wroth, C. P., 1987, "Direct Shear Tests on Reinforced Sand," Geotechnique, Vol. 37, No. 1, pp. 53-68.

Jewell, R.A. and Greenwood, J.H., 1988, "Long-Term Strength and Safety in Steep Soil Slopes Reinforced by Polymer Materials", *Geotextiles and Geomembranes*, Vol. 7, Nos. 1 and 2, pp. 81-118.

Kaliakin, V. N., Dechasakulsom, M., and Leshchinsky, D, 2000, "Investigation of the Isochrone Concept for Predicting Relaxation of Geogrids," *Geosynthetics International*, Vol. 7, No. 2, pp. 79-99.

Knight, M. A., Valsangkar, A. J., 1993, "Intrumentation and Performance of Tilt-Up Panel Wall," *Proceedings of the Geosynthetics '93 Conference*, Vancouver, BC, pp. 123-136.

Koutsourais, M., 1995, "Correlating the Creep Strain Component of the Total Strain as a Function of Load-Level for High-Tenacity Polyester Yarns, Geogrids, and Geotextiles," *Proceedings of the Geosynthetics '95 Conference*, Nashville, TN, Vol. 3, pp. 989-1002.

Kuhn, M. R. and Mitchell, J. K., 1993, "New Perspectives on Soil Creep," *Journal of Geotechnical Engineering*, ASCE, Vol. 119, No. 3, pp. 507-524.

Lade and Lee, 1976, "Engineering Properties of Soils," *Report UCLA-ENG-7652*, 145 pp. [As cited by Holtz and Kovacs (1981)].

Leclercq, B., Schaeffner, M., Delmas, Ph., Blivet, J. C., and Matichard, Y., 1990, "Durability of Geotextiles: Pragmatic Approach Used in France," *Proceedings of the Fourth International Conference on Geotextiles, Geomembranes, and Related Products*, The Hague, pp. 679-684.

Lee, K. L., Adams, B. D., and Vagneron, J. J., 1973, "Reinforced Earth Retaining Walls," *Journal, Soil Mechanics Division*, ASCE, Vol. 99, No. SM10, pp. 745-764.

Lee, W. F., 2000, *Internal Stability Analysis of Geosynthetic Reinforced Retaining Walls*, Ph.D. Dissertation, University of Washington, 355 pp.

Leflaive, E., 1988, "Durability of Geotextiles: The French Experience," *Geotextiles and Geomembranes*, No. 7, pp. 23-31.

McCrum, N.G., Buckley, C.P. and Bucknall, C.B., 1988, *Principles of Polymer Engineering*, Oxford University Press, Oxford, 391 pages.

McGown, A., Paine, N., and DuBois, D. D., 1984, "Use of Geogrid Properties in limit Equilibrium Analysis," *Proceedings Symposium on Polymer Grid Reinforcement in Civil Engineering*, Paper No. 1.4, pp. 1-5.

McMahon and Mann Consulting Engineers, 1996, *Addendum #6 Report Tensar Wall Instrument Readings, Tucson, Arizona*, Unpublished Report.

Montanelli, F., 2000 (personal communication).

Murray and Farrar, 1990, "Reinforced Earth Wall on the M25 Motorway at Waltham Cross," *Proceedings of the Institution of Civil Engineers*, Part 1, No. 88, 261-282.

Orsat, P., Khay, M., and McCreath, M., 1998, "Study on Creep-Rupture of Polyester Ttendons: Full Scale Tests," *Proceedings of the Sixth International Conference on Geosynthetics,* Atlanta, GA, Vol. 2, pp. 675-678.

Perkins, S.W., and Lapeyre, J.A., 1997, "In-Isolation Strain Measurement of Geosynthetics in Wide-Width Strip Tension Test," *Geosynthetics International*, Vol. 4, No. 1, pp. 11-32.

Powell, B., and Mohney, J., 1994, "Durability of Geotextiles Used in Reinforcement of Walls and Road Subgrade," Transportation Research Record 1439, Washington, DC, pp. 20-24.

Puig , J., Blivet, J. C., and Pasquet, P., 1977, "Earth Reinforced Fill with Synthetic Fabric," *Proceedings international Conference on the Use of Fabrics in Geotechniques*, Paris, Vol. 1, pp. 85-90.

Rimoldi, P., and Montanelli, F., 1993, "Creep and Accelerated Creep Testing for Geogrids," *Proceedings of the Geosynthetics '93 Conference*, Vancouver, BC, pp. 773-785.

Rowe, R. K., and Ho, S. K., 1993, "Keynote Lecture: A Review of the Behavior of Reinforced Soil Walls," *Earth Reinforcement Practice*, Ochiai, Hayashi, and Otani, ed's, Balkema, Rotterdam, pp. 801-830.

Sabatini, P. J., Pass, D. G., and Bachus, R. C., 1999, *Ground Anchors and Anchored Systems*, Geotechnical Engineering Circular No. 4, FHWA SA-99-015, Washington, DC, 281 pp.

Salman, A., Elias, V., and DiMillio, A., 1998, "The Effect of Oxygen Pressure, Temperature, and manufacturing Processes on Laboratory Degradation of Polyolefin Based Geosynthetics," *Sixth International Conference on Geotextiles, Geomembranes, and Related Products,* Atlanta, GA, Vol. 2, pp. 683-690.

Salman, A., Elias, V., Juran, I., Lu, S., and Pearce, E., 1997, "Durability of Geosynthetics Based on Accelerated Laboratory Testing," Geosynthetics '97, IFAI, San Diego, CA, pp. 217-234.

Saunders, D. 2001. The Performance of Two Full-Scale Reinforced Segmental Soil Retaining Walls, Master of Engineering Thesis, Civil Engineering Department, Royal Military College of Canada, May 2001, 304p.

Sawicki, A., 1999, "Rheological Model of Geosynthetic-Reinforced Soil", *Geotextiles and Geomembranes*, Vol. 17, pp 33-49.

Schlosser, F., Hoteit, N., and Price, D., 1993, "Instrumented Full Scale Freyssisol-Websol Reinforced Wall," Reinforcement Des Sols: Experimentations en Vraie Grandeur des Annees 80, Paris, pp. 299-320.

Steward, J., Williamson, R., and Mohney, J., 1977, *Guidelines for the Use of Fabrics in Construction and Maintenance of Low-Volume Roads*, Report No. FHWA-TS-78-205.

Tatsuoka, F. 1993, "Keynote Lecture: Roles of Facing Rigidity in Soil Reinforcing," *Earth Reinforcement Practice*, Ochiai, Hayashi, and Otani, ed's, Balkema, Rotterdam, pp. 831-870.

Thornton, J. S., Allen, S. R., and Thomas, R. W., 1997, "Approaches for the Prediction of Long Term Viscoelastic Properties of Geosynthetics from Short Term Tests," *Geosynthetics '97*, IFAI, Long Beach, CA, Vol. 1, pp. 277-291.

Thornton, J.S., 2001, "Characterization of Short and Long Term Creep and relaxation properties of a Polypropylene Geogrid", *Geosynthetics 2001*, IFAI, Portland, Oregon, pp. 835-845.

Vlachopoulos, N., 2000, *The Performance of Two Full-Scale Model Geosynthetic-Reinforced Walls: Segmental and Wrapped-Face*, M. S. Thesis, Royal Military College of Canada, Kingston, Ontario, 242 pp.

Walters, D. (2001) personal communication.

Washington State Department of Transportation, 1998, "Determination of Long-Term Strength of Geosynthetics," *WSDOT Test Method 925*, FOSSC Materials Laboratory, Tumwater, WA.

Wilding, M.A. and Ward, I.M., 1981, "Creep and Recovery of Ultra High Modulus Polyethylene", *Polymer*, Vol. 22, pp. 870-876.

Williams, J.G., 1980, *Stress Analysis of Polymers,* 2nd Edition, Ellis Horwood Limited, Chichester, John Wiley & Sons, New York, 360 pp.

Wilson-Fahmy, R. F., Koerner, R. M., and Fleck, J. A., 1993, "Unconfined and Confined Width Width Tension Testing of Geosynthetics," *Geosynthetic Soil Reinforcement Testing Procedures*, ASTM STP 1190, pp.

Yako, M. A., and Christopher, B. R., 1987, "The Application of Polymeric Reinforcement in Soil Retaining Structures," *NATO Advanced Study Institutes Series*, Kluwer Academic Publishers.

Yeo, K. C., 1985, *The Behavior of Polymeric Grids Used for Soil Reinforcement*, Ph.D. Dissertation, University of Strathclyde, pp.185 + Appendices.

Yuan, Z., Swan, R. H., Jr., and Bachus, R. C. 1998, "Soil Confinement Effect on Stress-Strain Properties of Geosynthetics," *Proceedings of the Sixth International Conference on Geosynthetics*, Atlanta, GA, pp. 523-528.

Zornberg, J. G., Sitar, N., and Mitchell, J. K., 1998(a), "Performance of Geosynthetic Reinforced Slopes at Failure," Journal of Geotechnical and Geoenvironmental Engineering, ASCE, Vol. 124, No. 8, pp. 670-683.

Zornberg, J. G., Sitar, N., and Mitchell, J. K., 1998(b), "Limit Equilibrium as basis for Design of Geosynthetic Reinforced Slopes," Journal of Geotechnical and Geoenvironmental Engineering, ASCE, Vol. 124, No. 8, pp. 684-698.

ADDITIONAL RESOURCES

Elias, V., DiMaggio, J., and DiMillio, A., 1997, "FHWA Technical Note on the Degradation-Reduction Factors for Geosynthetics," *Geotechnical Fabrics Report*, Vol. 15, No. 6, pp. 24-26.

Federal Highway Administration (FHWA), 1997, "Degradation Reduction Factors for Geosynthetics," *Federal Highway Administration Geotechnology Technical Note*.

Lescoutre, S. R., 1986, *The Development of a Large Scale Facility for Reinforced Soil Retaining Walls*, M.S. Thesis, Royal Military College of Canada, Kingston, Ontario, 294 pp.

Leshchinsky, D., Dechasakulsom, M., Kaliakin, V. N., and Ling, H. I., 1997, "Creep and Stress Relaxation of Geogrids," *Geosynthetics International*, Vol. 4, No. 5, pp. 463-479.

APPENDIX A: T_{MAX} MEASURED AND PREDICTED DISTRIBUTIONS AS A FUNCTION OF DEPTH BELOW THE WALL TOP
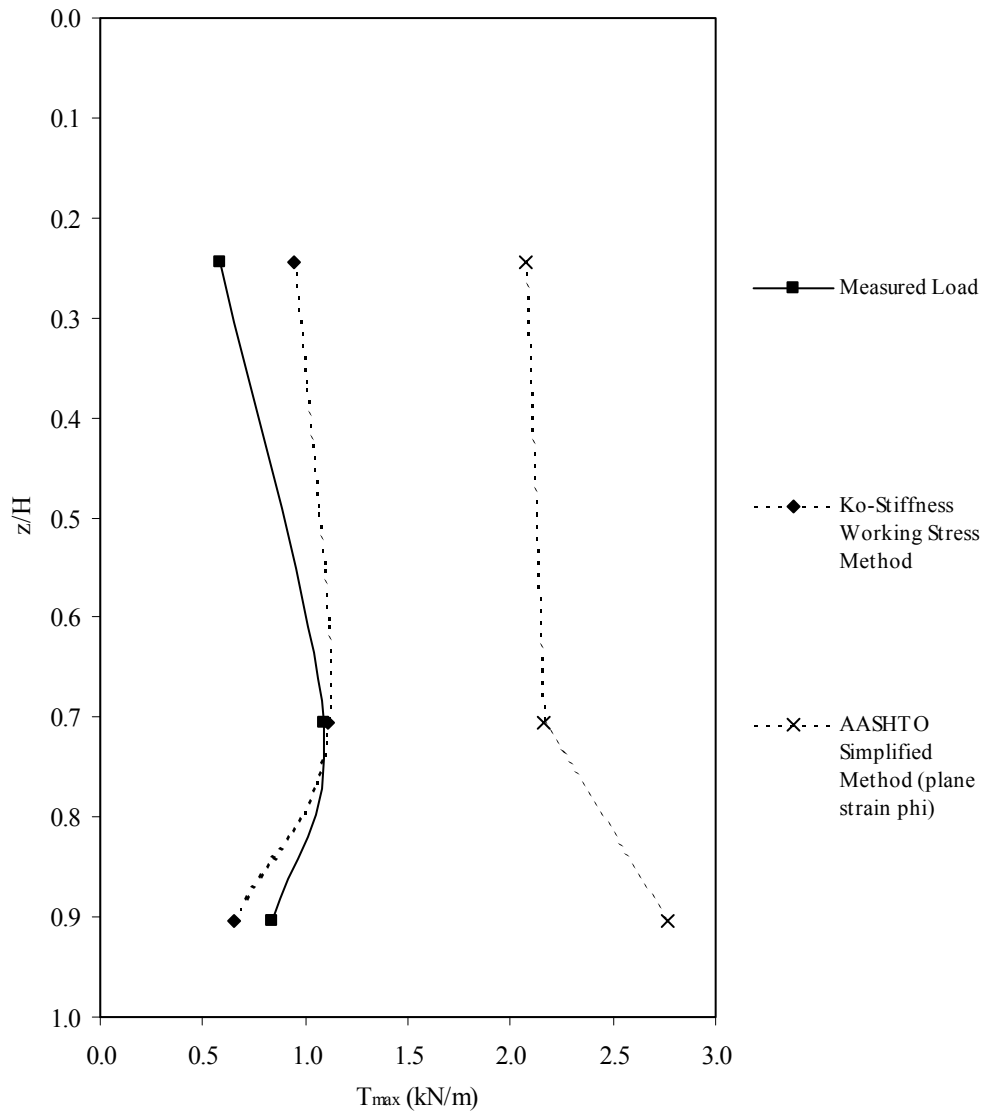
Figure A.1. Measured and predicted T_{max} as a function of depth below wall top for Wall GW5.
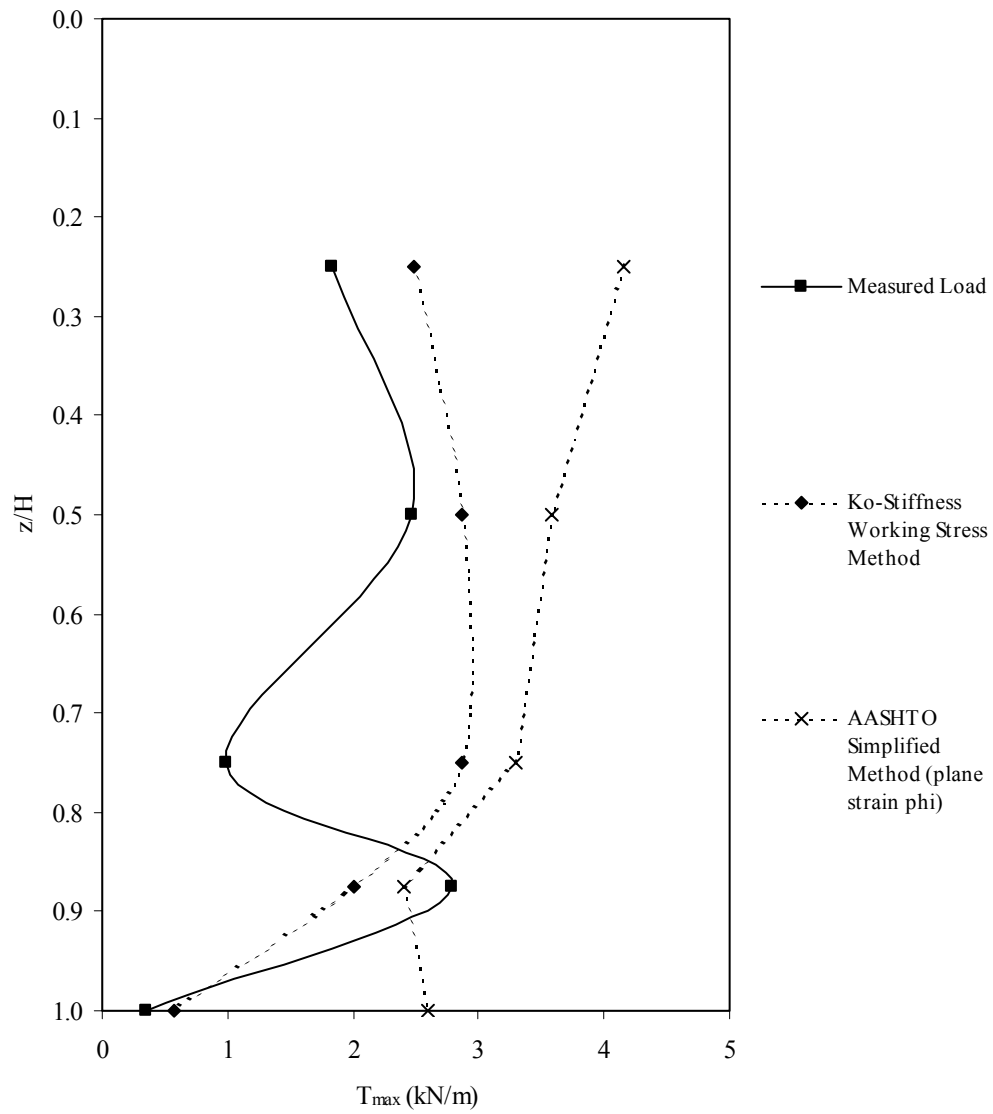
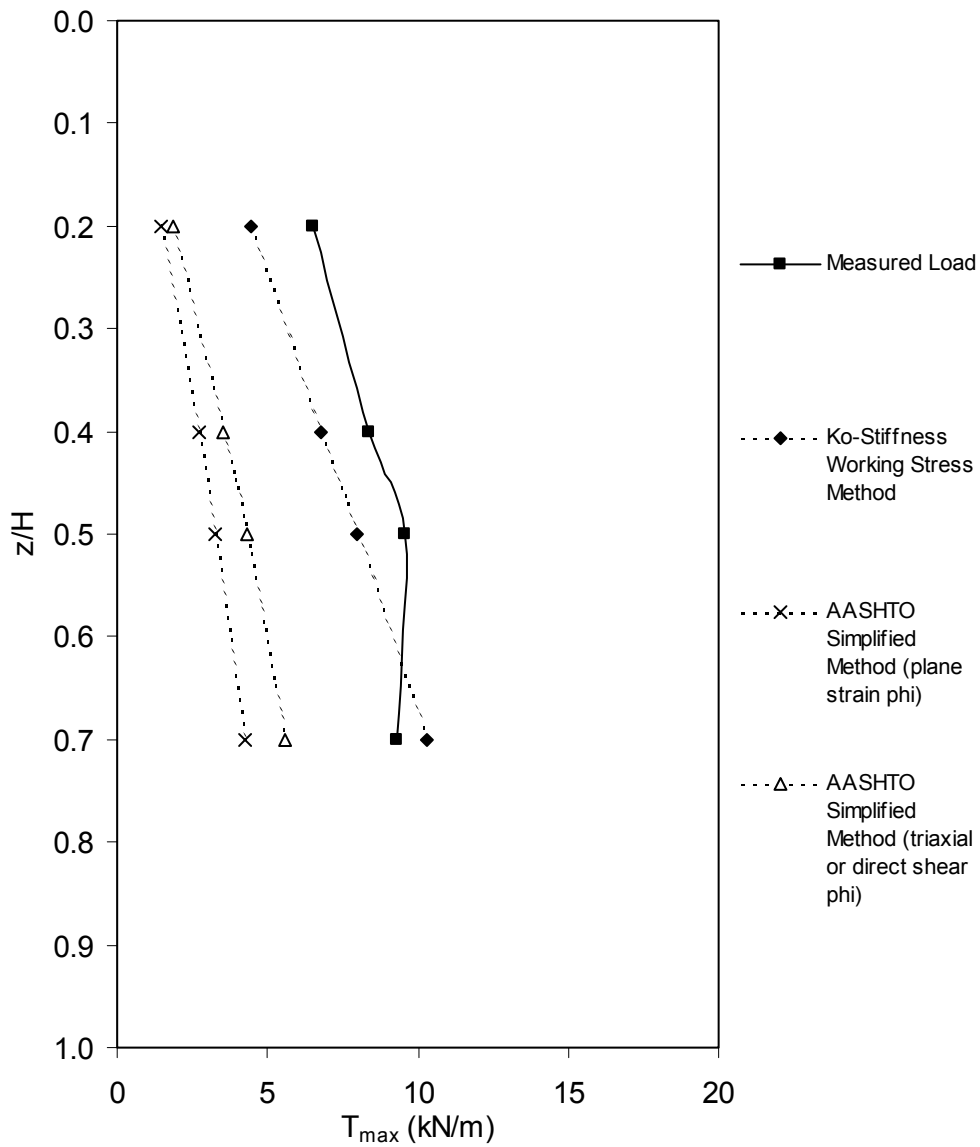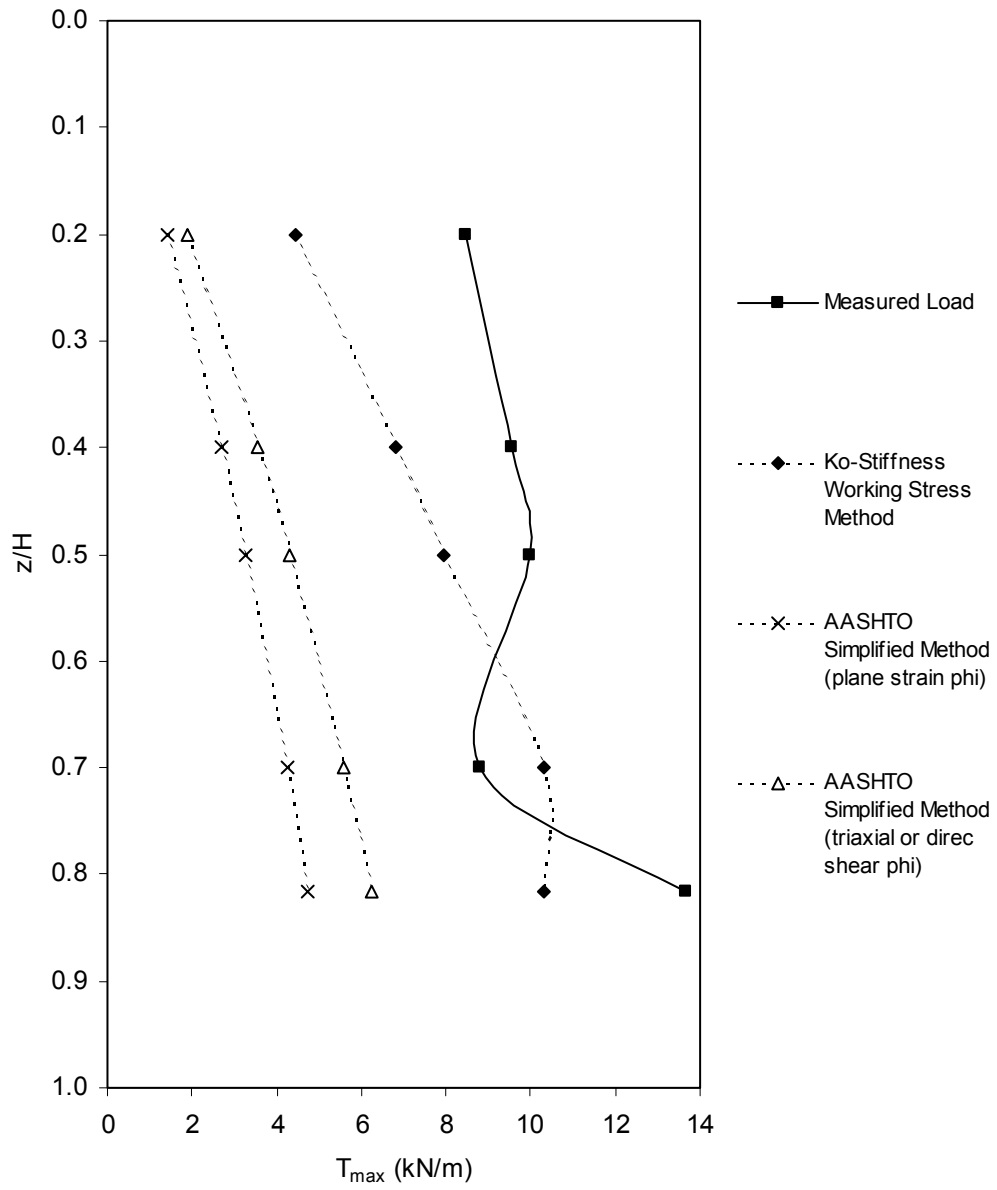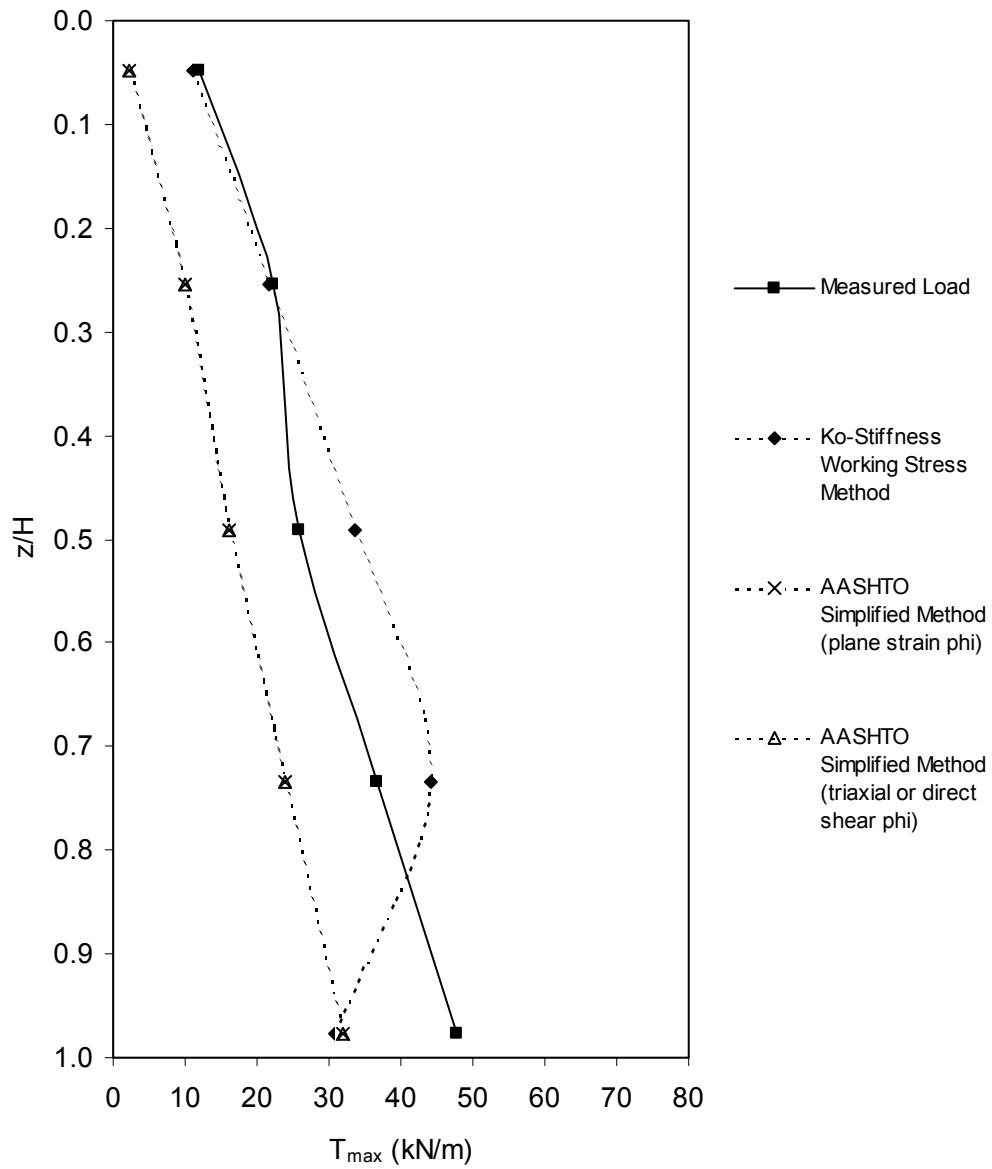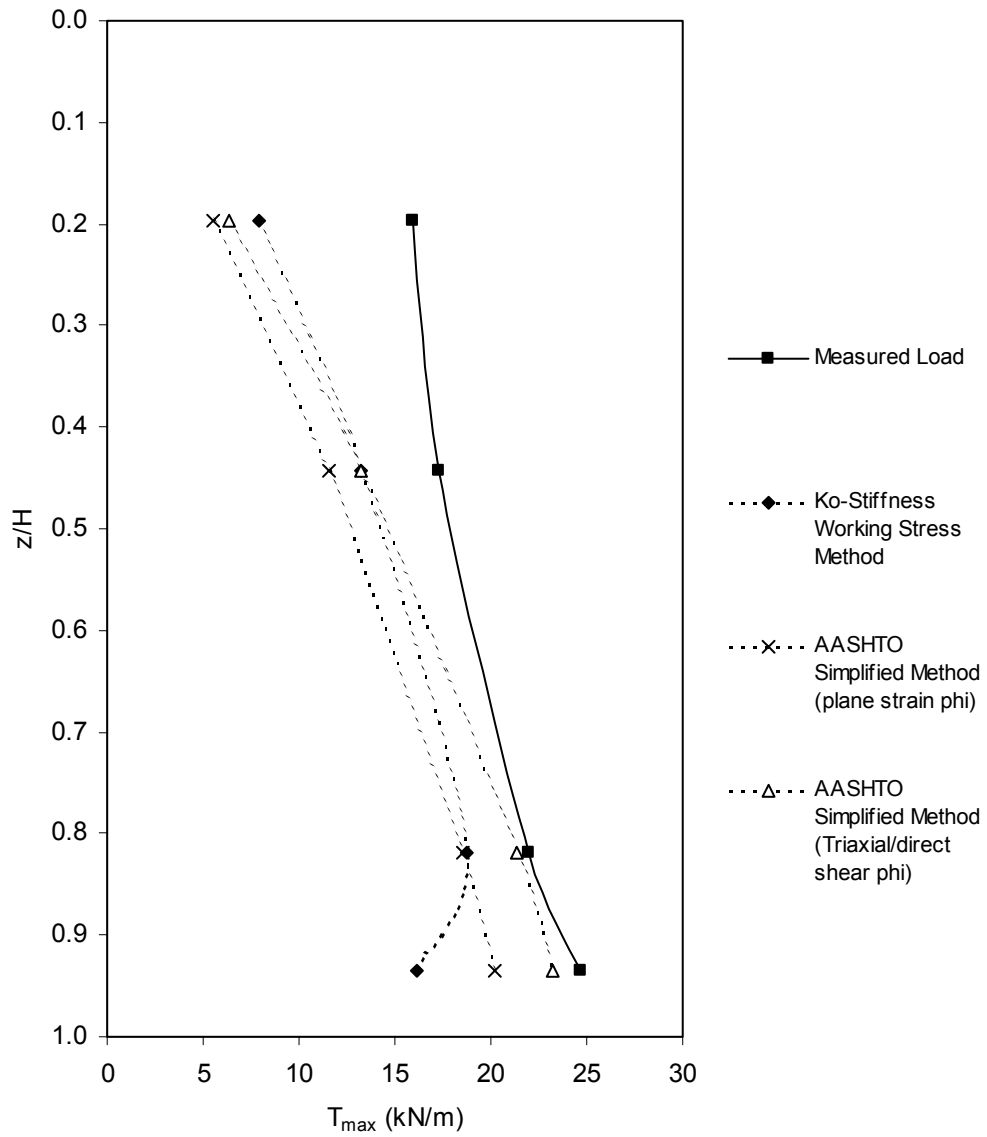Figure A.2. Measured and predicted T_{max} as a function of depth below wall top for Wall GW7 (Section J).
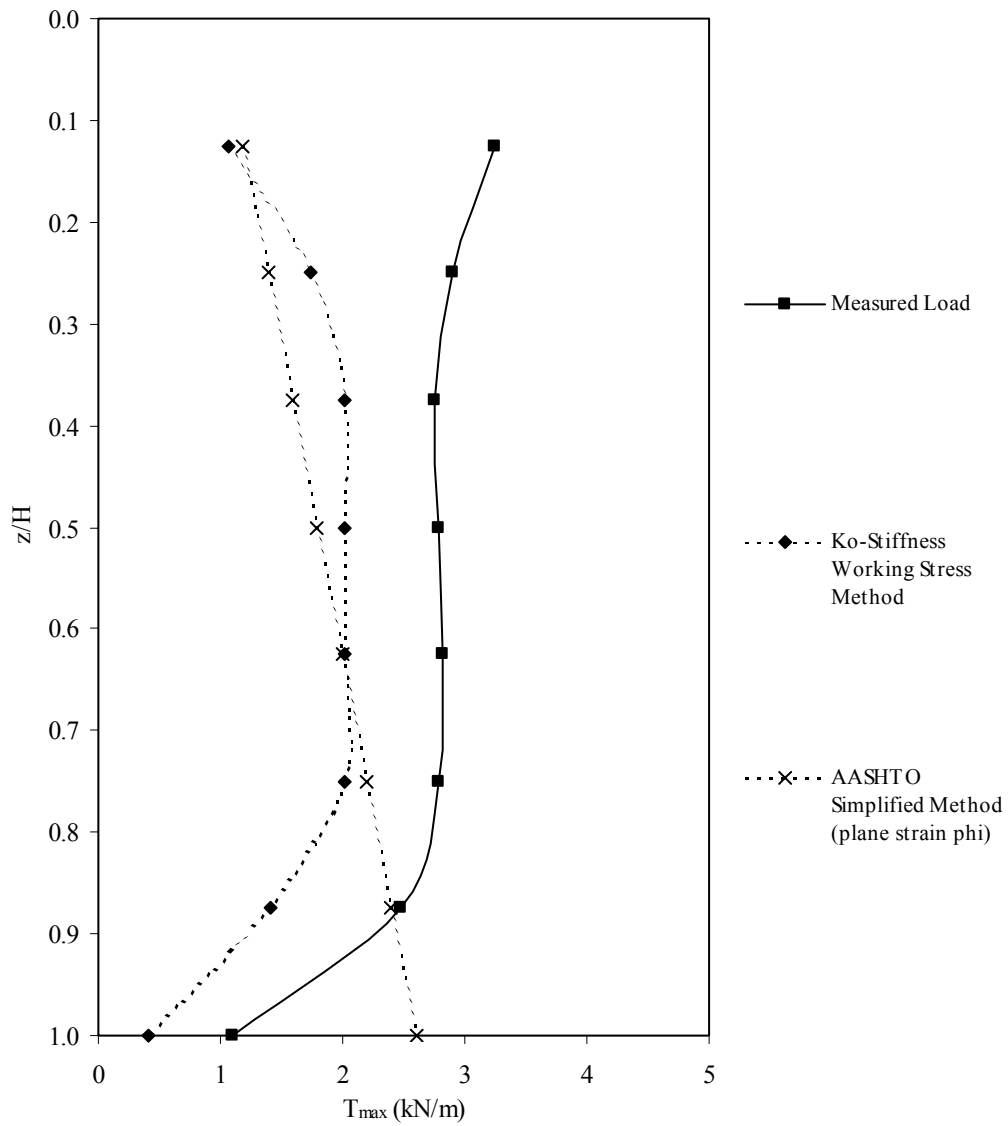
Figure A.3. Measured and predicted T_{max} as a function of depth below wall top for Wall GW7 (Section N).
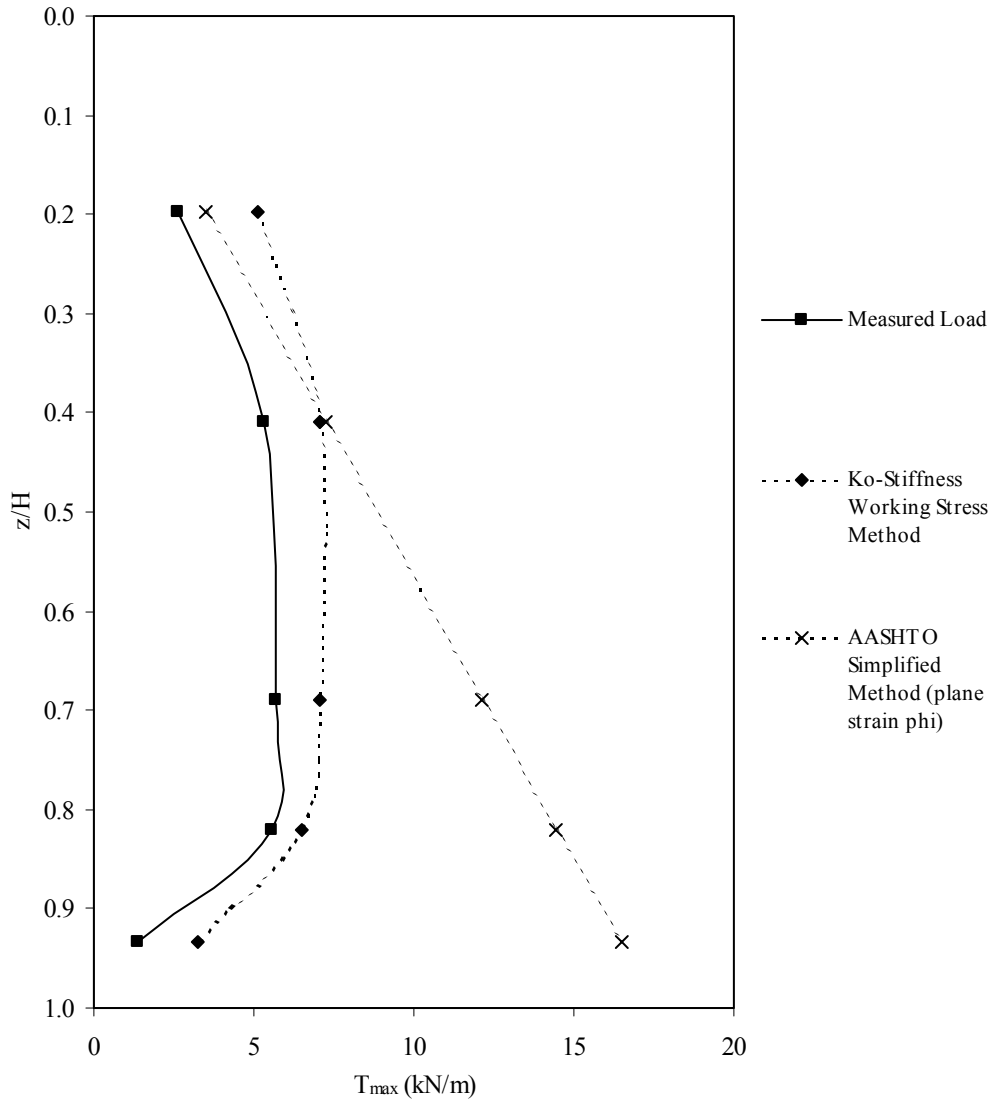
Figure A.4. Measured and predicted T_{max} as a function of depth below wall top for Wall GW8.
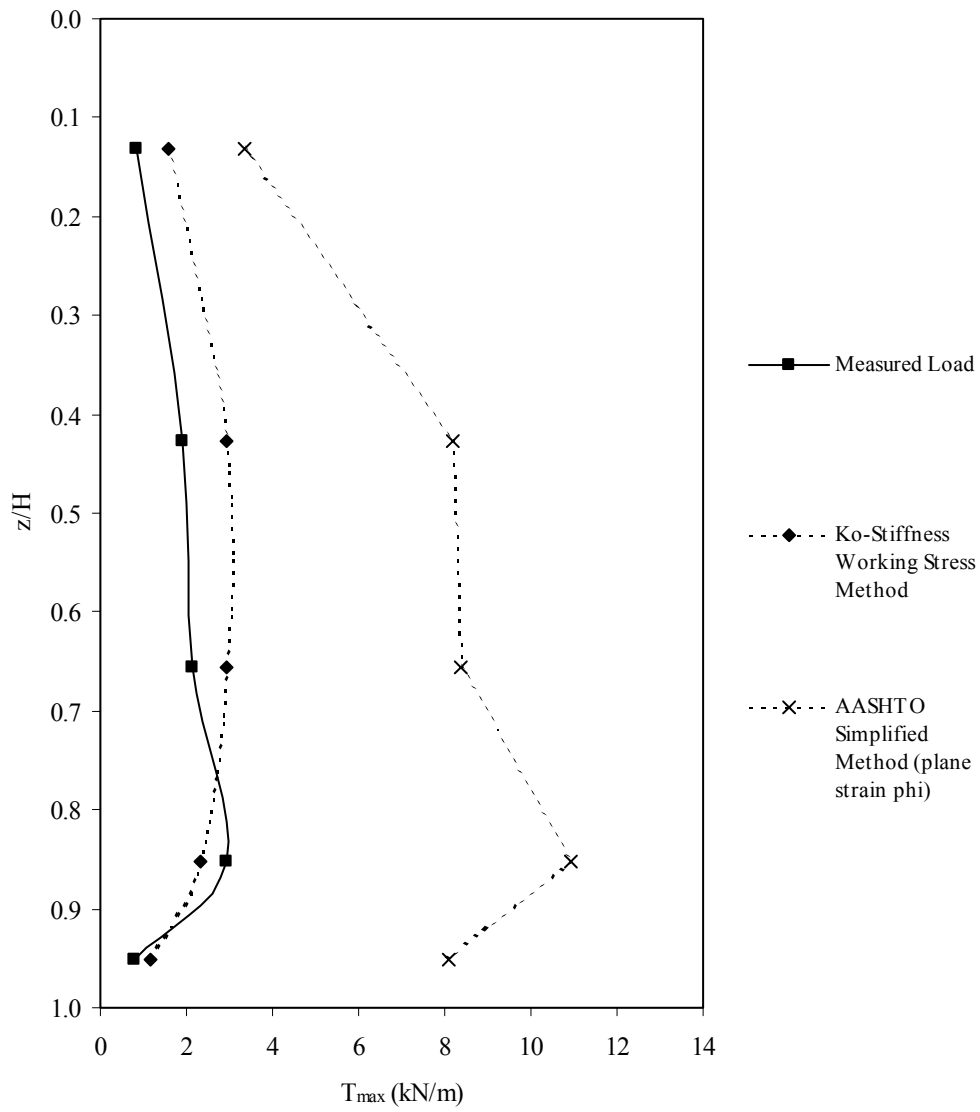
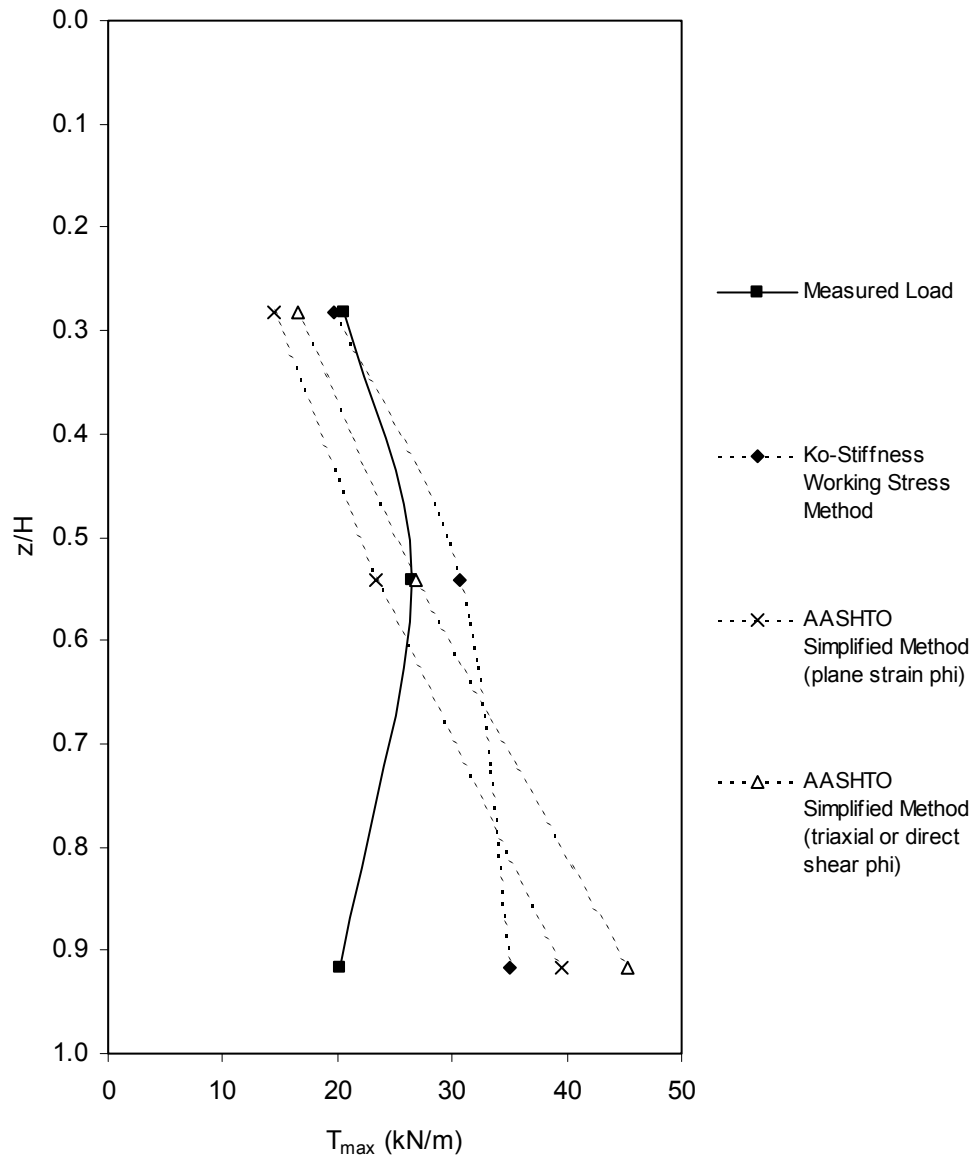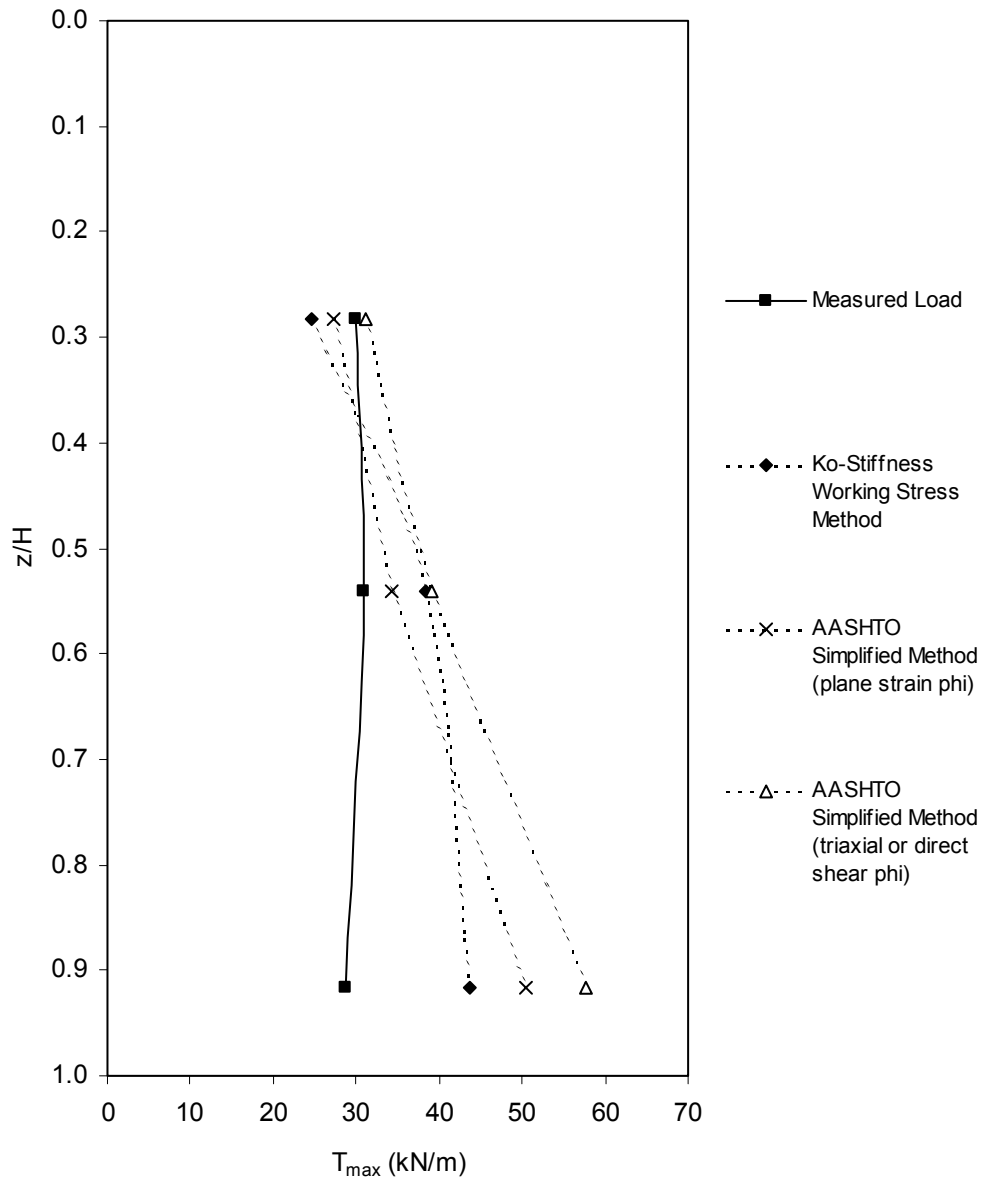Figure A.5. Measured and predicted T_{max} as a function of depth below wall top for Wall GW9 (no surcharge).
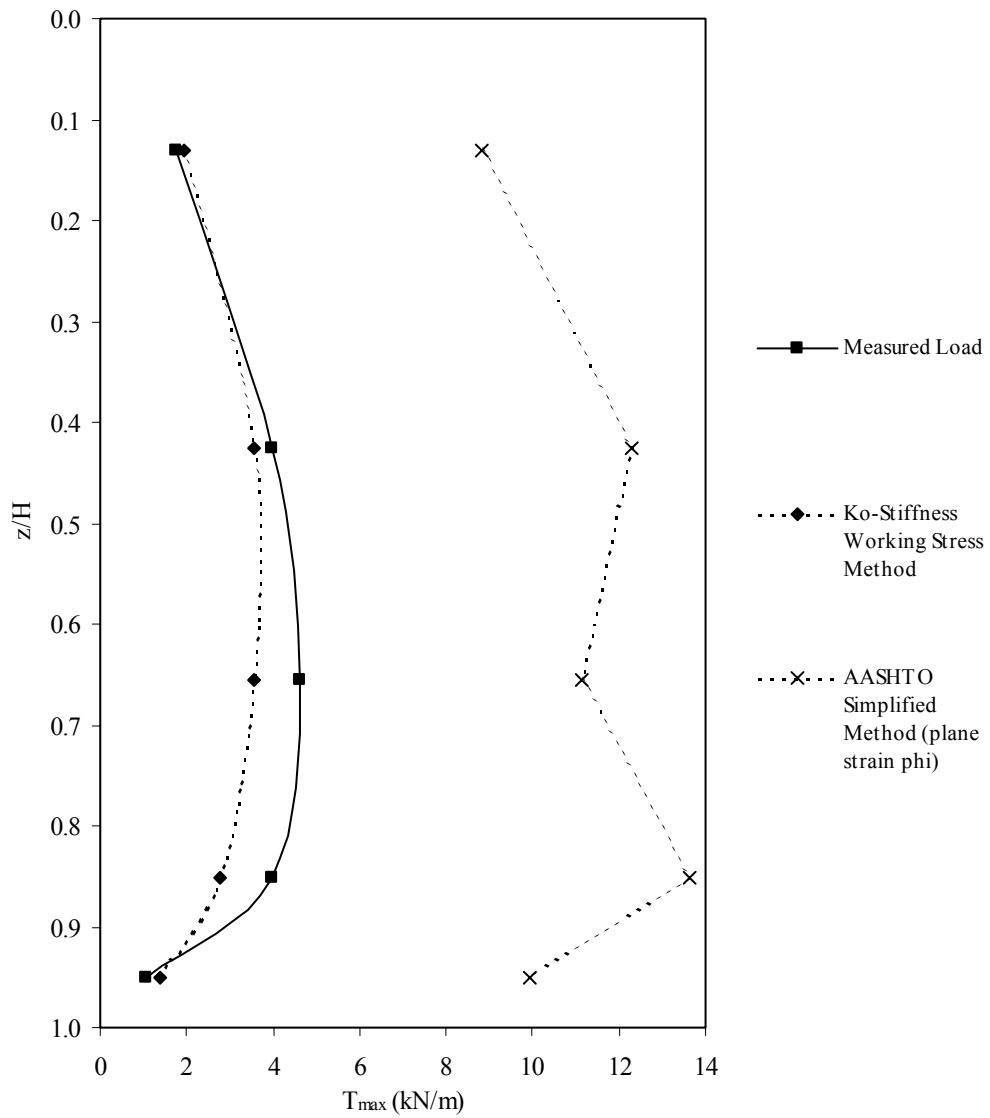
Figure A.6. Measured and predicted T_{max} as a function of depth below wall top for Wall GW9 (with surcharge).
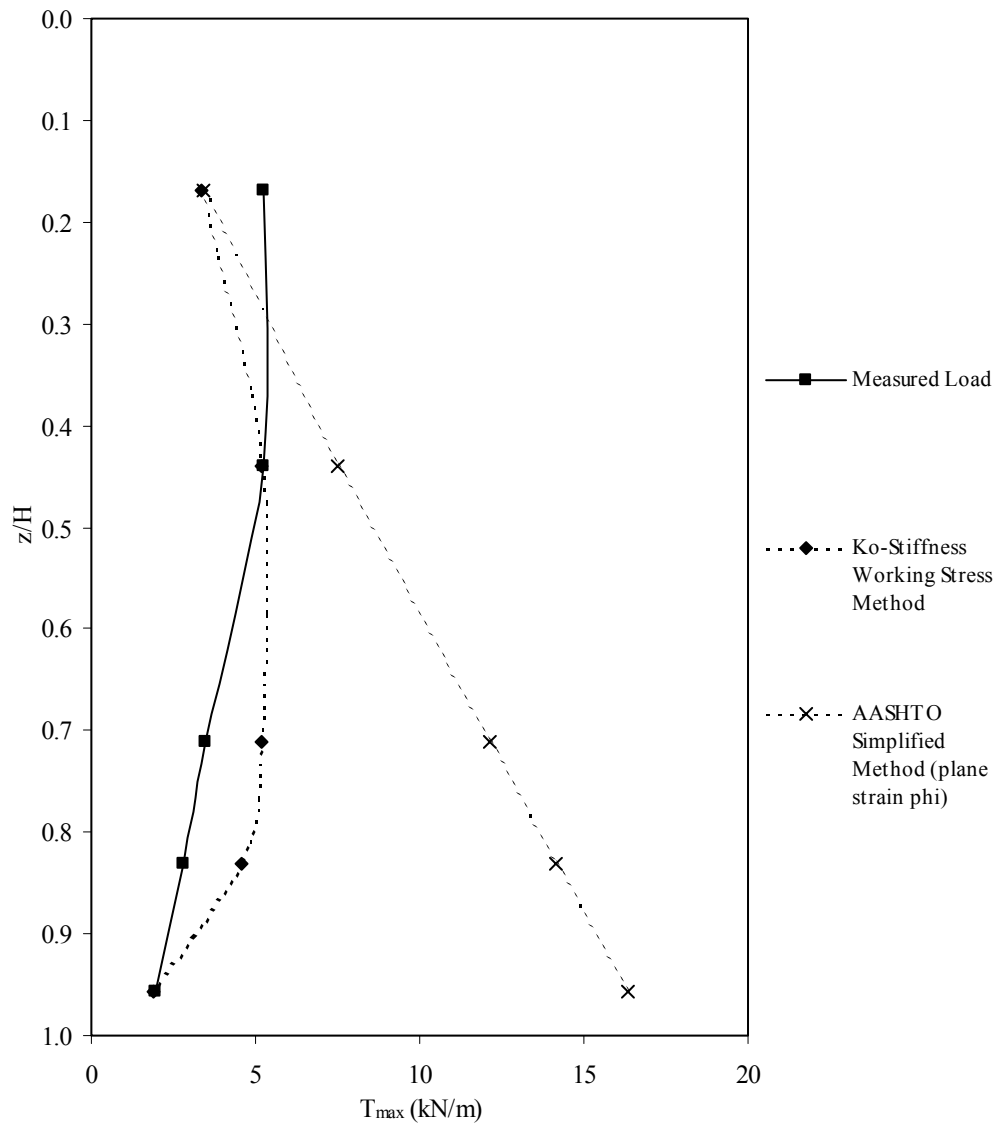
Figure A.7. Measured and predicted T_{max} as a function of depth below wall top for Wall GW10 (after water restraint removed).
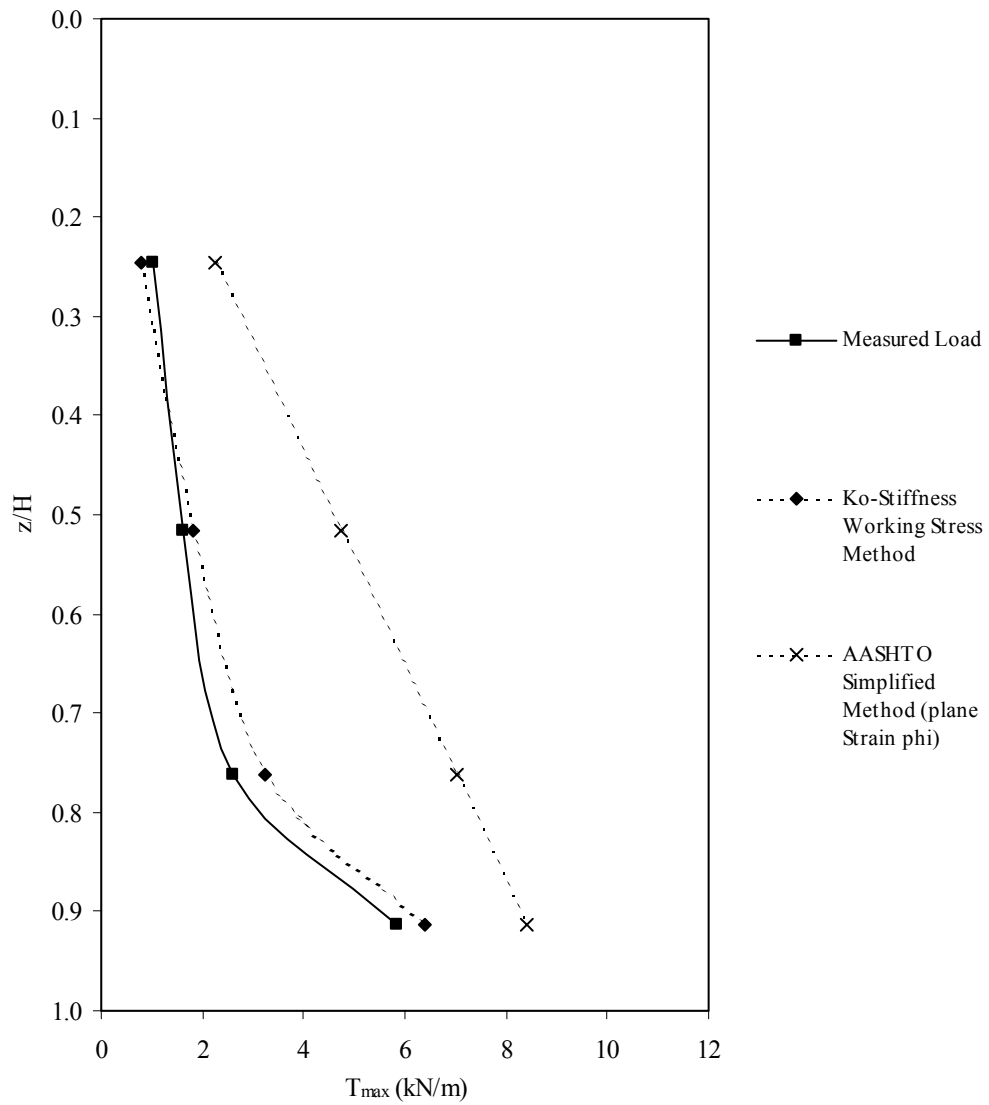
Figure A.8. Measured and predicted T_{max} as a function of depth below wall top for Wall GW16 (no surcharge).
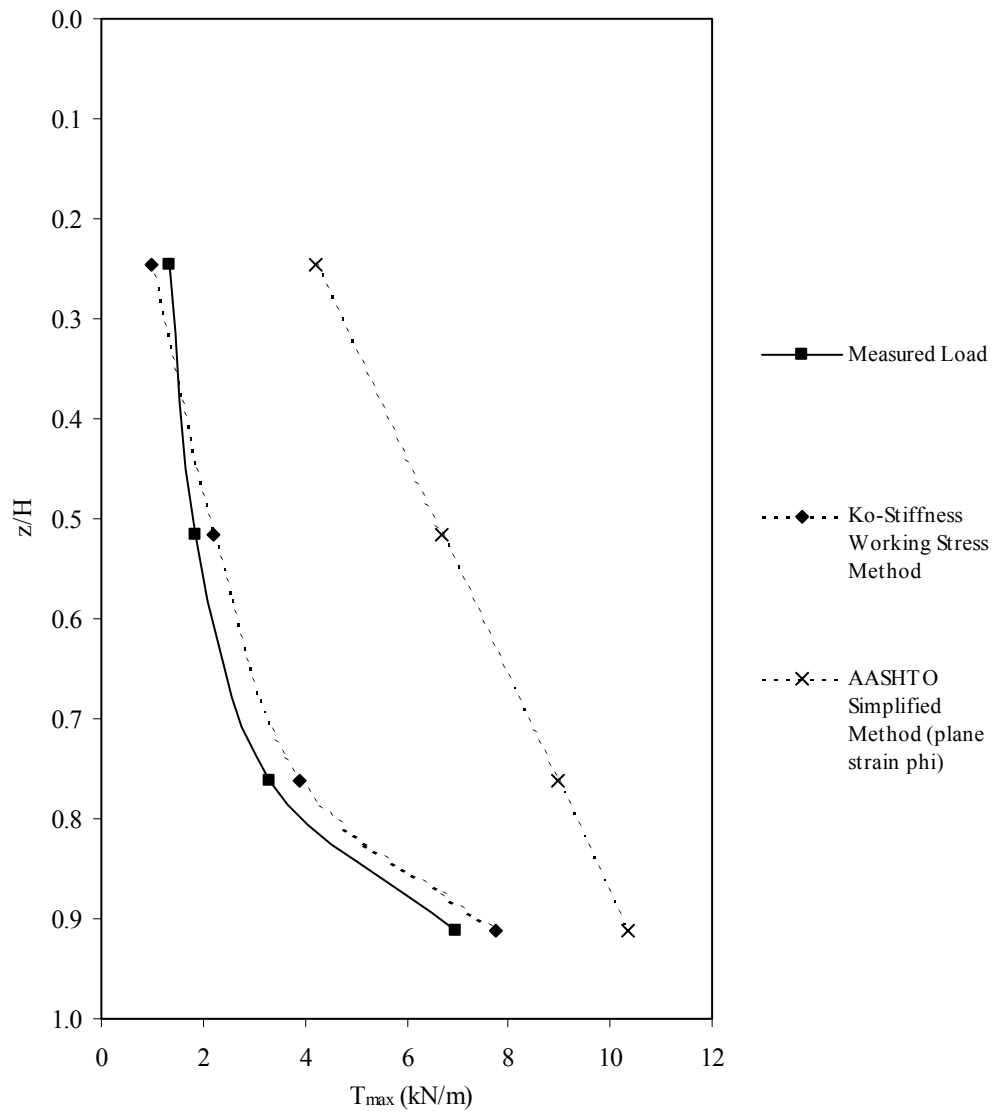
Figure A9. Measured and predicted T_{max} as a function of depth below wall top for Wall GW16 (with surcharge).
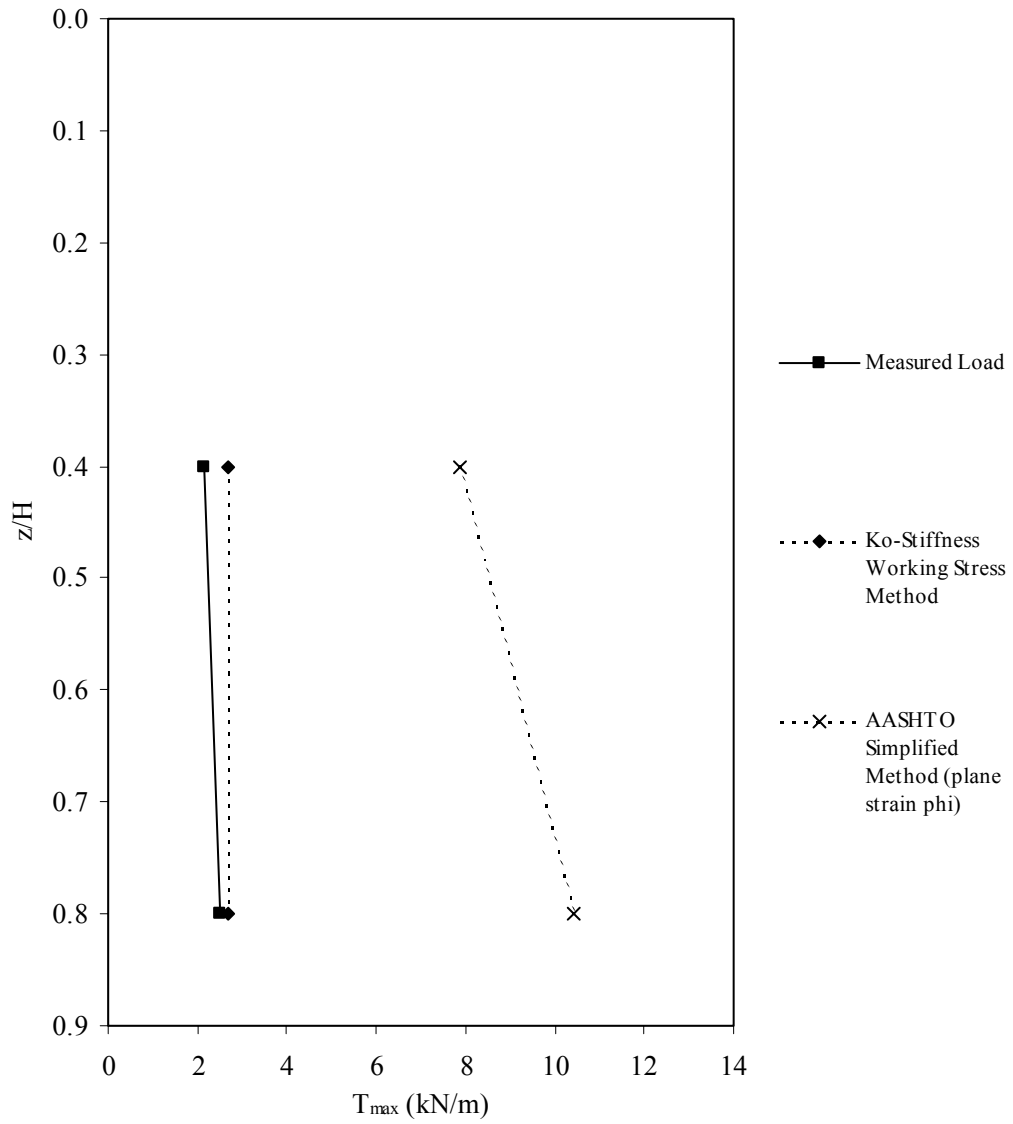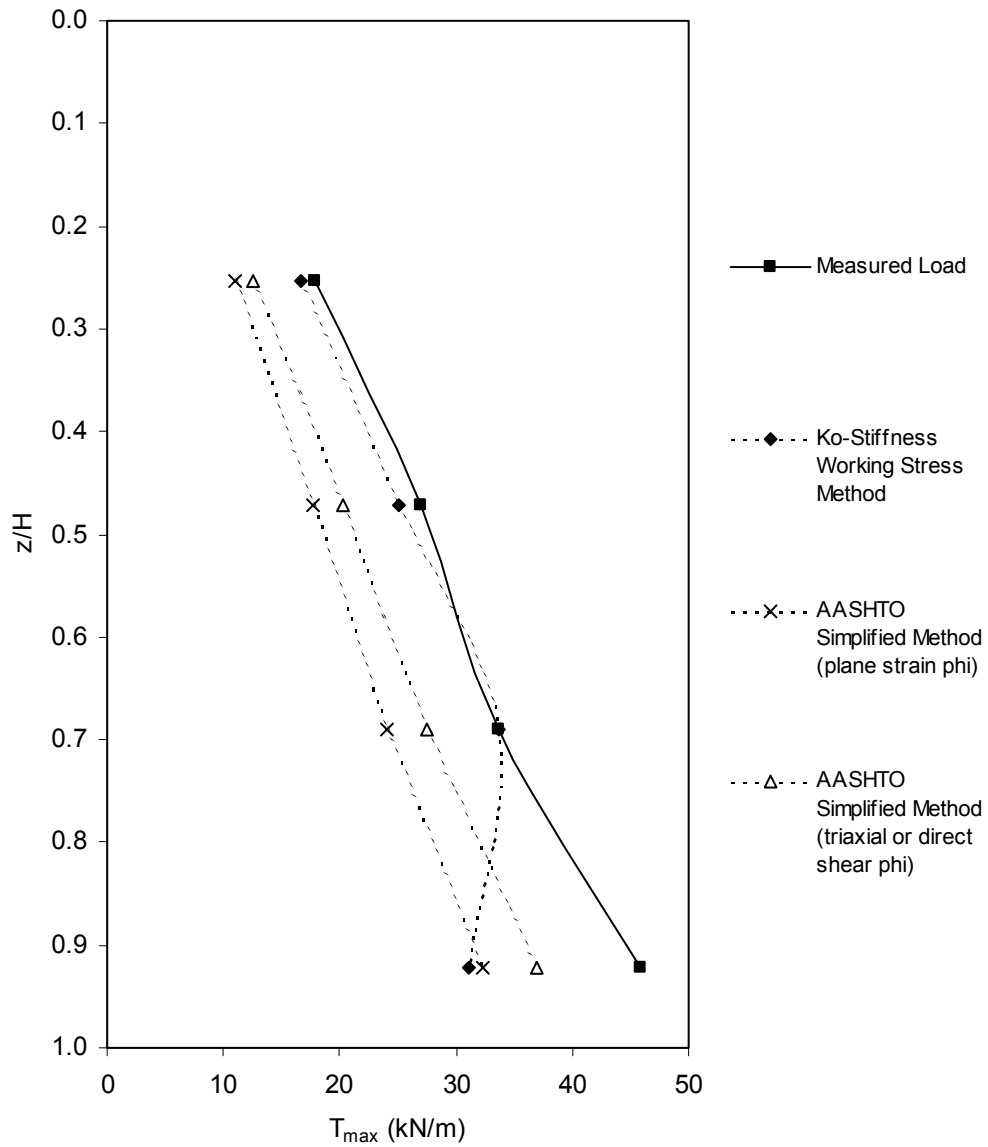
Figure A10. Measured and predicted T_{max} as a function of depth below wall top for Wall GW18.
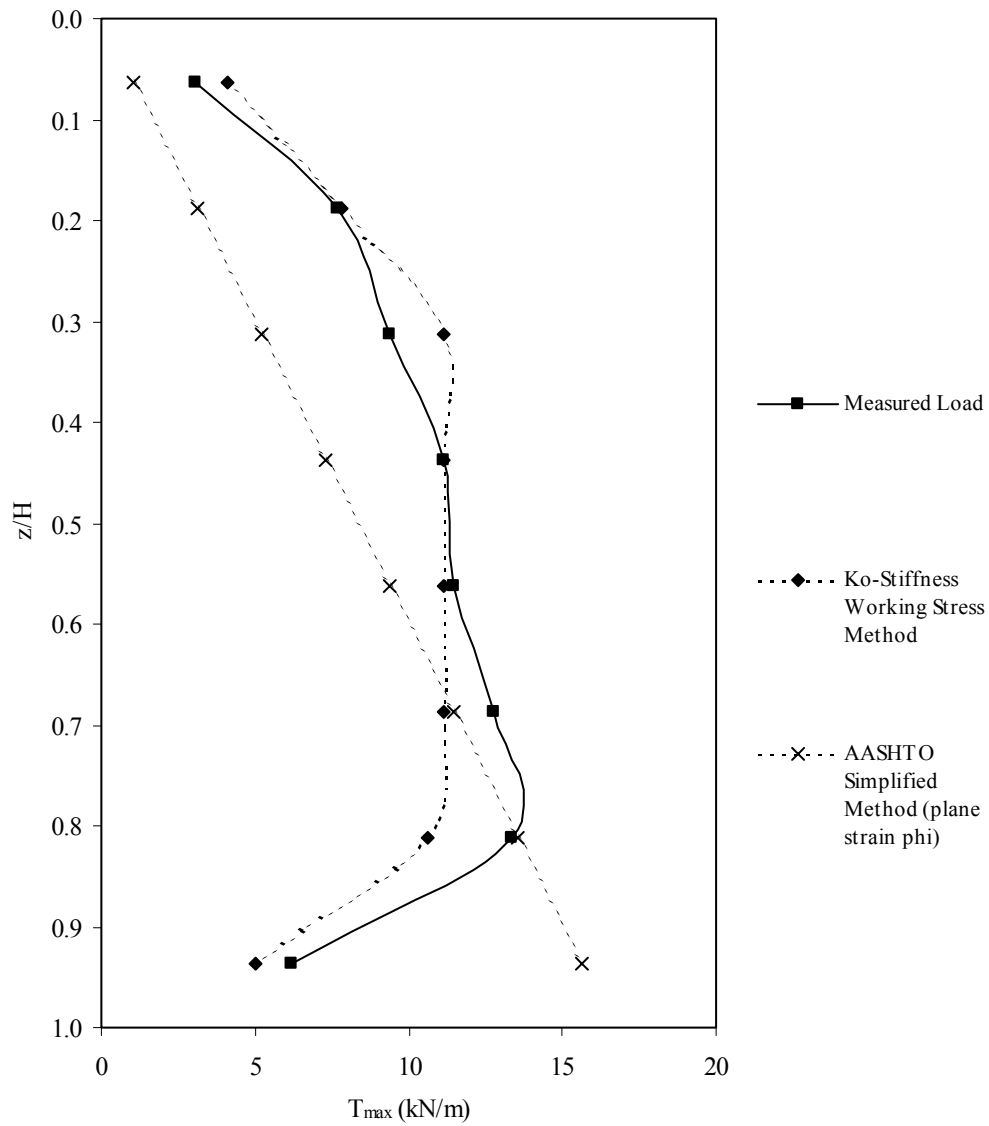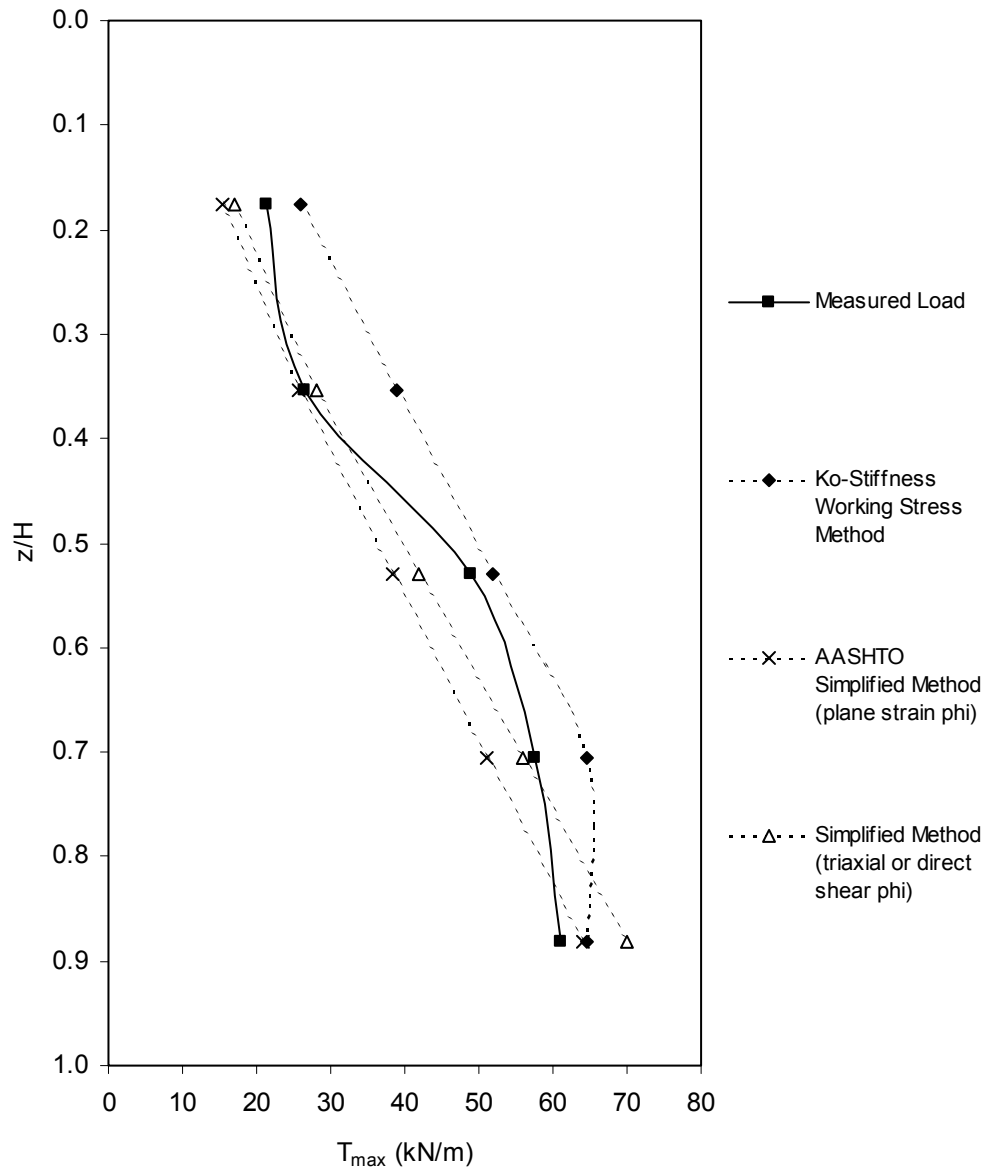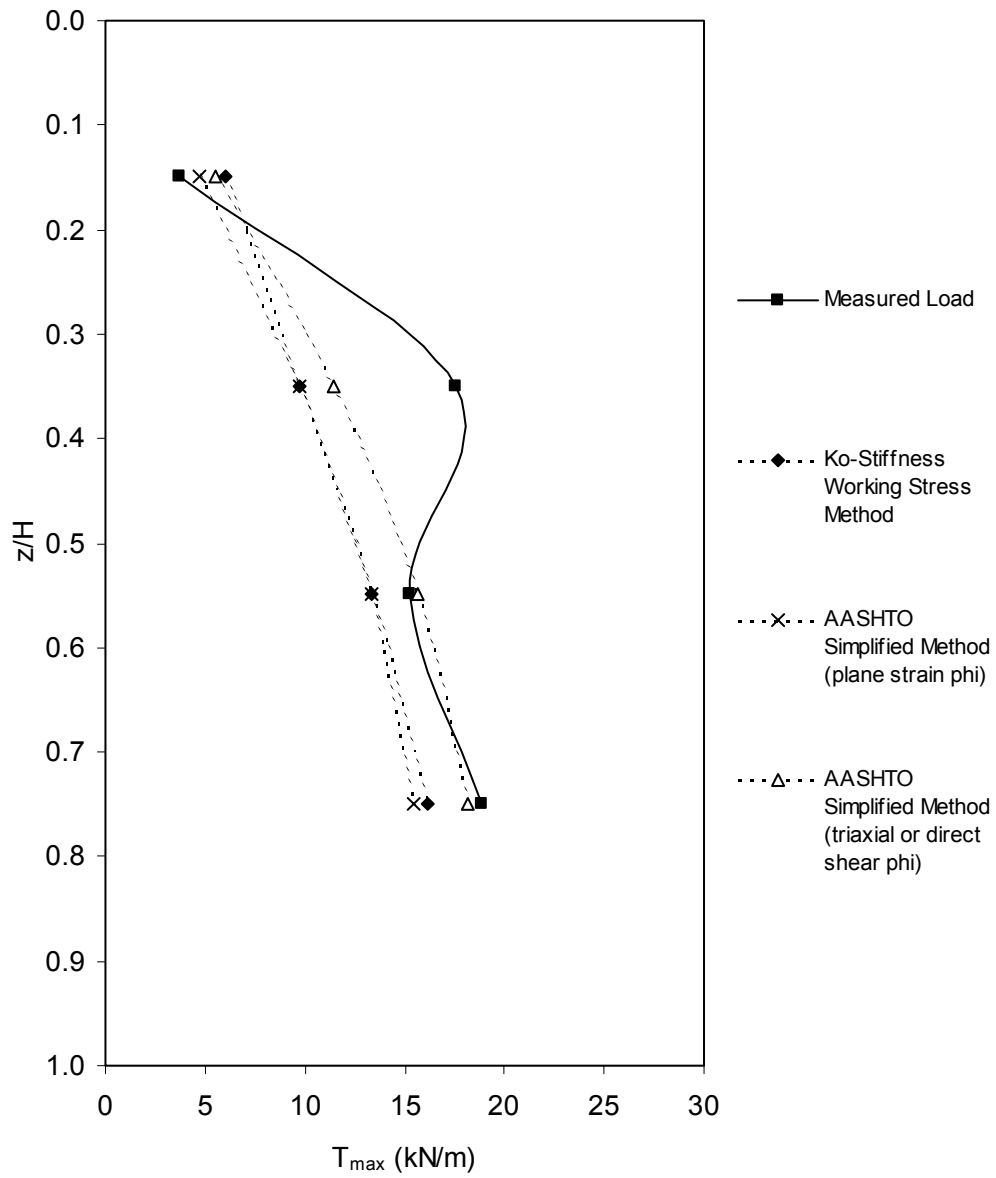
Figure A11. Measured and predicted T_{max} as a function of depth below wall top for Wall GW19.
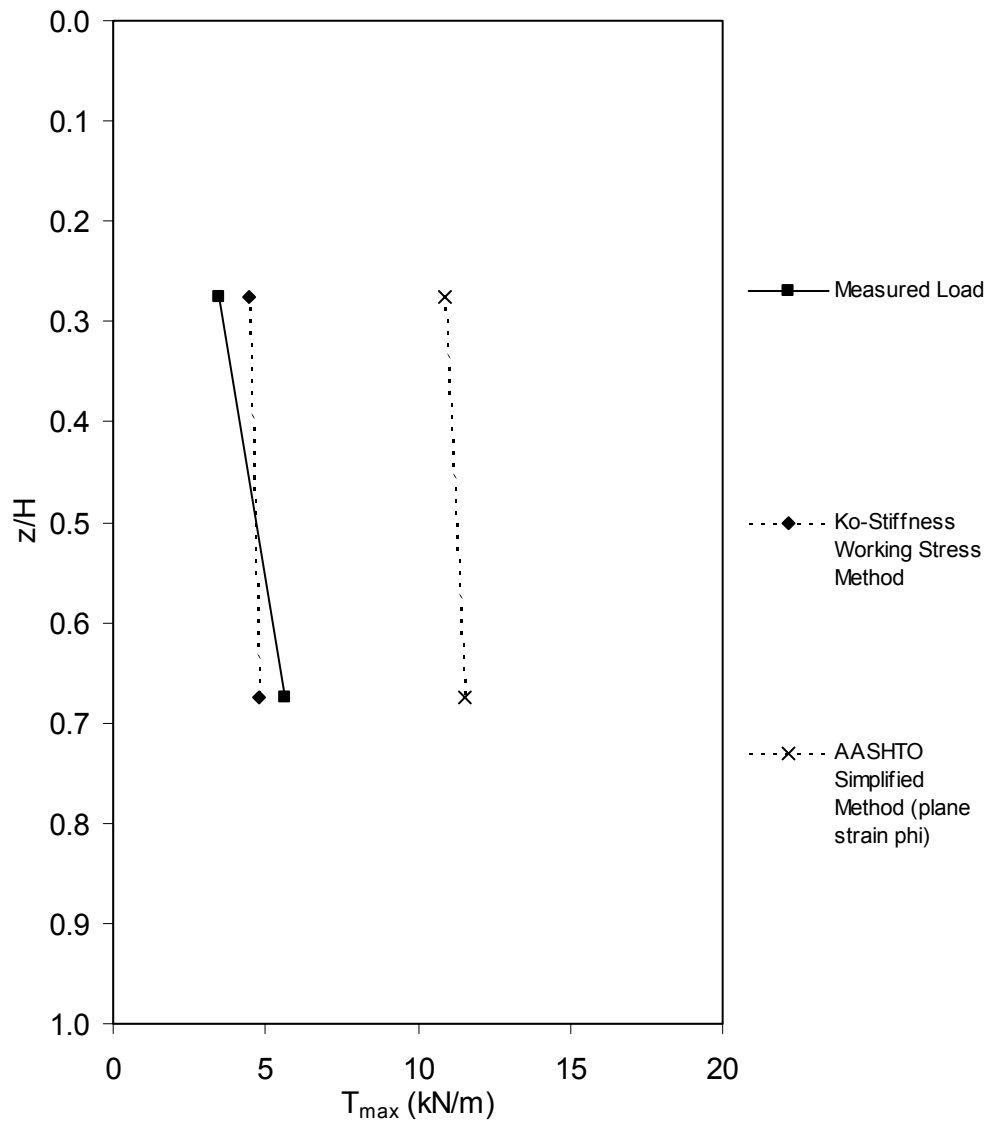
Figure A12. Measured and predicted T_{max} as a function of depth below wall top for Wall GW20, HDPE Section (with surcharge).
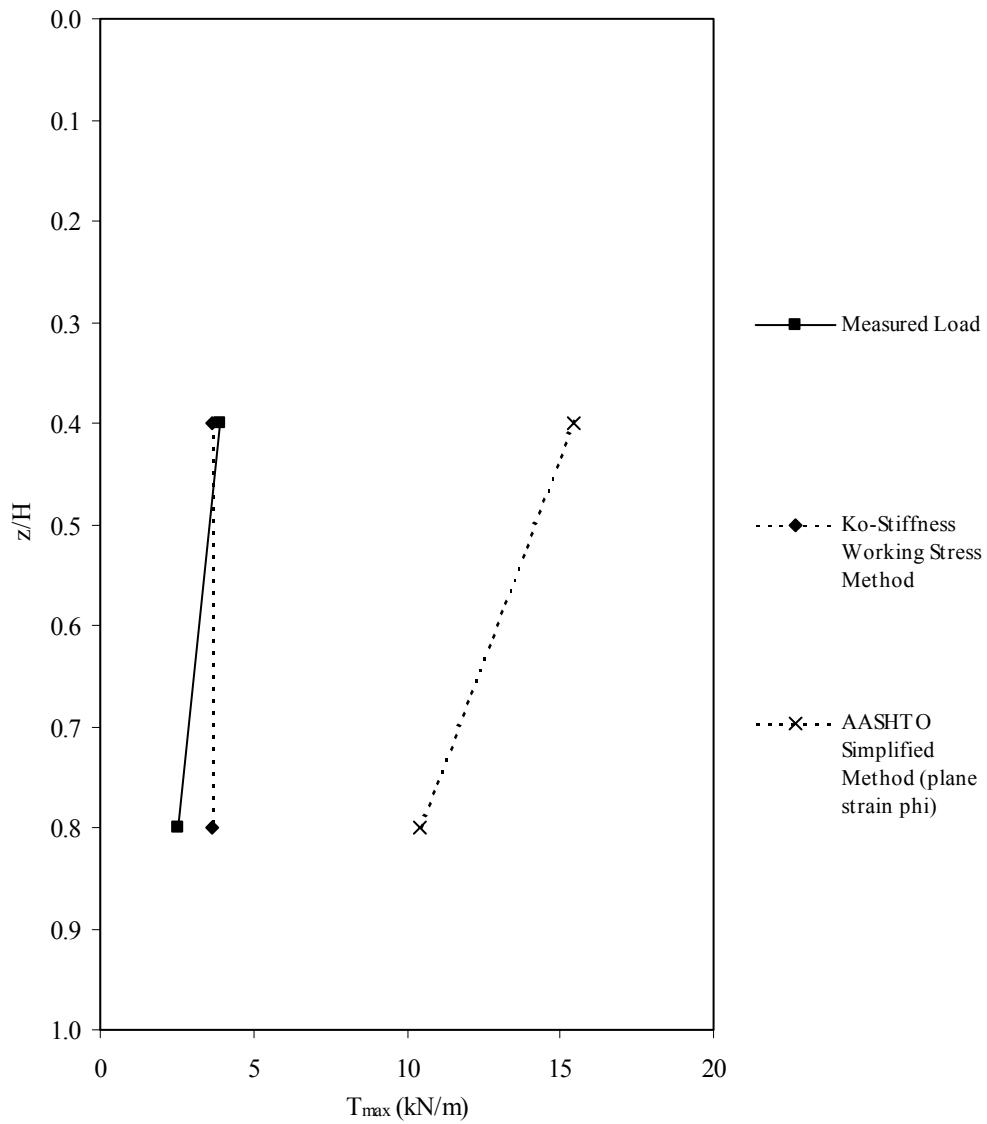
Figure A13. Measured and predicted T_{max} as a function of depth below wall top for Wall GW20, PP Section (with surcharge).
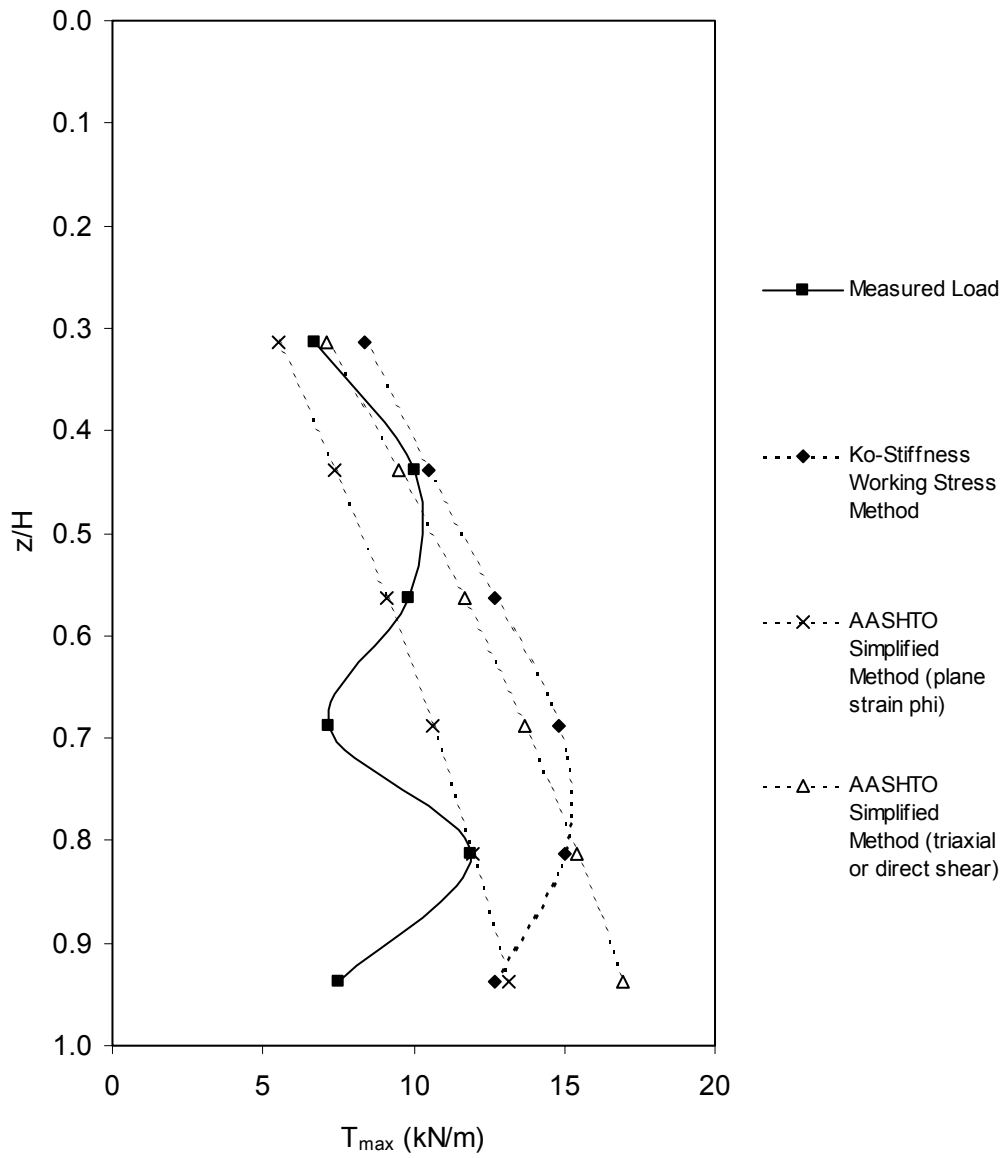
Figure A14. Measured and predicted T_{max} as a function of depth below wall top for Wall SS1.
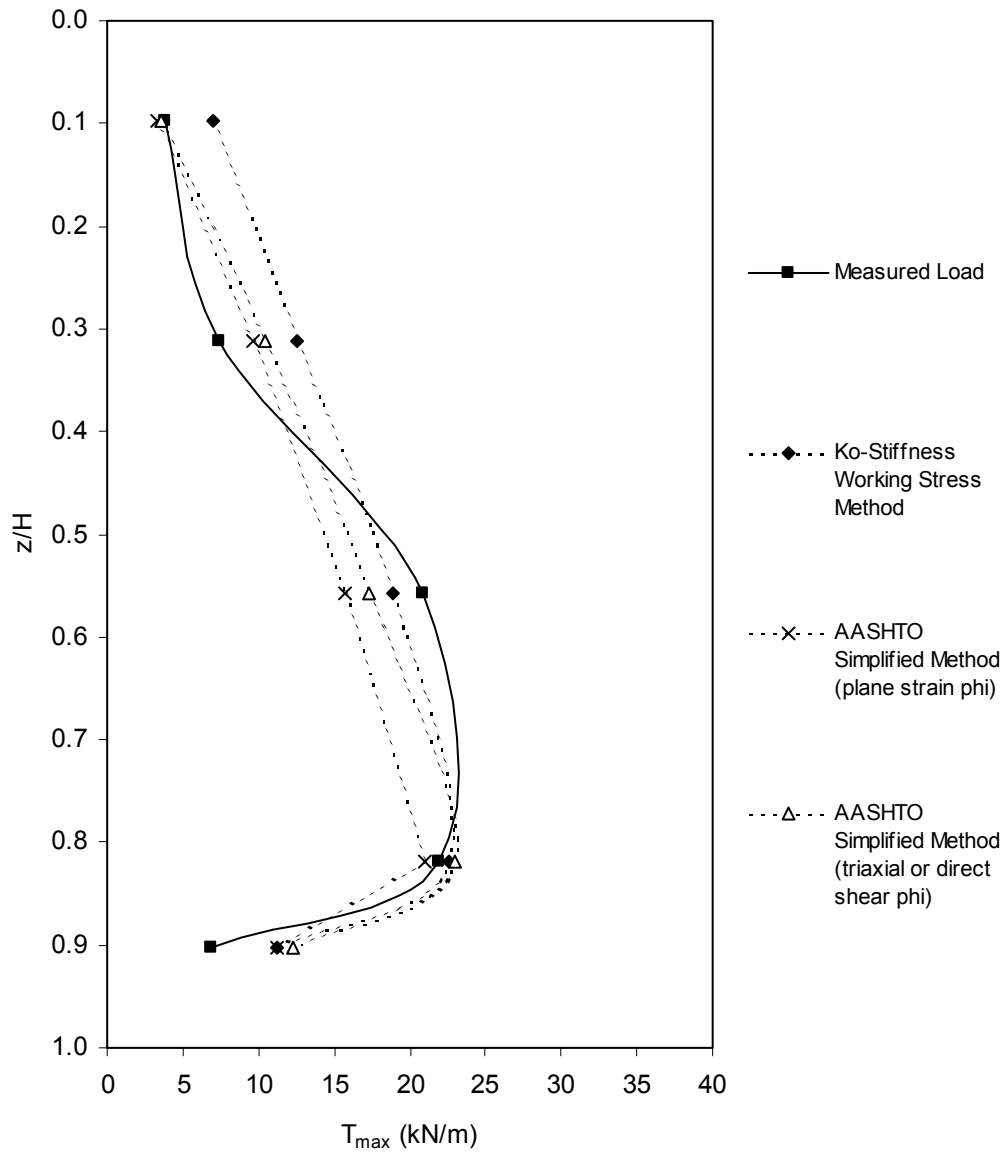
Figure A15. Measured and predicted T_{max} as a function of depth below wall top for Wall SS2.
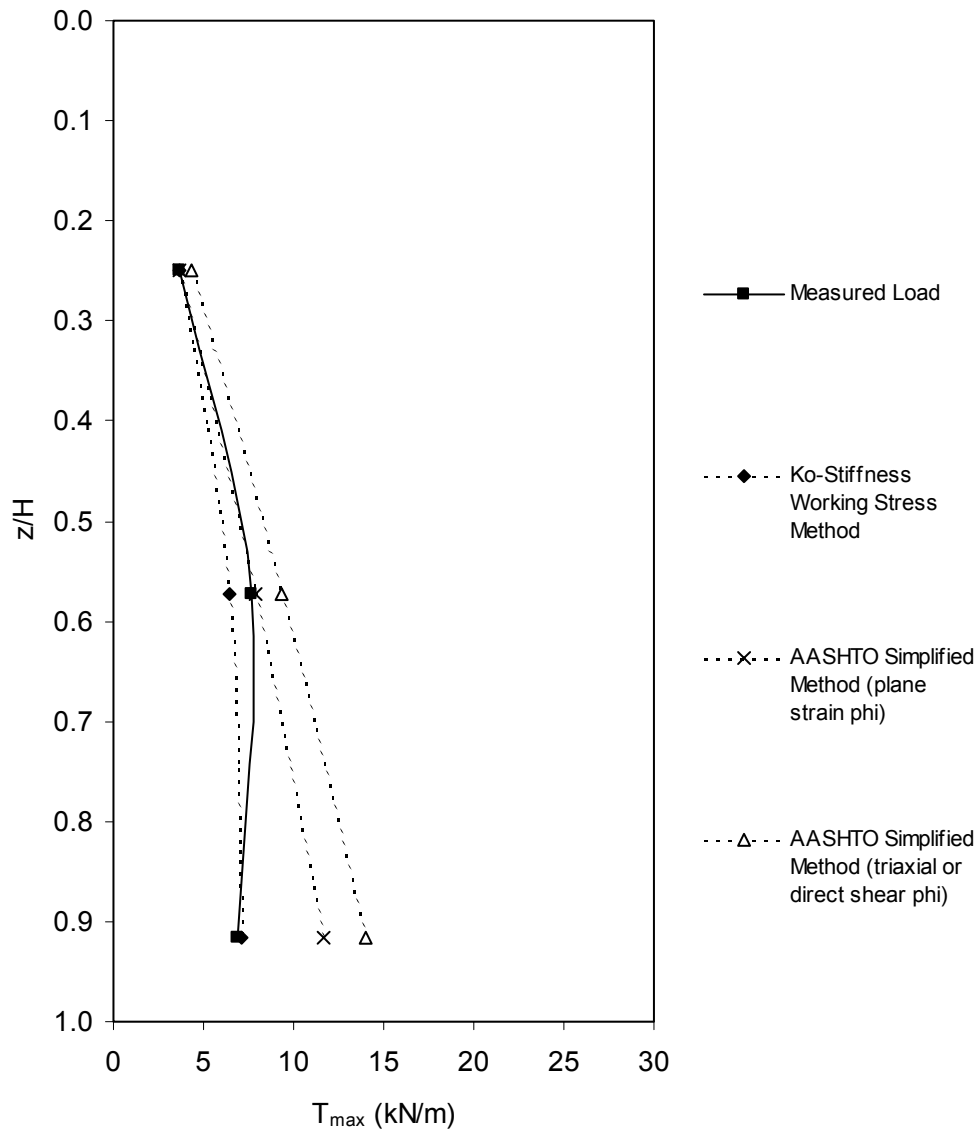
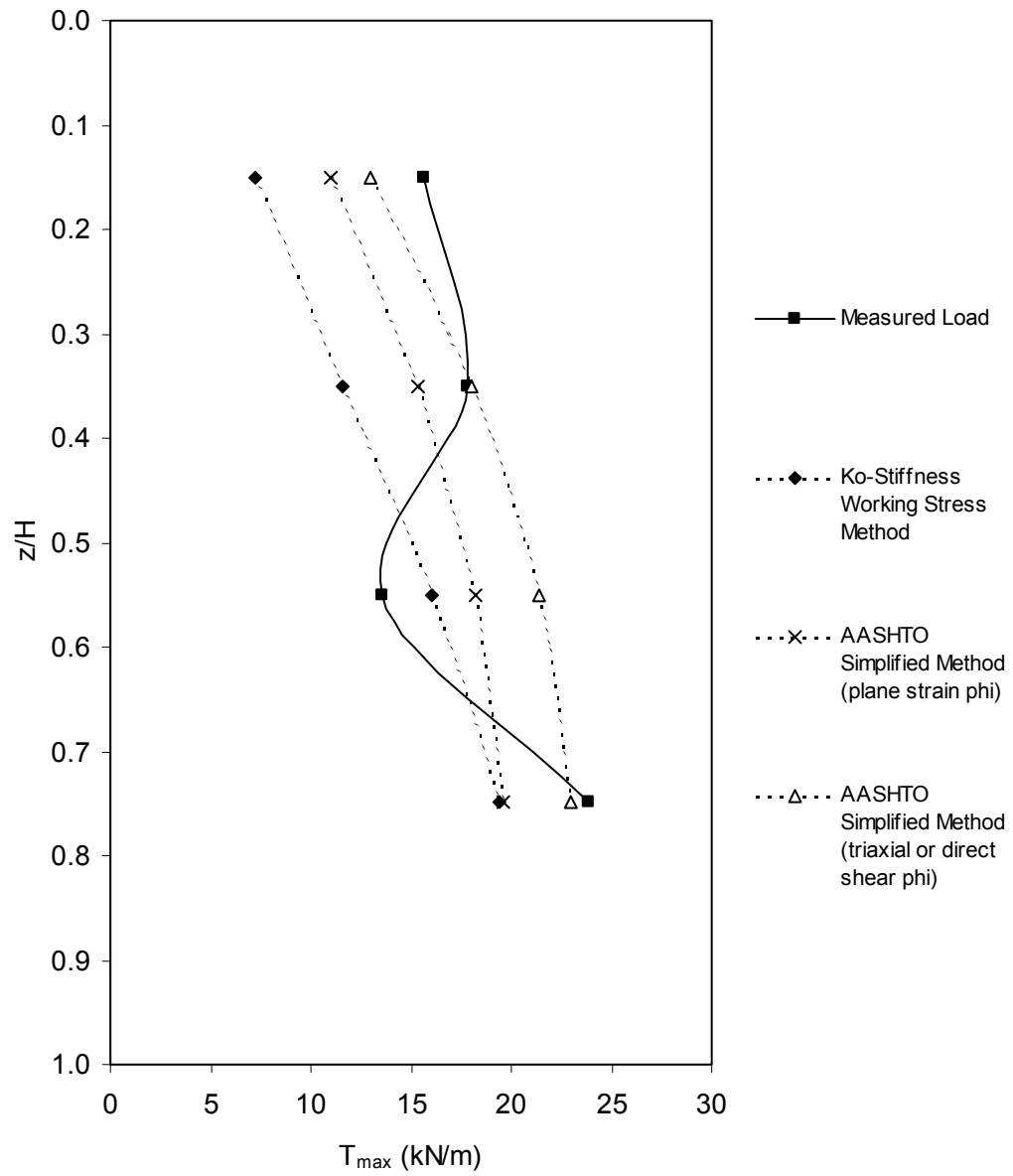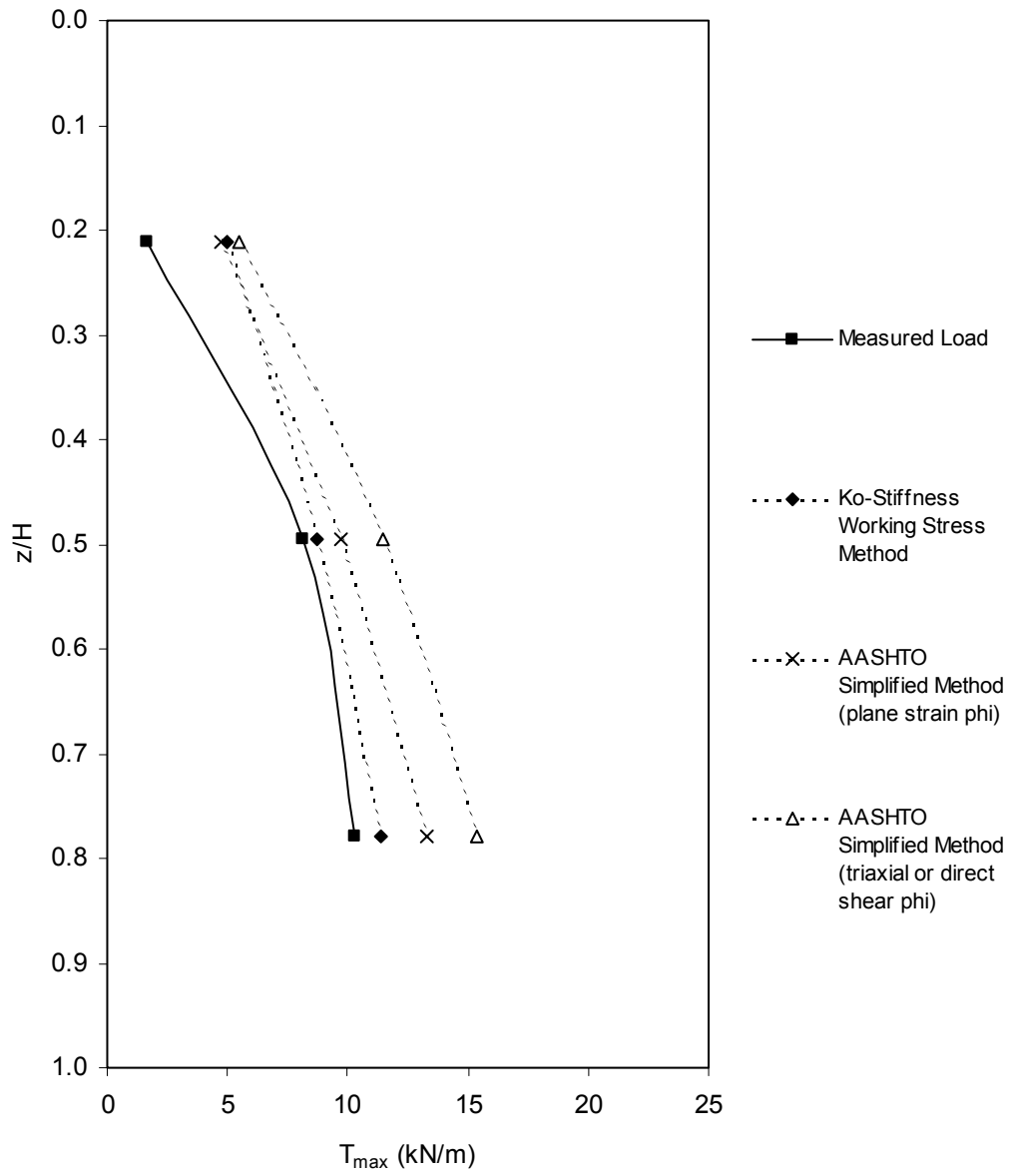Figure A16. Measured and predicted T_{max} as a function of depth below wall top for Wall SS3 (no surcharge).
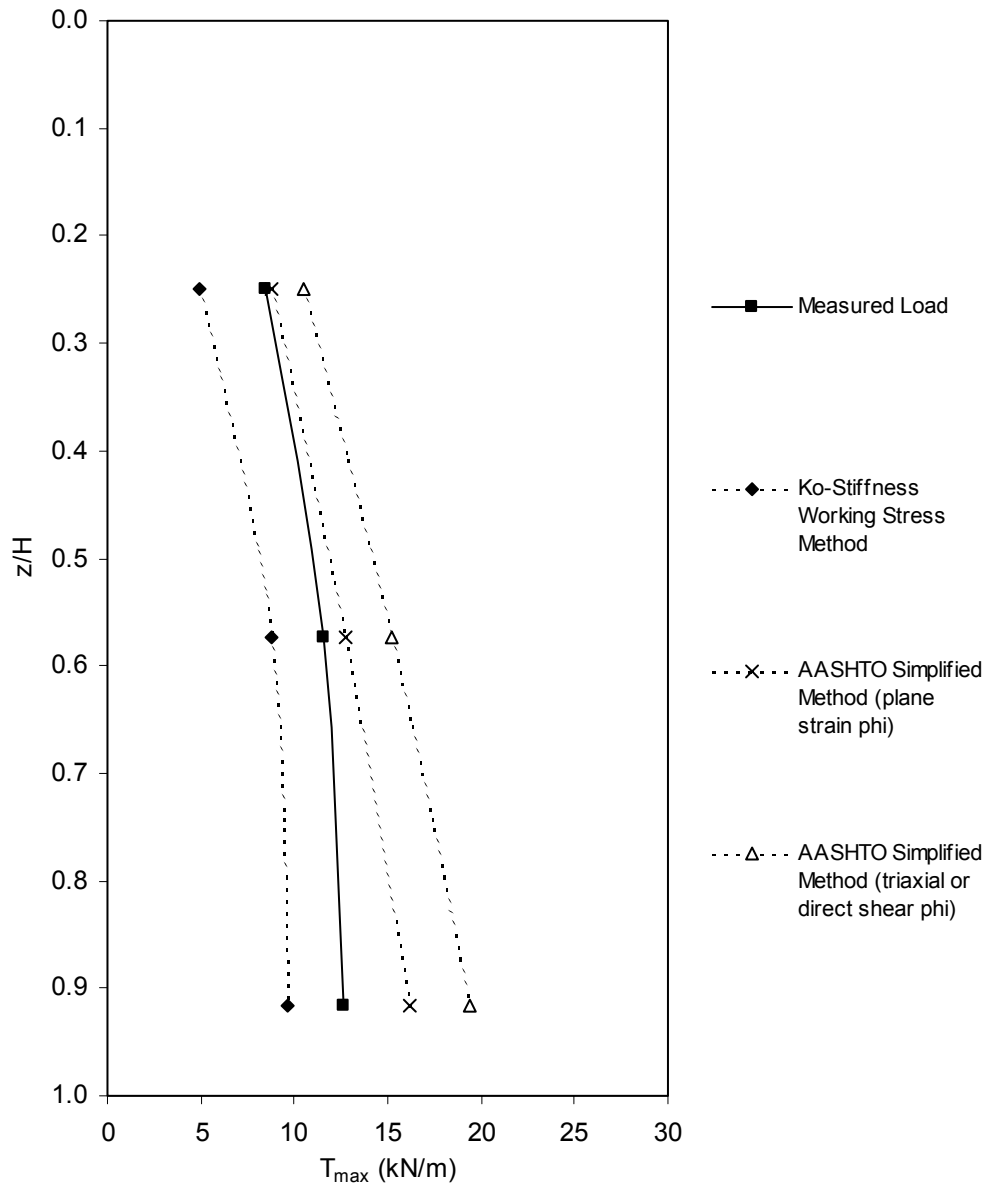
Figure A17. Measured and predicted T_{max} as a function of depth below wall top for Wall SS3 (24 kPa surcharge).
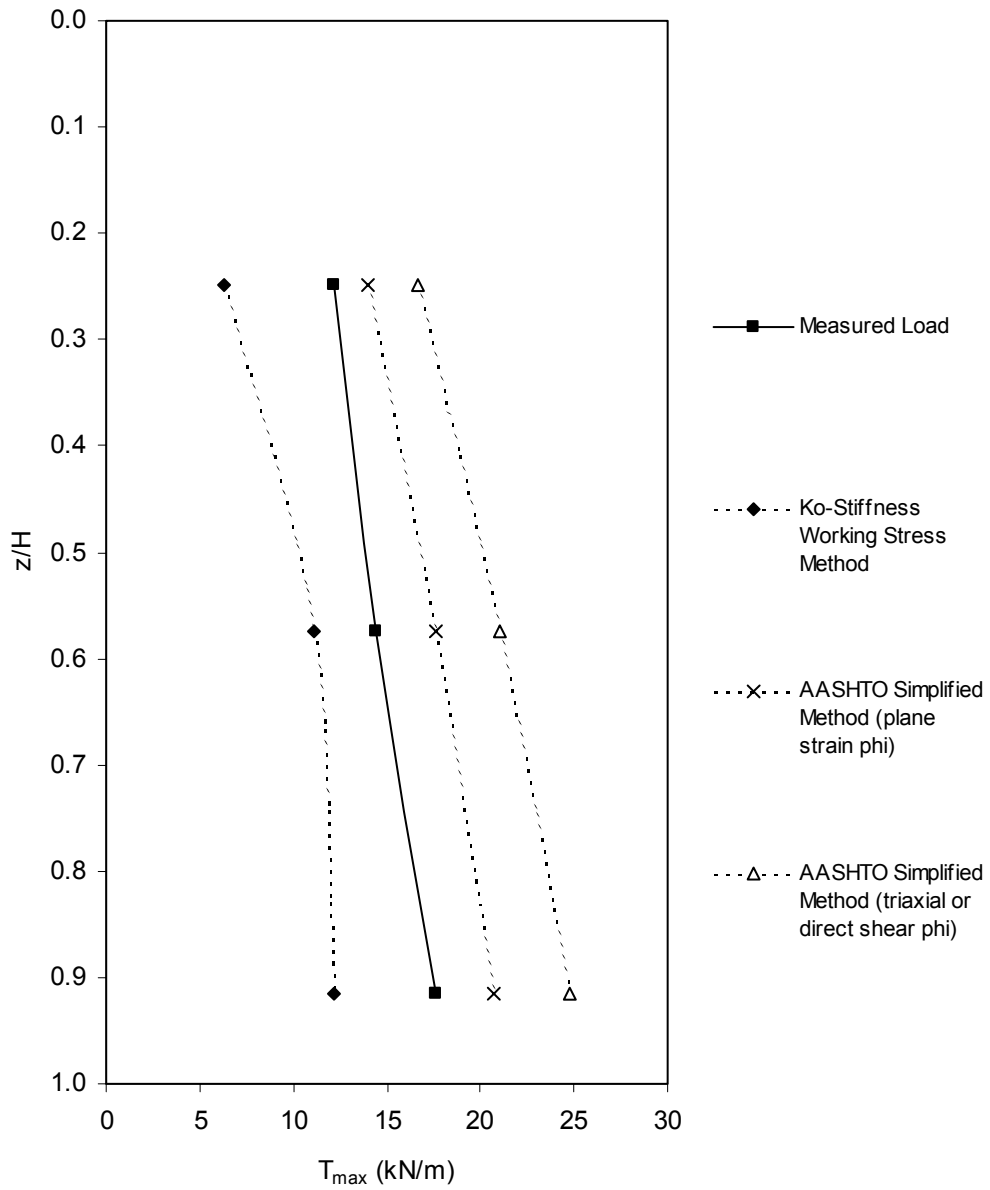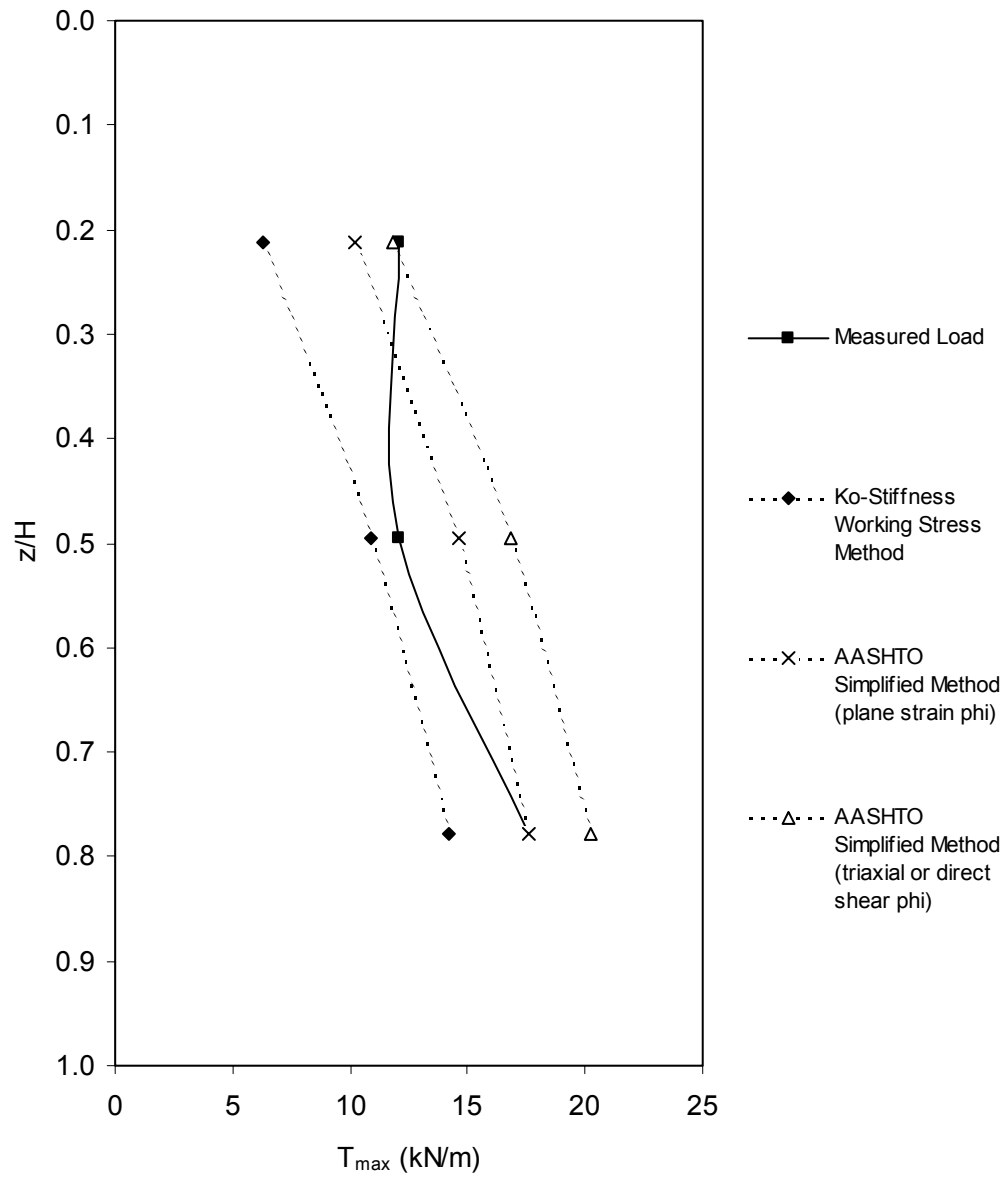
Figure A18. Measured and predicted T_{max} as a function of depth below wall top for Wall SS3 (48 kPa surcharge).
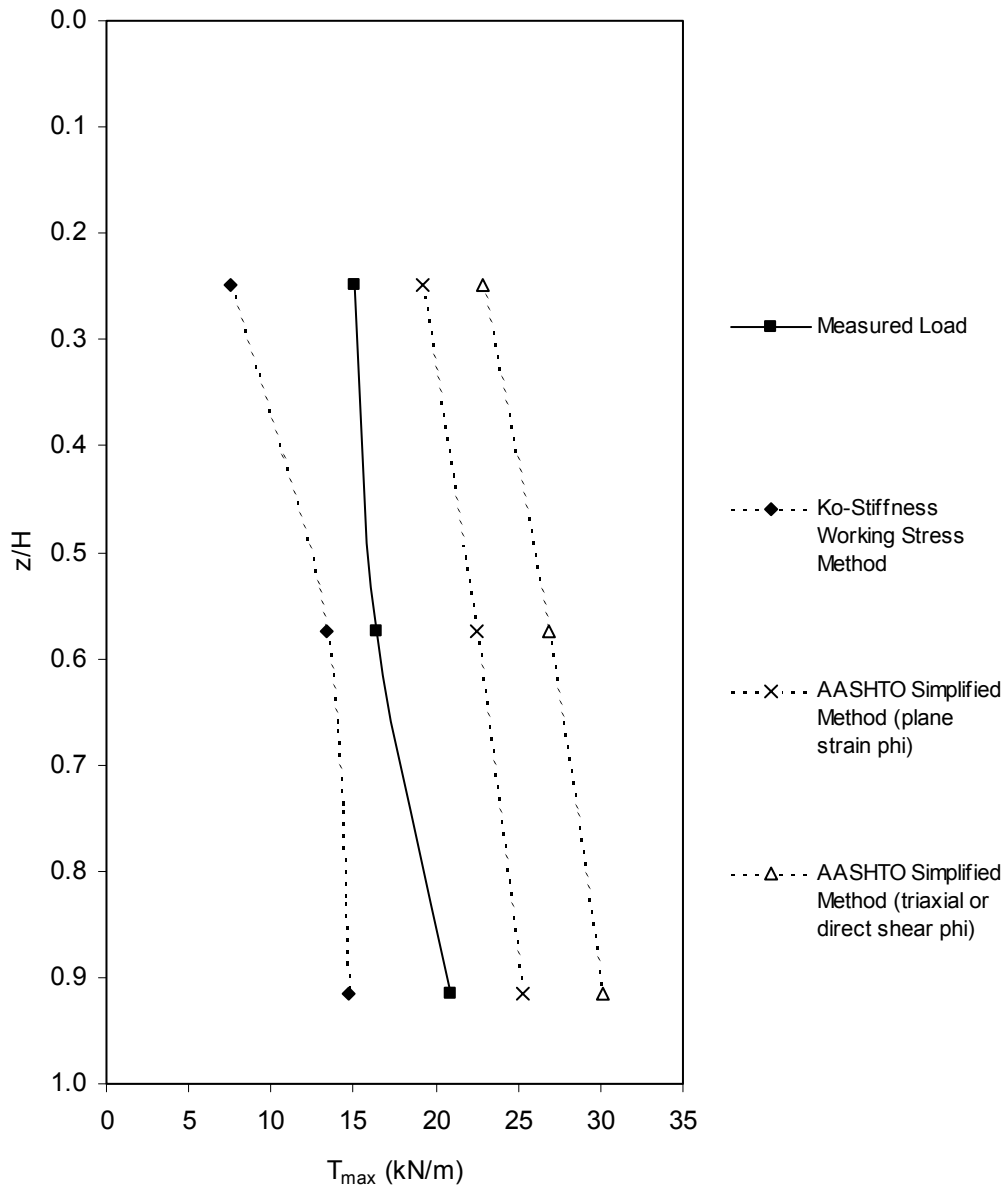
Figure A19. Measured and predicted T_{max} as a function of depth below wall top for Wall SS3 (72 kPa surcharge).
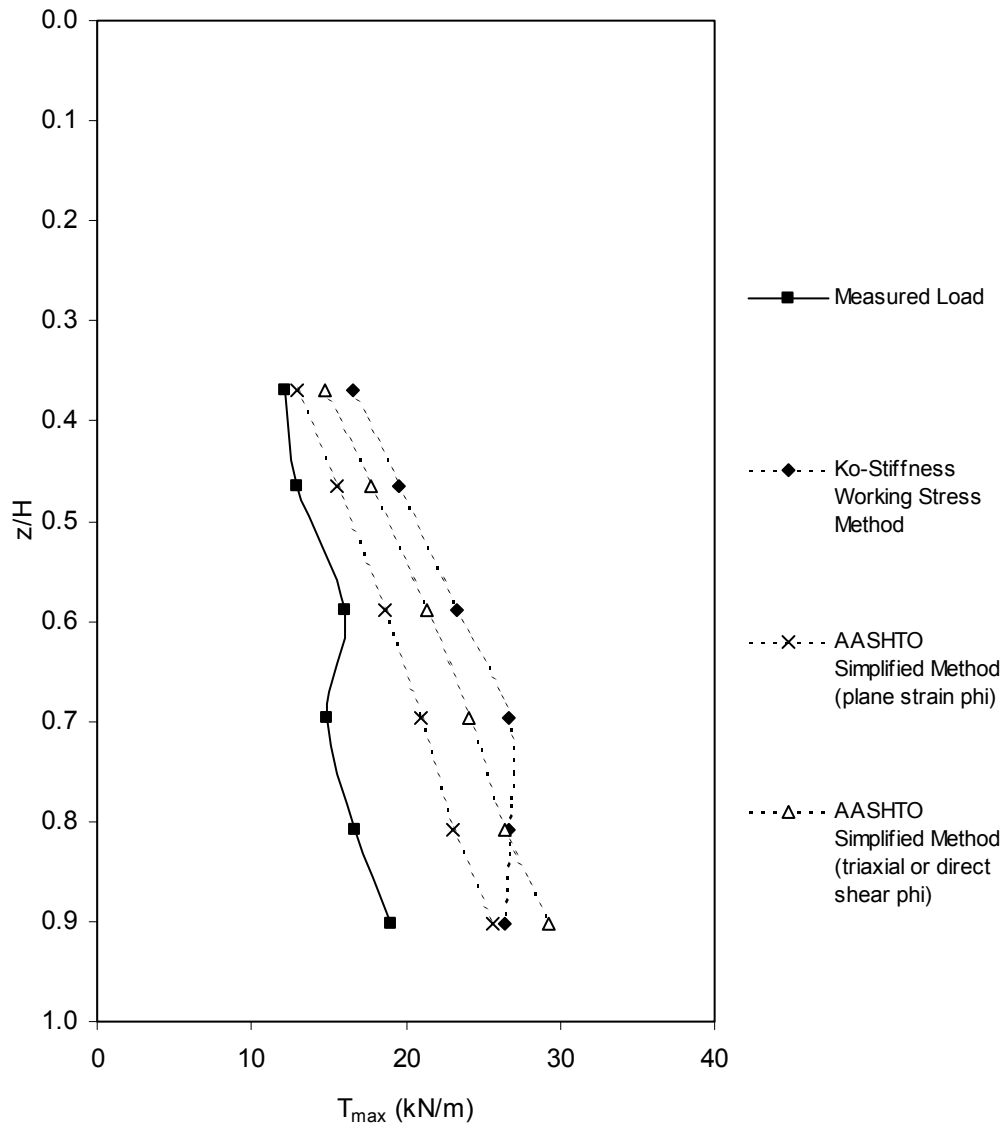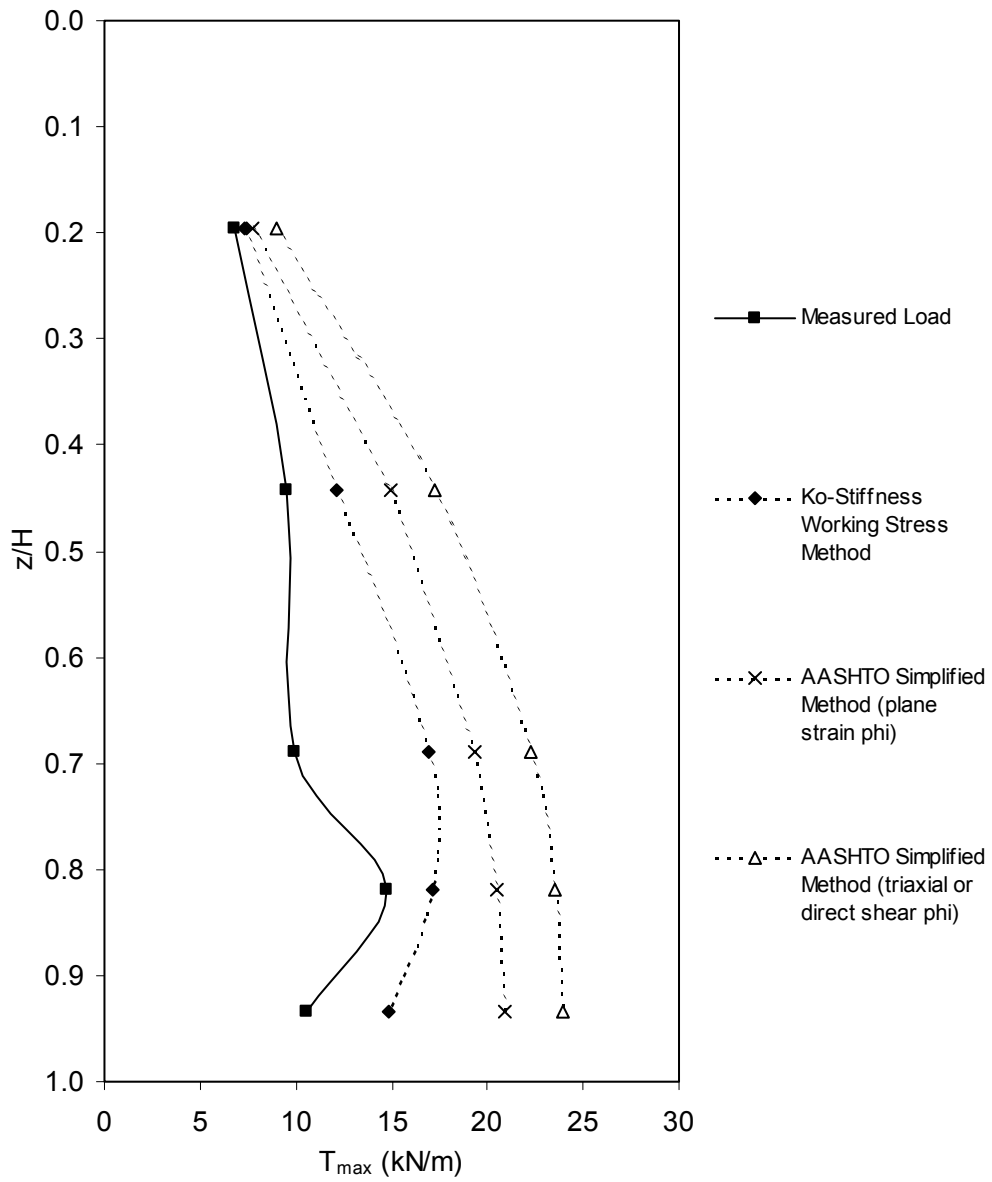
Figure A20. Measured and predicted T_{max} as a function of depth below wall top for Wall SS4.
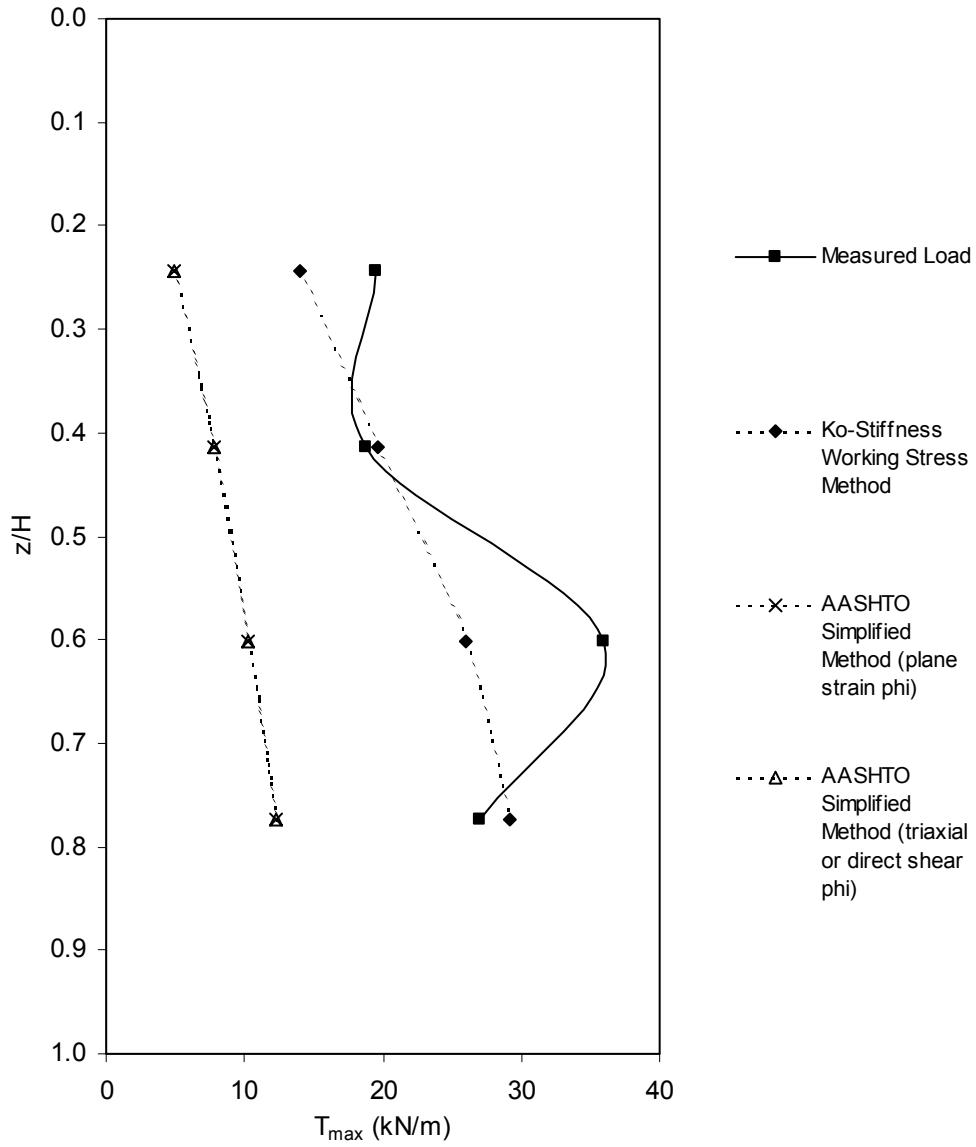
Figure A21. Measured and predicted T_{max} as a function of depth below wall top for Wall SS5.

Figure A22. Measured and predicted T_{max} as a function of depth below wall top for Wall SS6 (Section A).

Figure A22. Measured and predicted T_{max} as a function of depth below wall top for Wall SS6 (Section B).

Figure A23. Measured and predicted T_{max} as a function of depth below wall top for Wall SS10.

Figure A24. Measured and predicted T_{max} as a function of depth below wall top for Wall SS11.

Figure A25. Measured and predicted T_{max} as a function of depth below wall top for Wall SS12 (no surcharge).

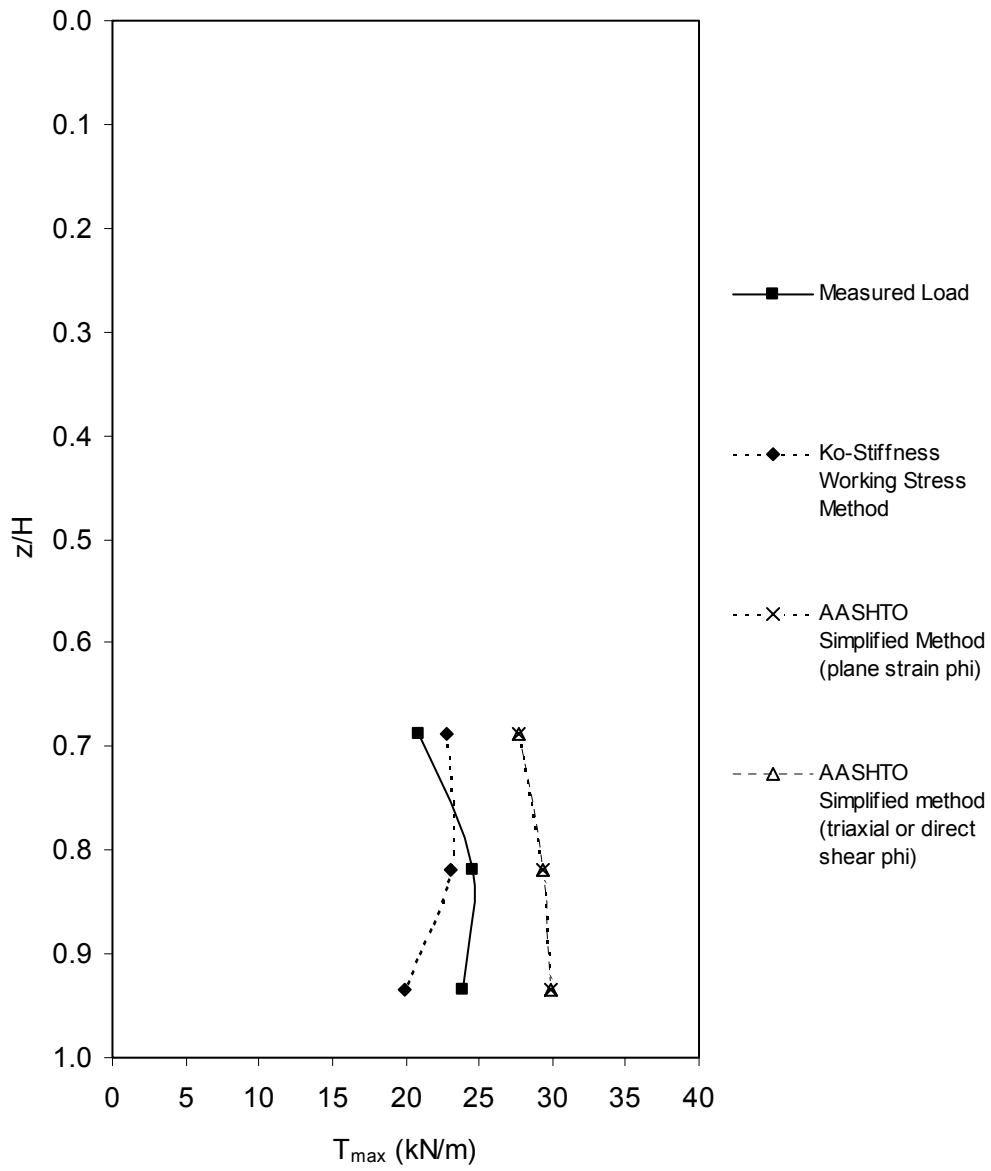Figure A26. Measured and predicted T_{max} as a function of depth below wall top for Wall SS12 (with surcharge).

Figure A27. Measured and predicted T_{max} as a function of depth below wall top for Wall SS14.

Figure A28. Measured and predicted T_{max} as a function of depth below wall top for Wall SS15.

Figure A29. Measured and predicted T_{max} as a function of depth below wall top for Wall BM1 (no surcharge).

Figure A30. Measured and predicted T_{max} as a function of depth below wall top for Wall BM1 (with surcharge).

Figure A31. Measured and predicted T_{max} as a function of depth below wall top for Wall BM2 (no surcharge).

Figure A32. Measured and predicted T_{max} as a function of depth below wall top for Wall BM2 (with surcharge).

Figure A33. Measured and predicted T_{max} as a function of depth below wall top for Wall BM3.

Figure A34. Measured and predicted T_{max} as a function of depth below wall top for Wall BM4.

APPENDIX B: LONG-TERM CREEP DATA FOR GEOSYNTHETIC WALLS
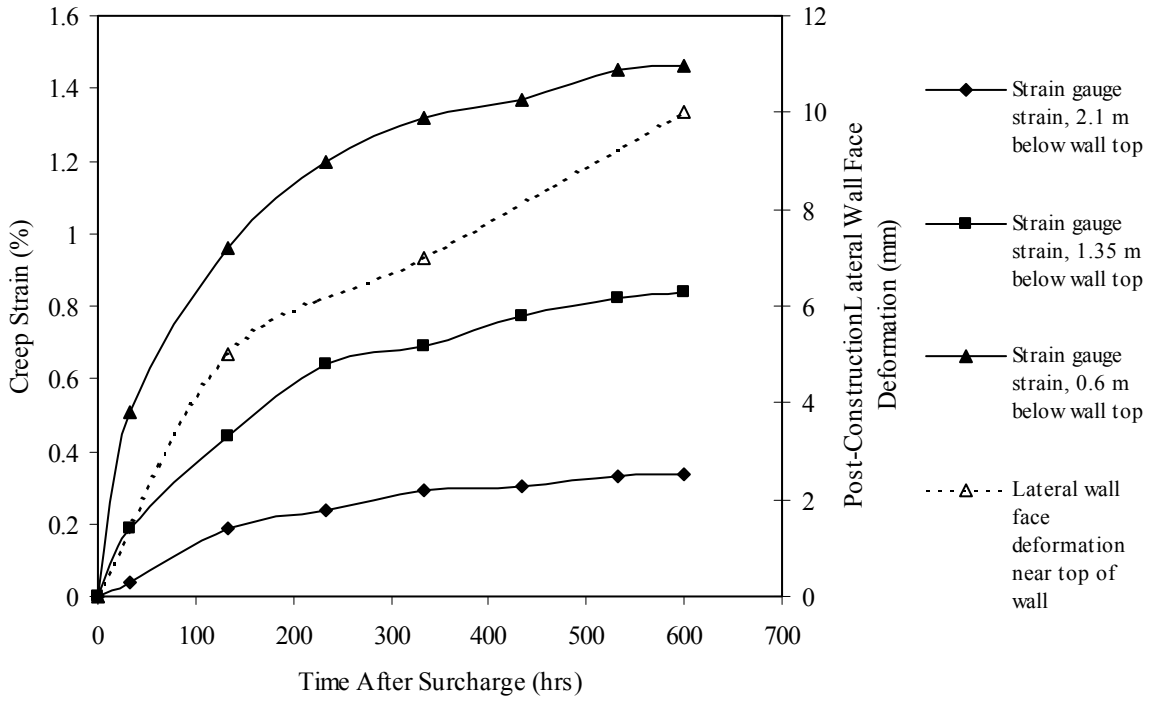
Figure B1. Comparison of measured creep strains and deformations for Wall GW11.
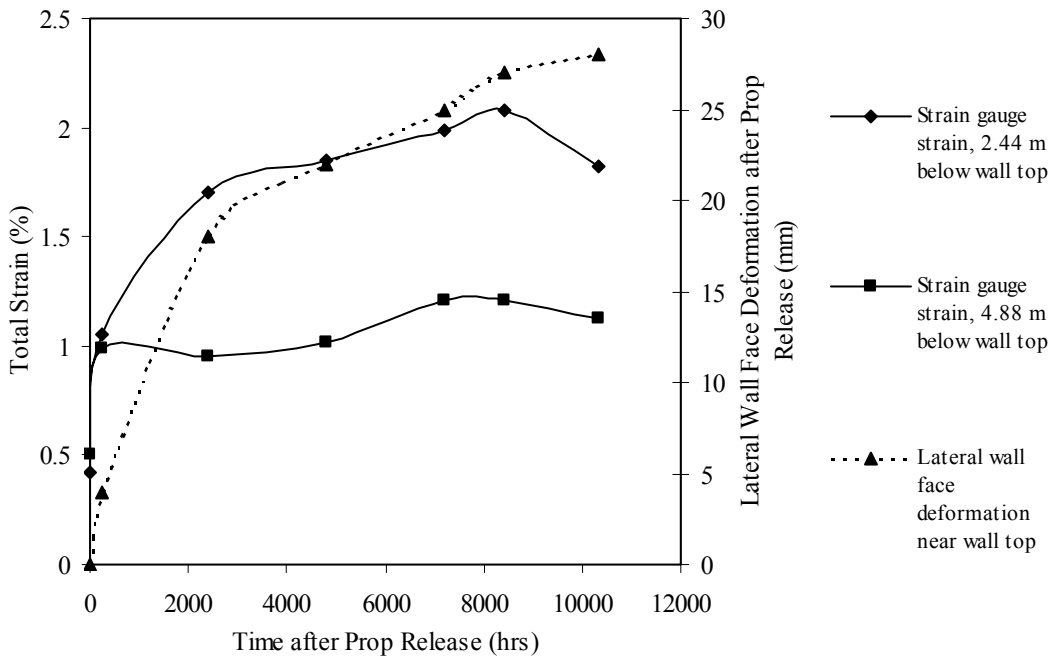
Figure B2. Comparison of measured creep strains and deformations for Wall GW18.
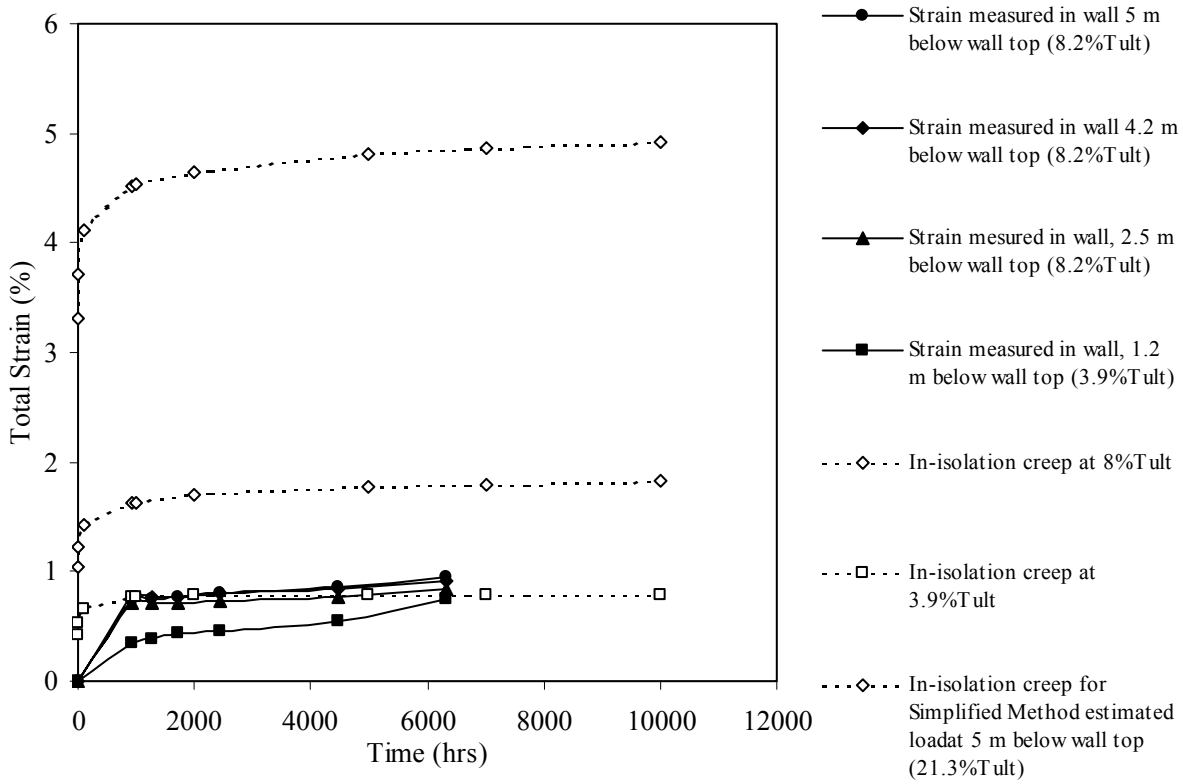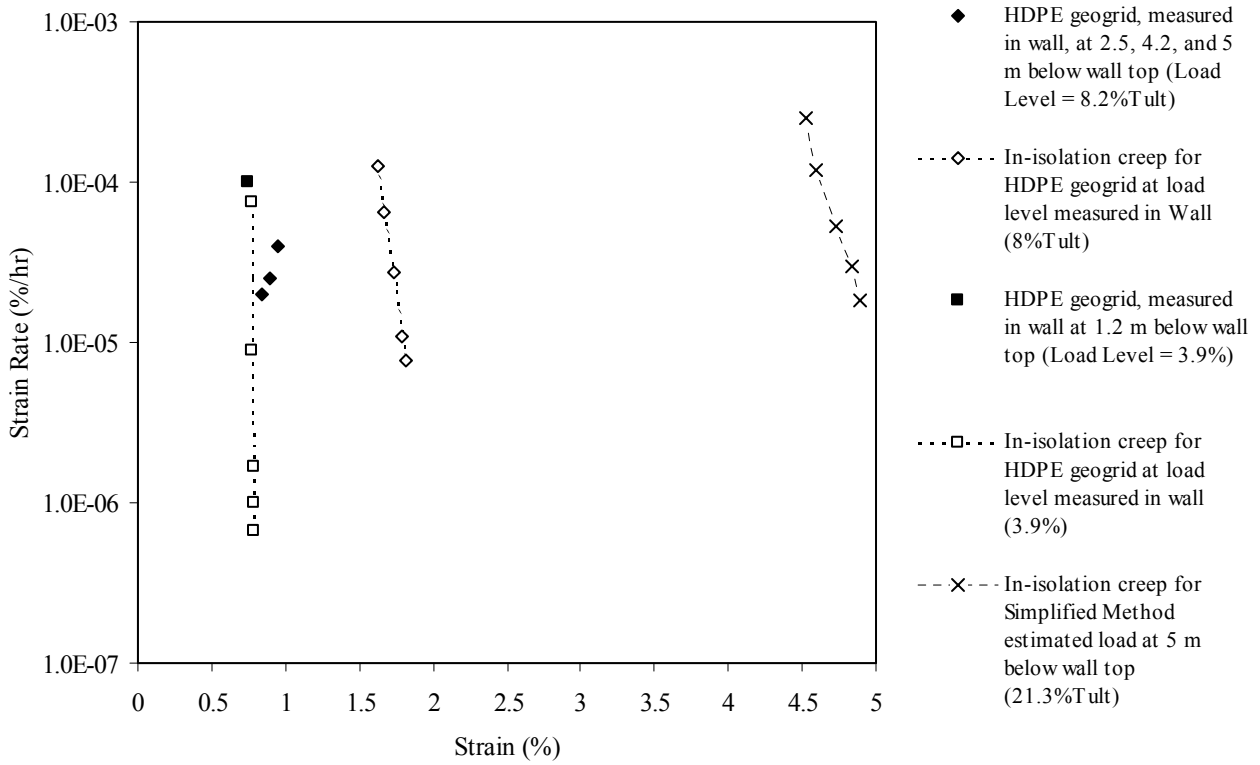
Figure B3. Wall GW8 long-term strains.
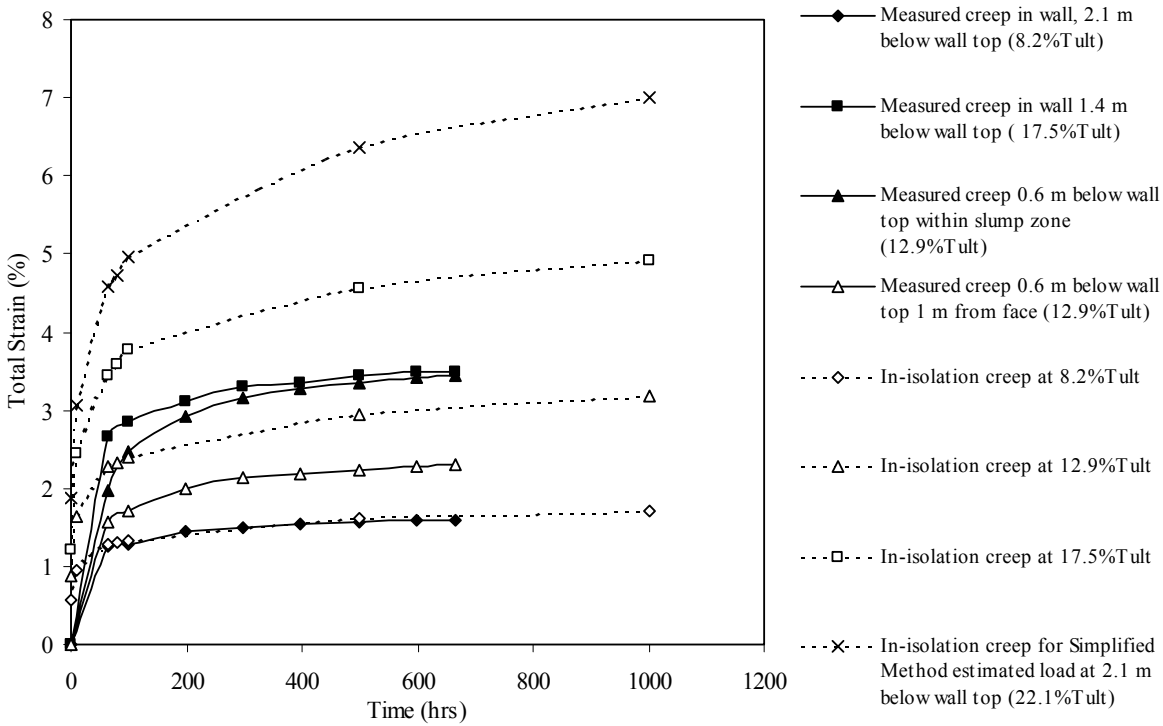
Figure B4. Long-term strain for Wall GW11.

Figure B5. Sherby-Dorn plot for Wall GW8—in-isolation vs. measured in wall.
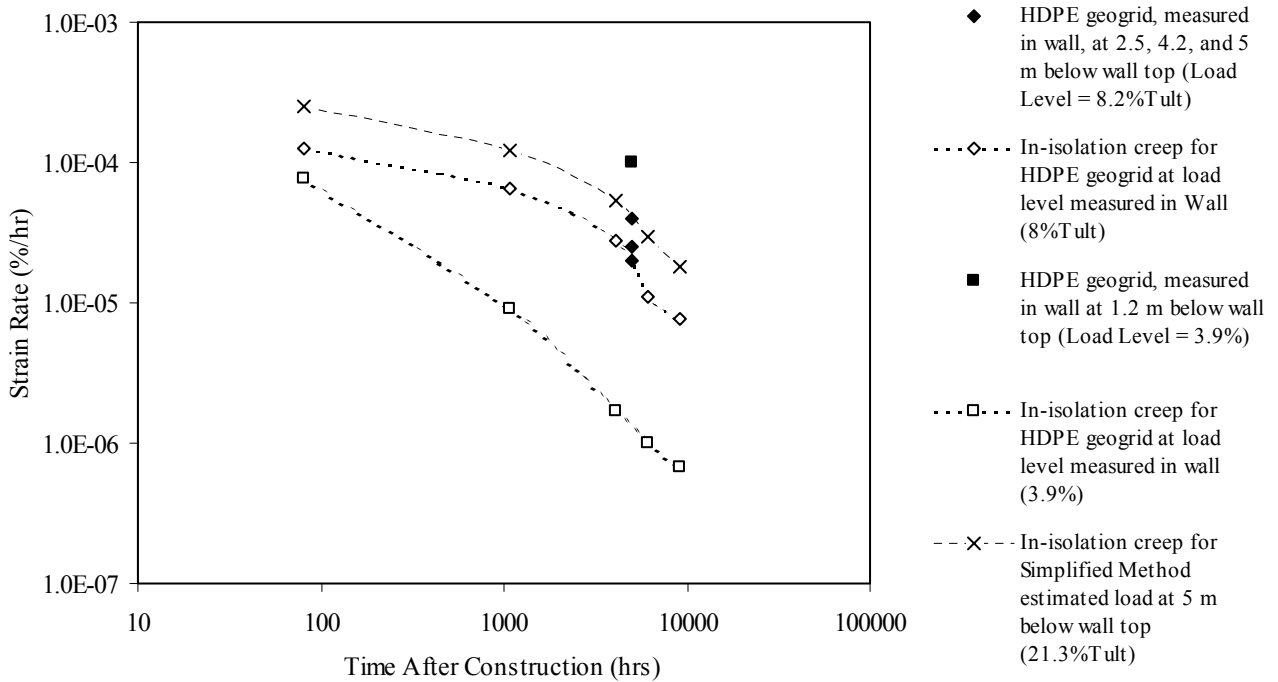

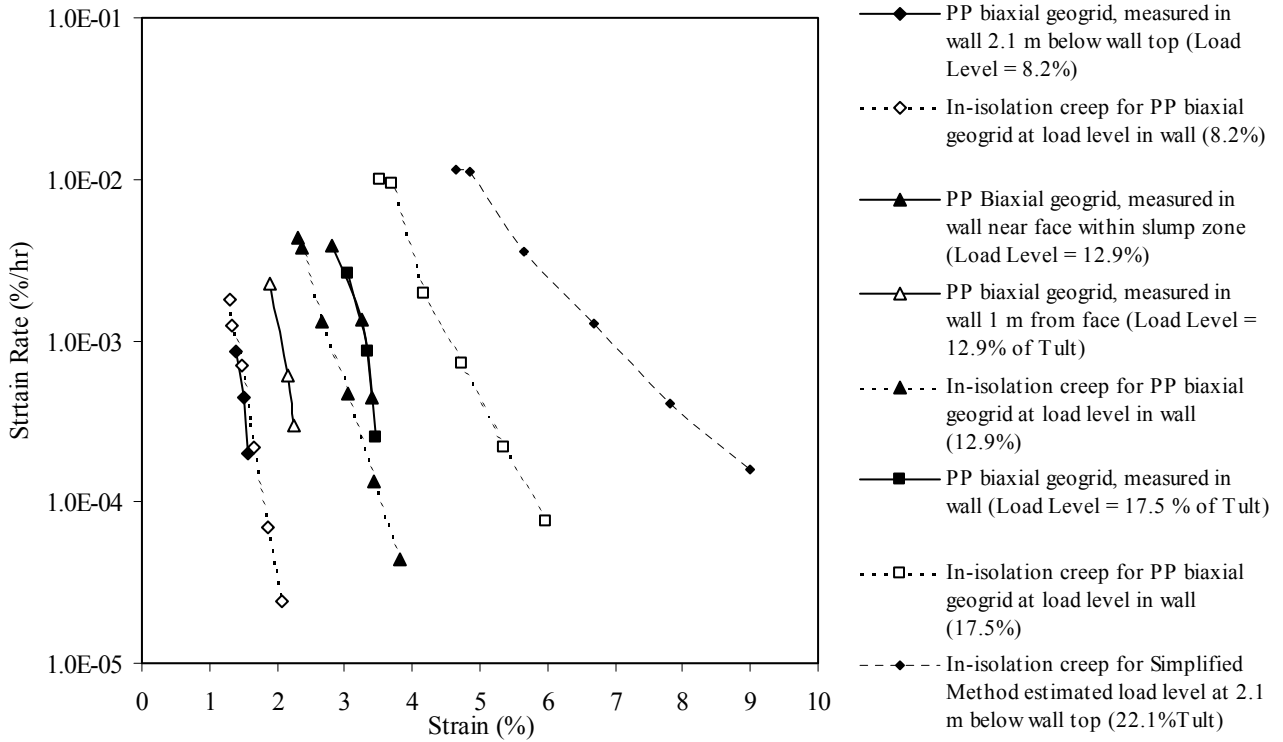Figure B6. Strain rate vs. time plot for Wall GW8—in-isolation vs. measured in wall.

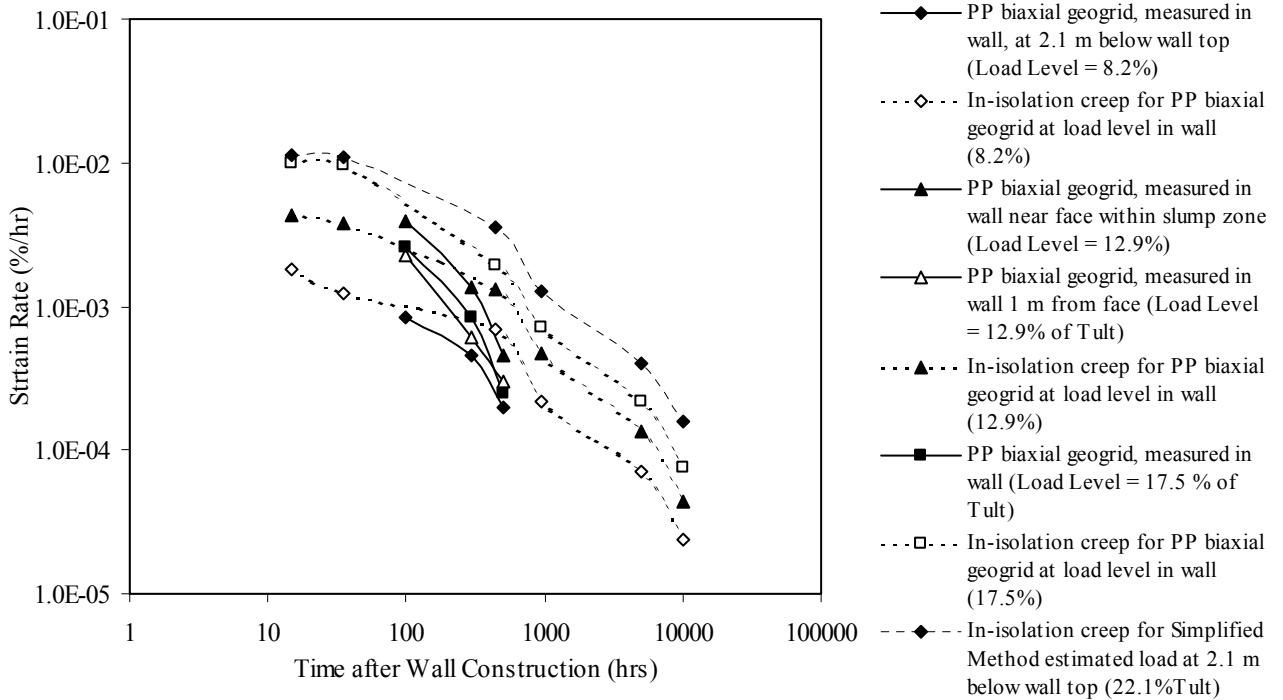Figure B7. Sherby-Dorn plot for Wall GW11—in-isolation vs. measured in wall.

Figure B8. Strain rate vs. time for Wall GW11—in-isolation vs. measured in wall.

APPENDIX C: NOMENCLATURE

a = constant coefficient

c = soil cohesion (kPa)

COV_1 = uncertainty in reinforcement strain measurements (%)

COV_2 = uncertainty in reinforcement secant modulus values (%)

COV_{total} = total uncertainty in estimated strain readings (%)

d = constant coefficient

D = demand (the total horizontal earth force to be carried by the reinforcement layers) (kN/m)

D_{actual} = demand based on the measured shear strength of the soil using plane strain peak friction angles (kN/m)

D_{design} = demand on the reinforcement layers based on the design value of soil shear strength (kN/m)

D_{tmax} = reinforcement load distribution factor (dimensionless)

FS = factor of safety

FS_{design} = design global factor of safety

H = height of the wall (m)

i = counter (1,2,3 …n)

J = tensile modulus of the reinforcement (kN/m)

J_1 = modulus of independent spring in the standard linear solid model

$J_{1\%}$ = secant modulus of the reinforcement at 1% strain (kN/m)

J_2 = modulus of second spring in the standard linear solid model

$J_{2\%}$ = secant modulus of the reinforcement at 2% strain (kN/m)

J_{ave} = average tensile modulus for all the reinforcement layers (kN/m)

J_c = creep modulus (kN/m)

J_{crs} = constant rate of strain modulus (kN/m)

J_{EQ} = delayed elastic modulus of the standard linear solid model

J_i = tensile modulus of an individual reinforcement layer (kN/m)

J_r = relaxation modulus (kN/m)

$\bar{J}(t)$ = mean value of the modulus averaged over the interval of time from 0 to t in a stress relaxation test (kN/m)

K = coefficient of lateral earth pressure (dimensionless)

K_a = active lateral earth pressure coefficient (dimensionless)

K_{abh} = horizontal component of active earth pressure coefficient accounting for wall face batter (dimensionless)

K_{ah} = horizontal component of active earth pressure coefficient (dimensionless)

K_{avh} = horizontal component of active earth pressure coefficient for vertical wall (dimensionless)

K_o = coefficient of lateral earth pressure at-rest (dimensionless)

K_r = lateral earth pressure coefficient (dimensionless)

n = total number of reinforcement layers in wall section

p_a = 101 kPa (atmospheric pressure)

P_{ah} = horizontal component of earth force (kN/m)

q = uniformly distributed surcharge pressure, or specifically the vertical stress due to traffic surcharge (kPa)

R = resistance (the total tensile capacity of the reinforcement layers in the structure) (kN/m)

R_{actual} = actual long-term resistance value (kN/m)

R_c = reinforcement coverage ratios (dimensionless)

$RD_{aldesign}$ = allowable long-term resistance-demand ratio (dimensionless)

R_{design}= long-term resistance value based on the design value of soil shear strength (kN/m)

$RD_{estimated}$ = estimated long-term resistance-demand ratio (dimensionless)

RD_{index} = index resistance-demand ratio (dimensionless)

$RD_{ultdesign}$ = ultimate design resistance-demand ratio (dimensionless)

RF = combined reduction factor to account for geosynthetic strength loss

RF_{actual} = actual strength reduction factor

RF_{CR} = reduction factor to account for strength loss due to creep

RF_D = reduction factor to account for chemical and biological degradation

RF_{design} = design reduction factor

RF_{ID} = reduction factor to account for installation damage

R_{index} = short-term resistance values (kN/m/m width of wall)

$R_{ultdesign}$= short-term resistance values based on the design value of soil shear strength (kN/m)

S = average soil surcharge depth above the wall top, or equivalent height of uniform surcharge pressure (m)

S_{global} = global reinforcement stiffness value (kN/m^2)

S_i = contributory unit face area (assumed equivalent to the vertical spacing of the reinforcement per unit length of wall) (m)

S_{local} = local reinforcement stiffness value (kN/m^2)

S_r = global reinforcement stiffness for the wall (kN/m^2)

S_v = tributary area for reinforcement layer (assumed equivalent to the vertical spacing of the reinforcement per unit length of wall) (m)

S_v^i = tributary area for reinforcement layer i (assumed equivalent to the vertical spacing of the reinforcement when analyses are carried out per unit length of wall) (m)

T, $T(t)$, T_i = reinforcement load at any time (kN/m)

$\dot{T}$ = reinforcement loading rate

T_{al}, T_{al}^i, $T_{aldesign}^i$ = long-term strength for reinforcement layer i (kN/m)

T_i = tensile capacity for reinforcement layer i (kN/m)

T_{max}^i, T_{max} = maximum measured or design reinforcement load in layer i (kN/m)

T_{max} = maximum tensile load in a reinforcement layer (kN/m)

T_{mxmx} = maximum reinforcement load from all layers in the wall (kN/m)

T_{ult} = short-term (index or ultimate) strength of the reinforcement (kN/m)

T_{ult}^i = short-term (index or ultimate) strength of the reinforcement for layer i (kN/m)

$T_{ultdesign}$, $T_{ultdesign}^i$ = ultimate design (index or ultimate) tensile strength for reinforcement layer i (kN/m)

z = depth to the reinforcement level relative to the wall top at the wall face (m)

z_i = depth below top of wall to reinforcement layer i (m)

α = constant coefficient

β = constant coefficient

δ = interface shear angle between wall facing and backfill soil (degrees)

$\varepsilon(t)$, ε_i = reinforcement strain at any time (dimensionless)

$\dot{\varepsilon}$ = reinforcement strain rate

Φ = influence factor = $\Phi_g \times \Phi_l \times \Phi_{fs} \times \Phi_{fb}$ (dimensionless)

Φ_{fb} = facing batter factor (dimensionless)

Φ_{fs} = facing stiffness factor (dimensionless)

Φ_g = global stiffness factor (dimensionless)

Φ_l = local stiffness factor (dimensionless)

ϕ = friction angle of the soil (degrees)

ϕ_{des} = design friction angle for the soil (degrees)

ϕ_{ds} = peak direct shear friction angle of the soil (degrees)

ϕ_{ps} = peak plane strain friction angle of the soil (degrees)

ϕ_{tx} = peak triaxial friction angle (degrees)

γ = unit weight of the soil (kN/m^3)

η = viscosity of the viscous element in the standard linear solid model

σ_1 = axial principal stress (kPa)

σ_3 = confining principal stress (kPa)

σ_h = lateral earth pressure acting over the tributary area (kPa)

τ_i = retardation times for the standard linear solid model

ω = wall batter

ψ = wall facing batter from vertical (degrees)

$\Omega_{1,2}$ = constant coefficient (dimensionless)